NATIONAL AND KAPODISTRIAN UNIVERSITY OF ATHENS
SCHOOL OF SCIENCE
DEPARTMENT OF GEOLOGY AND GEOENVIRONMENT

PhD THESIS

MARINE AGGREGATE DEPOSITS IN GREECE: SEDIMENTOLOGICAL - MINERALOGICAL AND GEOCHEMICAL STUDY – USAGE POSSIBILITIES

MARIANTHI ANASTASATOU

GEOLOGIST, MSc

ATHENS, 2020

NATIONAL AND KAPODISTRIAN UNIVERSITY OF ATHENS
SCHOOL OF SCIENCE
DEPARTMENT OF GEOLOGY AND GEOENVIRONMENT

PhD THESIS

MARINE AGGREGATE DEPOSITS IN GREECE: SEDIMENTOLOGICAL - MINERALOGICAL AND GEOCHEMICAL STUDY – USAGE POSSIBILITIES

MARIANTHI ANASTASATOU

GEOLOGIST, MSc

Supervisor

Michael Stamatakis, *Professor*

Advisory Committee

Michael Stamatakis, *Professor*

Athanasios Godelitsas, *Associate Professor*

Aristomenis Karageorgis, *Researcher A'*

Εξεταστική Επιτροπή

Michael Stamatakis, *Professor*

Athanasios Godelitsas, *Associate Professor*

Aristomenis Karageorgis, *Researcher A'*

Serafim Poulos, *Professor*

Ioannis Mitsis, *Assistant Professor*

Vasilios Kapsimalis, *Researcher A'*

Thomas Hasiotis, *Associate Professor*

ATHENS, 2020

To my parents, Spiros and Lemonia

To my family, George and Andriani

PREFACE

The present PhD dissertation was supported (2013 - 2015) by the research program THALES-MARE (MIS: 375655), funded by the Operational Programme "Education and lifelong learning, 2007-2013" of the Ministry of Education and Religious Affairs, Culture and Sports. Moreover, during the first two-years of my PhD studies (2013 - 2014) I received scholarship from the Antonios Papadakis Legacy, NKUA.

This dissertation was supervised by Professor Michael Stamatakis, to whom I would like to express immense gratitude. Firstly I would like to thank him for the guidance he provided me during my doctoral dissertation, but most of all I would like to thank him for his trust, kindness and continuous support. Prof. Michael Stamatakis gave me the opportunity to broaden my scientific horizons in different subjects by constantly transferring me knowledge and experience. I will always be grateful.

Moreover, I would like to thank namely the other members of my 7-member committee. I would like to thank Assoc. Professor Athanasios Godelitsas for his advices and Dr. Aristomenis Karageorgis, Research Director at HCMR, also for his advices and availability during my PhD studies. Moreover, I would like to thank Professor Serafim Poulos for his valuable guidance and knowledge he offered me, as this thesis wouldn't be completed without his contribution. I would like to acknowledge Dr Kapsimalis Vasileios, Research Director at HCMR, for his guidance during fieldwork, Assoc. Professor Thomas Hasiotis for the valuable remarks during the correction of this thesis and Ass. Professor Ioannis Mitsis for his contribution regarding mineralogical issues.

I would like extend my thanks to Dr Grigoris Roussakis, Senior Researcher at HCMR and to all HCMR team which was on-board during marine fieldwork. Moreover, I would like to express my gratitude to the late Professor Michael Collins for his coaching during my training on marine aggregates aspects at the University of Southampton.

Through the years of my PhD studies various researchers from different labs were of great help. Assistant Professor Maria Taxiarchou is acknowledged for providing me access to the Laboratory of Metallurgy, School of Mining and Metallurgical Engineering, NTUA, Mr Tzanis Emmanouil, Head of Group Concrete Laboratory, TITAN S.A., for his guidance regarding various technical tests at the laboratories of TITAN SA and Mrs Katerina Xinou, TITAN S.A., for providing me access to chemical analysis.

Professor Panagiotis Voudouris is acknowledged for his help during coastal sampling at Evia Island, Mr Vasileios Skounakis for his technical support during SEM/EDS analysis, Mrs Olga Koumoutsakou for her guidance at the determination density, Dr George Stamatakis for his contribution during mineralogical analysis and chlorines determination, Dr. George Economou, IGME, and Mrs Stefania Stamataki for providing me industrial samples and Ass. Professor Charalampos Vasilatos, whose help during these years was vital.

Furthermore, I would like to express my gratitude to Dr Aikaterini Karditsa for her support and significant contribution throughout my PhD studies. Specifically, I would like to thank her for her assistance in environmental aspects and for providing me the quantification prospect of marine aggregate deposits. Stelios Petrakis, PhD c., for his critical contribution at grain size analysis and GIS analysis, Konstantinos Aspiotis, PhD c., for his contribution at mineralogical analysis and my colleague Constantinos Mavrogonatos for his support especially during the last months of my studies.

On a more personal note, I would like to thank all my friends and especially my closest friend Antonia Tsoutsia as we went through a long part of this journey together. Of course, I owe a lot more than gratitude to my family, my parents Spiros and Nitsa and my sister Ioanna, as they supported me in all ways. Last but not least, I would like to thank my husband and colleague George Deligiannakis, as he tireless transfers me knowledge on GIS know-how and geological issues, but mostly for his support throughout these years.

ABSTRACT

The present PhD Thesis entitled “Marine Aggregate deposits in Greece: sedimentological - mineralogical and geochemical study ─ Usage possibilities” concerns the systematic investigation of the potential of Marine Aggregate (MA) deposits in Greece with respect to their industrial use. This thesis focuses on the research of various offshore modern sediments in the Greek continental shelf concerning their sedimentological, mineralogical and geochemical characteristics emphasizing the research of silica (quartz) sand. These offshore study areas are prioritized as potential MA deposits according their qualitative characteristics (such as grain size, mineralogy and geochemistry) of the sediments and significant environmental characteristics of the offshore areas.

Specifically, four offshore areas in the Greek territory, such as SE Evia, NW Crete, south and east Lesvos and NE Rhodes Island, were investigated regarding their potential to host MA deposits suitable for the construction industry. A few coastal areas, in central/eastern Evia Island, western Crete Island, north and east Peloponese, Milos, Samos and Kefalonia Island, were examined in order to suggest or not their potential for further offshore investigation. Moreover, selected industrial samples were employed as materials for evaluation and comparison to the study sediments.The suitability degree as aggregates for concrete was defined, according the performance of the materials from the qualified areas on specific technical tests.

In order to achieve the above goals, surficial offshore and coastal sediments and offshore gravity cores were collected. For the deterimination of the qualitative characteristics of the sediments were defined: the granulometric parameters, the density, the mineralogy by stereoscopy, XRD and SEM/EDS, the geochemistry by XRF method, the calcium carbonates and the chlorides. The technical tests that were employed in order to define the suitability degree of the proposed materials as aggregates in concrete were sand equivalent and methylene blue test. In the proposed areas, the spatial environmental restrictions that were applied are: *Posidonia oceanica* Natura zones, closure depth and proper distance from the coastline.

The offshore area of Evia Island is suggested as the most promising area and hosts MA deposits that cover 2.03 km^2 up to the water-depth of 50 m.The second most promising area is Kissamos Bay, NW Crete Island, which hosts MA deposit that covers 4.85 km^2 up to the isobath of 50 m.

This is the first time that an integrated study based on qualitative criteria regarding MA deposits is carried out in Greece.The suggested MA deposits and the proposed coastal areas for further investigation, contribute to the national potential for raw materials. However, for the final stage of MA deposits delimitation and exploitation, apart from the quantitative characteristics (oceanographic study), the local spatial planning issues should be considered in order to support the environmental, social and economic sustainability pillars.

ΠΕΡΙΛΗΨΗ

Η παρούσα διδακτορική διατριβή με τίτλο «Υποθαλάσσιες αποθέσεις (offshore placers) αδρανών υλικών στην Ελλάδα: ιζηματολογική – ορυκτολογική & γεωχημική μελέτη ─ Δυνατότητες αξιοποίησης τους» έχει ως αντικείμενο τη συστηματική διερεύνηση του δυναμικού των πιθανών Υποθαλάσσιων Κοιτασμάτων Αδρανών Υλικών (ΥΚΑΥ) στην Ελλάδα, σε σχέση με τη βιομηχανική χρήση των πρώτων, αυτών, υλών. Η παρούσα διατριβή επικεντρώνεται στην έρευνα σύγχρονων υπεράκτιων ιζημάτων στην ελληνική υφαλοκρηπίδα εξετάζοντας τα ιζηματολογικά, ορυκτολογικά και γεωχημικά χαρακτηριστικά τους, δίνοντας έμφαση στην έρευνα χαλαζιακής άμμου. Οι, υπο μελέτη, υπεράκτιες περιοχές προτεραιοποιούνται ως πιθανές θέσεις ΥΚΑΥ βάσει των ποιοτικών χαρακτηριστικών των ιζημάτων καθώς και βασικών περιβαλλοντικών χαρακτηριστικών τους.

Πιο συγκεκριμένα, στο πλαίσιο της παρούσας διατριβής, μελετήθηκαν τέσσερις υπεράκτιες περιοχές στην ελληνική υφαλοκρηπίδα σαν πιθανές θέσεις ΥΚΑΥ, οι οποίες βρίσκονται στη ΝΑ ν. Εύβοια, στη ΒΔ ν. Κρήτη, στη νότια και ανατολική ν. Λέσβο και στη ΒΑ ν. Ρόδο. Εν συνεχεία, μελετήθηκε υλικό από επιλεγμένες παράκτιες περιοχές, οι οποίες βρίσκονται στην κεντρική/ανατολική ν. Εύβοια, στη δυτική ν. Κρήτη, στη βόρεια και ανατολική Πελοπόνησο, στη ν. Μήλο, στη ν. Σάμο και στη ν. Κεφαλονιά, ώστε να προσδιοριστεί η δυνατότητα για περαιτέρω υπεράκτια έρευνα. Επιπλέον, μελετήθηκαν βιομηχανικά δείγματα ως υλικά για σύγκριση και αξιολόγηση των υπο μελέτη ιζημάτων. Ο βαθμός καταλληλότητας των υπο μελέτη ιζημάτων ως αδρανή σκυροδέματος προσδιορίστηκε, επιπροσθέτως, από εξειδικευμένες τεχνικές δοκιμές.

Για την επιτευξη των ως άνω στόχων, συλλέχθηκαν επιφανειακά υπεράκτια και παράκτια ιζήματα, καθώς και υπεράκτιοι πυρήνες βαρύτητας. Τα ποιοτικά χαρακτηριστικά των ιζημάτων προσδιορίστηκαν σύμφωνα με: την κοκκομετρία τους καθώς και των στατιστικών κοκκομετρικών παραμέτρων της, την πυκνότητα, την ορυκτολογία με στερεσκοπία, XRD και SEM/EDS, τη γεωχημεία με τη μέθοδο XRF, των χλωρϊόντων και του ανθρακικού ασβεστίου. Χρησιμοποιήθηκαν οι τεχνικές δοκιμές του ισοδύναμου άμμου και μπλε του μεθυλενίου, ώστε να προσδιοριστεί η καταλληλότητα των προτεινόμενων υλικών ως αδρανή σκυροδέματος. Τέλος, στις προτεινόμενες περιοχές εφαρμόστηκαν περιβαλλοντικοί χωρικοί περιορισμοί που αφορούν στις ζώνες Natura του είδους *Posidonia oceanica*, στο closure depth καθώς και στις κατάλληλες αποστάσεις από την ακτογραμμή.

Η πιο υποσχόμενη υπεράκτια περιοχή βρίσκεται στη ΝΑ ν. Εύβοια, η οποία προτείνεται πως φιλοξενεί ΥΚΑΥ που εκτείνονται σε 2,03 km^2 μέχρι την ισοβαθή των 50 m. Η επόμενη πιο ελπιδοφόρα περιοχή βρίσκεται στη ΒΔ ν. Κρήτη, στον κόλπο της Κισσάμου, η οποία προτείνεται πως φιλοξενεί ΥΚΑΥ που εκτείνεται σε 4,85 km^2 μέχρι την ισοβαθή των 50 m.

Είναι η πρώτη φορά που πραγματοποιείται μια ολοκληρωμένη μελέτη βασισμένη σε ποιοτικά και περιβαλλοντικά κριτήρια και αφορά ΥΚΑΥ στην ελληνική υφαλοκρηπίδα. Τα προτεινόμενα ΥΚΑΥ συμβάλλουν στην Εθνική Πολιτική για τον στρατηγικό σχεδιασμό και την εκμετάλλευση των Ορυκτών Πρώτων Υλών. Ωστόσο, για την τελική οριοθέτηση και εκμετάλλευση των προτεινόμενων ΥΚΑΥ, θα πρέπει να εξεταστούν τα ποσοτικά τους χαρακτηριστικά (ωκεανογραφική μελέτη) καθώς και να ληφθεί υπόψη ο τοπικός χωροτακτικός σχεδιασμός, ώστε να καλύπτονται οι πυλώνες της βιώσιμής ανάπτυξης.

CHAPTER 1. INTRODUCTION

1.1. Non-fuel Marine Mineral Deposits

Worldwide, non-fuel marine mining is carried out for several decades focusing on commodities such as aggregates, salt, cassiterite, gold and various other heavy minerals (Rona, 2008; Baker et al., 2016; Fig. 1.1). Naturally, all mineral commodities on-land mined, are also found in the marine environment (Cruickshank, 1988). However, only a small number of these marine minerals are currently exploited as current technical difficulties in seabed and substratum mining restrict large-scale exploitation of mineral resources and therefore, offshore mining industry is a relatively small economic sector (Baker et al., 2016).

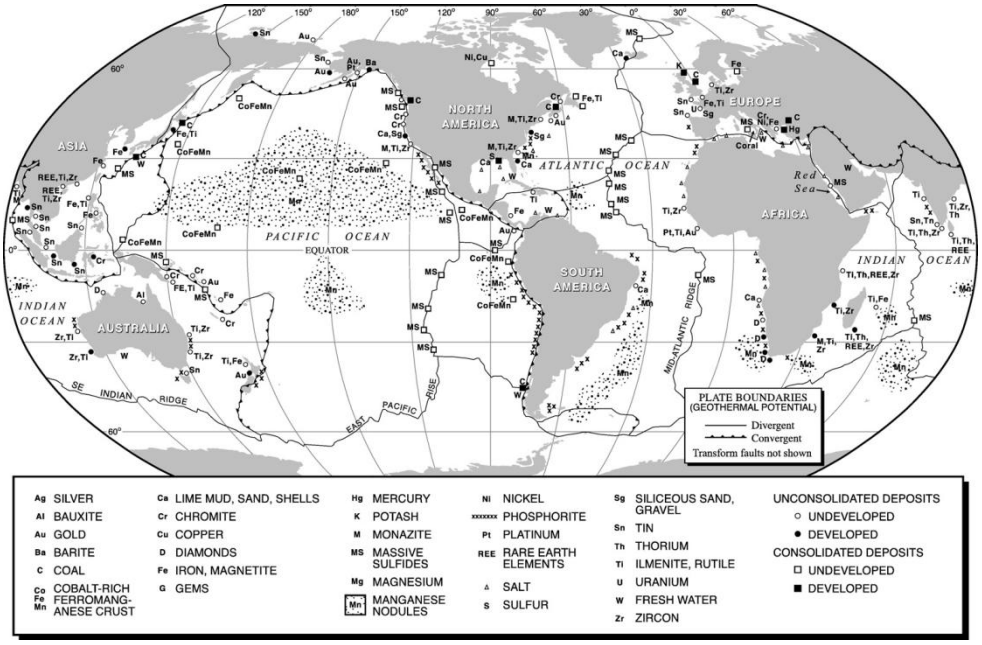

Figure 1.1. Global distribution of the currently known marine mineral resources (Rona, 2008).

Non-fuel marine mineral deposits can be obtained by: i) the continental margins; at water depths up to a few hundred meters and ii) the deep oceanic basins located at depths of several thousand meters (Cruickshank, 1988).

In the narrow continental shelves and especially nearby the coastal zone, marine placers mainly form modern deposits (e.g. beach placers, sediments sinks; USGS, 2014). Marine placers usually consist of metallic minerals of tin, tungsten, zinc, copper, iron and Rare Earth Elements – REEs, and native gold), or gems, which have been mechanically transported to the seafloor in a solid form (Cronan, 2003; Rona, 2008). Non- fuel marine

minerals and especially marine placers constitute a key sector to EU's Blue Growth Initiative, through coastal and seabed mining, as a potential contributor to growth and are included in the individual sectors of blue economy (COM(2012)494).

The formation of marine placers is a natural process that begins onland, where weathered rocks (sedimentary, igneous and metamorphic) are washed by streams and rivers, and terminates in the adjacent coasts where the sediment, which consists of gravel, sand, silt and clay, is accumulated. Among these detritus, primarily heavy minerals concentrations are formed by this physical-mechanical erosion process of bedrock minerals (USGS, 2014). Their concentration is a consequence of the higher density (>3.2 gr/cm^3) relative to the bulk eroded minerals (USGS, 2014). Factors, such as hardness, cleavage, density and solubility indicate the mineral resistance to mechanical activities applied during transport and define the distance of transportation without material change (Kudrass, 2000; Rona, 2008). According to Emery and Noakes (1968), the median transportation distance of detritus from a bedrock source to an offshore placer deposit is ~8 km. Sediments are carried from streams and rivers to a coastal area where they are deposited and/or distributed in various environments (Fig. 1.2) such as alluvial plains, deltas, the foreshore and shoreface, barrier islands, tidal lagoons and dunes (USGS, 2014). According to USGS (2014), the most significant placers are deposited in aeolian sand dunes and foreshore zone.

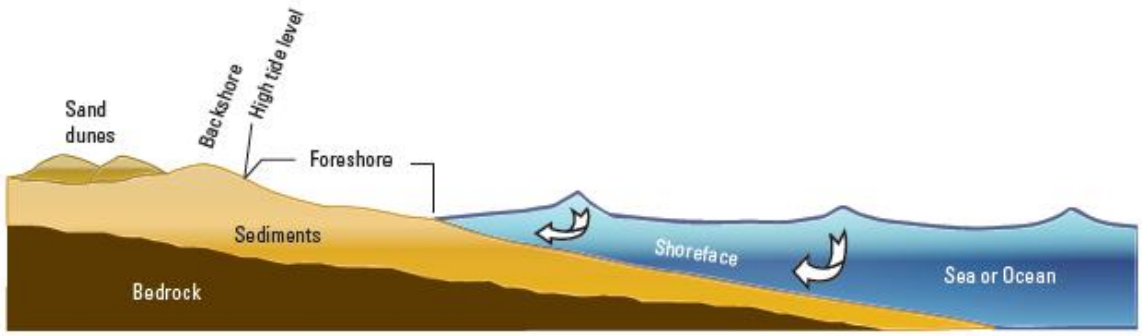

Figure 1.2. Schematic figure showing the shoreline depositional environment of marine placers (USGS, 2014).

Roy (1999) and USGS (2014) pointed out that the mature development of heavy mineral deposits is controlled by factors such as: i) long erosion periods, ii) moderately low rates of sediment supply, iii) strong and continuous wave action that drifts sand along the shore and/or onshore and iv) sea level fluctuations, especially sea transgressions. The sands in such areas are often well sorted, medium – fine grained and well rounded (Force, 1991).

According to Kudrass (2000) and Rona (2008), three generic types of placer deposits are identified: i) scattered beach placers of, relatively, light heavy minerals (< 6 g/cm^3; e.g. rutile, ilmenite, magnetite, monazite, garnet), ii) sunk fluviatile placers consist of sand and gravel containing heavy minerals (e.g. cassiterite, gold) and overlying river channels and, finally, iii) eluvial deposits. These placer deposits may lie above or below the present sea level (Rona, 2008). The operational activities of placers' exploitation concern deposits of Cretaceous to Holocene age (USGS, 2014). Particularly, they include recent deposits (Holocene) on modern coasts and other coastal deposits formed by sea level transgression and regressions during various periods of Quaternary, Tertiary and Cretaceous (USGS, 2014).

1.2. Continental Shelf

The continental shelf is a complex ecosystem where three environments interact: land, sea and atmosphere (Karditsa, 2010; Fig. 1.3). The continental shelf is a small part of continent submerged under relatively shallow sea water and covers about 5% of the earth's surface (Karditsa, 2010). According to Meade (1996), less than 5% of the sediments reaching the continental shelf from river systems escape the deep sea. Worldwide, the continental shelf hosts a wide range of natural resources and its proximity to land justifies the development as a primary area of human activities (Karditsa, 2010). Natural resources hosted in continental shelf are non-fuel mineral resources (heavy minerals, quartz-rich sand and gravel for concrete aggregate and other applications and aggregates for beach nourishment) and hydrocarbons. Moreover, the shelf area is used for aquaculture, navigation, fishing, waste disposal and renewable energy production from wave, tidal currents, wind and sun (Barrie and Conway, 2014; Chiocci and Chivas, 2014).

Continental shelves host unique archives of environmental changes arising from the interaction of sea, land and atmosphere, recorded in the depositional environment of the subsurface (Chiocci and Chivas, 2014; Gao and Collins, 2014). Consequently, sediment cores that may be collected on the shelf, due to the high depositional rate and terrestrial proximity, include local and global effects and have recorded human and environmental inputs (Chiocci and Chivas, 2014). The overall processes that control sedimentation on the continental shelf are the multifactorial result of interaction between endogenous (e.g. geodynamic) and exogenous (e.g. climatic) forces (Chiocci and Chivas, 2014). Moreover, the critical sediment distribution on the seafloor is the result of interaction between the sediment sources (e.g.

rivers, streams, estuaries, wind) and the sediment amount delivered to the shelf area and the hydrodynamic processes (e.g. waves, tides and currents) (Chiocci and Chivas, 2014).

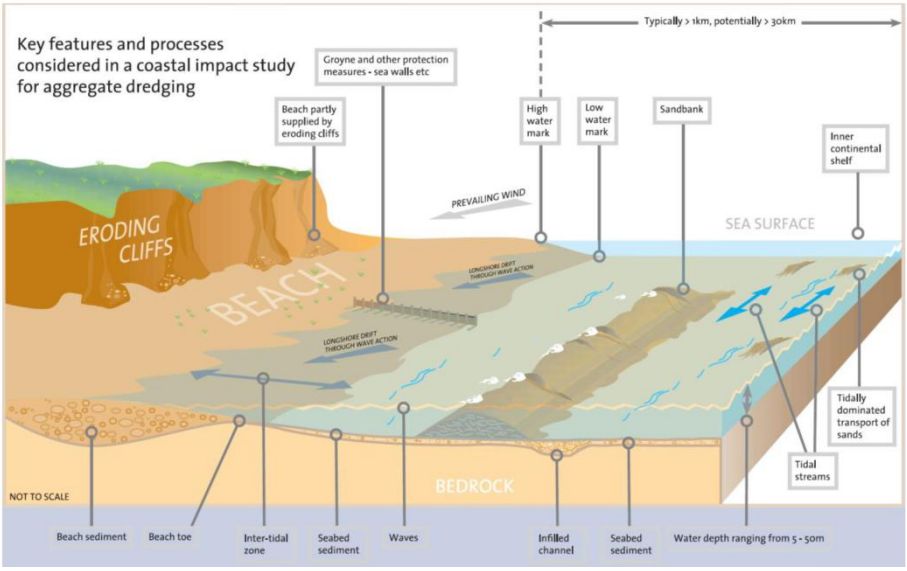

Figure 1.3. Typical features and processes occurring along the coastal areas (BMAPA, 2013).

According to the United Nations Convention on the Law of the Sea (UNCLOS), an international agreement as stated in Article 76 that defines the limits, the rights and responsibilities of the nation's towards their territorial water as: "the continental shelf of a coastal State comprises the seabed and subsoil of the submarine areas that extend beyond its territorial sea throughout the natural prolongation of its land territory to the outer edge of the continental margin, or to a distance of 200 nautical miles from the baselines from which the breadth of the territorial sea is measured where the outer edge of the continental margin does not extend up to that distance".

The inner continental shelf according to various dynamics may be distinguished into two main morphological zones: i) the nearshore zone and ii) the offshore zone (Fig. 1.4; 1.5). The nearshore zone extends seaward from the low water level up to the outer closure depth (e.g. Mangor et al., 2017). According to Krays et al. (1999), the closure depth is defined: "the depth of closure for a given or characteristic time interval is the most landward depth seaward of which there is no significant change in bottom elevation and no significant net sediment exchange between the nearshore and the offshore". Therefore, closure depth is critical as it separates two different zones (morphodynamically) along a beach profile at short/medium-term time scales (1–10 years): the active nearshore area and the significantly less active offshore area. Closure depth constitutes a crucial parameters in many coastal engineering projects, such as beach nourishment and aggregates dredging (Morang and Birkemeier,

2005). The offshore zone is defined as the zone off nearshore zone, the outer closure depth (e.g. Mangor et al., 2017).

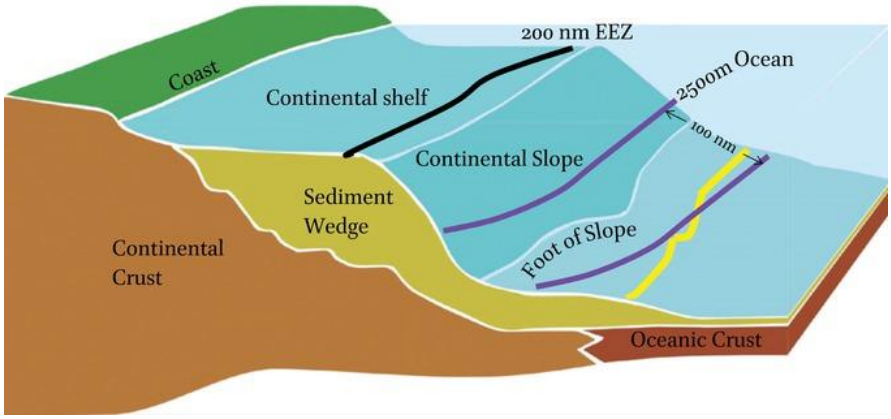

Figure 1.4. Schematic of the continental shelf according to UNCLOS (Mayer and Mosher, 2018)

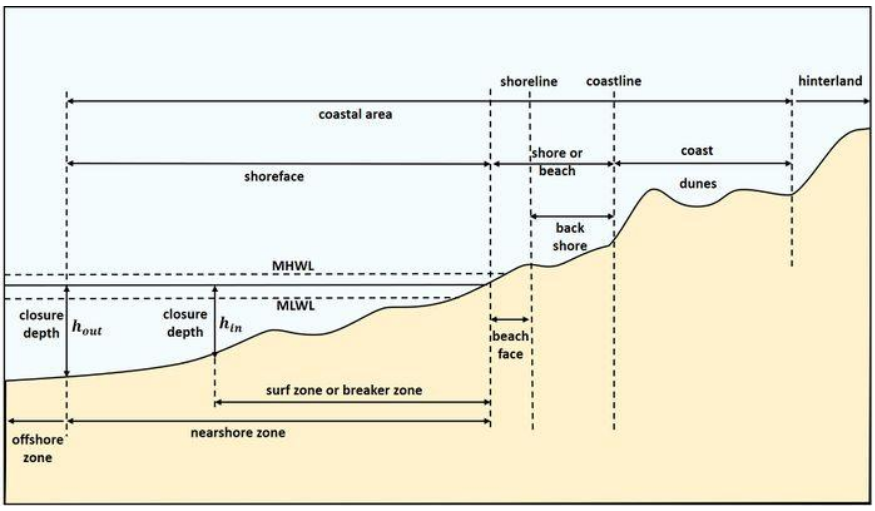

Figure 1.5. Schematic of the maritime zones (US Army Corps of Engineers, 1984).

1.3. Marine Aggregates

During the last decades Marine Aggregates (MA) exploitation increases due to the high demand for material supply regarding construction industry, coastal infrastructure projects and beach nourishment/replenishment projects (Phua, 2004; Velegrakis et al., 2010; Fig. 1.6). Sand and gravel are the fundamental and unrecognized materials of economies (UNEP, 2019), being the largest in volume mined solid-material extracted globally (UNEP, 2014). Until recently, sand and gravel were extracted mainly in river-beds and land-quarries; however, due to the decline of land-won, a shift to coastal and marine aggregates has occurred (UNEP, 2014). Currently, the increasing rates of the extracted sand and gravel exceed the natural replenishment rates; having a major impact to the ecosystem (UNEP, 2014, 2019)

Marine aggregates are non-metallic, natural occurring sediment deposits found in the inner continental shelf off the coast and consist of sand, gravels and shells/shell debris (Velegrakis et al., 2010).

Figure 1.6. a) Marine aggregates pumped from the ship onto the beach (Eastern Solent Coastal Partnership, www.escp.org.uk) and b) marine aggregates dredging on board (Marine Aggregates Dredging, www.hrwallingford.com).

1.3.1. Origin of Marine Aggregates Deposits

Sea levels fluctuations have led to the deposition of sand and gravel (marine aggregates) that currently lie on the sea-bed. Originally, these materials were deposited by rivers and streams, when their currently marine location was terrestrial and were re-worked during sea levels fluctuations (Fig. 1.7).

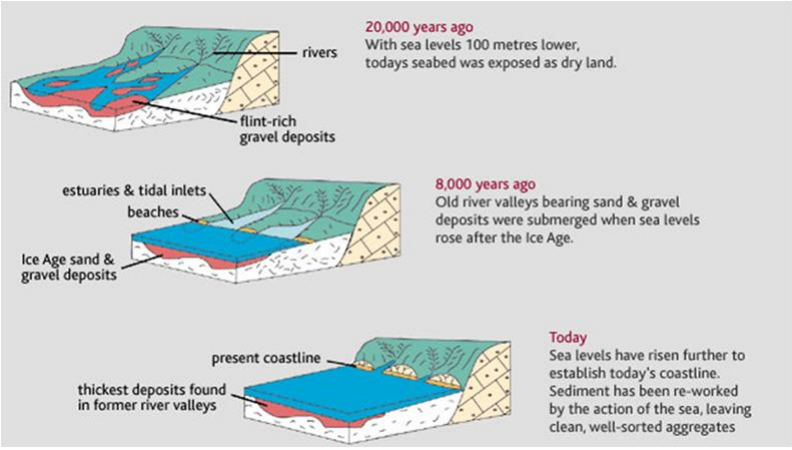

Figure 1.7. Schematic figure of how marine aggregates were formed (http://www.bmapa.org/).

Most of the exploitable marine aggregates deposits were formed during Quaternary (Velegrakis et al., 2010). The composition of marine aggregates varies greatly depending on the original bedrock source and mainly two kinds of deposits occur; relict and

contemporary/modern deposits (e.g. McManus, 1975; Velegrakis et al., 2010). Relict deposits were formed in the past, during Pleistocene, and under different environmental conditions than today (Velegrakis et al., 2010). Around European (especially northern) and during Pleistocene sea level lowstands, the continental shelves were drained by large periglacial river systems (e.g. Antoine et al., 2003) and relatively well sorted sediment material was deposited at the river thalweg, terraces, point bars and fans (Leeder, 1999; Velegrakis et al., 2010). These coarse grained deposits are usually buried under finer ones, although sometimes are found exposed on the present seafloor (Velegrakis et al., 2010).

Modern deposits are formed under the current hydrodynamic and sedimentary conditions and are related to high-tidal and/or wave energy, especially in shallow continental shelves (e.g. Vincent et al., 1998; Velegrakis et al., 2007). Depending the conditions, modern deposits could be subjected in significant material exchanges with the adjacent terrestrial and/or marine areas (Velegrakis et al., 2010). Based on their dynamics, modern deposits can be distinguished into (Velegrakis et al. 2010): i) sediment sinks, such as depositional centers that do not exchange sediment material with the surrounding areas and ii) sediment stores, such as depositional center with considerable material exchanges with the surrounding areas. According to the same authors, in active environments surficial sediment deposits are often mobile (stores) and may include sand sheets, sandbanks, sand ribbons, sand patches and submarine dune fields.

Furthermore, marine aggregates based on the origin and the environmental conditions are classified into two general schemes regarding their size, i.e. sand and gravel. Geologists use Folk (1980) grain size classification, according to which sands sizes range is 0.063 – 2 mm and gravels greater than 2 mm. However, marine aggregates industry uses different classification and classifies sand particles in the range 0.063 – 4 mm and gravel >4 mm.

1.3.2. Aggregates

Aggregates are inert, granular materials of natural or artificial (industrial) origin used either individually or in combination with cement, lime, bituminous binder or other aggregates (e.g. EN 12620:2002; BGS, 2007). Moreover, according to the classical concept, aggregates exhibit no chemical bonding properties between them and/or with the adhesive, only physical coherence (e.g. EN 12620:2002; BGS, 2007).

Aggregates are essential raw materials for construction industry and infrastructure on which our society depends. “Aggregates” is a generic term and various classifications may be applied based on their origin, size, shape, weight etc. Based on their origin, aggregates may be classified into three categories (e.g. UNEP, 2019): i) primary, ii) recycled and iii) manufactured aggregates (Fig. 1.8).

Figure 1.8. European statistics of aggregates’ categories for 2017 (UEPG, 2019).

Primary aggregates are materials from natural mineral resources, which have been subjected only to physical processing (i.e. crushing and sizing). Primary aggregates are crushed stone extracted in hard rock quarries, land-won sand and gravel excavated from pits, sand and gravel form rivers, lakes and beaches and marine aggregates (e.g. BGS, 2007; UNEP, 2019).

Recycled aggregates are re-processed inorganic materials derived from construction and demolition residuals (e.g. BGS, 2007; UEPG, 2019). Manufactured aggregated are materials resulting from industrial processes involving thermal or other modifications, such as furnace slugs or china clay residues (e.g. BGS, 2007; UEPG, 2019).

Based on their weight/density, aggregates are classified into three categories (EN 1097:2000; EN 12620:2002; GCCT, 2016): i) lightweight (<2 g/cm^3), ii) normal-weight (2-3 g/cm^3) and iii) heavy-weight aggregates (>3 g/cm^3). Based on their size, aggregated are classified into three categories (EN 933-1:1997; 12620:2002; GCCT, 2016): i) coarse (>4 mm), ii) fine (≤4 mm) aggregates and iii) filler (70% <0.063 mm). Furthermore, based on their shape aggregates may be classified into: rounded, angular, irregular, flaky, elongated or mixtures of them (e.g. BGS, 2007).

1.3.2.1. Silica Sand

Sand is a common material critical to society. The weathering of quartz-bearing formations (rocks) creates silica – rich or quartz sand. The highest quality sand deposits consist mainly of quartz with various types and amounts of other minerals (Shaffer, 2006). Quartz is a common mineral which comprises 35% of all rocks in the Earth's crust and occurs in many sand types (Shaffer, 2006).

Recent sand deposits are immature and generally angular particles are that become rounded with transport and maturity. Recent sands often contain various and relatively unstable minerals such as micas, while mature sand tends to contain one dominant mineral, such as quartz (Shaffer, 2006). In order to consider a material as silica or quartz sand, the quartz content must be more than 95% quartz and the iron oxide must be less than 0.6%. Lower quartz content corresponds to lower grades. High-purity sand (quartz sand) has numerous technological applications, such as water filtration, metal castings and glassmaking. The use of silica sand transfuses significant advantages, such as durability, excellent surface finish, hard surfaces and low water absorption (e.g. BGS, 2007).

1.4. Marine Aggregates Uses

Marine aggregates uses differ depending on the country. However, the main uses of marine aggregates are in the manufacture of concrete and in beach replenishment/nourishment projects. Furthermore, marine aggregates have multiple uses such as asphalt and coated products, masonry and paving blocks, drainage and fill materials, mortars, sports pitches, equestrian facilities, leisure facilities, horticulture products and steel manufacture.

In the case of marine aggregates uses in the manufacture of concrete, the applied requirements are these of common aggregates. The geological origin and, therefore, the mineralogical composition of marine aggregates are the same as the terrestrial sand and gravel. Moreover, the shape, strength and other physical characteristics are identical to land-based equivalents and therefore their properties (mechanical and chemical) are the same (http://www.marineaggregates.info). Marine aggregates generally host less fine-grained material, a significant factor for concrete applications (e.g. Velegrakis et al., 2010)

Additionally, siliciclastic marine aggregates consist of harder material than the terrestrial aggregates, as they have been processed with rigorous abrasion along the active coastal and inner shelf environments (e.g. Pettijohn et al., 1972). Dessert sand is not the optimum material for concrete as erosion process forms perfectly rounded grains which do not bind well in concrete applications (UNEP, 2014).

The only differences between marine aggregates and the majority of land-won aggregates are the chloride content and shell presence. Chlorides in marine aggregates, as well as in land-won aggregates, that is scheduled to be used as concrete component should be kept in perspective because two significant issues may arise: i) Alkali Silica Reaction (ASR) and ii) corrosion (BMAPA, 2020). Marine aggregates, as well as land-won aggregates, are susceptible to ASR. In washed aggregates the possible contribution to alkali of sodium and potassium aggregates are eliminated; however this has to be checked to comply with the relevant guidelines and restrictions in order to minimize the ASR risk (BMAPA, 2020). Moreover, there is a need to avoid corrosion in steel reinforced with concrete (EN 206-1:2000; BMAPA, 2000). Shell content in marine aggregates consists mainly of calcium carbonate, a compound that is stable in concrete (BMAPA, 2020). EN 12620 has two categories of shell content in coarse-grained aggregates; below and over 10%. No such a limit exists in fine-grained aggregates.

Qualitative characteristics of marine aggregates

According to various European and national restrictions (e.g. EN 933-1:1997; EN 1097:2000; EN 206-1:2000; EN 12620:2002; GCCT, 2016), aggregates and therefore marine aggregates, must comply with the following conditions, among others, in order to be eligible for using in concrete manufacturing.

- SO_3 content should be <1%, as it causes swelling
- Iron compounds should be <2%, as they cause swelling and spots (stains)
- Nitrates and halogens content, as they cause corrosion
- Lead and/or zinc compounds, as they reduce strength
- Chlorides should be <1%
- Phosphate compounds

- Siliceous clays content (Ca, K and Na) as they give rise to high volume changes on wetting and drying and are absorptive
- Components susceptible to corrosion, such as clay schists as they reduce strength
- Organic compounds
- Coal and lignite should be <1%, as they reduce strength
- Chert content (micro or crypto-crystallic quartz; specific weight<2.35 g/cm^3) should be <5% it is alkali-reactive
- Coarse – grained quartz intensely fractured, granulated and strained and containing secondary inclusions
- GCCT, 2016, suggests aggregates to avoid aggregates from rhyolite, opal, andesite and dolomites, as they cause swelling; zeolites as the react with the alkali of the cement.
- Anhydrous calcium chlorides should be <1%
- Shell content preferably to be <10% (obligatorily in coarse aggregates)

1.4.1. Life Cycle Assessment of Marine Aggregates

Life Cycle Analysis (LCA) is the process that assesses the impact of a product on the environment throughout its life and also increases the efficiency of the resource utilization (SARMA Glossary, 2011). It can also be used as a tool to Environmental Impact Assessment (EIA). The main points of LCA are to identify/quantify the environmental load involved, assess the possible environmental impacts and evaluate available options to reduce them (e.g. Blengini and Gabarino, 2011; SARMA Glossary, 2011).

Life Cycle Analysis of marine aggregates involves two phases: dredging/extraction and processing. The dredging phase includes two sub-phases, those of dredging and loading (Fig. 1.9). The processing phase comprises nine sub-phases: pre-treatment, storage, screening/grading, crushing/grinding, grain size sorting, washing, sorting by moisture, drying, grinding and end-products' storage (Korre et al., 2009). However, the specific processing procedures vary greatly depending on various parameters, such as the properties of the marine aggregates, the operating criteria, the waste products, the methods of collection and the availability of space and security (Barksdale, 1996).

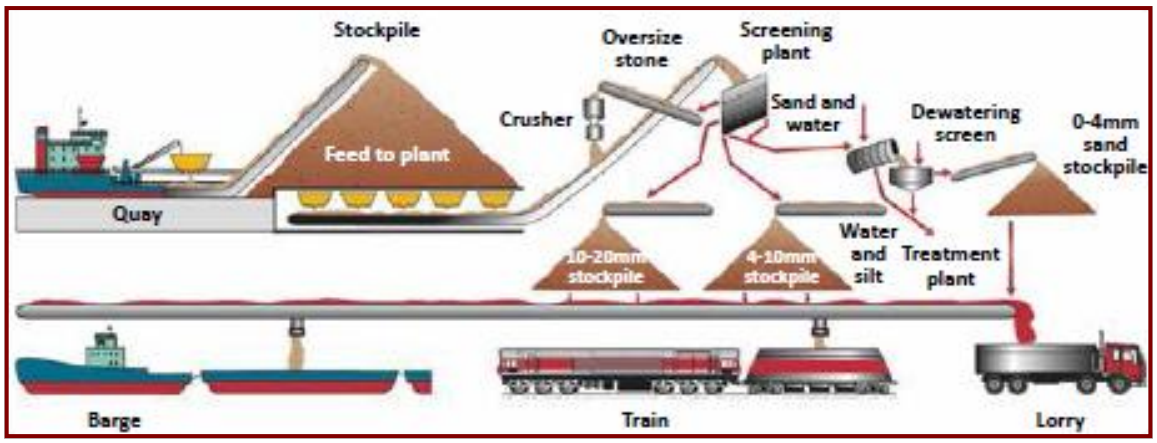

Figure 1.9. Life Cycle Analysis of marine aggregates at processing phase (Highley et al., 2007).

1.5. Legislative and Regulatory Framework – Environmental and Socio-economic Dimension

The link between Environmental, Social and Economic Sustainability constitutes a priority of the sustainability pillars of the Global Goals (UN SDG, 2015).

Legislative and Regulatory Framework

Marine aggregates extraction is governed by a number of legal regulatory measures in Europe. That legal regulatory framework is ruled by international conventions, European directives and national legislation. Greece has not validated all international conventions, which are as follows (Velegrakis et al., 2015).

The *United Nations Convention on the Law of the Sea (UNCLOS)*, which is opened for signature in 1982 and entered in force in 1994, states that the maritime zones for each country is delimited and the international legal framework on respect of usage, development and preservation is defined (e.g. Rona, 2008; Velegrakis et al., 2015). UNCLOS, 1982, recognizes a 200 nautical mile wide Exclusive Economic Zone (EEZ) under the authorization of adjacent coastal states (e.g. Rona, 2008). Furthermore, beyond the EEZ boundary an international zone “the Area” is declared as the “common heritage of mankind” area, wih the mineral resources under the United Nations’ jurisdiction (e.g. Rona, 2008).

The Barcelona Convention (1995), for the Protection of the Marine Environment and the Coastal Region of the Mediterranean whereas sixteen Mediterranean countries, including Greece, participate. The Barcelona Convention regulates the prevention and control of the

pollution that originates from exploration and exploitation activities in the seabed and its subsoil of the participating Countries (e.g. Velegrakis et al., 2015).

The ESPOO Convention, 1991, whereas the participating countries are expected to timely assess the environmental impacts of various activities, such as mining, extraction and processing (e.g. Velegrakis et al., 2015).

European and national legislation

Various EU Directives are related to marine aggregates operations and member states have to implement after adopting them in national legislation. These Directives mostly focus on the protection and sustainability of marine environment (Velegrakis et al., 2015). These are as follows:

- The Environmental Impact Assessment (EIA) Directive (85/337/EEC amended by 97/11/EC, 2003/35/EC and 2009/31/EC, codified by Directive 2011/92/EU further amended by 2014/52/EU)
- The Strategic Environmental Assessment Directive (SEA, 2001/42/EC) – Greek JMD 107017/28-8-2006 (OJG 1225/B/5-9-2006)
- The Council Directive on Conservation of Natural Habitats and of Wild Fauna and Flora (92/43/EC)
- Greek Law 3022/18-6-2002 (OGC 144/A/19-6-2002) – Barcelona Convention
- The Council Directive on Freedom of Access to Information on the Environment (2003/4/EC)
- The Raw Materials Initiative — meeting our critical needs for growth and jobs in Europe.COM (2008) 699, Communication from the commission to the European Parliament and the Council. SEC(2008) 2741.
- The Commission Decision on criteria and methodological standards on good environmental status (GES) of marine waters, 2010/477/EU,
- The Marine Strategy Framework Directive (2008/56/EC) – Greek Law 3983/16-6-2011 (OGC 144/A/17-6-2011)
- The Blue Growth, 2012; Communication from the Commission to the European Parliament, the Council, the European Economic and Social Committee and the Committee of the regions. Blue Growth opportunities for Marine and Maritime Sustainable Growth.

- The Directive on Maritime Spatial Planning, Directive 2014/ 89/EU. Commission of the European Communities.

Environmental and Socio-Economic Dimension

Globally, marine aggregates industry is an essential supplier of mineral resources. However, the increasing volumes of aggregates extracted from riverine and marine ecosystems are often not legally operated and result threatening the ecosystem (UNEP, 2019); this issue is often ignored by local policy makers and that problem remains unknown by the general public (UNEP, 2014). Sustainable development combines the socioeconomic development of a society with the the environment improvement (UNEP, 2019). Therefore, there is a need for regulating marine sand and gravel management in national and international level and furthermore these policy actions should include the scientific consulting and monitoring of these marine mining operations (UNEP, 2019).

The socioeconomic analysis as a decision-making tool regarding the marine environment has helped decision-making techniques; however, quite often there are overlaps between the social and the economic aspects (Newell and Woodcock, 2013). The tool designed by Dickie et al. (2010), uses socio-economic information in marine aggregates operations. This tool focuses on the interactions between the various uses of the marine environment (at local and regional level) and the requirements for such a context (Newell and Woodcock, 2013).

1.6. Future Demand of Marine Aggregates

Access to local aggregate resources is a fundamental and crucial issue both for the aggregates industry and for the European society. Marine aggregates resources are a mineral resource of high and increasing importance in the EU countries and the UK (Velegrakis et al., 2010). The EU aggregates sector represents a turnover of around €20-25 billion with an average price of 7-8 € per ton in 2009 (European Minerals Foundation, 2010). Aggregates are the largest mining industry in terms of volume production and the second most valuable after oil and gas (Menegaki and Kaliampakos, 2010). According to the EU project SARMA, the EU demand for aggregates is increasing at a rate of more than 4.2% per year.

Any prediction for the future demand of marine aggregates in not an easy process, as it depends on the economic growth of each country, the status of the construction industry, the international and European policies and regulations and the ability of the national construction industries to access markets and cooperates with other sectors (e.g. shipping companies). However, in some countries, e.g. UK, Netherlands and Belgium, marine aggregates demand is estimated to increase, due to on-going and /or new projects. The Global Aggregates Information Network (GAIN) estimates that by 2030 international aggregates demand will rise to 60 billion tons per year due to the increasing population, urbanization and economic growth (UNEP, 2019). This demand will derive from Asia (mainly India), Africa and Latin America (UNEP, 2019).

In Greece, many industries are active in aggregates sector and especially mining and/or use of silica sand as raw material. Indicatively, among these companies are Group TITAN S.A., Thrakon Group, Durostick S.A., Imerys, Sintecno Hellas, Lafarge (AGET Heracles), Kerakoll Hellas S.A., Mapei, Sibelco Hellas S.A., Mathios Reftactories S.A., MEVIOR S.A., Olympus S.A., e.t.c. However, due to lack of significant silica sand deposits, large amount of the required quartz-rich sand is imported. The imported quantities are estimated to be a few tens of thousands tons per year. Many cement companies use silica or quartz-rich sand as aggregate in concrete or ingredient in clinker. Industries related to building materials such as tiles and mortars, also use significant amounts of silica sand. Thrakon Company extracts quartz-rich sand from Ardas River in Evros, northern Greece for the production of insulating products. In the Greek market, bagged quartz sand (25 kg bags) costs ~170 €/ton, while quartz sand in big bags costs ~25 €/m^3.

1.7. Marine Aggregates Deposits

1.7.1. Marine Aggregates Deposits around the world

Globally, more sand and gravel are mined than any other material; however no reliable data exist for all countries (Krausmann, 2009; UNEP, 2014). Data are available either for certain developed countries or only data for cement production or no data (UEPG, 2019; UNEP, 2019; Table 1.1).

The exploitation of sand and gravel is ruled by safety, health and environmental regulations and restrictions, especially regarding crystalline silica exposure (USGS, 2020).

According to USGS (2020), USA plan to adopt new regulations through 2021, affecting various relative industries. The report of USGS (2020), predicts that these new restrictions will result in future sand and gravel operations being located further from high-population centres.

Table 1.1. World Mine Production and Reserves of Sand and Gravel (marine and land-won) (USGS, 2020).

COUNTRIES	2018	2019
United States	121000	110000
Australia	3000	3000
Bulgaria	7250	7300
Canada	2500	2500
France	9310	9300
Germany	7500	7500
India	11900	12000
Indonesia	5540	5500
Italy	14000	14000
Japan	2520	2500
Korea	4300	4500
Malaysia	10000	10000
Mexico	2360	2400
Netherlands	54000	54000
New Zealand	2320	2300
Poland	5120	5000
South Africa	2400	2400
Spain	35500	36000
Turkey	13500	14000
United Kingdom	4000	4000
Other countries	17200	21300
World Total (rounded)	**335000**	**330000**

According to Ross (2004), Steele et al. (2010) and USGS (2020), marine aggregates data vary significantly globally, however the largest producers seems to be the Japan, China, United States of America, United Kingdom and Netherlands (e.g. Fig. 1.10).

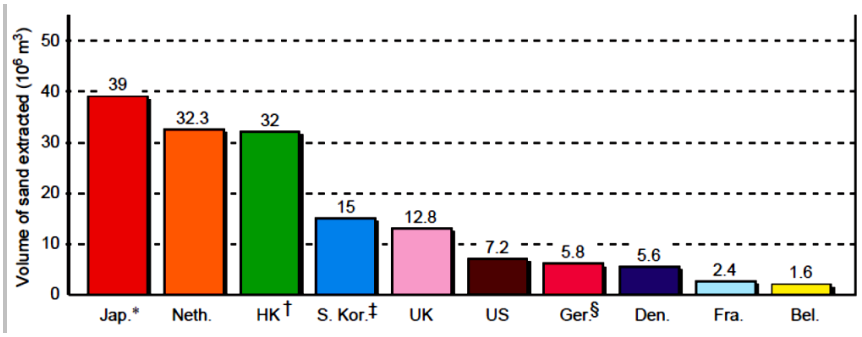

Figure 1.10. Global production of marine aggregates for 2002 (Roos, 2004; Steele et al., 2010).

China

The use of sand and gravel has a high correlation with the cement production. China hosts almost 60% of the global cement production (UNEP, 2019) due to construction boom (UNEP, 2014, 2019; Fig. 1.11). Therefore, China exploits sand and gravel (marine and land-won) from critical hotspots regarding extraction impacts (UNEP, 2019).

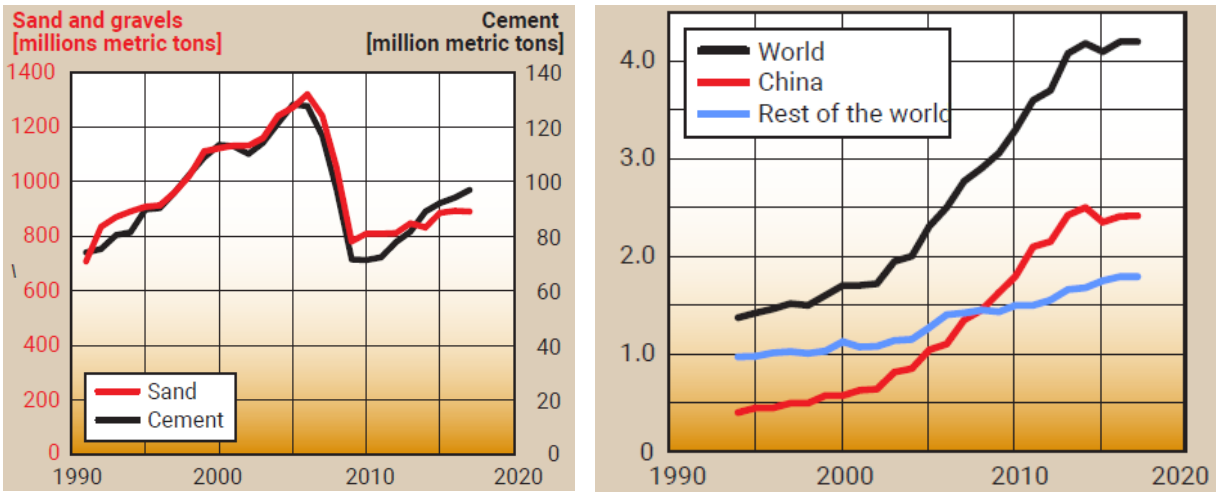

Figure 1.11. (a) Correlation of sand and gravel (marine and land-won) with cement production and (b) billion metric tons of cement globally (Krausmann, 2009; UNEP, 2019).

USA

Sand and gravel production in USA is intended for construction (e.g. private buildings, public construction projects) and industry (e.g. oil and gas sector). Concerning 2019, construction sand and gravel production was about 970 million tons; 4% increase compared to 2018 due to the continued growth of the private and public construction markets (USGS, 2020). In 2019, sand and gravel for industrial uses valued about $5.7 billion, from about 191 companies in 35 States (USGS, 2020).

European Union and the UK

According to the European Aggregates Association, in 2017 the production of marine aggregates remained at 2% compared with the previous year, i.e. 61 Mt; decreased production compared to 2009, 82 Mt. The largest producers in European region are the Netherlands, followed by the UK, Germany and Denmark (UEPG, 2019; Fig. 1.10 and 1.12).

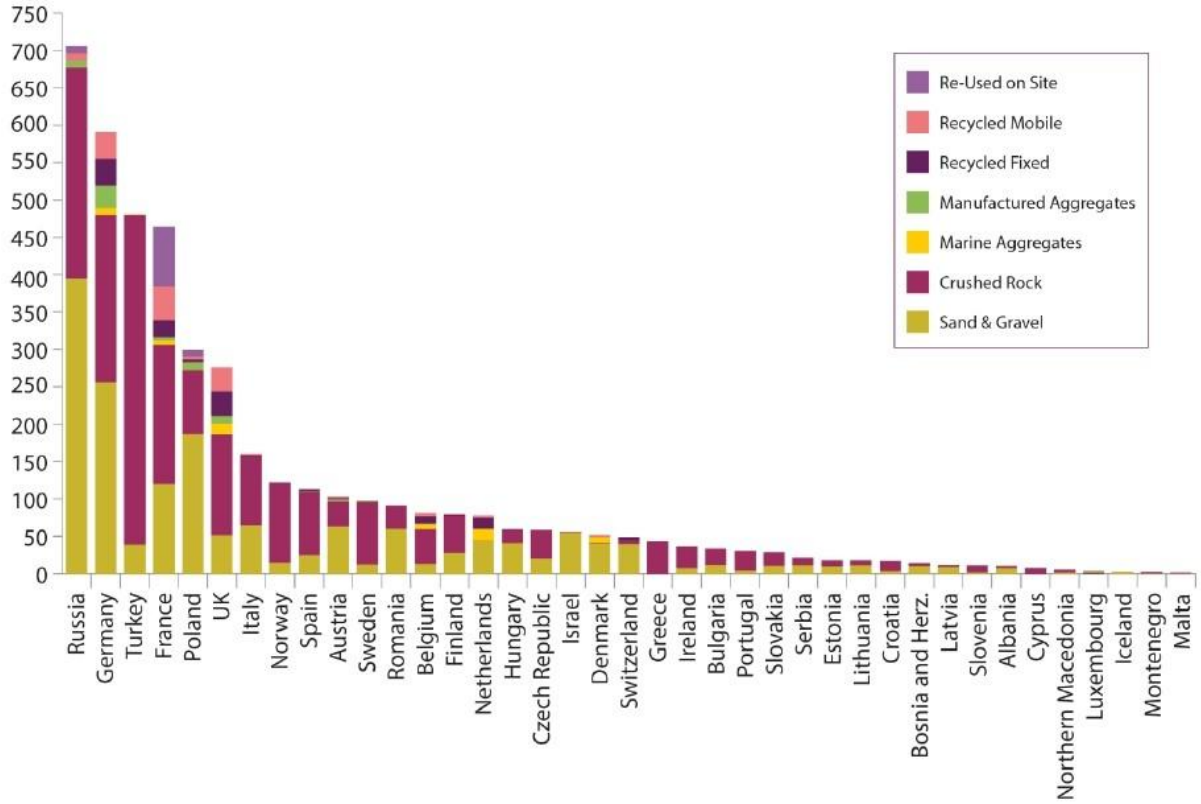

Figure 1.12. Annual aggregates production for 2017 in million tonnes by country and type (UEPG, 2019).

In the Netherlands marine aggregates operations increase since 1989, in response to the increasing demand of the construction industry and for fill and beach replenishment projects (ICES, 2005; Velegrakis et al., 2010). In the UK marine aggregates is a important resource. According to BMAPA, UK manages about 70 production licences and marine aggregates industry satisfies UK's sand and gravel need as follows: England and Wales 22%, London and the south east 31% and South Wales 90%. In France, marine aggregates production increases the last decade (Velegrakis et al., 2010; USGS, 2020). In Germany, during the last two decades the production increased greatly due to project led demand (Velegrakis et al., 2010; USGS, 2020). Belgium hosts great marine aggregates deposits, however during the last years the annual production remains stable due to high environmental concerns (e.g. stability and biodiversity; Velegrakis et al., 2010). Moreover, Belgium imports marine aggregates from the UK (Velegrakis et al., 2010). In Spain, marine aggregates exploitation is restricted only for beach replenishment projects and relevant operations take place both in the Atlantic and the Mediterranean inner continental shelf (ICES, 2006; Velegrakis et al., 2010).

1.7.2. **Marine Aggregates Deposits in Greece**

Along the Mediterranean European coast and therefore in Greece, no accurate data exist for marine aggregates production (Velegrakis et al., 2010).

1.7.2.1. ***Previous experience***

Aggregates in Greece are vital for the economy and society as they represent almost 45% of the total mineral/rock production (Tsakiris, 2012). Most of the aggregates materials are produced in land open quarries, which are estimated to be over 230 active, and most of them produce limestone aggregates (Litinas, 2008; Tsakiris, 2012).

In Greece, the gross value of aggregates, including sand and gravel (marine and land-won) exceed 300€ millions with an averages annual increase of 6% until 2009 (Tsirampidis and Fillipidis, 2013), followed by a decrease related to the recent economic crisis. According to Tsirampidis and Fillipidis (2013), operations of sand and gravel extraction are active in almost all the riparian areas of Greek rivers. Various construction works for the needs of "Olympic Games 2004" were implemented with sand and gravel aggregates from Axios River, which are considered to be of high quality (Tsirampidis and Fillipidis, 2013). Various quartz-rich sand and gravel deposits have been discovered over the last decades (Arvanitidis, 1998). According to Arvanitides (1998), a quartz-rich sand deposit is located in Kastoria (after treatment 94-96 wt% SiO_2 and 0.04 – 0.06 wt% Fe-oxides) and is estimated to host 1.2 million tons. However, according to various sources (e.g. https://www.pdm.gov.gr/), during 2015 – 2016 80 tn of quartz-rich sand required for the construction of Pramoritsa dam in Kastoria and were imported. Overall, Greek quartz and quartzite land-won reserves are expected to be $5.000*10^3$ tn (Tsirampidis and Fillipidis, 2013).

Marine aggregates extraction has been recorded since 1960s, mainly from the inner continental shelf of various Greek islands, such as Andros and Mykonos; the produced material was exploited from the construction industry (Velegrakis et al., 2010). During the 1980s, only a few organized operations for marine aggregates dredging and exploitation took place in Greece in areas such as NW Crete, Rhodes and S. Evia Island (Anastasatou et al., 2014). However, since the 1990s due to stricter environmental regulations most of the marine aggregates extraction operations have been terminated and only a few of them remained; offshore Trikeri (North Evian Gulf) and Southern Evia Island (Velegrakis et al., 2010). No available information exist for the annual extracted volumes of these marine aggregates operation, however they are estimated to be a few hundreds of thousands cubic meters (Velegrakis et al., 2010).

During recent years, the only information regarding an established company with marine aggregates dredging and exploitation operation was about a currently non-active company named “DRACHMI S.A.” in the area of Kavo D’Oro (Cape Kafireas), which was an occasional and not systematical activity. According to an internal technical report (2007) of TITAN Cement Company S.A. (pers. comm.) the dredging activity was carried out at 30 m depths and the annual production was estimated to be about 300.000 m^3, while co-production of 400 tn shells was involved. Concerning marine aggregates process after dredging, about 90% of the sea-water filtration was completed within the first three hours of the ship’s return trip to τthe unloading port. No further rinsing was performed in order to remove additional salt from the material, as this was not required from the end-users. The material was available in various Ionian and Aegean islands, as well as in yards with building materials throughout Greece.

Currently, the only known established company, which operates in marine aggregates dredging industry, is RAFINA Shipping Company (S.C.). The main activities of this company is dredging, transport and disposal of marine sand and gravel throughout Greece. RAFINA S.C. operates with the dredging ship “IRINI”, equipped with self-propelled trailing suction dredging system (Fig. 1.13). On board, the dredged material passes through a sieve, whereas the retained material (~0.1 % of the total) returns back to sea. Seawater is filtered on board and no further rinsing is applied. The dredged marine aggregates are delivered directly from the ship’s sandbox to the customer of each port indicated each time. The port often approached by IRINI ship area these of Piraeus, Keratsini, Chalkida, Lavrio, Lesvos Island, Volos, Chios Island, Mykonos Island, Kos Island, Samos Island and Rhodes Island (http://www.rafinashipping.gr).

Figure 1.13. Dredging ship “IRINI” of RAFINA S.C. (http://www.rafinashipping.gr)

1.7.2.2. ***Potential of Marine Aggregates around the Greek coastline***

In Greece, as in most Mediterranean countries, marine aggregates constitute a nearly unexploited potential resource with unclear national legal framework for their exploitation (Radzevičius, 2010), whilst any extraction activity occurs sporadically and more or less arbitrarily (Velegrakis et al., 2010). Particularly, high quality demand on marine aggregates (high quartz content) is crucial mainly in the construction industry due to their high strength/durability. Moreover, marine aggregates are crucial in coastal defence projects as resilience measure.

In Greece, the only scientific knowledge regarding marine aggregate deposits derives from the implementation of the research NSRF program MARE (Marine Aggregate Resources - NKUA, MIS 375655). During project's implementation, several promising areas in the Greek continental shelf of the Aegean were explored (e.g. Pascual and Jones, 2018), which appear to meet the requirement of industrial applications and products (Anastasatou et al., 2015; Stamatakis et al., 2015).

Promising areas of marine aggregates in Greece are narrow coastal valleys of "V" type that are incised the adjacent continental shelf and are filled with terrestrial sediments (Poulos et al., 2015). Coastal lithology provides information about the type of the terrestrial rocks that constitute the adjoining catchment. According to Poulos et al. (2015), the coastal lithology is classified into seven groups (Fig. 1.14): i) clastic sediments of Pleistocene – Quaternary age (25.4%), ii) carbonate formations (e.g. limestones, dolomites, marbles; 36.9%), iii) igneous formations (4.5%), iv) volcanic rocks (5.5%), v) metamorphic rocks (20.7%), vi) alterations of clastic sediments and carbonates; groups I and II (3.8) and vii) others (3.2%).

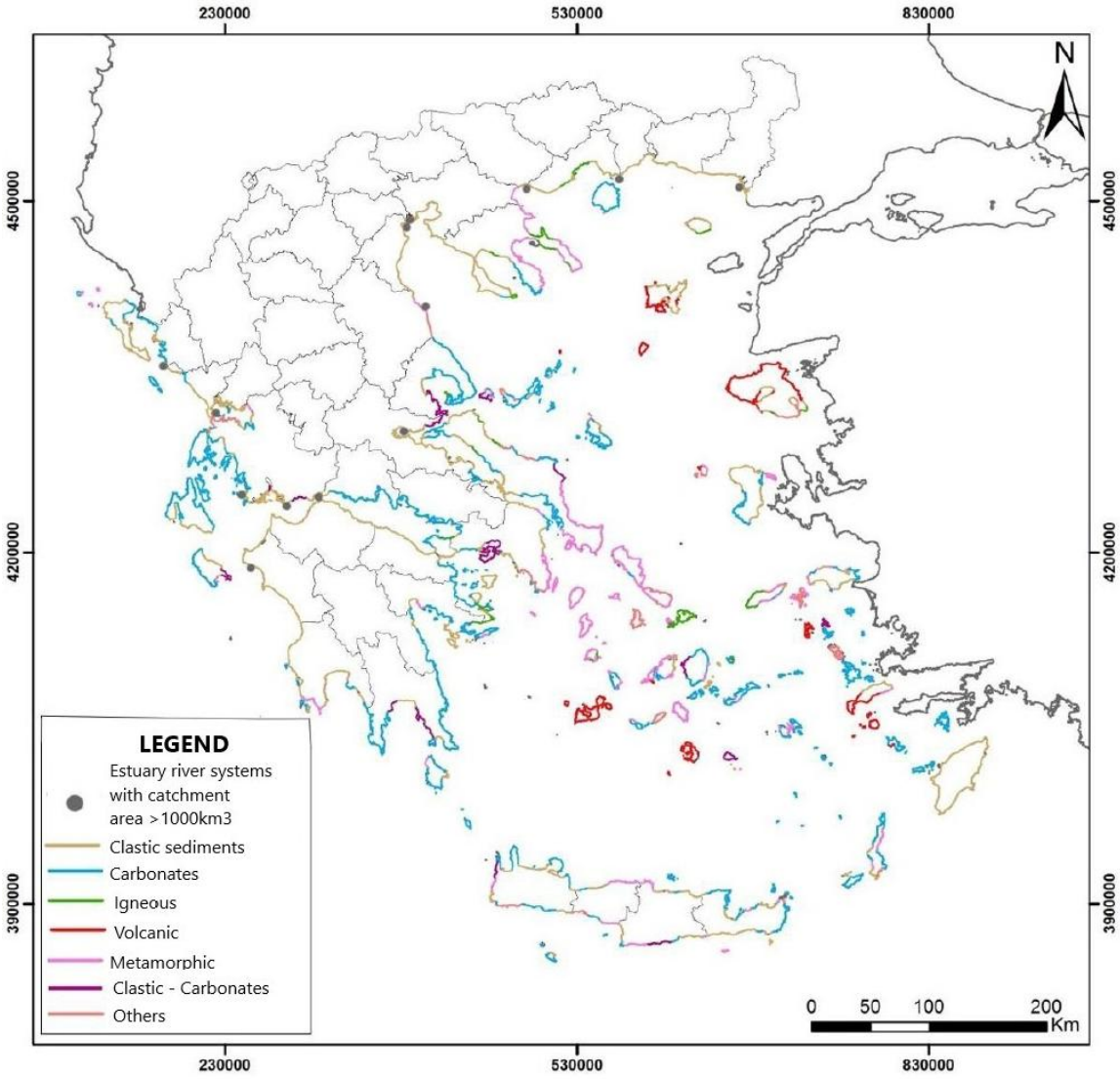

Figure 1.14. Lithological characterization of the Greek coastline according to IGME map (1983), and relevant publications (e.g. Evans, 1971; Kanellopoulos et al., 2007; Poulos, 2009, modified after Poulos et al., 2015).

1.8. Aim of the study

This dissertation investigates for the first time in a large scale the potential of Marine Aggregate deposits in Greece for industrial use. This thesis focuses on the systematic research of various offshore modern sediments of the Greek continental shelf concerning their sedimentological, mineralogical and geochemical characteristics emphasizing the research of silica (quartz) sand.

The aim of the present thesis is to prioritize the study areas (offshore and coastal) according the qualitative characteristics (such as grain size, mineralogy and geochemistry) of the sediments and selected environmental characteristics of the offshore areas (such as

closure depth, natura zones and distance from the coastline) as potential marine aggregates deposits. Moreover, the suitability degree of the sediments as aggregates for concrete is defined, according the performance of the materials from the qualified areas on specific technical tests and regarding their comparison to industrial sand and gravel.

CHAPTER 2. STUDY AREAS

2.1. SELECTION OF STUDY AREAS

There is no significant background scientific knowledge relative to the prospective of marine aggregates placer resources in Greece and no description relative to the mechanism leading to their formation. Therefore, in this chapter all data presented are based on the geological – lithlogical characteristics of each area and on limited information collected from studies or personal communications related to previous dredging activities.

The selection criteria of the offshore areas under study are based onto four significant axes, that could increase the possibilities of locating marine aggregates in the inner continental shelf. These selection criteria are:

i) Adjacent hinterland's geology/lithology
ii) Long sandy beaches at the adjacent coastal area
iii) Existence of streams/river mouths and delta areas
iv) Previous dredging activity in the wider area.

The coastal geology/lithology that favors the existence of quartz - rich sand deposits is mostly related to clastic and metamorphic formations, while marine aggregates with enriched calcium carbonate contents derive either from biogenic processes or carbonate formations. It is important to highlight that the largest share of demand concerns marine aggregates with high silica content, which are extremely rare in the Greek seas, as 70% of the terrestrial lithology consists of metamorphic or not carbonate formations (Fig. 1.13; Bornovas and Rontogianni, 1983).

According to Poulos (2009), the Aegean Sea receives 60-70 million tons per year of terrestrial material. Moreover, Poulos (2009), recognizes three sub-regions of the Aegean Sea regarding their sedimentological conditions: i) the North Aegean, where terrigenous material prevails ii) the South Aegean, which is dominated by biogenic material and iii) the Central Aegean being a transitional zone. This spatial distribution of sediments is probably attributed to the rates of sediment inputs and their proximity to river/stream mouth areas, the production of the surface waters, as well as the prevailing surface circulation patterns (Giresse et al., 2003; Poulos, 2009).

The coarse-grained land-derived sediments are deposited in the nearshore zone; however, some offshore deposits (e.g. Pehlivanoglou et al., 2009; Karageorgis et al., 2000)

are characterized as relict, due to the formation during sea-level lowstands from early Pleistocene to early Holocene (Ergin et al., 1998; Poulos, 2009). Modern sediment deposits are still under formation within the coastal area and controlled by the present hydro- and sediment- dynamic conditions.

The present dissertation investigates data from four promising areas on the Greek continental shelf, which are located (Fig. 2.1):

1) SE Evia Island (fulfils the criterions i, iii and iv)

2) NW Crete Island (fulfils the criterions i, ii, iii and iv)

3) S and E Lesvos Island (fulfils the criterions ii and iii) and

4) NE Rhodes Island (fulfils the criterions ii and iii)

Moreover, a few samples were collected from various coastal areas in order, either to form an integrated overview and support data from the offshore areas or to gain knowledge regarding the primary qualitative characteristics of the sediments from a few coastal areas. The latter reason will allow exploring these adjacent coastal areas to any offshore sediment deposits of potential marine aggregates with suitable characteristics regarding their exploitation. These coastal areas are (Fig. 2.1):

1) East – central Evia Island – South Evoikos Gulf,

2) NW and south Crete Island,

3) North and East Peloponnese (East Gulf of Corinth and Argolic Gulf),

4) Aegean Sea islands (Milos and Samos Islands),

5) SE Kefalonia Island

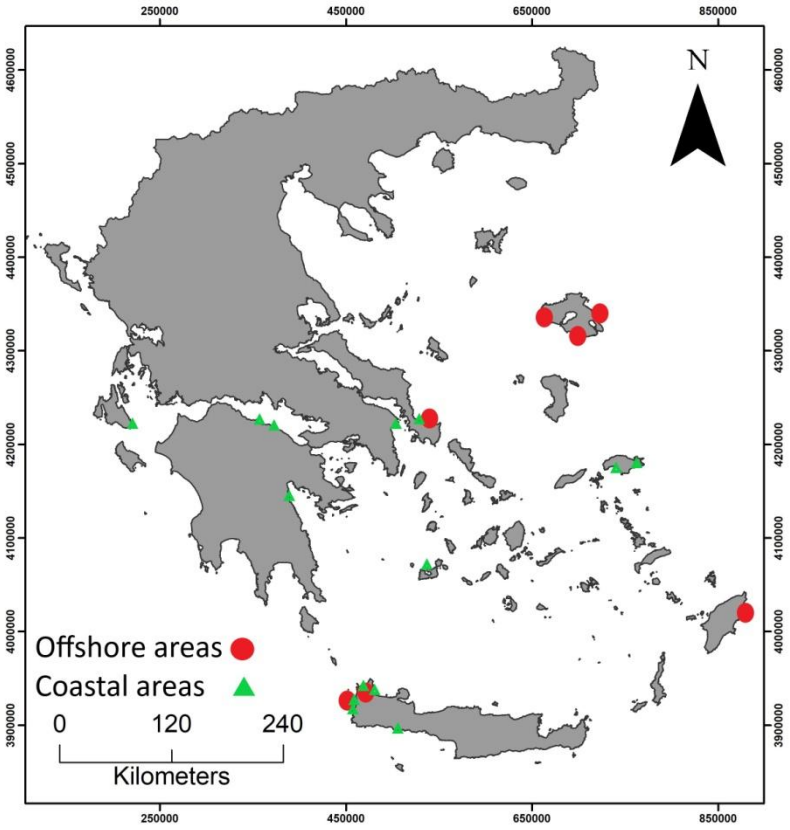

Figure 2.1. Map of Greece showing the offshore and coastal areas of the present thesis.

For comparison reasons, in the context of the present dissertation, samples were collected from areas that are either currently exploited as aggregates resources (Aliartos, Strymonas river, Kafireas Strait, Nairobi) or are examples of aggregates uses with no further processing (south England, NW Italy; beach replenishment examples). These industrial samples are located in the following areas:

1) Aliartos, central Greece

2) Strymonas river, northern Greece

3) Kafireas Strait

4) South England, UK (Boscombe, Bournemouth)

5) Tuscany, NW Italy

6) Nairobi sand (Nairobi, Kenya)

2.2. OFFSHORE AREAS

2.2.1. SE Evia Island

2.2.1.1. Physical Geography

Evia Island (Isl.) is located at the central part of Greece and is the second largest island of the country (Fig. 2.2). The extent of the island is 3.654 km^2 and the total length of the coastline is 677.8 km (Koufogiannis, 2015). The island is elongated and its' geographical direction is NW-SE. The Euripus Strait separates Evia Island from Biotia and the Greek mainland. The main mountains (Mt) of the island are: Dirfi Mt (1.743 m), Pyxaria Mt (1.341 m) and Ochi Mt (1.394 m), which is is located at the SE part of the island (Koufogiannis, 2015). Cape Kafireas is a promontory at the southeastern edge of Evia Island Cape Kafireas and the nearby north part of Andros Island delimit the Kafireas Strait, historically known as D'oro Passage, which is legendary for its' hideous winds and waves (Fig. 2.2; 2.3).

The offshore study area of Evia Island is located at the SE part of the island (Fig. 2.2; 2.3), off Karystos Municipality, Regional Unit of Evia, Region of Central Greece ("Cleisthenes I" Programme).

Figure 2.2. Map of Greece showing the study area off SE Evia Island

Figure 2.3. Satellite image showing the study area (red box) from Google Earth Pro. South of the study area and north of Andros Island is Kafireas Strait.

2.2.1.2. Geology of South Evia Island

Two major geotectonic units occur in South Evia Island, the relatively autochthonous Almiropotamos Unit and the overlying allochthonous Cycladic Blueschist Unit (CBU; Durr et al., 1978; Katsikatsos, 1986; Papanikolaou, 1987; Moustaka, 2011). However, the main geotectonic unit of the wider study area off Evia Island is CBU of which the northwestern part is found in southern part of the island (Fig. 2.4).

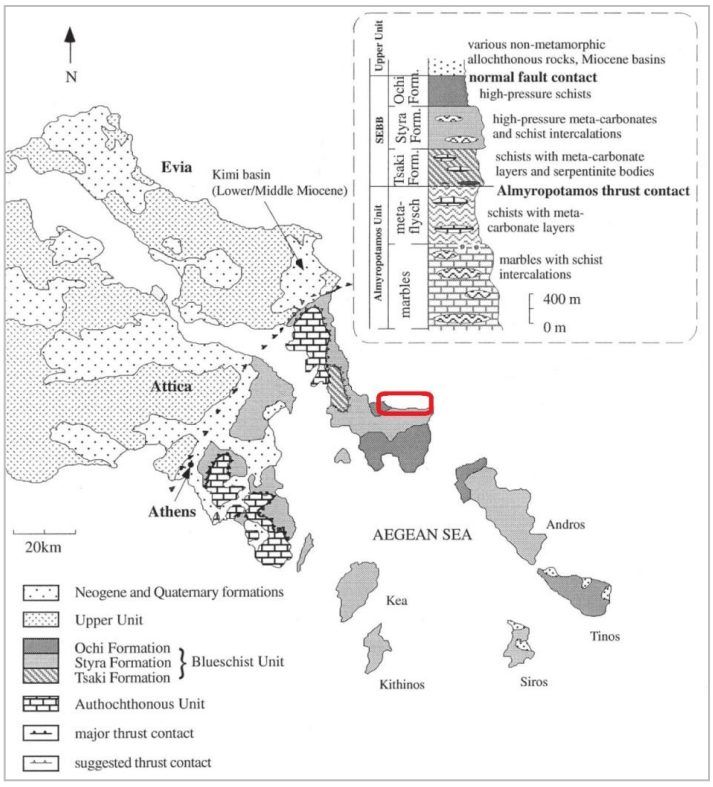

Figure 2.4. Generalized map showing the geological setting of Evia Island and the offshore study area (red box). Map is modified after Katsikatsos et al., 1986 and Shaked et al., 2000.

According to various researchers, who have focused their study on the Attico-Cycladic Zone (ACZ), the Pelagonian Zone underlies the ACZ, which consist of at least three main units/nappes formed during Alpine collision (Dürr et al., 1978; Papanikolaou, 1984; Chatzaras et al., 2013). The three main/major metamorphic units of Attico-Cycladic Zone, distinct from each other by thrust/normal faults, are (structurally lowest to highest): the Basal Unit, the Cycladic Blueschist Unit and the Upper Unit (Dürr et al., 1978; Papanikolaou, 1984, 1987; Forster and Lister, 2005; Voudouris et al., 2011; Chatzaras et al., 2013).

In Evia Island the Cycladic Blueschist Unit is observed to overlie Almyropotamos Unit (named "Basal Unit"), which is considered pertaining to the External Hellenides and it is appraise to have subjected mostly to low-temperature metamorphism (Pananikolaou, 1984; Katsikatsos et al., 1986; Voudouris et al., 2011). The Basal Unit (Almyropotamos Unit) is located exposed in tectonic windows at the Attica peninsula and on the islands of Tinos and Evia (Pananikolaou, 1987; Ring et al., 2007; Voudouris et al., 2011). However, according to Shaked et al. (2000) and Xypolias et al. (2012), this unit probably was affected by HP metamorphism followed by a greenschist facies overprint, although there is poor knowledge regarding the age of the events.

In Cyclades, after an initial Apline compressive facies accompanied by a high pressure/low temperature metamorphism (~15 kbar, 450-500 ^{o}C) during Upper Cretaceous – Middle Eocene (60-70 to 45-50 Ma), followed by the formations' emergence accompanied by broad metamorphic Greenschist/Amphibolitic facies (-7 kbar, 440-470 ^{o}C, locally ~650 ^{o}C) (Altherr & Schliestedt, 1979; Baltatzis, 1996; Bröcker & Franz, 1998; Bröcker & Enders, 1999). In particular, at Southern Evia Island geothermobarymetry implies an obduction process followed by cooling from Epidote-Blueschist facies (T_{max} ~ 450 ^{o}C, P_{min} ~ 11 kbar) to Pumpellyite/ Actinolite facies (T_{max} ~ 350 ^{o}C, P_{max} ~ 8kbar) (Katzir et al., 2000; Shaked et al., 2000). According to Malluski et al. (1981), the high-P metamorphism started on Evia Island at about 50 Ma.

The Cycladic Blueschist Unit at South Evia Island (or South Evia Blueschist Belt) consists of three distinct nappes, which from bottom to top are: the Tsaki, Styra and Ochi formations (Fig. 2.4; Katsikatsos et al., 1986; Shaked et al., 2000). The study area is related to Styra and Ochi formations (Fig. 2.4). Both Styra and Ochi nappes subjected to High-Pressure (HP) / Low – Temperature metamorphism at 0.7-0.9 GPa, 500-550 ^{o}C and 1.0- 1.2 GPa, 400-450 ^{o}C, respectively (Ring et al., 2007; Voudouris et al., 2011; Fig. 2.5). HP of the

Styra and Ochi nappes persisted until ~33Ma, when normal shearing started. After ~33 Ma, HP conditions began to decline; the rocks entered an exhumation stage and ultimately reequilibrated under greenschist facies conditions at ~21 Ma (Ring et al., 2007). The Styra nappe is overlain, through a SSW directed thrusting zone, Almyropotamos nappe (Shaked, 2000; Ring et al., 2007; Voudouris et al., 2011). According to Ring et al. (2007), coeval to Stryra- Basal Unit thrusting was normal faulting between Stryra and Ochi Nappe, following an extrusion wedge activated for about ~10 Ma.

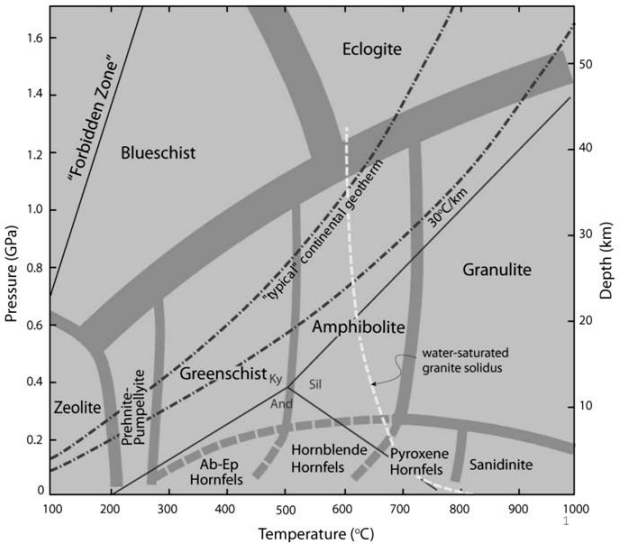

Figure 2.5. Temperature (^{o}C) – Pressure (GPa) – Depth (Km) diagram showing the generally accepted limits of the various metamorphic facies after Winter, 2011.

The Upper Unit, which is underlain by the Cycladic Blueschist Unit, is a non to weakly metamorphosed nappe, rarely exposed and consists of low to medium metamorphic rocks, Jurassic-Cretaceous ophiolites and Permian-Tertiary sediments (Dürr et al., 1978, Voudouris et al., 2011). According to Altherr and Siebel (2002), during the Miocene extension along Aegean Sea, a magmatic intrusion at the upper crust levels took place. The tectonic contiguity of the Upper Unit with the underlying CBU took place during early Miocene (Bröcker and Franz, 1998; Xypolias et al, 2012).

2.2.1.3. Geological formations of the adjacent hinterland

In the southern Evia Island the Cylcadic Blueschist Unit consists of Mesozoic metasediments and metavolcanics, while local intercalations of Hercynian anatectic basement (Jolivet et al., 2003; Xypolias et al., 2012) is represented by Styra and Ochi nappes, as metioned above. The Ochi nappe, as the uppermost CBU, embodies the ophioliitc melange

and consists of quartz and carbonate-rich schist, metagabbro, metabasalt, metarhyolite and piemontite-rich chert (Katzir et al., 2000; Ring et al., 2007). The underlying Styra nappe consists of quartzite, metapelites, metabauxite-bearong marble and seprentite lenses at the lowermost part (Ring et al., 2007). The Basal Unit (Almyropotamos nappe) comprised of Triassic to Middle Eocene metacarbonates (marbles) (Ring et al., 2007).

In the southern part of Evia Island, the rocks of the Ochi and Styra nappes are metamorphosed (schists) and contain blueschist to greenschist facies assemblages, as well as transitional varieties, and are fine-grained (Shaked et al., 2000; Ring et al., 2007; Fig. 2.6). The blueschist facies assemblages include Na-amphibole, epidote, albite, clinozoisite, white micas, quartz, sphene and opaques (Shaked et al., 2000). A Ca-amphibole - epidote - chlorite-albite assemblage is attributed to the transitional blueschist to greenschist facies conditions (Ring et al., 2007). The greenschist facies include epidote and albite porphyroblasts, which contain inclusions of earlier mineralogical components (e.g. phengite, glaucophane and e.t.c.), chlorite, stilpomelane, calcite, piemonite and accessories such as apatite, sphene and opaque minerals (Shaked et al., 2000). According to Ring et al. (2007), the rocks within the blueschist facies are strongly mylonitized and Na-amphiboles are acircular with high aspect ratio. These mylonitized blueschist facies were found at Cape Filagra and Mt Oiti (Fig. 2.7).

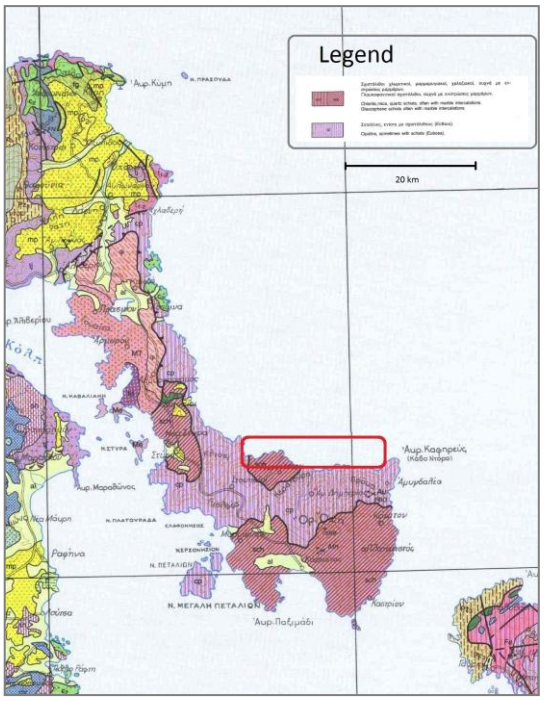

Figure 2.6. Geological map of the Southern Evia Island (Bornovas and Rontogianni- Tsiampaou, 1983).

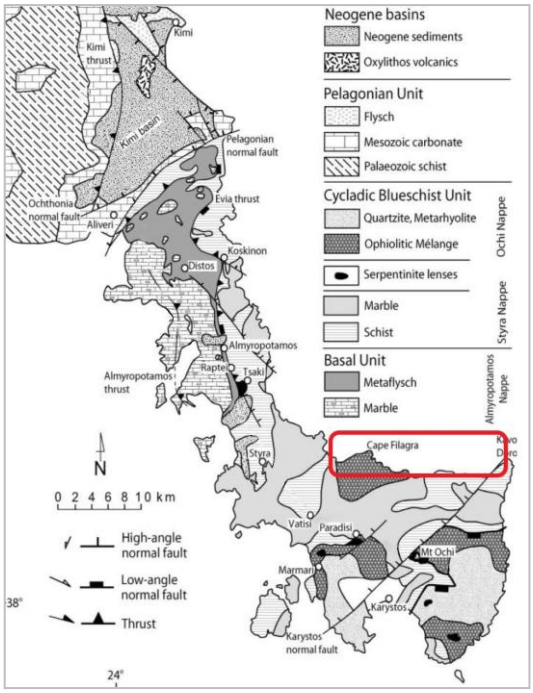

Figure 2.7. Geological map of southern Evia Island showing the adjacent onshore geological formations of the offshore study area (red box). Map modified after Jacobshagen, 1986; Katzir et al., 2000; Ring et al., 2007; Xypolias et al., 2003.

The Basal Unit (Almyropotamos) consists of marbles politic schists, which contain almost pure, coarse-grained calcite, detritus quartz, muscovite and chlorite (Shaked et al., 2000). In Evia Island, according to Shaked et al. (2000), it was observed that within the metapeletic sequence, glaucophane relicts and Si-rich phengites exist. According to Shaked et al. (2000), glaucophane was detected near the contact of Alyropotamos unit and Stryra nappe, and as inclusions/relicts within albite porphyroblasts near Koskina area (Fig. 2.7). These facts, according to Shaked et al. (2000), imply that the Basalt unit subjected to HP-metamorphism (~350 ^{o}C/8-10 kbar; 30-35 km depth). In local scale, glaucophane relicts are observed to be replaced by biotite and chlorite (Shaked et al., 2000). The Upper Unit, which is rarely exposed, consists of Permian to Mesozoic marbles intercalations, Late Cretaceous amphibolitic facies, ophiolites and felsic gneisses (Dürr et al., 1978; Katzir et al., 2000; Chatzaras et al., 2013).

2.2.2. NW Crete Island

2.2.2.1. Physical Geography

The island of Crete is located at the southern part of Greece, south of the Aegean Sea and is the largest island of the country (Fig. 2.1.). The extent of the island is 8336 km^2 and

the total length of the coastline is 1046 km. The island is elongated and its' geographical orientation is west to east; 260 km along the W-E axis and 60 km maximum width along the N-S axis (Sarris et al., 2005). Crete Island is surrounded to the south by the Libyan Sea, to the north by the Sea of Crete, to the west by the Myrtoon Sea and to the east by the Karpathion Sea (Sarris et al., 2005). The main mountains (Mt) of the island are: White Mts or Lefka Ori (2454 m), Idi Range or Psiloritis Mt (2456 m), Kedros Mt (1777 m), Dikti Mt (2148 m) and Thripti Mt (1.489 m).

The offshore study areas of Crete Island are two and located at the NW part of the island. Specifically, the two study areas are located at Kissamos and Sfinari Bay (Fig. 2.8). The offshore study area of Kissamos is located off Kissamos and Platania Municipality, Regional Unit of Chania, Region of Crete and the offshore study area of Sfinari is located off Kissamos Municipality, Regional Unit of Chania, Region of Crete ("Cleisthenes I" Programme).

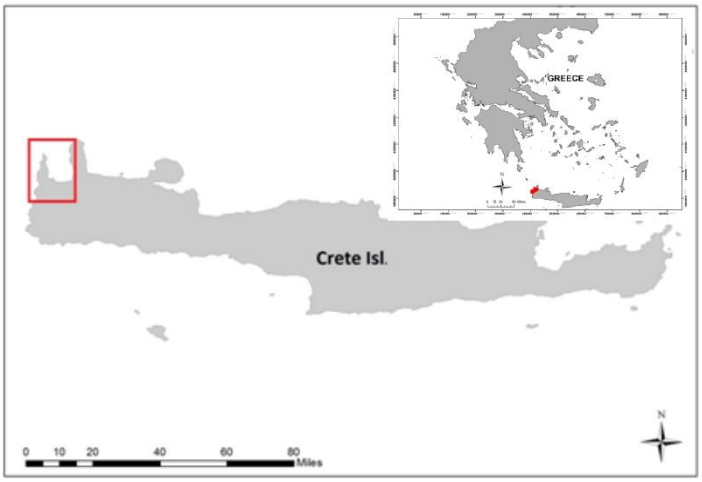

Figure 2.8. Map of Crete, Greece showing the wider study area off NW Crete Island.

2.2.2.2. Geology of NW Crete Island

Crete Island is a horst structure in the central forearc of the Hellenic subduction zone (Seidel et al., 2007) and is the most seismical active Mediterranean subduction zone, with sudbduction rate of oceanic North Africa plate beneath the continental Aegean microplate at ~35 mm/year (Reilinger et al., 2010; Vernant et al., 2014). The regional structure of western Crete, whereas the study areas off Kissamos and Sfinari are located, is dominated by an open E-W trending antiform (Fig. 2.9; Greiling, 1982).

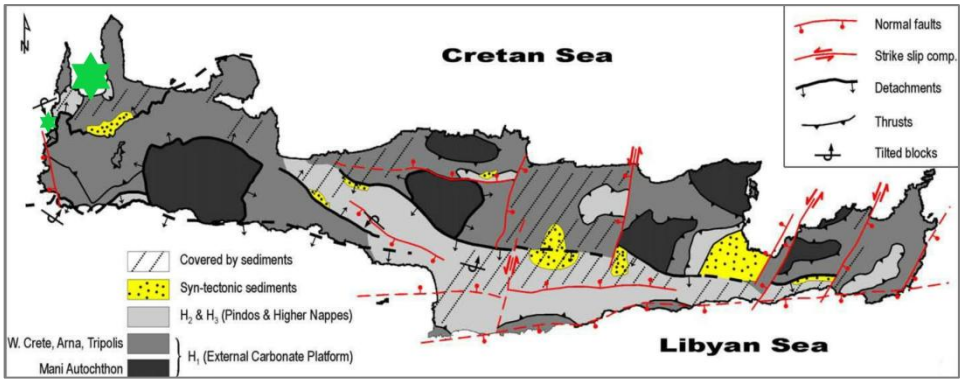

Figure 2.9. Simplified geotectonic map from Papanikolaou and Vassilakis, 2010, showing the Crete Island structure after the superposition of the extensional detatchments and various main normal/strike-slip faults in the pile of nappes. Study areas are shown with green stars (big star: Kissamos Bay; small star: Sfinari Bay).

The island of Crete is characterized by a complex and thick pile of nappes derived from different paleogeographic zones (Seidel et al., 2007; Ott et al., 2019). The island is characterized by pre-alpine and alpine rocks (complex nappe pile) and late alpine, Neogene sediments, that fill the basins between the mountains (Bonneau, 1984; Sarris et al., 2005).

According to Seidel et al. (1982) and Seidel et al. (2007), these nappes are subdivided into two groups of tectonic units; the upper and the lower. The upper units lack of Cenozoic metamorphism and the lower ones are subjected to HP/LT metamorphism (Seidel et al., 1982; Seidel et al., 2007). The HP/LT lower nappes are metamorphosed during Permian – Oligocene. These nappes are sedimentary and volcanic units that were stacked throughout subduction and following exhumed by extension (Jolivet and Brun, 2010; Ott et al., 2019). The Miocene – Pliocene marine basins, found nowadays above sea level, are the result of the forearc extension and are bounded by active normal faults (Papanikolaou and Vassilakis, 2010; Ott et al., 2019). The terrestrial Late Pliocene – Pleistocene basin deposits host indicators of the emergence of the island, the present elevation of the Neogene marine deposits indicate long-term uplift rates of minimum ~0.2 mm/year (Zacharias et al., 2008; Ott et al., 2019), while the quaternary paleoshorelines record ongoing uplift of Crete Island (Fig. 2.10; Gallen et al., 2014; Ott et al., 2019). According to Papanikolaou and Vassilakis (2010), the outline of the deformational history of Crete Island is summarized into the following three stages: i) the initial arc-parallel compressional phase, E-W trending, during Oligocene – Early Miocene age, ii) the following, also arc-parallel, extensional phase of E-W trending detachments during Middle – Miocene age and iii) the third extensional phase of normal

faults during Late Miocene – Quaternary age, which disrupt the previous two, arc-parallel, stages.

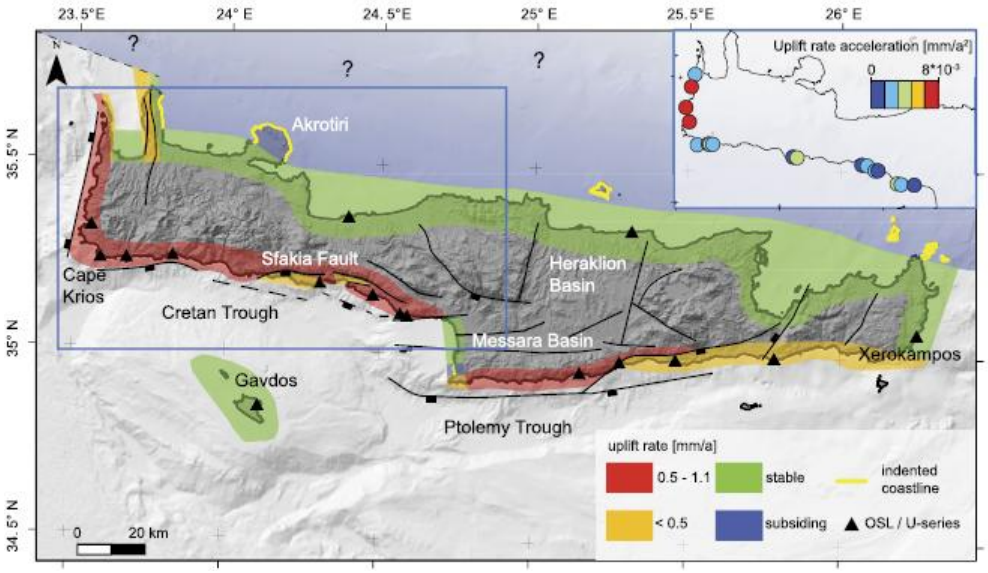

Figure 2.10. Map of Crete Island with the distribution of the Pleistocene uplift rates from Gallen et al., 2014; Ott et al., 2019.

In Crete Island, these nappes, from the upper to the lower ones are found stacked as follows: Asterousia nappe, Miamou nappe, Arvi nappe, Pindos - Ethia nappe, Tripolitza nappe, Phyllite nappe, Trypali Unit/nappe and Plattenkalk Group. The uppermost units (i.e. Pindos and Tripolitza Units) and the lowermost ones (i.e. Phyllite-Quartzite and Plattenkalk Units), are separated by normal detachment faults (Fassoulas et al., 1994; Jolivet et al., 1994; Seidel et al., 2007; Papanikolaou and Vassilakis, 2010). At the NW part of the island and, specifically, in the areas of Sfinari and Topolia the northern detachment of Crete can be observed, whereas Arna unit constitutes the footwall and Pindos and Tripolis units the hanging wall (Papanikolaou and Vassilakis, 2010; Fig. 2.9, 2.11).

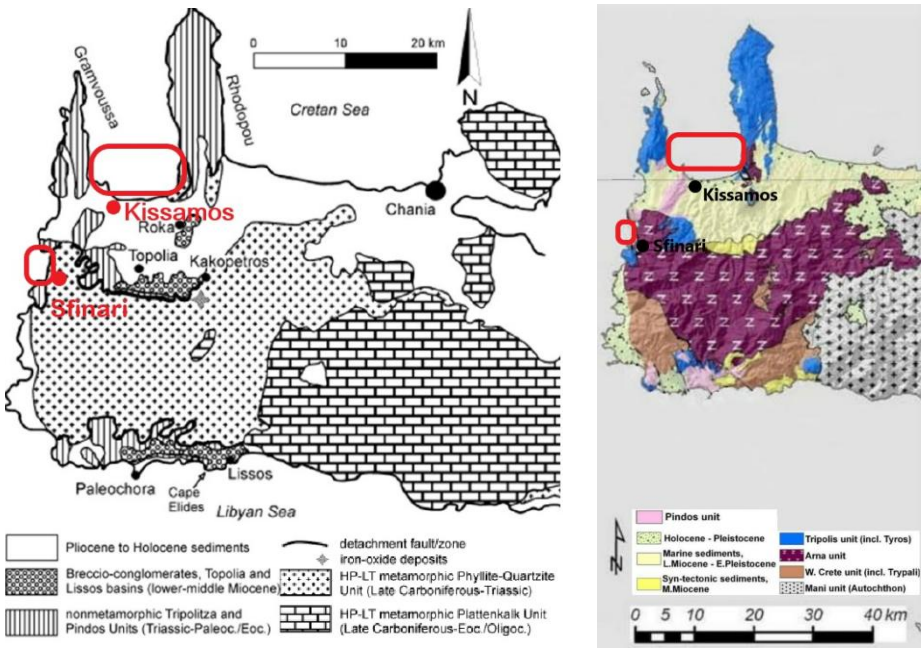

Figure 2.11. The offshore study areas on geological maps of western Crete Island from Seidel et al., 2007 (left) and Papanikolaou and Vassilakis, 2010 (right).

2.2.2.3. Geological formations of the adjacent hinterland

The wider, adjacent hinterland of the investigated offshore areas is located at western Crete Island. The surface area is characterized by a diversity of geological formations, including the following (Fig. 2.12; Seidel et al., 1982; Bornovas and Rontogianni-Tsiampaou, 1983; Seidel et al., 2007; Papanikolaou and Vassilakis, 2010):

- Quaternary deposits (Holocene and Pleistocene older fluvial terraces) composed of alluvial deposits in valleys, plains and coastal deposit, unconsolidated deposits of gravels, sand, clays and silts.
- Neogene deposits of Mio-Pliocene age composed of conglomerates, sand and sandstones, marls, clays/clayey material, marly limestones and gypsum.
- Tripolis zone (Upper Cretaceous - Eoocene) composed of undivided limestones and dolomites.
- Phyllites – Quartzite series, Permo-Triassic age, which consist of phyllites, quartzites, schists, limestones (marbles), meta-volcanic formations, dolomites and gypsum.
- Pindos unit formations of Jurassic – Eocene age consist of Upper Cretaceous Flysch, Cretaceous limestones and Jurassic cherts.

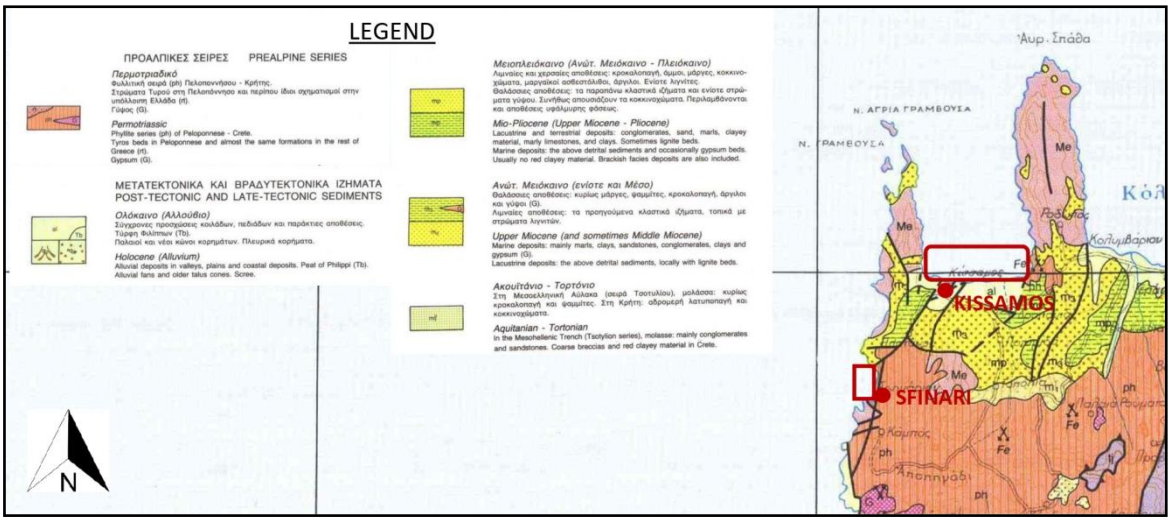

Figure 2.12. Geological map of NW Crete Island (Bornovas and Rontogianni- Tsiampaou, 1983).

According to Papanikolaou and Vassilakis (2010), the Phyllites – Quartzites series demonstrated the distinction of the Arna nappe from the underlying as well as overlying phyllites of Permo-Triassic age (Fig. 2.13). Tripolis flysch separates Tripolis limestones from Pindos nappes.

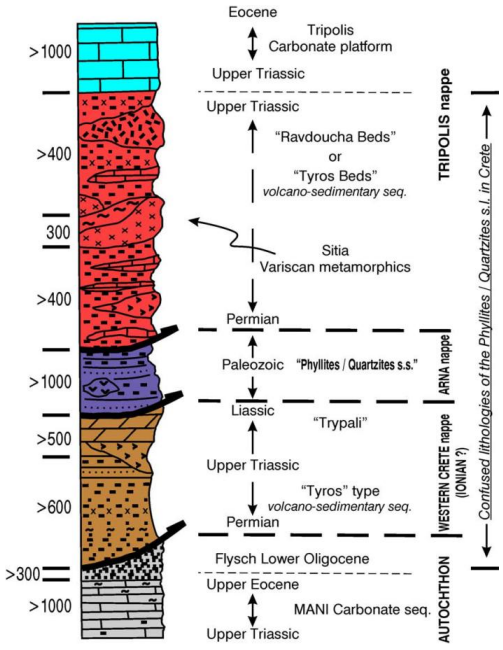

Figure 2.13. Tectono-stratigraphic column of 'Phyllite- Quartzites' series according to Papanikolaou and Vassilakis (2010).

South of Kissamos and east of Sfinari, a basin fill which is termed Topolia alluvial fan complex is located in the area of Topolia (Fig. 2.11; Seidel et al., 2007). At the present, the Topolia half-graben covers an outcrop area of about 15 km^2. The thickness of Topolia deposit is more than 500 m. The thickness of the clastic deposit decreases towards the north.

Moreover, towards the direction of sediments transport (increasing distance from the catchment) the particle size decreases as well as the grain size, while the clasts' roundness increases (Seidel et al., 2007). The basin fill classification is fanglomerates and this corresponds to a sedimentological model (Fig. 2.14) regarding alluvial fans, i.e. input material by huge clastic masses (Miall, 1996; Seidel et al., 2007). These alluvial fan complexes, such as Topolia clastic wedge, are the result of a large number of mass flow episodes with multiple sources (Seidel et al., 2007). According to Seidel et al. (2007), the particular structure and sedimentary characteristics of Topolia fan complex indicate an evolution associated with debris flow and water laid deposits (Fig. 2.6).

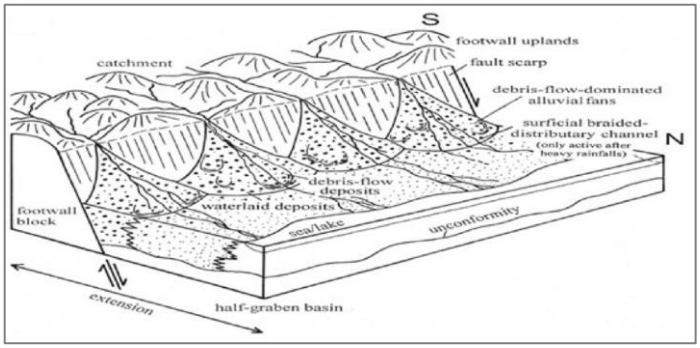

Figure 2.14. Schematic illustration of the sedimentological model of Topolia basin during the Middle Miocene. The alluvial fan is formed by debris-flow deposits. The clastic sediments are derived (catchment area) from the footwall (mountain range), which is separated from the hanging wall (basin floor) from the fault scrap of a normal fault (Seidel et al., 2007).

According to Papanikolaou and Vassilakis (2010), the detachment timing can be identified on the basis of the syntectonic clastic sediments of Topolia alluvial fan and the post-tectonic marine Neogene sediments (Fig. 2.12). Extensive field and laboratory investigations by Seidel et al. (2007), at the wider area of the Topolia alluvial fan, revealed that the breccio-conglomerates are derived mainly from the non-metamorphic upper tectonic units. During the depositional time, the bounding normal fault did not cross the detachment fault and the lower HP-LT metamorphic units were not exposed and therefore could not be the subject of erosional procedures (Seidel, 2003; Seidel et al., 2007). Whereupon, the predominant clastic facies are lagoonal limestones, fossiliferous limestones, biomicrites, biosparites, recrystallized limestones, partially dolomitized limestones, dolomites, dedolomites with fossil assemblages and microfacies suggesting Tripolitza Unit (Seidel, 2003; Seidel et al., 2007). Minor or trace clastic facies are small-sized (mm) quartz clasts and metamorphosed fragments are derived from the Cretaceous- Paleogene flysch of Pindos unit,

while micritic limestones with radiolarians, limestones with chert and calcarenites are probably derived from Pindos unit (Seidel, 2003; Seidel et al., 2007).

The marine Neogene sediments (Fig. 2.11; 2.12; 2.15), north of Topolia alluvial fan, mainly consist of detritus derived from Phyllite – Quartzite Unit, an HP-LP unit at the lower part of Cretan pile (Seidel, 2003; Seidel et al., 2007); further these sediments are underlain by coarse terrestrial sediments. This fact indicates that the HP-LT metamorphic unit of Phyllites-Quartzites was exposed at the latest ca. 10 Ma ago. According to Seidel (2003) and Seidel et al. (2007), fragments of the brecciоconglomerates are embedded in the coarse terrestrial sediments. This fact implies that at that time the synorogenic sediments of Topolia alluvial fan were already lithified and subjected to erosional processes (Seidel, 2003; Seidel et al., 2007).

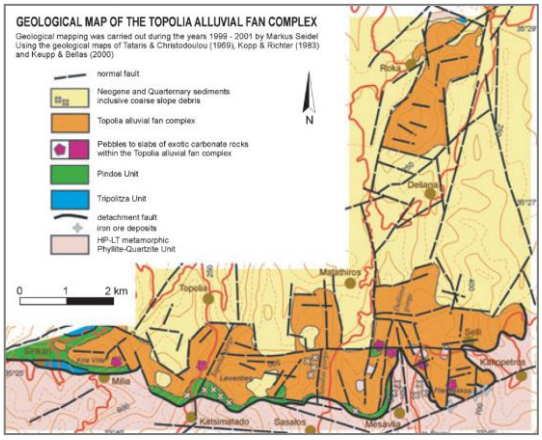

Figure 2.15. Geological map of the Topolia basin (Seidel et al., 2010).

2.2.3. Southern and eastern Lesvos Island

2.2.3.1. Physical Geography

Lesvos Island is located at the northeastern part of Aegean Sea and is the third largest island of Greece (Fig. 2.16; Zouros, 2010). The surface area of the island is 1633 km^2 and the total length of the coastline is 321 km. Lesvos Island has two mountains (Mt): the Lepetymnos (968 m) and Olympus (967 m). The eastern part of Lesvos Island faces the Turskish coast, separated by the narrow Mytilene Strait, whereas the narrowest point is ca. 5.5 km. The Lesvos Petrified Forest Geopark, a rare ecosystem consisting of fossilized trees which were covered by volcanic materials and petrified during Early Miocene (UNESCO, 2006), is located in the western part of the island. In the 2000, Lesvos Petrified Forest was

declared as a protected national monument of nature joined the European Geoparks Network and since 2004 belongs to the Global Geoparks Network by UNESCO (UNESCO, 2006).

The offshore study areas of Lesvos Island are three and located at southwest (Eresos), south (Vatera) and eastern (Mytilene Strait) part of the island (Fig. 2.16). The offshore study area of Eresos (Fig. 2.17) is located at the southeastern part of the island, off Skala Eresou area, Municipal Unit of Eresos – Antissa, West Lesvos Municipality, and Region of the Northern Aegean "Cleisthenes I" Programme. The offshore study area of Vatera (Fig. 2.17) is located at the south part of the island, off Vatera area, Municipal Unit of Polichnitos Programme, West Lesvos Municipality, Region of the Northern Aegean ("Cleisthenes I"). Finally, the offshore study area of Mytilene Strait (Fig. 2.17) is located at the eastern part of the island, off the wider area of Mytilene from Mytilene Airport to Skala Mistegnon, Municipal Unit of Mytilene and Loutropoli Thermis, Mytilene Municipality, Region of the Northern Aegean ("Cleisthenes I" Programme).

Figure 2.16. Map of Greece showing the study areas off Lesvos Island

Figure 2.17. Satellite image showing the study areas (red box) from Google Earth Pro.

2.2.3.2. Geology of southern and eastern Lesvos Island

Lesvos Island belongs to the Late Oligocene – Middle Miocene volcanic arc (Fig. 2.16) and the volcanic rocks extend across the central and west part of the island (Fig. 2.17; Lamera et al., 2001; Voudouris et al., 2019). These volcanic rocks are of shoshonitic to calc-alkaline character (Voudouris et al., 2019) and overlie the Metamorphic – Paleozoic basement of Sakarya Zone (Fig. 2.16; Koglin et al., 2009).

In the northern Aegean Sea, three major fault systems prevail, which are NW-, NE- to E- and NNW- trending (Jolivet and Brun, 2010; Voudouris et al, 2019). Since Miocene, these fault systems are associated with the propagation of the North Anatolian Fault (Jolivet and Brun, 2010; Voudouris et al, 2019). According to various researchers (i.e. Pe-Piper and Piper, 1993; Voudouris et al., 2019), three major calderas occur on Lesvos Island (Fig. 2.18).

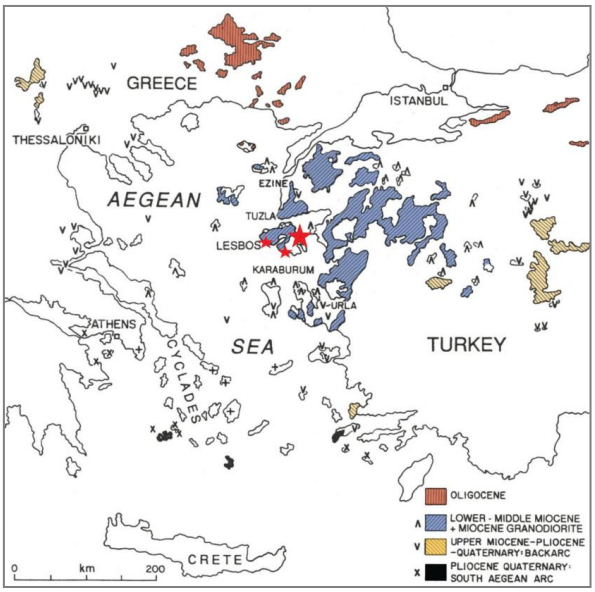

Figure 2.18. Generalized map of the Aegean Sea and the nearby areas of Greece and Turkey, showing Cenozoic volcanic rocks. Study areas are marked with red stars (after Helbling, 2011; Pe-Piper and Piper, 1993).

The geological formation of Lesvos Island can be divided into four main units as follows: i) the schist-marble unit, ii) the volcanosedimentary unit, iii) the untramafic unit and iv) the Cenozoic cover unit (Fig. 2.18; 2.19; Piper and Piper, 1993; Koglin, 2009).

i) The schist – Marble Unit (Fig. 2.18; 2.19) consists of a series schists, marbles and phyllites. The moderate metamorphism is up to greenschist facies conditions (Helbling, 2011; Pe-Piper and Piper, 1993; Koglin et al., 2009). The thickness regarding Permo-Carboniferous marbles and schists is estimated to be more than 400 m (Helbling, 2011).

ii) The volcanosedimentary Unit (Fig. 2.18; 2.19), also known as sub-ophiolitic mélange, consists of metabasalts and metagabbros along with schists, limestones and sandstones related to greenschists facies (Pe-Piper and Piper, 1993; Koglin et al., 2009). These volcanic formations are located in a series of stratovolcanoes of SW-NE direction (Helbling, 2011). According to Pe-Piper et al. (2001), this unit is overall strongly deformed apart from the Vatera outcrop. Moreover, the volcanosedimentary unit could be subdivided into two groups; the high – Ti MORB and the MORB-IAT transitional group and Papanikolaou (1999), suggested a Permian to Middle Triassic age.

iii) The ultramafic unit is thrusted over the volcanosedimentary unit and is exposed in two areas at the central/east and eastern part of the island, as shown in Figures 2.18 and 2.19. This unit has been extensively and variably serpentinized and both outcrops are of similar mineralogy (Katsikatsos et al., 1986; Koglin et al., 2009). This unit consists of ultramafic rocks, mainly harzburgite and lherzolite accompanied by minor dunite presence (Migiros et al., 2000).

iv) The Cenozoic unit (Fig. 2.18; 2.19) prevails at the island and consists mainly of Miocene - Pliocene high K-andesitic volcanic rocks and Neogene-Quaternary sediments (Hecht, 1972; Pe-Piper and Piper, 1993; Koglin et al., 2009).

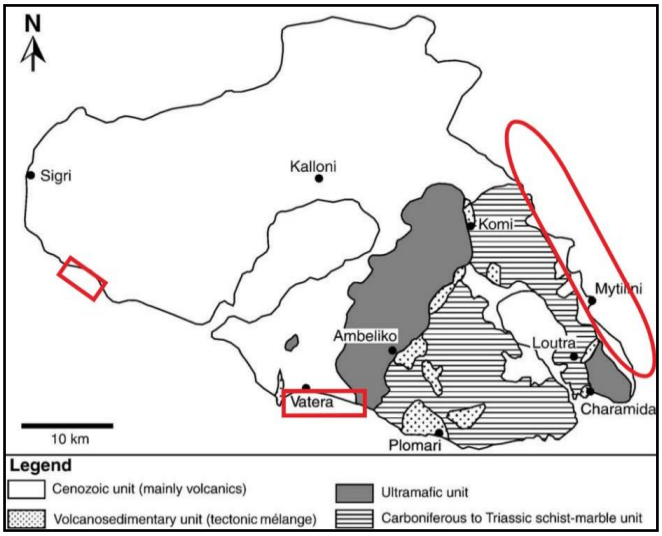

Figure 2.19. Simplified geological map of Lesvos Island (after Heght, 1972; Koglin et al., 2009) showing the offshore study areas (red frames).

According to Hecht (1974), Koglin et al. (2009), Pi-Piper and Piper (1993) and Voudouris et al. (2019), the Neogene volcanic rocks are divided into five (5) groups, which include from bottom to top: i) the lower Lava and Eresos Formation, ii) the Skoutaros Formation, iii) the acid volcanic unit including Sigri Pyroclastic Formation, Polychnitos and

Skopelos Ignimbrite and Kapi Rhyolite Formation, iv) the Sykamnea and Skalohorion Formation and v) the Mytilene Formation.

2.2.3.3. Geological formations of the adjacent hinterland

According to Gazis et al. (2017), the coastal geomorphology is controlled by the intensive erosion of the Miocene volcanic rocks, which cover the majority of the island's coast and specifically the southern coastal areas (i.e. Eresos and Vatera).

Eresos area

The adjacent hinterland of Eresos consists of the following geological formations (Fig. 2.20): Neogene-Quaternary sediments, Eresos Formation, a small outcrop of the volcanosedimentary unit and Sigri pyroclastics. Eresos Formation comprises of intense hydrothermally altered coarse grained porhyritic andesite with hornblende and biotite phenocrystal, interbedded with volcanic breccias (Helbling, 2011; Voudouris et al., 2019). The Sigri pyroclastics, which overlie the Lower Lava Unit in the wider Eresos area, consist of coarse volcanic ash, tuffs and volcanic breccias (Helbling, 2011; Voudouris et al., 2019).

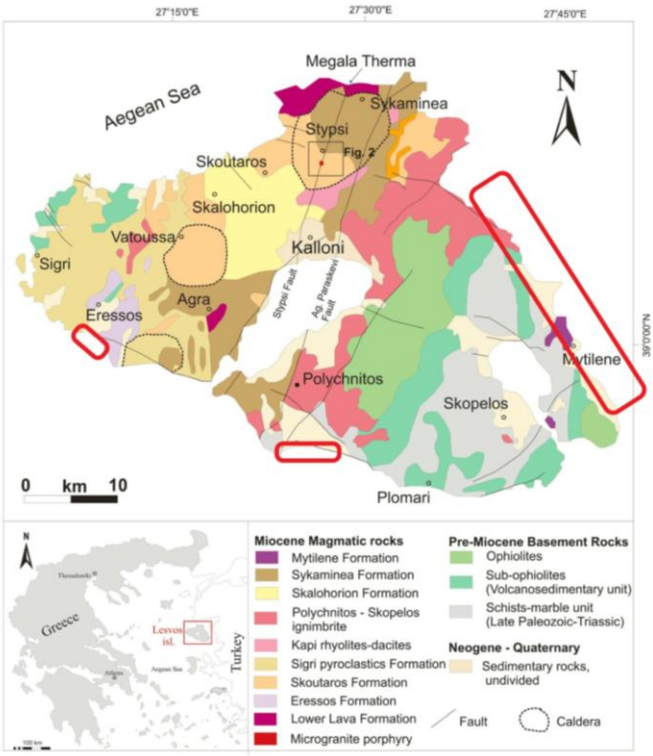

Figure 2.20. Generalized geological map of Lesvos Isl (Pe-Piper et al., 2019; Voudouris et al., 2019).

Vatera area

The adjacent hinterland of Vatera consists of the following geological formations (Fig. 2.20): Neogene – Quaternary sediments, Paleozoic – Triassic schists and marbles, Polychnitos Ignimbrite and minor outcrops of Sykamnea Formation and the Permian-Triassic volcanosedimentary unit. The mineralogy of Polychnitos Ignimbrite mainly consists of plagioclase (andesine and anorthoclase), K-feldspars and biotite (Lamera et al, 2001). Minor crystalline phases of clinopyroxene and traces of quartz, apatite, sphene and olivine also exist (Lamera et al., 2001). Moreover, Polychnitos Ignimbrite contains pumice fragments of two types: i) irregular, non flattened shape and spherical vésicules and ii) with eutaxitic texture, and, also lithic components 0% - 45%, mainly of volcanic origin and rarely of plutonic (Lamera et al., 2001). The Sykamnea Formation consists of andesite, dacite and minor pyroclastic (Voudouris, 2019). The volvanosedimentary unit of Vatera outcrop is almost undeformed pillow structures (Pe-Piper et al., 2001; Koglin et al., 2009).

According to Kelepertzis (2002), a nickeliferous laterite deposit occurs at the W-NW part of Vatera coastal area, which is derived from the secondary residual processes of the serpentinite of Profitis Ilias and Koukouvies areas.

Mytilene Strait

The adjacent hinterland of Mytilene Strait covers a large area with various geological formations and therefore is divided into the north and the south domains. *The northern part of Mytilene Strait* consists of (Fig. 2.20): the Polychnitos Ignimbrite, Skoutaros Formation and a small outcrop of Sigri pyroclastics. From bottom to top, the Skoutaros Formation includes pyroxene andesite lava flows, hornblende-biotite andesites and dacites interbedded with felsic pyroclastic rocks. *The southern part of Mytilene Strait* consists of (Fig. 2.20): Neogene-Quaternary sediments, the Mytilene Formation, the Paleozoic – Triassic schists and marbles, the Permian- Triassic volcanosedimentary unit and the ultramafic unit (known as ophiolites). The Mytilene Formation consists of andesite, basalt and minor felsic pyroclastics (Voudouris et al., 2019). Pe-Piper (1993), suggests an age of 16.8±0.9 Ma, which indicates that Mytilene Formation belongs to the main volcanic sequence of Lesvos Island (Helbling, 2011).

2.2.4. NE Rhodes Island

2.2.4.1. Physical Geography

The island of Rhodes is located at the southeastern part of the Aegean Sea (Fig. 2.21), Greece and is the largest of the Dodecanese islands of Greece. The extent of the island is 1400 km^2 and the total length of the coastline is 220 km. The shape of Rhodes Island is elongated and its' geographical orientation is NE to SW. The interior of the island is mountainous. The main mountains are: Attavyros Mt (1215 m), Profitis Ilias Mt (798 m), Akramitis Mt (825 m), Psalidi Mt (~555 m), which is located north of the study area. Rhodes Island is located 363 km E-SE from the Greek mainland and 18 km from the nearest Turkish shore.

Figure 2.21. Map of Greece showing the study area off SE Rhodes Island

The offshore study area of Rhodes Island is located at the SE part of the island, at Afantou Bay. The offshore study of Afantou Bay (Fig 2.22) is located off Municipal Unit of Afantou, Rhodes Municipality, Regional Unit of Rhodes, Region of South Aegean ("Cleisthenes I" Programme).

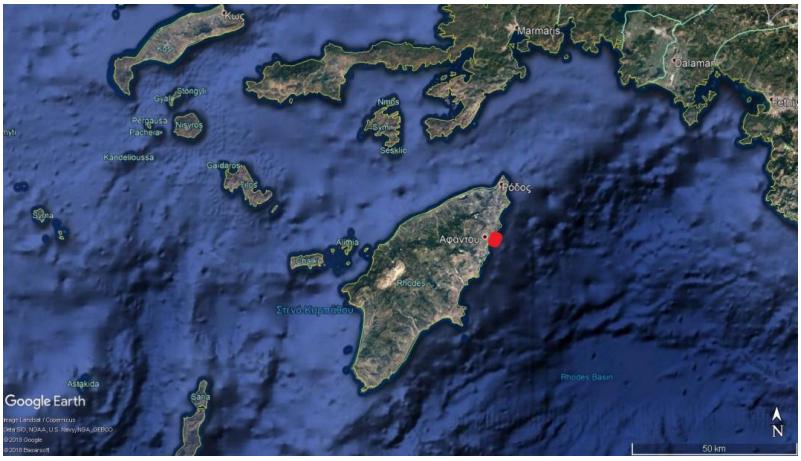

Figure 2.22. Satellite image showing the study area of Afantou, Rhodes Island (red box) from Google Earth Pro.

2.2.4.2. Geology of SE Rhodes Island

The geological basement of the island is composed by alpine calcareous series and ophiolitic complex formations. The alpine calcareous series are the Plattenkalk series (known as Attaviros Unit), the Tripolis series (locally known as Lindos Unit), the Pindos series (locally known as Profitis Ilias Unit) and the Pelagonian series, including the ophiolites (Agiadi, 2013). According to Papanikolaou et al. (1995), during Upper Oligocene, these alpine units were covered by clastic sequences of great thickness, which were deposited in the extensional basins (Fig. 2.23).

According to Papanikolaou et al. (1995) and Lekkas et al. (2007), Rhodes Island consists of a series of alpine units, which from bottom to top are as follows:

- Lindos Unit, which represents the island's lowermost and relatively autochthonous unit. This unit consists of black marble to cipolin marbles, phyllites and finally metamorphosed flysch of Upper Eocene – Lower Oligocene age.
- Laerma Unit, which is located in the area between Attabiros and Lindos, at the central part of the island. This unit consists of wild flysch with several alterations (clays, sandstones, bioclastic limestones), interbedded horizons of agglomerates and conglomerates (with ophiolites) and igneous olistholiths of Upper Eocene – Oligocene.
- Attabiros – Akramitis Unit, which consists of pelagic limestones with silex of Upper Jurrassic – Middle Eocene age.
- Archangelos Unit, which consists of a thick limestones sequence, dolomites (Upper Triassic – Lower Eocene age) and flysch (Lower Eocene age).

- Profitis Ilias Unit, which consists of agglomerated limestones with siles and red marls/radiolarites (Uppers Triassic – Upper Cretaceous age).
- Ophiolite Unit, which overlies either Archangeleos or Profitis Ilias Unit. This unit constists of (green) igneous rocks and often radiolarites.

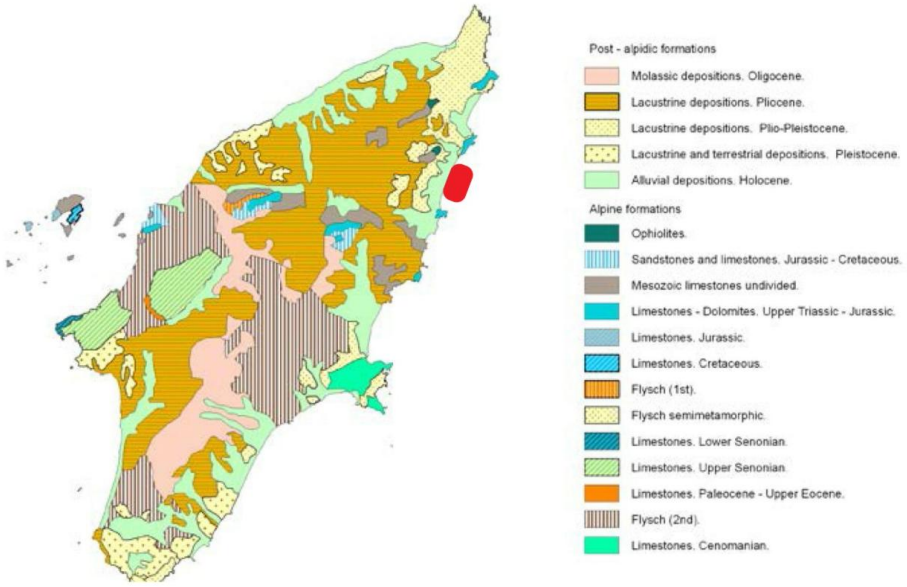

Figure 2.23. Geological map of Rhodes. The red box shows the offshore study area at Afantou Bay (Anagnostou et al., 2011).

2.2.4.3. Geological formations of the adjacent hinterland

In Rhodes Island Neogene and Quaternary marine sediments are widespread. This fact indicates that part of the island is recently emerged (Pirazzoli et al., 1989; Kontogianni, 2002). Since Pliocene, Rhodes Island syndepositional tectonism is controlled by N70^{o} trending strike-slip faults (Pirazzoli et al., 1989; Kontogianni et al., 2002; Agiadi, 2013). Moreover, during Pliocene and the most of the Pleistocene, the northeastern part of Rhodes Island, where the study area of Afantou belongs, was submerged (Agiadi, 2013). However, the NE part of the island experiences significant uplifting from Early-Middle Pleistocene until present (Pizzaroli, 1989; Cornée, 2006; Agiadi, 2013).

The wider area of Afantou has been subjected to significant uplifting tectonic movements of 2.9 m to 3.8 m during Holocene (Pirazzoli et al., 1989; Kontogianni et al., 2002; Kapsimalis et al., 2013), as shown in Figure 2.24.

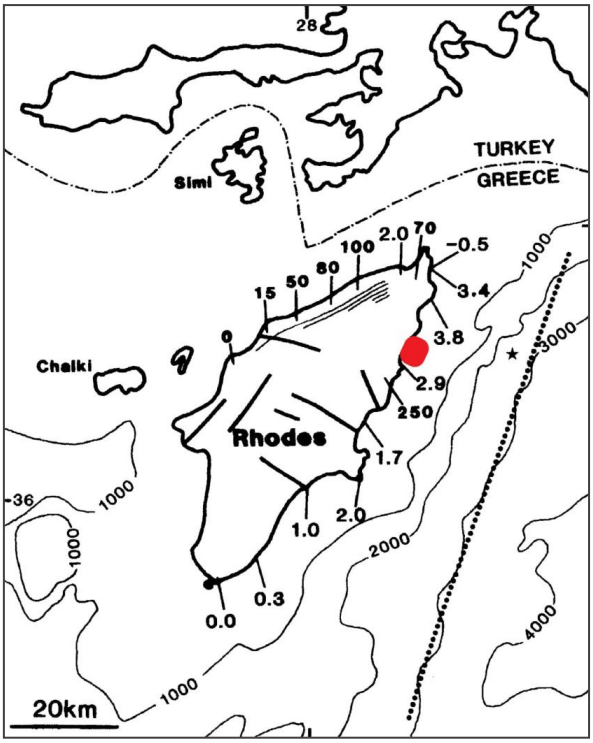

Figure 2.24. Coastal uplift in Rhodes Island. Decimal numbers suggest the maximum height of Holocene raised notches and the other numbers the height of terraces after Kontogianni et al., 2002, and Pirazzoli et al., 1989. Red box indicates tha stury area of Afantou Bay.

At the wider Afantou coastal area, beachrocks and sand dunes are observed (Verykiou-Papaspyridakou et al., 2004). Moreover, in the northern part of Afantou, the coast has high slopes and in some places is steep (Verykiou-Papaspyridakou et al., 2004). However, the long Afantou beach is developed on alluvial sediments.

2.3. VARIOUS COASTAL AREAS

East / central Evia Island – South Evoikos Gulf

The geological/lithological characteristics of the wider area, where the coastal areas of east/central Evia Island are located (Fig. 2.25) are thoroughly described in §2.2.1.

The coastal area of Schinias, which is located at south Evoikos Gulf (Fig. 2.25) is situated on alluvial – Holocene deposits. The adjacent hinterland comprises alpine basement rocks that belong to the metamorphic units of the Northern Cyclades and occur from Penteli Mt to south Evoikos Gulf (Papanikolaou and Papanikolaou, 2007). The Almyropotamos unit, which crops up the wider Marathon area, consists of phyllites appearing a metamorphosed

flysch underlain by a thick Mesozoic marble sequence (Katsikatsos, 1969; Papanikolaou and Papanikolaou, 2007). The relative autochthonous metomorphic Unit of Attica underlies Almyropotamos Unit and consists of marbles with dolomitic intercalations and schists (Papanikolaou, 2015).

NW and SW Crete Island

The geological/lithological characteristics of the wider area, where the coastal areas of NW and SW Crete Island are located (Fig. 2.25) is thoroughly described in §2.2.2.

North and East Peloponnese

The under study coastal areas of the northern Peloponnese are located at the southern onshore part of the Corinthian Gulf (Fig. 2.25). During the phases of Corinth Rift, terrestrial and marine sediments were deposited with thickness >2.8 km, that are now found at altitudes above 1.6 km (Dufaure, 1977; Skourtsos et al., 2016). The wider hinterland areas of the under-study coastal areas of Corinthian and Argolic Gulf (esat Peloponnese; Fig. 2.25) are dominated by formations of the Tripolis and Pindos Units. Tripolis Unit conists of a thick carbonate sequence of Up. Triassic – Upper Eocene age, underlain a volcanosedimentary complex of Upper Palaeozoic – Low Triassic age, known as Tyros Beds and followed by a flysch formation of Low Eocene – Oligocene age (Skourtsos at el., 2016). Pindos Unit consists of a sequence o limestones and cherts (pelagic sediments) of Mesozoic age capped by a flysch sequence of Palaeocene – Eocene age (Skourtsos et al., 2016).

Aegean Sea islands (Milos and Samos Islands)

The coastal area of Milos Island is located at the north/central part of the island (Fig. 2.25). Milos Island belongs to the central part of the active volcanic arc of the Aegean Sea (Middle Pliocene to present) and hosts volcanic lavas and tuffs which cover most of its surface (Fytikas et al. 1986; Anastasatou et al., 2019a). Milos Island is comprised mainly of Late Pliocene and Pleistocene volcanic, pyroclastic and volcanoclastic rocks of dacitic, andesitic and rhyolitic composition (Fytikas et al., 1986; Anastasatou et al., 2019a). Moreover, the island hosts a wide variety of coastal black sands (heavy minerals sands)

which are significantly enriched in titanomagnetite, ilmenite and barite. Black sands are the weathering products of mainly volcanic rocks, barite and polymetallic deposits (Anastasatou et al., 2019a). The under study coastal area is located at rhyolitic complexes and domes (Fytikas et al., 1986).

The coastal areas of Samos Island are located in the southeastern and south/central parts of the island (Fig. 2.25). Two main Neogene basins were formed on Samos Island; the Mytilini basin at the eastern part of the island and the Karlovassi basin situated in the western part, where one of the two coastal areas is located (Kantiranis et al., 2004). Specifically, the coastal area which is located in the south/central part of the island is situated on lacustrine deposits of Upper Miocene and at the adjacent hinterland pyroclastics of Mio-Pliocene occur (Stamatakis, 1989a). The coastal area which is located on the southeastern part of the island is supplied with sediments derived from the Ampelos formartion. Ampelos formation is part of the Bluschist Unit of Cyclades and consists of marbles (with metabauxite lenses), quartzites, bluechists and glaucophane – schists (Gessner et al., 2001; Kantiranis et al., 2004). It is important to note that authigenic silicates and silica polymorphs occur in the Miocene deposits of the basins (Stamatakis, 1989b).

SE Kefalonia Island

Kefalonia Island belongs to Ionian and Paxoi units, whereas the Ionian overlies Paxoi Unit. The southeasternmost edge of this thrust ends up at Skala area, where the study coastal area is located (Fig. 2.25). Paxoi Unit consists of Cretaceous limestones and dolomites, overlain by Paleogene thick limestones and also overlain by Upper Oligocene – Upper Miocene conglomeratic and brcciated limestones (e.g. Karymbalis et al., 2013). The Ionian Unit consists of Pantocrator limestones (Upper Triassic – Middle Lias) overlain by Ammonitico Rosso formation (Upper Lias – Middle Dogger). Thereinafter, in the area occur shales and limestones (Middle - Upper Dogger) overlain by Vigla limesotnes with chert intercalations (Upper Jurassic – Lower Cretaceous). Furthermore, breccias and limestones lie on the top of Palaeocene – Eocene age (e.g. Karympalis et al, 2013).

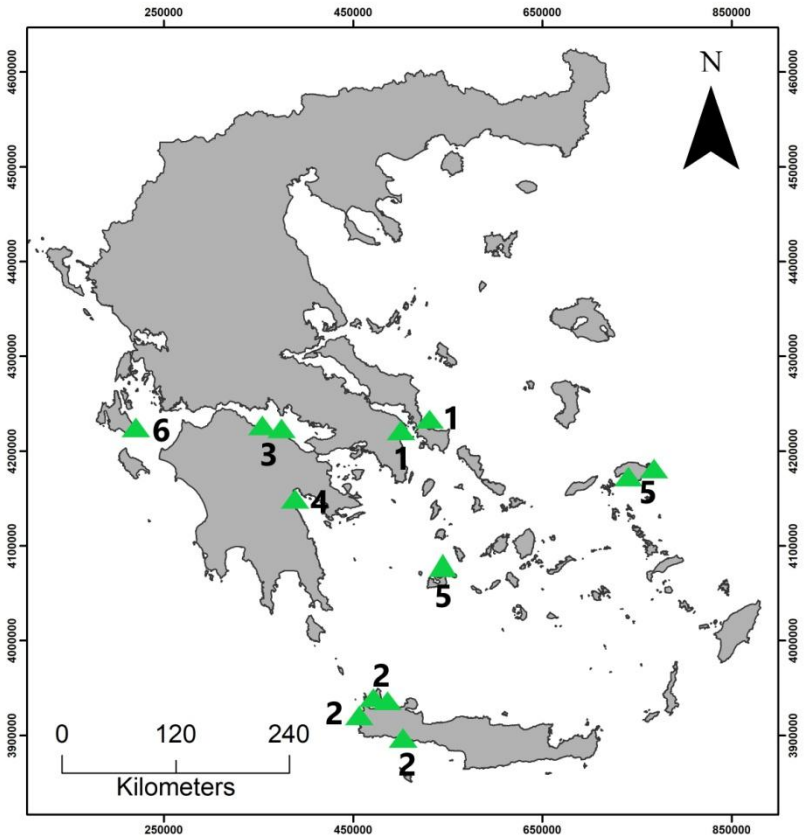

Figure 2.25. Map of Greece showing the under study coastal areas; 1: East / central Evia Island – South Evoikos Gulf, 2: NE and south Crete Island, 3: East Gulf of Corinth, 4: Argolic Gulf, 5: Aegean Sea islands (Milos and Samos Islands) and 6: SE Kefalonia Island

2.4. AREAS OF INDUSTRIAL SAMPLES

The selected industrial samples were obtained from various areas in Greece and abroad.

- Industrial samples from the southern UK coastline and specifically from the coastal areas of Bournemouth and Boscombe were collected during 2015, were a 17-year plan of beach replenishment was activated in order to protect Bournemouth and Boscombe coastline during 2015 – 2032 (Harlow, 2013). For example, during 2016, nearly 320.000 m^3 of sand was planned to be placed (pumped) onto Bournemouth beaches in order to avoid sand erosion (Harlow, 2013).
- The industrial coastal sample which was obtained from the beach Marina di Torre del Lago Puccini, located at Tuscany, NW Italy, is also a sample derived from a beach with systematic replenishment projects. Specifically, this beach belongs to the Region of Tuscany

Coastal Sediment Management Plan s into which the 215 km-long continental sandy coastline of Tuscany is replenished (Pranzini et al., 2020).

- Nairobi sand is a material similar to Sahara sand, which is a typical industrial material that Greek cement companies import in order to manufacture cement (clinker).
- The industrial sample from Aliartos area, central Greece, is a material from an active sand quarry exploited by a Greek company for construction applications.
- The industrial sample from Strymonas River, northern Greece, was obtained from a small company that at the time of collection held a local sand and gravel extraction permit at the riverbanks. This material was supplied to the construction market.
- Ultimately, the last industrial sample was obtained from the unique Greek company, which is active in the field of marine aggregates extraction and exploitation. Over a decade, southern from the study area of SE Evia Island, between Evia and Andros islands, it is known that marine aggregates uses other than concrete. Dredging is taking place from a small Greek company in a distance of >500 m from the coastline and at water depths of >30 m. This sample was obtained from Kafireas Strait, offshore of Evia Island and southern of the offshore study area of the present dissertation. This material is also used in the construction sector; however not as concrete aggregate.

CHAPTER 3. MATERIALS AND METHODS

3.1. FIELDWORK

For the purposes of the present thesis, one hundred and thirty two (132) samples were collected from offshore, coastal and terrestrial areas from Greece and abroad with various sediment sampler devices (box corer, gravity cores and Smith-McIntyre Grab), as well as by diving and swimming (manual sampling).

The sampling locations were selected on the basis of various characteristics that these areas should be eligible for dreadging and exploitation, as mentioned in §2.1. The most important criteria are specified as follows.

- The offshore areas should have certain water-depths (usually between 15 m and 70 m) to permit easy exploitation and the appropriate (short) distance from the coastline of more than 500 m.
- It is a benefit if the adjacent beaches of the offshore areas are quite long (>1 km length).
- The surrounding lithology of the adjacent hinterland of all areas should be able to provide suitable material (aggregates).
- Any information for pre-existing or present dredging activities is evaluated.

The precise offshore sample locations were selected after the analysis of the bathymetric and marine geophysical data that were acquired during purpose specific cruises (Thalis-Mare Project) in four island settings: Crete, Evia, Rodos and Lesvos. Extensive table for offshore, coastal and industrial samples are listed in Annex I.

3.1.1. Offshore Sampling areas

3.1.1.1. SE Evia Island

In June 2014, during the scientific cruise of R/V (Research Vessel) “Aegaeo” of the Hellenic Centre for Marine Research (HCMR), fourteen (14) surficial/subsurficial (up to ~20 cm depth) were collected with box corer and three (3) gravity cores, as shown in Figures 3.1 – 3.6. Extensive catalogue of sampling locations is provided in Annex I.

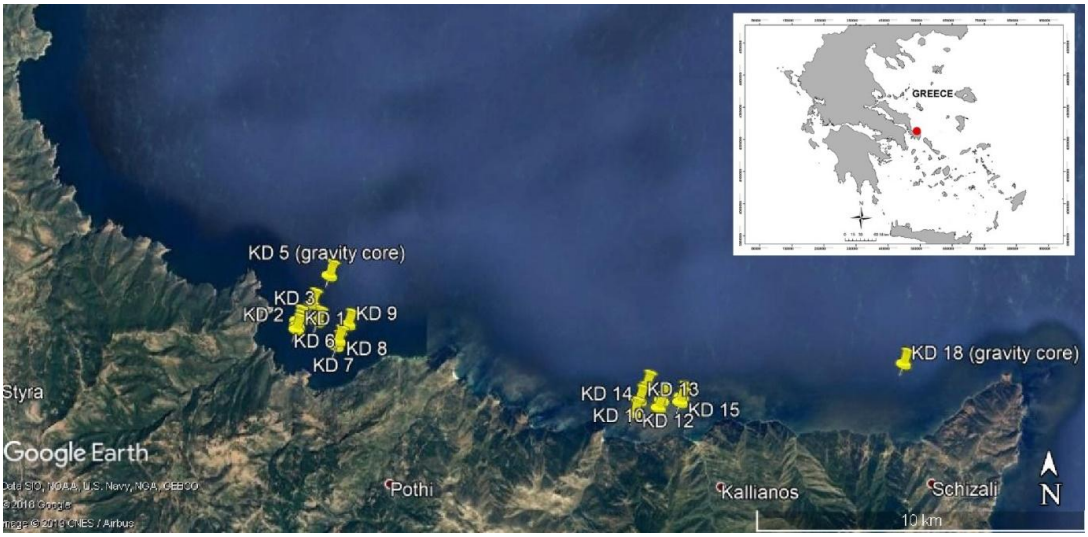

Figure 3.1. Sampling locations of the offshore surficial/sub-surficial samples and gravity cores at SE Evia Island from Google Earth Pro.

Figure 3.2. Box corer deployment for sediment sampling (left photo) and box corer recovery (right photo) on board R/V "Aegaeo".

Figure 3.3. Sample KD-7 with fine material (left photo) and KD-16 with coarser material (right photo) collected with box corer on R/V "Aegaeo".

Figure 3.4. Sea urchin collected with sample KD-16 (left photo; sea urchin returned to sea) and sample KD-15 with coarse material collected with box corer on board R/V "Aegaeo".

Figure 3.5. Gravity core sampler after a failed attempt (left photo) and gravity core ready for sampling (right photo) on board R/V "Aegaeo".

Figure 3.6. Gravity core sampling on board R/V "Aegaeo" and suitable preparation for safe transfer at the laboratories.

3.1.1.2. NW Crete Island

In May 2013, an offshore survey was carried out at Kissamos Bay and Sfinari area, with the R/V ALKYON of the Hellenic Centre for Marine Research (HCMR). During this survey, sixteen (16) offshore surficial sea-bottom sediment samples were collected from Kissamos Bay and three (3) offshore surficial sea-bottom sediment samples were collected from Sfinari offshore area. All samples were collected using Smith-McIntyre Grab, as shown in Figures 3.7-3.10. Extensive catalogue of sampling locations is provided in Annex I.

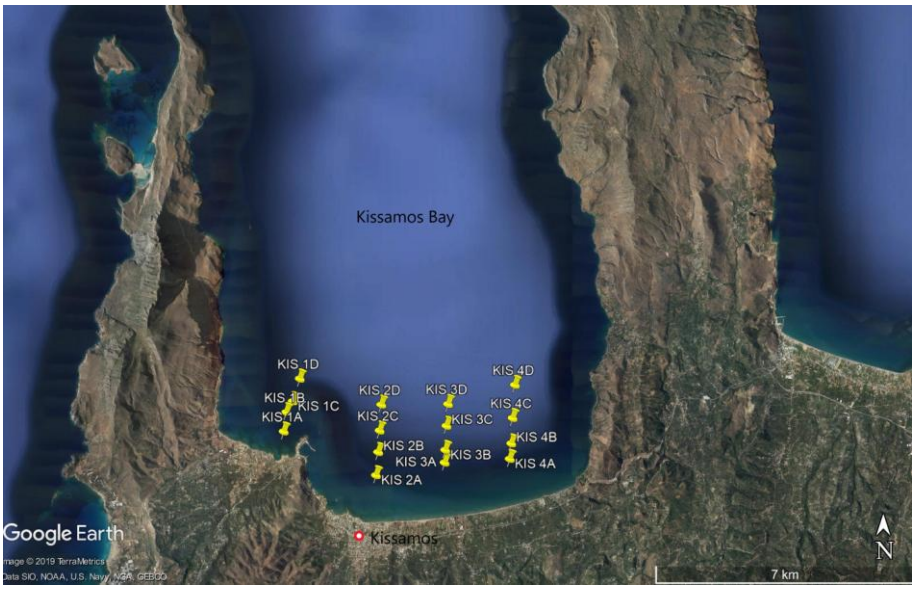

Figure 3.7. Sampling locations of the offshore surficial samples from Kissamos Bay, NW Crete Island from Google Earth Pro.

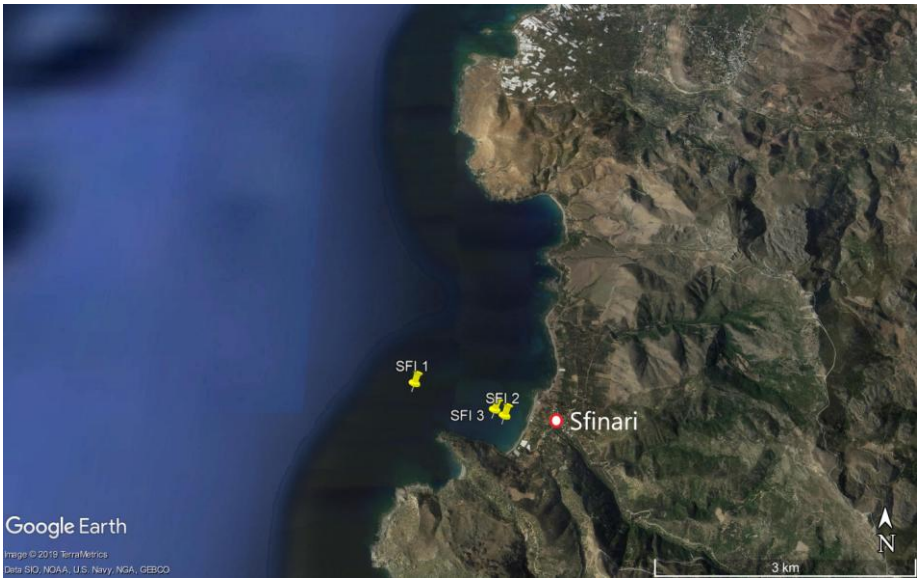

Figure 3.8. Sampling locations of the offshore surficial samples from Sfinari area, NW Crete Island from Google Earth Pro.

Figure 3.9. Smith-McIntyre grab preparation for sediment sampling (left photo) and Smith-McIntyre grab recovery filled with sediment sample (right photo) on board R/V "Alkyon".

Figure 3.10. Sample KIS-1D with fine material (left photo) and sample KIS1C with coarser (sand) material (right photo) collected with Smith-McIntyre grab on board R/V "Alkyon".

3.1.1.3. Southern and eastern Lesvos Island

In July 2014, an offshore survey was carried out at the southern and eastern part of Lesvos Island with the R/V ALKYON of the Hellenic Centre for Marine Research (HCMR). During this survey, three offshore areas were selected for study around southern and eastern part of Lesvos Island, Eresos, Vatera and Mytilene strait. In total thirty five (35) samples were collected, specifically nine (9) sediment samples were collected from the offshore area of Eresos, twelve (12) samples from the offshore area of Vatera and fourteen (14) offshore samples from Mytilene strait. All samples were collected using Smith-McIntyre Grab, as shown in Figures 3.11-3.17. Extensive catalogue of sampling locations is provided in Annex I.

Figure 3.11. Sampling locations of the offshore surficial samples from Eresos area, south Lesvos Island (Google Earth Pro).

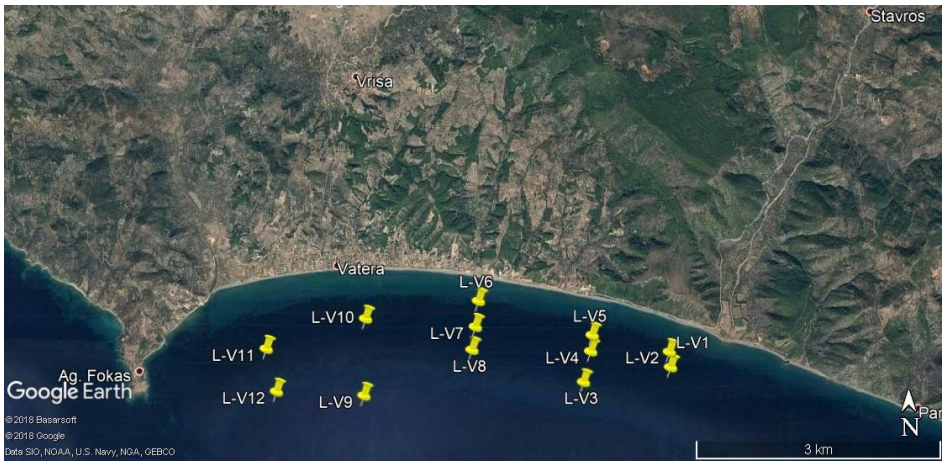

Figure 3.12. Sampling locations of the offshore surficial samples from Vatera area, south Lesvos Island (Google Earth Pro).

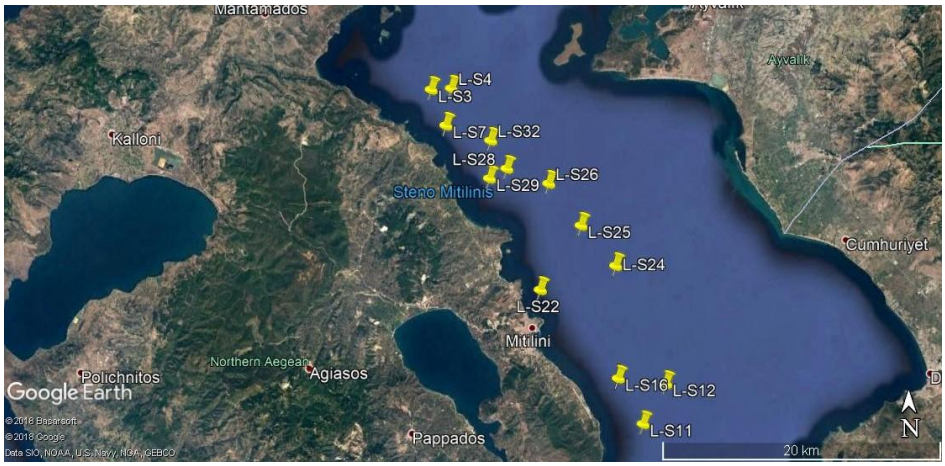

Figure 3.13. Sampling locations of the offshore surficial samples from Mytilene strait, eastern Lesvos Island (Google Earth Pro).

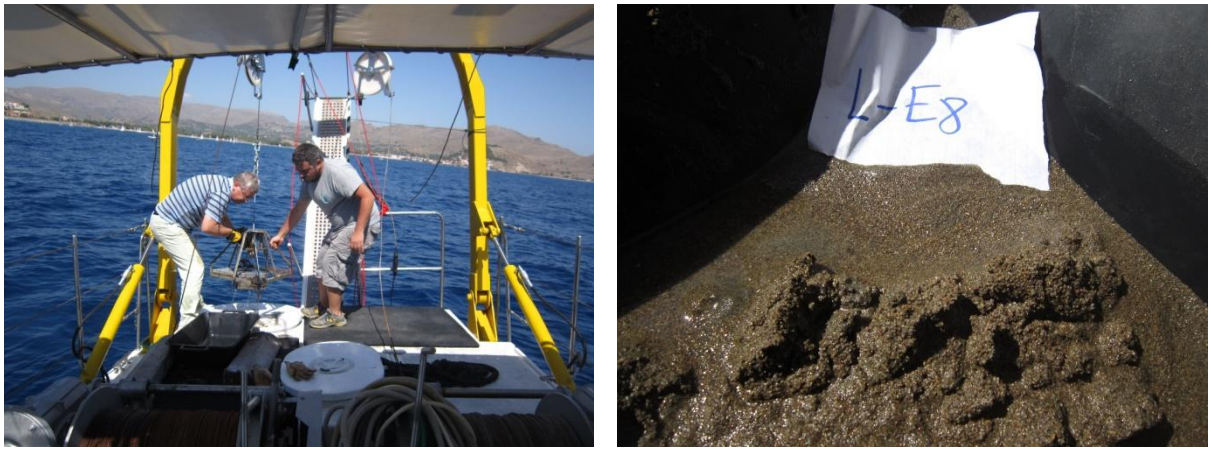

Figure 3.14. Smith-McIntyre grab filled with sediment sample on board R/V "Alkyon" (left photo) and sample L-E8 collected from the offshore area of Eresos with Smith-McIntyre grab (right photo).

Figure 3.15. Sample L-V3 (left photo) and sample L-V9 (right photo) with fine material collected from Vatera offshore area with Smith-McIntyre grab on board R/V "Alkyon".

Figure 3.16. Sample L-S11 (left photo) and sample L-S24 with fine material (right photo) collected from the offshore area of Mytilene strait with Smith-McIntyre grab on board R/V "Alkyon".

Figure 3.17. Sample with *Posidonia Oceanica* (left photo) and sample with sea-bottom flora and starfish (echinoderm) (right photo) collected from the wider offshore area of Mytilene strait with Smith-McIntyre grab on board R/V "Alkyon".

3.1.1.4. NE Rhodes Island

In November 2013, an offshore survey was carried out at Afantou bay located at the NE part of Rhodes Island with the R/V ALKYON of the Hellenic Centre for Marine Research (HCMR). During this cruise, twelve (12) offshore surficial sediment samples were collected using Smith-McIntyre Grab, as shown in Figures 3.18-3.19. Extensive catalogue of sampling locations is provided in Annex I.

Figure 3.18. Sampling locations of the offshore surficial samples from Afantou Bay, NE Rhodes Island (Google Earth Pro).

Figure 3.19. Sample AFA-3C (left photo) and sample AFA-3D with fine material (right photo) collected from the offshore area of Afantou Bay, NE Rhodes Island with Smith-McIntyre grab on board R/V "Alkyon".

3.1.2. Various Coastal Samples

Central – Eastern Evia Island

In November 2013, twelve (12) coastal sediment samples were collected from three beaches from the central – eastern part of Evia Island, as shown in Figures 3.20 – 3.23. Extensive catalogue of sampling locations is provided in Annex I.

Figure 3.20. Sampling locations of the surficial coastal samples from central-east Evia Island (Google Earth Pro).

Figure 3.21. View of the beach where samples NST-1&2 were collected (left photo) and sampling point of sample NST-3. Coastal sediments have a bright white color.

Figure 3.22. View of the beach where samples PSA-1&2 (left photo) and PSA-3&4 (right photo) were collected. Coastal sediments have a light grey color.

Figure 3.23. View of the beach where samples EV-1&2 (left photo) and EV-3&4 (right photo) were collected.

South Evoikos Gulf

In June 2012, two (2) coastal sediment samples were collected from Schinias beach located at the south Euboean Gulf, as shown in Figure 3.24. Extensive catalogue of sampling locality is provided in Annex I.

Figure 3.24. Sampling locations of the surficial coastal sample from Schinias beach, south Euboean Gulf (Google Earth Pro).

NW Crete Island

In July 2012, May 2013 and June 2014, fifteen (15) coastal samples were collected from NW and SW Crete Island, as shown in Figures 3.25 – 3.31. Extensive catalogue of sampling locations is provided in Annex I.

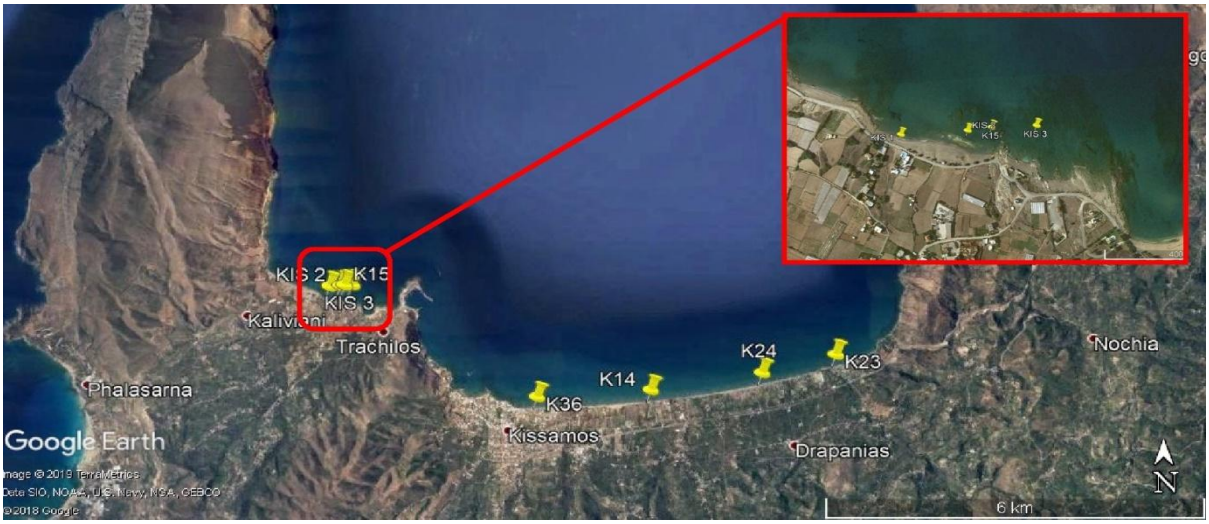

Figure 3.25. Sampling locations of the surficial coastal samples from Kissamos Bay, NW Crete Island (Google Earth Pro).

Figure 3.26. Part of the beach at Kissamos Bay, NW Crete Island., during samples collection.

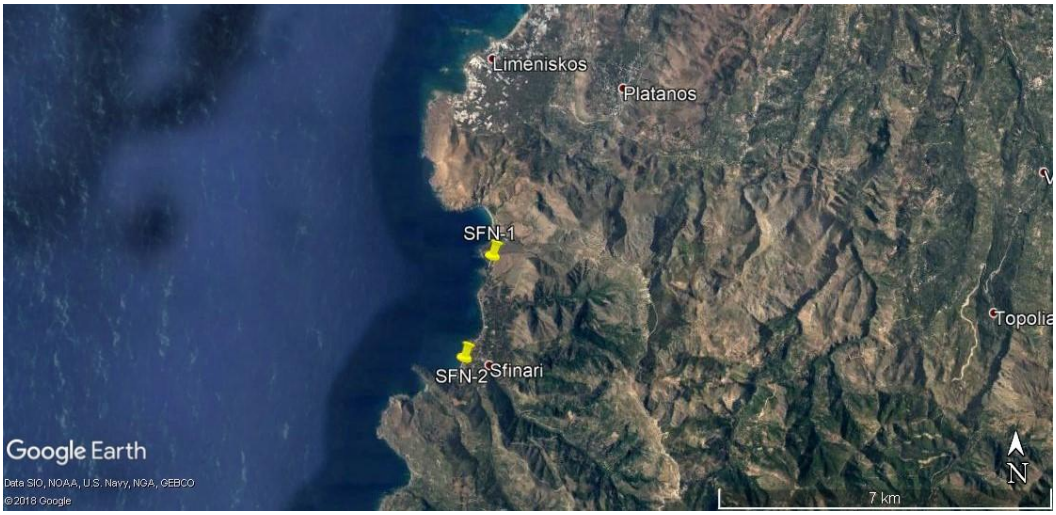

Figure 3.27. Sampling locations of the surficial coastal samples from Sfinari area, NW Crete Island (Google Earth Pro).

Figure 3.28. View of the Sfinari beach where coastal samples SFN-1 & 2 were collected. Coastal sediments have a dark color.

Figure 3.29. Sampling locations of the surficial coastal samples from Kampos area, western Crete Island (Google Earth Pro).

Figure 3.30. Sampling locality of the surficial coastal sample from Tavroniti area, NW Crete Island (Google Earth Pro).

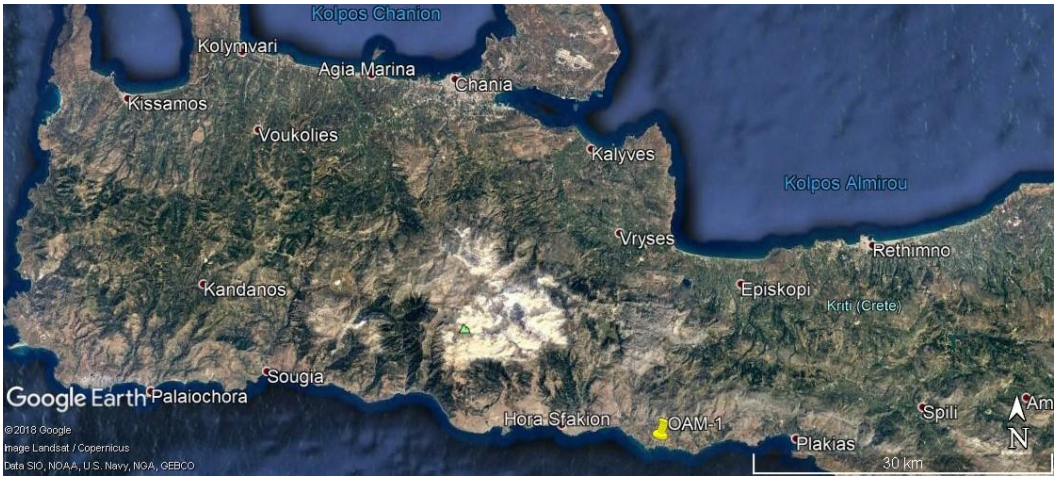

Figure 3.31. Sampling locality of the surficial coastal sample from Orthi Ammos area, southern Crete Island (Google Earth Pro).

North and East Peloponnese

In June 2012, five coastal sediment samples were collected from north and eastern Peloponnese. Specifically, four (4) samples were collected from Corinthian Gulf and one (1) sample from Argolic Gulf, as shown in Figures 3.32 – 3.33. Extensive catalogue of sampling locations is provided in Annex I.

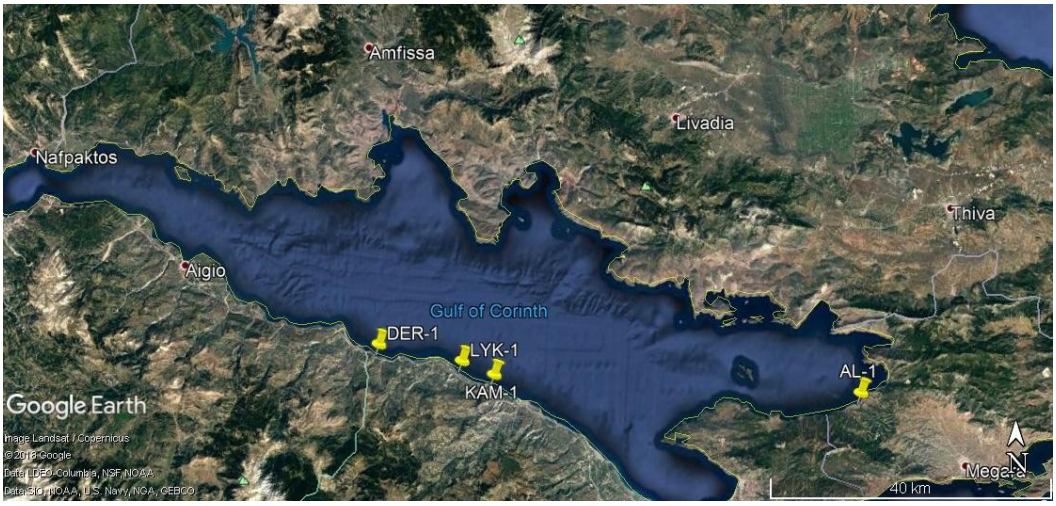

Figure 3.32. Sampling locations of the surficial coastal samples from the wider area of Corinthian Gulf, northern Peloponnese (Google Earth Pro).

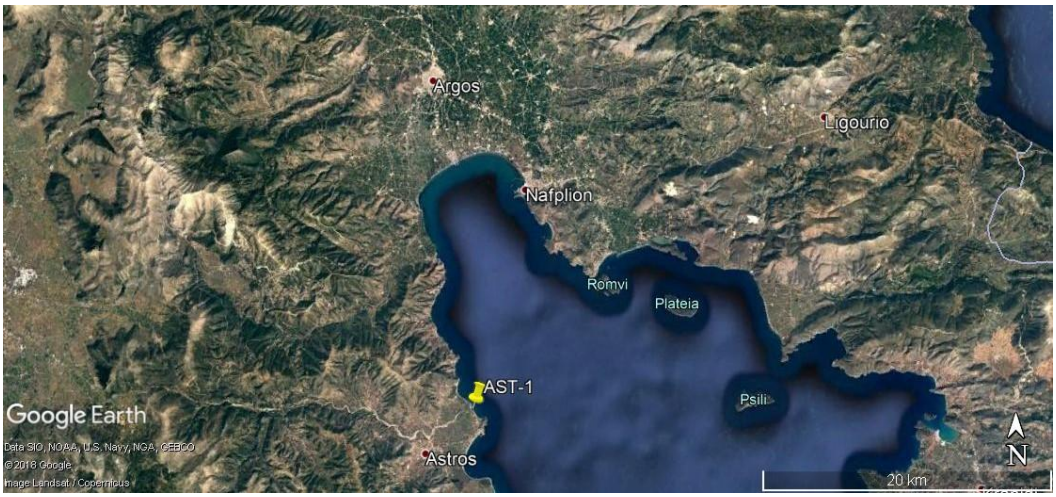

Figure 3.33. Sampling locality of the surficial coastal sample from the Argolic Gulf, eastern Peloponnese (Google Earth Pro).

Milos Island

In July 2012, one (1) coastal sample was collected from Plathiena beach, which is located at the northern Milos Island, as shown in Figure 3.34. Extensive catalogue of sampling locality is provided in Annex I.

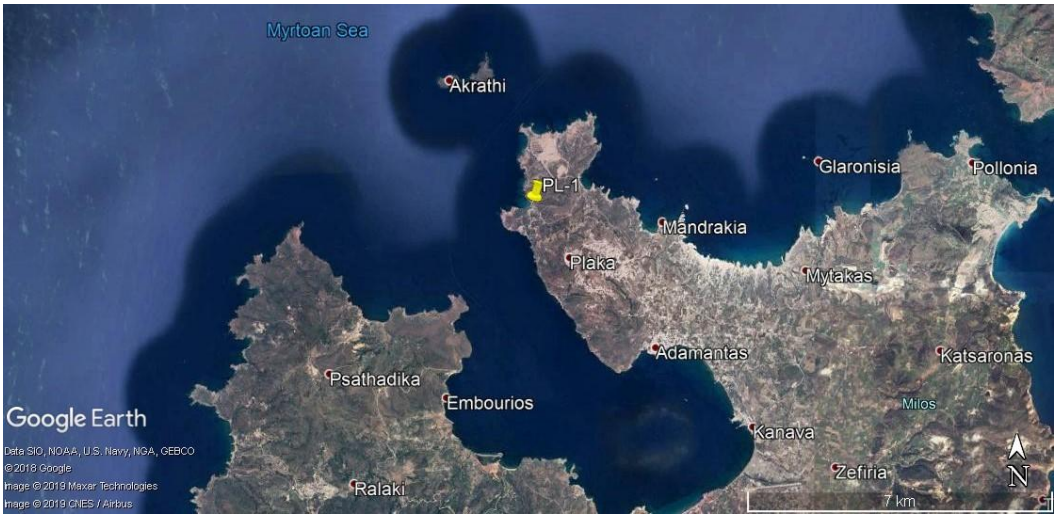

Figure 3.34. Sampling locality of the surficial coastal sample from Plathiena beach, north Milos Island (Google Earth Pro).

Samos Island

In July 2012, two (2) coastal samples were collected from Psili Ammos beach and Mpalos, at Samos Island, as shown in Figure 3.35. Extensive catalogue of sampling locations is provided in Annex I.

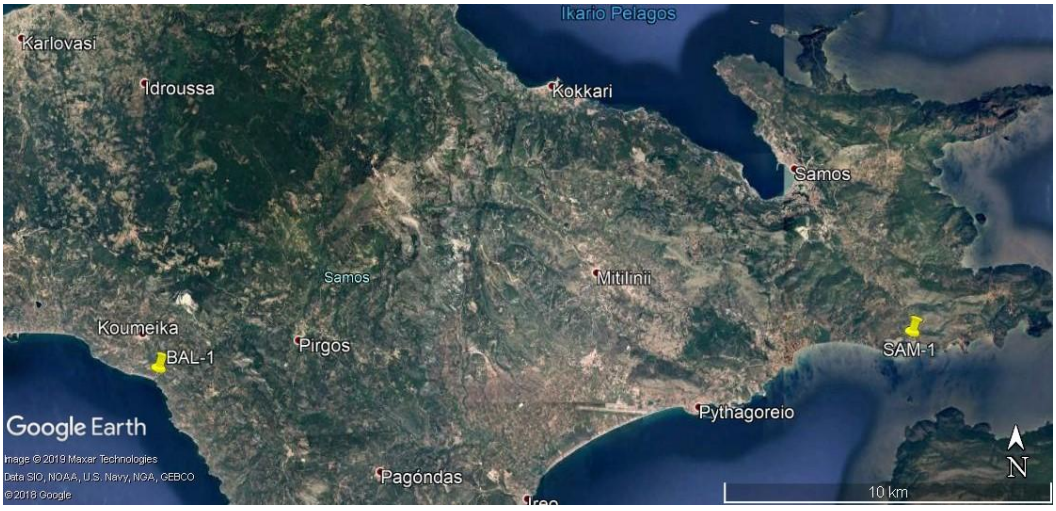

Figure 3.35. Sampling locations of the surficial coastal sample from Mpalos beach (samples BAL-1) and Psili Ammos beach (sample SAM-1), northern Samos Island (Google Earth Pro).

Kefalonia Island

In December 2018, one (1) coastal sample was collected from Skala beach, SE Kefalonia Island, as shown in Figures 3.36 – 3.37. Extensive catalogue of sampling locality is provided in Annex I.

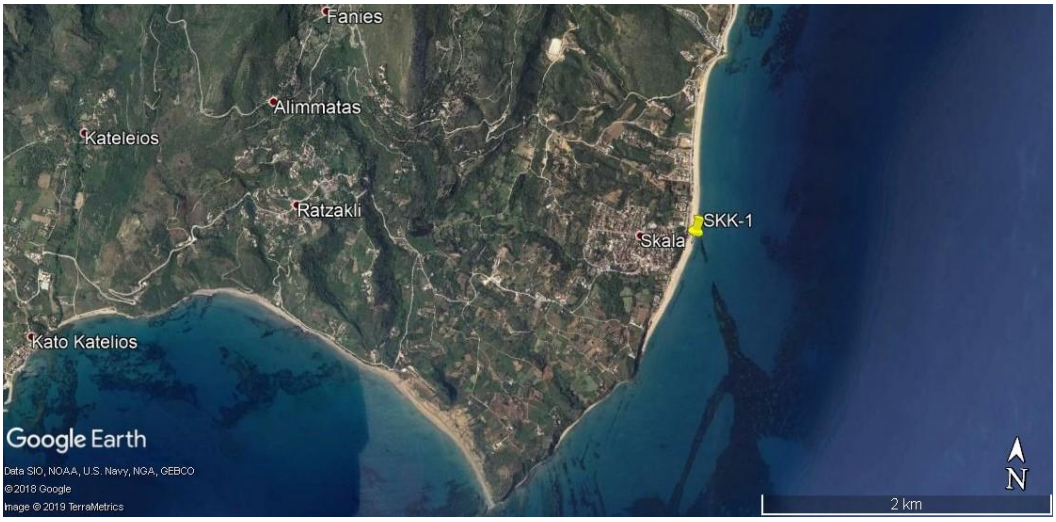

Figure 3.36. Sampling locality of the surficial coastal sample from Skala beach, SE Kefalonia Island (Google Earth Pro).

Figure 3.37. View of Skala beach where the coastal sample SKK-1 was collected.

3.1.3. Industrial Samples

South UK, Bournemouth and Boscombe areas

During March – April 2015, a visit took place at South UK for training and sampling. Sampling took place in the coastal areas of Bournemouth and Boscombe, where two (2) coastal sediment samples were collected from each beach of Bournemouth and Boscombe, respectively, as shown in Figures 3.38 – 3.40. Extensive catalogue of sampling locations is provided in Annex I.

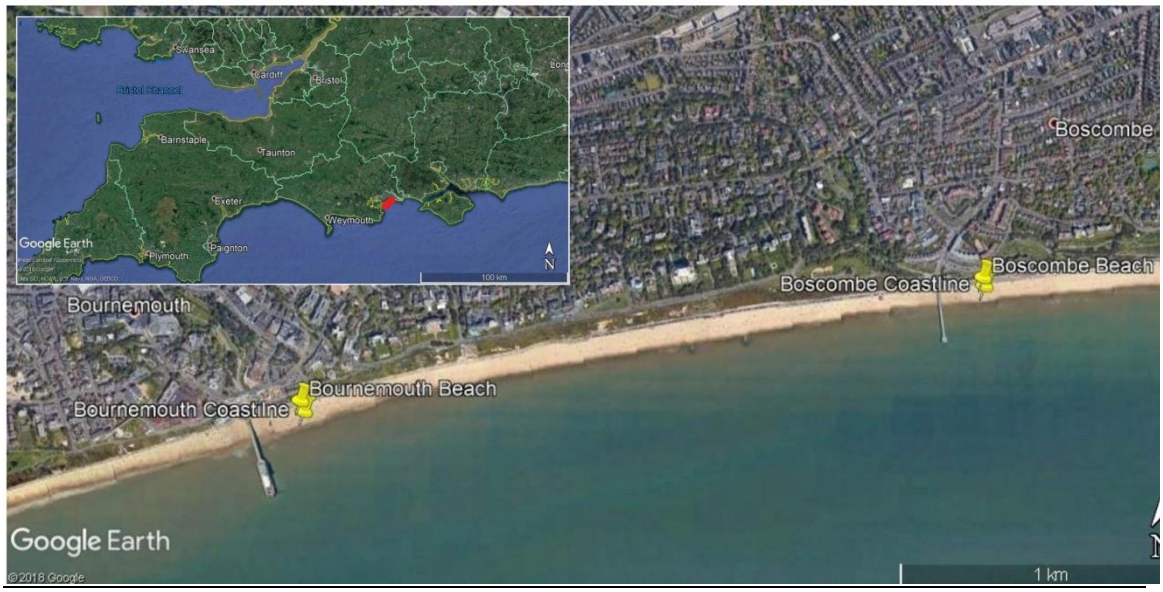

Figure 3.38. Sampling locations of the surficial coastal samples from Bournemouth and Boscombe beaches, south UK (Google Earth Pro).

Figure 3.39. View of Boscombe beach, south UK, where the coastal samples Boscombe Beach & Coastline were collected. Photos show the coastal infrastructure and therefore the need for beach nourishment projects in the area.

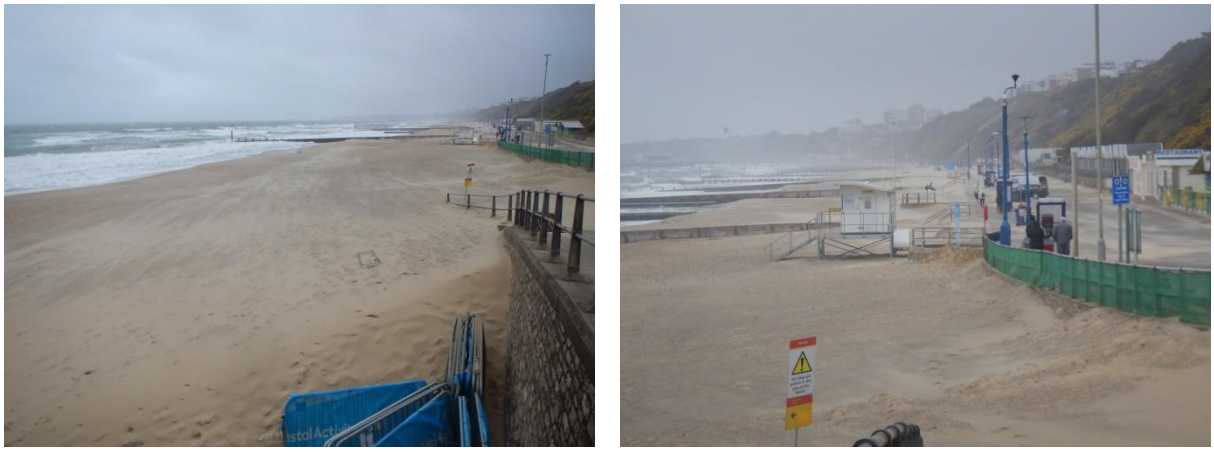

Figure 3.40. View towards Bournemouth beach, south UK, where the coastal samples Bournemouth Beach & Coastline were collected. Photos show the coastal infrastructure and therefore the need for beach nourishment projects in the area.

NW Italy

In July 2015, one (1) coastal sediment sample was collected from the beach Marina di Torre del Lago Puccini, which is located at Tuscany, NW Italy, as shown in Figure 3.41. Extensive catalogue of sampling locality is provided in Annex I.

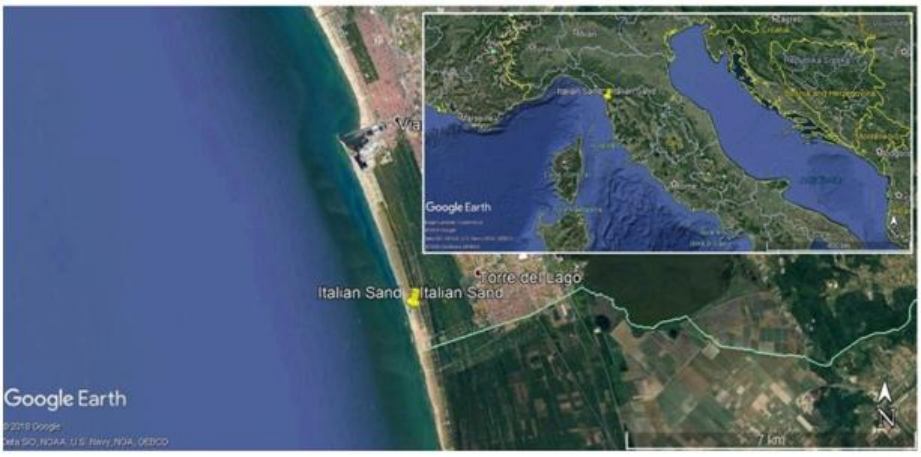

Figure 3.41. Sampling locality of the surficial coastal samples from the beach Marina di Torre del Lago Puccini, Tuscany, NW Italy (Google Earth Pro).

Aliartos

During 2014, two (2) terrestrial sediment samples were collected from Aliartos area, Viotia, central Greece, as shown in Figure 3.42. Extensive catalogue of sampling locations is provided in Annex I.

Figure 3.42. Sampling locations of the sediment terrestrial samples from Aliartos area, Viotia, central Greece (Google Earth Pro).

Strymonas River

During autumn 2015, two (2) sediment samples were collected on the bank of Strymonas River, NW of Sidirokastro, Northern Greece, as shown in Figure 3.43. Extensive catalogue of sampling locations is provided in Annex I.

Figure 3.43. Sampling locations of the sediment river samples from the bank of Strymonas river, NW of Sidirokastro, Northern Greece (Google Earth Pro).

Kafireas Stait, South Evia Island - North Kea Island

During 2014, a sediment sample was obtained from the company "RAFINA", a Greek shipping company whose main activity is the extraction, transportation and disposal of

marine aggregates. The sample was collected from the wider are between south Evia Island and north Kea Island, where the company is licensed for dredging activities.

3.2. LABORATORY METHODS

3.2.1. Grain Size Analysis

The determination of grain size analysis for all samples was performed at the Laboratory of Physical Geography, Section of Geography and Climatology, Department of Geology and Geoenvirnonment (DGG), National and Kapodistrian University of Athens (NKUA) and at the laboratories of Hellenic Geographical Military Service.

Grain size analysis was carried out by wet sieving (Folk, 1980) whilst grain size statistical parameters were further elaborated by Gradistat software v.8. The methodology followed for the grain size analysis is described below:

One hundered g of homogenized sediments was obtained from every sample (with high precision laboratory digital scale). Every sample was washed twice with tab water and stirred into a beaker. The purpose of this procedure is to remove salts and other impurities, such as wood, organisms and/or microorganisms, etc. The mixture remained for 24h in order the sediment to precipitate and then carefully remove the water (along with impurities). After, settled sediment was vigorously stirred with deionized water and calgon (sodium hexametaphosphate; 15g Calgon to 1.5 L of water) to separate fine-grained particles adhered to other grains. Then, the material was passed through a 63μm sieve.

Cores were sliced open and split into two halfs. One half was stored and archived. The other half was photographed and macroscopically observed in order to identify differences (in color, grain size, texture etc.) and to choose the frequency of sampling along the core. As a result, it was decided to collect one sample every ~10 cm and more samples at the upper 15 cm of each core as well as in any parts of the core considered to be of interest (different color, grain size, lenses, etc.).

Grain size analysis of the μm fraction >63 μm

The material remained on the above >63 μm sieve was placed into a labortory oven at 60 ^{o}C, until moisture totally removed. Prior and after the drying, each sample was weighed in

order to determine moisture content. After drying, a vibrator and sieves (brand CISA RP.08) were used in order to analyse the sediments. The sieves' nominal aoertures were 63 mm, 31.5 mm, 25.6 mm, 16 mm, 8 mm, 4 mm, 2.8 mm, 2 mm, 1.4 mm, 1 mm, 710 μm, 500 μm, 350 μm, 250 μm, 180 μm, 125 μm, 90 μm, 63 μm and <63 μm (tray). The nest of sieves was assembled with the coarsest screen at the top and the finest at the bottom and each sediment sample was mechanically agitated with an electric vibrator for ~20 min. After the end of vibration, the sediments retained in every sieve and collection tray were weighed (high precision laboratory digital scale – 4 digits) and tables were extracted for absolute, percent (%) and cumulative percent (%) w/w of each sample.

Grain size analysis of the fraction <63 μm

The material <63μm was collected in plastic bottles of 1.5 L (one sample in every bottle) and fine-grained samples were analyzed further for their grain size properties at the laboratories of the Hellenic Geographical Military Service. For the purpose of <63 μm fraction analysis a *Malvern Mastersizer* employs was used, which is based on laser diffraction techniques to measure the size of particles. The Malvern Mastersizer used Mie Theory and the principles of statioc light scattering (SLS) to calculate the size of particles in samples. The basic principle is to determine % v/v the grains for each fraction, as small particles scatter light at large angles and large particles scatter light at small angles.

Eventually, the results of grain size analysis of both the >63 μm and <63 μm fractions were merged and the final grain size results were extracted according to Folk, 1980 (Fig. 3.44).

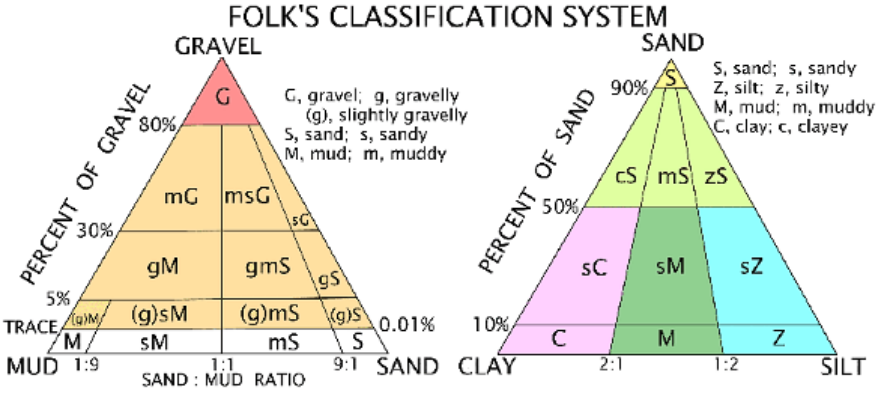

Figure 3.44. Folk's (1980) sediment classification scheme by the programme SEDCLASS modified from Poppe et al., 2014.

Statistical Parameters

According to Folk's methodology (1980) and with the contribution of sediment grain size analysis software the following statistical parameters of grain size were estimated: Mode (Mo), Median (Md), Graphic Mean (M_z), Inclusive Graphic Standard Deviation (σ_1), Inclusive Graphic Skewness (Sk_1) and Kyrtosis (K_G).

Specifically, according to Folk (1980):

- ***Mode (Mo)*** is the most frequently occurring particle diameter and it corresponds to the highest point on the frequency curve.
- ***Median (Md):*** $Md = Fd(d50)$

Median (Md) corresponds to the cumulative frequency of 50% and suggests that half of the particles are coarser than the median and half are finer.

- ***Graphic Mean (M_z):***

$$Mz = \frac{\phi 16 + \phi 50 + \phi 84}{3}$$

Determines the overall grain size of the sediment and characterize the sediment sample as coarser of finer than others. The Graphic Mean implies the magnitude of the force required for the transport of the sediment (wind or water force).

- ***Inclusive Graphic Standard Deviation (σ_1):***

$$\sigma_I = \frac{\phi 84 - \phi 16}{4} + \frac{\phi 95 - \phi 5}{6{,}6}$$

Inclusive Graphic Standard Deviation (σ_1) is a good measure of sorting and includes 90% of distribution. This formula suggests the degree of homogeneity or heterogeneity and rarely exceeds 10 value (extremely poorly sorted).

- **Inclusive Graphic Skewness (Sk_1):**

$$Sk_I = \frac{\phi 16 + \phi 84 - 2\phi 50}{2(\phi 84 - \phi 16)} + \frac{\phi 5 + \phi 95 - 2\phi 50}{2(\phi 95 - \phi 5)}$$

Skewness measures the degree of asymmetry and, also, the "sign", e.g. whenever a curve has an asymmetrical tail on the right or left. This formula includes 90% of the curve and expresses the degree of asymmetry of the cumulative curves of the sediments samples, characterizing the irregularity of the fractions' distribution of the grain size analysis.

Symmetrical curves have Sk_1=0, curves with excess of fine material (tail to the right) have positive skewness Sk_1>0 and those with excess of coarse material have negative skewness Sk_1<0. The more the skewness abstains from "0", the greater the degree of asymmetry. The absolute mathematical limits of the formula are +1.00 and -1.00, however rarely curves have values Sk_1 beyond +0.80 and -0.80 (Table 3.1).

- **Kurtosis (K_G):**

$$K_G = \frac{\phi 95 - \phi 5}{2{,}44(\phi 75 - \phi 25)}$$

Kurtosis is the quantitative formula used to describe deviance from the normality of the Gaussian formula. It measures the ratio between the sorting in the central portion and the sorting in the "tails" of the curve. Whenever the central portion is better sorted than the tails, then the curve is excessively peaked and called "leptokurtic". Whenever the tails are better sorted than the central portion the curve is flat-peaked and called "platykurtic" (Table 3.1). Strongly platykurtic curves are often bimodal with similar amounts of the two modes (M_o) and consequently a two-peaked frequency curves occurs. Therefore, the kurtosis distribution, for all graphical and statistical analysis of natural sediments, should be normalized using the transformation: $K_G/(1+ K_G)$.

Table 3.1. Classification of statistical parameters of grain size (Folk, 1980).

STATISTICAL PARAMETER	VALUES RANGE	CHARACTERIZATION
Inclusive Graphic Standard Deviation (σ_1)	<0.35	Very well sorted
	0.35-0.50	Well sorted
	0.50-0.71	Moderately well sorted
	0.71-1.00	Moderately sorted
	1.00-2.00	Poorly sorted
	2.00-4.00	Very poorly sorted
	>4.00	Extremely poorly sorted
Inclusive Graphic Skewness (Sk_I)	(+1.0) - (+0.30)	Strongly fine-skewed
	(+0.30) - (+0.10)	Fine-skewed
	(+0.10) - (-0.10)	Near symmetrical
	(-0.10) - (-0.30)	Coarse-skewed
	(-0.30) - (-1.00)	Strongly coarse-skewed
Kurtosis (K_G)	<0.67	Very platykurtic
	0.67-0.90	Platykurtic

0.90-1.11	Mesokurtic
1.11-1.50	Leptokurtic
1.50-3.00	Very leptokrutic
>3.00	Extremely leptokurtic

3.2.2. Stereoscopy

Selected samples (offshore, coastal and industrial samples) were chosen for stereoscopic observation. All these samples were studied under a Carl Zeiss Stemi 2000-C Stereo Microscope at the Laboratory of Inorganic and Analytical Chemistry, Department of Chemical Sciences, School of Chemical Engineering, National and Technical University of Athens (NTUA). Stereoscopic observation contributes to the determination of structure – microstructure of the grains (e.g. roundness and porosity), determination of impurities, determination of sorting in sediments, etc.

3.3.3. Density

Density measurements were performed for the majority of the offshore sediment samples and selected coastal and industrial samples. Density was determined with AccuPyc 1330 Pycnometer by Micromeritics which works by measuring the amount of displaced gas, herein helium gas. Density measurements with AccuPyc 1330 Pycnometer by Micromeritics performed at the Laboratory of Historical Geology – Paleontology, Section of Historical Geology – Paleontology, DGG, NKUA.

AccuPyc 1330 Pycnometer works as helium gas molecules quickly fill the tiniest pores of the sample chamber and then discharging it into another empty chamber allowing the computation of the sample's solid phase volume. The density of a sample material is determined as the mass of the material per unit volume. The precision mode achieves high repeatability.

3.3.4. Mineralogical Analysis – X-Ray Diffraction (XRD)

Mineralogical analysis was carried out for all samples. Measurements were conducted in powdered samples (powder <200 μm) by using a X-Ray Diffractiometer (XRD) at the Laboratory of Economic Geology and Geochemistry, Section of Economic Geology and Geochemistry, DGG, NKUA.

Crystalline, semi - crystalline and amorphous phases analysis was carried out by a Siemens D 5005 X-Ray Diffractometer with a Cu K_a radiation source at 40 kV, 40 mA and a graphite monochromator. The sampling interval of all measurements was 0.020°/step and 1.0 sec. step time. The evaluation of powdered XRD (PXRD) patterns took place with Eva 10.0 DIFFRACplus software package.

3.3.5. Scanning Electron Microscopy – Energy Dispersive Spectroscopy (SEM-EDS)

Representative samples were chosen to be analysed under a JEOL JSM-5600 Scanning Electron Microscopy (SEM) equipped with a backscatter electron detector (BSE) combined with a microanalyzer energy dispersive system (EDS) OXFORD LINK ISIS 300 with software ZAF correction quantitative analysis at the Laboratory of Economic Geology and Geochemistry, Section of Economic Geology and Geochemistry, DGG, NKUA. Accelerating voltage was of 20 kV, beam current of 0.5 nA, livetime of 50 sec and beam diameter of less than 2 microns. Microanalysis of free surfaces of sediment samples were coated with graphite and/or gold.

SEM/EDS analysis allows the study of micro to nano-scale features with magnification and provides the chemical elemental composition in or on the surface of the sediment samples. Also, it contributes to surface analysis, determination of inclusions and impurities, surficial salts presence, fatigue and corrosion of the grains and overall sample mapping.

3.3.6. Determination of Calcium Carbonates

The determination of carbonates (mainly $CaCO_3$ and $MgCO_3$ in %) is based on the volumetric analysis of the carbon dioxide (CO_2), which is produced during the application of hydrochloric acid solution HCl in the precipitate, as described in the following reaction:

$$CaCO_3 + 2HCl \rightarrow CaCl_2 + H_2O + CO_2^{\uparrow}$$

During the addition of the acid into the sample, foaming is observed, as an evidence of carbon dioxide's (CO_2) liberation and therefore the existence of carbonate salts.

The determination of total calcium carbonate was carried out in samples from gravity core at the Laboratory of Environmental Chemistry, Section of Inorganic Chemistry – Inorganic Chemical Technology – Environmental Chemistry, Department of Chemistry, NKUA.

The determination of carbonates was based on the weight difference before and after the addition of HCl to every sample. In a plastic container, 1g of sample was weighed, with accuracy of four decimal digits and the mass of the sediment was recorded (m_s). Then, the sediment was weighed together with a smaller container including 8ml HCl 6M (m_1). After withdrawing from the high precision laboratory digital scale, the acid was added to the precipitate and an exothermic reaction took place of gas HCl and CO_2 release. We time for one minute and weigh both containers with remaining precipitate and HCl (m_2).

The calculation of the carbonates percentage in the sediment is as follows:

$$\% \text{ Carbonates} = 100*(m_1-m_2)/m_s$$

3.3.7. Determination of Chlorides

Chlorides determination is a critical measurement in Marine Aggregates industry, as several issues are correlated with their presence, such as Alkali Silica Reaction (ASR) and Corrosion of Concrete Reinforcement (BMAPA, 2002). For the determination of chlorides content, 30 representative samples were selected; 10 samples from SE Evia Isl, 10 samples from NW Crete Island (Kissamos area) and 10 samples from NE Rhodes Island (Afantou area). Chlorides measurements were carried out at the Laboratory of Economic Geology and Geochemistry, Section of Economic Geology and Geochemistry, DGG, NKUA.

For every measurement, 100 g of each sample were placed in a graduated cylinder with tap and filter and then three successive washes with 100g of tap water were applied. The duration of every leaching was 10 minutes. The time interval between two successive leachings was 6 hours. The total chlorine content at each sample was measured with XRF analysis, while the soluble chlorine was determined using a HACH DR/4000 spectrometer, Method 8206, Mercuric Nitrate Method.

3.3.8. Chemical Analysis

Chemical analysis of major and trace elements was carried out with X-ray fluorescence (XRF) method. XRF spectrometry is a rather efficient quantitative technique to identify the elemental composition of any material (Barhoum et al., 2018). The determination of major and trace elements by XRF is accomplished by the interpretation of the behavior of atoms when they interact with radiation. XRF method is able to trace abundances at the ppm level. The X-rays of X-ray fluorescence are the characteristic X-rays of energy, lower than the incident X-rays, which are emitted from the sample. These fluorescent X-rays are used to identify the existence of elements, while their intensity is proportional to abundance of the elements, which are present in any sample (Barhoum et al., 2018). XRF analysis quite often is used to verify XRD results and vice versa.

For the purposes of this dissertation, three laboratories equipped with XRF Spectrometer were used the Laboratories of: i) TITAN SA, ii) Hellenic Centre for Marine Research (HCMR) and iii) NTUA. The first two laboratories are highly specialized in the geochemical analysis of aggregates and marine sediments, respectively.

Chemical analysis of major and trace elements with XRF method carried out in TITAN SA, Research, Development and Quality Department based in Kamari Viotia Cement Plant. For the analysis, a BRUKER SRS 3400 sequential X-ray spectrometer of WDS (Wavelength Dispersive Spectrometer) type was used operating at 50 kV, 69 mA with the AgRh tube and LIF, PET and OVE crystals. Chemical analysis of major and trace elements with XRF method was carried out in HCMR, Institute of Oceanography based in Anavyssos, Attica. For the analysis, a Philips PW-2400 XRF Spectrometer of WDS (Wavelength Dispersive Spectrometer) type was used. Chemical analysis was, also, carried out with XRF spectrometer SPECTRO XEPOS of SPECTRO Company at Laboratory of Metallurgy, School of Mining and Metallurgical Engineering, NTUA.The analysis method was TurboQuant. The samples were pressed to tablets of 32mm diameter using licowax as binder (CEREOX by Fluxana GMBH & Co) with a dilution factor approximate to 0.8.

3.3.9. Sand Equivalent Test

Sand Equivalent (SE) test is a rapid test which quantifies the relative abundance of fine-dust or clay-like materials in sand aggregates. The term “Sand Equivalent” expresses the

concept that most (fine) aggregates are mixtures of desirable coarse particles (e.g. sand-size particles and coarse particles) and undesirable clay/plastic fines and dust (ASTM, 2003). Sand equivalent test can be measured by standardized methods, such as ASTM D2419, AASHTO T176 and EN 933-8 (in Greece ELOT EN 933-8:2012).

For the purposes of this thesis, Sand Equivalent test carried out in TITAN S.A based in Kamari Viotia Cement Plant., Research, Development and Quality Department, Laboratory of Concrete Technology. The test carried out in representative mixtures of MA samples from two areas (Kissamos, Crete and SE Evia Island) and prior to Sand Equivalent Test, all samples (mixtures) were granulometrically analysed at the Laboratory of Physical Geography, Section of Geography and Climatology, Department of Geology and Geoenvirnonment, NKUA. The sieves' nominal aoertures were 16 mm, 8 mm, 4 mm, 2.8 mm, 2 mm, 1 mm, 500 μm, 250 μm, 180 μm, 125 μm, 63 μm and <63 μm (tray). The analytical procedure is according to § 3.2.1 Grain Size Analysis.

The procedure that was followed for SE determination concerns natural, fine aggregates passing the No. 4 (4.75 mm) sieve, according to Annex A of ELOT EN 933-8:2012. This procedure calculates the volume ratio of the clay to sand particles and is described below:

- 100 ml of standard concentrated solution of Formaldehyde, crystalline calcium chloride, glycerin and distilled water were poured into a graduated plastic cylinder.
- 120 g of the sample were weighed with a high precision lab digital scale and poured into the graduated plastic cylinder.
- The bottom of the graduated plastic cylinder was shaked in our hand in order to remove any trapped bubbles and to soak all the material.
- A rubber stopper was put to fit the plastic cylinder.
- The plastic cylinder was allowed to stand for 10 min.
- The graduated plastic cylinder was shaked into a mechanical device, which is designed to hold the cylinder in a horizontal position while subjecting to motion parallel to its length.
- The cylinder was removed from the mechanical device and afterwards we remove the rubber stopper and rinse any material from the stopper or the cylinder walls into the cylinder.
- Continue rinsing with the standard concentrated solution until 380 ml.
- The plastic cylinder was allowed to stand for exactly 20 min.

- The ***h1*** height of the suspended material was measured with a ruler (from the base of the cylinder).
- A weighting device was carefully placed (plumb) into the cylinder and allow it to rest on the sand.
- The ***h2*** height was measure with a ruler, from the surface where the plumb is in contact with the sand to the top of the cylinder/collar (a collar of the weighting device is attached to the top of the cylinder).

This procedure is implemented into two cylinders for every sample, in parallel.

The Sand Equivalent (SE) is expressed as the ratio of the height of the sand over the height of the clay.

SE = (Sand reading/Clay reading) * 100 = h2/h1 * 100

Higher SE values indicate "cleaner" aggregate (with less fine dust/clay-like material). According to ELOT EN 933-8:2012, the SE for 4 mm (SE_4) fraction is suggested to be:

- $SE_4 \geq 60$, for crushed aggregates
- $SE_4 > 70$, for natural formed aggregates, such as marine aggregates and aggregates from rivers.

3.3.10. Methylene Blue Test

Methylene Blue (MB) test is a reliable method to determine the amount of any potential harmful material in concrete aggregates, such as clay minerals and organic material. This test is carried out according to the ASTM C1777-15 and the EN 933-9 (in Greece ELOT EN 933-9:2013).

The methylene blue dye solution, known as methylthioninium chloride, consists of an organic base combined with acid (Taylor, 1985) and has the following formula: $C_{16}H_{18}N_3SCl$. The methylene blue contains a Cl^- ion and a large positively charged ion. As follows, methylene blue replaces the natural cations of clays (Taylor, 1985).

Ca-Na ***Clay*** + MB hydrochloride $\longrightarrow$ MB ***Clay*** + Ca-Na Chloride

Since, methylene blue dye solution as added to clay mixture, the MB positive ion removes the positive clay ions at the surface of the clay, continues until all other positive ions are expelled and up to point that clay mineral surfaces are attached to MB (Topal, 1996). Afterwards, MB ions replace clay positive ions in the interlayers. The remaining MB ions stay in solution.

When a methylene blue solution is added to a watery clay mixture, the positive methylene blue ion drives away the positive ions at the external surface of the clay. The process contiues until all the other positive ions have been expelled. Up to that point all the methylene blue attach to the clay mineral surfaces. Then the methylene blue ions replace the positive ions of the interlayers. From then on, the remaining methylene blue ions stay in solution. The maximum adsorption corresponds with the cation-exchange capacity (CEC).

For the purposes of this thesis, the Methylene Blue test was carried out in TITAN S.A based in Kamari Viotia Cement Plant., Research, Development and Quality Department, Laboratory of Concrete Technology. The test carried out in representative mixtures of MA samples from two areas (Kissamos, Crete and SE Evia Island). The procedure that was followed for MB determination concerns fine aggregates in the fraction between the 4mm and 2mm sieves, according to ELOT EN 933-9:2013. The procedure is as follows:

- 200 g of sample ($\boldsymbol{M_1}$) in the fraction between the 4 mm and 2 mm weighed in high precision lab digital scale)
- 500 ml of deionised water placed in a beaker.
- Add the 200 g of the sample in the beaker
- Stir the content of the beaker with a mixer for 5 min (600±60 r/min).
- Add 5 ml of MB solution into the beaker with a pipette.
- Stir the content of the beaker with a mixer for 1min (400±40 r/min).
- Place a filter paper on a watch glass.
- Take a drop from the solution into the beaker and deposit it onto the filter paper.
- The drop diameter should be between 8 mm and 12 mm.
- Observe if a circus of 1 mm thick is created around the drop.
- If not, add another 5 ml MB solution with a pipette, stir the content of the beaker with a mixer for 1 min (400±40 r/min) and place a drop into the filter paper.
- Repeat as many times, until a circus of 1mm thick is created around the drop.

- V_1 is the volume of MB solution added into the beaker until that circus of 1mm thick is created around the drop.

MB value = V1/M1*10

ELOT EN 933-9:2013 specifies that: a) MB value in 2mm fraction of sand, whether is crushed or natural sand, should be MB≤1.0 g/kg and b) when MB value in 2 mm fraction of sand, whether is crushed or natural sand, is MB≤0.8 g/kg, it is not necessary to perform SE test. According to Nikolaides et al. (2007), only a few countries include this test as a requirement in their nation specifications, such as France, USA and Greece (Greek Concrete Technology Regulation, 2016).

3.3.11. Data Correlation and Presentation

Grain size distribution and statistics were established according to established according to Folk (1980), nomenclature and Gradistat v.8 software (Blott and Pye, 2001). For the mapping and estimation of the spatial heterogeneity regarding the qualitative characteristics of the marine aggregates from the offshore areas, the ArcGis 10.2 software was used and more specifically the Inverse Distance Weighting (IDW) interpolation method. For the correlation of the qualitative characterics, a correlation matrix was built using the Correlation tool from from the Analysis ToolPak in Ecxel.

CHAPTER 4. RESULTS

In this chapter, the results of all the laboratory methods/techniques are presented. These results are presented in the context of an interdisciplinary approach to Marine Aggregates (MA) in Greece. The qualitative data include the following: physical characteristics (e.g. grain size analysis, density, SEM), texture (e.g. stereoscopy, SEM), mineralogy (e.g. XRD, SEM, stereoscopy), geochemistry (chemical analysis, chloride, total carbonates), environmental (e.g. chemical analysis, chlorides, carbonates, stereoscopy) and technical (e.g. sand equivalent, methylene blue) characteristics of MA.

4.1. GRAIN SIZE ANALYSIS

4.1.1. SE Evia Island – Offshore Samples

The results of the grain size analysis according Folk (1980) of the samples located at the offshore at the SE Evia Island are presented in the Table 4.1. Extensive catalogue with all the statistical parameters area presented in Annex II.

Table 4.1. Grain size analysis of the offshore samples of SE Evia Island, according to Folk classification (1980).

Samples	Folk Classification	Folk Abbreviation
KD-1	Slightly Gravelly Sand	**(g)S**
KD-2	Sand	**S**
KD-3	Sand	**S**
KD-6	Sandy Silt	**sZ**
KD-7	Silty Sand	**zS**
KD-8	Silty Sand	**zS**
KD-9	Slightly Gravelly Sandy Mud	**(g)sM**
KD-10	Gravel	**G**
KD-11	Silty Sand	**zS**
KD-12	Sand	**S**
KD-13	Slightly Gravelly Sand	**(g)S**
KD-14	Sandy Silt	**sZ**
KD-15	Gravelly Sand	**gS**
KD-16	Sandy Gravel	**sG**

Offshore samples from SE Evia Island are of various grain sizes. Samples KD-1-3, 10-13, 15-16 are coarser than the rest of samples. However, only samples KD-10 and KD-16 consist of gravel, whereas KD-6 and KD-14 consist mainly of silt.

4.1.2. SE Evia Island – Offshore Cores

The granulometrical results of the cores located off SE Evia Island are presented in the Table 4.2, while all the statistical parameters are presented in the Annex II.

Table 4.2. Grain size analysis of the offshore cores from SE Evia Island, according to Folk's classification (1980).

	Samples	Core's Depth (cm)	Folk Classification	Folk Abbreviation
CORE KD-4	**4-1**	0-2	Silty Sand	zS
	4-2	5-7	Silty Sand	zS
	4-3	10-12	Silty Sand	zS
	4-4	20-22	Silty Sand	zS
	4-5	30-32	Silty Sand	zS
	4-6	40-42	Silty Sand	zS
	4-7	50-52	Silty Sand	zS
	4-8	60-62	Silty Sand	zS
	4-9	70-72	Sandy Silt	sZ
	4-10	80-82	Silty Sand	zS
	4-11	90-92	Silty Sand	zS
	4-12	100-102	Silty Sand	zS
	4-13	110-112	Silty Sand	zS
	4-14	117-119	Silty Sand	zS
CORE KD-5	**5-1**	0-2	Silty Sand	zS
	5-2	5-7	Silty Sand	zS
	5-3	10-12	Silty Sand	zS
	5-4	20-22	Sandy Silt	sZ
	5-5	30-32	Sandy Silt	sZ
	5-6	40-42	Silty Sand	zS
	5-7	50-52	Silty Sand	zS
	5-8	60-62	Silty Sand	zS
	5-9	70-72	Silty Sand	zS
	5-10	80-82	Sandy Silt	sZ
	5-11	90-92	Sandy Silt	sZ
	5-12	100-102	Sandy Silt	sZ
	5-13	110-112	Sandy Silt	sZ

	5-14	120-122	Sandy Silt	sZ
	5-15	130-132	Sandy Silt	sZ
	5-16	140-142	Sandy Silt	sZ
	5-17	150-152	Sandy Silt	sZ
	5-18	160-162	Sandy Silt	sZ
	5-19	170-172	Sandy Silt	sZ
	5-20	180-182	Sandy Silt	sZ
	5-21	190-192	Sandy Silt	sZ
CORE KD-18	**18-1**	0-2	Sandy Silt	sZ
	18-2	5-7	Sandy Silt	sZ
	18-3	10-12	Sandy Silt	sZ
	18-4	15-17	Sandy Silt	sZ
	18-5	20-22	Sandy Silt	sZ
	18-6	30-32	Sandy Silt	sZ
	18-7	40-42	Sandy Silt	sZ
	18-8	50-52	Sandy Silt	sZ
	18-9	53-55	Sandy Silt	sZ
	18-10	60-62	Sandy Silt	sZ
	18-11	70-72	Sandy Silt	sZ
	18-12	80-82	Sandy Silt	sZ
	18-13	90-93	Sandy Silt	sZ
	18-14	100-102	Sandy Silt	sZ
	18-15	110-112	Sandy Silt	sZ
	18-16	120-122	Sandy Silt	sZ
	18-17	130-132	Sandy Silt	sZ
	18-18	137-139	Sandy Silt	sZ
	18-19	140-142	Sandy Silt	sZ
	18-20	150-152	Sandy Silt	sZ
	18-21	160-162	Sandy Silt	sZ
	18-22	170-174	Sandy Silt	sZ
	18-23	180-182	Sandy Silt	sZ
	18-24	190-192	Sandy Silt	sZ
	18_25	200-202	Sandy Silt	sZ
	18_26	207-209	Silty Sand	zS

Core KD-4 from the offshore area of SE Evia Island consists of silty sand apart from a horizon at 70-72 cm depth, which is sandy silt. Core KD-5 mainly consists mainly of sandy silt except of the uppermost layer 0-12 cm depth and a deeper layer 40-72 cm, which consist of silty sand. Core KD-18 consists of sandy silt apart from the deeper layer 207-209 cm, which consists of coarser material, silty sand.

4.1.3. NW Crete Island Offshore Samples

The grain size analysis data of the offshore samples, located at the NW Crete and specifically at Kissamos Bay and Sfinari area, are presented in the Table 4.3, while all the statistical parameters are presented in the Annex II.

Table 4.3. Grain size analysis of the samples located off Kissamos and Sfinari areas, NW Crete Island, according to Folk's classification (1980).

Samples	Folk Classification	Folk Abbreviation
KIS-1A	Gravelly Sand	gS
KIS-1B	Sand	S
KIS-1C	Slightly Gravelly Sand	(g)S
KIS-1D	Slightly Gravelly Muddy Sand	(g)mS
KIS-2A	Sand	S
KIS-2B	Sand	S
KIS-2C	Slightly Gravelly Sand	(g)S
KIS-2D	Slightly Gravelly Muddy Sand	(g)mS
KIS-3A	Sand	S
KIS-3B	Sand	S
KIS-3C	Slightly Gravelly Muddy Sand	(g)mS
KIS-3D	Slightly Gravelly Muddy Sand	(g)mS
KIS-4A	Sand	S
KIS-4B	Slightly Gravelly Sand	(g)S
KIS-4C	Slightly Gravelly Muddy Sand	(g)mS
KIS-4D	Slightly Gravelly Muddy Sand	(g)mS
SFI-1	Sand	S
SFI-2	Sand	S
SFI-3	Sand	S

Samples from Kissamos Bay mainly consist of sand. However, samples KIS-1A&B, KIS-2A&B, KIS-3A&B, KIS-4A&B are coarser than the rest of the samples. Samples from Sfinari area consist, exclusively, of sand.

4.1.4. Southern and Eastern Lesvos Island Offshore Samples

The results of the grain size analysis from the offshore areas of Eresos, Vatera and Mytilene strait are presented in the Table 4.4, while all the statistical parameters are presented in the Annex II.

Table 4.4. Grain size analysis of the samples located off southern and eastern Lesvos Island, according to Folk's classification (1980).

Samples	Folk Classification	Folk Abbreviation
L-E1	Sand	S
L-E2	Sand	S
L-E3	Slightly Gravelly Sand	(g)S
L-E4	Sand	S
L-E5	Sand	S
L-E6	Slightly Gravelly Sand	(g)S
L-E7	Slightly Gravelly Muddy Sand	(g)mS
L-E8	Sand	S
L-E9	Slightly Gravelly Sand	(g)S
L-V1	Slightly Gravelly Muddy Sand	(g)mS
L-V2	Slightly Gravelly Muddy Sand	(g)mS
L-V3	Slightly Gravelly Muddy Sand	(g)mS
L-V4	Slightly Gravelly Muddy Sand	(g)mS
L-V5	Slightly Gravelly Muddy Sand	(g)mS
L-V6	*Posidonia Oceanica*	
L-V7	Slightly Gravelly Muddy Sand	(g)mS
L-V8	Slightly Gravelly Muddy Sand	(g)mS
L-V9	Slightly Gravelly Muddy Sand	(g)mS
L-V10	Slightly Gravelly Sandy Mud	(g)sM
L-V11	Slightly Gravelly Muddy Sand	(g)mS
L-V12	Slightly Gravelly Muddy Sand	(g)mS
L-S3	Gravelly Muddy Sand	gmS
L-S4	Slightly Gravelly Muddy Sand	(g)mS
L-S7	Gravelly Muddy Sand	gmS
L-S11	Gravelly Sand	gS
L-S12	Slightly Gravelly Sand	(g)S
L-S16	Gravelly Muddy Sand	gmS
L-S19	Slightly Gravelly Sand	(g)S
L-S22	Gravelly Muddy Sand	gmS
L-S24	Gravelly Sand	gS
L-S25	Gravelly Sand	gS
L-S26	Slightly Gravelly Sand	(g)S
L-S28	Slightly Gravelly Muddy Sand	(g)mS
L-S29	Gravelly Muddy Sand	gmS
L-S32	Slightly Gravelly Muddy Sand	(g)mS

Offshore samples from Eresos, south Lesvos Island mainly consist of sand or gravelly sand. Offshore samples from Vatera area, south Lesvos Island consist of slightly gravelly

muddy sand, apart from sample L-V10, which consists of slightly gravelly sandy mud. Moreover, at position L-V6 no samples obtained as *Posidonia Oceanica* exists at the sea-bottom. Offshore samples from Mytilene strait, east Lesvos Island consist from gravelly muddy sand. Only samples L-S11-12, 19, 25-26 appear coarser, gravelly sand.

4.1.5. NE Rhodes Island Offshore Samples

The granulometrical results from the offshore samples located off Afantou Bay, NE Rhodes Island are presented below, while all the statistical parameters are presented in the Annex II.

Table 4.5. Grain size analysis of the samples located off Afantou Bay, Rhodes Island, according to Folk's classification (1980).

Samples	Folk Classification	Folk Abbreviation
AFA-1A	Sand	S
AFA-1B	Slightly Gravelly Sand	(g)S
AFA-1C	Slightly Gravelly Muddy Sand	(g)mS
AFA-1D	Slightly Gravelly Muddy Sand	(g)mS
AFA-2A	Sand	S
AFA-2B	Slightly Gravelly Sand	(g)S
AFA-2C	Slightly Gravelly Muddy Sand	(g)mS
AFA-2D	Slightly Gravelly Muddy Sand	(g)mS
AFA-3A	Sand	S
AFA3B	Gravelly Sand	gS
AFA-3C	Slightly Gravelly Muddy Sand	(g)mS
AFA-3D	Slightly Gravelly Sand	(g)S

The grain size of the samples from Afantou Bay, NE Rhodes Island, range from sand to gravelly muddy sand.

4.1.6. Various Coastal Samples

The grain size analysis data from various coastal areas in Greece are presented in Table 4.6, while all the statistical parameters are presented in the Annex II.

Table 4.6. Grain size analysis of the samples from various coastal areas, according to Folk's classification (1980).

Samples	Folk Classification	Folk Abbreviation
NST-1	Sandy Gravel	sG
NST-2	Slightly Sandy Gravel	(s)G
NST-3	Gravel	G
NST-4	Gravel	G
PSA-1	Sand	S
PSA-2	Gravelly Sand	gS
PSA-3	Sand	S
PSA-4	Sand	S
EV-1	Slightly Sandy Gravel	(s)G
EV-2	Sandy Gravel	sG
EV-3	Sandy Gravel	sG
EV-4	Slightly Sandy Gravel	(s)G
K-13	Slightly Gravelly Sand	(g)S
K-14	Sandy Gravel	sG
K-15	Sand	S
K-24	Gravelly Sand	gS
K-23	Slightly Gravelly Sand	(g)S
K-36	Sand	S
KIS-1	Gravelly Sand	gS
KIS-2	Sand	S
KIS-3	Slightly Gravelly Sand	(g)S
SFN-1	Gravel	G
SFN-2	Gravel	G
KAMP-1	Gravelly Sand	gS
KAMP-2	Sandy Gravel	sG
TAV-1	Gravelly Sand	gS
OAM-1	Sand	S
AST-1	Sandy Gravel	sG
KAM-1	Gravel	G
LYK-1	Gravelly Sand	gS
DER-1	Gravelly Sand	gS
AL-1	Sand	S
SXN-1	Sand	S
SXN-3	Sand	S
PL-1	Gravelly Sand	gS
SAM-1	Slightly Gravelly Sand	(g)S
BAL-1	Slightly Gravelly Sand	(g)S
SKK-1	Sandy Gravel	sG

Coastal samples have various grain sizes due to their variable geological origin. Coastal samples NST and EV from central/eastern Evia Island, consist mainly of gravel, while samples PSA, from the same area, and consist mainly of sand. Coastal samples from NW Crete Island (K, KIS, KAMP, TAV, OAM) are relatively coarse-grained (sand and gravel) and sample K-14 even coarser (sandy gravel). Coastal samples from Sfinari area (SFN), NW Crete Island are coarse (gravel). Sample AST-1 from Astros area (Argolic Gulf) is sandy gravel. Coastal samples from Corinthian Gulf (KAM, LYK, DER AL) are relatively coarse-grained (sand and gravel). Coastal samples from Schinias (SXN) are sands. Sample from Milos Island (PL) is gravelly sand, as well as samples from Samos Island (SAM, BAL). Finally, coastal sample from SE Kefalonia Island is sandy gravel.

4.2. STEREOSCOPY

Representative and selected sediment samples were studied under a Stereo Microscope, in order to determine the texture, shape and any impurities of the grains of the sampling areas under investigation: SE Evia Island (Fig. 4.1 – 4.2), NW Crete Island (Fig. 4.3), Lesvos Island, (Fig. 4.4) and industrial samples (Fig. 4.5).

SE Evia Island – Offshore Samples

Grain size does not fluctuate at the samples from Evia Island and grains are angular (Fig. 4.1). Quartz grains are transparent, shells are present in small amounts and glaucophane is appears in blue color (Fig. 4.1 a, g).

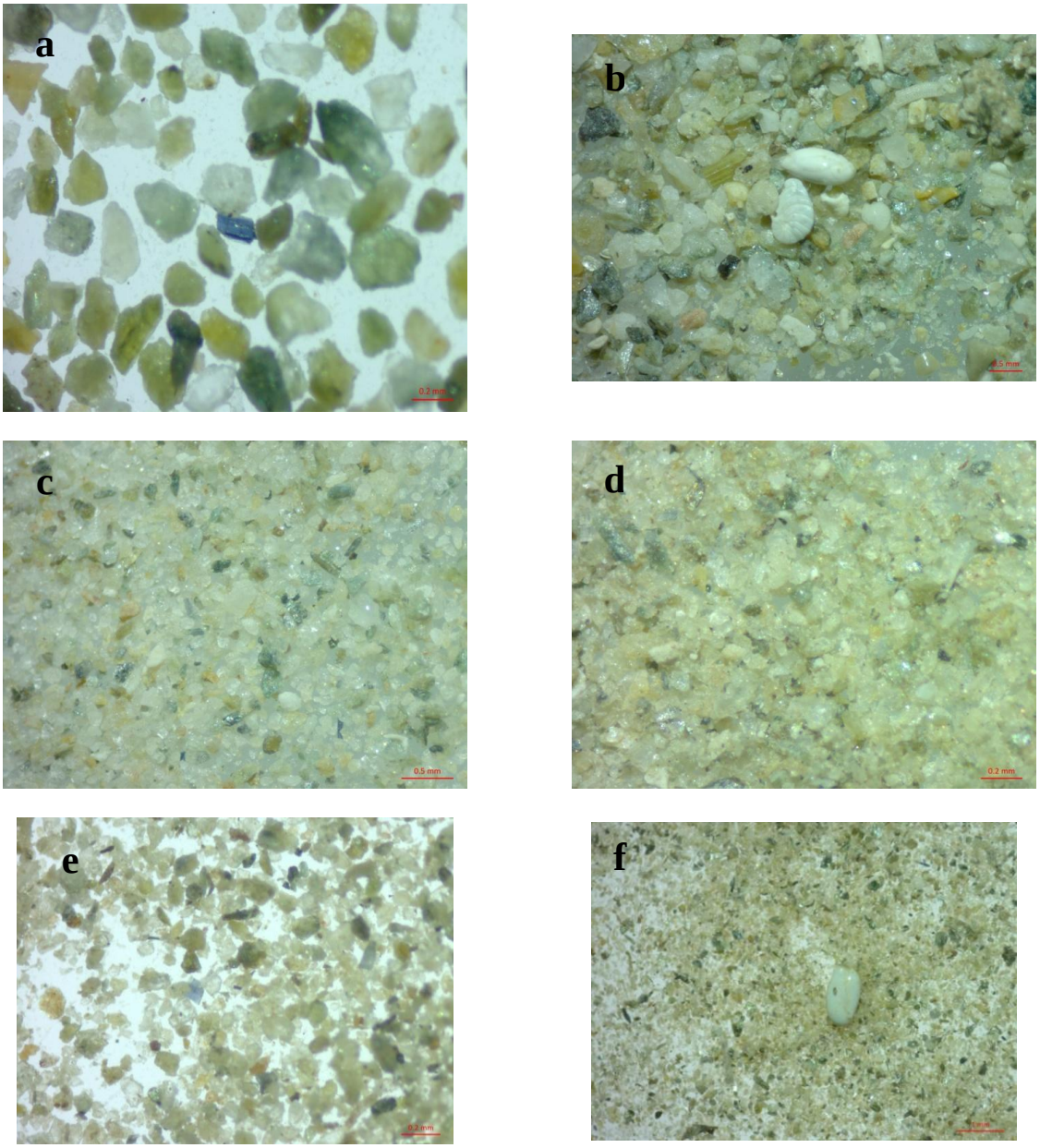

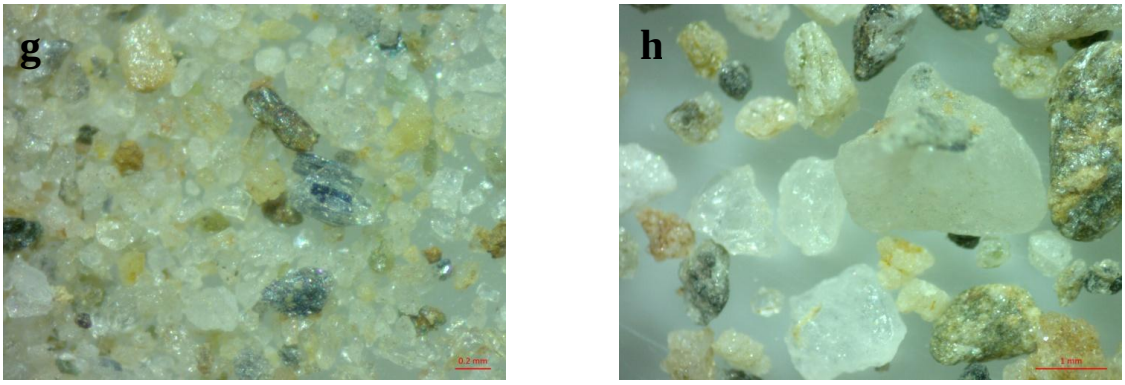

Figure 4.1. a) KD7, No 15; b) KD8, No 28; c) KD8, No 28; d) KD9, No11; e) KD9, No11; f) KD10, No45 g) KD13, No24; h) KD15 No49

SE Evia Island – Offshore Cores

Grain size of core samples varies significantly, as coarse grains were obserevd among the fine matrix (Fig. 4.2). Shells and micro-organisms are rarely observed (Fig. 4.2 f,g).

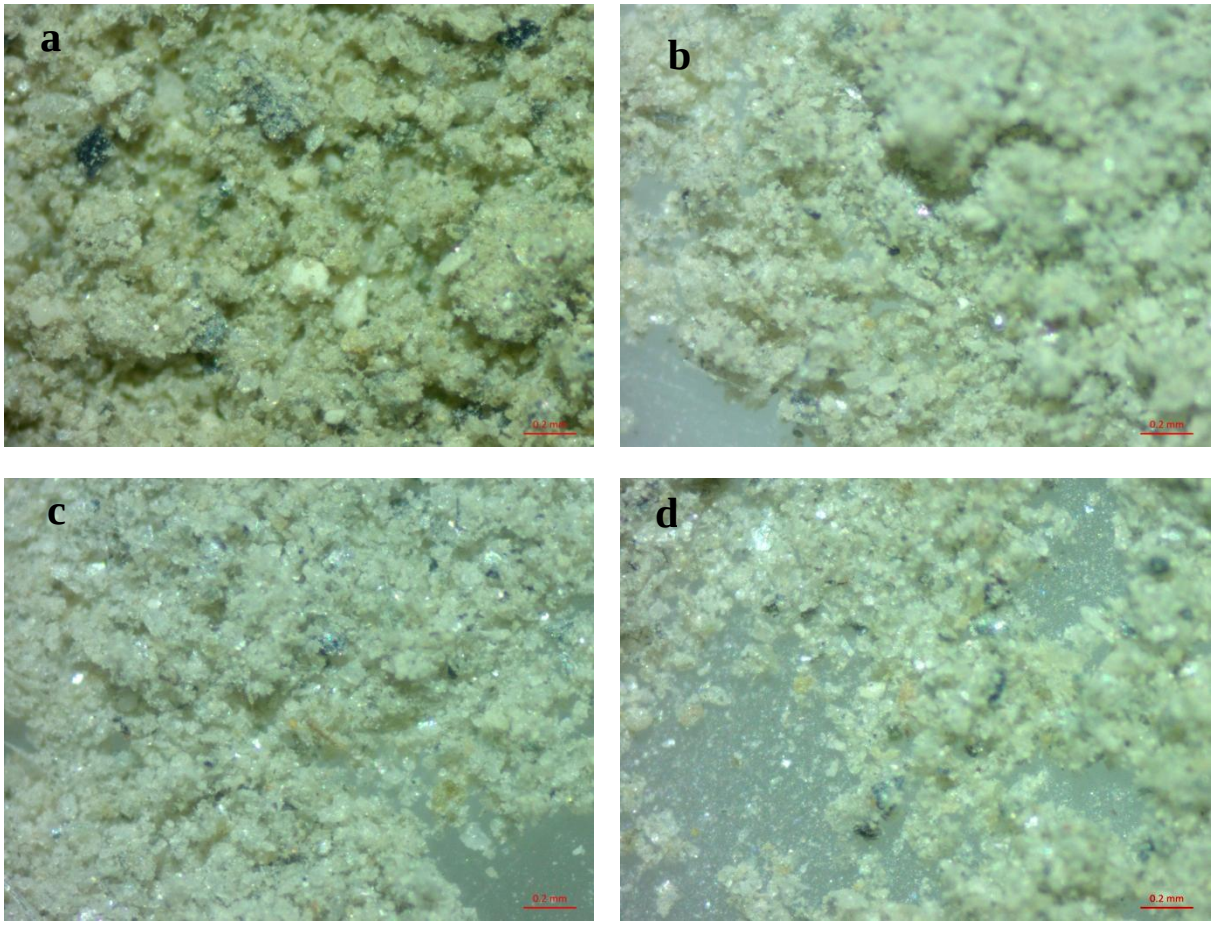

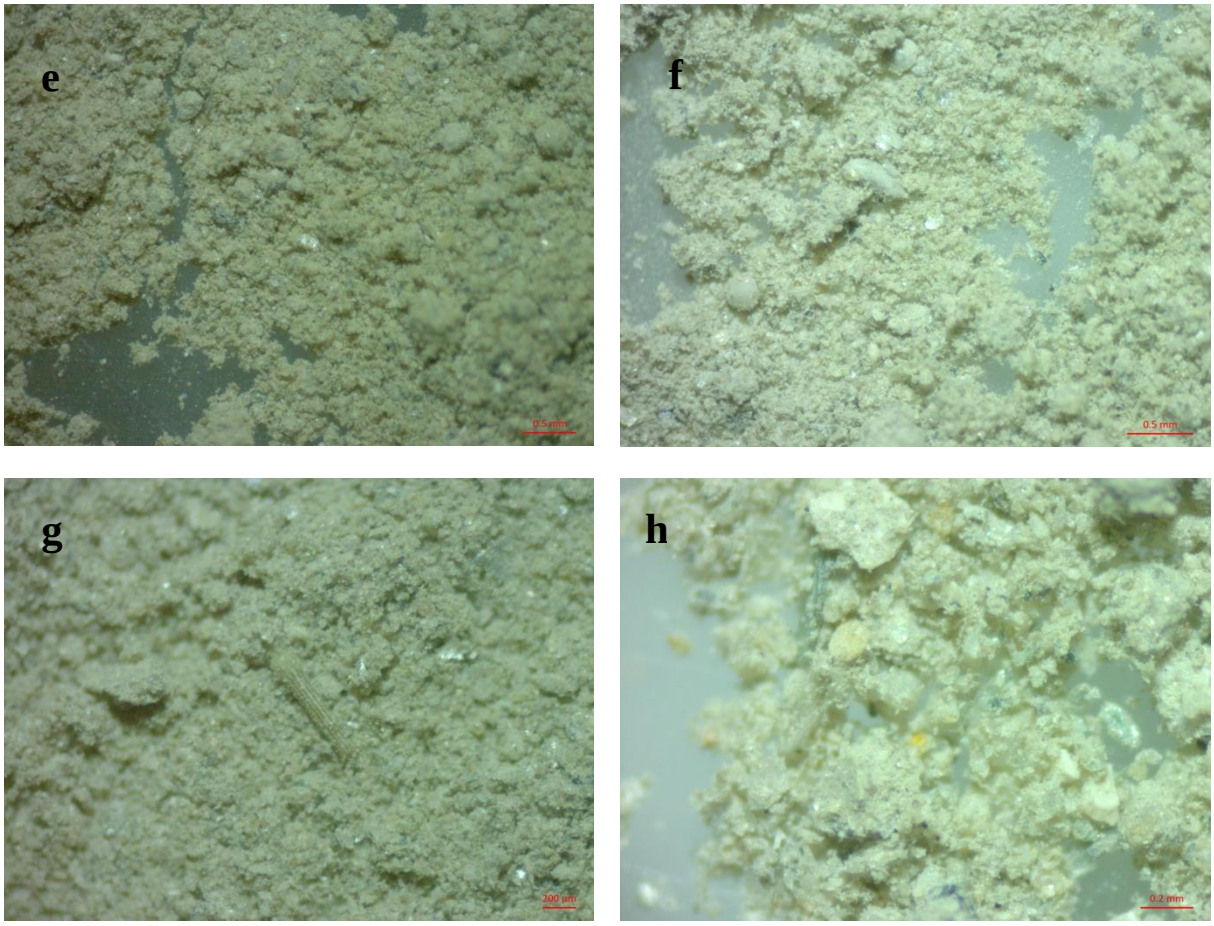

Figure 4.2. a) Core KD-5, 5-7; b) Core KD-5, 110-112; c) Core KD-5, 160-162; d) Core KD-5, 190-192; e) Core KD-18, 5-7; f) Core KD-18, 80-82; g) Core KD-18, 150-152; h) Core KD-18, 200-202.

NW Crete Island

Grain size in the shallow area of Kissamos Bay does not fluctuate, while in deeper areas varies significantly. Grains are sub-angular to rounded. Carbonate minerals were observed in light colors (mostly white and yellow). In Kissamos Bay, quartz grains are mostly transparent and shells and micro-organisms are present (Fig. 4.3 a-h), while in Sfinary Bay quartz grains are transparent to brownish and shells and micro-organisms are absent (Fig. 4.3 i, j).


a


b


c


d

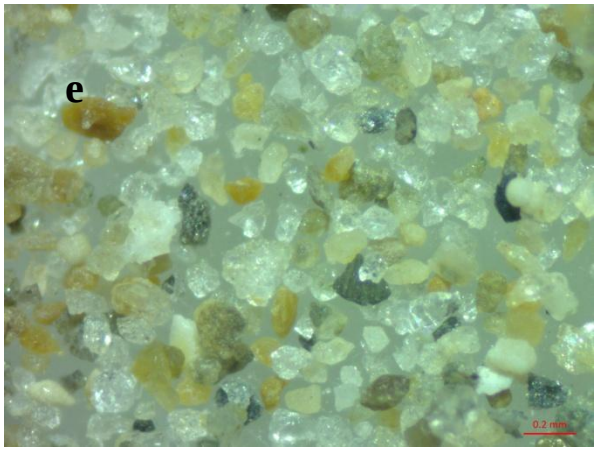
e

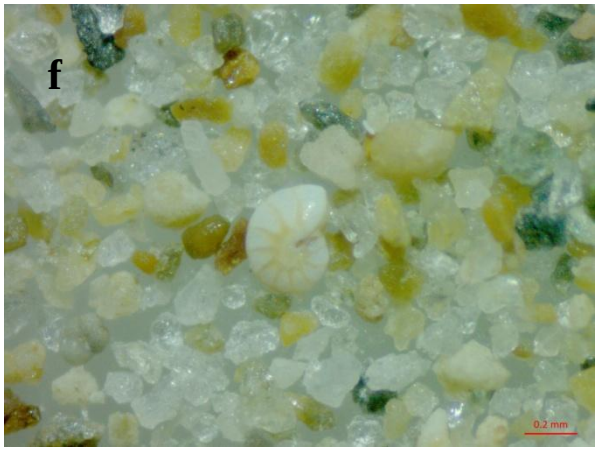
f

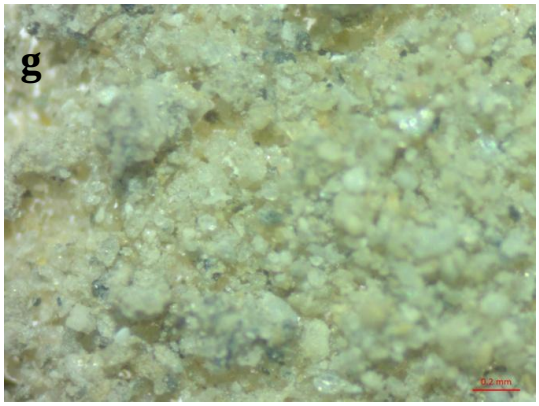
g


h

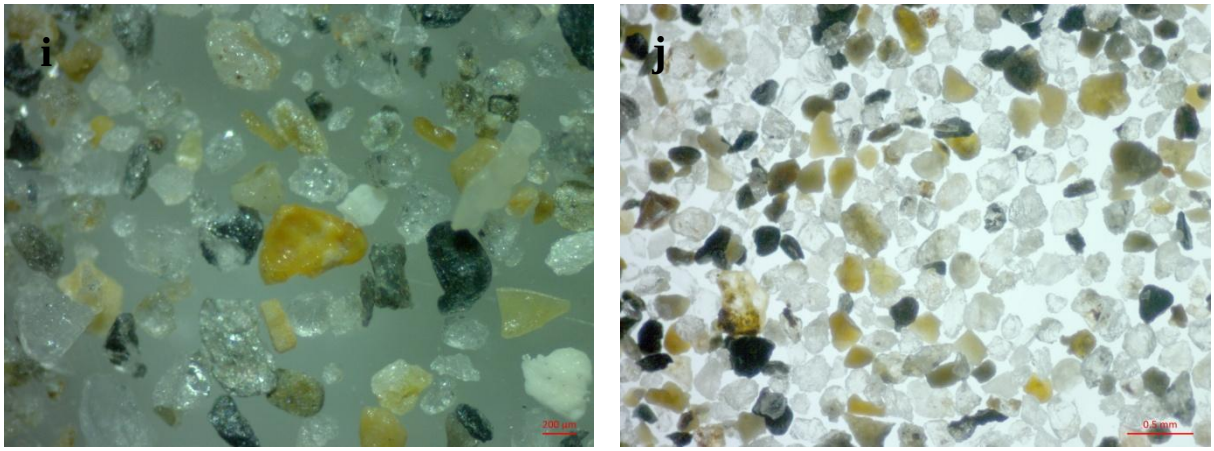

Figure 4.3. a,b) KIS-1A; c,d) KIS-1D; e,f) KIS-3A; g,h) KIS-3D; i) SFI-1, j) SFI-3

Southern and Eastern Lesvos Island

Grains are sub—angular and grain size is homogeneous (Fig. 4.4). Mafic minerals were often observed (Fig. 4.4 a,b,f), as well as shell fragments (Fig. 4.4 b, e, f).

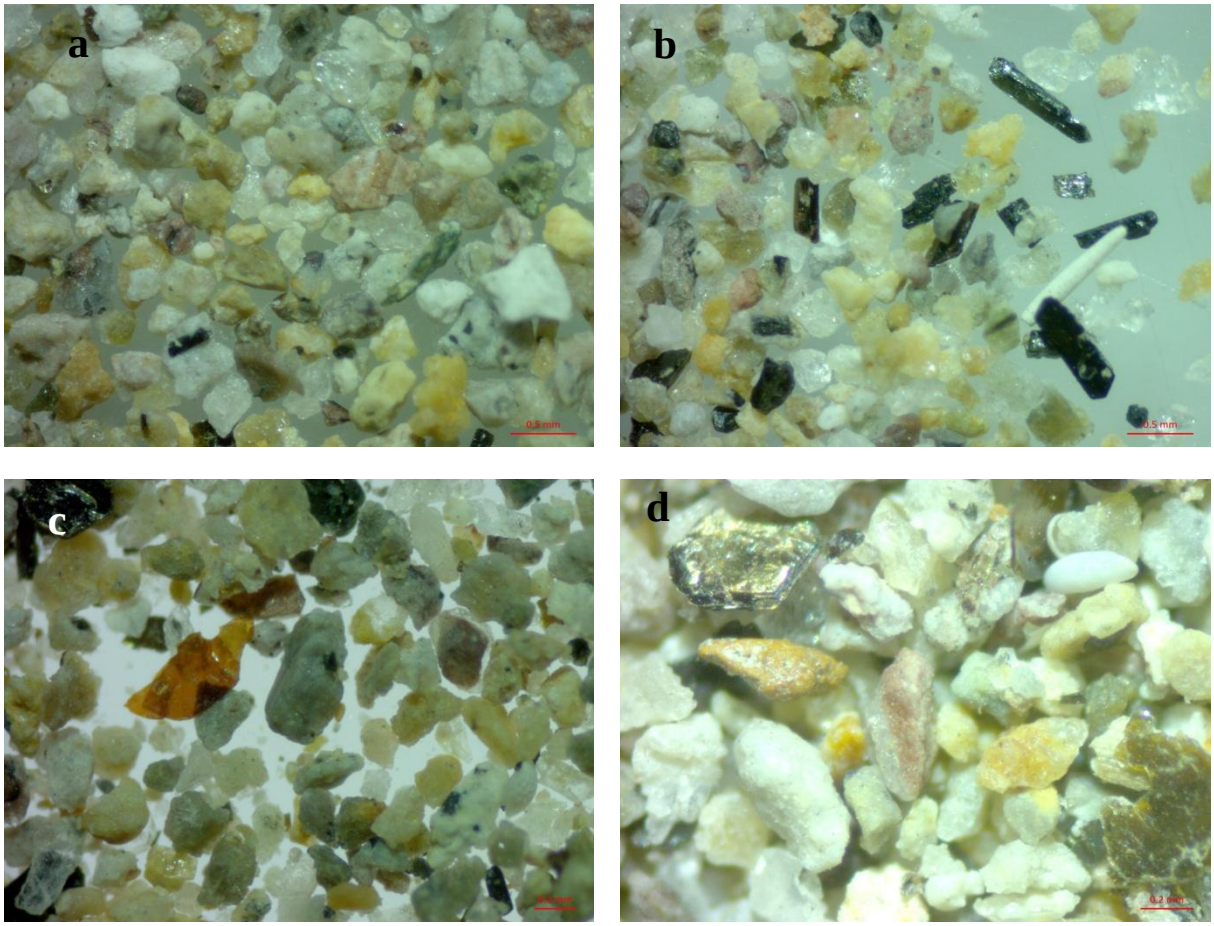

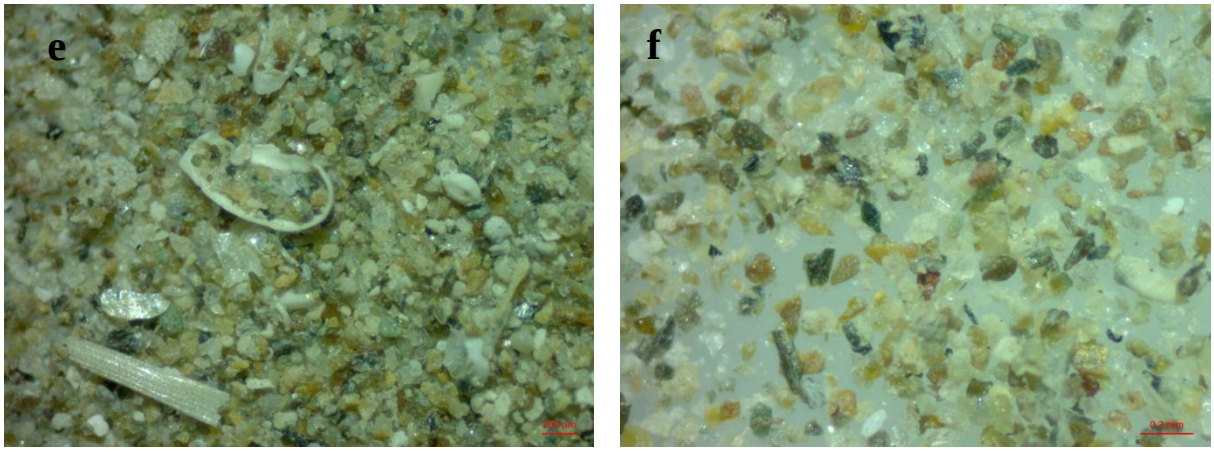

Figure 4.4. a,b) L-E1; c, d) L-E3, e,f) L-V12

Industrial Samples

Grains of Aliartos sample are sub-angular, quartz grains are white andvarious minerals, such as feldspars and calcite were observed (Fig. 4.5 a). Grains from Strymonas sample are angular, quartz grains are white to transparent and minerals of chlorite group are grayish (Fig. 4.5 b). Grains from Nairobi sand are rounded, quartz grains are transparent and, only, traces of others minerals were observed (Fig. 4.5 c, d). The same applies to UK samples (Fig. 4.5 e, f). Grain size of washed sample from Evia Island is quite homogeneous and fine material is absent (Fig. 4.5 h), while grain size of washed sample from Kissamos Bay (Fig. 4.5 a) varies significantly as coarse grains participate in the sandy matrix (Fig. 4.5 j).

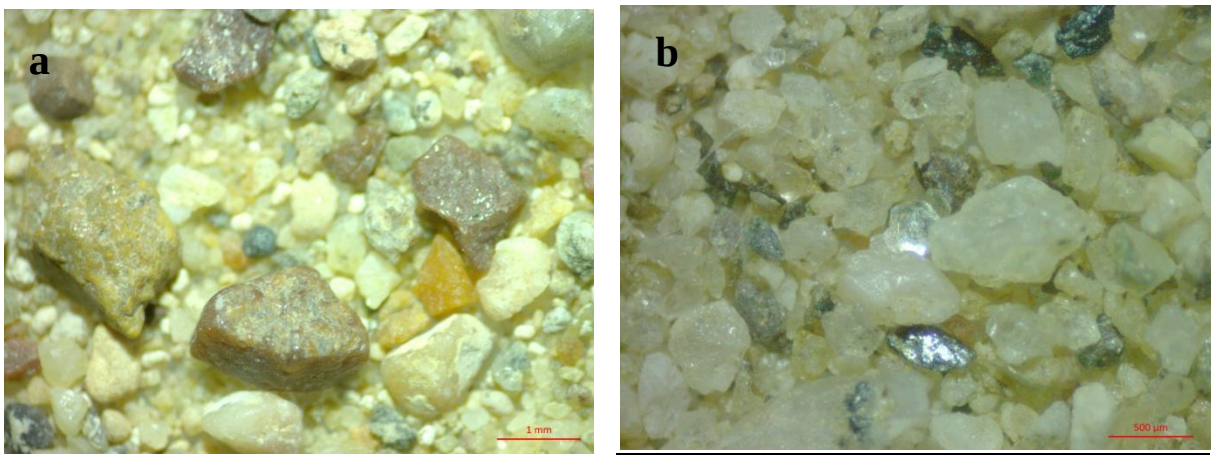

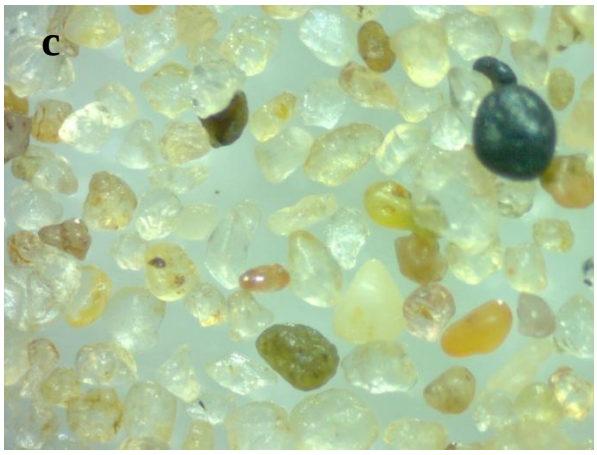
c


d


e
0.5 mm

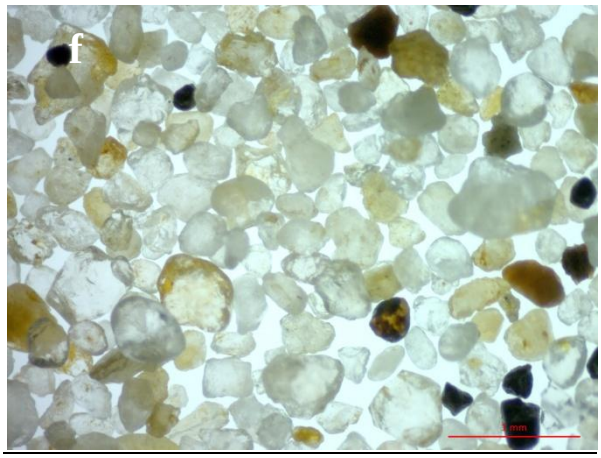
f

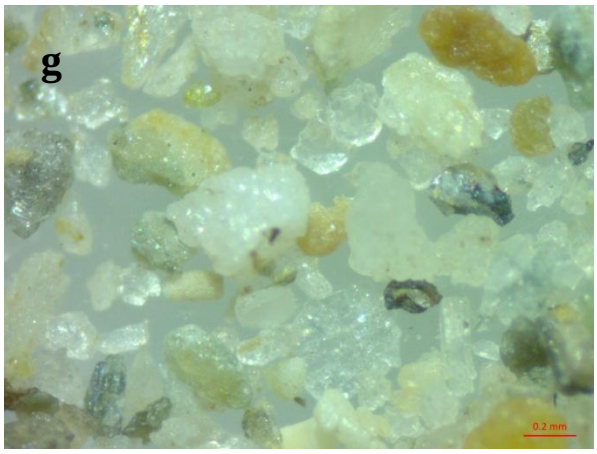
g
0.2 mm

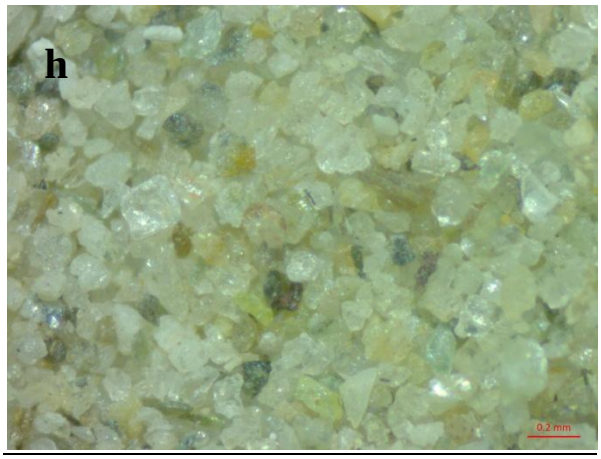
h
0.2 mm

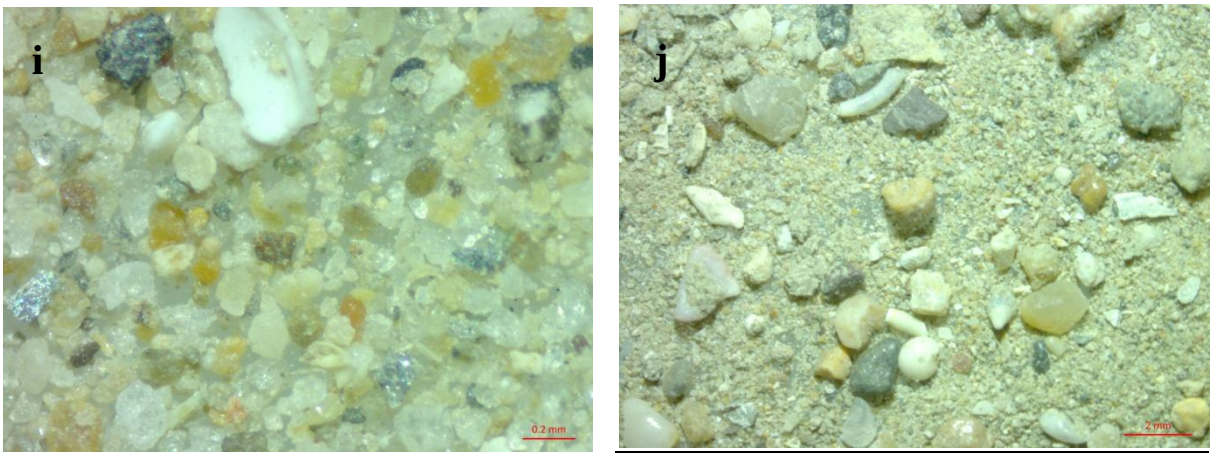

Figure 4.5. a) Aliartos 1, b) Strymonas 1, c, d) Nairobi, e,f) Boscombe coast, g) EV-W, h) EV-W-washed, i) KIS, j) KIS-washed.

4.3. DENSITY

The results of density measurements (expressed in g/cm^3) are presented in the Table 4.7.

Table 4.7. Density results of selected samples.

SAMPLES	AVERAGE SPECIFIC GRAVITY (Relative Density) (g/cm^3)	SAMPLES	AVERAGE SPECIFIC GRAVITY (Relative Density) (g/cm^3)
KD-1	2.63	**L-E1**	2.69
KD-2	2.64	**L-E2**	2.60
KD-3	2.67	**L-E3**	2.67
KD-6	2.64	**L-E4**	2.63
KD-7	2.81	**L-E5**	2.62
KD-8	2.73	**L-E6**	2.70
KD-9	2.61	**L-E7**	2.64
KD-10	2.69	**L-E8**	2.70
KD-11	2.65	**L-E9**	2.62
KD-12	2.67	**L-V3**	2.61
KD-13	2.65	**L-V12**	2.62
KD-14	2.62	**AFA-1A**	2.74
KD-15	2.64	**AFA-1B**	2.70
KD-16	2.71	**AFA-1C**	2.68
Core KD-18_0-2	2.65	**AFA-1D**	2.69
Core KD-18_53-55	2.66	**AFA-2A**	2.76
Core KD-18_100-102	2.68	**AFA-2B**	2.72

Core KD-18_140-142	2.56	**AFA-2C**	2.69
Core KD-18_180-182	2.67	**AFA-2D**	2.71
Core KD-18_207-209	2.69	**AFA-3A**	2.81
KIS-1A	2.64	**AFA-3B**	2.72
KIS-1B	2.63	**AFA-3C**	2.75
KIS-1C	2.66	**AFA-3D**	2.75
KIS-1D	2.58	**Italian Sand**	2.65
KIS-2A	2.67	**Bournemouth Beach**	2.69
KIS-2B	2.63	**Bournemouth Coastline**	2.65
KIS-2C	2.62	**Boscombe Beach**	2.70
KIS-2D	2.64	**Boscombe Coastline**	2.61
KIS-3A	2.64	**Nairobi**	2.69
KIS-3B	2.65	**Strymonas 1**	2.66
KIS-3C	2.60	**Aliartos 1**	2.63
KIS-3D	2.65	**GK**	2.63
KIS-4A	2.65	**KIS**	2.66
KIS-4B	2.62	**KIS washed**	2.63
KIS-4C	2.55	**EV-W**	2.67
KIS-4D	2.53	**EV-W-washed**	2.70
SFI-1	2.65	**EV-E**	2.67
SFI-2	2.64	**EV-E-washed**	2.70
SFI-3	2.68		

Offshore samples from SE Evia Island (KD) exhibit high density values in relation to core samples from the same area and from samples Kissamos Bay, Crete. Samples from Sfinari Bay, Crete exhibit slightly lower density values in relation to offshore SE Evia Island samples. Samples from Afantou display the higher density values, while these from Eresos, Lesvos exhibit the lower ones. Samples from Nairobi and south UK coastline display, quite, high values. Finally, washed samples from Crete and Evia Island, definitely, exhibit higher density values than the unwashed ones.

4.4. X-RAY DIFFRACTION (XRD)

The mineralogical analyses of the offshore and coastal samples are presented in Tables 4.9 - 4.18, while the list of the abbreviations is given in the followingTable 4.8.

Table 4.8. List of abbreviation used in mineralogical evaluations.

Explanatory Note	
Quartz	**Qz**
beta-Quartz	**β-Qz**
Albite	**Ab**
Calcite	**Cal**
Magnesian Calcite	**MgCal**
K-Feldspar	**Kfs**
Biotite	**Bt**
Illite/Muscovite	**Ilt/Ms**
Galena	**Gn**
Chlorite Group	**ChlG**
Edenite	**Ed**
Actinolite	**Act**
Sepiolite	**Sep**
Gypsum	**Gp**
Serpentine Group	**Srp**
Halite	**Hl**
Talc	**Tlc**
Cristobalite	**Crs**
Glaucophane	**Glc**
Stilbite	**Stb**
Dolomite	**Dol**
Goethite	**Gth**
Mn-Oxides	**Mn-Ox**
Orthoclase	**Or**
Anhydrite	**Anh**
Aragonite	**Arg**
Hematite	**Hem**
Smectite Group	**SmeG**
Bassanite	**Bas**
Celestine	**Clt**
Clinochrysotile	**Cctl**
Augite	**Aug**
Major Mineral	**MJ**
Medium Mineral	**MD**
Trace Mineral	**TR**
Minor Mineral	**tr**

4.4.1. SE Evia Island – Offshore Samples

Mineralogical analysis (qualitative and semi-quantitative) of the offshore samples from SE Evia Island was carried out for fourteen samples (Table 4.9).

Table 4.9. XRD mineralogical analysis of the seabed samples from SE Evia Island

SAMPLES	Qz	Ab	Cal	ChlG	Ilt/Ms	Glc	Tlc	Ed	Mn-Ox
KD-1	MJ	MD	TR	TR	TR	TR	TR		TR
KD-2	MJ	MD	TR	TR	TR	TR	TR		TR
KD-3	MJ	MD	TR	TR	TR	TR	TR		TR
KD-6	MJ	MD	TR	TR	TR	TR	TR		TR
KD-7	MJ	MD	TR	TR	TR	TR	TR	TR	TR
KD-8	MJ	MD	TR	TR	TR	TR		TR	
KD-9	MJ	MJ	TR	TR	TR	TR	TR		TR
KD-10	MJ	TR	TR	TR	TR				
KD-11	MJ	TR	TR	TR	TR		TR		TR
KD-12	MJ	MD	TR	TR	TR	TR	TR		TR
KD-13	MJ	MD	TR	TR	TR	TR	TR		TR
KD-14	MJ	MD	TR	TR	TR	TR	TR		TR
KD-15	MJ	TR	TR	TR	TR				TR
KD-16	MJ	TR	TR	TR	TR				

Quartz is the major mineral in all samples, while albite being the second most significant mineral phase. Calcite, chorites and clay minerals occur in trace amounts in all samples and talc and Mn-oxides occur in trace amounts in most of the samples. Glaucophane appears as trace mineral in samples KD-1 to KD-9, KD-12 to KD-14. Edenite occurs only in samples KD-7&8.

4.4.2. SE Evia Island – Offshore Cores

Mineralogical analysis (qualitative and semi-quantitative) of the offshore core samples from SE Evia Island was carried out for forty-four samples (Table 4.10).

Table 4.10. XRD mineralogical analysis of the offshore core samples from SE Evia Island

CORE	Core's Depth	Qz	Ab	Cal	Ilt/Ms	ChlG	SmeG	Glc	Or	Anh	Tlc	Ed	Mn-Ox
KD-4	5_7	MJ	MJ	MD	TR	TR		TR	TR	TR	TR	TR	
KD-4	40_42	MJ	MD	MD	TR	TR		TR	TR	TR	TR	TR	
KD-4	70_72	MJ	MD	MD	MD	MD		TR	TR	TR	TR	TR	
KD-4	100_102	MJ	MJ	MD	TR	MD		TR	TR	TR	TR	TR	
KD-4	110_112	MJ	MD	MD	TR	MD		TR	TR	TR	TR	TR	
KD-4	117_119	MJ	MD	MD	TR	MD		TR	TR	TR	TR	TR	
KD-5	0_2	MJ	MD	MD	TR	MD		TR	TR	TR	TR	TR	TR
KD-5	5_7	MJ	TR	MD	TR	MD		TR	TR	TR	TR	TR	TR
KD-5	10_12	MJ	TR	TR	TR	TR		TR	TR	TR	TR	TR	TR
KD-5	20_22	MJ	MD	MD	TR	MD		TR	TR	TR	TR	TR	TR
KD-5	30_32	MJ	TR	TR	TR	MD		TR	TR	TR	TR	TR	TR

KD-5	40_42	MJ	TR	MD	TR	MD		TR	TR	TR	TR	TR	TR
KD-5	50_52	MJ	TR	MD	TR	MD		TR	TR		TR	TR	TR
KD-5	60__62	MJ	MD	MD	TR	MD		TR	TR	TR	TR	TR	TR
KD-5	80_82	MJ	MJ	MD	TR	MD			TR	TR	TR		TR
KD-5	90_92	MJ	MD	MD	TR	MD		TR	MJ/MD	TR	TR	TR	TR
KD-5	110-112	MJ	MD	MD	TR	MJ		TR	MJ/MD	TR	TR	TR	TR
KD-5	120_122	MJ	MD	MD	TR	MJ		TR	MJ/MD	TR	TR	TR	TR
KD-5	130_132	MJ	MD	MD	TR	MJ	TR	TR	MJ/MD	TR	TR	TR	TR
KD-5	140_142	MJ	TR	MJ/MD	TR	MJ	TR	TR	TR	TR	TR	TR	TR
KD-5	160_162	MJ	MD	MD	TR	MD	TR	TR	TR	TR	TR	TR	TR
KD-5	170_172	MJ	MD	MD	TR	MD	TR	TR	TR	TR	TR	TR	TR
KD-5	180-182	MJ	MJ	MD	TR	MJ/MD	MD	TR	TR	TR	TR	TR	TR
KD-5	190-192	MJ	MD	MD	TR	MD	TR	TR	TR	TR	TR	TR	TR
KD-18	5_7	MJ	MD	MD	MD	MJ		TR	TR	TR	TR	TR	TR
KD-18	15_17	MJ	MD	MD	MD	MD		TR	TR	TR	TR	TR	TR
KD-18	20_22	MJ	MD	MD	MD	MJ		TR	TR	TR	TR	TR	TR
KD-18	30_32	MJ	MD	MD	MD	MJ		TR	TR	TR	TR	TR	TR
KD-18	50_52	MJ	TR	TR	MD	MD		TR	TR	TR	TR	TR	TR
KD-18	53_55	MJ	TR	TR	MD	MD		TR	TR	TR	TR	TR	TR
KD-18	60_62	MJ	TR	TR	MD	MJ		TR	TR	TR	TR	TR	TR
KD-18	80_82	MJ	TR	TR	MD	MJ		TR	TR	TR	TR	TR	TR
KD-18	90_92	MJ	TR	TR	MD	MD		TR	TR	TR	TR	TR	TR
KD-18	100_102	MJ	TR	TR	MD	MJ			TR		TR	TR	TR
KD-18	110_112	MJ	TR	TR	MD	MJ		TR		TR	TR	TR	TR
KD-18	120_122	MJ	TR	TR	MD	MJ		TR		TR	TR	TR	
KD-18	130_132	MD	TR	TR	MJ	MJ		TR	TR	TR	TR	TR	TR
KD-18	137_139	MJ	TR	MD	MD	MJ	TR	TR	TR	TR	TR	TR	TR
KD-18	140_142	MJ	TR	MD	MD	MJ	TR	TR	TR	TR	TR	TR	TR
KD-18	150_152	MJ	MD	MD	MD	MJ	TR	TR	TR	TR	TR	TR	TR
KD-18	160_162	MJ	TR	MD	MD	MJ	TR	TR	TR	TR	TR	TR	TR
KD-18	180_182	MJ	TR	TR	MD	MJ		TR	TR	TR	TR	TR	TR
KD-18	190_192	MD	TR	TR	MJ	MJ		TR	TR	TR	TR	TR	TR
KD-18	200_202	MJ	TR	TR	MD	MJ		TR	TR	TR	TR	TR	TR

Samples from Core KD-4 display quartz as major mineral, albite as secondary mineral phase. Clay minerals, amphiboles and chlorite group minerals occur as trace minerals. Samples from Core KD-5 display the same mineralogical composition as Core KD-4, apart from smectite group minerals that exist as trace mineral in core depth deeper than 130 cm and orthoclase which occurs as major mineral in a horizon at core depths 90-132 cm. Samples from Core KD-18 display quartz and chlorite group minerals as the main mineralogical phases. Moreover clay minerals occur as the second most significant minerals. Albite and

calcite occur as medium to trace minerals, while amphiboles and Mn-oxides are present as trace minerals.

4.4.3. NW Crete Island Offshore Samples

Mineralogical analysis (qualitative and semi-quantitative) of the offshore samples from Kissamos and Sfinari areas, NW Crete Island was carried out for nineteen samples (Table 4.11).

Table 4.11. XRD mineralogical analysis of the seabed samples from Kissamos and Sfinari areas, Crete Island

SAMPLES	Qz	Ab	Cal	MgCal	Dol	Arg	Ilt	ChlG	Hem	Hl	SmeG
KIS-1A	MJ	TR	MD/TR	MD/TR		TR	TR	-	TR	-	-
KIS-1B	MJ	-	MD/TR	TR	TR	TR	TR	-	-	-	-
KIS-1C	MJ	TR	MD/TR	MD/TR	TR	TR	TR	TR	-	-	-
KIS-1D	MJ	TR	MD	MD	TR	TR	TR	-	-	-	-
KIS-2A	MJ	TR	TR	TR	TR	-	TR	TR	-	-	TR
KIS-2B	MJ	TR	MD/TR	-	-	-	TR	TR	-	-	TR
KIS-2C	MJ	TR	TR	-	TR	-	TR	TR	-	-	-
KIS-2D	MJ	TR	MD/TR	-	-	TR	TR	TR	-	-	TR
KIS-3A	MJ	MD/TR	MD/TR	TR	TR	-	TR	TR	-	-	TR
KIS-3B	MJ	TR	MD/TR	-	-	-	TR	TR	-	-	TR
KIS-3C	MJ	TR	MD/TR	-	TR	-	TR	TR	-	-	-
KIS-3D	MJ	TR	MD/TR	TR	TR	-	TR	TR	-	-	-
KIS-4A	MJ	TR	TR	-	TR	-	TR	TR	-	-	TR
KIS-4B	MJ	TR	TR	-	-	-	TR	TR	-	TR	TR
KIS-4C	MJ	TR	MD/TR	TR	TR	TR	TR	TR	-	TR	TR
KIS-4D	MJ	TR	MD/TR	-	TR	-	TR	TR	TR	-	TR
SFI-1	MJ		TR	TR			TR	TR			TR
SFI-2	MJ		TR	TR			TR	TR			TR
SFI-3	MJ		TR	TR	TR		TR	TR			TR

Mineralogical analysis of Kissamos' samples showed that quartz is the main mineral and calcite is the second significant crystalline phase. Magnesian calcite and aragonite appear as medium to trace mineral mostly in samples KIS-1. Albite, clay minerals and chlorite group minerals occur as trace mineral in most of the samples. Samples from Sfinari area display quartz as the major mineral, whereas calcite, clay minerals and chlorite group minerals occur as trace minerals.

4.4.4. Southern and Eastern Lesvos Island Offshore Samples

Mineralogical analysis (qualitative and semi-quantitative) of the offshore samples from Eresos, Vatera and Mytilene, southern and eastern Lesvos Island was carried out for thirty-four samples (Tables 4.12 - 14).

Eresos

Table 4.12. XRD mineralogical analysis of the seabed samples from Eresos area, Lesvos Island

SAMPLES	Qz	Ab	Cal	Kfs	Bt	Ed	Hl
L-E1	MD	MJ		TR	TR	TR	TR
L-E2	MD	MJ	TR	TR	TR	TR	
L-E3	TR	MJ	TR	TR	TR	TR	TR
L-E4	MJ	MJ		TR	TR	TR	
L-E5	MD	MJ		TR	TR	TR	
L-E6	TR	MJ		TR	TR	TR	
L-E7	TR	MJ	TR	TR	TR	TR	TR
L-E8	TR	MJ			TR	TR	
L-E9	TR	MJ		TR	TR	TR	TR

The mineralogical analysis of samples from Eresos area showed that the primary mineral is albite, while quartz is the second most significant phase. Pottasium feldspars, micas and amphiboles occur as trace minerals.

Vatera

Table 4.13. XRD mineralogical analysis of the seabed samples from Vatera area, Lesvos Island

SAMPLES	Qz	Ab	Cal	Kfs	Ilt/Ms	ChlG	Ed	Act	Sep	Srp	Hl	Tlc
L-V1	MJ	MD	TR		TR	TR	TR		TR			TR
L-V2	MJ	MD	TR		TR	TR	TR			TR		TR
L-V3	MJ	MD	TR		TR	TR	TR					TR
L-V4	MJ	MD	TR		TR	TR	TR			TR		TR
L-V5	MJ	MD	TR		TR	TR	TR			TR	TR	TR
L-V6	***Posidonia oceanica***											
L-V7	MJ	MD	TR		TR	TR	TR			TR	TR	
L-V8	MJ	MD	TR	TR	TR	TR	TR			TR		TR
L-V9	MJ	MD	TR		TR	TR	TR			TR	TR	
L-V10	MJ	MD	TR	TR	TR	TR		TR			TR	
L-V11	MJ	MD	TR	TR	TR	TR	TR			TR		
L-V12	MJ	MD	TR	TR	TR	TR	TR			TR	TR	

Samples from Vatera area exhibit quartz as the major crystalline phase and albite as an abundant mineral. Calcite, clay minerals, chlorite group minerals, amphiboles and serpentine group minerals occur as trace minerals.

Mytilene Strait

Table 4.14. XRD mineralogical analysis of the seabed samples from Mytilene Strait, Lesvos Island

SAMPLES	Qz	β-Qz	Ab	Cal	MgCal	Kfs	Ilt/Ms	ChlG	Ed	Act	Gp	Hl	Tlc	Crs	Stb	Dol	Gth
L-S3	MJ	TR	MD	MJ		TR	TR	TR	TR	TR							
L-S4	MJ	TR	MJ	MD	TR	TR	TR	TR	TR	TR		TR	TR				
L-S7	MJ	TR	MD	MD	TR	TR	TR	TR	TR	TR		TR					
L-S11	MD	TR	TR	TR	MJ	TR			TR			TR					
L-S12	MD	TR	TR	TR	MD	TR	TR			TR			TR	TR			
L-S16	MJ	MD		MD	MJ		TR	TR					TR				TR
L-S19	MJ	TR	TR	TR	MD	TR				TR							TR
L-S22	MJ	TR	TR	MD	TR	TR	TR	TR	TR	TR				TR			
L-S24	MJ	TR	MD	TR	TR	MD	TR			TR							
L-S25	MJ	TR	MJ	MD	TR	TR	TR	TR	TR	TR	TR	TR	TR				TR
L-S26	MD	MD	TR	MJ	TR	MJ	TR	TR									TR
L-S28	MD	TR	MD	MJ		TR	TR	TR		TR		TR				TR	
L-S29	MD		TR	MJ	TR	TR	TR	TR		TR		TR	TR	TR	TR	TR	
L-S32	TR		TR	MJ		TR	TR	TR		TR			TR				

Mineralogical analysis of samples from Mytilene Strait showed that quartz is the main mineralogical phase, while albite and calcite occur as the second significant minerals. Beta-quartz, magnesian calcite, potassium feldspars, clay minerals and amphiboles occur as trace minerals in most of the samples. Goethite occur as trace miner in a few samples, gypsum occurs as trace mineral only in sample L-S25 and cristobalite and stilbite occur in sample L-S29.

4.4.5. NE Rhodes Island Offshore Samples

Mineralogical analysis (qualitative and semi-quantitative) of the offshore samples from Afantou Bay, NE Rhodes Island was carried out for twelve samples (Table 4.15).

Table 4.15. XRD mineralogical analysis of the seabed samples from Afantou Bay, NE Rhodes Island

SAMPLES	Qz	Ab	Cal	MgCal	Kfs	Dol	Arg	ChlG	Act	Cctl	Aug
AFA 1A	MJ	MD	MJ		TR	MJ		TR	TR	tr	
AFA 1B	MJ	TR	MJ		TR	MD		TR	TR	tr	
AFA 1C	MJ	MD	MJ		TR	MD		TR	TR	tr	
AFA 1D	MJ	MD	MJ		TR	MD		TR	TR	tr	
AFA 2A	MD	TR	MJ		TR	MJ		TR	TR	tr	
AFA 2B	MD	TR	MJ		TR	MD		TR	TR	tr	
AFA 2C	MD	TR	MJ		TR	MD		TR	TR	tr	
AFA 2D	MD	TR	MD		TR	MJ		TR	TR	tr	
AFA 3A	MD	TR	MJ			MJ	tr	TR	TR	tr	tr
AFA 3B	MD	TR	MJ			MD	TR	TR	TR	tr	tr
AFA 3C	MD	TR	MJ			MD	TR	TR	TR	tr	tr
AFA 3D	TR		MD	MJ			MD				

Samples from Afantou Bay showed that calcite is the main minerlogical phase, while quartz and dolomite are also abundant minerals. Albite, potassium feldspars, amphiboles and clay minerals occur as trace minerals in most of the samples, while clinochrysotile occurs as minor mineral.

4.4.6. Various Coastal Samples

Mineralogical analysis (qualitative and semi-quantitative) of coastal samples from various areas along Greece was carried out for thirty-three samples (Table 4.16 - 17).

Table 4.16. XRD mineralogical analysis of coastal samples from various coastal areas.

SAMPLES	Qz	Ab	Cal	MgCal	Dol	Arg	Ilt/Ms	ChlG	SmeG	Or	San	Hem	Bas
NST-1	MJ	TR	TR				TR	TR					
NST-2	MJ	TR	TR							TR	TR		
NST-3	MJ	TR	TR							TR	TR		
NST-4	MJ	TR									TR		
EV-1	MJ	TR	TR					TR		TR			
EV-2	MJ	TR	TR				TR	TR		TR			
EV-3	MJ	TR	TR				TR	TR		TR			
EV-4	MJ	TR	TR				TR	TR		TR			
K-13	MJ	TR	MD	tr	tr	TR	TR	TR	TR				
K-14	MJ		MD	TR	tr	tr	tr	TR					tr
K-15	MJ		MJ/MD	MD/TR		TR	tr	tr				TR	
K-23	MJ		TR		tr	TR	TR	tr				tr	
K-24	MJ	TR		tr	tr	tr	tr	tr	tr				
K-36	MJ		MD/TR	TR	TR	tr	tr	tr	tr				

KIS-1	MJ	TR	TR										
KIS-2	MJ		TR	TR									
SFN-1	MJ		TR		TR								
SFN-2	MJ		TR				TR						

Coastal samples from Evia Island (NST & EV) consist of quartz as the major crystalline phase and albite, calcite, clay minerals and potassium feldspars as trace minerals. Coastal samples from Kissamos Bay, Crete (K) consist, mainly, of quartz and secondary from calcite, while coastal samples from Sfinari consist, mostly, of quartz.

Table 4.17. XRD mineralogical analysis of coastal samples from various coastal areas.

SAMPLES	Qz	Ab	Cal	MgCal	Dol	Ilt/Ms	ChlG	SmeG	Glc	Act	Or	Ed	Mn-Ox	San	Clt	Bt
KAMP-1	MJ		TR		TR		TR									TR
KAMP-2	MJ		TR		TR	TR	TR									
TAV-1	MJ		TR			tr	TR									
OAM-1	MJ		TR	TR	TR							TR				
AST-1	MJ	TR	MD	TR		tr	TR		TR	TR			TR			
KAM-1	MJ	TR	MJ		TR	TR	TR									
LYK-1	MJ	TR	MD		TR											
DER-1	MJ	TR	MJ		TR	TR	TR									
AL-1	MJ	TR	TR												TR	
SXN-1	MJ	TR	TR			TR	TR	TR								
SXN-3	MJ	TR	TR			TR	TR	TR								
PL-1	MJ			Tr										TR		
SAM-1	MJ	MD	TR								TR			TR		
BAL-1	MJ	TR	MD		Tr	tr	TR									
SKK-1	MJ		TR													

Coastal samples from Kampos (KAMP), Crete Island, consist of quartz as the major crystalline phase and calcite, dolomite and clay minerals as trace minerals. The mineralogical analysis of the coastal samples from Argolic (AST) and Corinthian Gulf (KAM, LYK, DER, AL) showed that quartz and calcite are the main mineralogical phases. Samples from Schinias (SXN) showed that quartz occurs as major mineral and albite, clay minerals and calcite as trace minerals. Samples from Milos (PL) and Kefalonia (SKK) Island showed that quartz is their major and almost excusive mineral.

4.4.7. Industrial Samples

Mineralogical analysis (qualitative and semi-quantitative) of industrial samples from various areas worldwide was carried out for eleven samples (Table 4.18).

Table 4.18. XRD mineralogical analysis of industrial samples.

SAMPLES	Qtz	Ab	Cc	ChlG	Ill/Ms	Glc	Or	Tlc	Hl
Italian Sand	MJ	TR	TR						
Bournemouth Beach	MJ		TR						
Bournemouth Coastline	MJ		TR						TR
Boscombe Beach	MJ	TR	TR						
Boscombe Coastline	MJ								
Nairobi	MJ			tr					
Strymonas 1	MJ	TR	TR	MD	TR		TR	TR	
Strymonas 2	MJ	TR	TR	MD	TR		TR	TR	
Aliartos 1	MJ	TR	TR	MD	TR	TR	TR	TR	
Aliartos 2	MJ	TR	TR	MD	TR	TR	TR	TR	
GK	MJ	MJ	TR	TR	TR	TR	TR	TR	

The major mineral of industrial samples collected from abroad is quartz; however, there are some traces of albite and/or calcite. The mineralogical analysis of the industrial samples from Greece revealed that quartz is the most abundant mineral, while chlorite group minerals occur are of medium content. Moreover, other minerals, such as albite, calcite, talc, potassium feldspars, glaucophane and micas occur as trace minerals.

4.5. SCANNING ELECTRON MICROSCOPY – ENERGY DISPERSIVE SPECTROSCOPY (SEM-EDS)

Representative samples were studied under SEM-EDS from each offshore area (Fig. 4.6-4.30), as well as industrial samples (Fig. 4.31 - 4.53).

4.5.1. SE Evia Island – Offshore Samples

Regarding sample KD-7, Figure 4.6 involves a quartz grain, while Figure 4.7 shows an illite grain (semi-quantitative microanalysis a) with iron oxides (semi-quantitative microanalysis b). Details of sample KD-10 display in Figure 4.8, where a quartz grain appears (semi-quantitative microanalysis a) covered with iron oxides probably of biogenic

origin (semi-quantitative microanalysis b) and Figure 4.9, where a calcareous shell occurs. Figure 4.10 shows an epidote grain with Cu-Zn oxides.

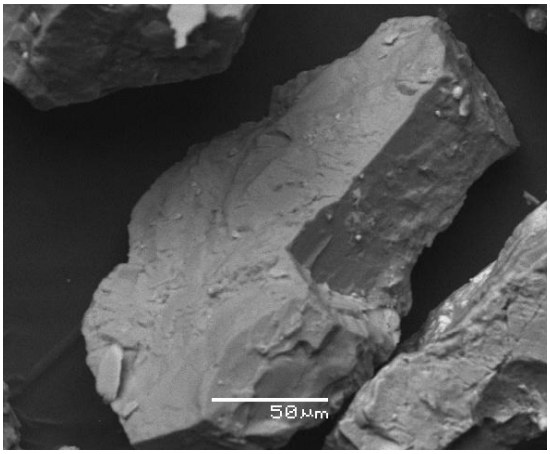

Figure 4.6. SEM microphotograph, showing details of sample KD-7.

Semi-quantitative microanalysis (%) EDS:

SiO_2	*98.72*

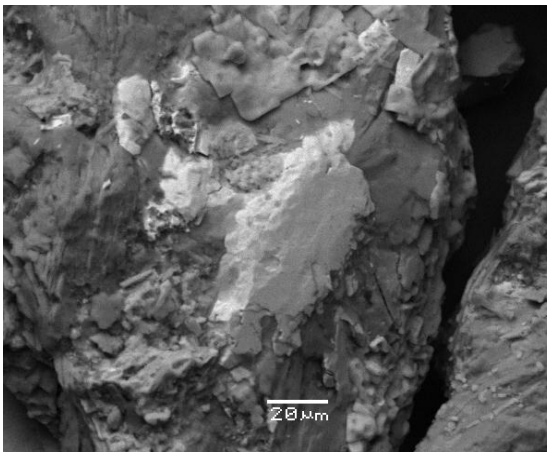

Figure 4.7. SEM microphotograph, showing details of sample KD-7.

Semi-quantitative microanalysis (a) (%) EDS:

SiO_2	*52.95*
Al_2O_3	*27.31*
K_2O	*11.69*
Fe_2O_3	*4.66*

Semi-quantitative microanalysis (b) (%) EDS:

Fe_2O_3	*98.35*

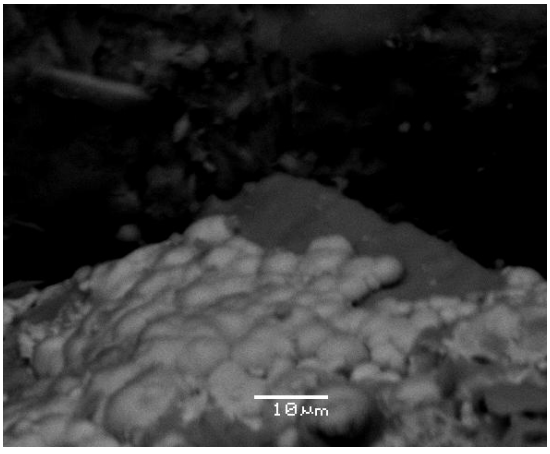

Figure 4.8. SEM microphotograph, showing details of sample KD-10.

Semi-quantitative microanalysis (a) (%) EDS:

SiO_2	*97.62*

Semi-quantitative microanalysis (b) (%) EDS:

Fe_2O_3	*89.77*
Cu2O	*0.88*

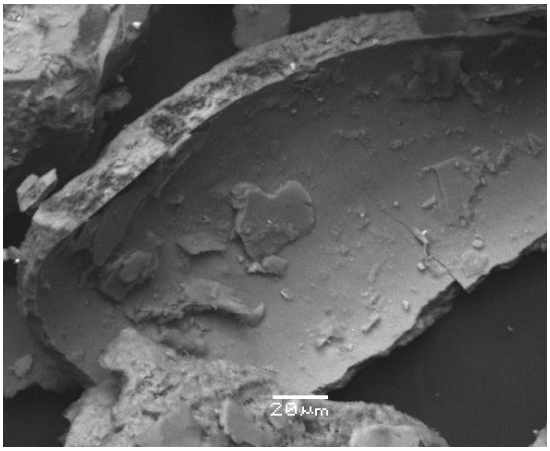

Figure 4.9. SEM microphotograph, showing details of sample KD-10.

Semi-quantitative microanalysis (%) EDS:

CaO	*54.22*

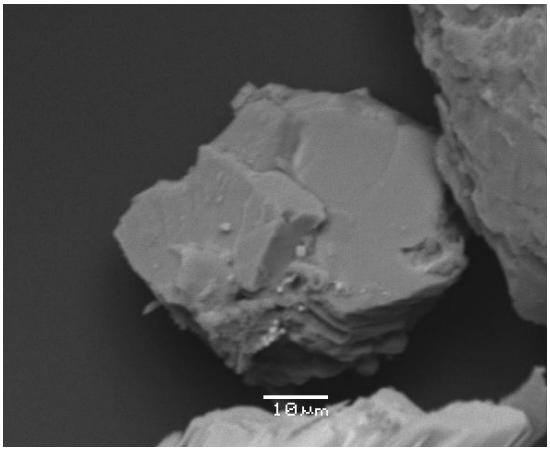

Figure 4.10. SEM microphotograph, showing details of sample KD-8.

Semi-quantitative microanalysis (%) EDS:

SiO_2	*29.57*
Al_2O_3	*11*
Fe_2O_3	*35.21*
CaO	*16*
Cu_2O	*3.5*
ZnO	*3.2*

4.5.2. SE Evia Island – Offshore Cores

Figure 4.11 (Evia Core KD-5, depth 5-7 cm) shows an illite grain, while figure 4.12 (Evia Core KD-5, depth 60-62 cm) and Figure 4.13 (Evia Core KD-18, depth 150-152 cm) show a Cu-Zn oxide grain. Figure 4.14 reveals a barite grain (Evia Core KD-18, depth 150-152 cm), while Figure 4.15 shows a Ce- Monazite grain (Evia Core KD-18, depth 80-82 cm).

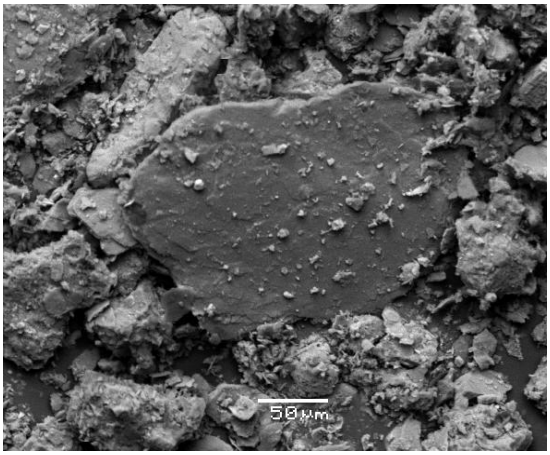

Figure 4.11. SEM microphotograph, showing details of sample Core KD-5, depth 5-7 cm.

Semi-quantitative microanalysis (%) EDS:

SiO_2	*56.39*
Al_2O_3	*25.19*
Fe_2O_3	*2.54*
K_2O	*11.84*
MgO	*2.89*

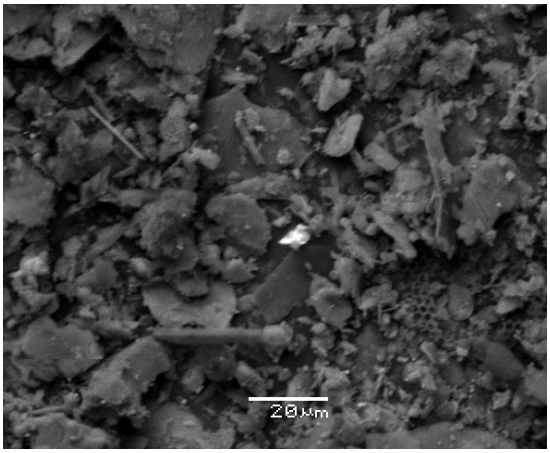

Figure 4.12. SEM microphotograph, showing details of sample Core KD-5, depth 60-62 cm.

Semi-quantitative microanalysis (%) EDS:

Cu_2O	*48.85*
ZnO	*34.28*

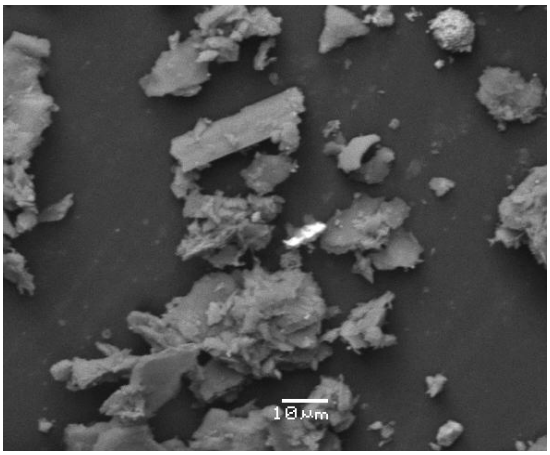

Figure 4.13. SEM microphotograph, showing details of sample Core KD-18, depth 150-152 cm.

Semi-quantitative microanalysis (%) EDS:

Cu_2O	*51.62*
ZnO	*43.66*

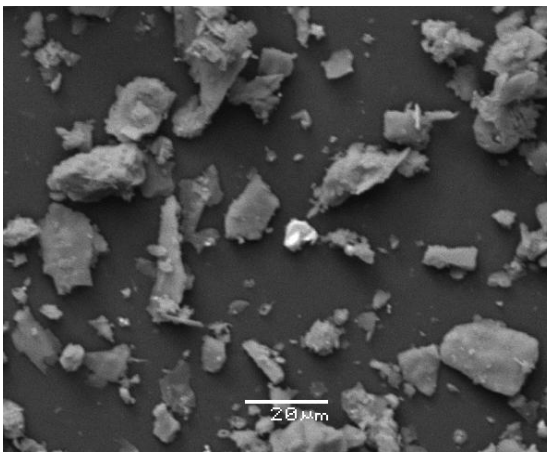

Figure 4.14. SEM microphotograph, showing details of sample Core KD-18, depth 150-152 cm.

Semi-quantitative microanalysis (%) EDS:

BaO	*59.80*
SO_4	*31.35*

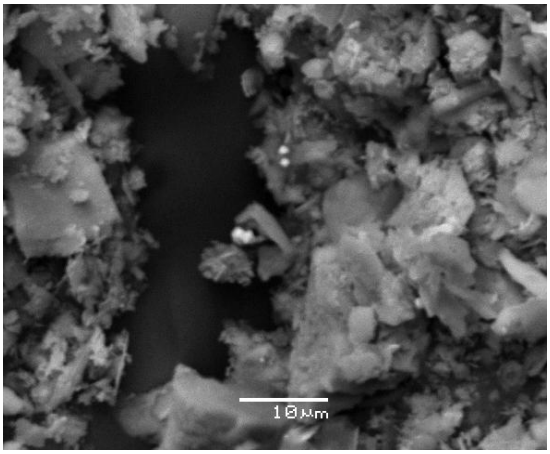

Figure 4.15. SEM microphotograph, showing details of sample Core KD-18, depth 80-82 cm.

Semi-quantitative microanalysis (%) EDS:

La_2O_3	*20.61*
Ce_2O_3	*45.15*
Pr_2O_3	*2.84*
ThO_2	*2.11*
Nd_2O_3	*15.27*
P_2O_5	*14.02*

4.5.3. NW Crete Island Samples Offshore Samples

Regarding samples from Kissamos Bay, NW Crete Island SEM-EDS analysis revealed the following. Figure 4.16 displays a slightly eroded quartz grain crystal in which the facets have been preserved. Also, Figure 4.17 displays a highly eroded quartz grain where no facets can be detected. Figure 4.18 shows Cu-Zn oxides (semi-quantitative microanalysis b) on a quartz grain (semi-quantitative microanalysis a). Figure 4.19 displays a clinochlore grain buried in smaller fragments. Regarding samples from Sfinari Bay, western Crete Island SEM-EDS revealed the following. Figure 4.20 display iron oxides (semi-quantitative microanalysis b) on a quartz grain (semi-quantitative microanalysis a). Figure 4.21 shows a calcite grain.

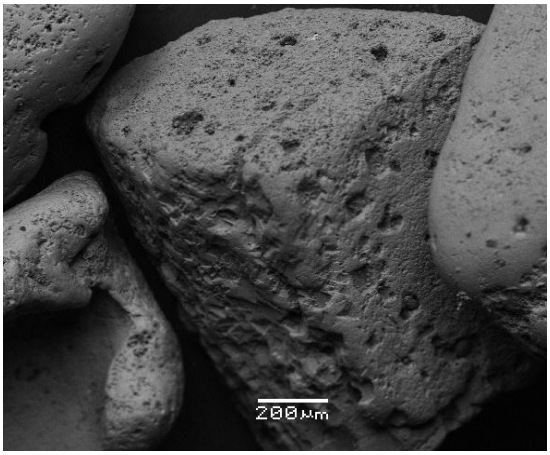

Figure 4.16. SEM microphotograph, showing details of sample KIS-1A.

Semi-quantitative microanalysis (%) EDS:

SiO_2	*99.35*

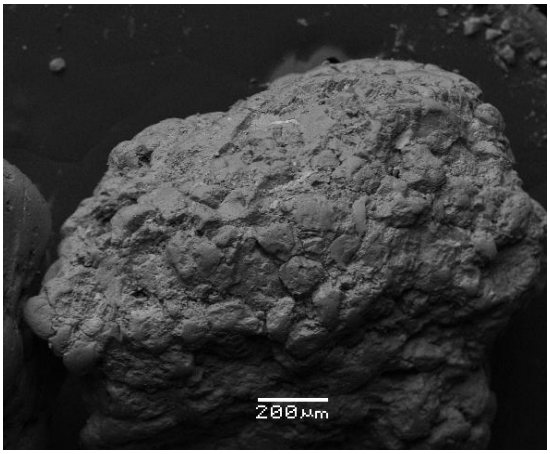

Figure 4.17. SEM microphotograph, showing details of sample KIS-1A.

Semi-quantitative microanalysis (%) EDS:

SiO_2	*97.35*

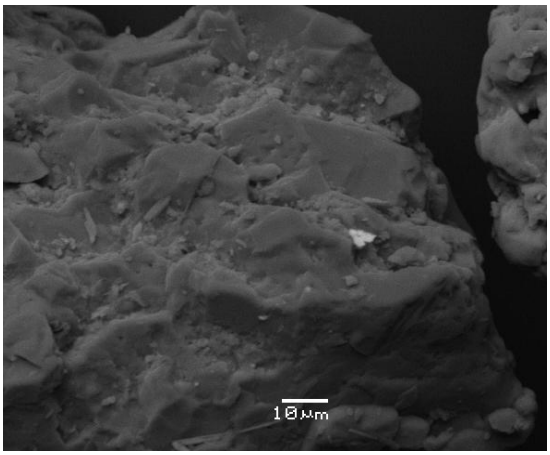

Figure 4.18. SEM microphotograph, showing details of sample KIS-3A.

Semi-quantitative microanalysis (a) (%) EDS:

SiO_2	*98.43*

Semi-quantitative microanalysis (b) (%) EDS:

Cu_2O	*56.16*
ZnO	*39.68*

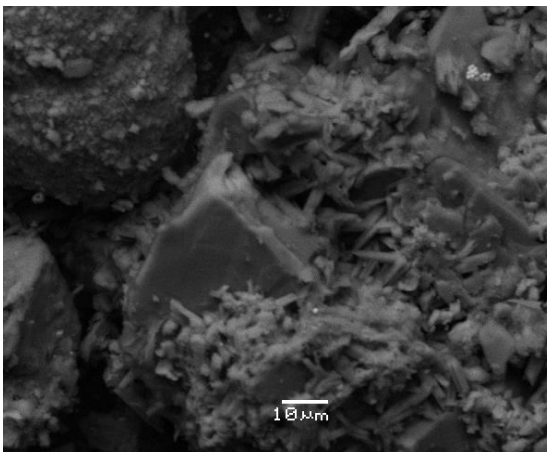

Figure 4.19. SEM microphotograph, showing details of sample KIS-3D.

Semi-quantitative microanalysis (%) EDS:

SiO_2	*26.78*
Al_2O_3	*22.37*
MgO	*12.75*
Fe_2O_3	*28.83*

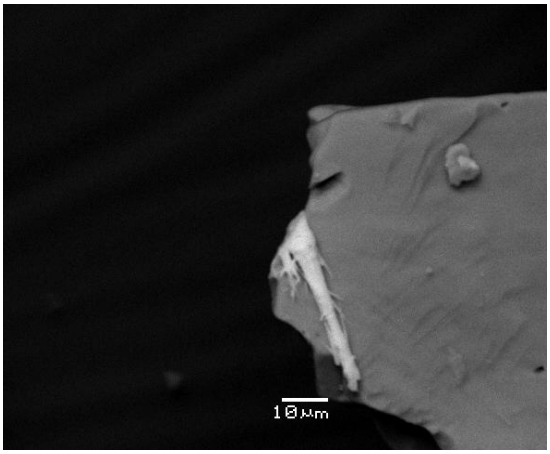

Figure 4.20. SEM microphotograph, showing details of sample SFI-1.

Semi-quantitative microanalysis (a) (%) EDS:

SiO_2	*99.34*

Semi-quantitative microanalysis (b) (%) EDS:

Fe_2O_3	*96.78*

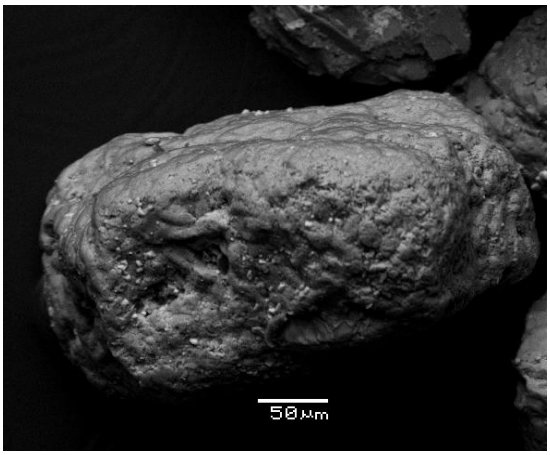

Figure 4.21. SEM microphotograph, showing details of sample SFI-1.

Semi-quantitative microanalysis (%) EDS:

CaO	*55.23*

4.5.4. Southern and Eastern Lesvos Island Offshore Samples

Figure 4.22 involves a grain of biotite mica observed in sample L-E1, while Figure 2.23 shows Pb-oxides (white spot; semi-quantitative microanalysis b) on a grain of eroded albite (semi-quantitative microanalysis a). Figure 4.24 displays a highly eroded calcite grain and Figure 4.25 a zircon grain. Regarding samples from Mytilene Strait, Figure 4.26 reveals a small grain of iron oxides, while Figure 4.27 shows a general image of sample L-S24.

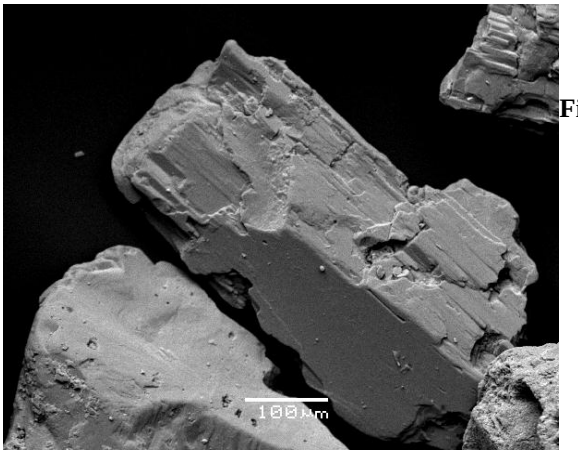

Figure 4.22. SEM microphotograph, showing details of sample L-E1.

Semi-quantitative microanalysis (%) EDS:

SiO_2	*50.93*
Al_2O_3	*14.25*
MgO	*11.20*
Fe_2O_3	*8.96*
K_2O	*14.66*

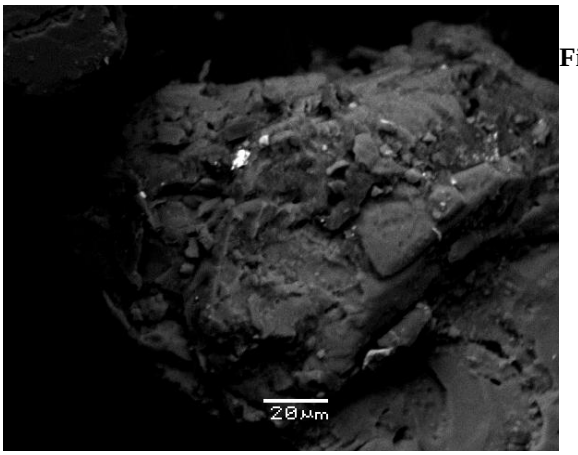

Figure 4.23. SEM microphotograph, showing details of sample L-E1.

Semi-quantitative microanalysis (a) (%) EDS:

SiO_2	*58.44*
Al_2O_3	*19.43*
Na_2O	*4.77*
CaO	*17.36*

Semi-quantitative microanalysis (b) (%) EDS:

PbO	*85.45*

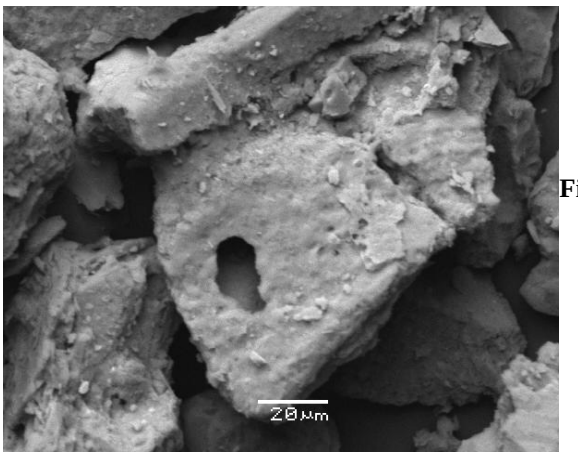

Figure 4.24. SEM microphotograph, showing details of sample L-V12.

Semi-quantitative microanalysis (%) EDS:

CaO	*55.89*

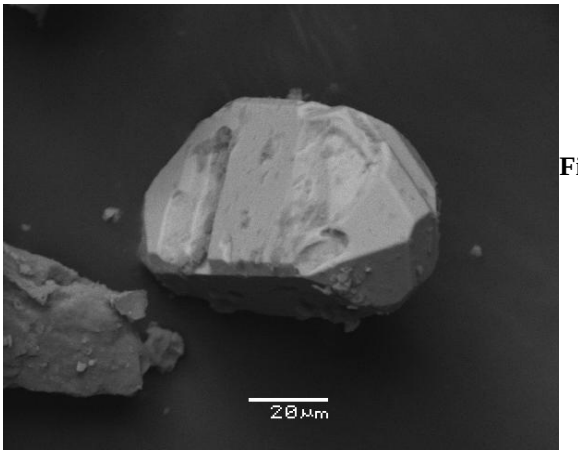

Figure 4.25. SEM microphotograph, showing details of sample L-V12.

Semi-quantitative microanalysis (%) EDS:

SiO_2	*32.65*
ZrO_2	*59.56*

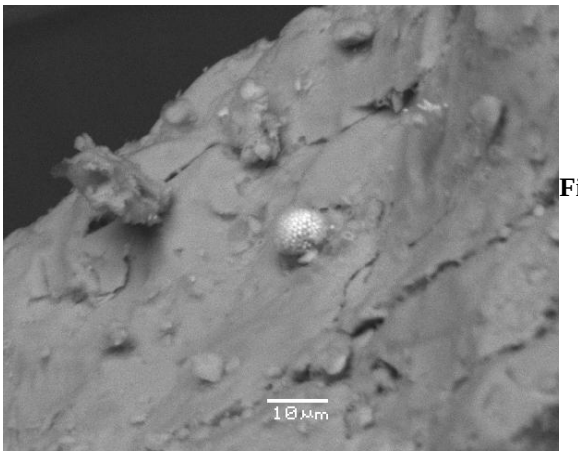

Figure 4.26. SEM microphotograph, showing details of sample L-E24.

Semi-quantitative microanalysis (a) (%) EDS:

Fe_2O_3	*97.62*

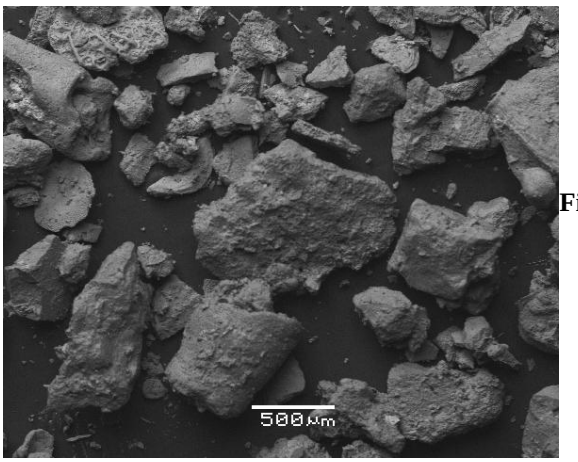

Figure 4.27. SEM microphotograph, showing details of sample L-S24.

4.5.5. NE Rhodes Island Offshore Samples

Regarding Afantou Bay samples, SE Rhodes Island Figures 4.28 - 29 reveal a general aspect of the samples and Figure 4.30 shows a calcite grain.

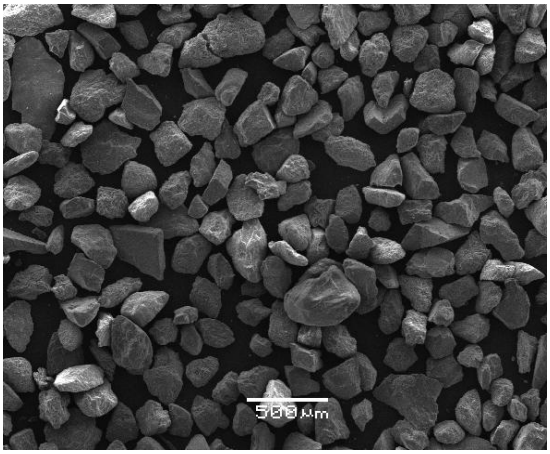

Figure 4.28. SEM microphotograph, showing details of sample AFA-3A.

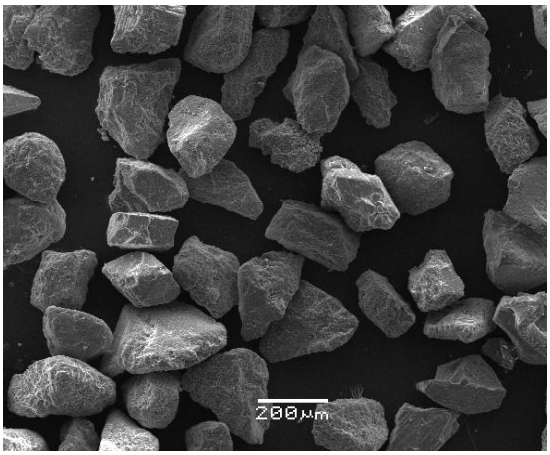

Figure 4.29. SEM microphotograph, showing details of sample AFA-3A.

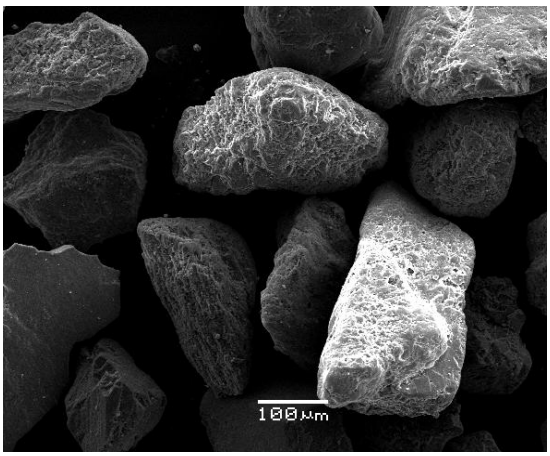

Figure 4.30. SEM microphotograph, showing details of sample AFA-3A.

Semi-quantitative microanalysis (%) EDS:

CaO	*53.69*

4.5.6. Industrial Samples

Figure 4.31 displays a general view of Aliartos-1 sample; Figure 4.32 shows an eroded grain of quartz and Figure 4.33 reveals a rounded calcite grain. Figure 4.34 reveals a general aspect of Boscombe-Coastline sample; Figure 4.35 iron oxides on an albite grain and Figure 4.36 a grain of quartz. Figure 4.37 shows a general aspect of Strymonas-1 sample;

Figure 4.38 a zircon grain and Figure 4.39 a Ce-monazite outcrop. Figure 4.40 shows a general aspect of samples from Nairobi sand. Figure 4.41 displays a part of a typical quartz grain from Nairobi sand, while Figure 4.42 shows a rounded zircon crystal. Regarding artificial industrial mixtures, Figure 4.43 shows a general view from KIS-washed sample and Figure 4.44 a calcite grain. Figure 4.45 displays a general aspect of KIS sample and Figure 4.46 shows a calcite grain involving salts (lower part of the grain). Figure 4.47 reveals a general aspect of EV-W-washed sample; Figure 4.48 shows a grain of edenite amphibole and Figure 4.50 reveals a residual Cu-Zn grain. Figure 4.51 shows a general aspect of EV-W sample showing angular grains; Figure 4.52 reveals a Ti-magnetite grain and 4.53 shows a a quartz grain with conchoidal fracture.

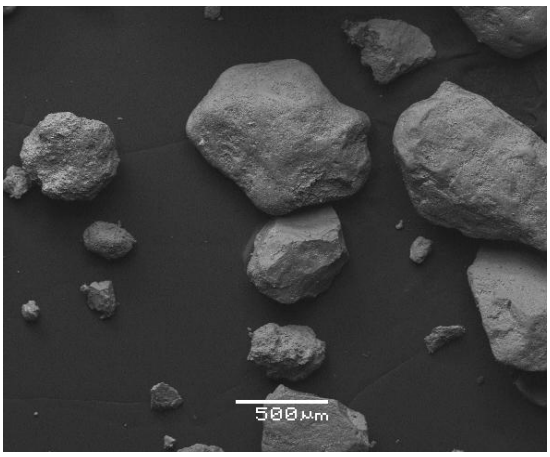

Figure 4.31. SEM microphotograph, showing details of sample Aliartos-1.

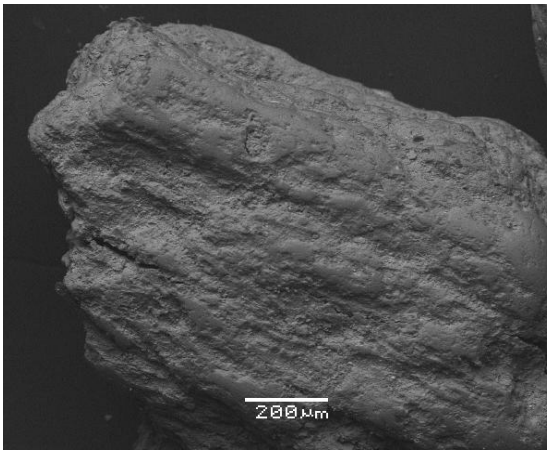

Figure 4.32. SEM microphotograph, showing details of sample Aliartos-1.

Semi-quantitative microanalysis (%) EDS:

SiO_2	*98.29*

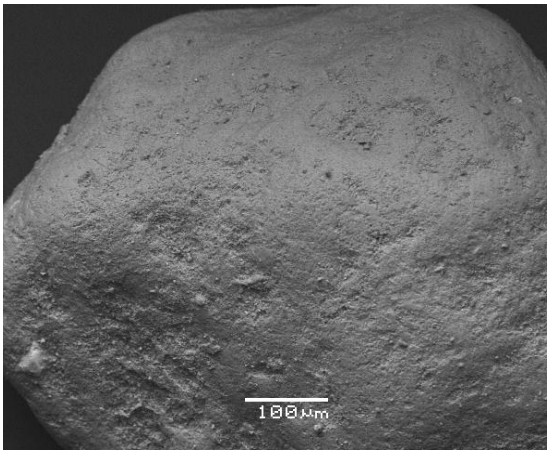

Figure 4.33. SEM microphotograph, showing details of sample Aliartos-1.

Semi-quantitative microanalysis (%) EDS:

CaO	*51.53*

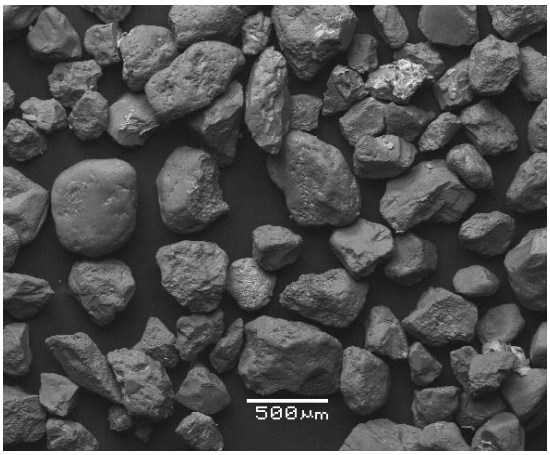

Figure 4.34. SEM microphotograph, showing details of sample Boscombe-Coastline.

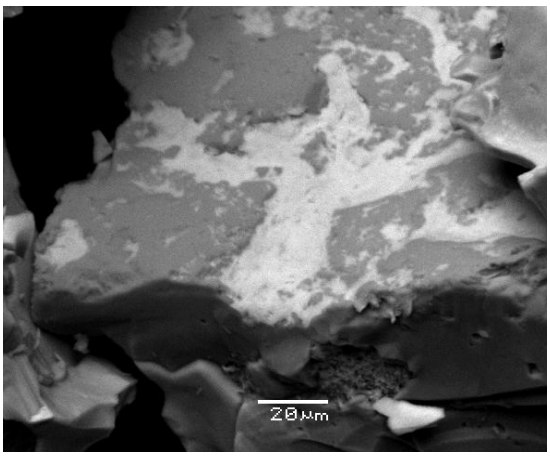

Figure 4.35. SEM microphotograph, showing details of sample Boscombe-Coastline.

Semi-quantitative microanalysis (a) (%) EDS:

Fe_2O_3	*96.82*

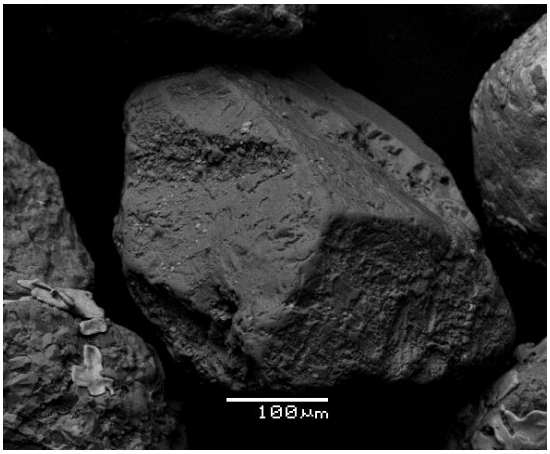

Figure 4.36. SEM microphotograph, showing details of sample Boscombe-Coastline.

Semi-quantitative microanalysis (%) EDS:

SiO_2	*98.12*

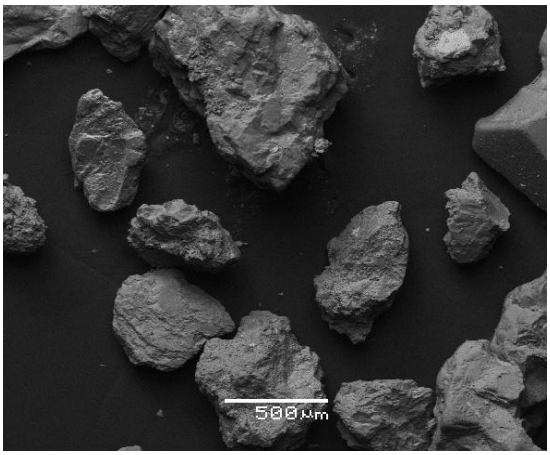

Figure 4.37. SEM microphotograph, showing details of sample Strymonas-1.

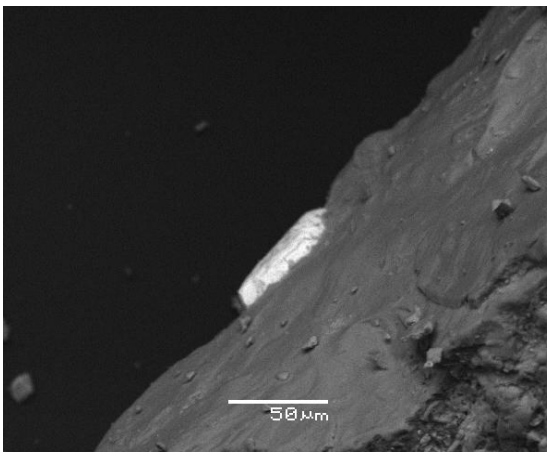

Figure 4.38. SEM microphotograph, showing details of sample Strymonas-1.

Semi-quantitative microanalysis (%) EDS:

SiO_2	*30.79*
ZrO_2	*64.31*

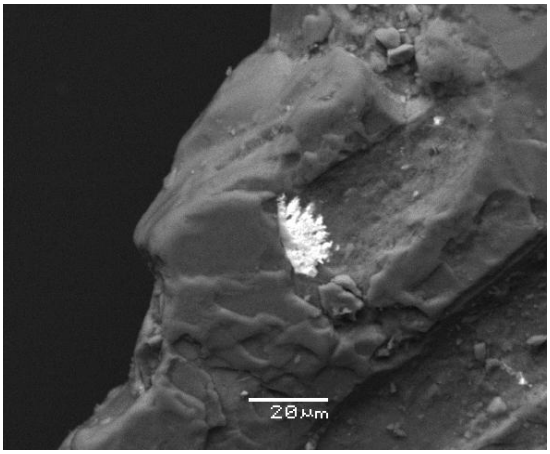

Figure 4.39. SEM microphotograph, showing details of sample Strymonas-1.

Semi-quantitative microanalysis (%) EDS:

La_2O_3	*4.15*
CeO_2	*23.81*
ThO_2	*15.96*
Nd_2O_3	*15.23*
P_2O_5	*40.84*

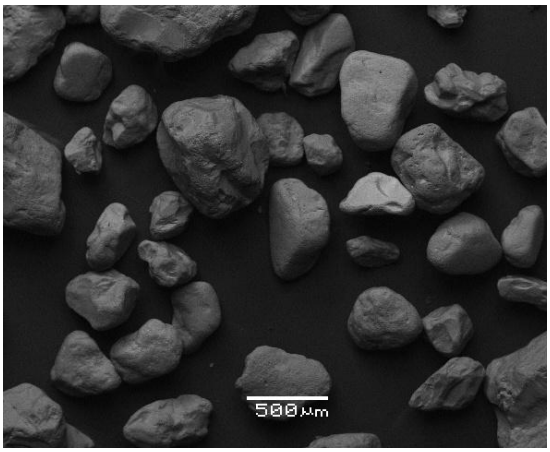

Figure 4.40. SEM microphotograph, showing details of sample Nairobi.

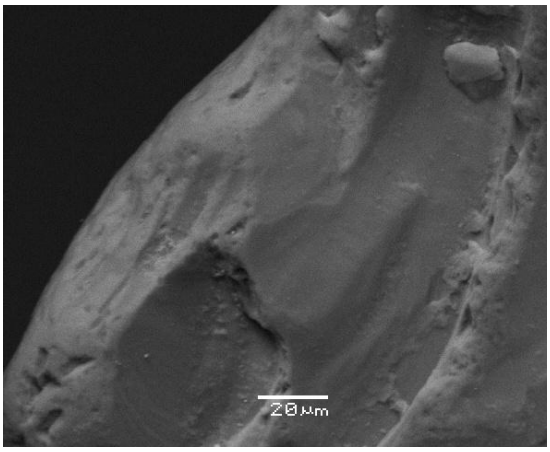

Figure 4.41. SEM microphotograph, showing details of sample Nairobi.

Semi-quantitative microanalysis (%) EDS:

SiO_2	*99.87*

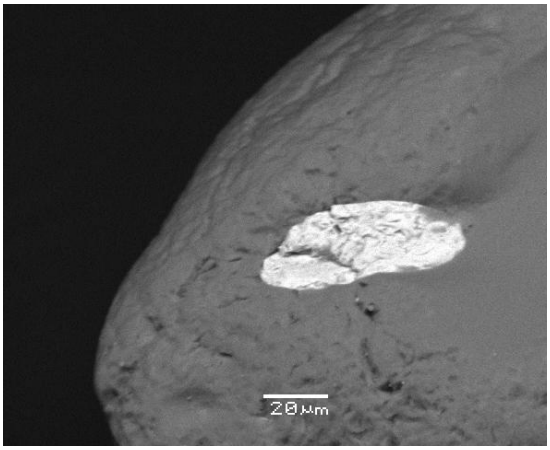

Figure 4.42. SEM microphotograph, showing details of sample Nairobi.

Semi-quantitative microanalysis (%) EDS:

SiO_2	*31.53*
ZrO_2	*64.73*

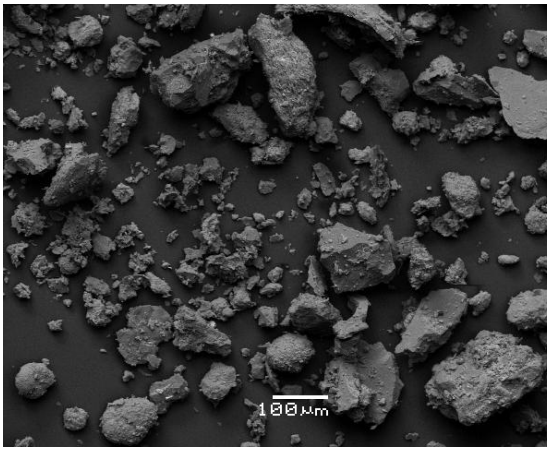

Figure 4.43. SEM microphotograph, showing details of sample KIS-washed.

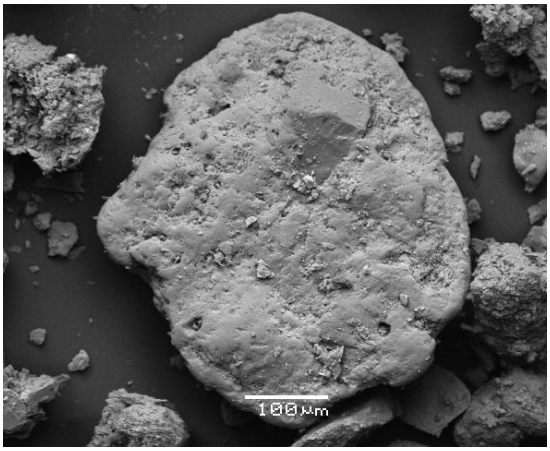

Figure 4.44. SEM microphotograph, showing details of sample KIS-washed.

Semi-quantitative microanalysis (%) EDS:

CaO	*52.74*

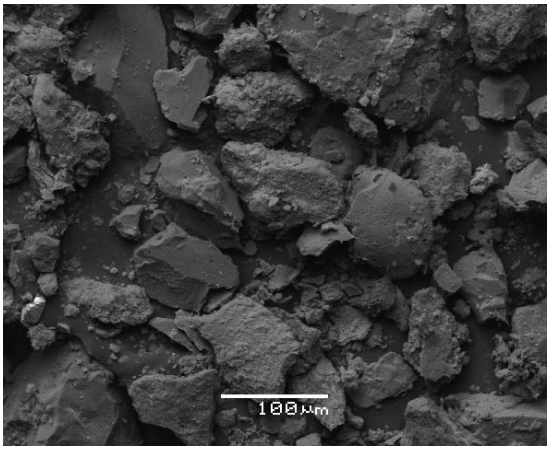

Figure 4.45. SEM microphotograph, showing details of sample KIS.

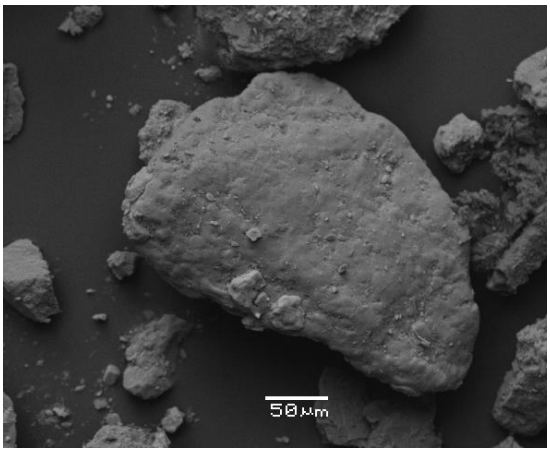

Figure 4.46. SEM microphotograph, showing details of sample KIS.

Semi-quantitative microanalysis (%) EDS:

CaO	*56.44*

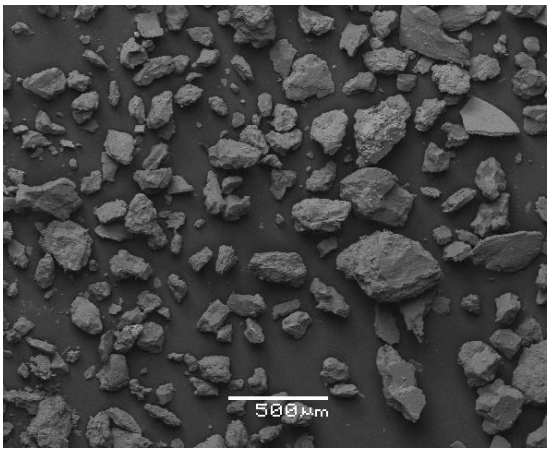

Figure 4.47. SEM microphotograph, showing details of sample EV-W-washed.

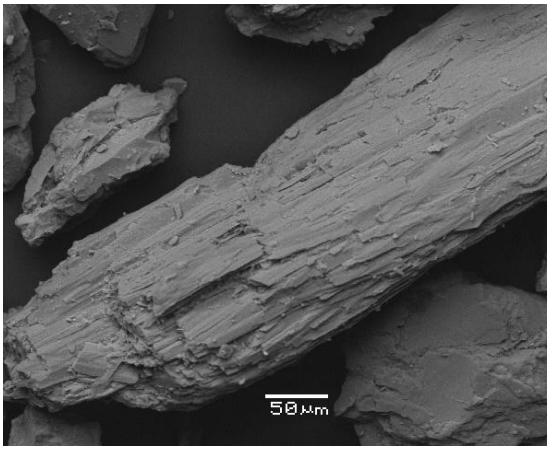

Figure 4.48. SEM microphotograph, showing details of sample EV-W-washed.

Semi-quantitative microanalysis (%) EDS:

SiO_2	*59.09*
Al_2O_3	*2.16*
MgO	*21.76*
CaO	*15.37*

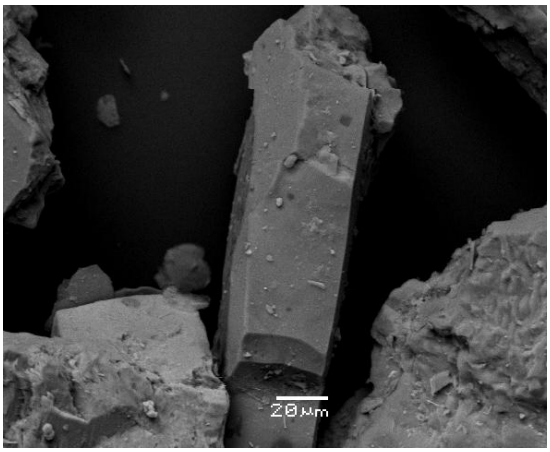

Figure 4.49. SEM microphotograph, showing details of sample EV-W-washed.

Semi-quantitative microanalysis (%) EDS:

SiO_2	*99.2*

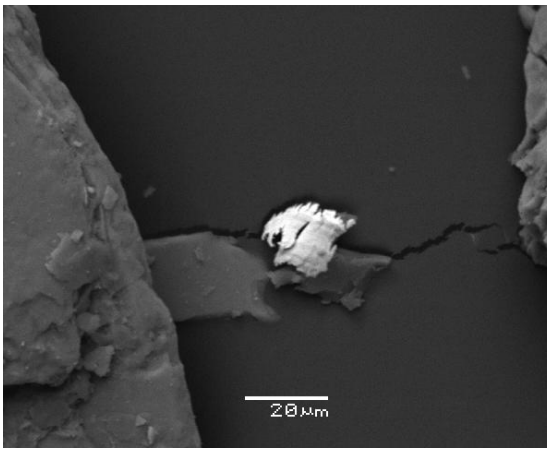

Figure 4.50. SEM microphotograph, showing details of sample EV-W-washed.

Semi-quantitative microanalysis (%) EDS:

Cu_2O	*59.84*
ZnO	*41.74*

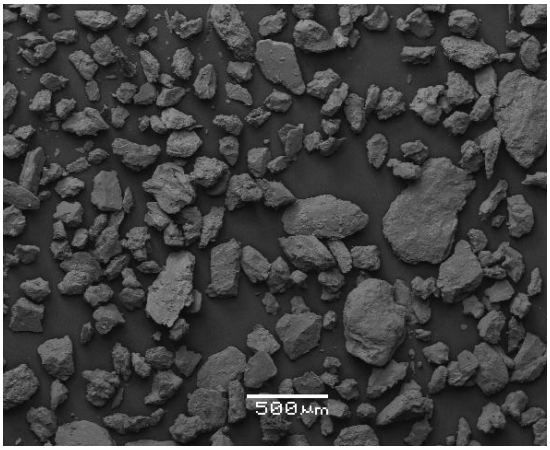

Figure 4.51. SEM microphotograph, showing details of sample EV-W.

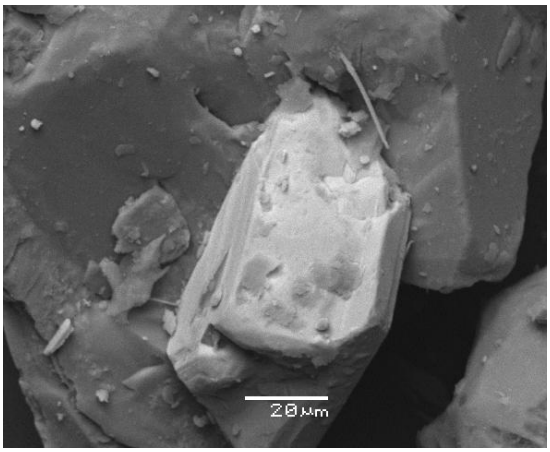

Figure 4.52. SEM microphotograph, showing details of sample EV-W.

Semi-quantitative microanalysis (%) EDS:

Fe_2O_3	*92.02*
TiO_2	*7.9*

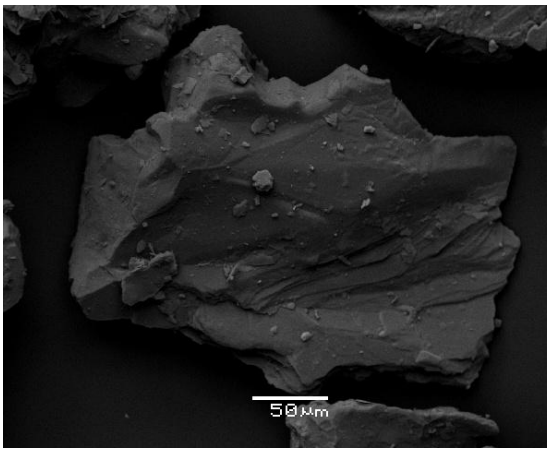

Figure 4.53. SEM microphotograph, showing details of sample EV-W.

Semi-quantitative microanalysis (%) EDS:

SiO_2	*99.09*

4.6. DETERMINATION OF CALCIUM CARBONATES

Calcium carbonate content was determined for selected samples. Specifically, $CaCO_3$ content (%) was determined for SE Evia Island cores and offshore samples from Lesvos Island. The results of the determination of calcium carbonates content are presented in the Tables 4.19 - 20.

Table 4.19. Calcium Carbonates content (%) of SE Evia Island core samples.

CORE N^{o}	Core's Depth	$CaCO_3$ %	CORE N^{o}	Core's Depth	$CaCO_3$ %
KD-18	*0-2*	6.40	**KD-4**	*40-42*	8.49
KD-18	*5-7*	7.18	**KD-4**	*50-52*	7.99
KD-18	*10-12*	9.20	**KD-4**	*60-62*	6.60
KD-18	*15-17*	9.41	**KD-4**	*70-72*	3.44
KD-18	*20-22*	8.93	**KD-4**	*80-82*	7.07
KD-18	*30-32*	9.17	**KD-4**	*90-92*	8.67
KD-18	*40-42*	7.00	**KD-4**	*100-102*	9.46
KD-18	*50-52*	5.85	**KD-4**	*110-112*	9.26
KD-18	*53-55*	7.65	**KD-4**	*117-119*	8.22
KD-18	*60-62*	9.41	**KD-5**	*0-2*	9.06
KD-18	*70-72*	11.40	**KD-5**	*5-7*	9.58
KD-18	*80-82*	10.83	**KD-5**	*10-12*	10.85
KD-18	*90-93*	8.37	**KD-5**	*20-22*	9.44
KD-18	*100-102*	10.23	**KD-5**	*30-32*	6.59
KD-18	*110-112*	10.78	**KD-5**	*40-42*	7.22
KD-18	*120-122*	10.78	**KD-5**	*50-52*	9.29
KD-18	*130-132*	11.45	**KD-5**	*60-62*	11.28
KD-18	*137-139*	8.67	**KD-5**	*70-72*	9.78
KD-18	*140-142*	8.29	**KD-5**	*80-82*	9.51
KD-18	*150-152*	7.91	**KD-5**	*90-92*	8.40
KD-18	*160-162*	6.95	**KD-5**	*100-102*	8.07
KD-18	*170-174*	7.45	**KD-5**	*110-112*	9.46
KD-18	*180-182*	7.90	**KD-5**	*120-122*	9.63
KD-18	*190-192*	7.76	**KD-5**	*130-132*	10.19
KD-18	*200-202*	6.12	**KD-5**	*140-142*	9.97
KD-18	*207-209*	6.47	**KD-5**	*150-152*	10.55
KD-4	*0-2*	7.06	**KD-5**	*160-162*	10.49
KD-4	*5-7*	6.92	**KD-5**	*170-172*	10.02
KD-4	*10-12*	6.92	**KD-5**	*180-182*	10.21
KD-4	*20-22*	8.00	**KD-5**	*190-192*	8.04
KD-4	*30-32*	8.94			

The average calcium carbonate content (%) of core KD-5 is higher than that of the other two cores. Core KD-4 displays the lowest $CaCO_3$ content (%).

Table 4.20. Calcium Carbonates content (%) of southern and eastern Lesvos Island surficial samples.

SAMPLE	$CaCO_3$ %	SAMPLE	$CaCO_3$ %
L-E1	0.24	**L-S3**	20.34
L-E2	2.21	**L-S4**	16.92
L-E3	0.87	**L-S7**	16.02
L-E4	0.28	**L-S9**	34.25
L-E5	0.39	**L-S11**	38.21
L-E6	0.75	**L-S12**	21.04
L-E7	2.96	**L-S16**	14.71
L-E8	0.50	**L-S17**	20.15
L-E9	0.62	**L-S18**	19.61
L-V1	4.01	**L-S19**	14.71
L-V2	2.97	**L-S22**	18.81
L-V3	8.73	**L-S24**	16.90
L-V4	5.27	**L-S25**	15.90
L-V5	6.57	**L-S26**	35.51
L-V7	8.18	**L-S28**	20.59
L-V8	11.43	**L-S29**	19.98
L-V9	6.65	**L-S32**	26.17
L-V10	4.60		
L-V11	4.36		
L-V12	5.50		

The $CaCO_3$ content (%) of Eresos's samples is very low (0.24-2.96%), calcium carbonate values of samples from Vatera area are quite higher (~4-11%) and these from Mytilene Strait are high, ranging from ~15 % to ~38%.

4.7. DETERMINATION OF CHLORIDES

One of the most important parameters for the industrial utilization of Marine Aggregates as raw material for the production of building materials is their chlorine content. On the contrary, the issue of the chlorine content regarding the utilization of Marine Aggregates in beach replenishment and nourishment projects does not exist. The chlorine content determination of leaching is presented in Table 4.21 and Figure 4.54.

Table 4.21. Successive leaching for chlorine determination.

SAMPLES	Initial average Cl from XRF analysis (ppm)	1st Leaching (ppm)	2nd Leaching (ppm)	3rd Leaching (ppm)	4th Leaching (ppm)
Kissamos, Crete Isl.	3300	2204	660	136	33
Afantou, Rhodes Isl.	2700	1533	340	65	27
SE Evia Isl.	1700	1288	200	68	7

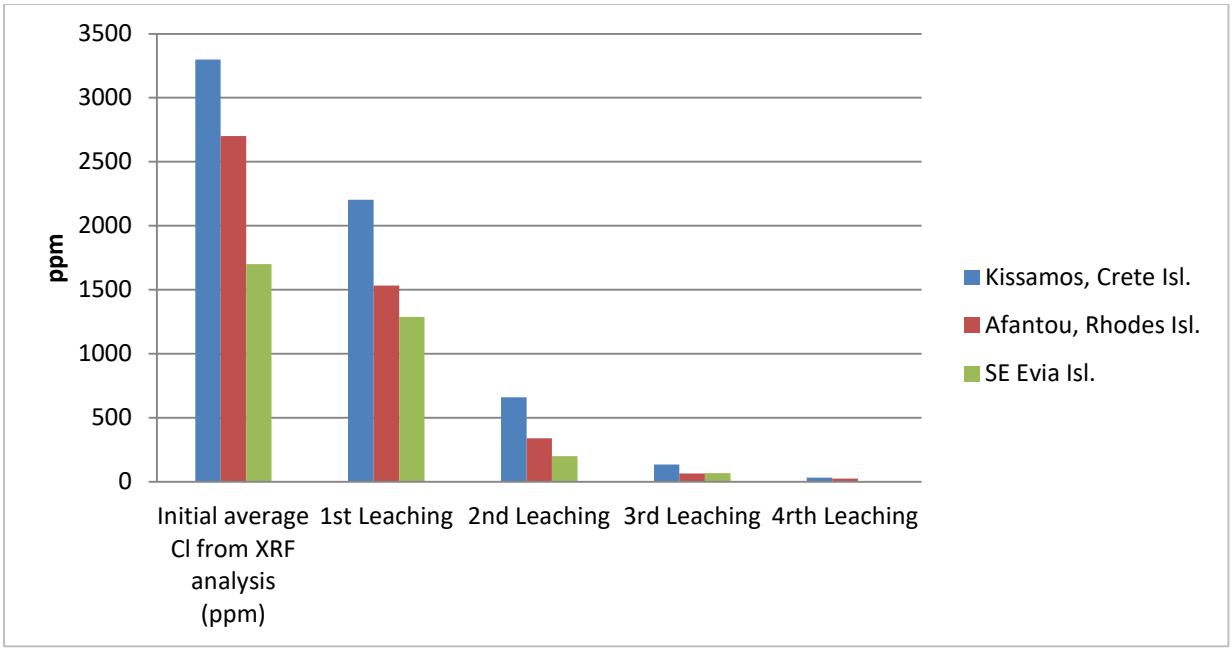

Figure 4.54. Graphic illustration of chlorine content in successive leachings.

Sample from SE Evia Island retains less chlorine than the other samples, as shown from the initial chlorine values. Moreover, after the fourth leaching, chlorine content approached zero values.

4.8. CHEMICAL ANALYSIS

The geochemical analysis of the offshore sediment samples, the offshore cores, the coastal and industrial samples includes both qualitative and quantitative identification of major and trace elements. Foremost, the study of major elements provides information regarding the general chemical composition of the samples. However, the study of trace element gives information about the physicochemical conditions in the environment of deposition, the origin of the sediments (primary sources), the sediments' pathways form the source to the current depositional environment and the possible impacts from anthropogenic activities.

The full database of the results of major and trace elements are listed in the ANNEX III. The following figures display the most siginificant variations and contents of major and trace elements per area.

4.8.1. SE Evia Island – Offshore Samples

Major Elements

In Figure 4.55, SiO_2 content varies from ~60% to ~86%, while CaO content varies from 1.5% to 15%. Samples with low SiO_2 values have high CaO values and vice versa.

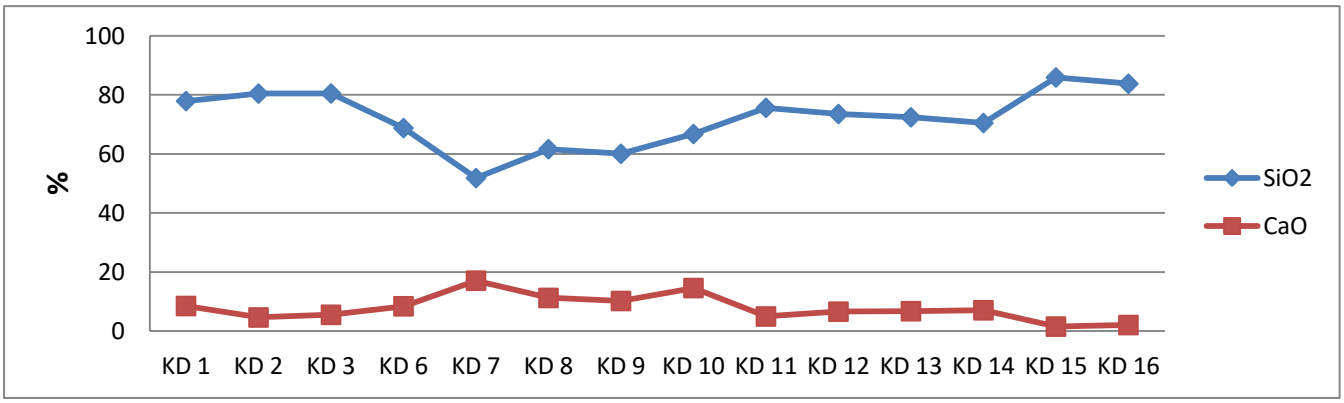

Figure 4. 55. Graphical illustration of the major components SiO_2 and CaO from SE Evia Island offshore samples.

In Figure 4.56, Al_2O_3 content varies significantly from almost zero to ~7%. Fe_2O_3 displays values from 1.22% to 3.82%. Na_2O and K_2O values are at low levels ~0-2.5%.

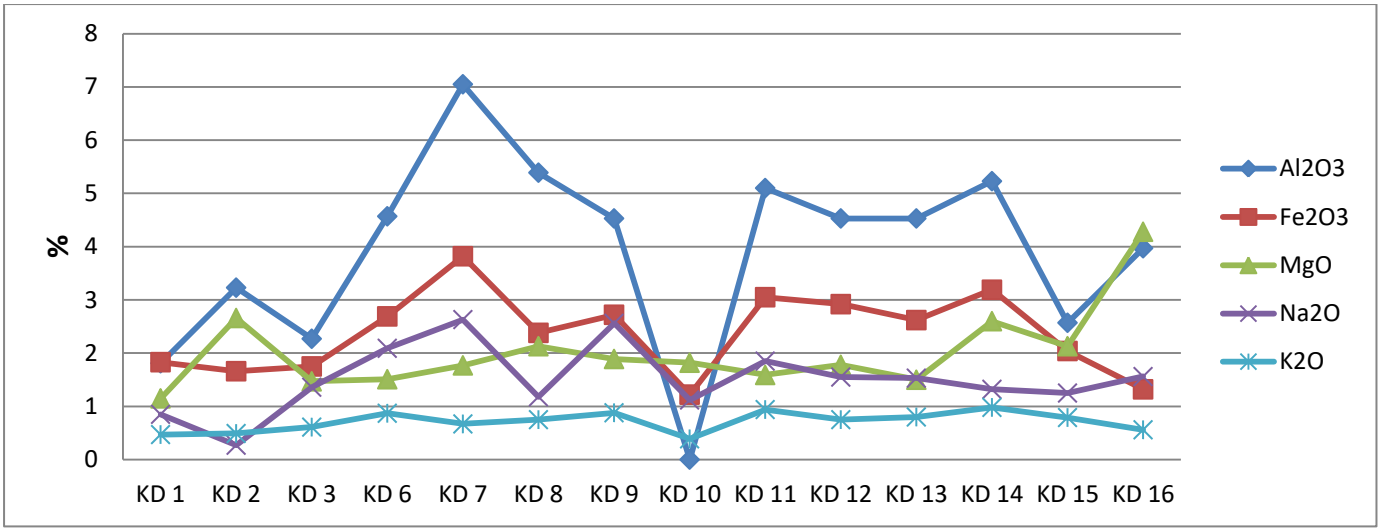

Figure 4.56. Graphical illustration of the major components Al_2O_3, Fe_2O_3, MgO, Na_2O and K_2O from SE Evia Island offshore samples.

Trace Elements

In Figure 4.57, Ba and Br have the matching variations; however Ba values are significant higher than Br. Relevant variations apply for Zn and Zr. Ce displays a different pattern.

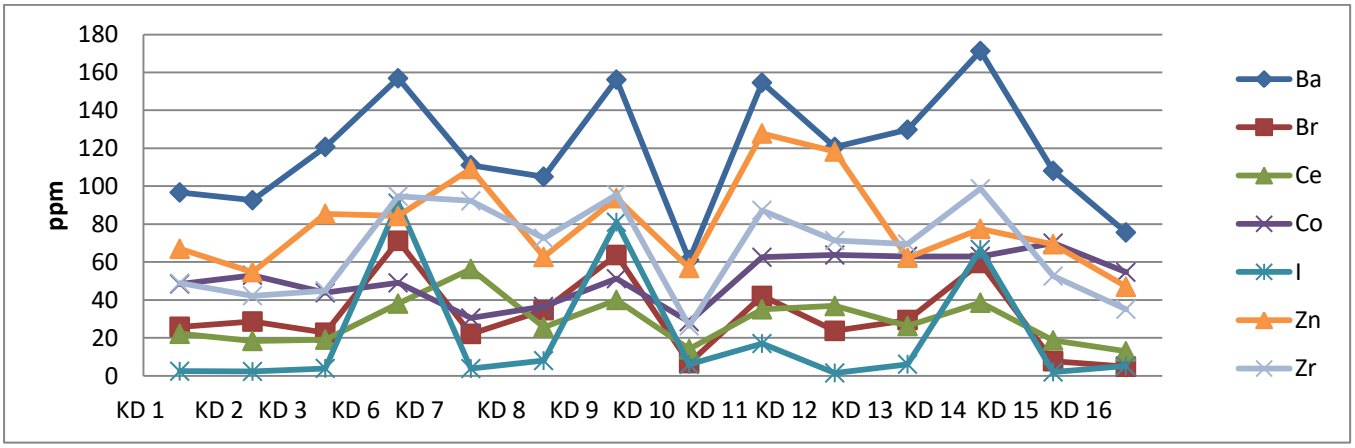

Figure 4.57. Graphical illustration of the trace elements Ba, Br, Ce, Co, I, Zn and Zr from SE Evia Island offshore samples.

In Figure 4.58, Cr, Ni and Cu display a similar pattern; Sr shows higher values in samples KD7-11 and Cl values range from 1200-1900 ppm.

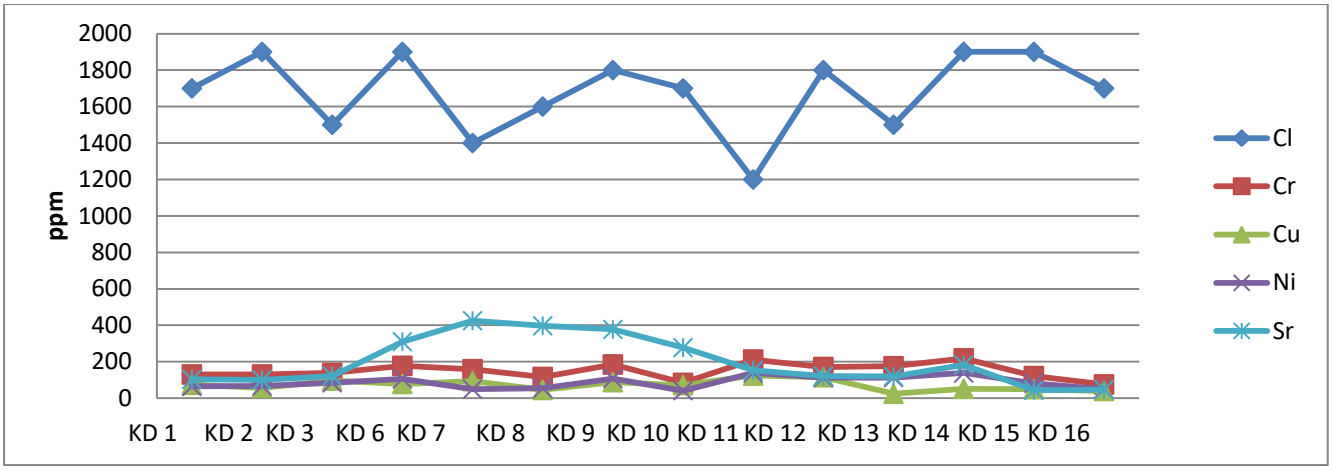

Figure 4.58. Graphical illustration of the trace elements Cl, Cr, Cu, Ni and Sr from SE Evia Island offshore samples.

4.8.2. SE Evia Island – Offshore Cores

Major Elements

In Figure 4.59, SiO_2 content varies from ~35% to ~43%, while CaO content varies from 9% to 16.5%. Samples with low SiO_2 values have high CaO values and vice versa. Fe_2O_3 and MgO follow the same pattern and range from ~4.5% to ~7.5%.

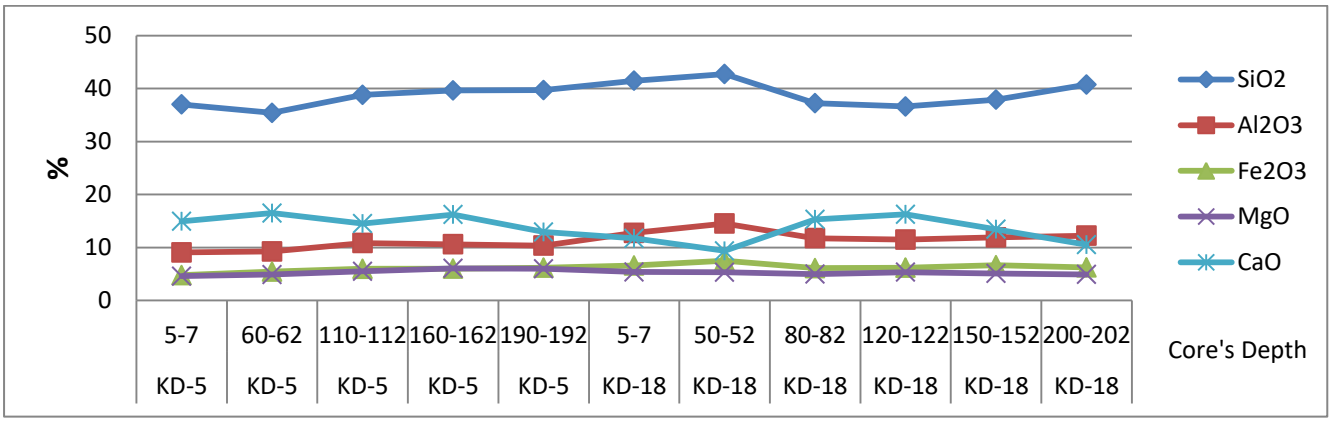

Figure 4.59. Graphical illustration of the major components SiO_2, Al_2O_3, Fe_2O_3, MgO and CaO from SE Evia Island core samples.

In Figure 4.60, TiO_2 values are low in all samples. Na_2O and K_2O display the same pattern and have values <3%. SO_3 display values <1%, apart from samples KD-5, 60-62 cm depth and KD-18, 150-152 cm depth, which are slightly higher at 1.27% and 1.12%, respectively.

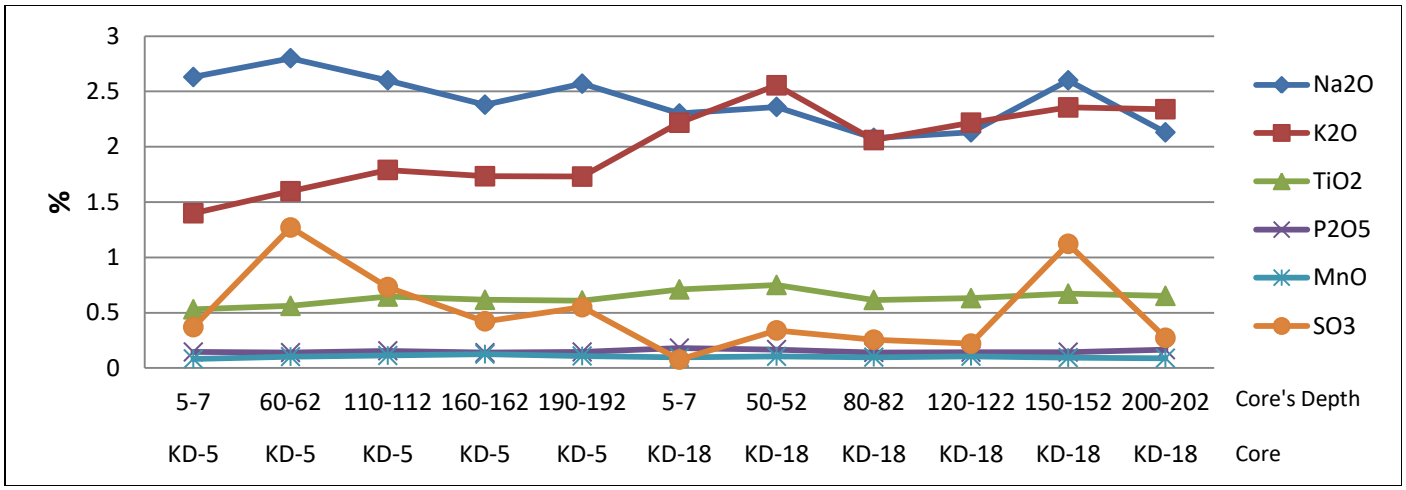

Figure 4.60. Graphical illustration of the major components Na_2O, K_2O, TiO_2 and SO_3 from SE Evia Island core samples.

Trace Elements

In Figure 4.61, Sr, Cr, and Ba values range from ~160-490ppm; while Mn values display higher values from 639 ppm to 969 ppm. Rb values are relatively low (<100 ppm) apart from sample KD-18, 150-152 cm core depth where Rb reaches 3242 ppm.

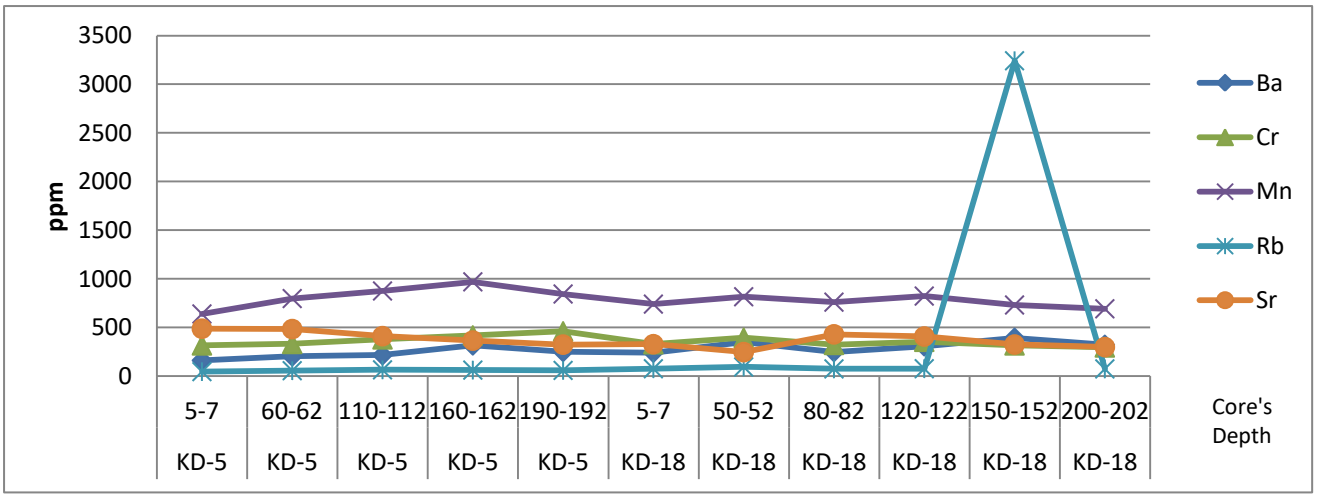

Figure 4.61. Graphical illustration of the trace elements Ba, Cr, Mn, Rb and Sr from SE Evia Island core samples.

In Figure 4.62, Cu, Co and V display the same pattern, however in different value' ranges, ~27-63 ppm, 74-101 ppm and 114-181 ppm, respectively. Moreover, V is slightly

enriched in samples from core KD-18. Sample KD-18, 50-52 cm core depth, seems to be relatively enriched in all elements.

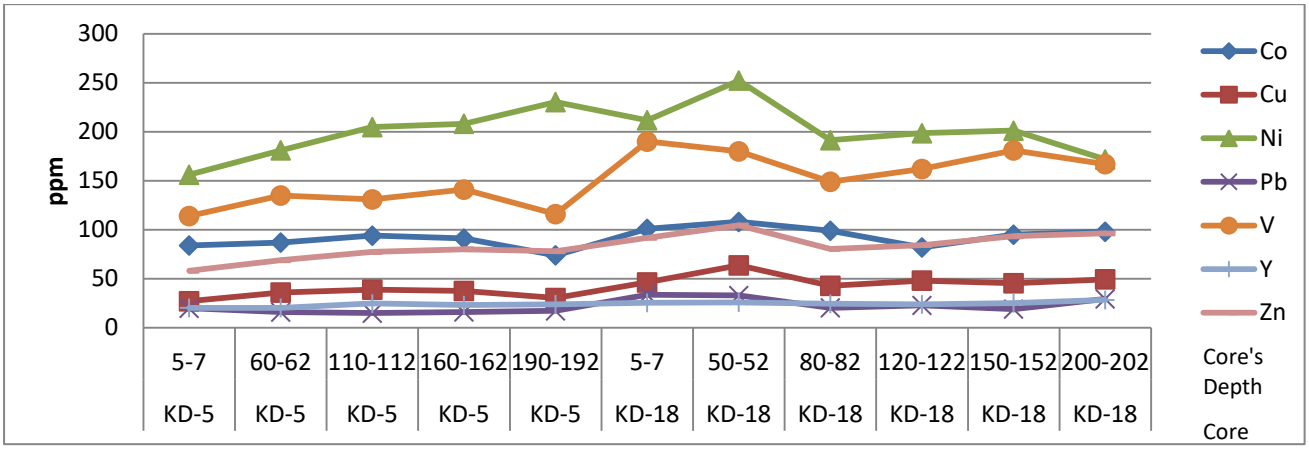

Figure 4.62. Graphical illustration of the trace elements Co, Cu, Ni, Pb, V, Y and Zn from SE Evia Island core samples.

4.8.3. NW Crete Island Offshore Samples

Major Elements

In Figure 4.63, SiO_2 and CaO have inverse patterns. SiO_2 content varies from ~30% to ~82%, while CaO content varies from ~6.5% to ~32%.

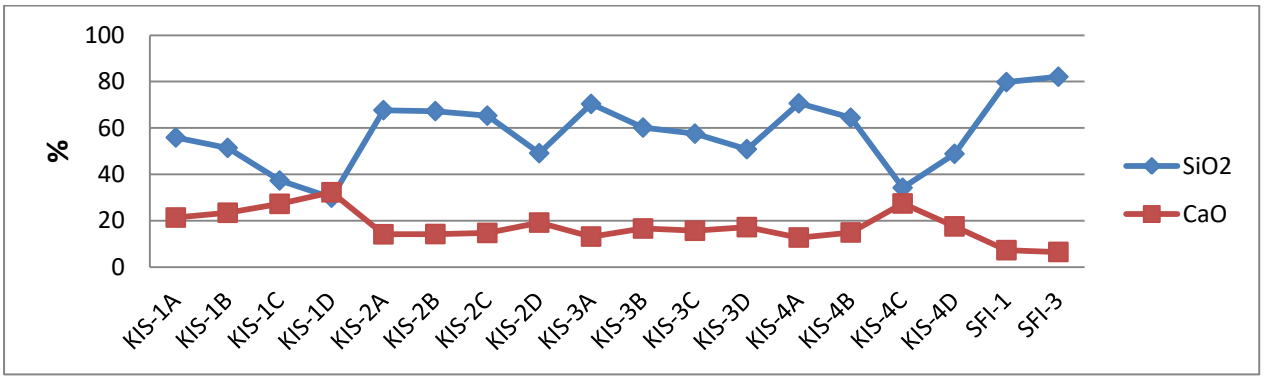

Figure 4.63. Graphical illustration of the major components SiO_2 and CaO from NW Crete Island offshore samples.

In Figure 4.64, Al_2O_3 content in SFI samples is lower than KIS samples. SO_3 content is <1% apart from samples KIS-4C (1.17%). Fe_2O_3 content varies from 0.62% to 2.46%.

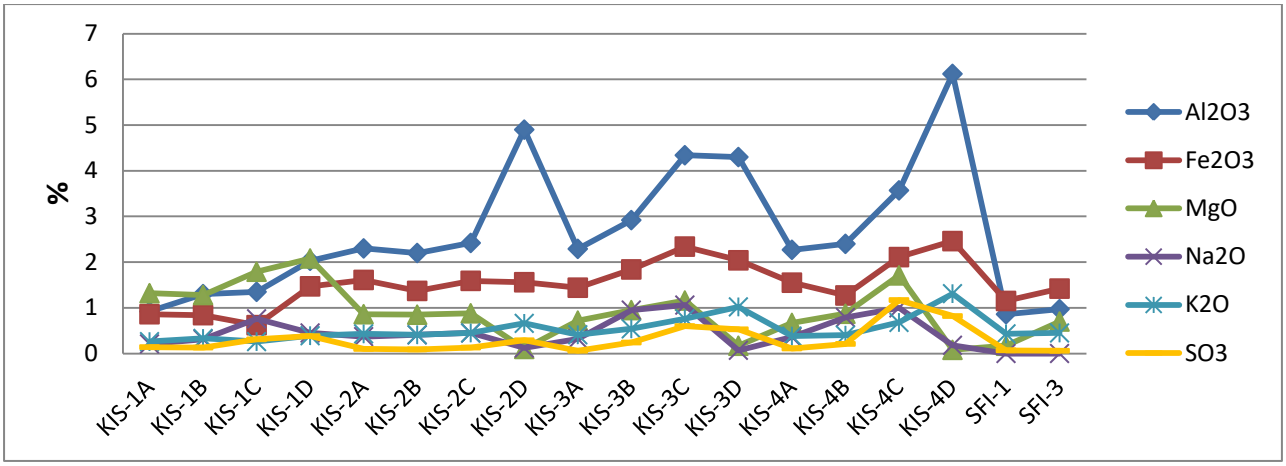

Figure 4.64. Graphical illustration of the major components Al_2O_3, Fe_2O_3, MgO, Na_2O, K_2O and SO_3 from NW Crete Island offshore samples.

Trace Elements

In Figure 4.65, Sr content display relatively high values in samples KIS-1D and KIS-4D. SFI samples display lower values relatively to KIS samples in all elements apart from Zr. In Figure 4.66, the elements that display similar patterns are: Ce-La-Nd, Th-Sc and Ni-Cu.

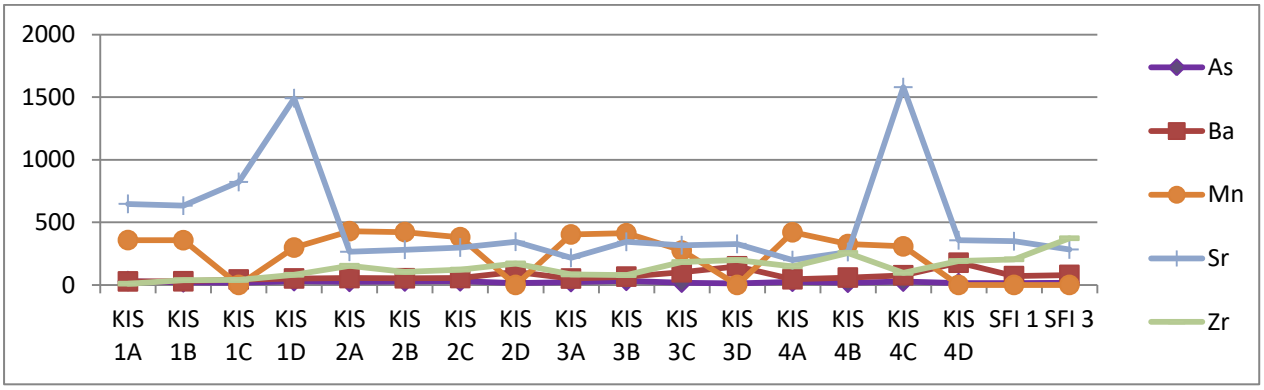

Figure 4.65. Graphical illustration of the trace elements As, Ba, Mn, Sr and Zr from NW Crete Island offshore samples.

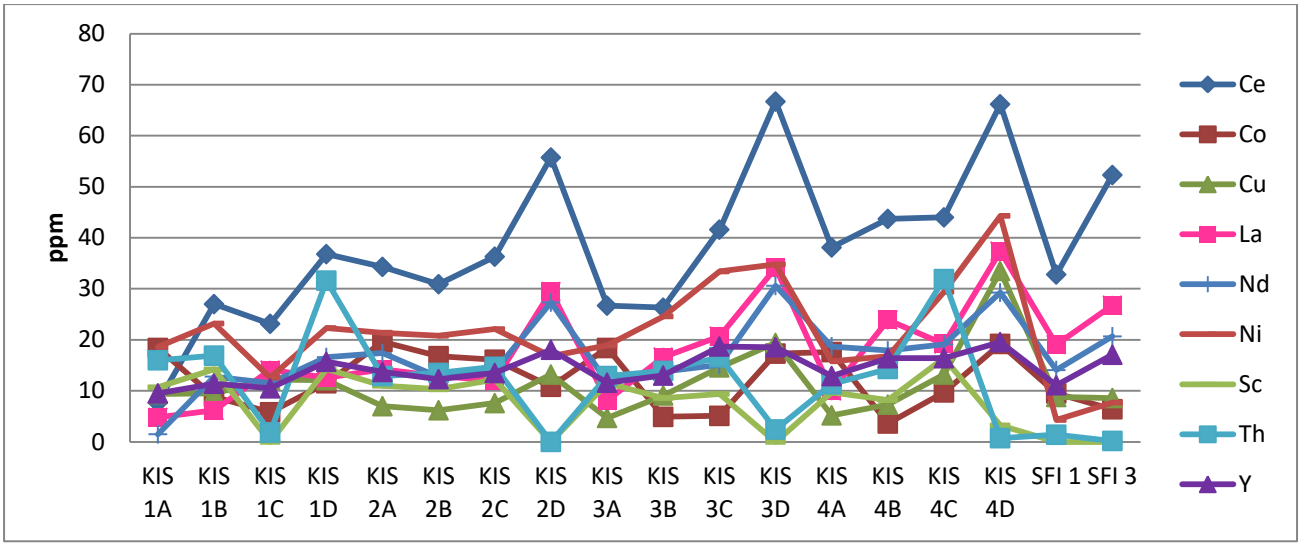

Figure 4.66. Graphical illustration of the trace elements Ce, Co, Cu, La, Nd, Ni, Sc, Th and Y from NW Crete Island offshore samples.

4.8.4. NE Rhodes Island Offshore Samples

Major Elements

In samples from Afantou Bay, Rhodes Island (Fig. 4.67), SiO_2 and MgO display inverse patterns. Moreover SiO_2 content displays low values. CaO values range ~30-40%. In Figure 4.68, Al_2O_3 and Fe_2O_3 display similar pattern apart from last sample AFA-3D. MnO, K_2O and Na_2O display values below 1%.

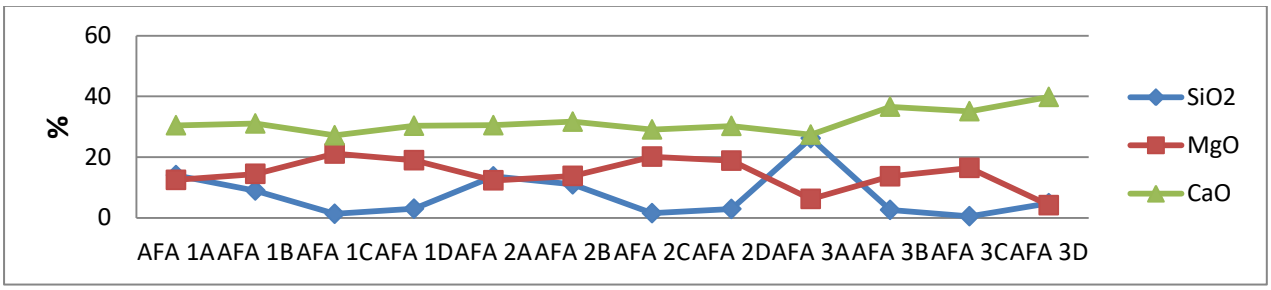

Figure 4.67. Graphical illustration of the major components SiO_2, MgO and CaO from NE Rhodes Island offshore samples.

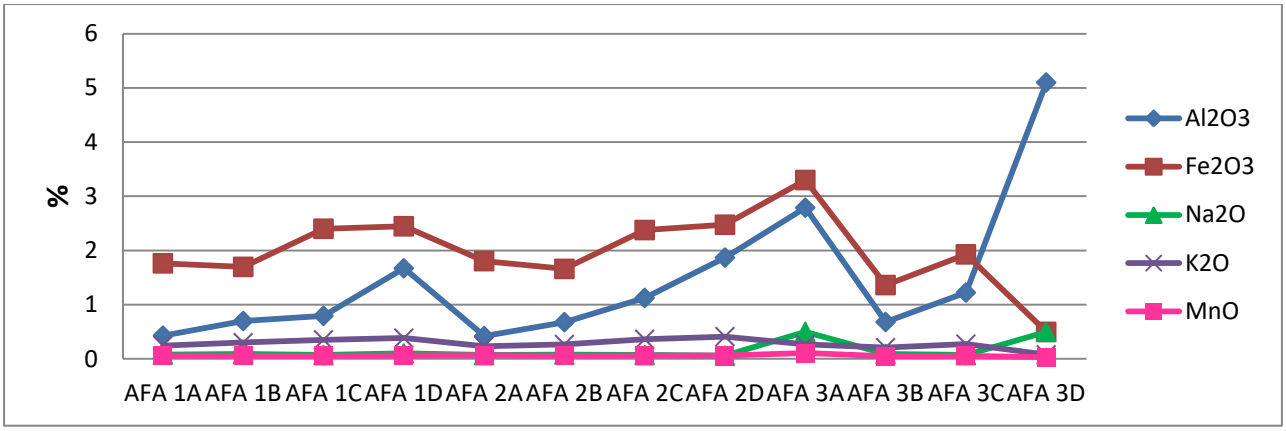

Figure 4.68. Graphical illustration of the major components Al_2O_3, Fe_2O_3, Na_2O, K_2O and MnO from NE Rhodes Island offshore samples.

Trace Elements

In Figure 4.69, Cr shows quite increased values. Cl content varies ~1500-2500 ppm. In Figure 4.70, the elements that display similar patterns are: Zn-V and Ba-Ce-La.

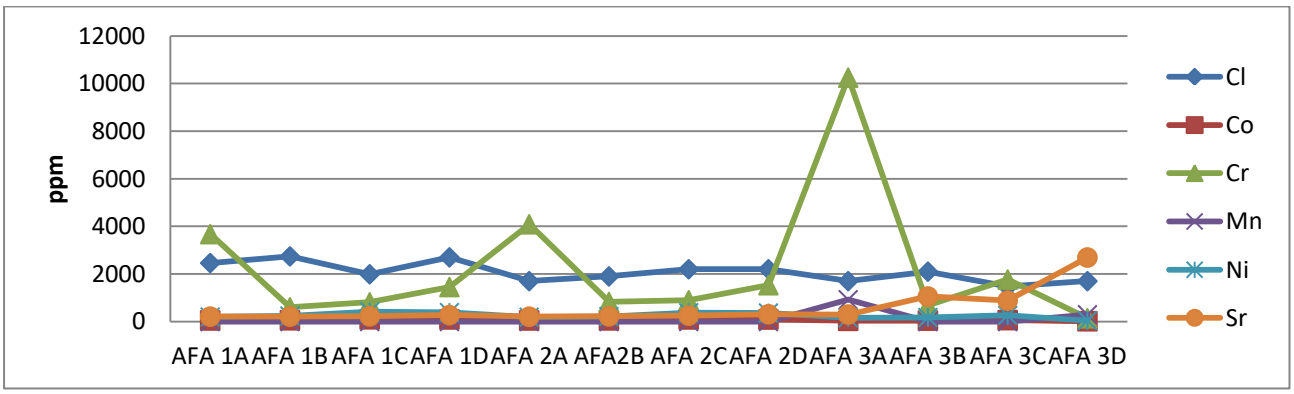

Figure 4.69. Graphical illustration of the trace elements Cl, Co, Cr, Mn, Ni and Sr from NE Rhodes Island offshore samples.

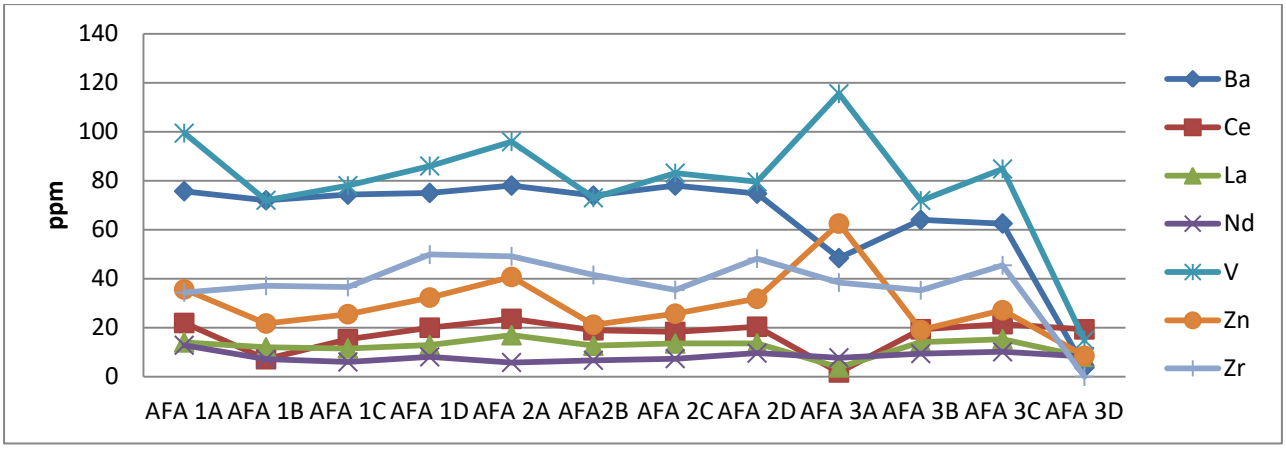

Figure 4.70. Graphical illustration of the trace elements Ba,Ce, La, Nd, V, Zn and Zr from NE Rhodes Island offshore samples.

4.8.5. Various Coastal Samples

Major Elements

In Figure 4.71, SiO_2 content varies from ~70% to ~94%, while CaO content varies from 0.5% to 14%. Samples with low SiO_2 values have high CaO values and vice versa, so SiO_2 and CaO content have inverse patterns. In Figure 4.72, Al_2O_3, Na_2O and K_2O display similar patterns; SO_3 content is below 1% and Fe_2O_3 content is <1% in NST samples and ~1% in EV samples.

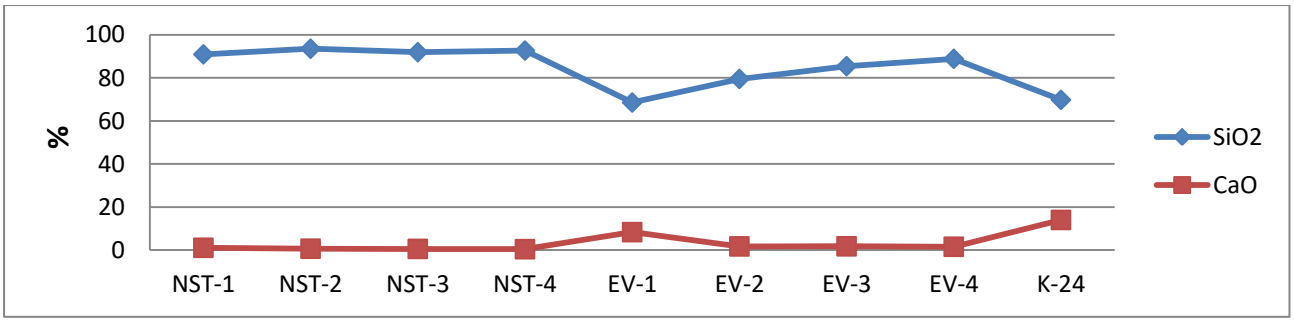

Figure 4.71. Graphical illustration of the major components SiO_2 and CaO from various coastal samples.

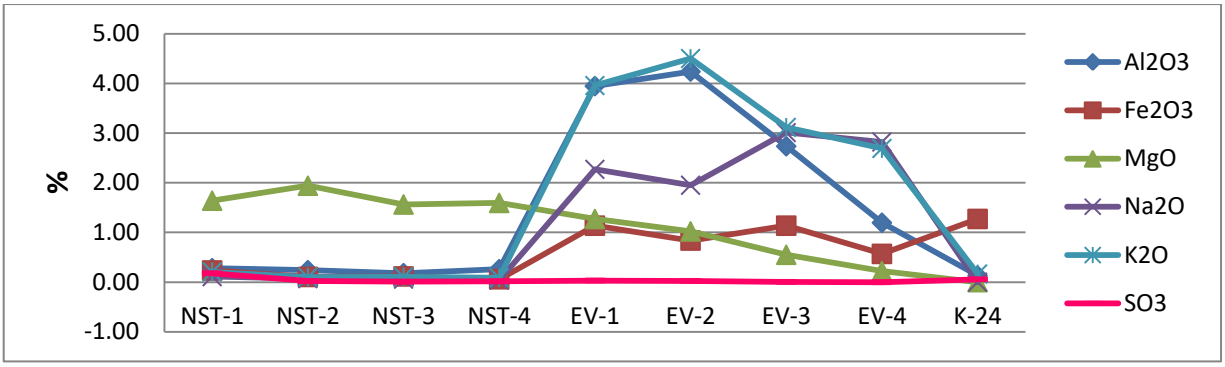

Figure 4.72. Graphical illustration of the major components Al_2O_3, Fe_2O_3, MgO, Na_2O, K_2O and SO_3 from various coastal samples.

Trace Elements

In Figure 4.73, Ce, La, Rb, Y, Nd and V follow similar pattern and Zr is enriched in EV samples.

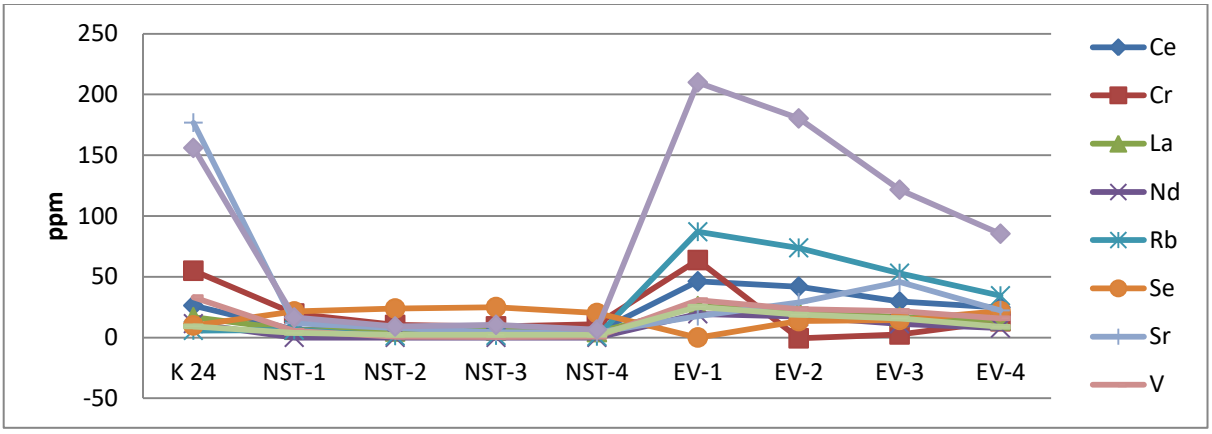

Figure 4.73. Graphical illustration of the trace elements Ce, Cr, La, Nd, Rb, Se, Sr, V, Y and Zr from various coastal samples.

4.8.6. Industrial Samples

Major Elements

In Figure 4.74, SiO_2 content varies from ~60% to ~87%, while CaO content varies from 1% to 14%. Samples with low SiO_2 values have high CaO values and vice versa. Al_2O_3 varies from ~0.1% to ~11.3%. In Figure 4.75, SO_3 and MnO content is below 1%; Fe_2O_3 content is >2% in GK sample and MgO content is slightly enriched in UK samples (Bournemouth and Boscombe).

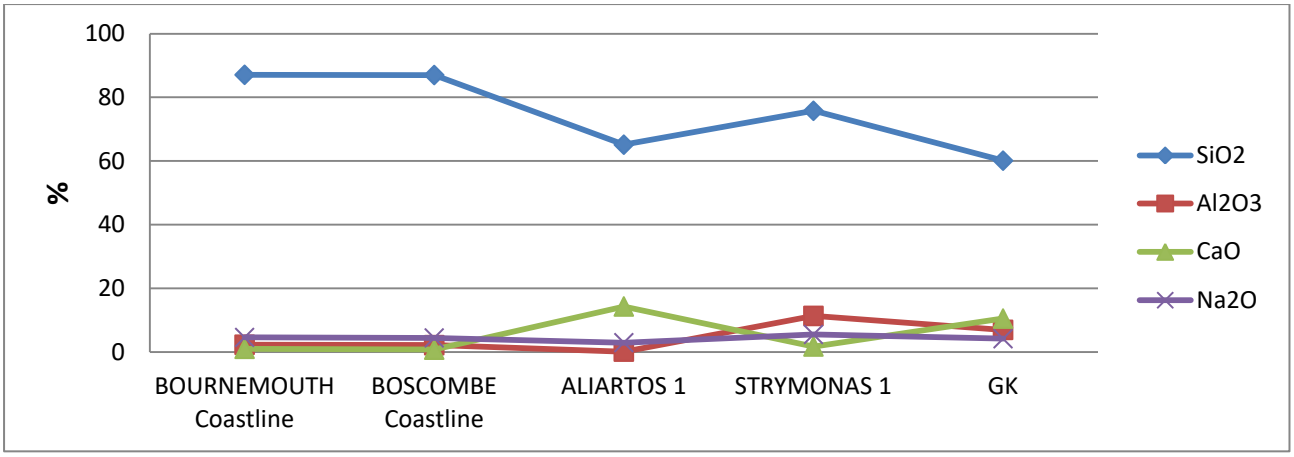

Figure 4.74. Graphical illustration of the major components SiO_2, Al_2O_3, CaO and Na2O from various industrial samples.

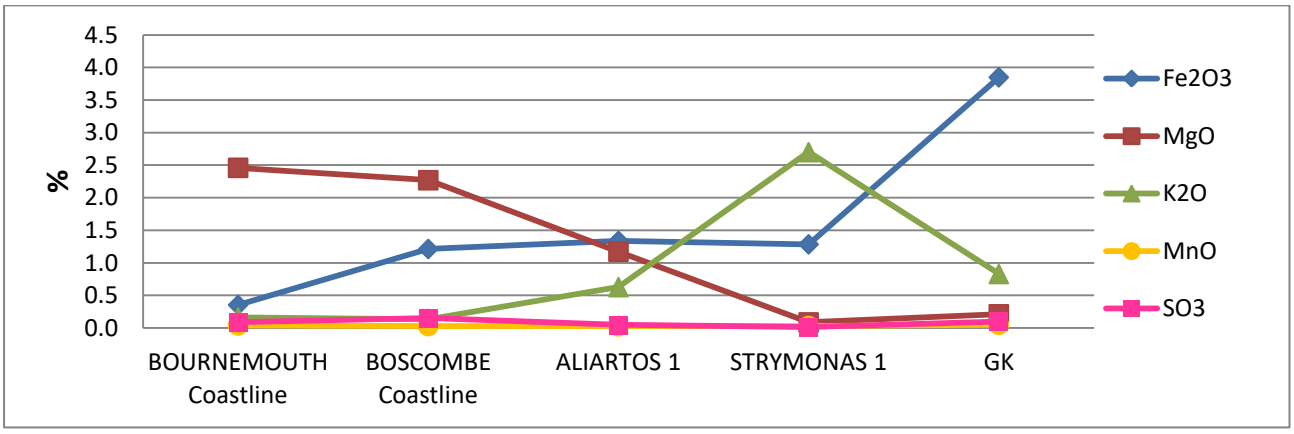

Figure 4.75. Graphical illustration of the major components Fe_2O_3, MgO, K_2O, MnO and SO_3 from various industrial samples.

Trace Elements

In Figure 4.76, Ba is enriched in Strymonas-1 sample; Sr is slightly enriched in Greek samples and Mn in Aliartos-1 and Strymonas-1 samples. In Figure 4.77, Cu is slightly enriched in GK sample and Zr quite enriched in UK samples.

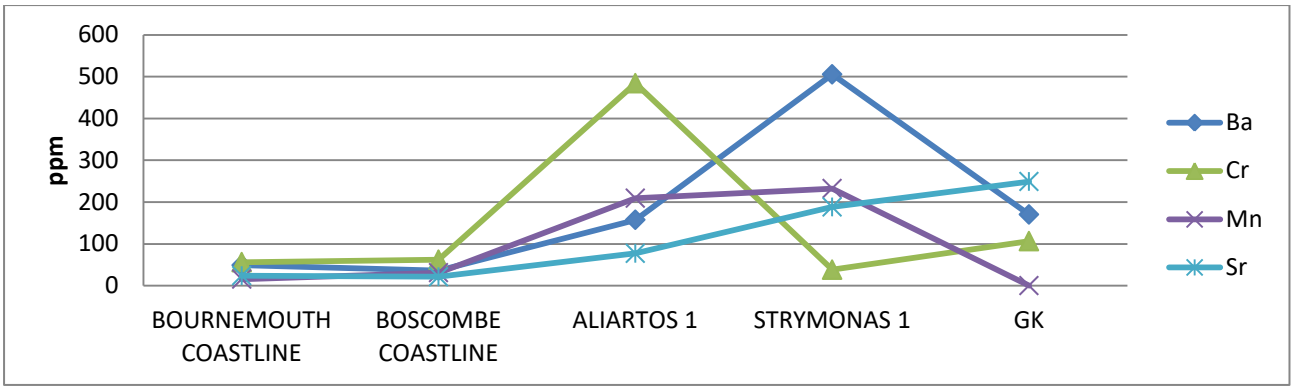

Figure 4.76. Graphical illustration of the trace elements Ba, Cr, Mn and Sr from various industrial samples.

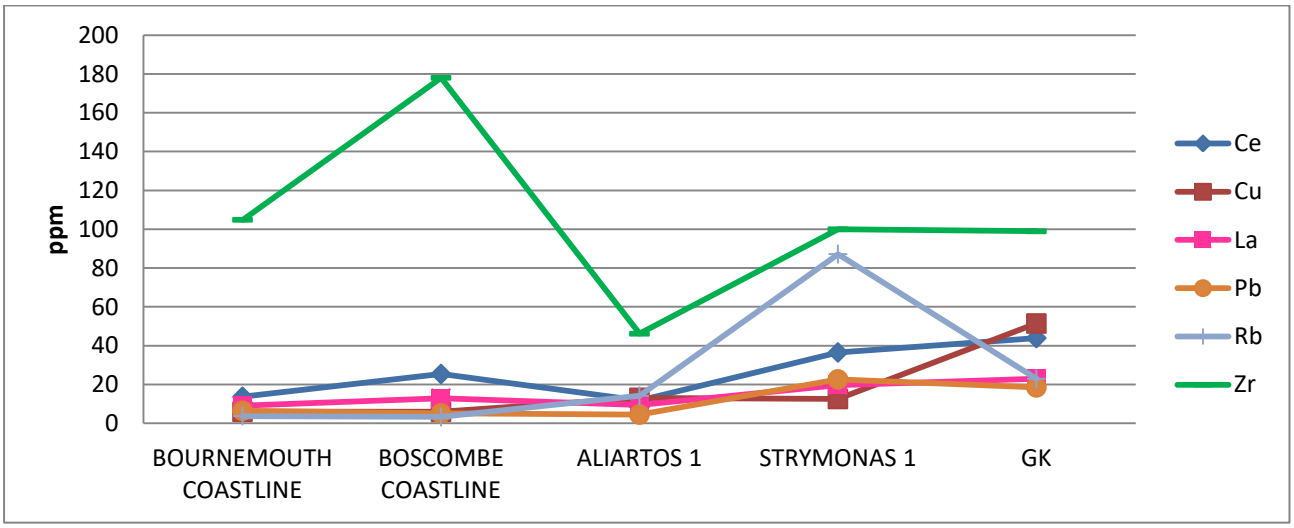

Figure 4.77. Graphical illustration of the trace elements Ce, Cu, La, Pb, Rb and Zr from various industrial samples.

4.9. SAND EQUIVALENT TEST

Sand equivalent test was performed according to EN 933-8. Prior to Sand Equivalent and Methylene Blue Testing, an analysis of particle size distribution was made, in order to determine that samples belong to sand and gravel fraction (Fig. 4.78).

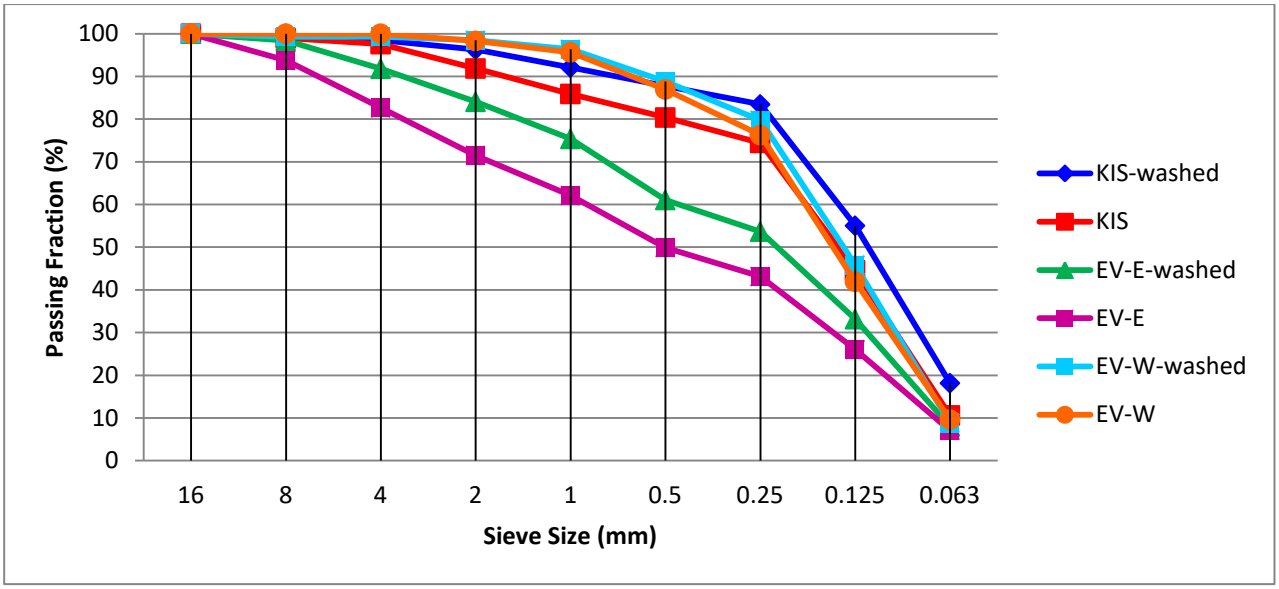

Figure 4.78. Grain size analysis for artificial mixtures of marine aggregates.

Particle size distribution varies among aggregates from different areas, as well as among washed and non-washed aggregates from the same area. Results imply that EV-E samples are coarser than other samples and KIS samples the most fine-grained. Furthermore, non-washed samples are coarser than the corresponding washed ones. Remarkably, the grain size differences decline towards the extreme sieve values (16mm, 0.063mm).

Sand Equivalent values of the marine aggregates tested show significant variations between the two different areas (Table 4.22); Kissamos Bay, NW Crete Island and SE Evia Island, with KIS samples having substantially lower values than the EV ones. Moreover, the difference between washed and non-washed samples is crucial, as the washed ones display consistently higher SE values in all areas and sub-areas.

Table 4.22. Sand Equivalent results.

Sample	Parameter	Sample 1	Sample 2
KIS-washed	*Sample Weight (gr)*	120	120
	h1	15.5	15.2
	h2	8.5	8.3
	100(h2/h1)*	54.8	54.6
	SE$_4$	**54.7**	
KIS	*Sample Weight (gr)*	120	120
	h1	21.7	22.1
	h2	7.4	7
	100(h2/h1)*	34.1	31.7
	SE$_4$	**32.9**	
EV-E-washed	*Sample Weight (gr)*	120	120
	h1	11.9	11.8
	h2	8.7	8.8
	100(h2/h1)*	73.1	74.6
	SE$_4$	**73.85**	
EV-E	*Sample Weight (gr)*	120	120
	h1	14	13.5
	h2	7.8	7.9
	100(h2/h1)*	55.7	58.5
	SE$_4$	**57.1**	
EV-W-washed	*Sample Weight (gr)*	120	120
	h1	12.2	12.3
	h2	9.5	9.1
	100(h2/h1)*	77.9	73.9
	SE$_4$	**75.9**	
EV-W	*Sample Weight (gr)*	120	120
	h1	14.8	14.8
	h2	8.4	8.3
	100(h2/h1)*	56.8	56.1
	SE$_4$	**56.5**	

4.10. METHYLENE BLUE TEST

Methylene Blue test was performed according to ASTM C1777-15 and the EN 933-9 and was conducted in order define any active and harmful clay minerals (Fig. 4.79). Methylene Blue values exhibit important variations between the two different areas (Table 4.23); Kissamos Bay, NW Crete Island and SE Evia Island, with KIS samples having significantly higher values than the EV ones. The results of washed samples point towards the decrease of MB values. Specifically, MB values of Evia Island washed samples (EV-E-washed and EV-W-washed) display values <1g/kg.

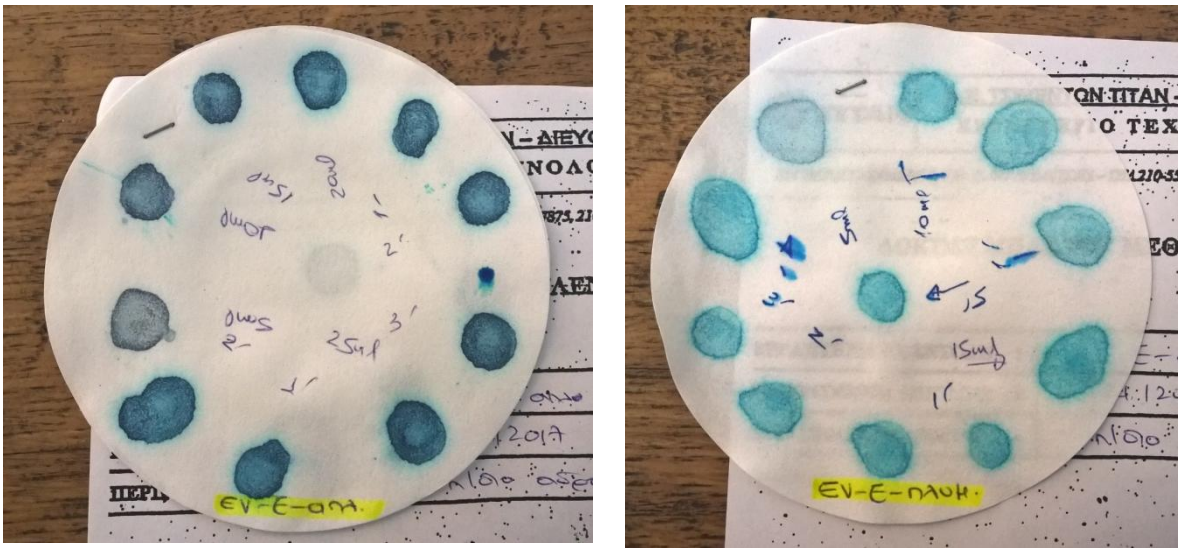

Figure 4.79. Spots tests for specifying the end point and accordingly the total volume of the added MB for samples: (a) EV-E and (b) EV-E-washed.

Table 4.23. Methylene Blue results.

Sample	Parameter	Result
KIS-washed	*M1*	222.80
	V1	30.00
	MB	1.47
KIS	*M1*	204.30
	V1	50.00
	MB	2.24
EV-E-washed	*M1*	203.20
	V1	15.00
	MB	0.74
EV-E	*M1*	206.30
	V1	25.00
	MB	1.21
EV-W-washed	*M1*	215.50
	V1	15.00
	MB	0.70
EV-W	*M1*	203.00
	V1	27.00
	MB	1.33

CHAPTER 5. DISCUSSION

The discussion of the results of this thesis is developed and presented in the context of an interdisciplinary approach, as marine aggregates deposits are characterized by a multitude of factors; some of which must coexist and/or could be exclusion criteria and others help to prioritize them according to the end-use of marine aggregates.

This chapter consists of four sections: i) the first section, which is the most important, investigates thoroughly each offshore area by integrating and interpreting all data arose from fieldwork and laboratory analysis; ii) the second section investigates some keynote factors, with focus on quality, of the coastal areas that indicate the possibility of marine aggregates' existence in the corresponding offshore areas; iii) the third section determines the qualitative characteristics of the industrial samples in order to set a baseline regarding the performance of the investigated marine aggregates and iv) the fourth section evaluates the results from the technical tests implemented in the aggregates from the promising marine aggregates deposits according to the current regulations and legislation.

5.1. MARINE AGGREGATES POTENTIAL IN THE OFFSHORE AREAS

5.1.1. SE Evia Island

The offshore area of Evia Island is located at the SE part of the island. The coastal area of the studied offshore area mainly consists of steep cliffs with streams (Fig. 5.1). Cape Filagra, located at the hinterland coastal area at the western part of the study area, hosts mylonitized blueschist to greenschist facies assemblages/metamorphosed schists, which include Na-amphibole, clinozoisite, white micas, quartz, chlorite, stilpomelane, calcite sphene, opaque minerals, epidote and albite porphyroblasts, which contain inclusions of e.g. glaucophane (Shaked et al., 2000; Ring et al., 2007). The hinterland coastal area eastern of Cape Filagra to Cavo D'Oro hosts marbles, quartzite, carbonate-rich schists, metapelites, metabauxite-bearing marble and seprentite lenses (Shaked et al., 2000; Ring et al., 2007).

Figure 5.1. View of the coastal area, which is adjacent to the offshore area of Evia Island. The coastal area consists mostly of steep cliffs and streambeds.

The interpretation of the results from the analysis of the obtained offshore surficial samples and cores from SE Evia Island (Fig. 5.2) is developed below.

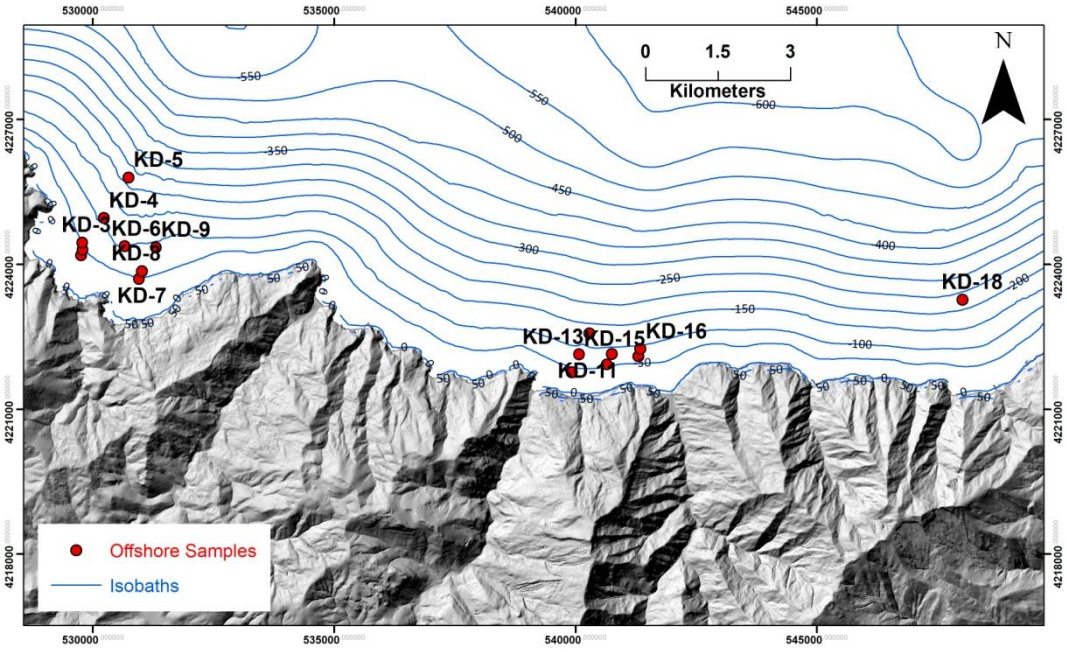

Figure 5.2. Shaded onshore relief map and general bathymetry of Kissamos Bay including sampling points.

Grain size

Grain size analysis of the studied areas offshore SE Evia Island revealed that the predominant sediment type is sand with slight transition to gravel (Fig. 5.3). Seven sedimentary classes have been identified according to Folk's (1980) classification and present a differentiation between the eastern and western sub-area. These classes are (Fig. 5.4): i)

Gravels (G), ii) sandy Gravels (sG), iii) gravelly Sand (gS), iv) Sand (S), v) silty Sand (Zs), vi) gravelly sandy Mud (gsM) and v) sandy Silt (sZ).

At water depths between 10 and 20m sand content is >99% and at water depths 20-50 m sand content is >83%. However, at samples KD 10 and 16 the gravel content reaches 90% and at sample KD11 the mud fraction is ~50% with the remaining percentage representing sand (Annex II-Grain Size Analysis). Therefore, the surficial sediments of the eastern sub-area are coarser than the western sub-area. At waters depths deeper than 50 m the mud fraction is >55 %. Furthemore, mud fraction percentages decrease eastwards. Especially, at the eastern sub-area sand fraction is observed at depths >35 m which probably indicates reslict sands (Karditsa, 2010). The increased sand content along the coastline and the grain size zonal distribution are attributed to wave action, while the existence of fine material at intermediate depths, as sample KD11, is probably attributed to fine-grained terrestrial (stream) inputs and local water circulation (Karditsa, 2010).

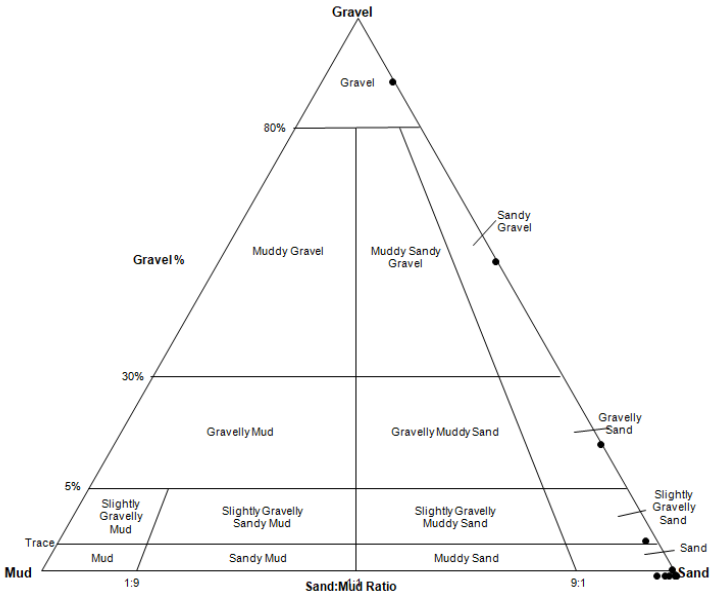

Figure 5.3. Grain-size classification of the surficial sea-bottom sediment samples collected offshore SE Evia Island, according to Folk (1980).

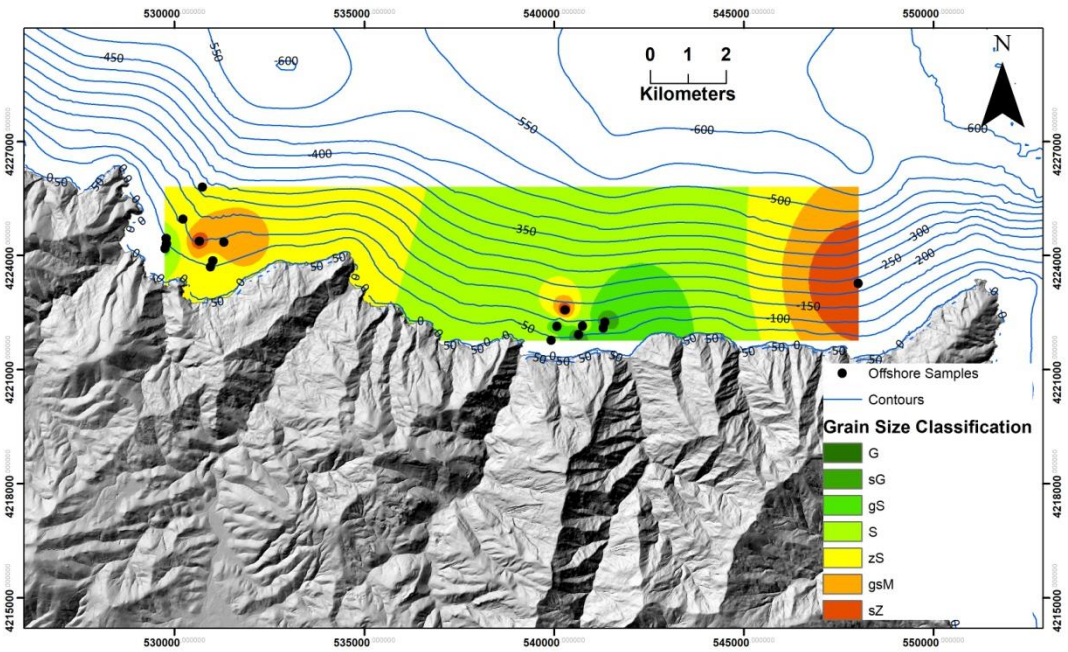

Figure 5.4. Spatial distribution of the sediment granulometric types offshore SE Evia Island

Poorly sorted sediments are found at depths >40 m, while moderately well sorted sediments are associated with shallower areas with high sand content. The eastern sub-area, where gravel fraction is relatively high, exhibits sediments of moderately well - sorting. Near - symmetrical skewness is observed in shallower depths and fine skewness in deeper areas. Better sorting means a more uniform sample in terms of grain sizem usually associated with wave action. Regarding kurtosis, a leptokurtic zone is observed at depths between 20 m and 40 m and mesokurtic in shallower and deeper areas, a fact that may suggest variable wave regime and sedimen sources (Friedman, 1962; Mohtar et al., 2017).

Offshore core KD-4 has 1.2m length and was acquired at 76 m water depth (Fig. 5.5). Along the entire core sediments are characterized as silty sands apart from the layer of 0.65 – 0.75 m, which is characterized as sandy silts. This shift is also observed in $CaCO_3$ content, which also declines from 0.65 m to 0.75 m following the reduction of sand content. Along the core sediments are poorly sorted, strongly fine skewed and leptokurtic (Annex II-Grain Size Analysis). The average content of $CaCO_3$ is ~7.7 %.

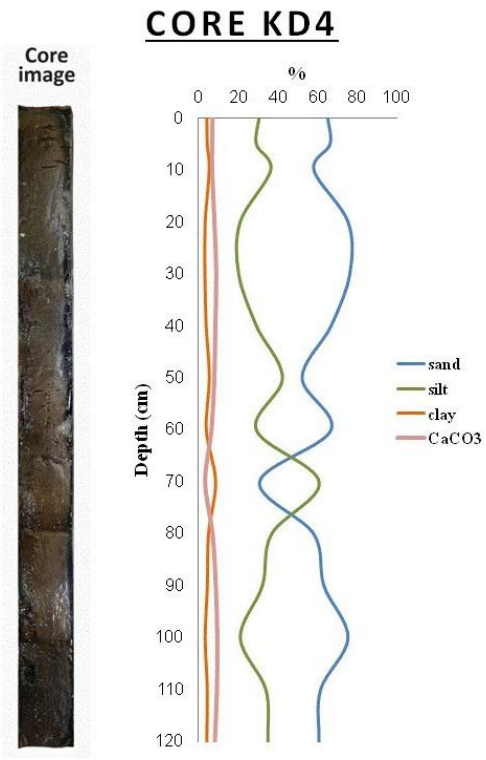

Figure 5.5. Grain size and $CaCO_3$ analysis of core KD-4.

The offshore core KD-5 (1.95 m in length) was acquired at 144 m of water depth (Fig. 5.6). Sediments of the the upper 0.15m are characterized as silty sands, followed by finer sediments (sany silts) at the part from 0.15 m to 0.35 m, shifting again to silty sand below 0.35 m and up to 0.75 m with the remaining part of the core (0.75 – 1.95 m) being sandy silt. $CaCO_3$ content follows the grain size alterations during the first 1.3 m of the core, remains stable from 1.3 m to 1.8 m and then declines within the deeper part of the core. The average content of $CaCO_3$ is ~9.4%, higher as expected from core KD-4. Core KD-5 was obtained in the same sub-area but at greater water depth than core KD-4 and, therefore, $CaCO_3$ percentage indicates the degree of marine influence. Sediments along the core are poorly sorted, strongly fine skewed and mesokurtic at the first half of the core (0-0.85 m), and fine skewed and leptokurtic at its deeper half (0.85 – 1.95 m) (Annex II-Grain Size Analysis).

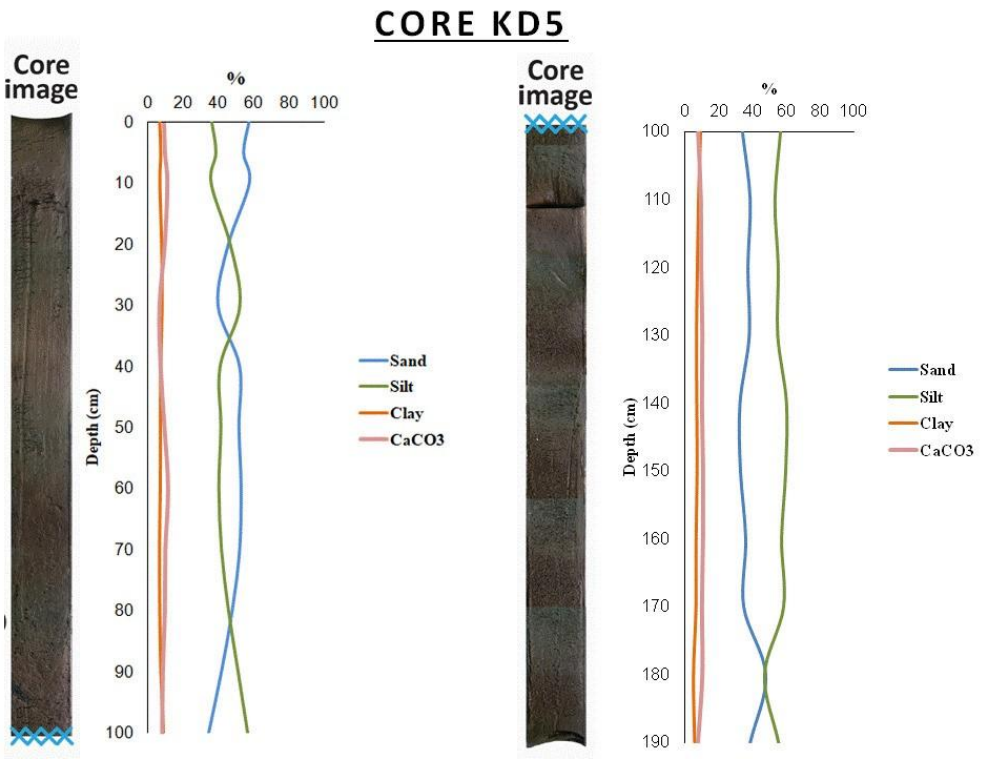

Figure 5.6. Grain size and $CaCO_3$ analysis of core KD-5.

The offshore core KD-18 (2.1 m in length) was acquired in 218 m water depth (Fig. 5.7). It consists of sandy silt, apart from its deepest 5 cm (2.05-2.1 m depth) that is characterized as silty sand. $CaCO_3$ content does not follow grain size distribution as calcium carbonate increases within the layer of 0.7-1.35 m part of the core. The average content of $CaCO_3$ is ~8.5%, lower than core KD-5, which was obtained on shallower area. Sediments along the entire core are very poorly sorted, fine skewed and leptokurtic when mud fraction is >70% (Annex II-Grain Size Analysis); this indicates rather quiscident condtions of deposition.

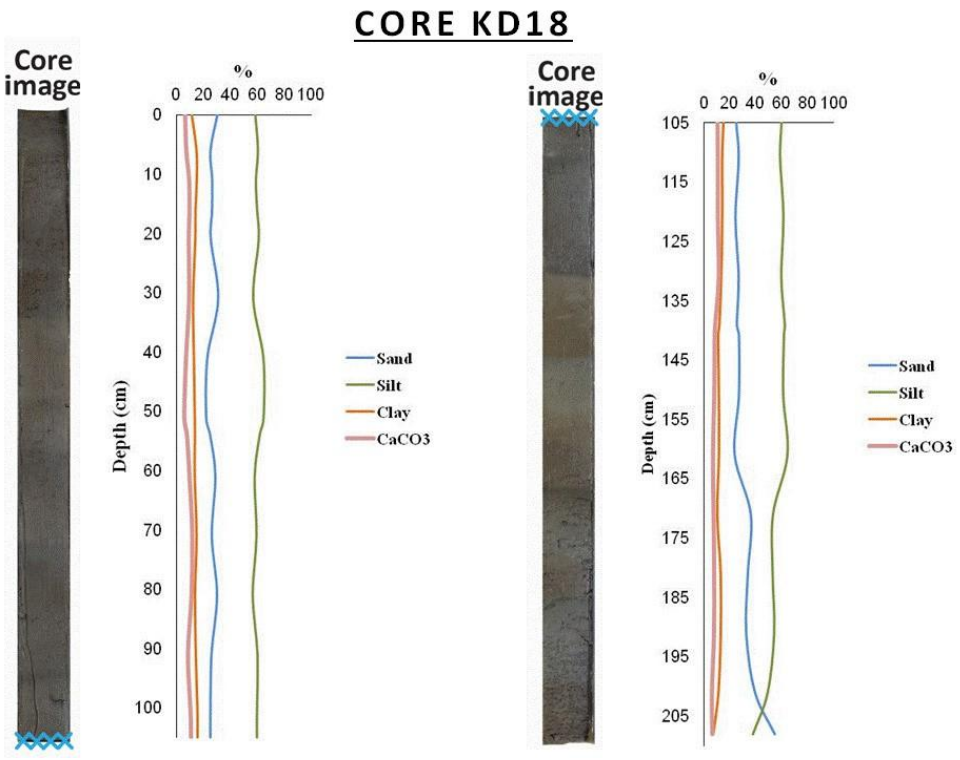

Figure 5.7. Grain size and $CaCO_3$ analysis of core KD-18.

Physical characteristics of the sediments

Density values regarding core KD-18 increases with depth up to 1 m depth, then decrease at the horizon of 1.4m depth and again increases up to the deepest point of the core. Overall, ensity values at the offshore area of SE Evia Island range between 2.61 and 2.80 gr/cm^3, with the higher values located in shallow depths at the western part of the studied area (Fig. 5.8). There is no direct relation between grain size and density and, therefore, higher density values maybe affected by a number of factors such as grain size, mineralogy and geochemistry.

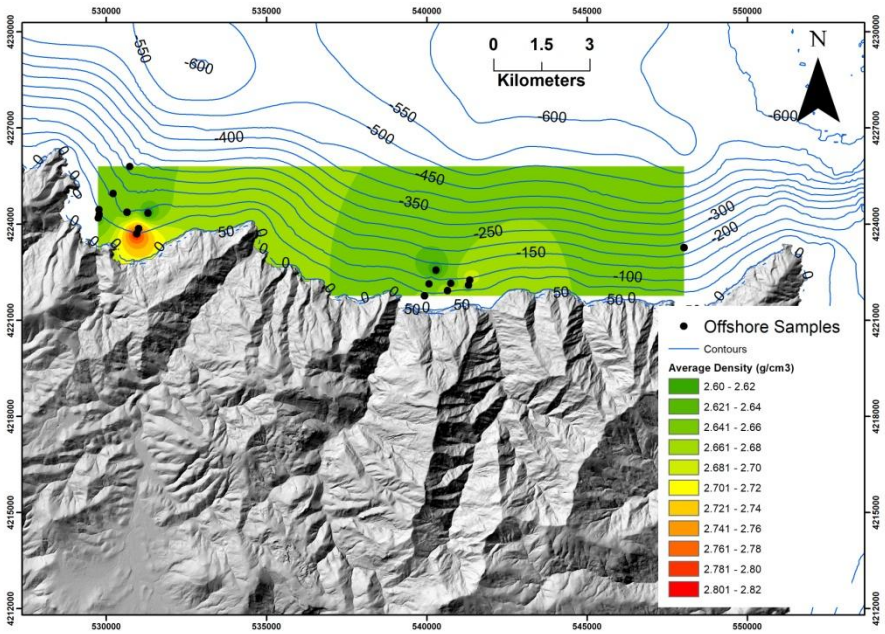

Figure 5.8. Spatial distribution of the density in surficial sediment offshore SE Evia Island Depth contours in blue color.

Microscopic analysis (Stereo-microscopy/ SEM-EDS)

Surficial sediments

The textural analysis of the surficial sediments offshore SE Evia Island through stereo-Microscope and SEM/EDS revealed great amounts of quartz, less of albite (Fig. 4.1), schist and small amounts of glaucophane (Fig. 4.1a, g), carbonates and organic material (Fig. 4.1b, c, f and Fig. 4.9). Furthemore, according to microscopic observations, quartz grains at the western part of the study area (Fig. 4.1a – e, Fig. 4.6 and Fig. 4.8), most probably derived from Ochi nappe, are less overworked and stressed than those from the central – eastern study area (Fig. 4.1g-h). Quartz grains from the central-eastern part of the area are probably derived from Styra nappe and therefore had been submitted in high pressure conditions. All quartz grains from the offshore study area of Evia Island are transparent, coarse-grained and angular; the latter observation indicates no intense near bed currents.

Quartz is considered as the most suitable mineral that is able to recordon its surface textural features of different formation processes and/or depositional environments (Warrier et al., 2019). Conchoidal fractures, in grains that lack pronounced cleavage direction and develop breakage patterns, are a consequency of the energy involved during their formation

(e.g. Mahaney, 2002) and correlated with their size. These features are very common in quartz grains (Margolis and Krinsley, 1974; Warrier et al., 2019).

Microscopic analysis with SEM/EDS also revealed iron oxides, often of biogenic origin, that secondarily covers clay minerals (Fig. 4.7) and quartz grains (Fig. 4.8); this fact suggests a supply of material from the onshore oxidized zone. Moreover, SEM/EDS analysis detected epidote grains with Cu-Zn oxides, probably derived from the adjacent mineralizaton zone which is located in the broad area of Kallianou (Voudouris et al., 2011).

Core sediments

Microscopic analysis of the cores offshore SE Evia Island revealed grains of Cu-Zn oxides in all three cores (e.g. Fig. 4.12-13) which most likely have been derived from the adjacent onshore area of Kallianou (Voudouris et al., 2011). The fact that Cu-Zn oxides were detected also in the sediment column of the cores that were collected in deeper waters implies that these oxides are spatially distributed from shallow to greater depths and that Cu-Zn supply is not temporal but rather constant. Furthermore, Ce- Monazite and barite grains were detected (Fig. 4.14 - 15), especially at the eastern part of the study area (core KD-18). The stereoscopic study displayed the abundance of finer material (Fig. 4.2) mixed with carbonates and organic material (Fig. 4.2f - g). However, glaucophane grains were able to be traced (Fig. 4.2c), indicating the diachronic and constant supply from the blueschist metamorphic facies.

Mineralogy - XRD

Surficial sediments

The mineralogical analysis of the surficial sediments offshore SE Evia Island revealed that quartz is the dominant mineral throughout the area (Table 4.9). Sediments that have a high percentage of quartz and feldspars have a high compositional maturity (Warrier et al., 2019). This fact is characteristic of the depositional environment of the offshore area of Evia Island Albite (Fig. 5.9a) appears to have higher content at the western part of the area probably attributed to the direct terrigenous supply from the metamorphosed facies of Cape Filagra. Furthermore, the spatial distribution pattern of albite is similar to grain size distribution, with higher albite content associated to the finer fraction (Fig. 5.4; 5.9a). Calcite occurs as trace mineral throughout the area, as well as chlorite group minerals and

illite/muscovite (Table 4.9, Fig. 5.9). Terrigenous calcite presence may be attributed to marbles intercalations that are hosted onshore (Shaked et al., 2000; Ring et al., 2007). Chlorite group minerals are major crystalline phase at the surficial sample of core KD-18, obtained at the eastern part of the area at water depths >200m. Glaucophane is found in traces at the western/central part of the area and is absent at the central/eastern (Fig. 5.9c), a fact that is related to the blueschist facies onshore and especially albite porphyroblasts which contain inclusions of glaucophane (Shaked et al., 2000). Glaucophane content was also detected in stereoscope images as in the case of Figure 4.1a, g. K –feldspars are only present in deeper areas and specifically at the surficial samples obtained from cores (Fig. 5.9d). Talc occurs as trace mineral in most of the samples and is probably related to blueschist metamorphism of south Evia (Katzir et al., 2000).

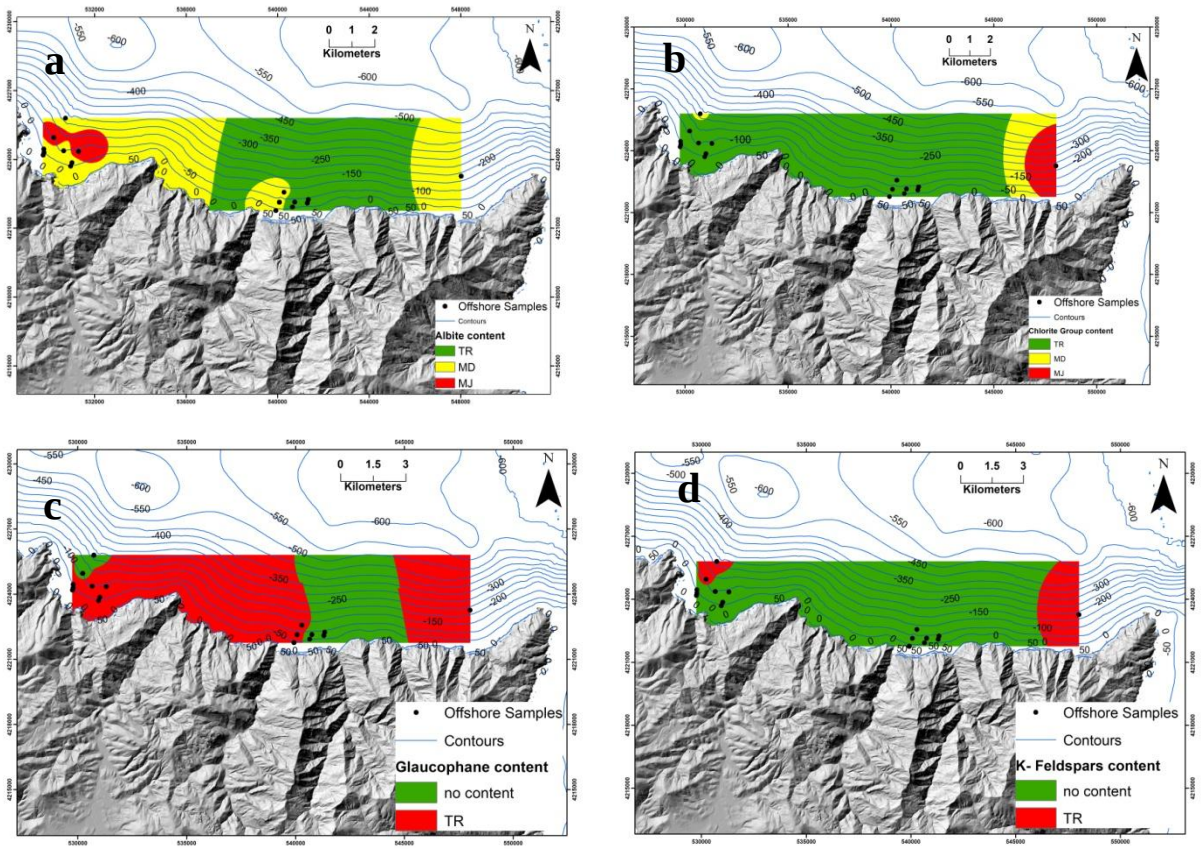

Figure 5.9. Abundance and distribution of: (a) albite, (b) chlorite group minerals, (c) glaucophane and (d) K-feldspars in surficial sediments offshore SE Evia Isl (MJ: major, MD: medium, TR: trace). Depth contours in blue color.

Core KD-4 (76m water depth) contains quartz as the major crystalline phase throughout the 1.2 m length (Table 4.10). Moreover, albite content occurs as major mineral at

the upper layer (0.4 m) and then substantially decreases between 0.4 m and 1 m, to increase again from 1 m to 1.1 m and then back declines up to 1.2 m (Fig. 5.10). Calcite content is exhibits medium content throughout the core (Fig. 5.10). Illite/muscovite occurs as trace mineral thhroughout the core apart from the layer of 0.7 m depth whereas its' content increases to medium content (Fig. 5.10). This fact is probably attributed to increased terrestrial (fluvial) inputs at the past, when that horizon was at the surface (e.g. Friedman, 1962; Karditsa, 2010; Ramadan, 2019). Chlorite group minerals content confirm this assumption, as it also increases below 0.7 m. K-feldspars, glaucophane, talc and edenite occur as trace minerals throughout the core (Table 4.10), suggesting constant sediments supply from the hinterland. At core KD-4, illite/muscovite is correlated to silt fluctuations and albite to sand fluctuations (Fig. 5. 5; Fig. 5.10).

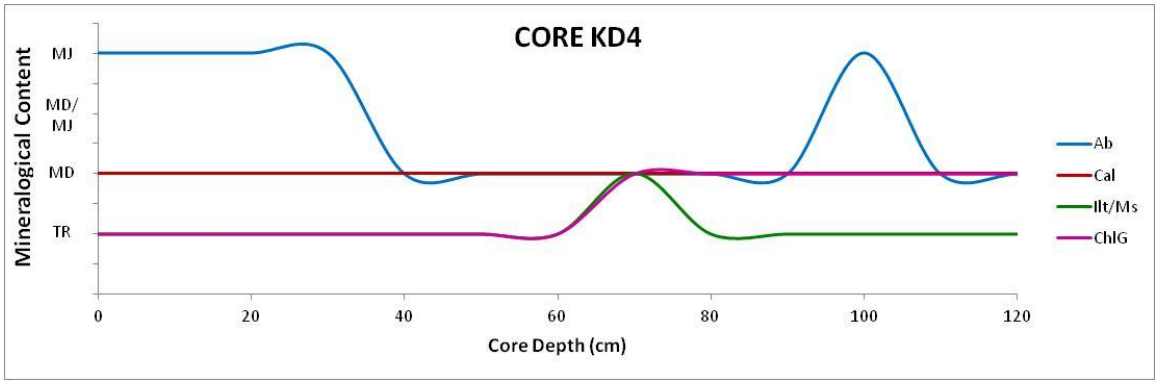

Figure 5.10. Downcore abundance of albite (Ab), calcite (Cal), illite/muscovite (Ill/Ms) and chlorite group (ChlG) of core KD-4 depth (MJ: major, MD: medium, TR: trace).

Core KD-5 (144m water depth), also, contains quartz as the dominant mineral throughout the ~2m core length (Table 4.10; Fig. 5.11). Although core KD-5 was obtained at the same area as core KD-4, the albite content clearly differs. Mineralogical analysis revealed that albite occurs as mineral of medium content at the seabed surface, declines to trace mineral up to 0.6 m depth, then increases to medium/major content along its length. Calcite presents medium content along the cores' length, apart from the horizons of 0.1 m and 0.3 m. Chlorite group minerals occur are of medium content, apart from the horizon of 0.1 m. The decrease of calcite and chlorite group minerals content that is observed at the 0.1 m horizon is suggesting reduced sediments supply from the central part of the onshore area. Glaucophane, K-feldspars, plagioclase, talc, edenite and Mn-oxides occur as trace to minor crystalline

phases along its length. At core KD-5, albite content is correlated to sand fluctuations (Fig. 5.6; 5.11).

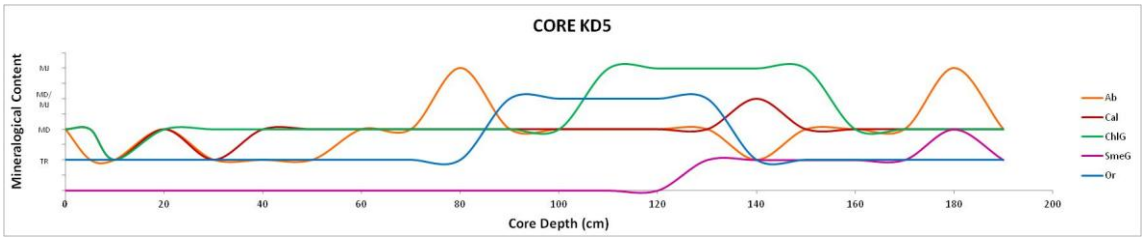

Figure 5.11. Downcore abundance of albite (Ab), calcite (Cal), chlorite group (ChlG), smectite group (SmeG) and orthoclase (Or) KD-5 depth (MJ: major, MD: medium, TR: trace).

Core KD-18 (~2 m length) was obtained at the eastern part of the study area, across cores KD-4 and KD-5, in higher water depth (218 m). Quartz also revealed as the major mineralogical phase, slightly reduced to medium content in the horizons of 1.3 m and 1.9 m (Fig. 5.12). Illite/muscovite presents exactly opposite pattern, as increases its' content (from medium to major mineral) in the horizons of 1.3 m and 1.9 m (Fig. 5.12). This fact clearly suggests the higher stream/river sediments discharge at the past, whereas chlorite group minerals content increased against quartz content (e.g. Friedman, 1962; Karditsa, 2010; Ramadan, 2019). Smectite group minerals only appear as trace minerals in the layer 1.37 – 1.62 m. Calcite occurs as mineral of medium content at the upper horizon (0-0.3 m) and as trace mineral further to the rest of the core apart from the horizon of 1.37 m – 1.62 m, where also shows medium content (Fig. 5.12). Glaucophane, K - feldspars, plagioclase, talc, edenite and Mn-oxides occur as trace to minor crystalline phases along its length (Table 4.10). The overall mineralogical alterations from 1.2 m to 2 m suggest a higher energy environment (Mohtar et al., 2017). At core KD-18, quartz and slightly albite contents are correlated to sand percentile fluctuations (Fig. 5.7; 5.12), while illite/muscovite content is positively related to density.

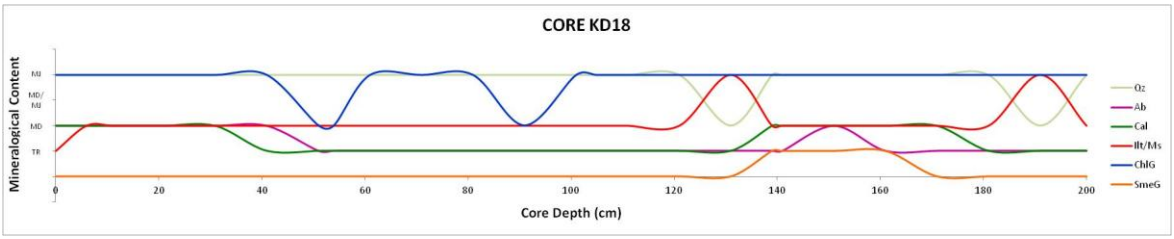

Figure 5.12. Mineralogical distribution according core's KD-18 depth. Downcore abundance of quartz (Qz), albite (Ab), calcite (Cal), illite/muscovite (Ill/Ms), chlorite group (ChlG) and smectite group (SmeG) of core KD-18 depth (MJ: major, MD: medium, TR: trace).

Geochemistry

Surficial sediments

The determination of major elements in the surficial sediments offshore SE Evia Island revealed that SiO_2 content varies between 60% and 80% (Annex III- Chemical Analysis) with the eastern subarea to display higher values than the western sub-area (Fig. 5.13a). This coincides with the fact that coarser material prevails at the eastern area confirming also the microscopic observations for the presence of coarse – grained quartz. As water depth increases (up to ~200m) SiO_2 content decreases to lower percentages (~40%) indicating no SiO_2-rich sediment deposits in greater water depths. CaO content varies substantially between 1.5% and 17% (Fig. 5.13b). The spatial distribution of CaO content is inverse to SiO_2, with low CaO values appear at the eastern sub-area and greater values at the western sub-area (e.g. Fig. 4.55). This pattern highlights the different origin of SiO_2 and CaO, with the former deriving from terrigenous sources and the latter from authigenic carbonates of biogenic origin (calcitic shells and shell-fragments). Fe_2O_3 content varies close to ~2-3% (Fig. 5.13c), with the eastern sub-area displaying slightly lower values. SO_3 values are <1% throughout the study area, with the exception of sample KD-8 located at the western sub-area (Annex III- Chemical Analysis). The spatial distribution of Al_2O_3 reveals lower values at the eastern sub-area, relatively to the western sub-area, while relatively higher values are present at greater water depths (Fig. 5.13d). This fact is positively related with the presence of aluminosilicate clay minerals and negatively related with the presence of quartz. MgO content varies between ~1.5% and 4%, showing its' highest values at the eastern sub-area (Fig. 5.13e), becoming more abudant at greater depths in both areas (surficial core samples). K_2O content displays low values throughout the study area, probably due to the absence of K-feldspars at the onshore onshore sediments (Fig. 4.56; Annex III- Chemical Analysis).

The chemical analysis of surficial sediments offshore SE Evia Island for trace elements revealed the disintegration and decomposition of the metamorphic rocks from the hinterland must have contributed heavy metals to the study area. Barium concentration displays higher values at greater depths (Fig. 5.14a) and Ba is related to barite occurrences observed at SEM/EDS, especially at core KD-18 at the eastern part of the study area. The elements Co, Cr, Cu, Mn, Ni and V exhibit similar spatial distribution patterns with Ba (Fig. 5.14-15). These elements are spatially correlated with the Al_2O_3 distribution and they are related to the presence of aluminosilicate minerals (Karageorgis et al., 2009). Moreover, Ce, La and Nd are quite correlated as they display similar spatial distribution patterns (Annex IV, Tables IV.1; Fig. 5.14-15). Furthermore, CaO and Sr patterns are positively correlated (Annex IV, Tables IV.1), revealing their common origin, such as carbonates and their spatial distribution patterns show increasing values towards the eastermost and westernmost areas, especially in greater depths (Fig. 5.13b; 5.15f). Pb and Sb (Fig. 5.15d-e) display similar spatial distribution patterns showing an increase at central study area. This encrichment is attributed to the supply material from the metalliferous Kallianou area (Voudouris et al., 2011). Tellurium enrichment in the sediments of the westernmost area (Fig. 5.15g) is also attributed to the sediment supply from the adjacent Kallianou area.

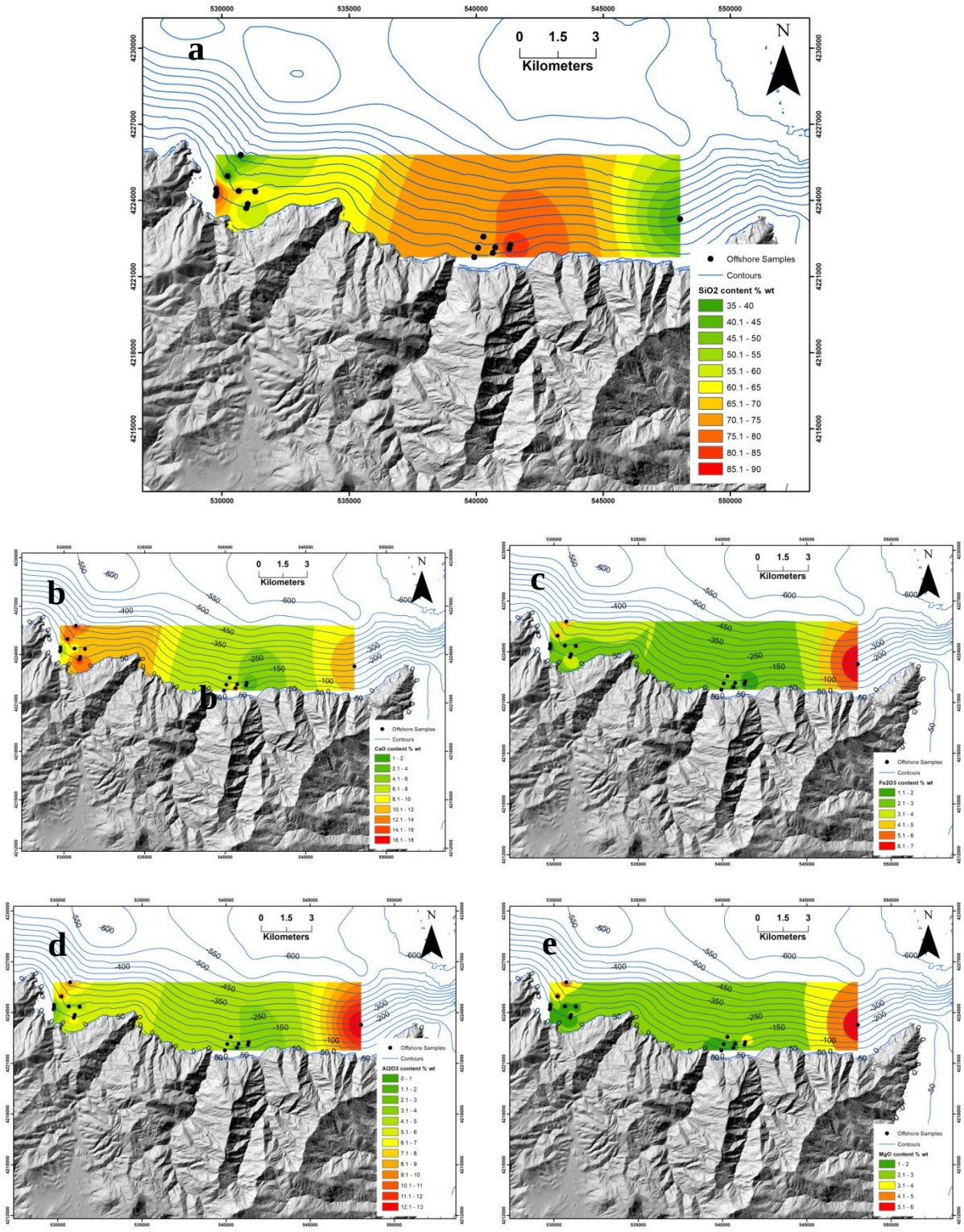

Figure 5.13. Spatial distribution patterns of major elements (% wt) in surficial sediment samples offshore SE Evia Island: (a) SiO_2, (b) CaO, (c) Fe_2O_3, (d) Al_2O_3 and (e) MgO. Depth contours in blue color.

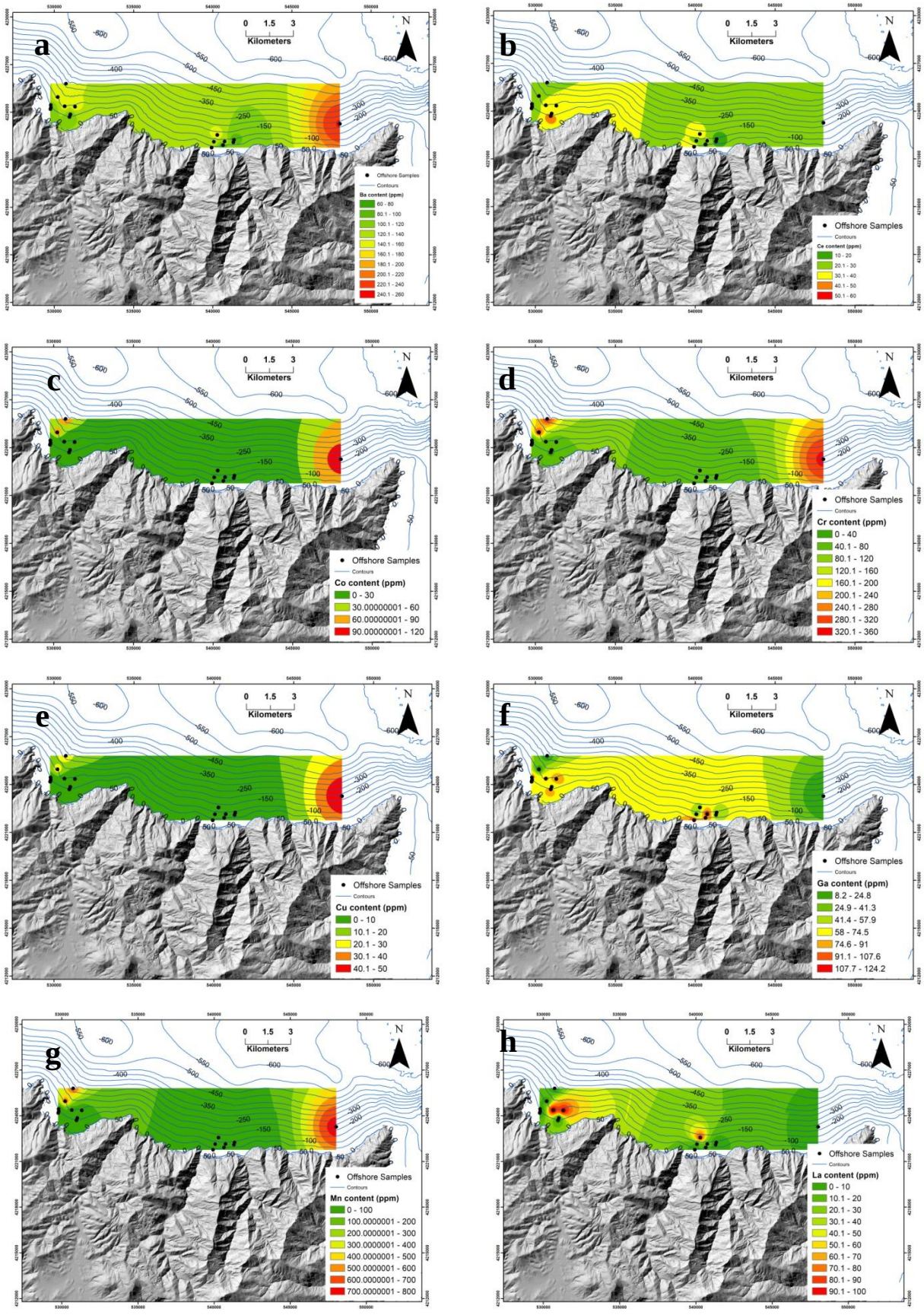

Figure 5.14. Spatial distribution patterns of trace elements (ppm) in surficial sediment samples offshore SE Evia Island: (a) Ba, (b) Ce, (c) Co, (d) Cr, (e) Cu, (f) Ga, (g) Mn and (h) La. Depth contours in blue color.

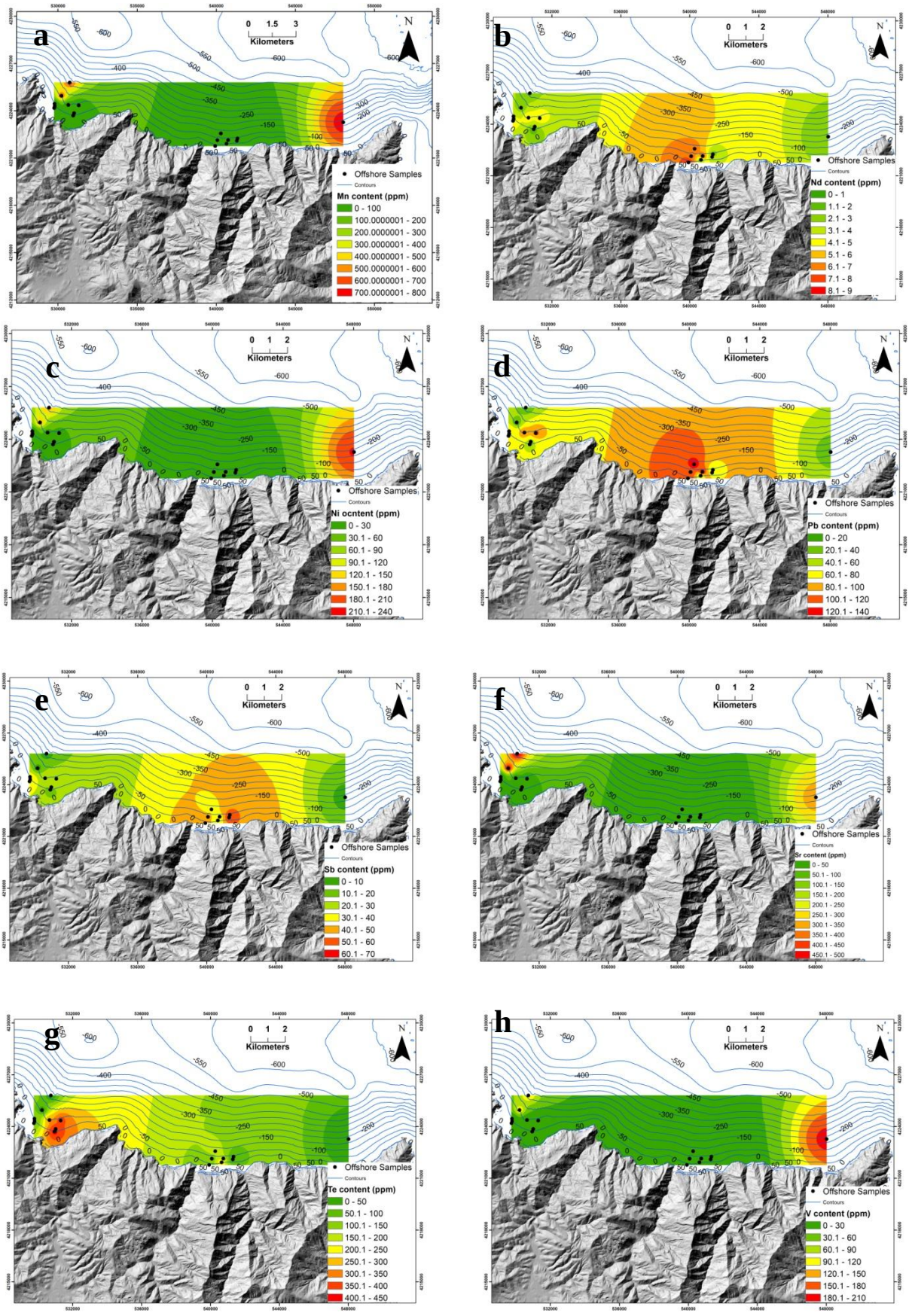

Figure 5.15. Spatial distribution patterns of trace elements (ppm) in surficial sediment samples offshore SE Evia Island: (a) Mn, (b) Nd, (c) Ni, (d) Pb, (e) Sb, (f) Sr, (g) Te and (h) V Evia Island Depth contours in blue color.

Core sediments

Chemical analysis of major elements from the cores KD-5 and KD-18 revealed that SiO_2 content prevails throughout the cores (Fig. 5.16-17). However, a decline of SiO_2 content is noticed at the 0.5-0.7 m layer of core KD-5 (144m water depth) and 0.8-1.2 m layer of core KD-18 (218m water depth). SiO_2 distribution pattern is positively correlated with Al_2O_3 pattern and negatively correlated with CaO pattern (Annex IV, Tables IV.1), which across the corresponding horizons increases its' content (Fig. 5.16-17). Especially in core KD-18, the Fe_2O_3 content follows the same distribution pattern such as of SiO_2 and Al_2O_3 (Fig. 5.16-17).This implies that the general sediment input derives from the metamorphic facies, apart from the corresponding horizons, whereas the sediment discharge derived from marble intercalations increases. SO_3 remains generally ~<1% throughout the cores. The same pattern applies also to TiO_2 content, apart from the deepest layer of core KD-5, which increases significantly (~13%). Low sand and quartz contents suggest at low compositional maturity of the sediments in water depths greater than 100 m, indicating the absence of any relicts marine aggregates deposits (Velegrakis, 2010; Warrier et al., 2019).

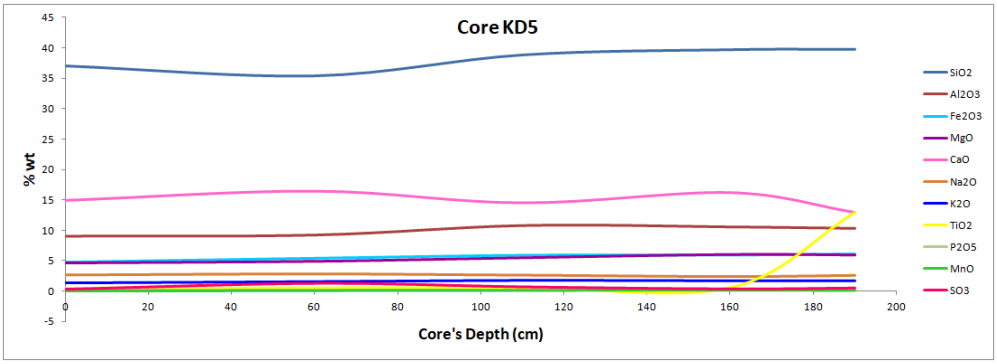

Figure 5.16. Major elements distribution according core's KD-5 depth.

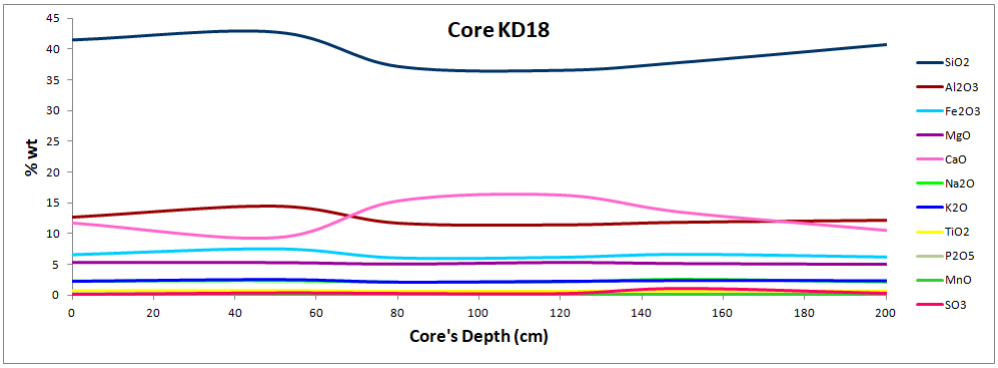

Figure 5.17. Major elements distribution according core's KD-18 depth.

Chemical analysis of trace elements from the core KD-5 located at the western sub-area of SE Evia Island show that Mn, Zn, Cu and Co present the same distribution pattern (Fig. 5.18a-b). Moreover, these elements show a rather weak correlation (Annex IV, Tables IV.1) with Al_2O_3 distribution pattern indicating their common origin of aluminosilicate minerals (Karageorgis et al., 2009). Chlorine content declines in both cores as depth decreases (Fig. 5.18c, d) and there is no correlation with the respective SiO_2 distribution pattern, which is probably attributed to the proximity of the upper layer with the sea-water column. Concerning the core KD-18, Ba, Cr, Cu, Co, Mn, Ni, Pb and Zn are positively correlated (Annex IV, Tables IV.1), displaying similar distribution patterns and, as such, indicating a common origin (Fig. 5.18c-d). Sr content is strongly correlated with CaO content (Annex IV, Tables IV.1), both displaying almost identical distribution patterns, suggesting their common origin from carbonates (probably biogenic).

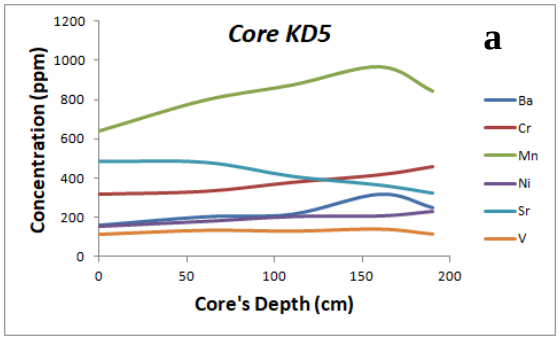

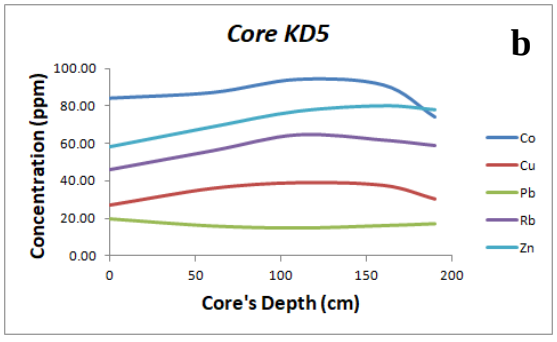

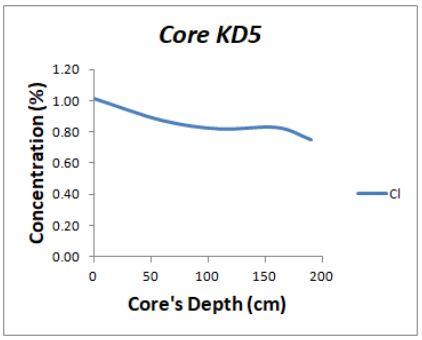

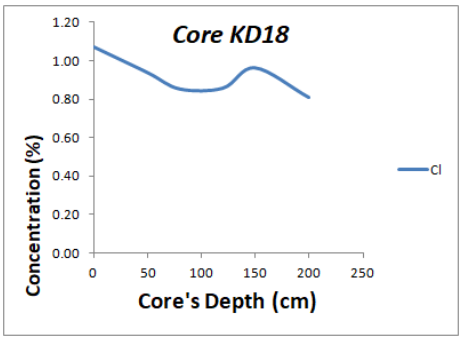

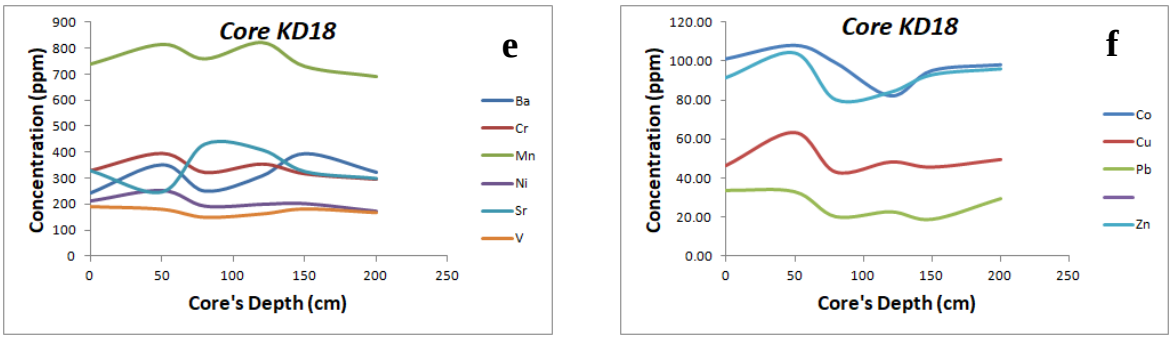

Figure 5.18. Trace elements (a, b, e, f) and chlorine (c, d) distribution according cores KD-5 and KD-18 depth.

<u>Potential of the area off SE Evia Island to host marine aggregates deposits for uses in the construction industry</u>

The abovementioned physical, mineralogical and geochemical characteristics configure various potential sub-areas for MA dredging offshore SE Evia Isl. The critical factors that arise from their study can be summirized as follows:

- Interpretation of grain size data resulted into the determination of a sub-area, whereas grains fraction is sand and coarser than sand.
- Semi-quantitative quartz content is uniform throughout the study area, although SiO_2 content varies. Therefore according to SiO_2 content, two sub-maps were created with SiO_2 content above 70% and 80%, respectively (Fig. 5.19). This differentiation aims to determine two eligible sub-areas, one with material of premium quality (>80%) and another of lower quality (>70%).
- Albite is enriched in greater depths; areas that are already excluded from grain size exclusion factor. All the other minerals are if minor interest, as they occur at the most as trace minerals throughout the area and/ or are slightly enriched in greater depths (>100m).
- Regarding Fe_2O_3 content, the study area was limited to the two sub-areas with Fe_2O_3 content below 2%, as required from various European and national restrictions (§1.4).
- CaO content has been differentiated below 5% and 10%, respectively, aiming to determine two eligible sub-areas, one with material of premium quality (<5%) and another of lower quality (<10%).

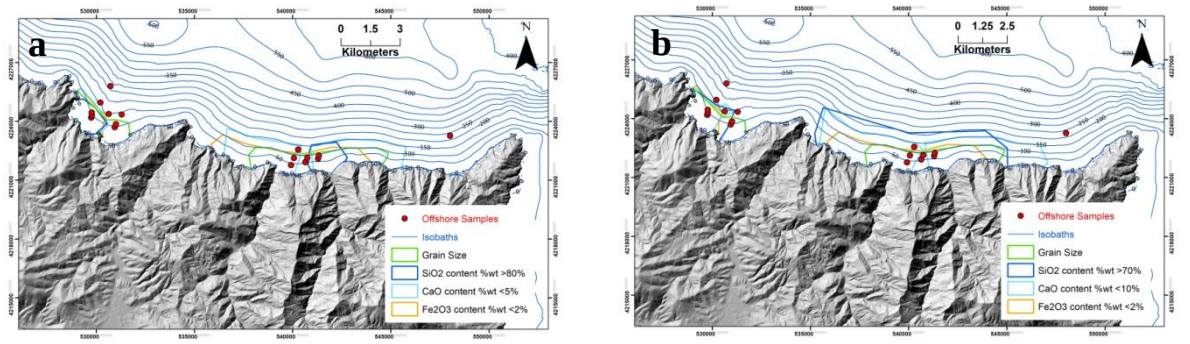

Figure 5.19. Shaded onshore relief map with the restricted offshore sub-areas of SE Evia Island according grain size, SiO_2, CaO and Fe_2O_3 content; (a) sub-areas with material of high quality and (b) sub-areas with material of lower quality.

No national restrictions apply regarding the required distance that any dredging activities should comply with. Therefore, according to the National Regulation for Mining and Quarrying activities (2011), a minimum distance of 100m is required for any extraction and exploitation activities. However, this restriction legally applies onshore. According to the 'Framework for safety in the offshore hydrocarbon exploration and exploitation activities', 2016, which incorporated the European Directive 13/30/EU, a minimum distance of 500m from any activity (e.g. port, beach, fish farms etc.) is required for the activities regarding hydrocarbon exploration and exploitation. Taking into consideration all the above, a minimum distance of 300 m from the coastline is introduced (Fig. 5.20), as 100 m distance from the coastline may affect the coastal area and 500 m is required for activities regarding hydrocarbons. Moreover, the under-study offshore area is relatively isolated and any extraction activities will not be in visual contact with inhabited areas.

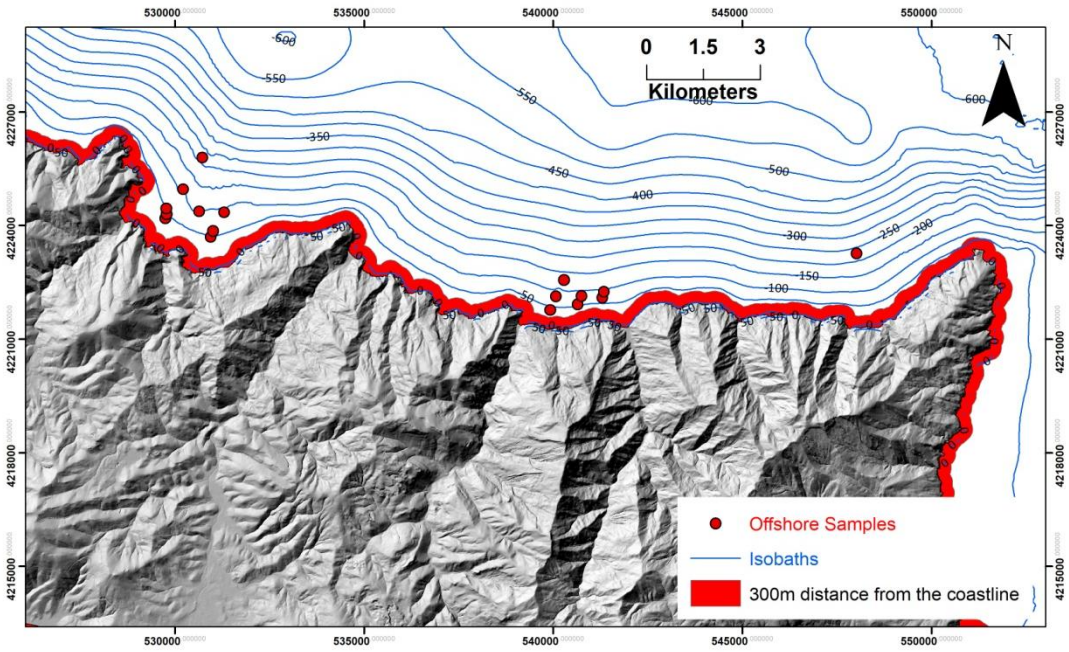

Figure 5.20. Shaded onshore relief map with the restricted offshore area of 300 m distance from the coastline, SE Evia Island.

Another critical factor for the delimitation of the potential offshore dredging area is closure depth, which represents the maximum water depth in which sea-bottom sediments are mobile (§1.3). Any dredging activity shallower than the closure depth will impact the onshore coastal area and the sediments balance will be disrupted (§1.3). According to Athanassoulis and Skarsoulis (1992) and Hallermeier's, (1978, 1981), equation for maximum closure depth for the offshore area of SE Evia Island is estimated to be at water depths of 12-15 m (Fig. 5.21).

Moreover according, to various practices worldwide and especially in North Europe, it is known that the common operational water depth is below 50 m. However, there are international examples, such as sand and gravel dredging in Palm Islands, Dubai, which dredgers operated up to 100 m water depth. Of course, the capabilities of the dredging vesels operating in Greece must be considered and evaluated if these activities will take place.

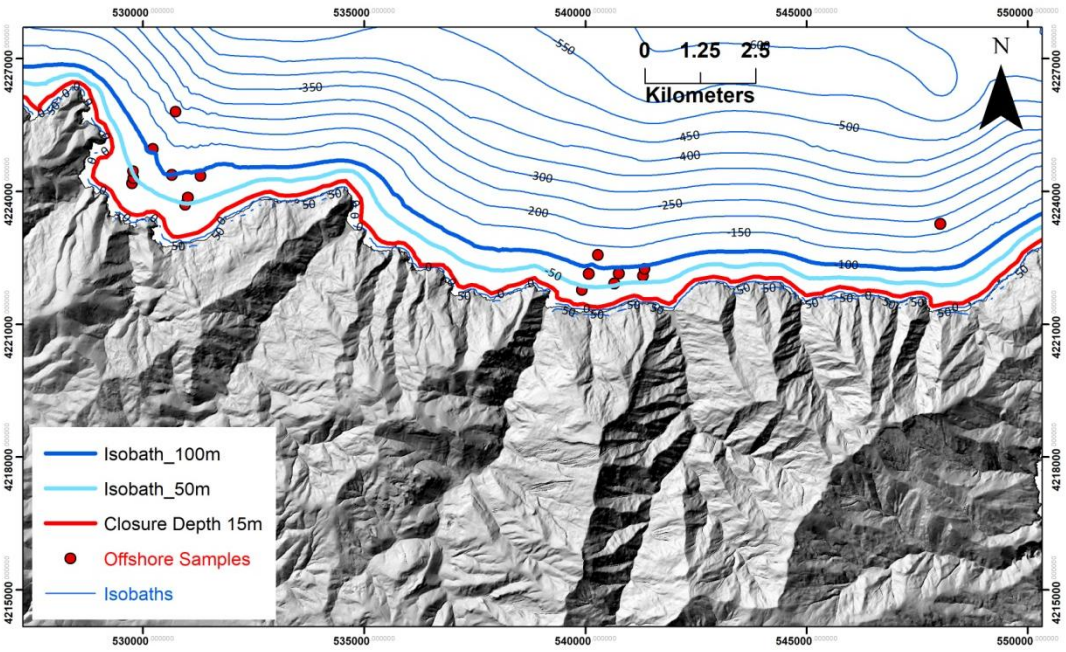

Figure 5.21. Shaded onshore relief map with the restrictions of closure depth in 15 m distance from the coastline, SE Evia Island.

In the wider area off SE Evia Island the Natura2000 site (GR2420001) "OROS OCHI – KAMPOS KARYSTOU – POTAMI – AKROTIRIO KAFIREFS – PARAKTIA THALASSIA ZONI" is located hosting meadows of the *Posidonia oceanica* (1120 Natura Habitat Code), which is endemic to the Mediterranean Sea and recognised as a priority habitat type for conservation under the Habitats Directive 92/43/CEE (Díaz-Almela and Duarte, 2008). These meadows present significant environmental restriction for any dredging activities. Hence, with respect to the seafloor extend of oceanic meadows, a 300 m buffer zone is applied (Fig. 5.22).

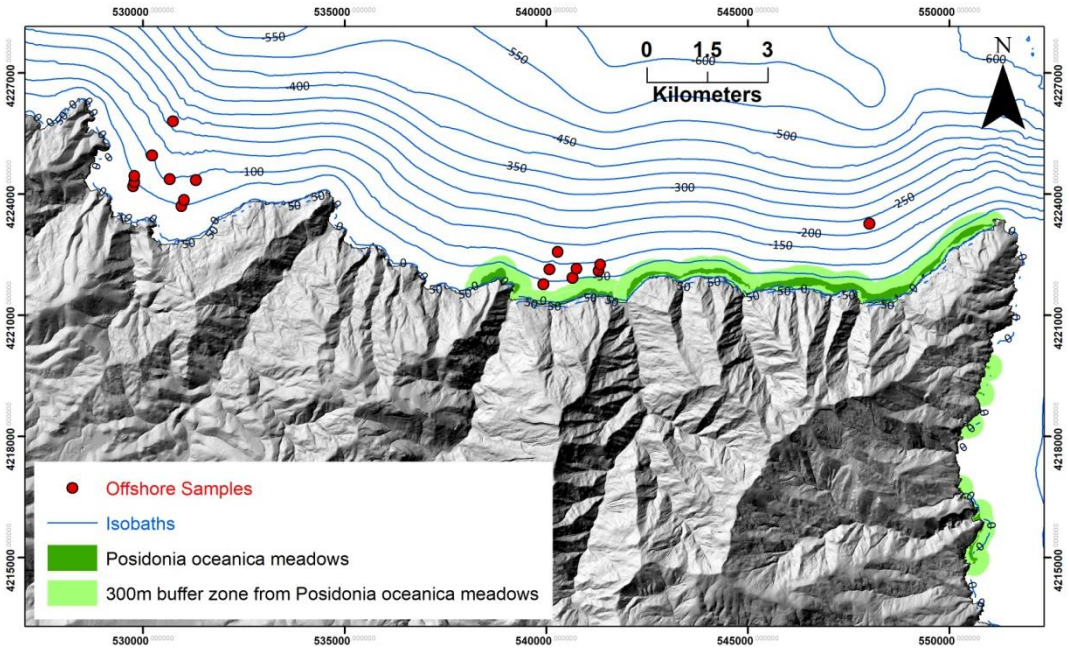

Figure 5.22. Shaded onshore relief map with the restrictions of Posidonia oceanic meadows with 300 m buffer zone, SE Evia Island.

Therefore, the offshore area of Evia Island is hosts marine aggregates deposits up to the water-depth of 50m, that cover 2.03 km^2 (Fig. 5.23). If these MA deposits extend over the isobath of 100 m, then, the MA deposits covers an area of 3.2 km^2 (Fig. 5.24). Furthermore, a sub-area at the western part of the offshore area of SE Evia Island, host a MA deposit with characteristics of high quality (e.g. SiO_2> 80% w/w) and covers 0.85 km^2 (Fig. 5.25).

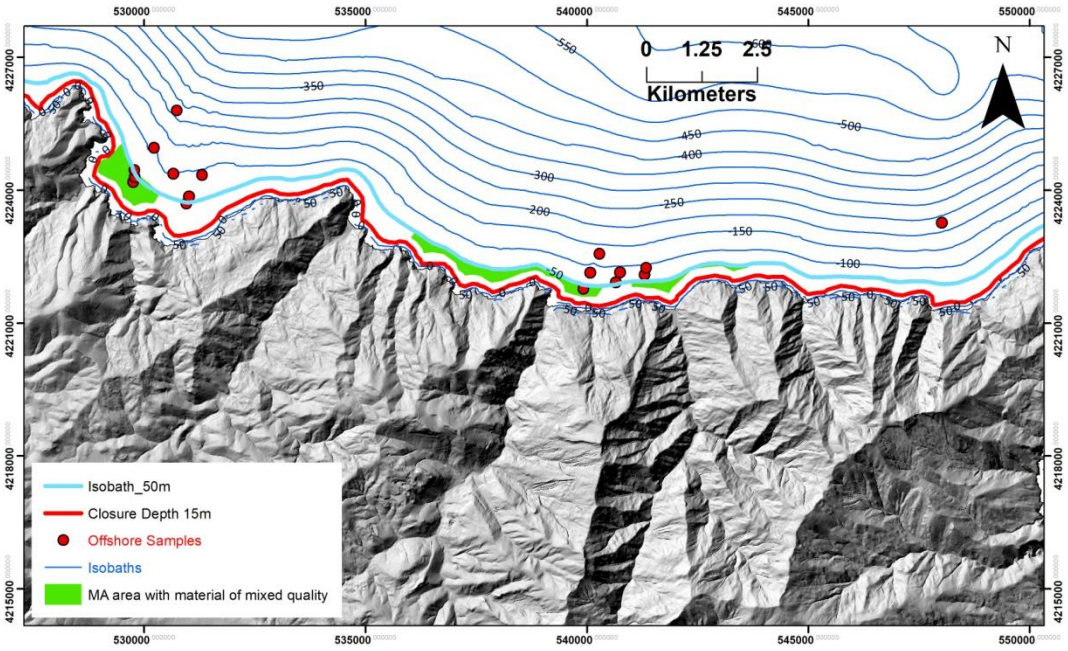

Figure 5.23. Shaded onshore relief map showing the potential offshore area with Marine Aggregates deposits of mixed quality (high and lower) shallower than water depths of 50 m, SE Evia Island.

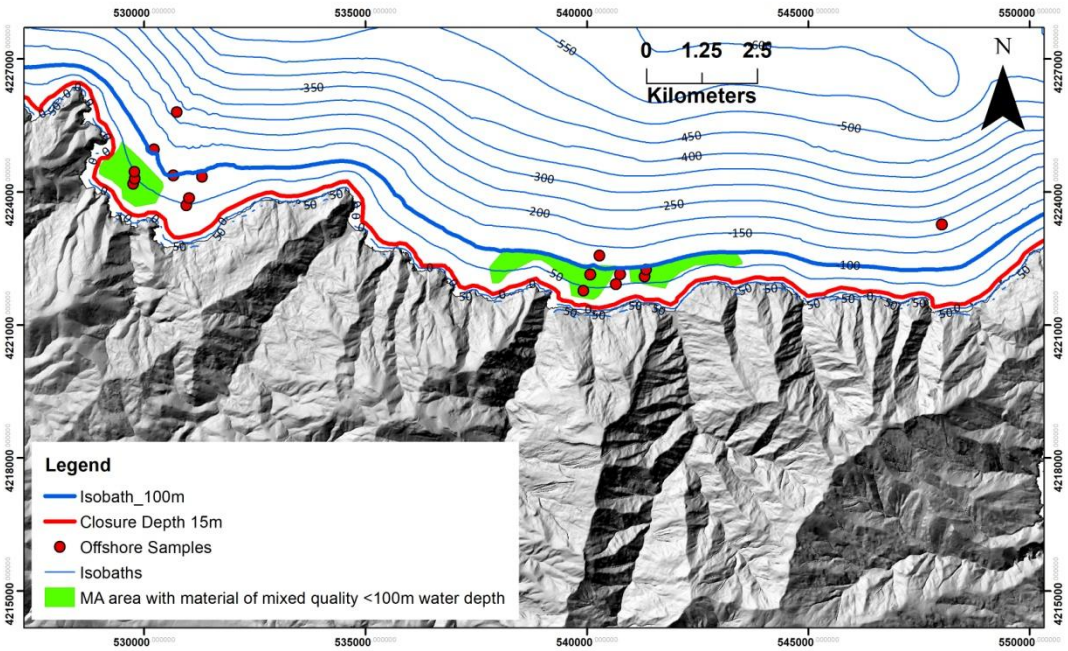

Figure 5.24. Shaded onshore relief map showing the potential offshore area with Marine Aggregates deposits of mixed quality (high and lower) shallower than water depths of 100 m, SE Evia Island.

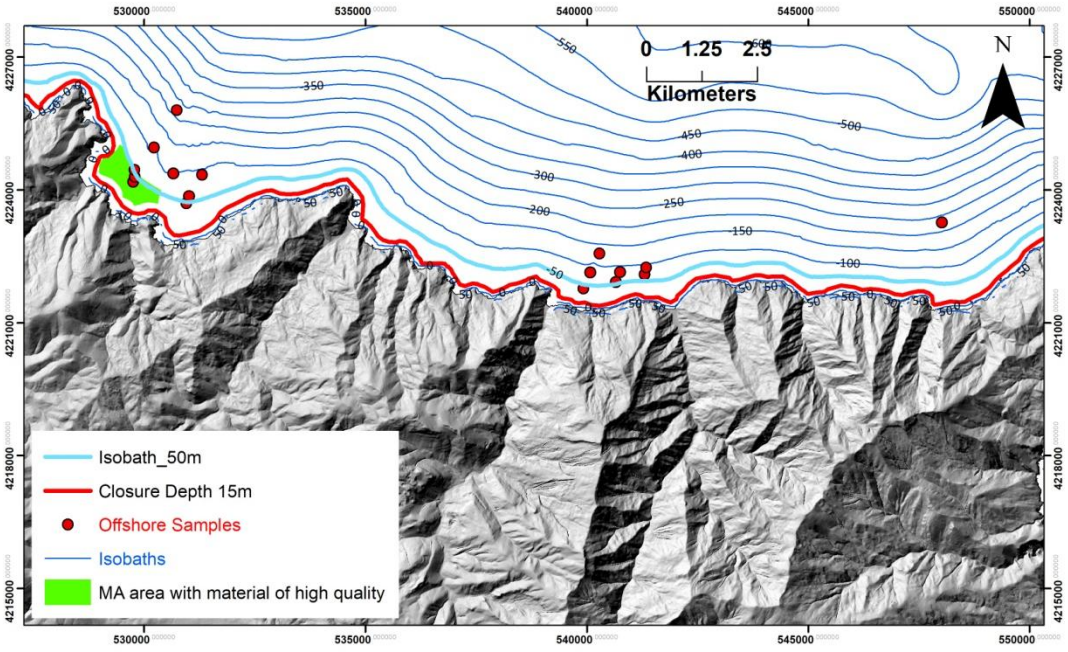

Figure 5.25. Shaded onshore relief map showing the potential offshore area with Marine Aggregates deposits of high quality shallower than water depths of 50 m, SE Evia Island.

5.1.2. NW Crete Island

The two offshore study areas of Crete Island are located at the SW part of the island, in Kissamos and Sfinari Bay. The coastal area of Kissamos Bay consists of Quaternary (Holocene and Pleistocene older fluvial terraces of unconsolidated deposits of gravels, sand, clays and silts) and Neogene deposits (conglomerartes, sand and sandstones, marls, clays/clayey material, marly limestones and gypsum). These sediments are derived from Pindos (Flysch, limestones and cherts) and Tripolis (individed limestones and dolomites) geotectonic units and also from Phyllites-Quartzite series (Bornovas and Rontogianni-Tsiampaou, 1983; Papanikolaou and Vassilakis, 2010; Seidel et al., 1982; Seidel et al., 2007). The coastal area of Sfinari Bay is mainly supplied with sediments from Phyllites-Quartzite series; however the outer parts of the Bay may supply the coastal and offshore area with sediments from the non-metamorphic Pindos Unit (Bornovas and Rontogianni- Tsiampaou, 1983; Papanikolaou and Vassilakis, 2010; Seidel et al., 1982; Seidel et al., 2007).

5.1.2.1. Kissamos Bay

The interpretation of the results from the analysis of the obtained coastal and offshore surficial sediment samples from the Kissamos Bay, NW Crete Island (Fig. 5.26) is developed below.

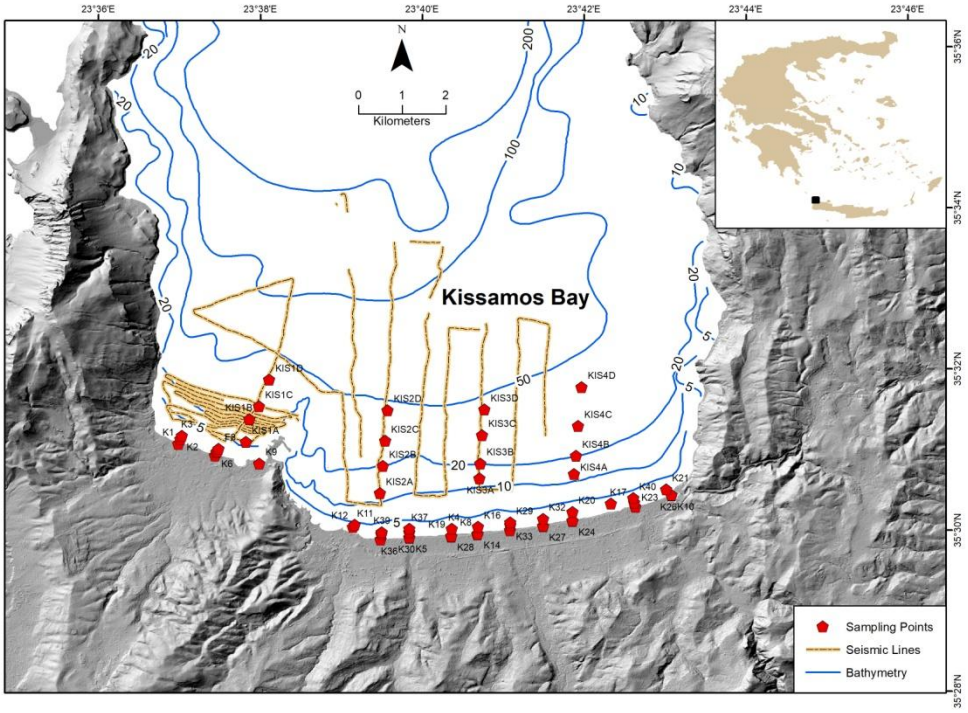

Figure 5.26. Shaded onshore relief map and general bathymetry of Kissamos Bay including sampling points and seismic lines (Anastasatou et al., 2019).

Grain size

The studied offshore area of Kissamos Bay are sandy i.e. sand, gravelly sand, and muddy sand (Fig. 5.27). Nearshore sediment are the sand-gravel mixtures, while onshore sediment is gravel (Fig. 5.28).

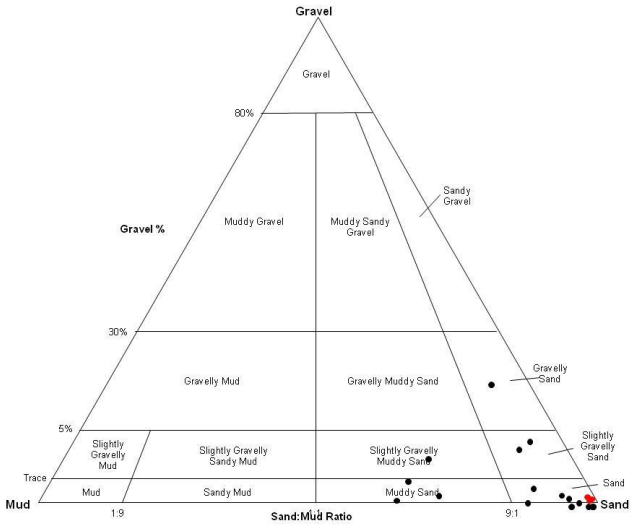

Figure 5.27. Grain-size classification of the surficial sea-bottom sediment samples collected offshore Kissamos (black circles) and Sfinari Bay (red circles) according to Folk (1980).

In Kissamos Bay the surficial coastal sediment samples are relatively coarse-grained (sandy). Specifically, five sedimentary classes have been identified according to Folk's (1980) classification that also roughly present an almost zonal distribution from shallow to deeper water depths: i) Gravels (G), ii) sandy Gravels (sG), iii) gravelly Sands (gS), iv) gravelly muddy Sands (gmS) and v) Sands (S) (Fig. 5.28).

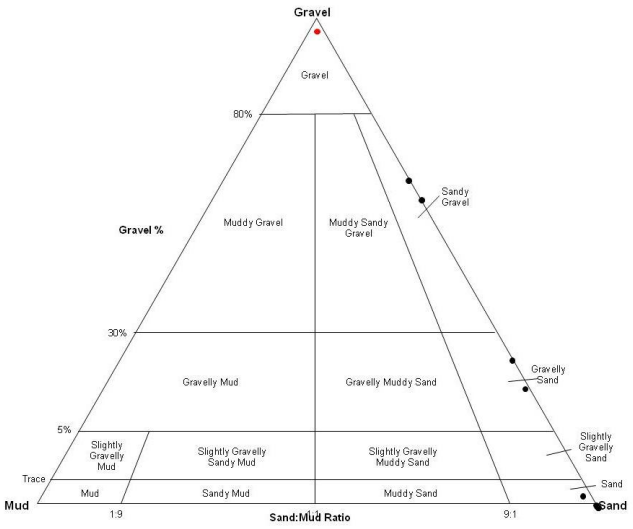

Figure 5.28. Grain-size classification of the coastal sediment samples from Kissamos (black circles) and Sfinari Bay (red circles) according to the Folk (1980).

Regarding sand content, the surficial sediments consist mainly of sand (90-100%) at water depths between 10 and 30 m with the only exception in front of western part of the bay where sand is 82% with the remaining percentage representing gravels (Annex II-Grain Size Analysis; Anastasatou et al., 2019). Gravel fraction (15-65%) is observed at the coastal western and central part of the bay (Fig. 5.29). Mud fraction ranges from 38% to 25% with the greatest values observed in depths over 35-40 m, declining eastwards (Anastasatou et al., 2019). At the central part, sand fraction is observed in depth >35 m which probably indicates residual sands. This zonal distribution of reducing grain size while depth is increasing and then transition to residual sand is typical of most continental shelves (Karditsa, 2010). Similar examples occur at the Mediterranean, which distribute sea-bottom surficial sediments under the similar hydrodynamic conditions, such as the continental shelf of Ebro's river in Spain and the Gulf of Lyon, France (Palanques et al., 1990; Diaz et al., 1996; Ulses et al., 2008; Karditsa, 2010). Moreover, at the eastern part of the bay gravels can be found in depths >30m.

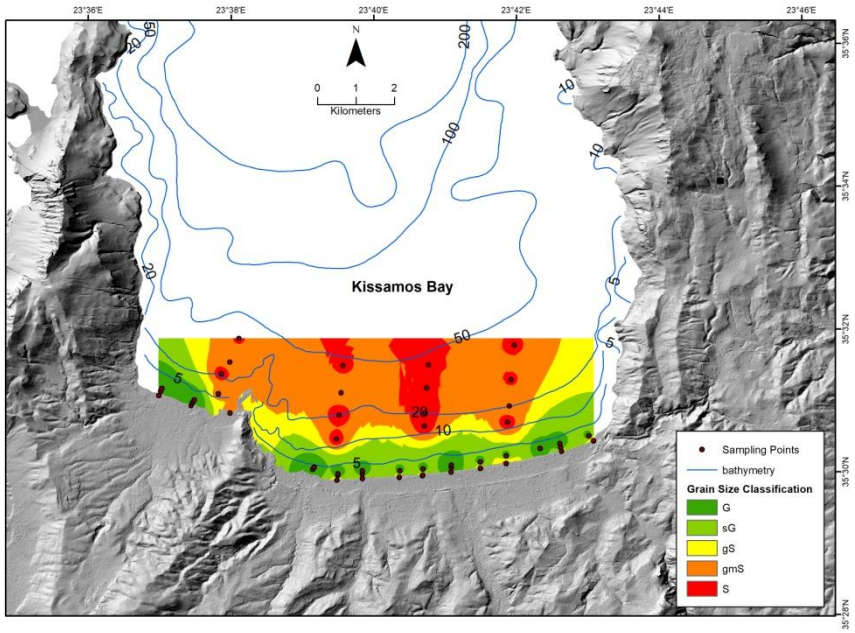

Figure 5.29. Spatial distribution pattern of the granulometric types of the offshore samples in Kissamos Bay. Depth contours in blue color.

According to the grain size statistical parameters regarding Kissamos Bay, the surficial sediment are moderately well sorted, coinciding with the areas with higher sand content, while poorly sorted sediments were found in muddy beds in larger water depths and towards the eastern part of the Bay. Poor sorting indicates that the sediments were transported

for relatively short distances from their source areas (Ramadan et al., 2019) and/or that are not that reworked. Negative skewness values (excess of coarse material) are observed at shallower depths and positive at deeper areas (excess of finer material); the latter indicates the existence of suspended fine material (Kontopoulos, 2004). Samples are classified from leptokurtic, at the western part of the bay, to mesokurtic at its eastern part. This fact suggests the higher energy environment (Friedman, 1962; Mohtar et al., 2017) at the eastern part of the bay.

Physical characteristics of the sediments

Density values at the area of Kissamos Bay, NW Crete Island vary between 2.53 g/cm^3 to 2.67 g/cm^3 (Fig. 5.30), with the higher values are mostly observed at the central and shallower part of the bay. There is a spatial relation between grain size and density in the area as well as with various mineralogical and geochemical factors at the area. As it is expected, higher sand fraction is positively related to greater density values.

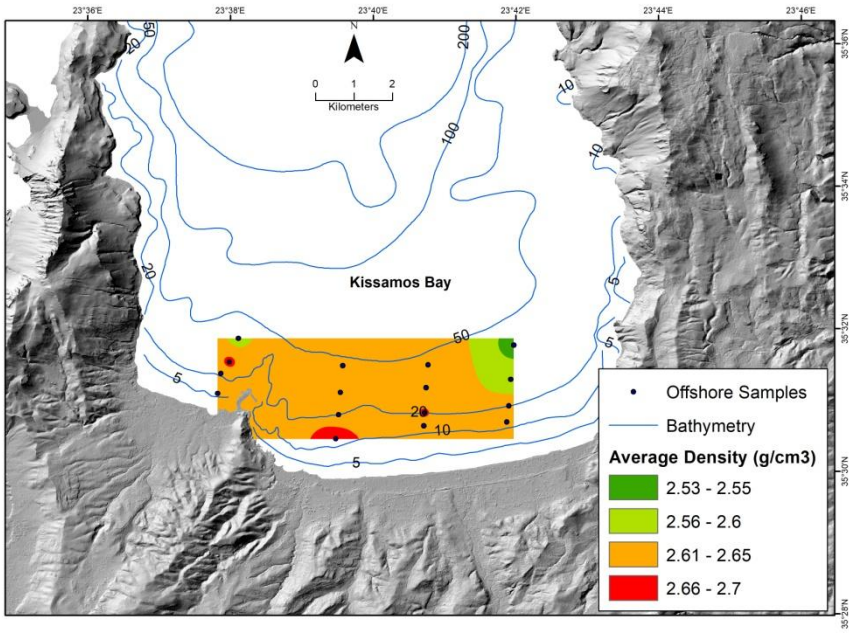

Figure 5.30. Spatial distribution pattern of the density of the surficial sediments offshore Kissamos Bay, NW Crete Island.

Microscopic analysis (Stereo-microscopy/ SEM-EDS)

Stereo- microscopic observations revealed sub-angular quartz grains, rounded calcite grains, sub-rounded feldspar crystals and small amounts of other carbonates and organic material (Anastasatou et al., 2019; Fig. 4.3 a,b,e,f). Quartz grains are mostly transparent and brownish. Moreover, samples from greater depths (Fig. 4.3c, d, g, h) contain clearly more fine - grained material, greater amounts of carbonates and organic material.

SEM/EDS analysis revealed the degree of the sediments' grains corrosion, which is greater in carbonate minerals. However, SEM-EDS analysis identified various siliceous in various degrees of preservation (Anastasatou et al., 2019), such as those presented in Figure 4.16 (a quartz grain with preserved facets) and in Figure 4.17 (same sample KIS-1A) displaying a highly eroded quartz grain. Furthermore, siliceous and calcareous shells were detected, such as radiolarian and foraminifera, bivalves and gastropods (Anastasatou et al., 2019). Moreover, analysis revealed various grains of metal oxides such as Fe, Cu, Cr, Ni, Zn and Mn (e.g. Fig. 4.18; Anastasatou et al., 2019). Based on geological and textural characteristics, it is suggested that quartz grains are mostly derived from the phyllite - quartzite series.

Mineralogy - XRD

The mineralogical analysis of the surficial sediments of Kissamos Bay, NW Crete Island revealed that quartz is the dominant mineral throughout the study area (Table 4.11). Albite is a trace/minor mineral, however increases its' content at the shallow central part of the study area (Fig. 5.31a). Albite' spatial distribution is positively related with density. Calcite occurs as mineral of medium content at the deeper western part and as trace to medium/trace mineral in the remaining study area (Fig. 5.31b). Spatial distribution pattern of calcite is correlated with those of magnesian calcite and aragonite (Fig. 5.31b, c, e; Annex IV, Tables IV.2), showing enrichment at the western part of the bay; that is mostly attributed to the abundance of marine shells (Fig. 5.31d, e; Anastasatou et al., 2019). Smectite and chlorite group minerals are absent at the western part of the bay and occur as trace minerals at the central and part of the study area (Fig. 5.31f, g).

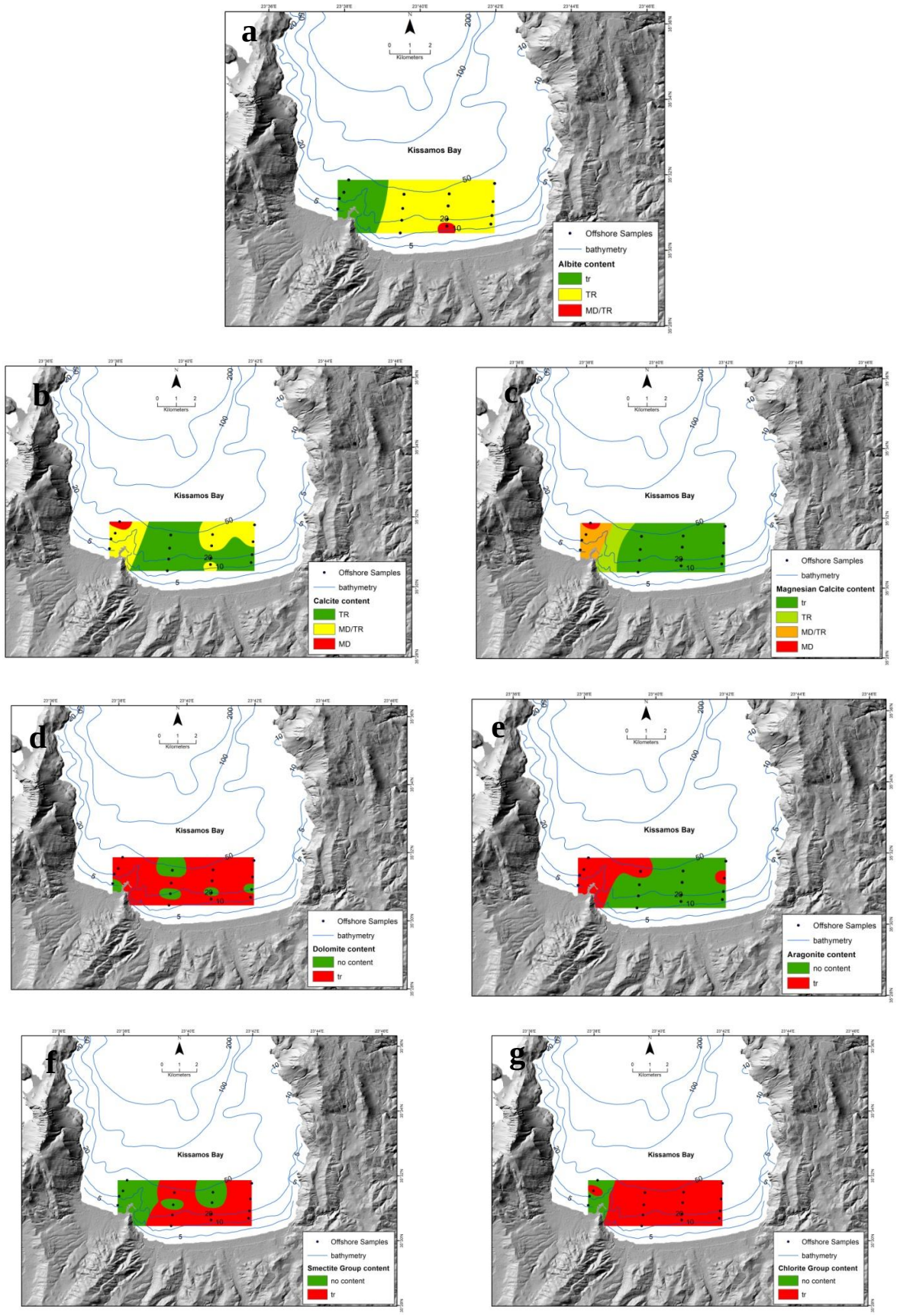

Figure 5.31. Abundance and spatial distribution of: (a) albite, (b) calcite, (c) magnesian calcite, (d) dolomite, (e) aragonite, (f) smectite group minerals and (g) chlorite group minerals of the surficial sediment samples of Kissamos Bay, NW Crete Island (MJ: major, MD: medium, TR: trace). Depth contours in blue color.

Geochemistry

Chemical analysis of the major elements from the surficial sediments of Kissamos Bay, NW Crete Island revealed that SiO_2 content varies significantly between ~30% and70% and display higher values at the central and eastern part of the bay in water depths <35 m (Annex III – Chemical Analysis). SiO_2 distribution pattern displays a similar picture with grain size pattern, as coarser material is associated with increased SiO_2 presence (Fig. 5.32a). Al_2O_3 content presents low values at the eastern and shallow central/western parts of the bay (Fig. 5.32b). Fe_2O_3 content, also, increases eastwards and towards deeper depths (Fig. 5.32c) and having a similar pattern with Al_2O_3 indicates their correlation with iron-rich clay minerals. CaO content increases at the deeper part of the eastern bay area (Fig. 5.32d) being positively related with calcite, magnesian calcite and aragonite distribution patterns. K_2O content increases eastwards and at greater depths (Fig. 5.32e), similar to Fe_2O_3 and Al_2O_3. SO_3 is below 1% throughout the area, apart from the deeper western area (Annex III – Chemical Analysis), where values are >1%. SO_3 content is attributed to the onshore presence of gypsum (Stamatakis et al., 2015), which was not detected by XRD-mineralogical analysis, probably due to <1% content.

Chemical analysis of the trace elements from the surficial sediments of Kissamos Bay, revealed that Ba, Br, Ce, Cr, Cu, La, Nd, Pb, V and Zn (Fig. 5.33-34) are correlated (Annex IV, Tables IV.2) and display similar distribution patterns, as their content increase eastwards and at greater depths. Moreover, their pattern present similarities with Al_2O_3, Fe_2O_3 and K_2O patterns; suggesting their relation to aluminosilicate minerals. As and Mn display relatively enriched content at the shallow and central part of the bay (Fig. 5.33-34), with their distribution patterns correlated with density pattern and higher sand content.

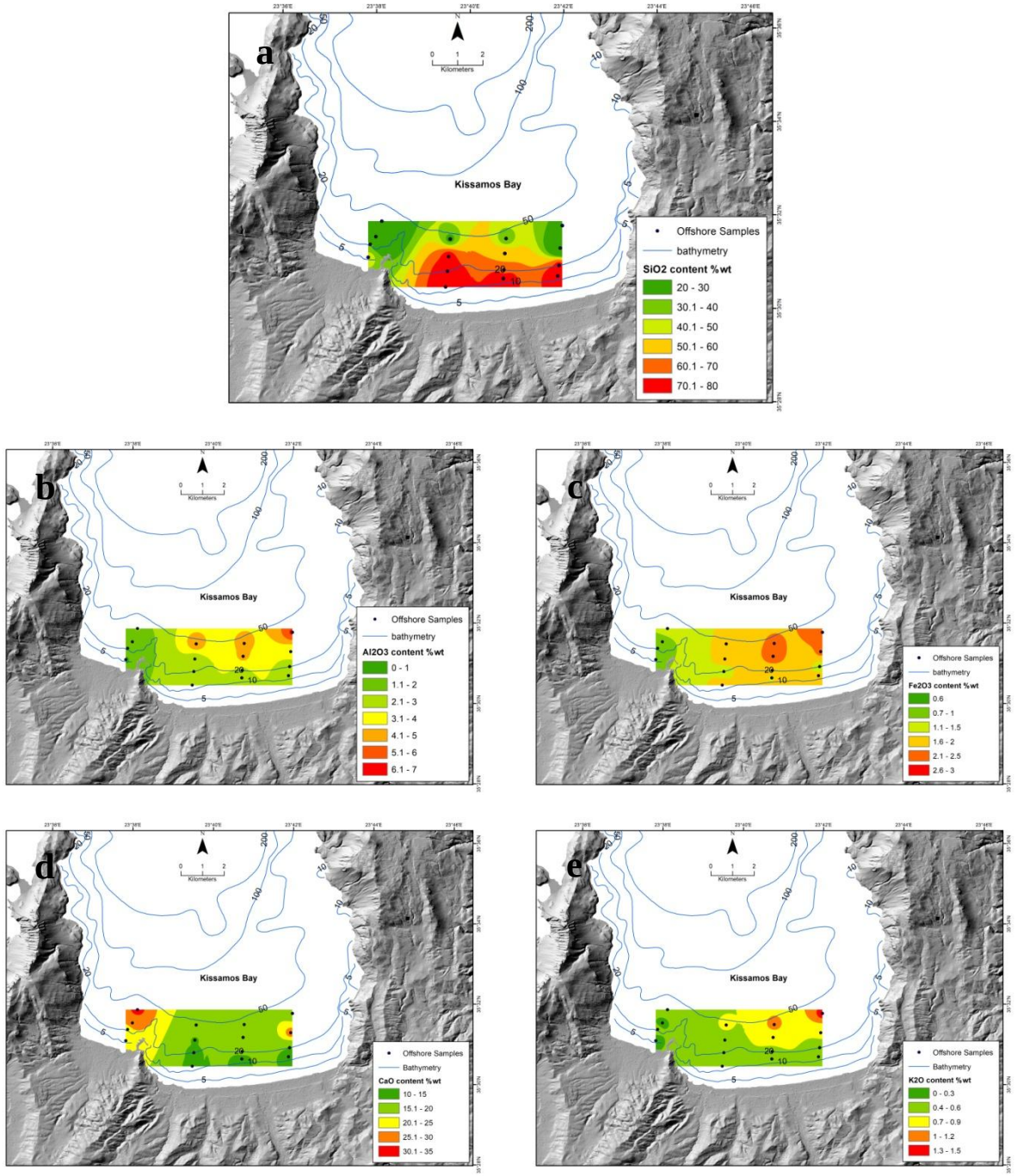

Figure 5.32. Spatial distribution patterns of major elements (%) in surficial sediment samples offshore Kissamos Bay, NW Crete Isl: (a) SiO_2, (b) Al_2O_3, (c) Fe_2O_3, (d) CaO and (e) K_2O. Depth contours in blue color.

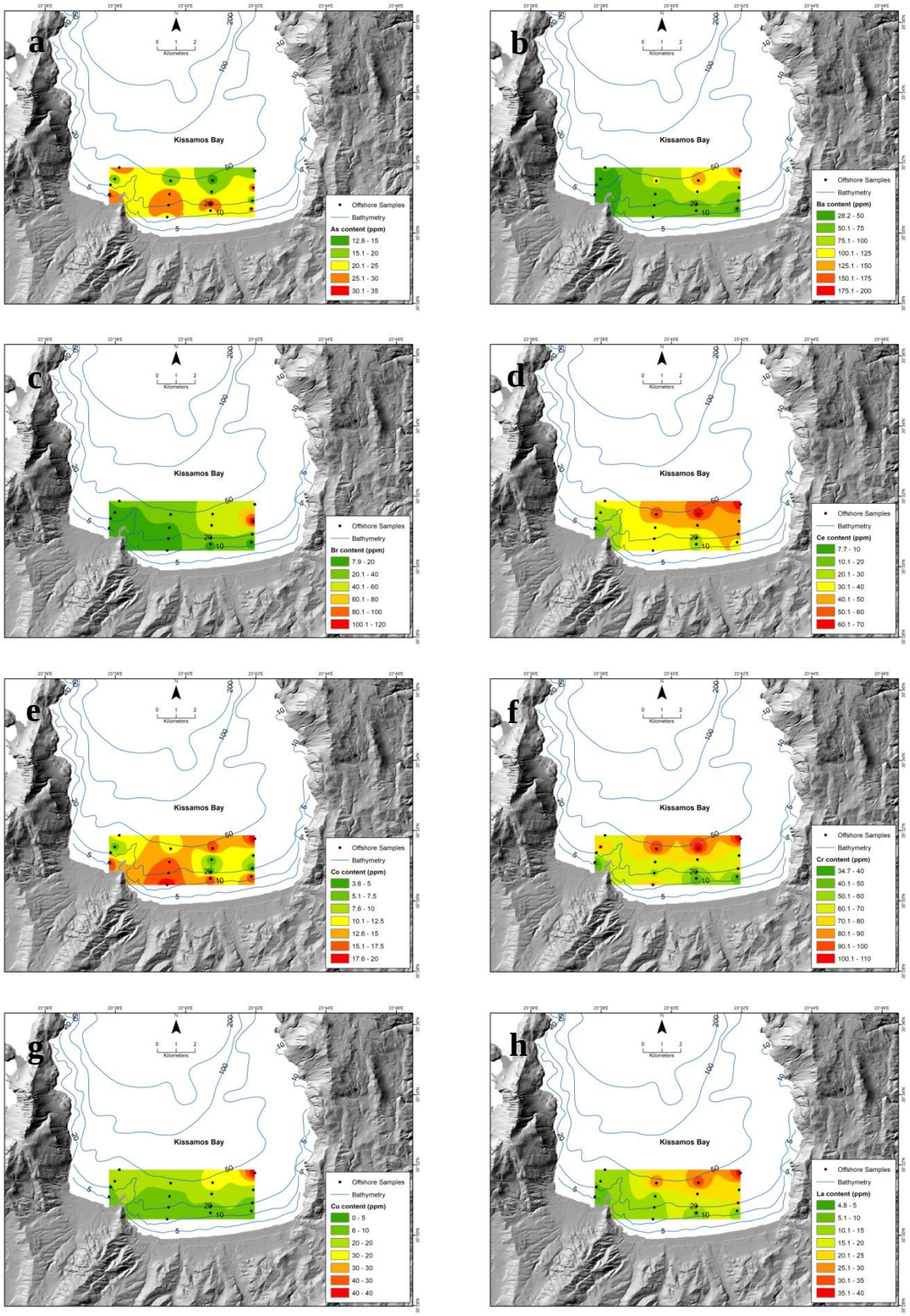

Figure 5.33. Spatial distribution patterns of trace elements (ppm) in surficial sediment samples offshore Kissamos Bay, NW Crete Island: (a) As, (b) Ba, (c) Br, (d) Ce, (e) Co, (f) Cr, (g) Cu and (h) La. Depth contours in blue color.

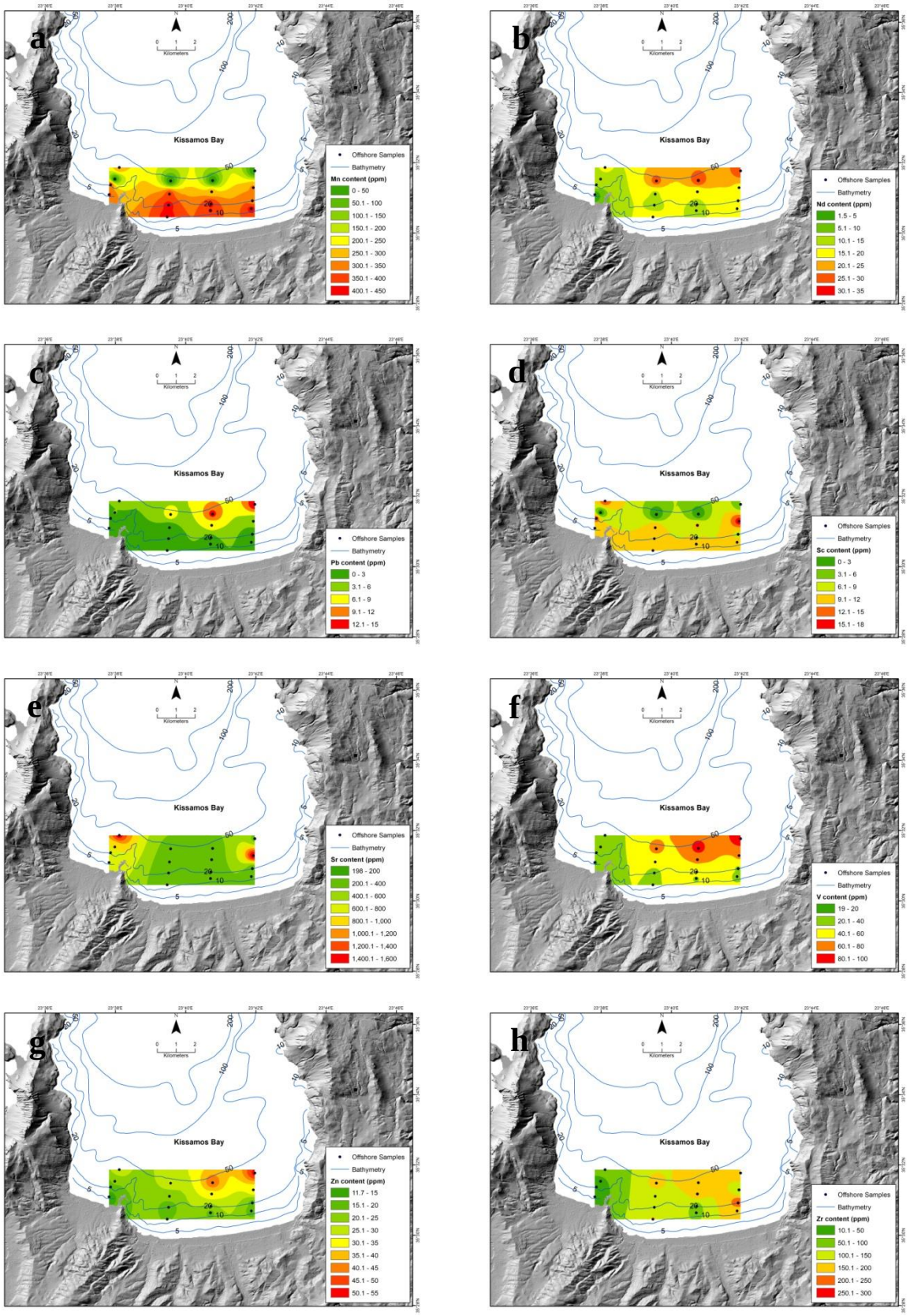

Figure 5.34. Spatial distribution patterns of trace elements (ppm) in surficial sediment samples offshore Kissamos Bay, NW Crete Island: (a) Mn, (b) Nd, (c) Pb, (d) Sc, (e) Sr, (f) V, (g) Zn and (h) Zr. Depth contours in blue color.

Potential of the area of Kissamos Bay, NW Crete Island to host marine aggregates deposits for uses in the construction industry

The aforementioned physical, mineralogical and geochemical characteristics designate various potential sub-areas for MA dredging in the case of Kissamos Bay (Fig. 5.35). The critical factors that arise from the physical, mineralogical and geochemical characteristics of the offshore area of Kissamos Bay according the corresponding sampling are:

- Determination of a sub-area, whereas grain fraction is coarser than sand.
- Quartz content is uniform throughout the study area, however SiO_2 content varies greatly. Therefore according to SiO_2 content, a sub-area with SiO_2 content above 70% was identified,
- According to Fe_2O_3 content, the study area was limited to a sub-area with Fe_2O_3 content below 2%, as required from various European and national restrictions (§1.4).
- According to CaO content, also as SiO_2, a sub-area created with CaO content below 25%.
- A sub-area of SO_3 content below 1% content below 1%, as required from various European and national restrictions (§1.4) was identified.
- Calcite and magnesian calcite content created two sub-areas whereas their mineralogical content is below medium content.

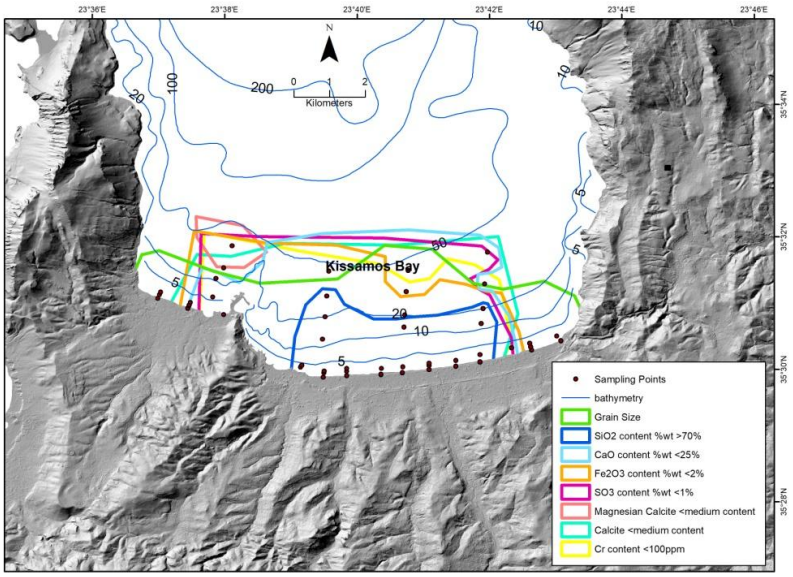

Figure 5.35. Shaded onshore relief map with the restricted area of Kissamos Bay, NW Crete Island according grain size, calcite, magnesian calcite, SiO_2, CaO, SO_3, Fe_2O_3 and Cr content.

As mentioned in §5.1.1, no national restrictions apply regarding the required distance that any dredging activities should comply with. Therefore, according to the National Regulation for Mining and Quarrying activities (2011) and to the "Framework for safety in the offshore hydrocarbon exploration and exploitation activities" (2016), which incorporated the European Directive 13/30/EU, a minimum distance of 500m from the coastline is introduced (Fig. 5.36), with respect to the touristic and inhabited coastal area.

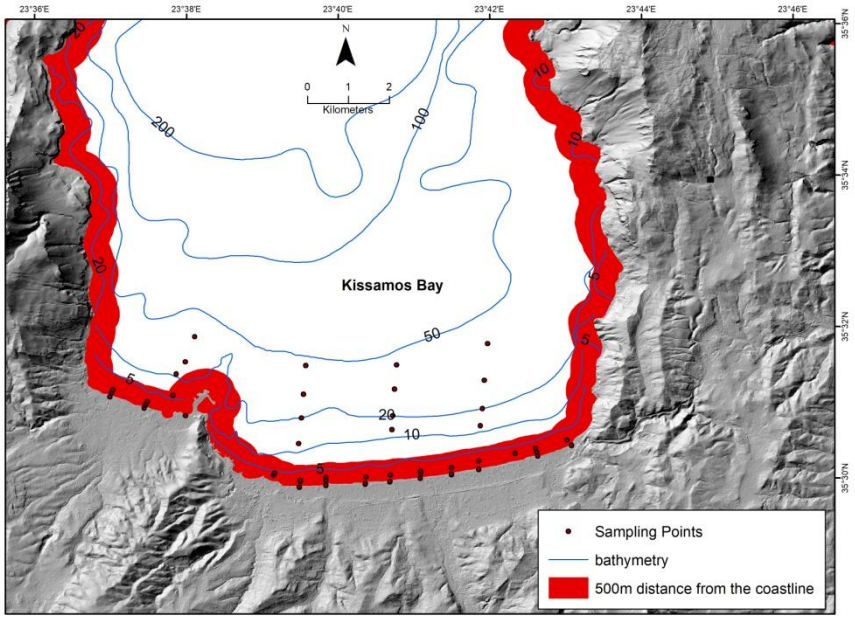

Figure 5.36. Shaded onshore relief map with the restricted offshore area of 500 m distance from the coastline, Kissamos Bay, NW Crete Island.

According to Athanassoulis and Skarsoulis (1992), and Hallermeier's (1978, 1981), equation for maximum closure depth for the offshore area of SE Evia Island is estimated to be at water depths of 10-12 m (Fig. 5.37).

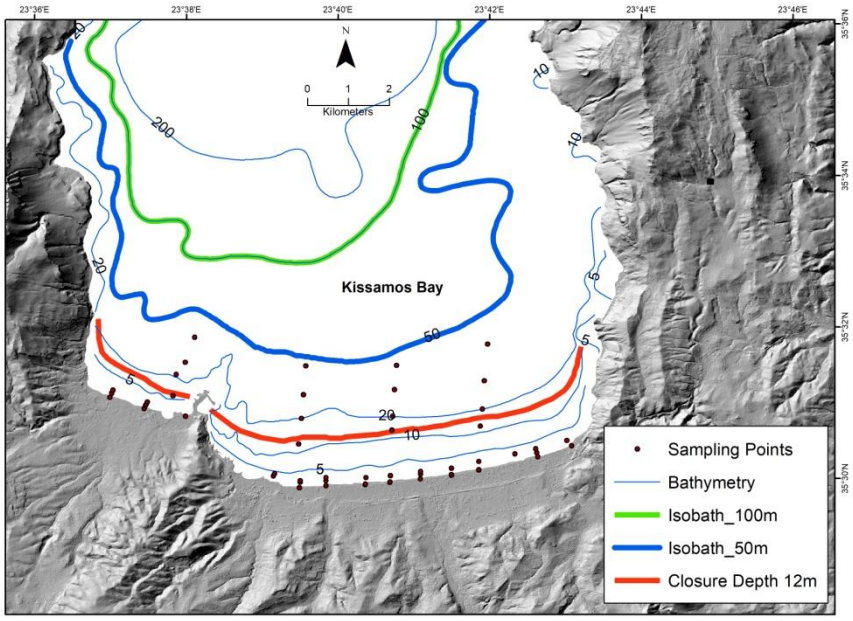

Figure 5.37. Shaded onshore relief map with the restrictions of closure depth in 12 m distance from the coastline, Kissamos Bay, NW Crete Island.

In the wider offshore area of Kissamos Bay, a Natura2000 Site (GR4340001) is located "IMERI KAI AGRIA GRAMVOUSSA - TIGANI KAI FALASARNA - PONTIKONISI, ORMOS LIVADI - VIGLIA" is located. This area hosts meadows of the protected species *Posidonia oceanica* (1120 Natura Habitat Code), as shown in Figure 5.38. Hence, a 300 m buffer zone is applied (Fig. 5.38), for the restriction for any dredging activity.

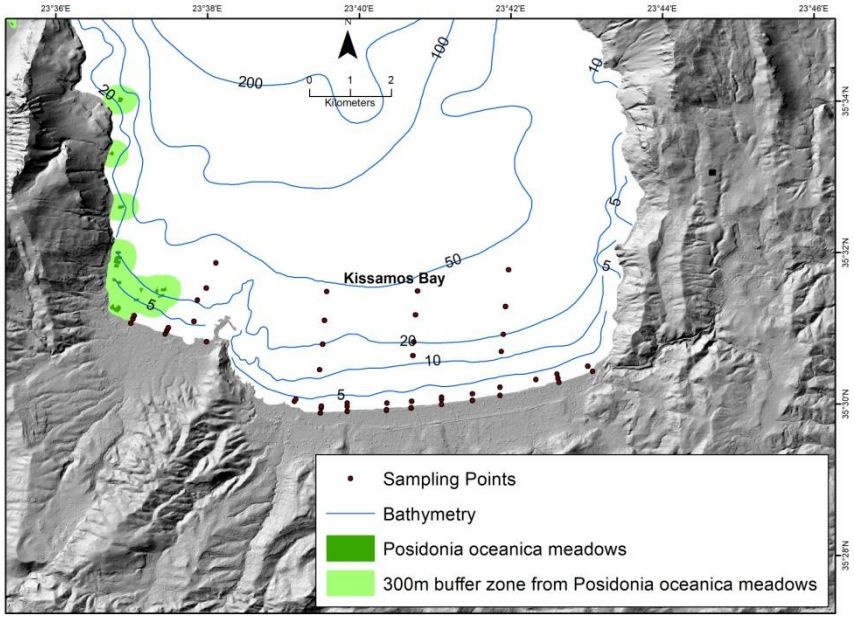

Figure 5.38. Shaded onshore relief map with the restrictions of Posidonia oceanic meadows with 300 m buffer zone, Kissamos Bay, NW Crete Island.

Anastasatou et al. (2019) have studied the offshore area of Kissamos Bay, NW Crete regarding the existence of any marine aggregates deposits in the wider area. Bathymetric and geophysical survey was conducted in order to locate and quantify the dimensions of the potential deposit, whilst benthic analysis of the sediments was carried out in order to determine its environmental status (Anastasatou et al., 2019). The interpretation of the geophysical records revealed an area of ~19 km^2 between the 10 and 150 m isobaths, consisting of relatively coarse-grained sediments, whose greater thickness is 7 m and it is found along the shallower part of the coastal area (Fig. 5.39). Moreover, benthic analysis revealed the absence of sensitive and/or protected macrofauna species, such as *Posidonia oceanica* meadows or *Cymodocea nodosa* (Anastasatou et al., 2019).

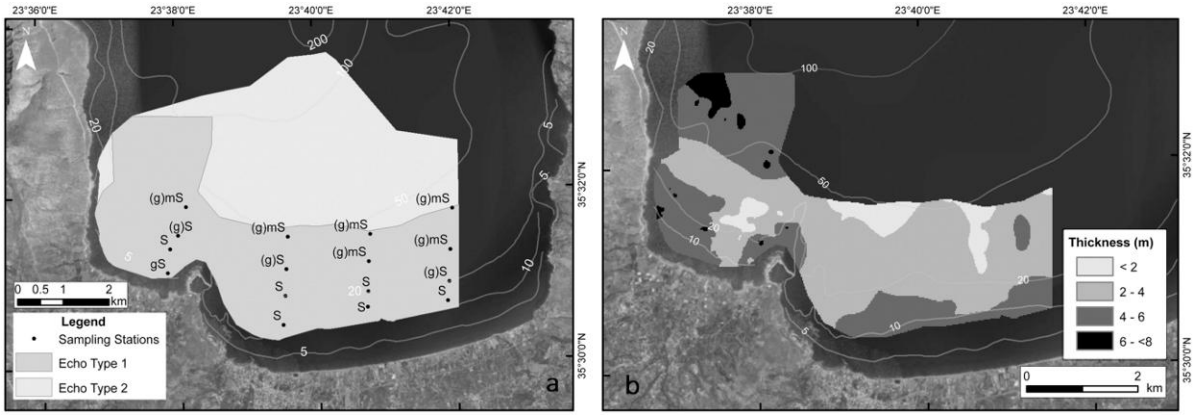

Figure 5.39. Echo Types distribution map (left) and thickness of the coarse-sediment marine aggregates' deposit (right) from Anastasatou et al., 2019.

Taking into consideration the aforementioned, the offshore area of Kissamos Bay, hosts a marine aggregates deposit, up to the water-depth of 50m, that covers 4.85 km^2 (Fig. 5.40).

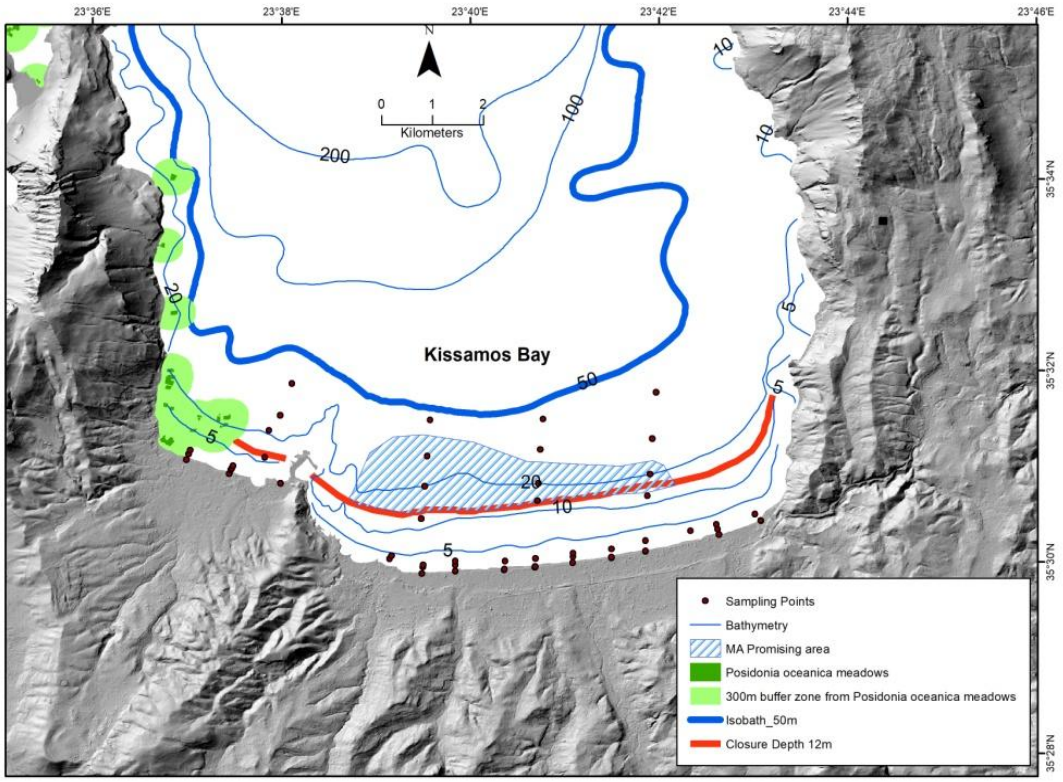

Figure 5.40. Shaded onshore relief map showing the promising offshore area with Marine Aggregates deposits of good quality shallower than water depths of 50 m, Kissamos Bay, NW Crete Island.

The offshore area of Sfinari Bay, west Crete Island revealed material that display high qualitative characteristics for uses into the construction industry. Therefore, this area is highly proposed to be further investigated as probably hosts MA deposits suitable for the construction industry.

5.1.2.2. Sfinari Bay

The interpretation of the results from the analysis of the obtained coastal and offshore surficial samples of Sfinari Bay, west Crete Island (Fig. 3. 10; 3.30) is developed below. However, due to limited offshore sampling, no spatial distribution maps are presented.

Grain size

The studied offshore area of Sfinari Bay revealed that the main trend of the grain size is sand (Fig. 5.27). Sand content is ≥99% (Annex II-Grain Size Analysis) in water depths between ~8m and 32.5m. This fact implies similar sand content in greater depths and perhaps the existence of modern and relict sand deposits. Grain size statistical parameters revealed that sediments are moderately well sorted, indicative of areas with higher sand content (e.g. Ramadan et al., 2019). Skewness degree is near symmetrical and sediments switch from leptokurtic to mesokurtic as depth increases.

Physical characteristics of the sediments - Microscopic analysis (Stereo-microscopy/ SEM-EDS)

In Sfinari Bay, density values of surficial sediment generally decrease as depth increases; this fact is related with the sand content of samples, as higher sand content is related to higher density values (Table 4.7; Annex II-Grain Size Analysis).

According to stereoscopic macroscope observations Sfinari samples (Fig. 4.3i, j) contain great amount of quartz grains, a few round calcite grains and minor clay grains. Notably, fine fraction is absent in both shallow and deeper surficial sediments, revealing the well sorting degree, most probably due to high wave activity, which denotes high compositional maturity of the deposit (Warrier et al., 2019). This fact is an advantage for any future use of the corresponding material. SEM/EDS analysis at sediments from Sfinari Bay proved the secondary existence of various iron oxides in other mineral grains, such as quartz

(e.g. Fig. 4.20). Other grains, such calcite (Fig. 4.21) were rarely observed. Quartz grains are derived from the onshore phyllite - quartzite formations.

Mineralogy - XRD

Mineralogical analysis of the surficial sediments of Sfinari Bay showed that quartz is the dominant mineral (Table 4.11), while other and equally distributed minerals of minor content, such as calcite, magnesian calcite and clay minerals (i.e. illite, smectite and chlorite group minerals) were detected.

Geochemistry

Chemical analysis of the major elements from the surficial sediments of Sfinari Bay, revealed that SiO_2 content is ~80% through the study area (Fig. 4.63; Annex III – Chemical Analysis). CaO content is ~7%, Fe_2O_3 <1%, SO_3 ~0.1% and Al_2O_3 <1% (Fig. 4.64; Annex III – Chemical Analysis). Regarding trace minerals analysis, Zr displays quite enriched values (~200-370ppm) and is related to high SiO_2 content. Sr displays values of ~280 – 350 ppm that are correlated to CaO content (Annex IV, Tables IV.2). Ce (~30-50ppm) and La (~20=30ppm) content is related to phyllite-quartzite series.

The overall, chemical analysis of major and trace elements from the offshore surficial sediments from Sfinari Bay revealed the existence of a promising MA deposit with no impurities.

Potential of the area of Sfinari Bay, west Crete Island to host marine aggregates deposits for uses in the construction industry

The above physical, mineralogical and geochemical characteristics determine high qualitative material for uses into the construction industry. The critical factors that determine these great qualitative characteristics, according the corresponding though limited sampling, are:

- Grain size data defined the existence of well sorted and mature sand.
- Quartz content is uniform and high throughout the study area and other minerals only exist as trace crystalline phases
- SiO_2 content is ~80%

- According to Fe_2O_3, the display content below 2%, as required from various European and national restrictions (§1.4).
- CaO content also is below 7%.
- SO_3 content is below 1%, as required from various European and national restrictions (§1.4).

Therefore, the limited offshore sampling in the offshore area of Sfinari Bay, west Crete revealed an area with promising qualitative characteristics and further in-situ investigation may reveal potential marine aggregates deposits.

5.1.3. Southern and eastern Lesvos Island

The three offshore study areas of Lesvos Island are located at the SW (Eresos), south (Vatera) and eastern (Mytilene Strait) part of the island. The coastal geomorphology of these areas is mainly controlled by the high erosional rate of the adjacent to coastline volcanic rocks, which cover the majority of the island's coast (Hasiotis et al., 2020). The wider coastal area of the island is tideless (Tsimplis, 1994) and the overall sediment supply is constrained as the drainage system is ephemeral. Hasiotis et al., (2020) investigated the three areas using a bathymetric, geophysical and sedimentological dataset and studied the coarse-grained deposits of the areas, however, under the context of their potential to be used for nourishment purposes. Thus, mainly the grain-size distribution and preliminary results of XRD analysis were evaluated and the prioritization of their potential to serve as marine aggregates was also based in various local spatial planning issues (*Posidonia oceanica* distribution, human activities, appropriate port distance etc). Therefore, some of the results / considerations mentioned below stem from that study.

In Eresos Bay, the main volume of the sediment supply is derived from Chalandras river, which is dammed (Velegrakis et al., 2008; Chatzipavlis et al., 2012). According to Hasiotis et al. (2020), in Eresos relatively steep slopes prevail (up to 20%) at water depths between 12-35m and at distance of ~600m from the coastline. At the eastern part of Eresos Bay and deeper than the 35m isobath, the slope gradients decrease (Hasiotis et al., 2020). In Vatera Bay, at water depths up to 100m small slopes prevail (<8%) which eastwards increase slightly and deeper than 100m steep slopes dominate (>50%) (Hasiotis et al., 2020). Furthemore, according to Hasiotis et al. (2020), a shipwreck was detected in the eastern part

of Vatera Bay at water depths ~25m, fact that might disturb marine aggregates distribution. Two small and ephemeral streams are located at the coastal area of Vatera. Mytilene Strait can be divided into two parts; the north and the south. At the southern part the 30m isobath, which is the mean deeper limit of *Posidonia oceanica*, is ~1.5 km off the coastline, while in the northens this isobaths appears closer. Along the entire study area of Mytilene Strait very small slopes are observed, particularly deeper than 30 m slope is approximately < 2.8 % (Hasiotis et. al, 2020).

The coastal part of the study areas (Fig. 5.41), Eresos, Vatera and Mytilene Strait offshore area, consists of the following geological formations: volcanic tuffs and lavas (i.e., Eresos Formation, the Miocene Polychnitos Ignimbrite, Mytilene volcanic formation) and ophiolites and metamorphic rocks, such as schists, phylites, greywacke and marbles (Kelepertzis and Velitzelos, 1992; Voudouris et al., 2019; Hasiotis at al., 2020). According to Hasiotis et el. (2020), during Holocene sea-level rise, the coastline of the eastern part of the island was flooded, leaving coarse-grained sediments further offshore and therefore, it is expected that the adjacent offshore areas might host potential marine aggregates deposits, that are left behind transgression procedure.

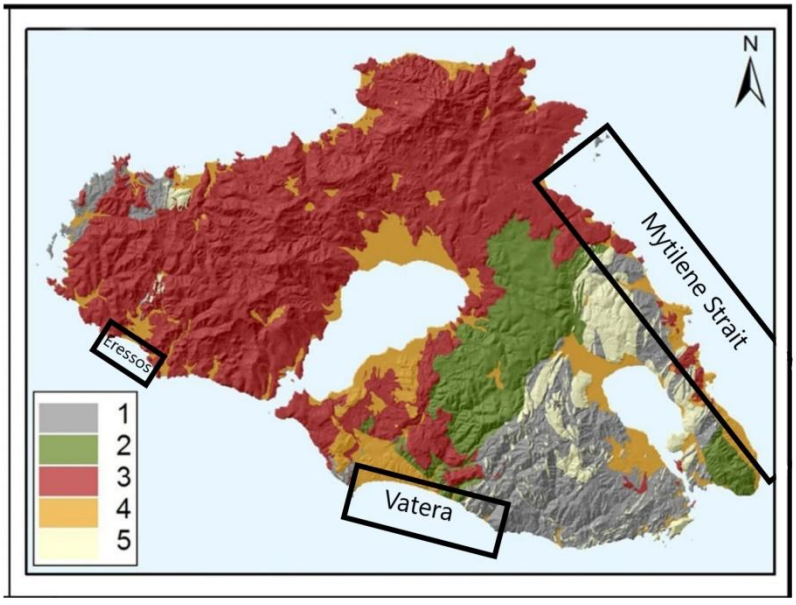

Figure 5.41. Map modified from Hasiotis el al., 2020, of general geology of Lesvos Island; 1: schists and phyllites; 2: peridotites; 3: basalts, ignimbrites, volcanic material; 4: Quaternary deposits; 5: marbles and limestones.

The interpretation of the results from the analysis of the obtained offshore surficial samples from the southern and eastern Lesvos Island (Fig. 5.42) is developed below.

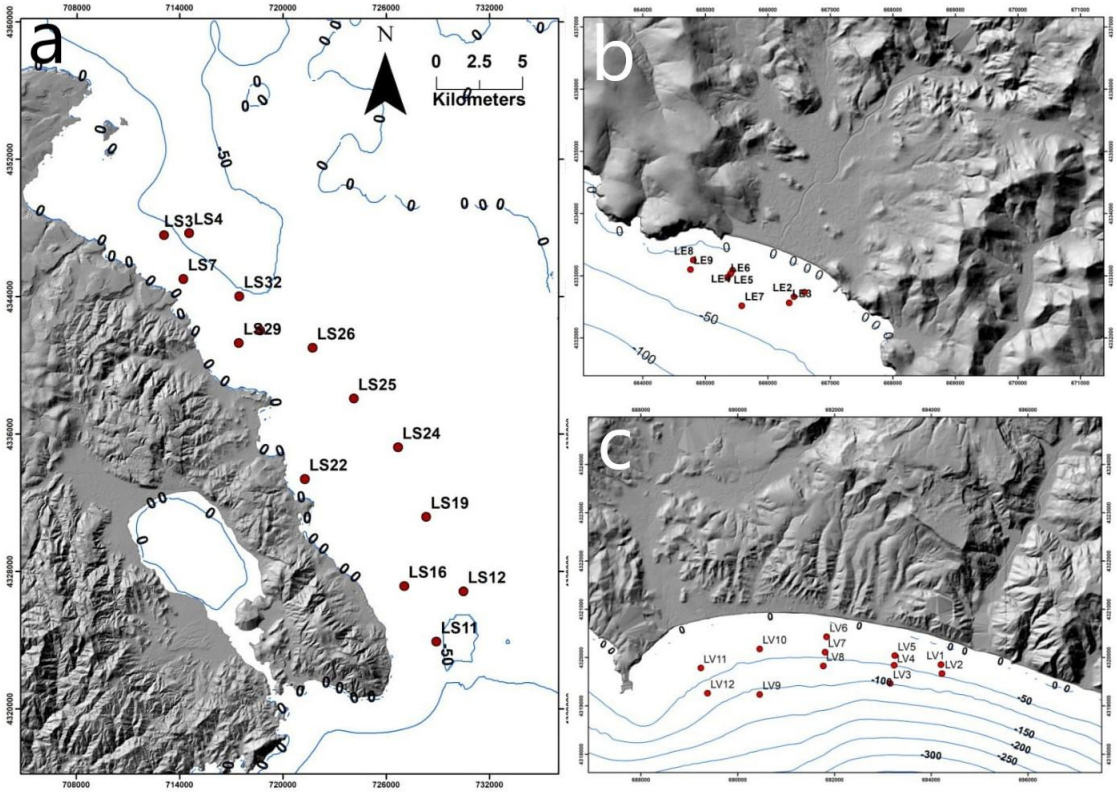

Figure 5.42. Shaded onshore relief map and general bathymetry including the sampling points of the offshore study areas of (a) Mytinene Strait, (b) Eresos and (c) Vatera. Depth contours in blue color.

5.1.3.1. Eresos area

Grain size

The studied offshore area of Eresos Bay revealed (Fig. 5.43) three sedimentary classes according to Folk's (1980) classification: i) gravelly Sand (gS), ii) gravelly muddy Sand (gmS) and iii) Sand (S) with sand content >80%. Moreover, coarse sand fraction > 50% was located at water depths of 18 - 30m mixed with Posidonia leaves/roots (Hasiotis et al., 2020; Fig. 5.44). Sample LE7, which is located at higher depth than the others contain 81.8% sand and 17.6% silt fraction (Annex II-Grain Size Analysis). Gravel fraction is observed in water depths between 43.5m and 47m. According to Hasiotis et al. (2020), the seismic profiles verified the presence of sandy material locally with shells and/ or shell fragments in Eresos

and furthermore, the structure and location of the marine sediment in Eresos suggest that they might constitute relict sands trapped offshore during the Holocene transgression.

The grain size analysis of the statistical parameters (Annex II-Grain Size Analysis) revealed that all offshore sediments from Eresos area are moderately to moderately well sorted. Well sorting indicates that the sediments are quite reworked (Ramadan et al., 2019). Coarse skewed sediments are observed in shallower depth and at the eastern part of Eresos study area. Regarding kyrtosis, no specific pattern was identified and samples are classified from leptokurtic to platykurtic with the excpetion of the eastern part of Eresos bay where they are classified as mesokurtic, suggesting a more energetic environent (Friedman, 1962; Mohtar et al., 2017).

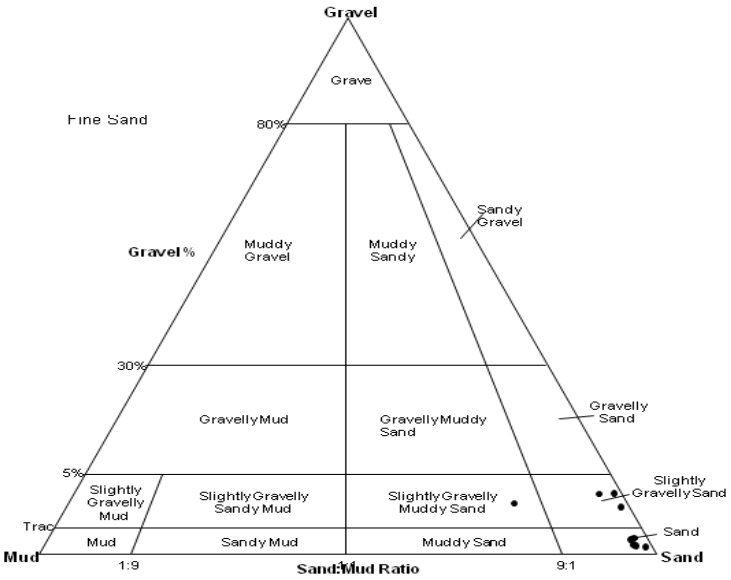

Figure 5.43. Grain-size classification of the surficial sea-bottom sediment samples collected offshore Eresos area, southern Lesvos Island, according to the Folk (1980).

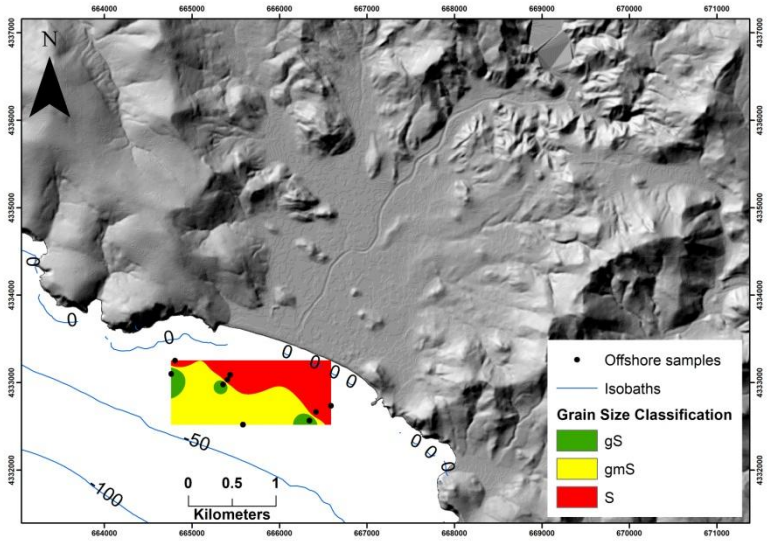

Figure 5.44. Spatial distribution pattern of the granulometric types of the offshore samples in Eresos area, southern Lesvos Island. Depth contours in blue color.

Physical characteristics of the sediments

Density values at the area off Eresos bay vary between 2.6 and 2.70 g/cm^3 (Fig. 5.45) with the higher values mostly observed at the western sector of the study area, whereas also coarse fraction occurs.

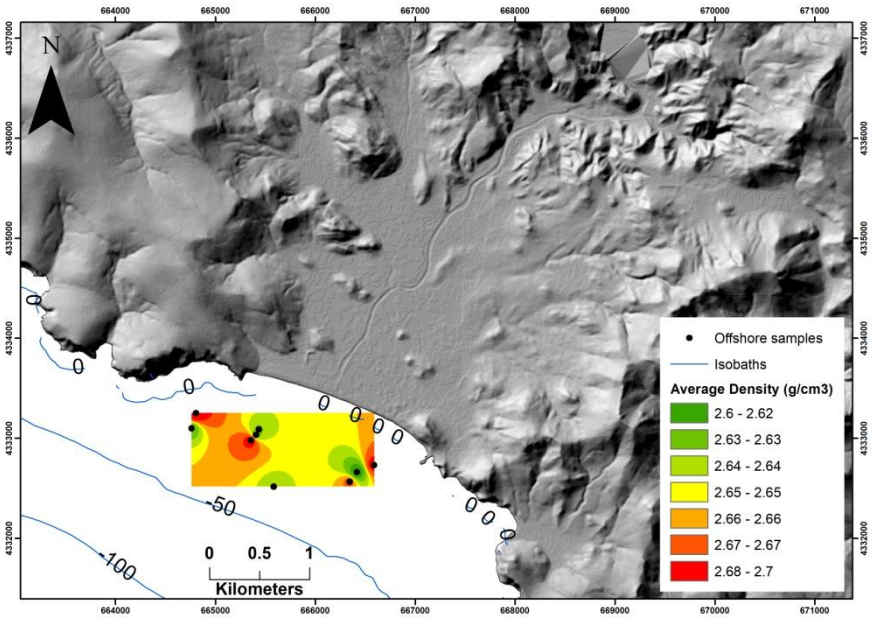

Figure 5.45. Spatial distribution of the density in surficial sediments offshore Eresos area, southern Lesvos Island. Depth contours in blue color.

Microscopic analysis (Stereo-microscopy/ SEM-EDS)

The stereoscopic microscope analysis of the surficial sediments off Eresos area, revealed the presence of sub-angular quartz grains, feldspars (Fig. 4.4a - d) and mafic minerals (Fig. 4b), which are also observed at SEM/EDS analysis (Fig. 4.22). Moreover, the absence of clayey material is discrete, which coincides with grain size analysis. SEM/EDS analysis revealed oxides of heavy metals lying on eroded grains, such as Pb-oxides that are detected on an albite grain (Fig. 4.23).

Mineralogy - XRD

The mineralogical analysis of the surficial sediments off Eresos area revealed that albite is the dominant mineral throughout the area (Table 4.12). Quartz is the second most significant crystalline phase, especially in shallower depths, with medium content eastwards that decline western wards (Hasiotis et al., 2020; Fig. 5.46a). Quartz's higher content is related with higher sand content. Calcite's trace content is observed at the deeper – eastern part of the area (Fig. 5.46b). Other minerals, such as potassium feldspars, mafic minerals and amphiboles were recognized in minor amounts (Table 4.12; Hasiotis et al., 2020). The findings of the present mineralogical study are similar to those given for the beach material by Velegrakis et al. (2008). The quartz, plagioclase, edenite and biotite content is related to Eresos Formation, which consists of coarse-grained andesite with hornblende and biotite phenocrysts (Pe-Piper and Piper, 1993; Hasiotis et al., 2020).

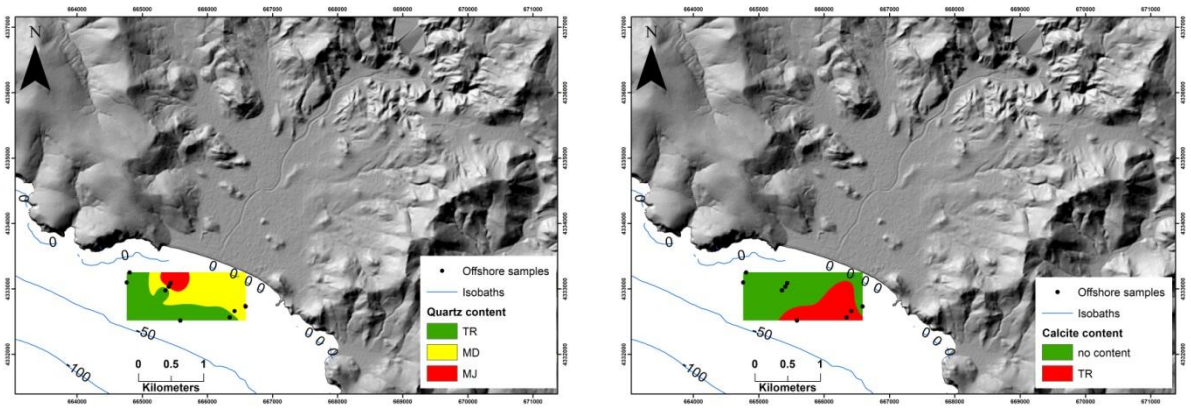

Figure 5.46. Abundance and spatial distribution of: (a) quartz and (b) albite of the surficial sediment samples offshore Eresos area, southern Lesvos Island (MJ: major, MD: medium, TR: trace). Depth contours in blue color.

Carbonates content (Fig. 5.47) is determined in low levels, suggesting the absence of any input from biogenic material. $CaCO_3$ content slightly increases at higher depths.

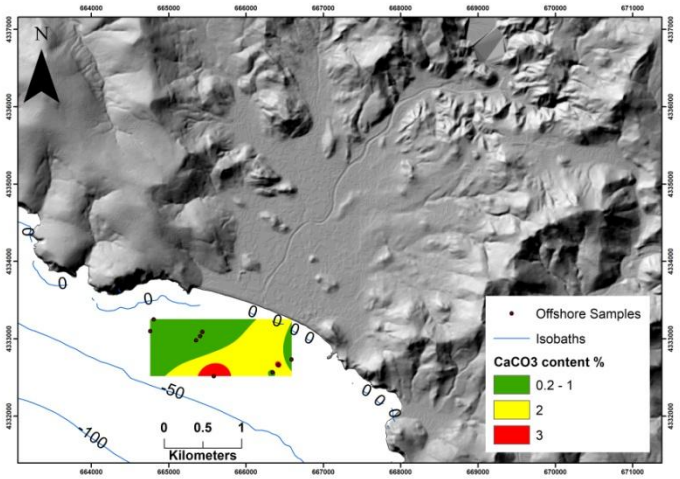

Figure 5.47. Spatial distribution patterns of $CaCO_3$ content % of the surficial sediment samples off Eresos area, southern Lesvos Island. Depth contours in blue color.

Potential of the area off Eresos, south Lesvos Island to host marine aggregates deposits for uses in the construction industry

The above physical, mineralogical and geochemical characteristics arise concerns regarding any future uses of the offshore material in the construction industry. The factors that display advantages and disadvantages are:

- Grain size data defined the existence of moderately to well sorted and mature (reworked) sand to slightly gravelly (muddy) sand. This output is considered as a positive factor.
- Carbonates content is low, suggesting the absence of any input from biogenic material. This factor is, also, considered as a positive one.
- Quartz content is the major crystalline phase; although it is expected that the SiO_2 content would not exceed 60-70%. This factor is considered as a disadvantage.
- From the mineralogical and SEM/EDS analysis, Fe_2O_3 and/ or SO_3 content is expected to exceed the European and national restrictions (§1.4). This factor is also considered disadvantageous.

Therefore, the offshore area of Eresos is hardly expected to host suitable aggregates for any future uses for the construction industry. However, any further chemical analysis would define the ultimate potential of the area.

The study of Hasiotis et al. (2020), found that the marine aggregates deposit covers 1 km^2, denoting a potential volume of 0.5 - $2*10^6$ m^3 that could be mainly for nourishment purposes.

5.1.3.2. Vatera area

Grain size

The offshore study area at Vatera revealed the presence of four sedimentary classes according to Folk's (1980) classification: i) gravelly Sand (gS), ii) gravelly muddy Sand (gmS), iii) Sand (S) and iv) gravelly sandy Mud (gsM) (Fig. 5.48). Grain size analysis revealed that sediments from the eastern part contain higher percentages of sand (58.28% - 70.37%) than these from the western part (36.8% - 67.97%). Respectively, mud fraction content is higher at the western part of Vatera area (29.89% - 53.5%) and lower at the eastern part (26.78% - 33.63%). Coarse fraction varies between 0.23% and 4.24%. At the central and shallow part of the area *Posidonia oceanica* was identified (Fig. 5.49). Acoustic data interpretation of the area confirmed the existence of dense *Posidonia oceanica* meadows growing over sandy beds (Hasiotis et al., 2020).

The grain size analysis of the statistical parameters revealed that all offshore sediments from Vatera area are poorly sorted (Annex II-Grain Size Analysis). This fact suggests that sediments were transported for relatively short distances from their source areas (Ramadan et al., 2019) and/or that have not been hydrodynamically reworked. Fine skewed sediments were observed at the eastern part of the area and strongly fine skewed sediments at the western part (Annex II-Grain Size Analysis). This change in skewness implies the existence of fine material or sediment winnowing (Friedman, 1961; Duane, 1964; Dora et al., 2011). Samples are classified from leptokurtic to very leptokurtic, suggesting the low energy environment that exists in the area (Friedman, 1962; Mohtar et al., 2017).

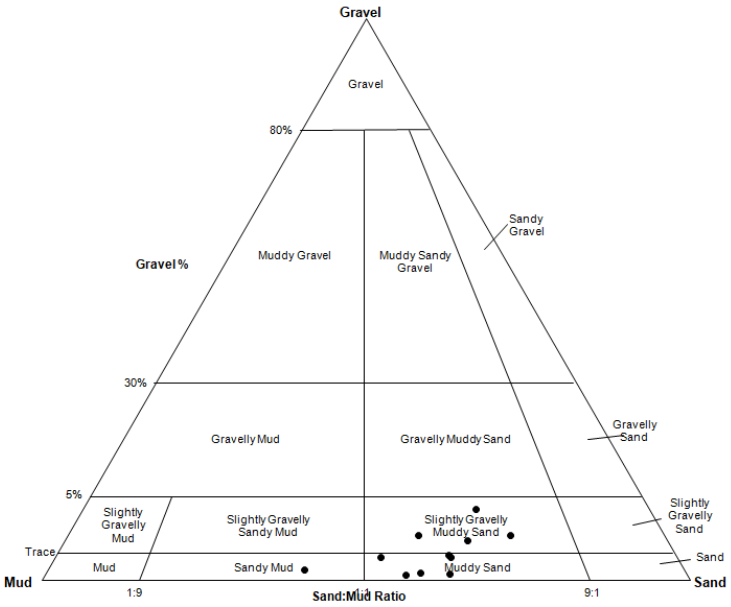

Figure 5.48. Grain-size classification of the surficial sea-bottom sediment samples collected offshore Vatera area, southern Lesvos Island, according to the Folk (1980).

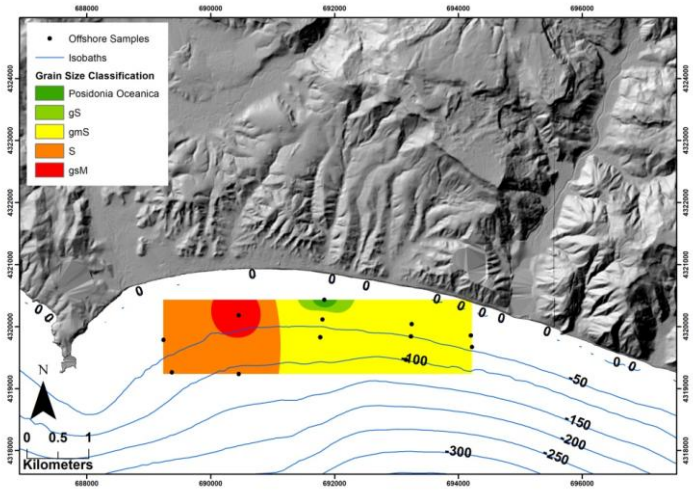

Figure 5.49. Spatial distribution pattern of the granulometric types of the offshore samples from Vatera area, southern Lesvos Island. Depth contours in blue color.

Physical characteristics of the sediments

The textural analysis of the surficial sediments off Vatera area revealed abundance of clayey material (Fig. 4.4e, f), while microscopy revealed significant amounts of carbonates and organic material. Overall, sediments from Vatera area are poorly sorted.

Mineralogy

The mineralogical analysis of the surficial sediments off Vatera area revealed quartz as the dominant crystalline phase and albite as a mineral of medium content (Table 4.13). Potassium feldspars reveals only trace amounts at the western part of the area (Fig. 5.50a), while talc displays trace amounts at the eastern part of the study area (Fig. 5.50c). Serpentine group minerals (Fig. 5.50b), edenite, illite/muscovite and chlorite group minerals are also observed in trace amounts (Table 4.13).

There is a clear difference regarding the prevailing mineralogical phases between Eresos and Vatera area, even though they are adjacent. This fact indicates their diverse origin. Mineralogy of Vatera area is associated with the Pre-Miocene schists-marble unit and the Miocene Polychnitos Ignimbrite (Migiros et al., 2000; Lamera et al., 2001).

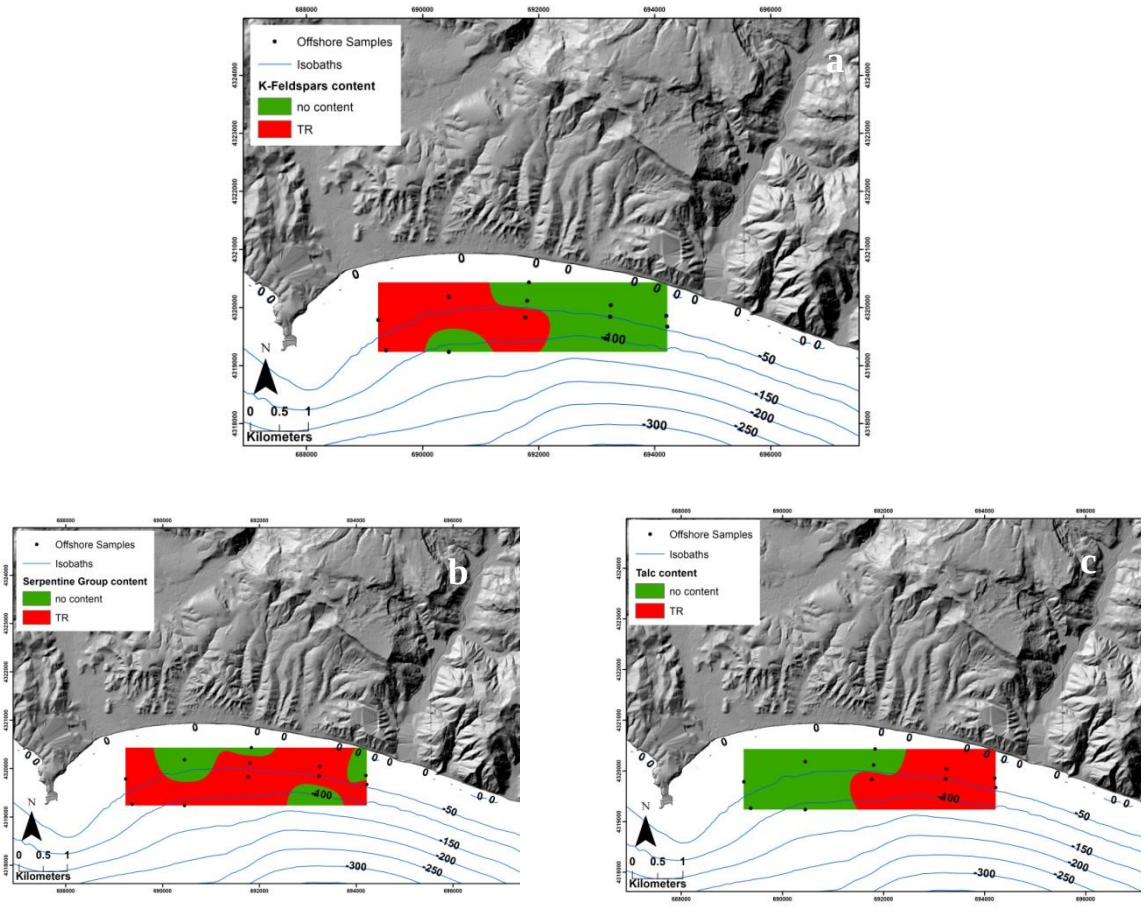

Figure 5.50. Abundance and spatial distribution of: (a) K-Feldspars, (b) serpentine group minerals and (c) talc of the surficial sediment samples offshore Vatera area, southern Lesvos Island (MJ: major, MD: medium, TR: trace). Depth contours in blue color.

Calcium carbonates content (Table 4.20) varies between ~3% and 11.5%. Spatial distribution pattern reveals higher content as depth increases at the central part of the bay (Fig. 5.51). $CaCO_3$ content is a significant factor that differentiates Eresos and Vatera area, suggesting the higher input of biogenic, in origin, material (e.g. Spagnoli et al., 2010); the latter was justified by microscopic observations.

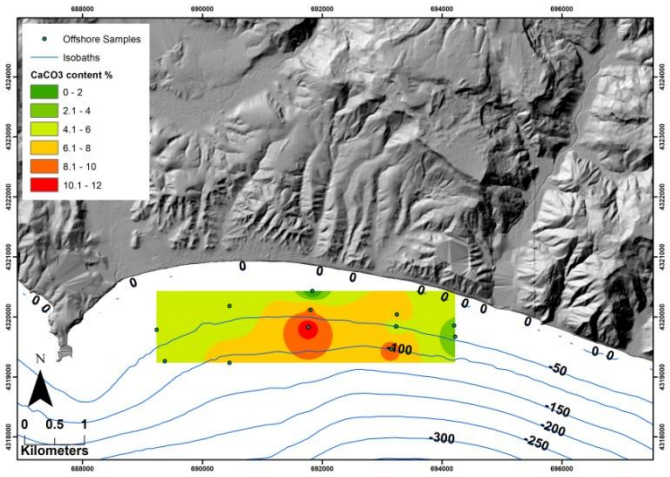

Figure 5.51. Spatial distribution patterns of $CaCO_3$ content % of the surficial sediment samples off Vatera area, southern Lesvos Island. Depth contours in blue color.

<u>Potential of the area off Vatera, south Lesvos Island to host marine aggregates deposits for uses in the construction industry</u>

The above physical, mineralogical and geochemical characteristics define that the offshore study area of Vatera is unsuitable for any future uses of the offshore material in the construction industry. The factors that display significant disadvantages are:

- Grain size data defined the existence of poorly sorted and immature muddy sand to slightly gravelly muddy sand and sandy mud.
- The textural analysis revealed abundance of clayey material and significant amounts of carbonates and organic material.
- Carbonates content varies from ~3% to 1.5%, suggesting the presence of biogenic material. According to GCCT (2016), shell content should always be below 10%.
- Various mineralogical assemblages were determined, such as clays and talc implying the unsuitability of the material as aggregates for concrete, according to various European and national restrictions (§1.4).

Therefore, the offshore area of Vatera, south Lesvos Island, is not expected to host suitable aggregates for any future uses for the construction industry.

However, Hasiotis et al. (2020), proposed an area of ~1.7 km^2 between 40 and 55 m water depth (suggesting a maximum volume of $0.85*10^6$ to $3.4*10^6$ m^3) that can be further investigated in the context of nourishment material.

5.1.3.1. Mytilene Strait area

Grain size

The studied offshore area of Mytilene (- Asia Minor) Strait revealed the presence of two main sedimentary classes according to Folk's (1980) classification: i) gravelly Sand (gS) and ii) gravelly muddy Sand (gmS) (Fig. 5.52-53). Hasiotis et al. (2020) has shown that seabed has very small gradients (<2.8% especially deeper that 30m) with <1m local micro-relief. Bathymetrical data of Hasiotis et al. (2020), revealed that the study area of Mytilene Strait can be subdivided into two sub-areas (north and south) according to their maximum depths of ~60m and 50m, respectively. At the northern part, whereas gravelly muddy sand fraction prevails, the isobath of 30m appears to be at a distance of ~1.5 km off the coastline (Hasiotis et al., 2020). At the southern part, whereas gravelly sand fraction prevails, the isobath of 30 m appears to be closer (Hasiotis et al., 2020). It has to be mentioned that the 30 m isopleth corresponds the mean deeper limit of *Posidonia oceanica* prairies (Hasiotis et al., 2020).

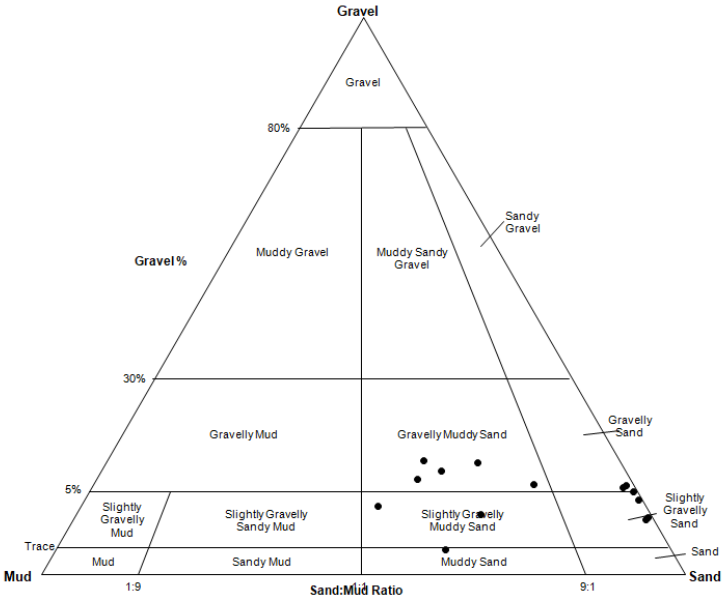

Figure 5.52. Grain-size classification of the surficial sea-bottom sediment samples collected offshore Mytilene Strait area, southern Lesvos Island according to the Folk (1980).

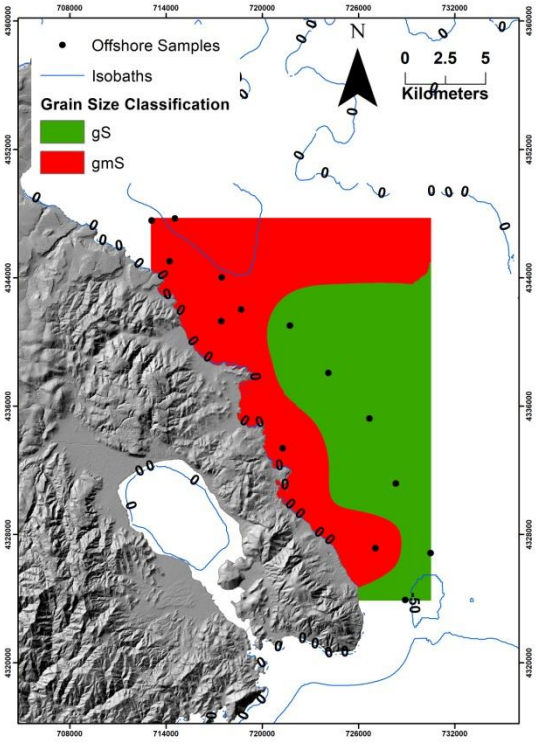

Figure 5.53. Spatial distribution pattern of the granulometric types of the offshore samples from Mytilene Strait, eastern Lesvos Island. Depth contours in blue color.

Grain size analysis revealed a grouping of gravelly muddy sand at the northern area as well as at the shallower studied area, while gravelly sand prevails at the southern and deeper

area. At the northern part, the higher mud percentages coincide with greater depths, which act as fine-grained materials sediment traps (Martsuka, 2009). Furthermore, according to Hasiotis et al. (2020), the increase of finer fraction at the northern part is related to sediment input from ephemeral rivers that discharge to the northwest. At the southern and deeper area, sand fraction varies between 91.45% and 96.15% (Annex II-Grain Size Analysis). Moreover, sand has a transition from finer to coarser fraction to the south (Hasiotis et al., 2020). Gravel fraction has a wide range at the northern part (3.3% - 12.73%) and is <8% at the southern part (Annex II-Grain Size Analysis).

The grain size analysis of the statistical parameters revealed that all surficial sediment samples from Mytilene Strait are poorly to very poorly sorted (Annex II-Grain Size Analysis). Poorly sorting suggests short distance transportation of the sediments from their source areas (Ramadan et al., 2019) and/or that are not that reworked. No pattern is identified in skewness degree and sediments are classified as strongly fine, fine, near symmetrical and coarse skewed (Annex II-Grain Size Analysis).

Physical characteristics of the sediments - Microscopic analysis (Stereo-microscopy/ SEM-EDS)

Microscopic analysis of the surficial sediments revealed the poorly sorting degree and the existence of angular to sub-angular grains (Fig. 4.27) which exhibit low textural maturity. SEM/EDS analysis detected iron oxides, probably of biogenic origin (Fig. 4.26).

Mineralogy - XRD

The mineralogical analysis of the surficial sediments from Mytilene Strait reveals the mineralogical complexity of the offshore area. Quartz content is the main crystalline phase of the area, displaying higher values at the southern part (Fig. 5.54a). Off Thermi's thermal springs and at the southernmost part of the strait low quartz and high beta-quartz content is observed, suggesting silica-rich volcanic rocks (Fig. 5. 54a-b; Hasiotis et al., 2020). Albite and calcite are the second most significant minerals of the study area (Fig. 5. 54d-e). Albite pattern reveals major/medium content at the northern and central part of the strait and decreases off Thermi's thermal spring and at southern part. Calcite also displays similar spatial pattern. However, the spatial distribution pattern of magnesian calcite is not related with calcite's (Fig. 5. 54f), indicating sediment input other other than terrigenous at the southern area of the strait (Spagnoli et al., 2010). Cristobalite displays trace content at the central and shallow study area (Fig. 5.54c). Dolomite, stilbite and galena occur only off Thermi's thermal springs as trace minerals (Fig. 5.55a; 56c). Clay minerals, such as illite and chlorite group minerals (Fig. 5.55c-d), occur in higher content at the central/northern part of the strait. Gypsum, talc, actinolite and edenite (Fig. 5.55e-f; 56a-b) occur sporadically as trace/minor minerals. Goethite is observed at the central/sourthern part of the strait and especially in grater depths (Fig. 56e). The mineralogical composition of Mytilene Strait's sediments coincides with the study of Martsouka et al. (2009).

The mineralogical patterns of the sediments from Mytilene Strait reveal that: a) sediments from the northern strait are associated with Polychnitos Ignimbrite Formation and b) sediments from the southern part are related to the pre-Miocene basement rocks and the Mytilene volcanic Formation (Hasiotis et al., 2020).

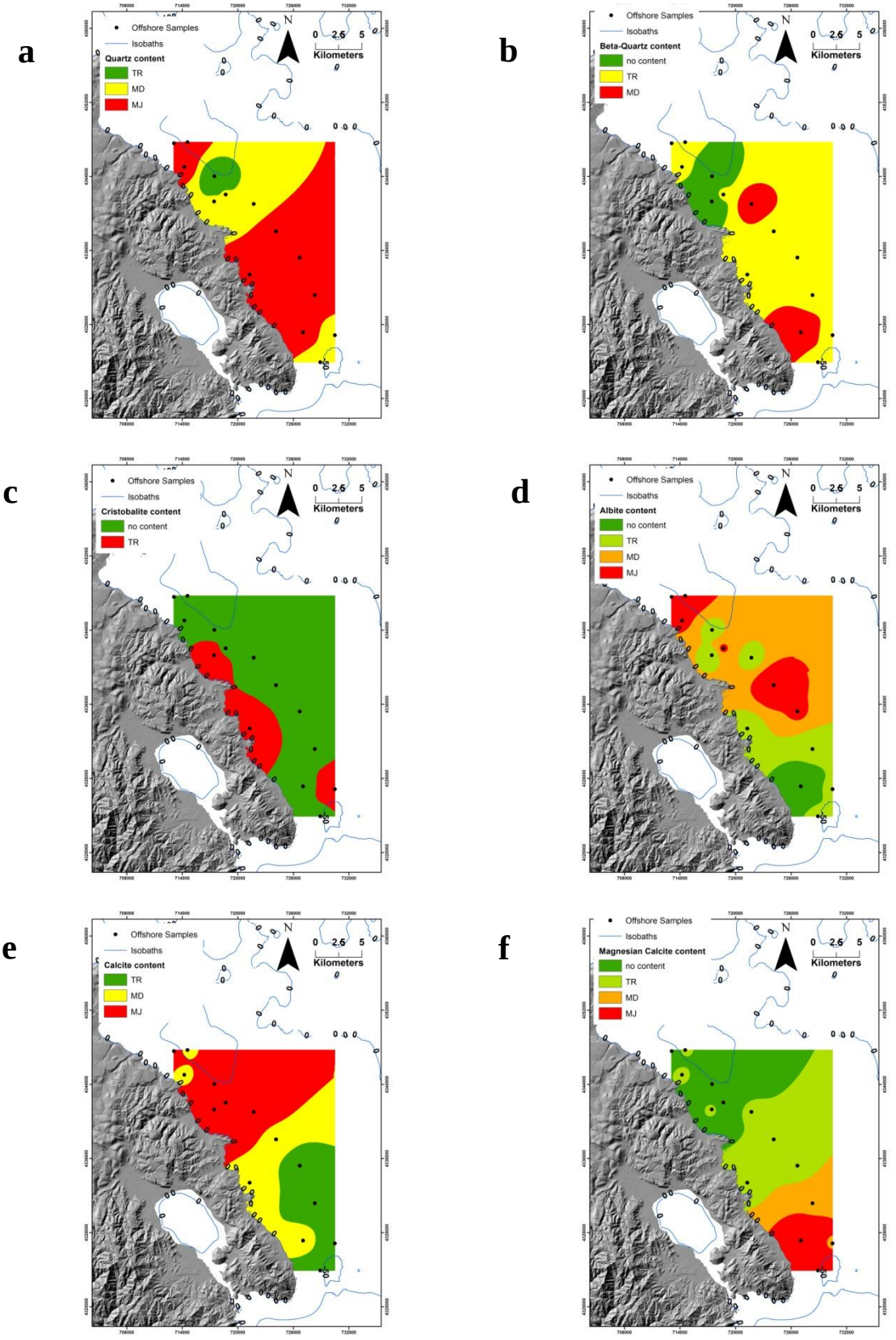

Figure 5.54. Abundance and spatial distribution of: (a) quartz, (b) b-quartz, (c) cristobalite, (d) albite, (e) calcite, (f) magnesian calcite of the surficial sediment samples offshore Mytilene Strait, eastern Lesvos Island (MJ: major, MD: medium, TR: trace). Depth contours in blue color.

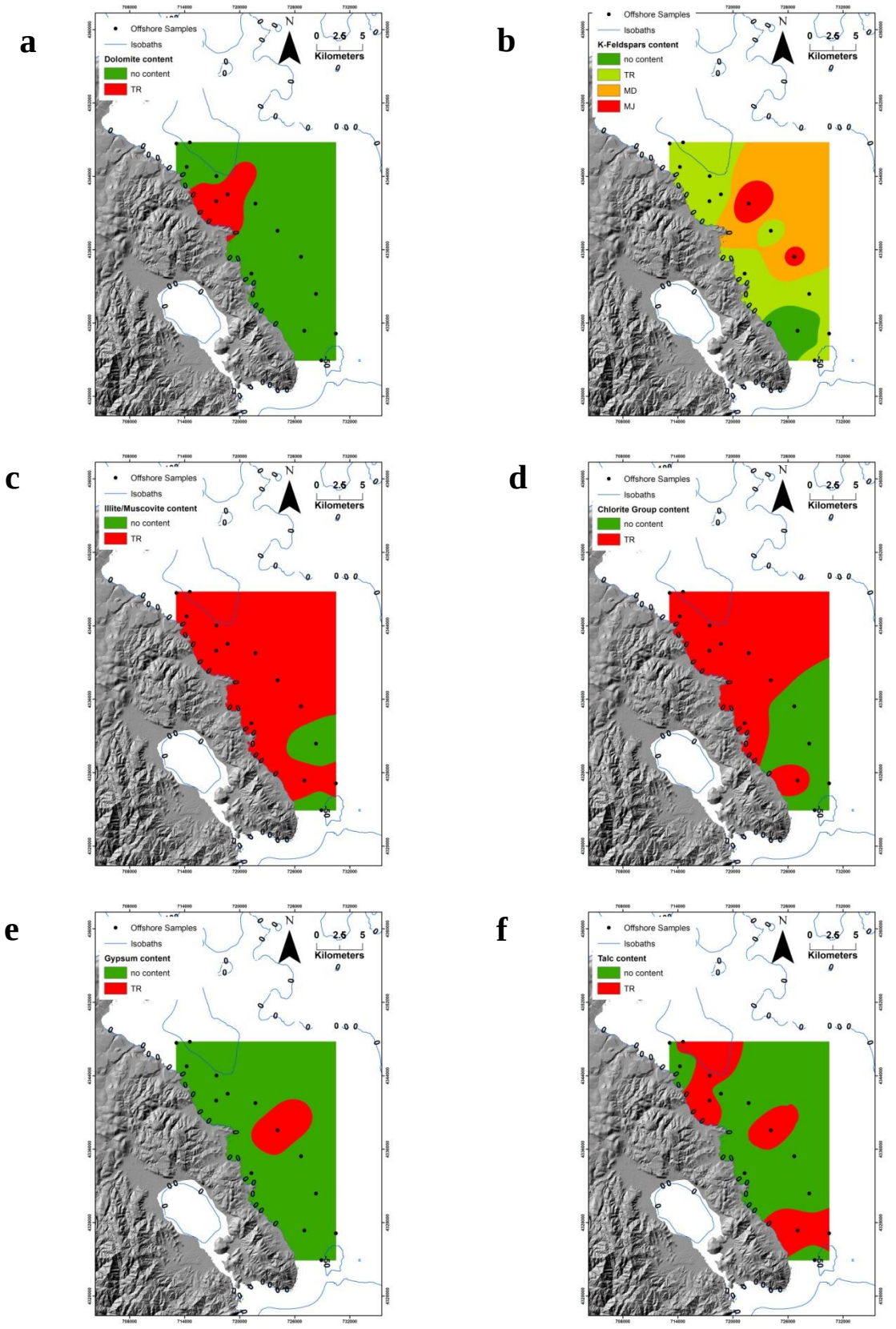

Figure 5.55. Abundance and spatial distribution of: (a) dolomite, (b) K - Feldspars, (c) illite/muscovite, (d) chlorite group minerals, (e) gypsum, (f) talc of the surficial sediment samples offshore Mytilene Strait, eastern Lesvos Island (MJ: major, MD: medium, TR: trace). Depth contours in blue color.

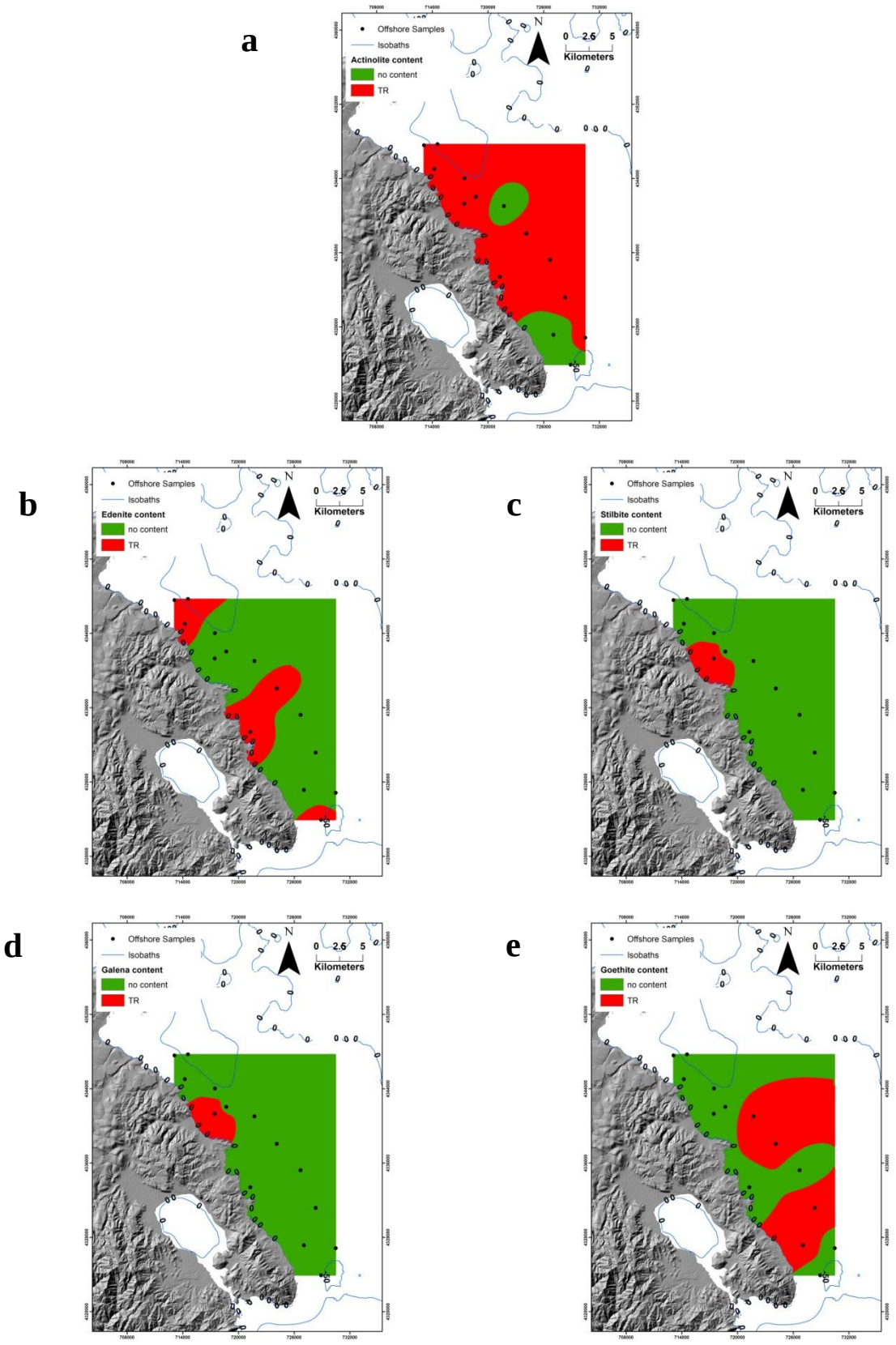

Figure 5.56. Abundance and spatial distribution of: (a) actinolite, (b) edenite, (c) stilbite, (d) galena and (e) goethite of the surficial sediment samples offshore Mytilene Strait, eastern Lesvos Island (MJ: major, MD: medium, TR: trace). Depth contours in blue color.

Calcium carbonates analysis revealed significant content, which varies between 14% and 38% (Table 4.20). $CaCO_3$ content is higher at southern part of the strait as well as at the deeper/northern part, coinciding with magnesian calcite content (Fig. 5.57). The distribution of high $CaCO_3$ percentages throughout the strait suggests a great disadvantage for any potential use of the sediments from the construction industry.

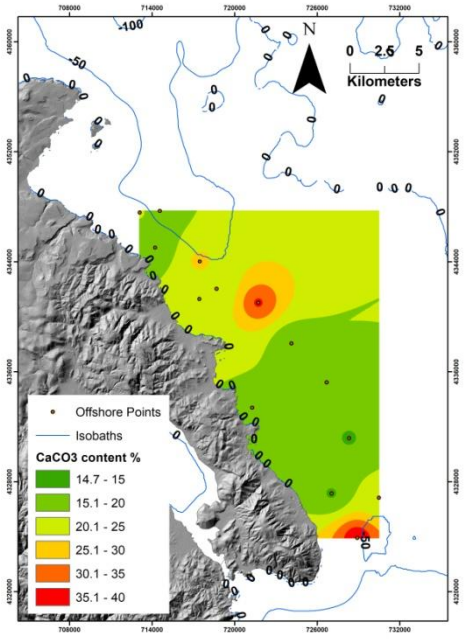

Figure 5.57. Spatial distribution patterns of $CaCO_3$ content % of the surficial sediment samples off Mytilene Strait area, southern Lesvos Island. Depth contours in blue color.

Potential of the offshore area of Mytilene Strait, east Lesvos Island to host marine aggregates deposits for uses in the construction industry

The above physical, mineralogical and geochemical characteristics define that the offshore study area of Mytilene Strait, east Lesvos Island, is unsuitable for any future uses of the offshore material in the construction industry. The factors that display significant disadvantages are:

- Grain size data defined the existence of poorly sorted gravelly sand to gravelly muddy sand and muddy sand with low textural maturity. This factor is especially a drawback at the northern as well as at the shallower area.

- Carbonates content is high and varies between 14% and 38%, suggesting the significant input from biogenic material; these percentages are forbidden according to GCCT (2016), in aggregates for concrete.

- Wide mineralogical study was determined crystalline phases, such as clays, gypsum, talc, feldspars, aphiboles and cristobalite implying the unsuitability of the material as aggregates for concrete, according to various European and national restrictions (§1.4).

Therefore, the offshore area of Mytilene Strait, east Lesvos Island, is not expected to host suitable aggregates for any future uses for the construction industry.

On the other hand, according to Hasiotis et al. (2020), a significant area of 71.2 km^2, suggesting maximum volumes of marine aggregates (35.6 - 142.5*10^6 m^3), as showed in Figure 5.58.

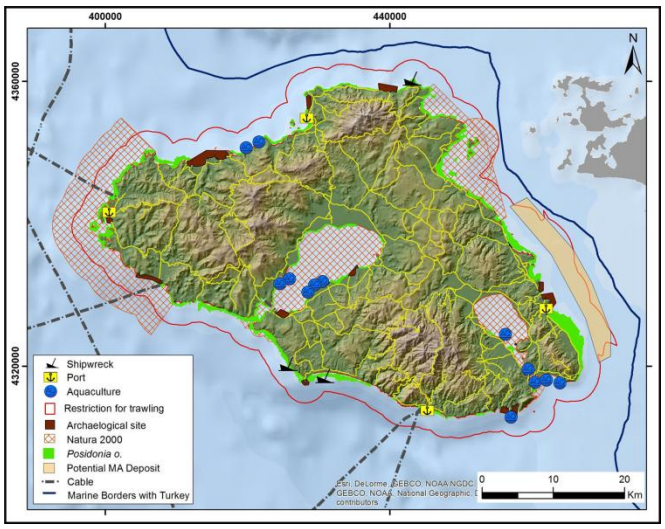

Figure 5.58. General map presenting the potential MA deposit in Mytilene Strait, east Lesvos Island from Hasiotis et al., 2020.

5.1.4. NE Rhodes Island

The offshore area Afantou Bay (Fig. 5.59) is located at the NE part of Rhodes Island Afantou beach is long (~6.3 km) and the coastal morphology is relatively smooth (Kapsimalis et al., 2013). Various streams and rivers flow across the coastal area with N-S direction, such as Potos, Psalidokampos and Loutanis rivers; Pelemonis and Platirema streams (Verikiou-

Papaspiridakou et al., 2004). Furthermore, along the backshore of Afantou beach a series of small sandy dunes is observed, which are highly affected from anthropogenic interventions (Verikiou-Papaspiridakou et al., 2004). The coastal area of Afantou Bay consists of alluvial deposits and postalpine marine sediments of Pliocene age such as limestones with silex, marls and radiolarites derived from Profitis Ilias unit (Mutti et al. 1970; Lekkas et al. 2007). Marine sediments such as sands, clays, conglomerates and sometimes gupsum beds of Plio-Plistocene occur in the hinterland (Mutti et al. 1970; Lekkas et al. 2007, Tsoutsia et al., 2014). Moreover, undivided limestones and dolomites of Mesozoic – Eocene age occur in the area of Vagia – Kolympia (Mutti et al. 1970; Tsoutsia et al., 2014).

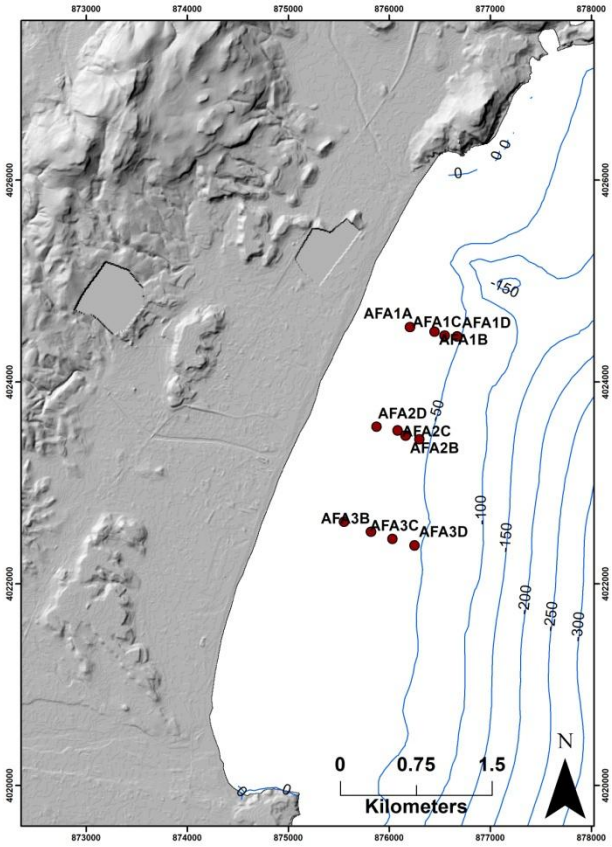

Figure 5.59. Shaded onshore relief map and general bathymetry including the sampling points from the offshore study area of Afantou Bay, NE Rhodes Island. Depth contours in blue color.

According to Kapsimalis et al. (2013), the offshore area of Afantou Bay hosts two main morphological features: a submarine canyon located at the SE part and a rocky shoal at the southern part (Fig. 5.60). No *Posidonia Oceanica* meadows were detected at the bay and in the central part the bottom deepens gradually and eventually has a shelf-break at 75-90m

water depths (Kapsimalis et al., 2013). The maximum width of the continental shelf occurs in the southern part of the bay and does not exceed 2 km (Kapsimalis et al., 2013).

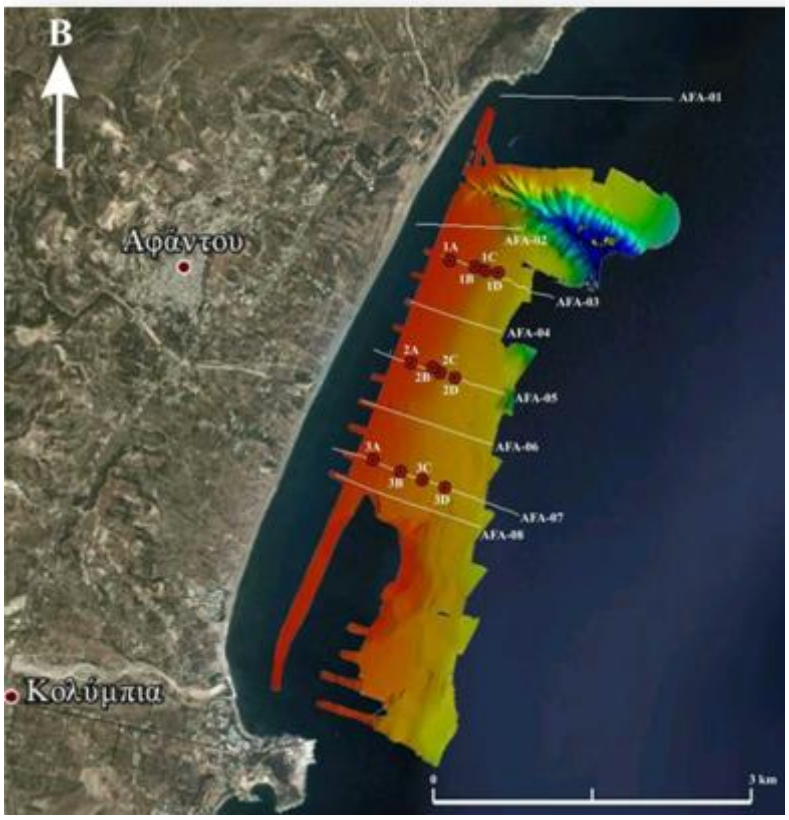

Fig. 5.60. Bathymetry, seismic lines and sampling positions in the Afantou Bay (Kapsimalis et al., 2013).

The interpretation of the results from the analysis of the obtained offshore surficial samples from the Afantou Bay, NE Rhodes Island (Fig. 5.59-60) is developed below.

Grain size

Grain size analysis of the studied offshore area of Afantou Bay revealed three sedimentary classes according to Folk's (1980), classification: i) gravelly Sands (gS), ii) gravelly muddy Sands (gmS) and iii) Sands (S) (Fig. 5.61 - 62). According to Kapsimalis et al. (2013), two distinctive morphological features exist in Afantou Bay: a rocky 'shoal' located at the southern area and a submarine canyon at northeastern part of the bay. Furthemore, at the central part of the bay seabed has gradually slopes with a shelf-break at 75 – 90m water depth (Kapsimalis et al., 2013). Kapsimalis et al. (2013), also, noticed that no *Posidonia oceanica* prairies exist in the studied area of Afantou Bay.

In the studied area, sand content varies from 72.71% to 95.76% (Annex II-Grain Size Analysis). Samples exhibit zone distribution and in general are finer as depth increases (Tsoutsia et al., 2014), which is typical in most continental shelves (Karditsa, 2010). The bay area at water depths of 15 – 35m consists of medium to fine sand (Kapsimalis et al., 2013). However, mud content is significant lower than sand in all samples and is ranging between 4.23% and 27.18% (Annex II-Grain Size Analysis). Gravel fraction is below 1% in all samples apart from the southern part of the bay whereas it reaches almost 10% in water depth of 25m. Furthermore, grain size differentiates in deeper samples at the southern part of the bay, as gravel impurities are present (Tsoutsia et al., 2014). In opposition, the other deeper studied locations do not host gravel fraction.

At the northern part of the bay sediments are moderately to poorly sorted as depth increases, when at the southern part are moderately, poorly, very poorly and again moderately sorted. This fact is probably attributed to the high sand content (~95%) and low near bed hydrodynamic conditions. There is also a differentiation between the northern and the southern area concerning skewness. At the northern and central part of the studied area, sediments are nearly symmetric to strongly fine skewed with increasing depth, while at the southern part sediments are strongly fine skewed to near symmetrical (Annex II-Grain Size Analysis). The same grouping is observed regarding kurtosis, whereas sediments are extremely leptokurtic to leptokurtic at the southern part, suggesting low energy environment at this part (Friedman, 1962; Mohtar et al., 2017). In opposition, at the remaining of the studied area, sediments are mesokurtic to very leptokurtic as depth increases (Annex II-Grain Size Analysis).

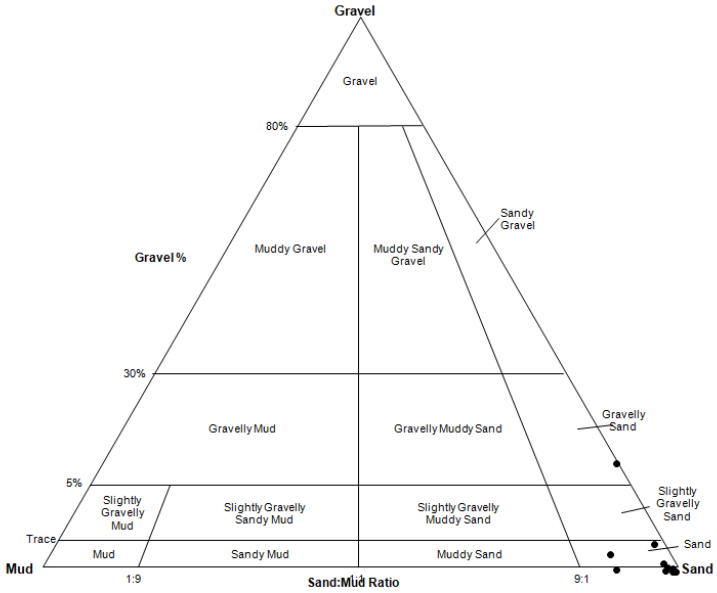

Figure 5.61. Grain-size classification of the surficial sea-bottom sediment samples collected offshore Afantou Bay, NE Rhodes Island according to the Folk (1980).

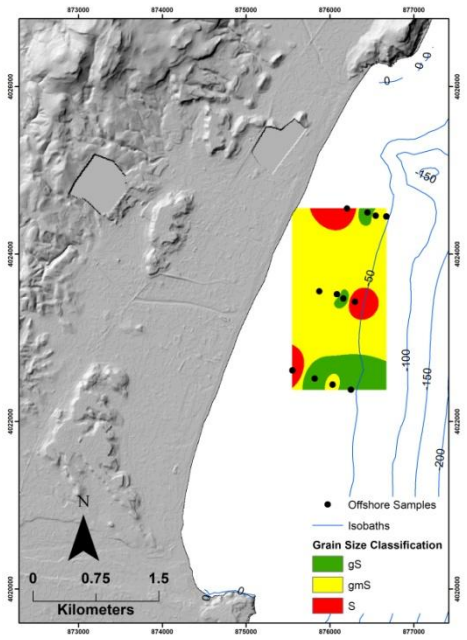

Figure 5.62. Spatial distribution pattern of the granulometric types of the offshore samples from Afantou Bay, Rhodes Island. Depth contours in blue color.

Physical characteristics of the sediments

Density values at the area of Afantou Bay, NE Rhodes Island are ranging between 2.68 and 2.8 gr/cm^3 (Fig. 5.63). The higher values are mostly observed at shallow depths and specifically at the southern part of the bay. As also noticed in Kissamos Bay, higher density values are related with higher sand fraction content.

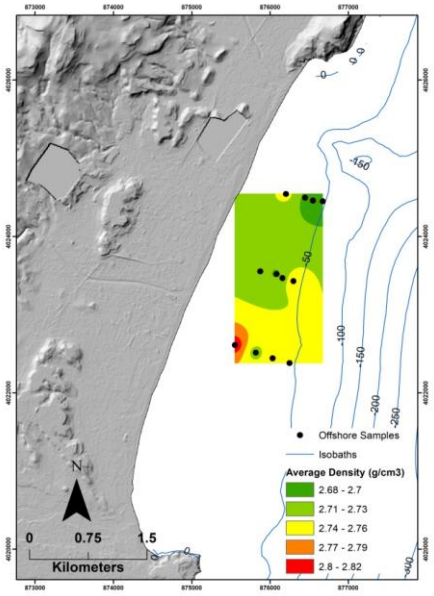

Figure 5.63. Spatial distribution of the density in surficial sediments offshore Afantou Bay, Rhodes Island. Depth contours in blue color.

Microscopic analysis (Stereo-microscopy/ SEM-EDS)

The textural analysis of the surficial sediment of Afantou Bay revealed the abundance of calcitic material (Fig. 4.28-29). Grains are sub-angular and well sorted indicating a medium textural maturity. Grains from different minerals do not display significant textural differences in shape and grains do not display stress signs. No metallic minerals were observed, however SEM/EDS analysis detected Cr-oxides lying over calcite and albite grains. Furthermore, macroscopic observations revealed a plurality of skeletal remains of marine organisms (Tsoutsia et al., 2014).

Mineralogy - XRD

The mineralogical analysis of the surficial sediments from Afantou Bay, revealed that calcite is the dominant crystalline phase (Fig. 5.64d). Spatial distribution of quartz and albite is similar (Fig. 5. 64a,b), displaying higher content at the northern part of the bay (major/medium), slightly lower content at the central part (medium/trace) and significantly lower content at the southern part (trace/minor/no content). Potassium feldspars are detected as trace mineral only at the central and northern part of the bay (Fig. 5.64c). Magnesian calcite and aragonite display content only at the southern part of the bay and mostly at greater depths (Fig. 5.64e-f). Dolomite, chlorite group minerals, actinolite and clinochrysotile display similar distribution patterns, showing no content at the southern and deeper part of the study area and trace content at the rest of the area (Table 4.15; Fig. 5.65a, b, c, e). Pyroxenes (e.g. augite; Fig. 5.65c) also occur only at the southern part of the bay and present spatial correlation with density.

The distinct differentiation of the southern area in relation to the central/northern is probably due to: i) the existence shells and skeletal remains of marine organisms, ii) the low terrestrial sediments discharge by the Pelemonis and Loutanis torrents and iii) the presence of strong marine currents compared to the northern area. Furthermore, the proximity of the southern area from Kolympia rocky area supports the development of hard-bottom benthic biocommunities (Plaiti et al., 2006) and has a different geological background in relation to the northern part of the Bay (Mutti et al. 1970; Tsoutsia et al., 2014).

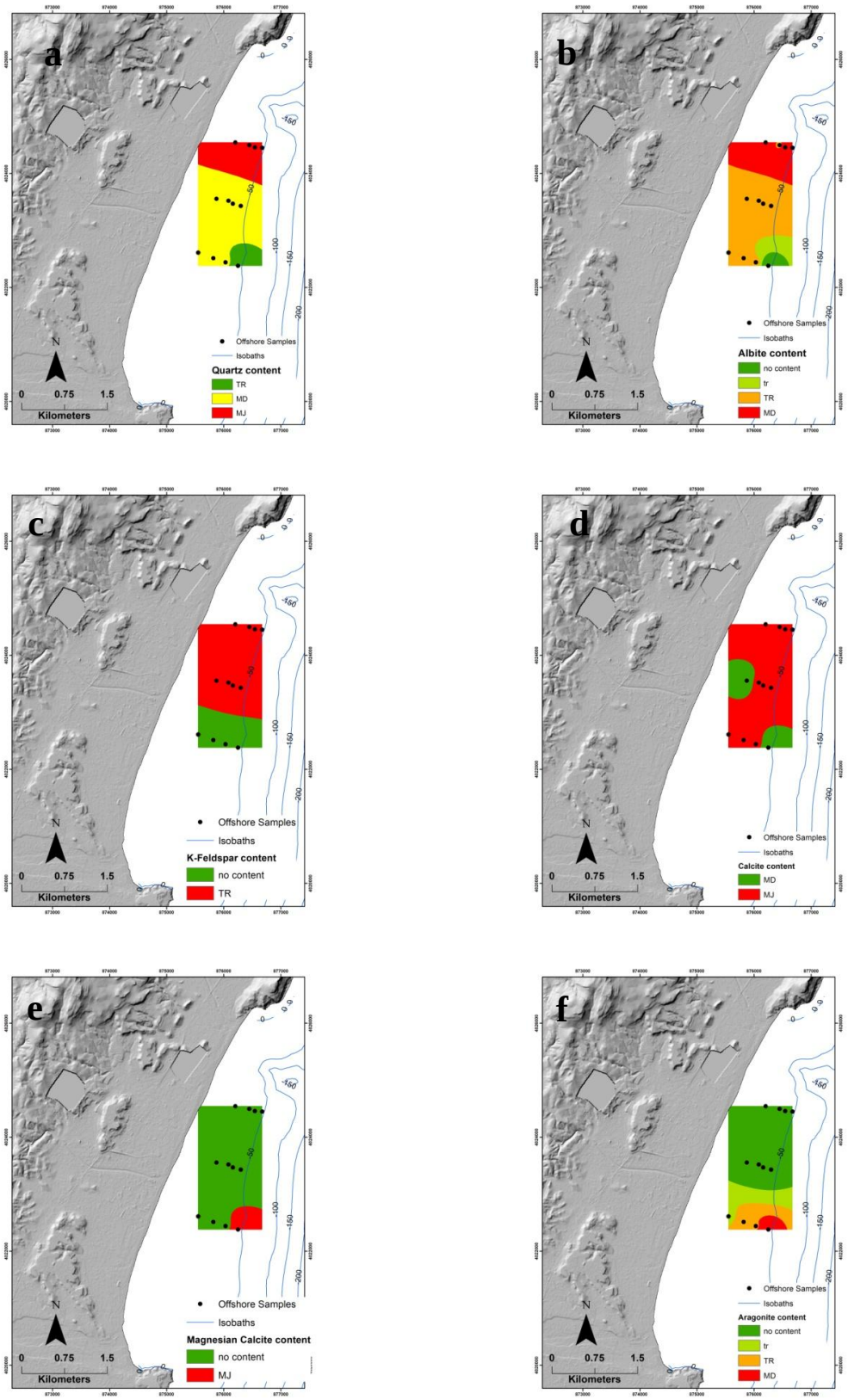

Figure 5.64. Abundance and spatial distribution patterns of: (a) quartz, (b) albite, (c) K-Feldspar, (d) calcite, (e) magnesian calcite and (f) aragonite of the surficial sediment samples offshore Afantou Bay, NE Rhodes Island. Depth contours in blue color.

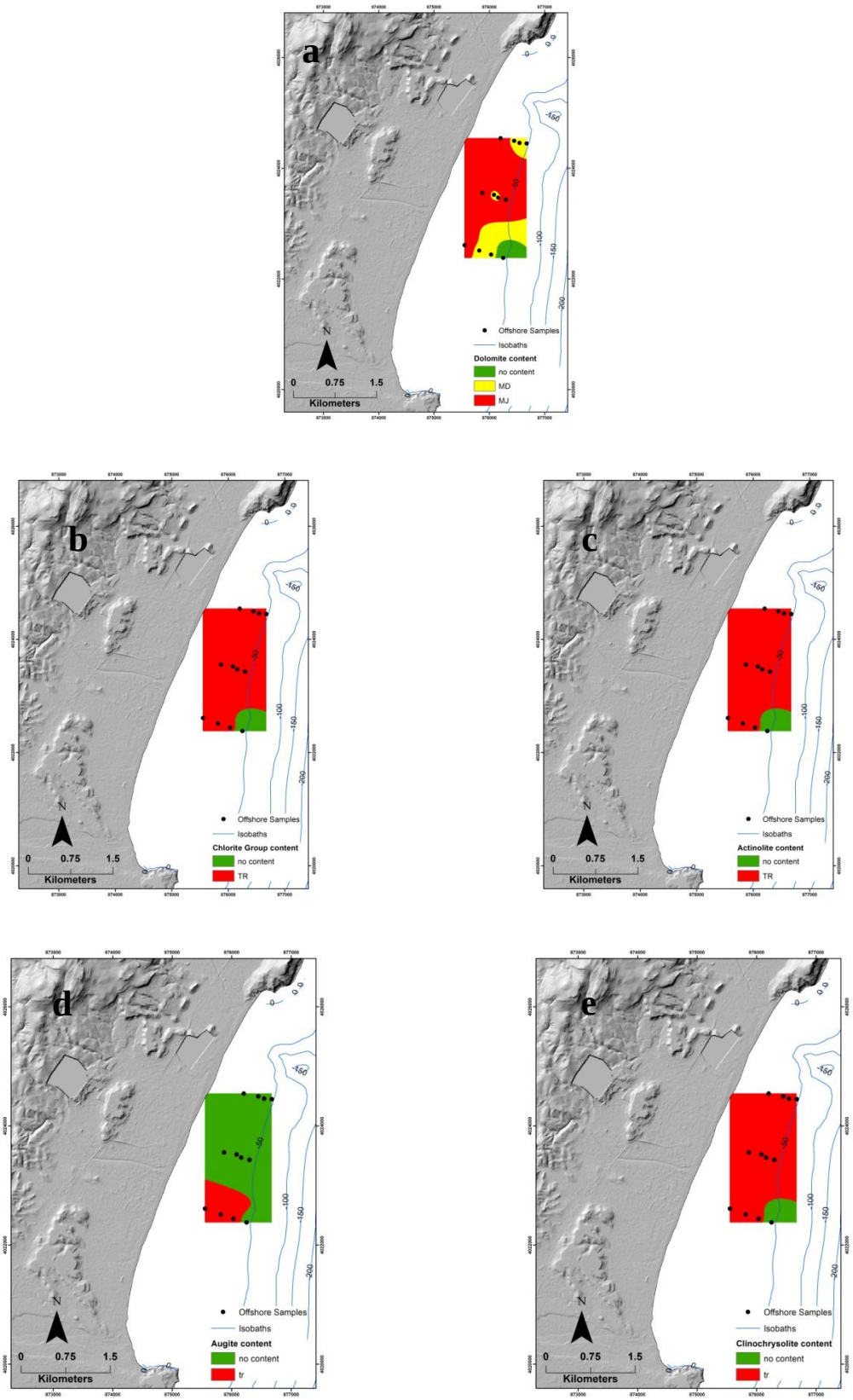

Figure 5.65. Spatial distribution patterns of mineralogical content of (a) dolomite, (b) chlorite group minerals, (c) actinolite, (d) augite and (e) clinchrysotile of the surficial sediment samples of Afantou Bay, NE Rhodes Island. Depth contours in blue color.

Geochemistry

SiO_2 content is generally extremely low and varies between ~0.5-26% (Annex III – Chemical Analysis), displaying slightly higher content at the southern/shallow part of the study area (Fig. 5.66a). SiO_2 distribution pattern is similar to density pattern. CaO (~27 – 40%), Al_2O_3 (~0.5-5%) and SO_3 patterns are similar and being enriched at the southern part of the bay (Fig. 5.66b, d, f). These patterns are also related to those of magnesian calcite and aragonite. Fe_2O_3 content is higher at shallower depths, reaching 3.3% (Fig. 5.66c). MgO content is higher at the central/northern part of the bay and shows positive correlation with dolomite.

Arsenic and strontium show enrichment at the southern/ deeper part of the study area (Fig. 5.67a; 68e), as CaO, Al_2O_3, SO_3, calcite and aragonite. Chromium, manganese and zinc show similar patterns, as they are slightly enriched at the southern/shallow area (Fig. 5.67c, f 5.68d), displaying positive correlation with Si and density (Annex IV, Tables IV.3). Barium and cobalt display higher content at the central/ southern part (Fig. 5.67b, d).

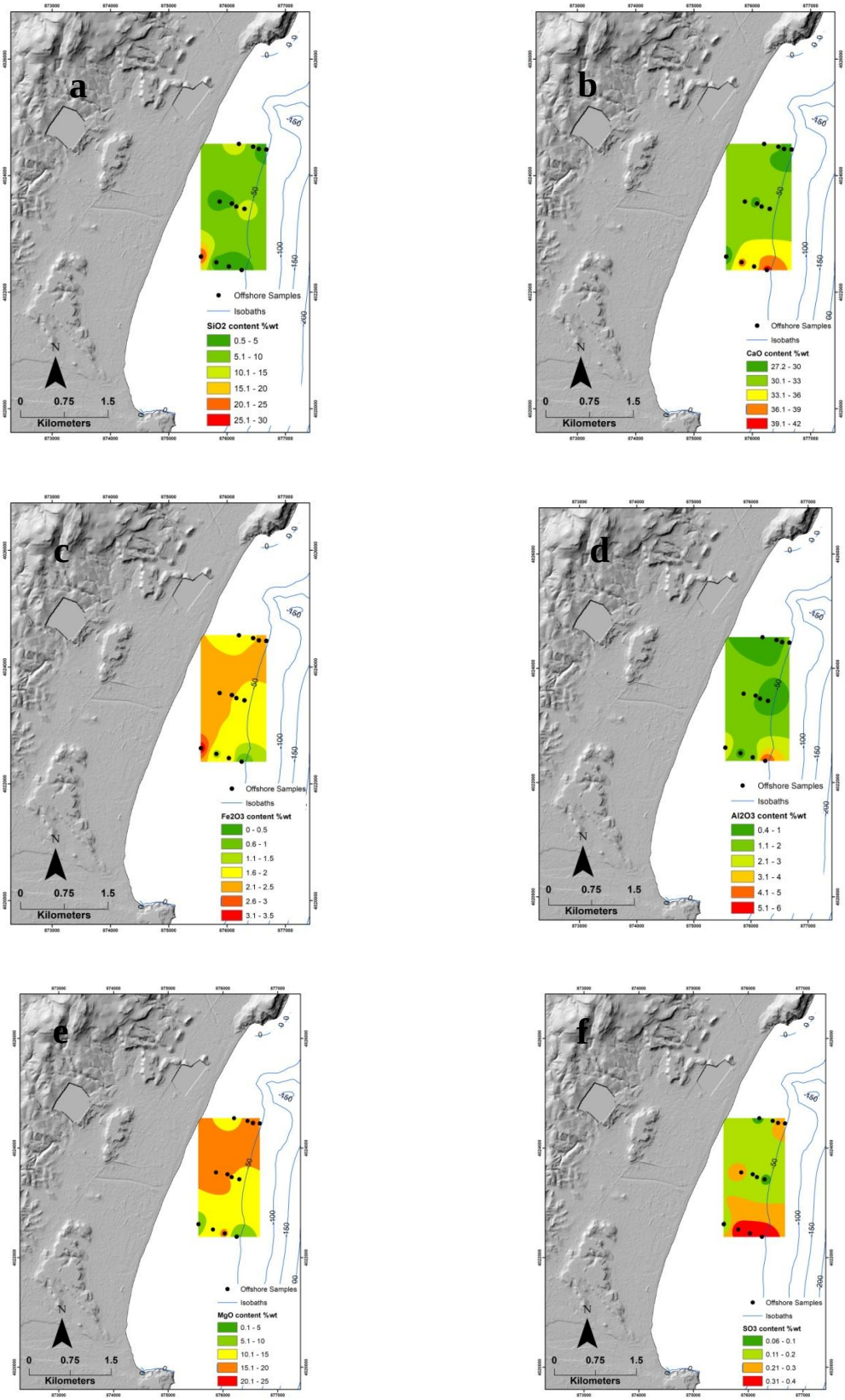

Figure 5.66. Spatial distribution patterns of major elements (%) in surficial sediment samples offshore Afantou Bay, NE Rhodes Island: (a) SiO_2, (b) CaO, (c) Fe_2O_3, (d) Al_2O_3, (e) MgO and (f) SO_3. Depth contours in blue color.

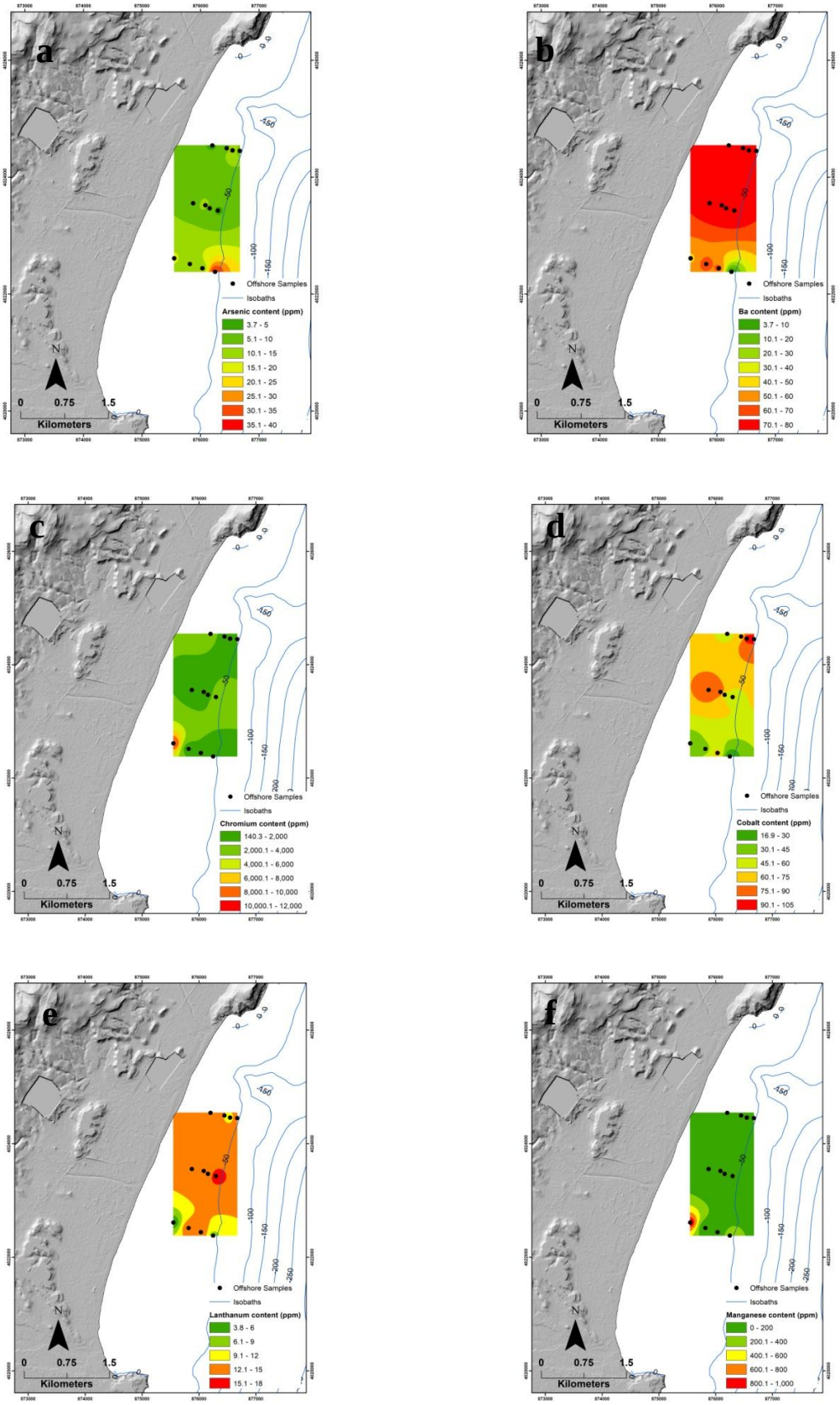

Figure 5.67. Spatial distribution patterns of trace elements (ppm) in surficial sediment samples offshore Afantou Bay, NE Rhodes Island: (a) As, (b) Ba, (c) Cr, (d) Co, (e) La and (f) Mn. Depth contours in blue color.

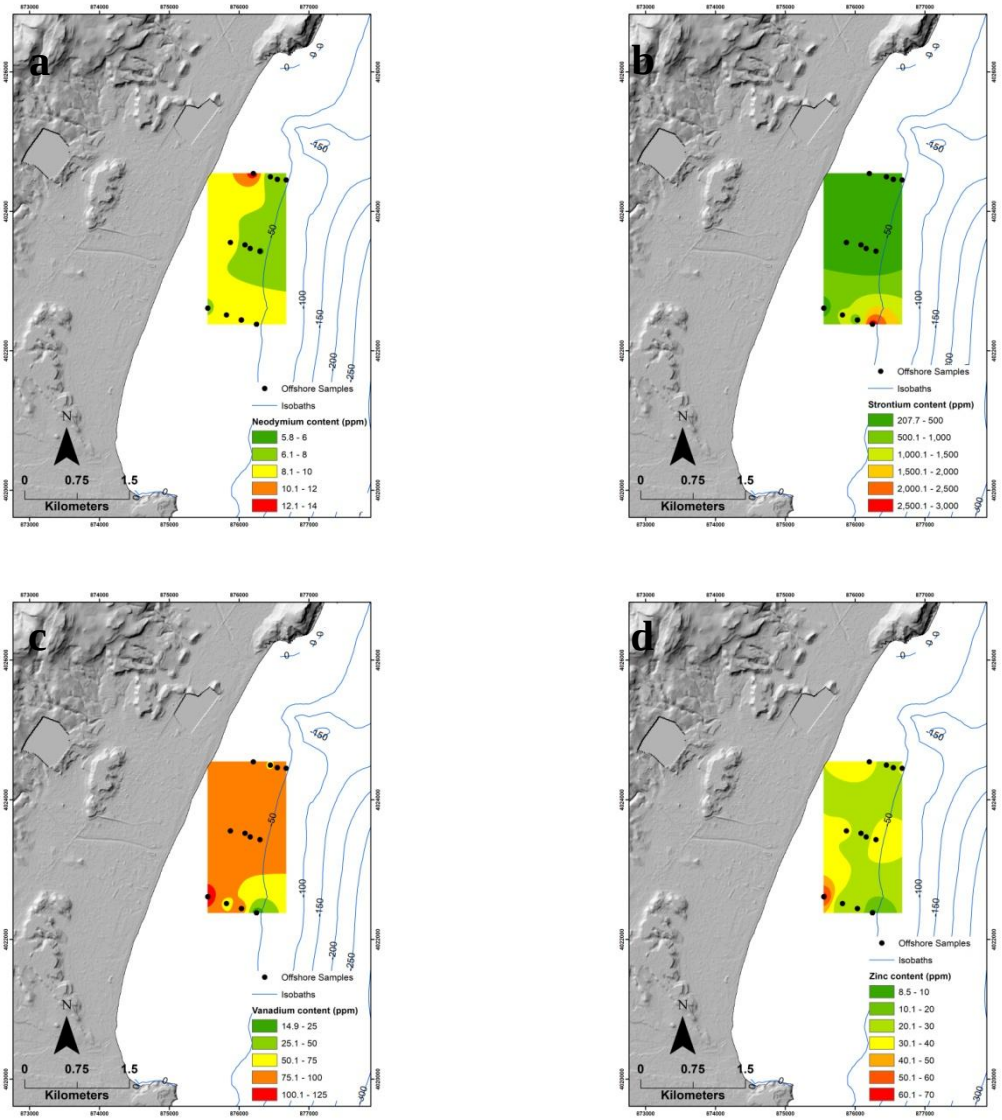

Figure 5.68. Spatial distribution patterns of trace elements (ppm) in surficial sediment samples offshore Afantou Bay, NE Rhodes Island: (a) Nd, (b) Sr, (c) V and (d) Zn. Depth contours in blue color.

Potential of the offshore area of Afantou Bay, NE Rhodes Island to host marine aggregates deposits for uses in the construction industry

The above physical, mineralogical and geochemical characteristics suggest that the offshore study area of Afantou Bay, NE Rhodes Island is unsuitable for any future uses of the offshore material in the construction industry. The factors that display mainly significant disadvantages are:

- Grain size data defined the existence moderately to poorly sorted sand to gravelly sand. This factor consists the only advantage

- Textural analysis revealed the great abundance of calcitic material
- Calcite is the major mineral and the sediments consist of various crystalline phases such as clays, dolomite, magnesian calcite, aragonite, actinolite, clinochrysotile and pyroxenes implying the unsuitability of the material as aggregates for concrete, according to various European and national restrictions (§1.4).
- Fe_2O_3 content is above 2%, which is not permitted according to various European and national restrictions (§1.4).
- CaO content varies between 27% and 40%
- Various metals are enriched in the study area.

Therefore, the offshore area of Afantou Bay, NE Rhodes Island, does not host suitable aggregates for any future uses for the construction industry.

Kapsimalis et al. (2013), performed a survey at the offshore area of Afantou Bay and they estimated an area of 0.65x106 m^2 that hosts marine aggregates, suggesting volumes that can reach up to 1.3-2.0 $*10^6 m^3$. Marine aggregates deposit was found in water depth of 13 - 35m and *Posidonia oceanica* meadows were detected, only sparse appearances of the invasive green alga Caulerpa racemosa var. cylindracea (Kapsimalis et al., 2013)

5.2. MARINE AGGREGATES POTENTIAL IN VARIOUS ONSHORE COASTAL AREAS

East – central Evia Island – South Evoikos Gulf

East – central Evia Island

Regarding the east/central Evia Island coastal areas, grain size analysis revealed the variances between these successive areas. From north to south, coastal areas NST, PSA and EV revealed that their main grain size trend is sandy gravel to gravel, sand and sandy gravel, respectively (Fig. 5.69a, b, c). These three coastal areas are located northern of the offshore area of Evia Island and their grain size analysis displays slightly coarser fraction than the offshore area (Fig. 5.3 – 5.4).

NST samples (the northern coastal area) present gravel content >73.6% while the remaining percentage represents sand, PSA samples contain sand content >88.4% with the remaining percentage representing gravel and EV samples (the southern coastal area and

nearest to the offshore) contain gravel content >79.4% with the remaining percentage representing sand (Annex II – Grain Size Analysis). The surficial coastal samples that were obtained directly from the coastline in all areas (NST2, 4; PSA2, 4; EV2, 4) are moderately sorted and symmetrical to coarse skewed. The hydrodynamics due to wave activity contribute to the reworking of the beach material and to the removal of fine material. On the contrary, coastal samples from the beach (NST1, 3; PSA1, 3; EV1, 3) are poorly sorted and symmetrical to fine skewed. This fact is probably attributed to the absence of nearbed wave-induced activity and current's actions, which are between the most critical sorting factor at the coastal environment (e.g. Mohtar et al., 2017).

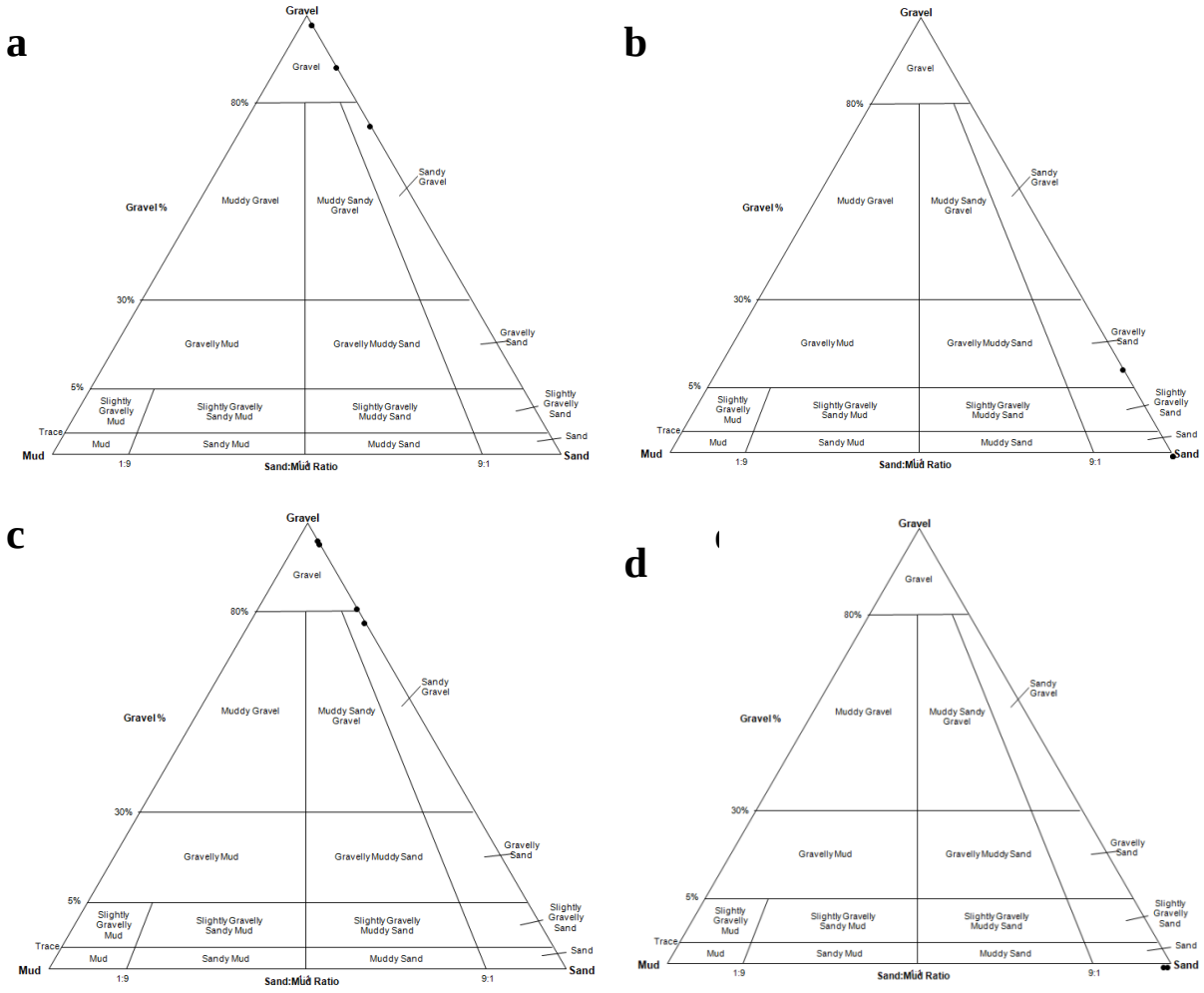

Figure 5.69. Grain-size classification of the coastal sediment samples from the areas of central/eastern Evia Island and south Evoikos Gulf, according to Folk (1980); (a) NST samples, (b) PSA samples, (c) EV samples and (d) Schinias samples.

The mineralogical analysis of the samples from east/central Evia Island indicated quartz as the dominant mineral (Table 4.16). The mineralogical analysis of the northern coastal area (NST samples) also indicated calcite, albite and potassium feldspars as trace minerals, while clay minerals occur as minor only in samples obtained from the beach, whereas hydrodynamic conditions are absent to remove the finer material. The south coastal area (EV samples), display the same mineralogical content, apart from the relatively higher mineralogical content of clay minerals (illite and chlorite group minerals). The higher content of clay minerals cannot be related to the any grain size differences, therefore may be attributed to the mineralogy (quality) of fluvial sediment inputs.

The sediments from north coastal area, east/central Evia Island (NST samples) present notable higher SiO_2 content >91% (Annex III – Chemical Analysis) and extremely low iron, potassium, sulfur, aluminium, sodium and calcium oxides (all <1%). Moreover, trace elements were detected in low levels. The sediments from the south coastal area, east/central Evia Island (EV samples) display lower SiO_2 content of 68-89%. Moreover, other major elements vary significantly; e.g. CaO 1.5-8.3%, K_2O 2.7 – 4.5%, Al_2O_3 1.2-4% and Na_2O 2-3%.

The above data suggest that nearshore and most probably the adjacent offshore area of the northern coastal zone of east/central Evia Island may host marine aggregates with excellent qualitative characteristics regarding the construction industry. This conclusion arises from various factors:

- Granulometry of the coastal sediments presents mostly coarse fraction implying that the adjacent offshore area is expected to host sand and gravel. Finer fraction may participate at an insignificant rate up to water depths of 70-100 m. This fact is strengthened from the good sorting degree of the coastal sediments.
- Mineralogy and geochemistry of the coastal sediments consists mostly of silica (quartz) in high percentages. The absence of any impurities, such as shell content, feldspars, clay minerals, sulphate, aluminum and iron oxides and other harmful components that are restricted according to various European and national restrictions (§1.4), indicates also their absence in greater depths.
- Finally, the absence of the clay fraction and any other mineralogical and geochemical content that silica suggests the naturally low chloride content of the marine

material. This is a critical factor for the construction industry, as the opposite requires detailed and successive washings of the material with water.

Sediments from the southern coastal of east/central Evia Island do not display the same qualitative characteristics. Grain size characteristics are similar to these of the northern area; however that contain higher CaO, K_2O, Al_2O_3 and Na_2O, which are expected to be higher at the adjacent offshore area. These factors may or may not be proved significant disadvantages, though an offshore sampling will define the final suitability of the material regarding construction industry.

Schinias area

Grain size analysis from the coastal area of south Evoikos Gulf (Schinias area), revealed that the main trend is sand, with sand fraction content to be ~99% and samples to be moderately well sorted (Fig. 5.69d; Annex II – Grain Size Analysis). The mineralogical analysis of the sample from the coastal Schinias area, south Evoikos Gulf, revealed quartz as the major mineral (Table 4.17). Moreover, calcite, albite and clay minerals occur as trace minerals.

Sample from Schinias area displays similar mineralogical content with samples from the southern coastal area of east/central Evia Island (EV samples), apart from the additional content of smectite group as trace minerals. However, the comparison semi-quantitative XRD patterns suggests the distinctively lower quartz content and therefore the enriched content carbonates, feldspars and various clay minerals (e.g. illite, chlorite and smectite group minerals).

On the basis of the above, this area does not seem to have potential to host offshore marine aggregates with suitable qualitative characteristics regarding construction industry.

NW and south Crete Island

Kissamos area

Onshore/nearshore sediments from Kissamos Bay located at the eastern part of the bay are finer than those at the central and western part (Fig. 5.29). Grain size analysis trend revealed that samples vary from sand to sandy gravel (Fig. 5.28; 5.70), while this trend

generally follows an eastwards direction. This direction coincided with sorting classification, as samples are poorly to moderately well sorted, respectively, due to the excess of sand content at the eastern part of the bay (Annex II-Grain Size Analysis).

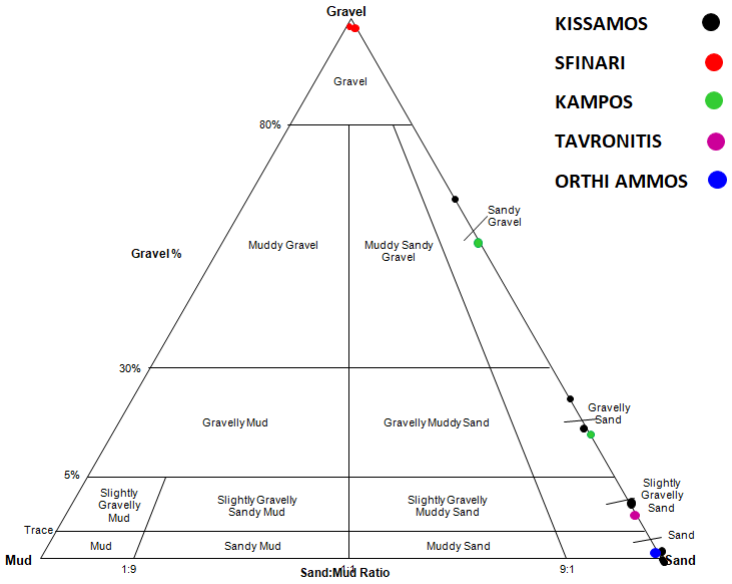

Figure 5.70. Grain-size classification of the coastal sediment samples from the areas of NW and south Crete Island according to Folk (1980).

The mineralogical analysis of the coastal sediments from Kissamos Bay revealed quartz as the main crystalline phase. However, calcite occurs as mineral of medium content and especially major/medium content at the western part of the bay (Table 4.16). This fact is directly correlated with the enriched content of calcite (Fig. 5.31b) and CaO (Fig. 5.32d), also at the western part of bay. Albite is almost absent at the western coastal part and occurs as trace mineral at the rest of the coastal part of the bay. Regarding albite, it seems that it is evenly distributed from the coast to the seawards. Magnesian calcite occurs as trace mineral at the central/east coastal part and as major/medium mineral at the west coastal part of the bay, which coincides with spatial distribution of magnesian calcite at the offshore are. Aragonite, dolomite and various clay minerals occur as trace mineral through the whole coastal area. Moreover, at the central area, bassanite occurs as trace mineral, which is attributed to the gypsum formations of the hinterland (§2.2.2.3; Fig. 2.13).

The chemical analysis of the coastal sediments at the east part of the bay showed that silica content is ~70%, which is expected to be lower in greater depths and carbonates are ~14%, which are expected to be higher in greater depths (Fig. 4.71-72; Annex III – Chemical

analysis). Sulphate, aluminium, potassium and sodium oxides display significantly low values <1% and iron oxides content is ~1.3%, which expected to be higher in greater depths. All expectations are confirmed from the corresponding offshore spatial distribution patterns of SiO_2 and CaO (Fig. 5.31a,b). Trace elements do not display any significant enrichment.

Sfinari area

The coastal sediments from Sfinari area, western Crete Island, are classified as gravel (>99%) and moderately well sorted (Fig. 5.28; 5.70; Annex II-Grain Size Analysis). Also, the sediments from the adjacent nearshore area are moderately well sorted and sandy (>99%), implying a clear zoning distribution from the beach to greater depths and stable hydro- and sediment- dynamic conditions. The mineralogical analysis of Sfinari area samples, west Crete Island, revealed that the dominant mineralogical phase is quartz (Table 4.16). Moreover, calcite, magnesian calcite and dolomite occur as trace minerals. The coastal mineralogy coincides with the offshore mineralogical status of Kissamos Bay, with the exception of the significant enrichment in clay minerals, such as illite, chlorite and smectite group minerals that are observed in greater depths due the hydro- and sediment- dynamics (Table 4.11; Fig. 5.31f,g).

Other coast areas from Crete Island

Sample from Tavronitis area, east of Kissamos Bay, is classified as moderately sorted, gravelly sand (Annex II-Grain Size Analysis; Fig. 5.70). The coastal sediments from Kampos area, western Crete Island, are located south of Sfinari area and according to their grain size analysis are classified as gravely sand to sandy gravel, moderately to poorly sorted respectively (Fig. 5.70; Annex II-Grain Size Analysis). This fact implies a different dynamic environment than Sfinari. Furthermore, sample from Orthi Ammos, south Crete Island, is classified as well sorted sand (Fig. 5.70; Annex II-Grain Size Analysis).

The coastal sediments from Kampos area, western Crete Island, present quartz as the main mineral and calcite, dolomite and clay minerals (illite and smectite group minerals) as trace minerals. The presence of clay minerals in the coastal area imply the different sediments supply and/or hydro- and sediment- dynamics that prevail in the area, that the northern Sfinari area. This fact also verified by the interpretation of the grain size data, mentioned above. The mineralogical analysis of the sample Tavronitis area display quartz as the

prevailing mineral, calcite as trace mineral and clay minerals (illite and chlorite group minerals) as minor minerals (Table 4.17). Sample from Orthi Ammos, south Crete Island, display, also, quartz as the major mineral, various carbonates, such as calcite, magnesian calcite and dolomite as trace minerals, as well as edenite also detected as trace mineral, probably derived from the amphibolite schists that occur in the hinterland (Fig. 2.10-12).

From the above data, the characteristics of the nearshore Kampos area does not suggest that the adjacent offshore area hosts marine aggregates suitable for the construction industry, being poor in quartz content In addition, the sediments' sorting degree is not promising. The same conclusion applies also to the offshore Orthi Ammos area as its associated nearshore area is rich in amphiboles. Sediments from the nearshore area of Tavronitis present similar qualitative characteristics (moderately well sorted, same mineralogical content) as those from Kissamos Bay. However, emphasis should be given on the coastal geomorphological and oceanographic characteristics that may vary significantly from those in the Kissamoes Bay of the Tavronitis adjacent offshore area in order the potential prospecting of MA to be defined.

North and East Peloponnese (East Gulf of Corinth and Argolic Gulf)

Argolic Gulf

Grain size analysis, revealed that sample from Argolic Gulf (Astros area) is classified as sandy gravel, however very poorly sorted with ~59% of gravel content (Fig. 5.71; Annex II-Grain Size Analysis).

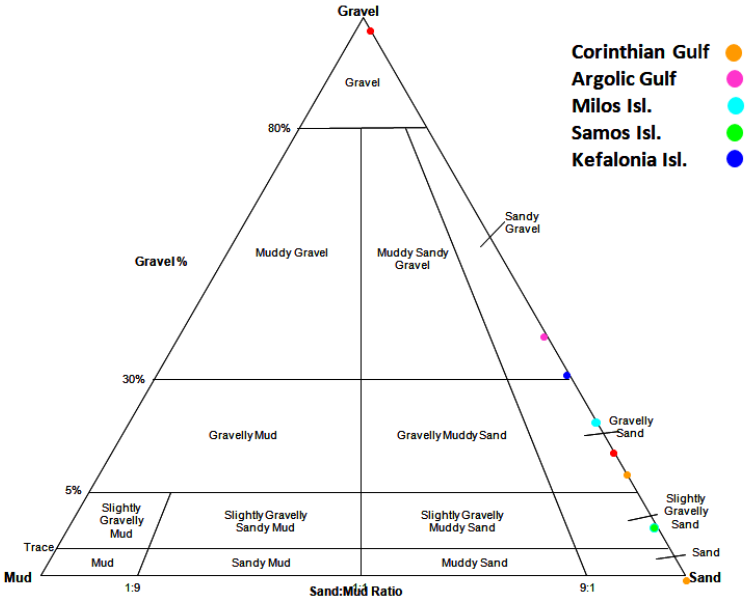

Figure 5.71. Grain-size classification of the coastal sediment samples from various coastal areas, according to Folk (1980).

Mineralogical analysis revealed that sample from Argolic Gulf (Astros area) displays quartz as major mineral and calcite as the second most important crystalline phase originated from the carbonate sequences of Pindos Unit (§2.3). Moreover, magnesian calcite occurs as trace mineral implying the marine origin of the sediments. Albite, clay minerals (illite and chlorite group minerals) and amphiboles, such as glaucophane and actinolite, also occur as trace/minor minerals (Table 4.17).

The poor sorting degree and the rich mineralogical content of the sediments from Argolic Gulf imply that its adjacent offshore area does not host potential marine aggregates deposits with suitable characteristics for the construction industry.

Corinth Gulf

Grain size analysis, revealed that samples from Corinthian Gulf are classified as gravelly sand to gravel, moderately (Kamari area) to poorly sorted (Fig. 5.71; Annex II-Grain Size Analysis). Sample from Kamari area contains ~99% gravel content, while the other samples contain ~85-90% sand content (Annex II-Grain Size Analysis). Mineralogical analysis of samples from Corinthian Gulf revealed quartz and calcite as the major crystalline

phases. Albite, dolomite and clay minerals (illite and chlorite group minerals) occur as trace minerals.

The moderately to poor sorting degree and the variable mineralogical content of the sediments from Corinth Gulf imply that its adjacent offshore area does not host potential marine aggregates deposits with suitable characteristics for the construction industry.

Aegean Sea islands (Milos and Samos Islands)

Milos Island

Grain size analysis of Milos Island sample classified it as poorly sorted, gravely sand with ~85% of sand content (Fig. 5.71; Annex II-Grain Size Analysis). Mineralogical analysis of sample from Plathiena, north Milos Island, revealed that quartz is the major crystalline phase, while only sanidine occurs as trace mineral implying the hydrothermal influence on the sediments and the magnesian calcite as minor mineralogical phase (Table 4.17).

The mineralogical status of the sediments from Milos Island indicates that the adjacent offshore area may host potential marine aggregates deposits at its adjacent offshore area exclusively regarding their suitability for the construction industry. However, in order ensure suitability for industrial use, a chemical analysis is required to determine any impurities.

Samos Island

Grain size analysis of samples from Samos Island revealed that they are classified as well sorted, slightly gravelly sand with ~99% of sand content (Fig. 5.71; Annex II-Grain Size Analysis). The mineralogical analysis of the sample from Balos beach, west Samos Island, revealed that quartz is the major mineral and calcite the second most abundant mineral. Moreover, albite, dolomite and clay minerals (illite and chlorite group minerals) occur as trace minerals (Table 4.17). Mineralogical content of the ample from the Psili Ammos beach, east Samos Island displays differences. Quartz is also the major mineral; however albite is second most abundant mineral. Moreover, calcite and potassium feldspars (orthoclase and sanidine) occur as trace minerals (Table 4.17).

The rich mineralogical content of the sediments from Samos Island suggest that the adjacent offshore areas do not host any potential marine aggregates deposits being suitable for the construction industry.

SE Kefalonia Island

Grain size analysis, revealed that sample from Skala area, SE Kefalonia Island classified as moderately sorted, sandy gravel with ~67% of sand content (Fig. 5.71; Annex II-Grain Size Analysis). The mineralogy of the sample revealed quartz as the dominant crystalline phase and calcite as trace mineral, which is derived from the carbonate sequences of Ionian and Paxoi Units (§2.3).

The relatively enriched silica content at sediments from Skala area is attributed to the formation of Pleistocene silica sand deposit located onshore and nearby the coastal area (Kontopanou, 2019). The resource of the silica material is the intercalated silica cherts at the Mesozoic limestones of Ionian Unit (§2.3). Probably, through various procedures, $CaCO_3$ dissolved and silica transported in short distances and deposited. However, the SiO_2 varies significantly at the Pleistocene onshore sand deposit (68 – 95%). The average silica content is expected to be slightly enriched at the coastal area of Skala, thus it contains significantly high $CaCO_3$ content >20% (Kontopanou, 2019) and this fact deteriorates its' quality. Furthermore, chert origin may imply micro or crypto-crystallic quartz which is harmful for concrete aggregates (§1.4) as they are alkali-reactive.

5.3. QUALITATIVE CHARACTERISTICS OF INDUSTRIAL SAMPLES

Physical characteristics, mineralogy and geochemistry of industrial samples were examined, in order to determine their qualitative characteristics and to compare them with those of the offshore areas under investigation that probably host marine aggregates deposits, i.e. the offshore areas of SE Evia Island and Kissamos Bay, NW Crete Island

Industrial samples from ***Bournemouth and Boscombe, southern UK coastline*** were collected from replenished beaches. Mineralogical analysis revealed that the major crystalline phase is quartz and calcite only occurs as trace mineral (Table 4.18). Stereo-microscpoic observations (Fig. 4.5 e, f) and SEM/EDS analysis (Fig. 4.34; 4.36) revealed the good sorting degree of the samples and the sub-angular to rounded shape of the grains, implying that the

material is reworked. Moreover, SEM/EDS analysis (Fig. 4.34) detected stains of iron oxides in various grains in both samples. Chemical analysis showed that SiO_2 is ~87% in both samples suggesting the high quartz content. Al_2O_3 varies 2-2.3% and Fe_2O_3 between 0.35-1.2% (Annex III – Chemical Analysis) probably derived from fragments or clasts of silicate minerals (Mathers et al., 2014). This material, although it used for beach replenishment projects, is suitable for concrete applications, due to its' high purity. This fact is confirmed by the figures of the intertemporal use of marine aggregates (since) derived from the entire UK coastline into various projects, such us underground stations, terminals and athletic infrastructures (e.g. Highley et al., 2007).

Similar qualitative characteristics are noticed into the western sub-area off SE Evia Island, at the southern coastal area of east/central Evia Island (EV samples) and at Sfinari Bay, suggesting that the corresponding materials are suitable for various uses in the construction industry.

Sediment sample from ***Marina di Torre del Lago Puccini, located at Tuscany, NW Italy***, was collected from the beach which is part of a replenishment sand project at the coastline of Tuscany. The mineralogical analysis revealed that quartz is the prevailing crystalline phase and albite and calcite occur as minerals of trace content. The mineralogical qualitative analysis showed that the only difference from the UK samples is the additional albite content at the Italian sample. However, the semi-quantitative analysis suggests that the quartz content at the Italian sand is significantly lower than that in UK samples.

Nairobi sand, Kenya is an industrial material similar to Sahara sand, which is used for cement manufacture (clinker). The mineralogical analysis revealed that quartz is the dominant and almost exclusive mineral and only minor amounts of chlorite group minerals were detected (Table 4.18). Stereo-microscopy and SEM/EDS analysis revealed the excellent sorting degree of the materials, the rounded shape of the grains (Fig. 4.40-42) and Nairobi sand displays the highest specific weight among the industrial samples, ~2.69 g/cm^3. Moreover, SEM/EDS revealed grains of titanium-iron oxides (probably ilmenite).

Such qualitative characteristics display sediments from Sfinari, west Crete Island and northern coastal sediments from east/central Evia Island (NST samples); however Greek marine aggregates display more angular shape.

Industrial sample from ***Aliartos area, central Greece***, was collected from an active quarry which extracts aggregates for construction applications. The mineralogical analysis revealed quartz as the major mineral, chlorite group as minerals of medium content and albite, calcite, illite/muscovite, glaucophane, orthoclase and talc as trace mineral (Table 4.18). Stereo-microscopic (Fig. 4.5a) and SEM/EDS (Fig. 4.31 - 33) analysis revealed the poor sorting degree and the angular to sub-angular shape of the grains. Chemical analysis showed that SiO_2 content is ~65%, CaO content ~14% and Fe_2O_3 and MgO content ~1-1.5% (Annex III – Chemical Analysis).

The profile of the aggregates from Aliartos area display quite inferior or equivalent features to these from the offshore areas of SE Evia Island and Kissamos Bay and Sfinari Bay, NW Crete Island.

Samples from ***Strymonas River, northern Greece***, are an industrial material (sand and gravel) which is currently used from the wider construction industry. The mineralogical analysis revealed quartz as the prevailing crystalline phase and chlorite group minerals as minerals of medium content. Furthermore, albite, calcite, illite/muscovite, feldspars and talc were detected as trace minerals (Table 4.18). Stereo-microscopic (Fig. 4.5b) and SEM/EDS (Fig. 4.37) analysis determined that sediments are poorly to moderately sorted. The chemical analysis showed that SiO_2 content is ~75%, Al_2O_3 is ~11% and is probably related to the significant existence of clay minerals, CaO is ~1% due to the carbonates and Fe_2O_3 ~1.3% (Annex III – Chemical Analysis). Moreover, SEM/EDS analysis (Fig. 4.38) detected various zircon and Ce-monazite grains, suggesting their origin from the Maronia Plutonic Complex in Northern Greece (Papadopoulos et al., 2019).

The material from Strymonas River is suitable for uses of the wider construction industry (e.g. roads, mortars etc); however is unsuitable as aggregates for concrete manufacturing due to its' high clay minerals content, which is forbidden according to various European and national restrictions (§1.4).

Bulk sample from ***Kafireas Strait, off south Evia Island*** was collected from a currently licensed marine aggregates dredging area and is an industrial material that is used from the wider construction industry in various uses other than concrete. The mineralogical analysis that quartz and albite are the major mineralogical phases and calcite, clay minerals, feldspars, glaucophane and talc are trace minerals (Table 4.18). Chemical analysis showed that SiO_2 content is ~60%, Al_2O_3 is ~10.5% and is probably related to the significant existence of

feldspars, CaO is ~10% due to the carbonates and Fe_2O_3 ~4% (Annex III – Chemical Analysis).

Marine aggregates from Kafireas Strait are correctly used from the wider construction industry in uses other than concrete, as they contain Fe_2O_3 >2%, which is restricted according to various European and national restrictions (§1.4). Moreover, the high content of feldspars is harmful in concrete aggregates, as they contain alkalis in their structure and are able to release them in conditions of high alkalinity (Ferraz et al., 2017).

5.4. TECHNICAL TESTS OF THE OFFSHORE MARINE AGGREGATES AS CONCRETE AGGREGATES

A series of critical technical tests were applied to the material obtained from the two promising areas off SE Evia Island and Kissamos Bay, Crete Island. These tests were performed i) in order to determine the suitability degree of the respective materials as concrete aggregates and also ii) to perceive in hindsight the efficiency of the criteria, such as the physical characteristics, grain size, mineralogy and geochemistry of the final qualified materials as concrete aggregates.

Grain size data were interpreted according to GCCT (2016), and grain size analysis is performed due to ELOT EN 933.01. Grain size data display according to GCCT (2016), is a factor which determines their suitability as concrete aggregates in reinforced or unreinforced concrete or defines the need for further processing.

The display of the grain size data of the offshore areas of SE Evia Island and Kissamos Bay, Crete Island revealed that grain size curves for both washed (§4.7) and unwashed samples from both areas are above the subzones D and E (Fig. 5.72). This fact implies that all samples have excess of required fine fraction, which demands great amounts of water and give a high probability of cement cracking (EN12620, 2002; GCCT, 2016). Therefore, the materials from the under study offshore areas should be subjected into further mechanical processing in order to remove the undesired percent of fine fraction. This procedure will allow the aggregates to be used in reinforced concrete (EN12620, 2002; GCCT, 2016). As noticed, washing of the samples did not improve their performance regarding the desirable sub-zones D and E.

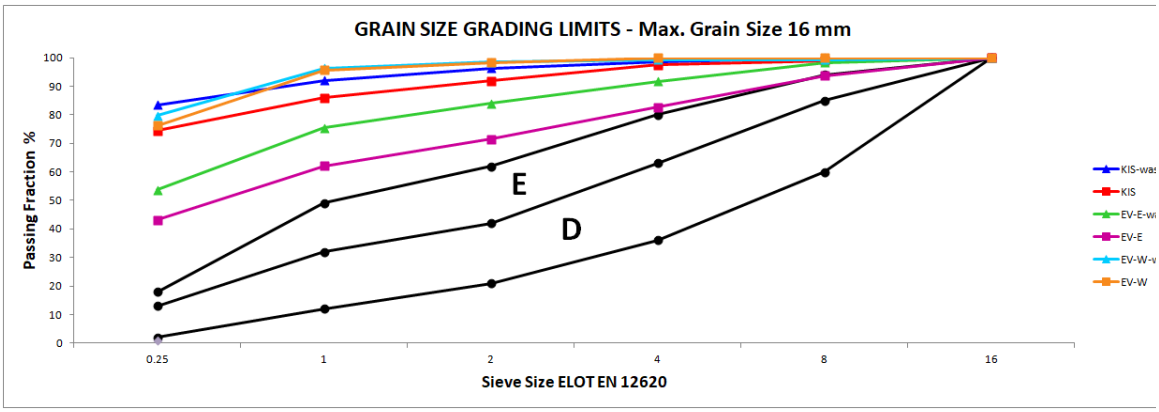

Figure 5.72. Grain size curves of aggregates mixtures from the offshore areas of SE Evia Island and Kissamos Bay, Crete Island according to GCCT (2016).

As mentioned in §3.3.9. ***Sand Equivalent (SE) test*** quantifies the relative abundance of fine-dust or clay-like materials in sand aggregates. However, SE test is not able to distinguish the difference between a swelling and not swelling clay, such is i.e. a kaolinite versus a bentonite mineral (Fournari and Ioannou, 2019). Therefore, SE test must be co-evaluated with mineralogical analysis and Methylene Blue (MB) test.

According to GCCT (2016),, SE should be >70 for collected sand and gravel, such as marine aggregates. The results of sand equivalent test show significant fluctuations in the case of washed and not washed material. This fact indicates that washing procedure removes part of the fine fraction that is harmful for the concrete. According to SE tests, unwashed material of all samples is not suitable for concrete aggregates (Fig. 5.73a). Washed materials from both offshore sub-areas of SE Evia Island is suitable as they display SE values >70. Washed material from Kissamos Bay, NW Crete needs further processing (grain size process) in order to qualify for concrete aggregates.

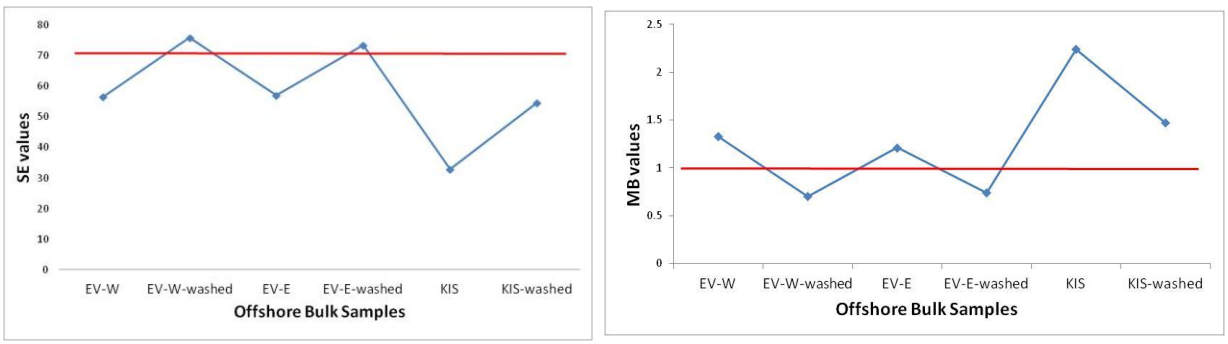

Figure 5.73. (a) Sand equivalent and (b) methylene blue tests of the offshore bulk samples. Red line is the threshold that GCCT, 2016, sets for the collected aggregates from natural resources.

In opposition to SE tests, ***Methylene Blue (MB) test*** quantifies the reactive clay fraction (e.g. swelling bentonite) that the fine fraction of the aggregates may contain (e.g. Fournari and Ioannou, 2019). According to GCCT (2016), MB values for aggregates (either crushed or collected) should be ≤ 1.0 g/kg. As also observed to SE, MB results indicate that the unwashed material of all samples is not suitable for concrete aggregates; the washed material of both offshore areas from SE Evia Island is suitable for concrete aggregates and the washed material of Kissamos Bay, NW Crete Island is unsuitable and need further processing (Fig. 5.73b).

Both SE and MB tests reveal that the material from the offshore area of SE Evia Island is superior to that of Kissamos Bay. Marine aggregates from Kissamos Bay contain clay minerals that could be harmful to concrete due to their ability to absorb water and therefore to contribute to the decline of concrete strength. Furthermore, SE and MB results indicate their good relation; however both tests remain complementary and cannot replace each other, as they detect different clay minerals (Fournari and Ioannou, 2019).

Chlorides are present in aggregates and especially in marine aggregates and their contribution to concrete should be in perspective as two major issues relevant to chlorides arise in concrete: i) corrosion and ii) alkali silica reaction (ASR; e.g. Sirivivatnanon et al., 2011). Chloride is considered to be the most aggressive ion that contributes to the corrosion of reinforced concrete (Barberon et al., 2005). Only free chloride is responsible for depassivation and corrosion in concrete (e.g. Byfors et al., 1986). Marine aggregates are susceptible to ASR, like the equivalent land-based aggregates (BMAPA, 2002). Therefore a small contribution to available alkali from the chloride content is taking place and restrictions to chloride content also minimize the risk for ASR (BMAPA, 2002).

According to GCCT (2016), in concrete containing steel reinforcement marine aggregates may contain up to 0.04% chlorides w/w, even if these marine aggregates are not washed. In concrete containing prestressing steel reinforcement marine aggregates always should be subjected to washing procedure; however chlorides also should be below 0.04% w/w.

According to Table 4.21, all samples prior washing were above the restricted chlorides content (GCCT, 2016). After the first wash, marine aggregates from SE Evia Island

almost reached the desired limit, whereas marine aggregates from Kissamos Bay, NW Crete Island, required a second wash in order to approach the GCCT limit (5.71a). Therefore, marine aggregates from SE Evia Island are suitable as concrete aggregates after the first to second wash and those from Kissamos Bay are suitable after the second to third wash. As noticed in Table 4.21, after the fourth wash chlorine leachates approach zero. Material from Afantou Bay, NE Rhodes Island was included for comparison reasons and the results indicate that according to this factor are also unsuitable, as after four successive washes, chloride limit is still violated (Fig. 5. 74a). Furthermore, chlorine reduction is carried out at a corresponding rate in samples from SE Evia and NW Crete Island during successive rinses and at a significantly lower rate in samples from NE Rhodes Island (5.71b).

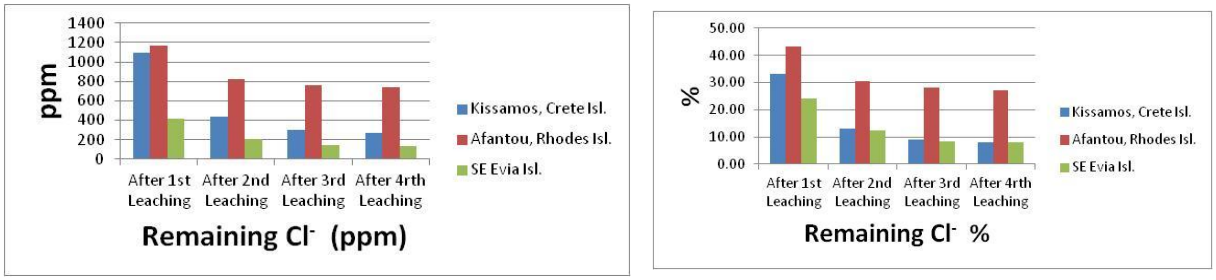

Figure 5.74. Graphic illustration of the remaining chlorine content after successive washes with tab water.

CHAPTER 6. CONCLUSIONS

This is the first time that an integrated study based on qualitative criteria regarding Marine Agrgegates deposits is carried out in Greece.The present PhD thesis investigates thoroughly four offshore areas in the Greek territory regarding their potential to host marine aggregates (MA) deposits suitable for the construction industry. A few coastal areas were, also, examined in order to suggest or not their potential for further offshore investigation. Moreover, selected industrial samples were employed as materials for evaluation and comparison to the under study marine aggregates.

The sedimentological, mineralogical and geochemical characteristics of the sediments revealed their potential as Marine Aggregates suitable for cement production. Emphasis was given to the chlorine content and, as expected, sediments with high quartz and low clay minerals content carry relatively low chlorine content. Furthermore, at each offshore area the most important environmental spatial restrictions, such as closure depth, *Posidonia oceanica* meadows and appropriate distance from the coastline, were applied, in order to identify the most prominent areas that are probably hosting marine aggregates deposits. According to the qualitative criteria, the environmental restrictions and the technical tests, the study areas were prioritized as possible to host MA deposits.

The offshore areas that comply with all the qualitative physical, mineralogical and geochemical characteristics that are suitable for the construction industry and take into consideration all the environmental restrictions which arise from the current European and national legislation, regulation and practices are located at SE Evia Island and NW Crete Island (Kissamos). The offshore area of Evia Island is suggested as the most promising area and hosts MA deposits that cover 2.03 km^2 up to the water-depth of 50 m and 3.2 km^2 over the isobath of 100 m. These sediments show high compositional maturity and purity, such as suitable grain size with good sorting, high quartz content, low clay minerals and chlorine content. However, the promising areas are downscaled from the environmental restriction of the natura zones.The second most promising area is Kissamos Bay, NW Crete Island which hosts MA deposit that covers 4.85 km^2 up to the water-depth of 50 m. This deposit has slightly inferior qualitative characteristics than SE Evia Island, mostly due the increased calcite and chlorine content. The identification of MA deposit in Kissamos Bay justifies the empirical past dredging activities that took place in the area.

Regarding the other offshore areas, the study of Sfinari Bay, west Crete Island, revealed material that displays high qualitative characteristics for uses into the construction industry and therefore, this area is highly proposed to be further investigated as probably hosts MA deposits. Morever, it is noticed that these sediments are strongly related to the phyllite-quartzite series. At Lesvos Island, the offshore area of Eresos is hardly expected to host suitable aggregates for any future uses for the construction industry, however, it is suggested that the material should be further investigated. The offshore areas of Vatera and Mytilene Strait do not host suitable aggregates for uses from the construction industry. Ultimately, also, the offshore area of Afantou Bay, NE Rhodes Island, does not host suitable aggregates for any uses from the construction industry.

The study of various coastal samples revealed the following promising areas that may suggest further investigation at the adjacent offshore areas, if the oceanographical and environmental characteristics confirm it. These areas are: i) the northern coastal area of east/central Evia Island, where the sediments display the highest qualitative characteristics among all studied samples (offshore and coastal), ii) the southern coastal area of east/central Evia Island, where the sediments display inferior qualitative characteristics of those from the northern coastal area, however it is suggested to investigate the adjacent offshore area and iii) the coastal area of northern Milos Island, which it is suggested that it should be further investigated as the mineralogical status of the coastal sediments is positively evaluated.

The mineralogy and geochemistry of the offshore sediments is strongly related to the geology/lithology of the adjacent hinterland. Moreover, alike placer deposits, the mineralogical composition of the sediments is related to the grain size and the distance from the coastline, as the coarser and/ or heavier grains accumulate near the coastline and the lighter ones spread deeper.

The suggested MA deposits and the proposed coastal areas for further investigation, contribute to the national potential for raw materials. However, for the final stage of MA deposits delimitation and exploitation, the local spatial planning issues should be considered in order to support the environmental, social and economic sustainability pillars.

REFERENCES

AASHTO T 176, 2017. Standard Method of Test for Plastic Fines in Graded Aggregates and Soils by Use of the Sand Equivalent Test. American Association of State Highway and Transportation Officials (AASHTO), pp. 13.

Agiadi, K., 2013. Investigation of the Plio-Pleistocene eastern Mediterranean Ichthyofauna and paleoenvironmental representations on Rhodes and Crete Islands. PhD Thesis, National and Kapodistrian University of Athens, pp. 241.

Altherr, R., Seidel, E., 1977. Speculations on the geodynamic evolution of the Attic–cycladic crystalline complex during alpidic times. Proceedings of the VI. Colloquium on the Geology of the Aegean Region, Athens, 1, 347–52.

American Society for Testing and Materials (ASTM), 2003. Annual Book of ASTM Standards, Volume 04.03, Road and Paving Materials; Vehicle-Pavement Systems. ASTM International. West Conshohocken, PA.

Anagnostou, C., Sioulas, A., Hatiris, G. A., Karageorgis, A., Chronis, G., 2011. Erosion: A human induced threat for the NW coasts of Rhodes Island (SE Greece). MEDCOAST 11, 2, 781-786.

Anastasatou, M., Tsoutsia, A., Stamatakis, M., Velegrakis, A., Poulos, S., Kapsimalis, V., 2014. Review on marine aggregates deposits in Europe and their uses. 10th International Congress of the Hellenic Geographical Society, Thessaloniki, 22 – 24/10/2014.

Anastasatou, M., Tsoutsia, A. , Stamatakis, M., Roussakis, G., Kapsimalis, V., Voudouris, P., Mitsis, I., Petrakis, S., Karditsa, A., Poulos, S., Panagiotopoulos, I., Koukounari, I., Hasiotis, Th., Aspiotis, K., Stamatakis, G., Papavlassopoulou, N., 2015. The relation between the coastal hinterland bedrock and the nature of the offshore sea bedded sediments. Examples from the Aegean Sea, Greece. 11th Panhellenic Symposium on Oceanography and Fisheries, Mytilene, Lesvos island, Greece. pp. 1061-1064.

Anastasatou, M., Karditsa, A., Petrakis, S., Tsoutsia, A., Kapsimalis, V., Foutrakis, P., Hasiotis, T., Roussakis, G., Evangelopoulos, A., Poulos, S., Stamatakis, M., 2019. Marine Aggregates Deposits of Kissamos Bay, Crete, Greece. Proceedings of 14th International

MEDCOAST Congress on Coastal and Marine Sciences, Engineering, Management & Conservation, 22–26 Oct. Marmaris Turkey, 221–232.

Anastasatou M., Stamatakis M., Karageorgis A., 2019a. Mineralogy and geochemistry of beach black sands along the coastline of Milos and SW Kimolos Islands, Greece. 15th Biennial Meeting of the Society for Geology Applied to Mineral Deposits, Glasgow, UK, Vol.2, pp. 885-888.

Antoine, P., Coutard, J.P., Gibbard, P.L., Hallegouet, B., Lautridou, J.P., Ozouf, J.C., 2003. The Pleistocene rivers of the English Channel region. Journal of Quaternary Science, 18(3-4), 227-243.

Arvanitidis, N., 1998. Northern Greece's industrial minerals: production and environmental technology developments. Journal of Geochemical Exploration 62, 217-227.

ASTM C1777-15, 2015. Standard Test Method for Rapid Determination of the Methylene Blue Value for Fine Aggregate or Mineral Filler Using a Colorimeter, ASTM International, West Conshohocken, PA. www.astm.org

ASTM D2419-14, 2014. Standard Test Method for Sand Equivalent Value of Soils and Fine Aggregate, ASTM International, West Conshohocken, PA. www.astm.org.

Athanassoulis, G.A., Skarsoulis, E.K., 1992. Wind and Wave Atlas of the Northeastern Mediterranean Sea. Athens: National Technical University of Athens, Laboratory of Ship and Marine Hydrodynamics.

Baker, E., Gaill, F., Karageorgis, A., Lamarche, G., Narayanaswamy, B., Parr, J., Raharimananirina, C., Santos, R., Sharma, R., Tuhumwire, J., 2016. Offshore Mining Industries. In The First Global Integrated Marine Assessment; World Ocean Assessment I; United Nations (UN): New York, NY, USA.

Baltatzis, E., 1996. Blueschist-to-greenschist transition and the P-T path of prasinites from the Lavrion area, Greece. Mineralogical Magazine, 60, p. 551-561.

Barberon, F., Bouny, V.B., Zanni, H., Bresson, B., Caillerie, J.B., Malosse, L., Zehong, G., 2005. Interactions between chloride and cement-paste materials. Magn. Reson. Imag. 23, 267–272.

Barhoum, A., García-Betancourt, M.L., Rahier, H., Van Assche, G., 2018. Chapter 9 - Physicochemical characterization of nanomaterials: polymorph, composition, wettability, and thermal stability. Eds: Ahmed Barhoum, Abdel Salam Hamdy Makhlouf In Micro and Nano Technologies, Emerging Applications of Nanoparticles and Architecture Nanostructures, pp. 255-278, https://doi.org/10.1016/B978-0-323-51254-1.00009-9.

Barksdale, R.D. (editor), 1996. The Aggregate Handbook. Third edition. National Stone Association. Braun-Brumfield, Inc. USA.

Barrie, J.V., Conway, K.W., 2014. Seabed characterization for the development of marine renewable energy on the Pacific margin of Canada. Continental Shelf Research, 83, 45–52.

BGS, 2007. Construction Aggregates. Mineral Planning Factsheet, pp. 30.

Blengini G.A., Gabarino E., 2011. Life Cycle Assessment (LCA) Guidelines; Activity 3.3 (Recycling). http://www.sarmaproject.eu/.

Blott, S.J., Pye, K., 2001. GRADISTAT: a grain size distribution and statistics package for the analysis of unconsolidated sediments. Earth Surface Processes and Landforms, 26, 1237-1248.

BMAPA, 2002. Marine Aggregates in Concrete, pp.2.

BMAPA, 2013. Marine aggregate dredging and the coastline: a guidance note. The Crown Estate, pp. 52. ISBN: 978-1-906410-50-6.

BMAPA, 2020. Marine aggregates in concrete. The Crown Estate, pp. 2.

Bonneau, M., 1984. Correlation of the Hellinides nappes in the South-East Aegean and their tectonic reconstruction, Geological Society of London, special Publications, 17, 517-527.

Bornovas, J., Rontogianni-Tsiambaou, Th., 1983. Geological Map of Greece, Scale: 1:500.000. Institute of Geology and Mineral Exploration, 2nd Edition.

Brocker, M., Kreuzer, H., Matthews, A., Okrusch, M., 1993. 40Ar/39Ar and oxygen isotope studies of polymetamorphism from Tinos Island, Cycladic blueschist belt. J. Metamorph. Geol. 11, 223–240.

Bröcker, M., Franz, L., 1998. Rb–Sr isotope studies on Tinos Island Cyclades, Greece: additional time constraints for metamorphism, extent of infiltration-controlled overprinting and deformational activity. Geol. Mag. 135-3, 369–382.

Burgess, J., Foulkes, L., Jones, P., Merighi, M., Murray, S., Whitacre, J., 2017. Law of the Sea – A policy primer. LL.M. Program in International Law + Fletcher Maritime Studies Program, Tufts University, p. 93.

Byfors, K., Hansson, C. M., Tritthart, J., 1986. Pore solution expression as a method to determine the influence of mineral additives on chloride binding. Cement Concrete Research, Vol. 16, No. 5, pp. 760-770.

Chatzaras, V., Dörr, W., Finger, F., Xypolias, P., Zulauf, G., 2013. U-Pb single zircon ages and geochemistry of metagranitoid rocks in the Cycladic Blueschists (Evia Island): Implications for the Triassic tectonic setting of Greece. Tectonophysics. 595-596. 125-139.

Chatzipavlis, A., Monioudi, I., Velegrakis, A. F., Andreadis, O., 2012. Case Scenario Investigation of Beach Nourishment in Eresos Beach, Lesvos, Greece. Proceedings of the International Offshore and Polar Engineering Conference.

Chiocci, F.L., Chivas, A.R., 2014. Continental Shelves of the World: Their Evolution During the Last Glacio-Eustatic Cycle. Geological Society, London, Memoirs, 41, 1–5.

Cornée, J.J., Moissette, P., Joannin, S., Suc, J.P., Quillévéré, F., Krijgsman, W., Hilgen, F., Koskeridou, E., Münch, P., Lécuyer, C., Desvignes, P., 2006. Tectonic and climatic controls on coastal sedimentation: Late Pliocene-Middle Pleistocene of northeastern Rhodes, Greece. Sedimentary Geology, 187, 159-181.

Cronan, D. S., 2003. Marine Placers. In: Sedimentology. Encyclopedia of Earth Science, pp. 864 - 869. ISBN: 978-1-4020-3609-5.

Cruickshank, M.J., 1988. Marine mining. In: General Geology. Encyclopedia of Earth Science. Springer, Boston, MA.

Diaz, J.I., Nelson, C.H., Barber, J.H.Jr., Gro, S., 1990. Late Pleistocene and Holocene sedimentary facies on the Ebro continental shelf. Marine Geology, 95: 333-352.

Díaz-Almela E., Duarte C.M., 2008. Management of Natura 2000 habitats. 1120 *Posidonia beds (Posidonion oceanicae). European Commission

Dickie, I., Hime, S., Lockhart-Mummery, E., Ozdemiroglu, E., Tinch, R., 2011. Including the Socio-Economic Impacts of Marine Aggregate Dredging in Decision-Making. http://www.eftec.co.uk/home.

Dora, G.U., Kumar, S.V., Philip, C., Glejin J., Vinayaraj, P., Gowthaman, R., 2011. Textural characteristics of foreshore sediments along Karnataka shoreline, west coast of India. International Journal of Sediment Research – Int. J. Sediment Res., 26, 364-377. 10.1016/S1001-6279(11)60100-5.

Dufaure, J.J., 1977. Néotectonique et morphogenèse dans une péninsule méditerranéenne: la Péloponnèse, Revue de Géographie Physique et de Géologie Dynamique, 19(1), 27-58.

Duane, D.B., 1964. Significance of skewness in recent sediments, Western Pamlico Sound. North Carolina. Journal of Sedimentary Petrology, Vol. 34, No. 4, pp. 864-874.

Dürr, S., Altherr, R., Keller, J., Okrusch, M., Seidel, E., 1978. The Median Aegean Crystalline Belt: stratigraphy, structure, metamorphism, magmatism. In Alps, Apennines, Hellenides (eds H. Closs, D. H. Roeder & K. Schmidt), pp. 455–77. IUGS Report no.38. Stuttgart: Schweizerbart.

ELOT EN 933-8, 2012. Tests for geometrical properties of aggregates – Part 8: Assessment of fines – Sand Equivalent Test. Hellenic Organization for Standardization S.A.

ELOT EN 933-9, 2013. Tests for geometrical properties of aggregates – Part -9: Assessment of fine – Methylene Blue Test. Test. Hellenic Organization for Standardization S.A.

Emery, K.O., Noakes, L.C., 1968. Economic placer deposits of the continental shelf. Committee for co-ordination of joint prospecting for mineral resources in Asian offshore areas. Technical Bulletin 1, 95.

EN 933-1:1997. Tests For Geometrical Properties Of Aggregates - Part 1: Determination Of Particle Size Distribution - Sieving Method.

EN 1097:2000. Tests for mechanical and physical properties of aggregates. Determination of particle density and water absorption.

EN 206-1:2000. Concrete. Specification, performance, production and conformity.

EN 12620:2002. Aggregates for Concrete.

Ergin, M., Kazan, B., Yucesoy-Eryilmaz, F., Eryilmaz, M., Okyar, M., 1998. Hydrographic, deltaic and benthogenic controls of sediment dispersal in the Gulf of Iskenderum, SE Turkey (E. Mediterranean). Estuarine Costal & Shelf Science 46, 493–502.

European Commission, 2012. COM (2012) 494, Communication from the Commission to the European Parliament, the Council, the European Economic and Social Committee and the Committee of the regions. Blue Growth opportunities for Marine and Maritime Sustainable Growth. Brussels.

European Minerals Foundation, 2010. The 11th European Minerals Forum "The EU Raw Materials Initiative – What next?". Proceedings, pp. 51.

Evans, G., 1971. The recent sedimentation of Turkey and the adjacent Mediterranean and Black seas: A rreveiw. In: Cambell, A.S., (Ed.), Geology and history of Turkey, Petroleum Exploration Society of Libya, Tripoli, pp. 385–406.

Fassoulas, C., Kilias, A., Mountrakis, D., 1994. Postnappe stacking extension and exhumation of high-pressure/lowtemperature rocks in the island of Crete, Greece. Tectonics, 13, 127–138.

FEK 136, 28/07/2016. Framework for safety in the offshore hydrocarbon exploration and exploitation activities, incorporation of the European Directive 13/30/EU.

Ferraz, A., Fernandes, I., Soares, D., Santos S.A., Quinta-Ferreira, M., 2017. Assessment of the Alteration of Granitic Rocks and its Influence on Alkalis Release. IOP Conference Series: Earth and Environmental Science, 95, 022001. 10.1088/1755-1315/95/2/022001.

Friedman, G.M., 1961. Distinction between dune, beach and river sands from their textural characteristics. Journal of Sedimentary Petrology, 31, 514-529.

Folk, R., 1980. Petrology of sedimentary rocks. Hemphill Publishing Company, Texas, pp.190.

Force, E.R., 1991. Geology of titanium-mineral deposits: Geological Society of America Special Paper 259, p.112.

Forster, M.A., Lister, G.S., 2005. Several-distinct tectono-metamorphic slices in the Cycladic eclogite-blueschist belt, Greece. Contr. Miner. Petrol., 150, 523–545.

Fournari, R., Ioannou, I., 2019. Correlations between the Properties of Crushed Fine Aggregates. Minerals, 9, 86; doi:10.3390/min9020086.

Fytikas, M., Innocenti, F., Kolios, N., Manetti, P., Mazzuoli, R., Poli, G., Rita, F., llari, L., 1986. Volcanology and petrology of volcanic products from the island of Milos and neighbouring islets. J. Volcanol. Geotherm. Res. 28:297–317.

Gallen, S.F., Wegmann, K.W., Bohnenstiehl, D.R., Pazzaglia, F.J., Brandon, M.T., Fassoulas, C., 2014. Active simultaneous uplift and margin-normal extension in a forearc high, Crete, Greece. Earth Planet. Sci. Lett., 398, 11–24.

Gao, S., Collins, M.B., 2014. Holocene sedimentary systems on continental shelves. Marine Geology, 352, 268–294.

Gazis, I.Z., Hasiotis, T., Velegrakis, A.F., Anastasatou, M., Kapsimalis, V., Stamatakis, M., Poulos, S., 2017. The potential of marine aggregate deposits off a highly eroded coastal area in Lesvos Island (Greece)-Implications for coastal management. 15th International Conference on Environmental Science and Technology, pp. 4.

GCCT, 2016. Greek Code of Conrete Technology. GG. 1561/b/02.06.2016.

GRMQ, 2011. Greek Regulation for Mining and Quarrying Activities, FEK122714/06/11.

Gessner, K., Ring, U., Passchier, C.W., Güngör, T., 2001. How to resist subduction: evidence for largescale out-of-sequence thrusting during Eocene collision in western Turkey. Journal of the Geological Society, London, 158, 769-784

Giresse, P., Buscail, R., Charriere, B., 2003. Late Holocene multisource material input into the Aegean Sea: depositional and post-depositional processes. Oceanolo- gica Acta 26, 657–672.

Greek Concrete Technology Regulation, 2016. FEK1561/ 02-06-2016.

Greiling, R., 1982. The metamorphic and structural evolution of the Phyllite-Quartzite Nappe of western Crete. Journal of Structural Geology, 4, 3, 291-297.

Hallermeier, R.J., 1978. Uses for a calculated limit depth to beach erosion. Proceedings, Coastal Engineering 1978:1493–1512.

Hallermeier, R.J., 1981. A profile zonation for seasonal sand beaches from wave climate. Coastal Eng. 4:253–277.

Harlow, D., 2013. Bournemouth beach management (000303). Full Business Case, BCP Council, pp. 20.

Hasiotis, Th., Gazis, I.Z., Anastasatou, M., Manoutsoglou, E., Velegrakis, A. F., Kapsimalis, V., Karditsa, A., Stamatakis M., 2020. Searching for potential marine sand resources to mitigate beach erosion in island settings, Marine Georesources & Geotechnology. doi.org/10.1080/1064119X.2020.1721623.

Hecht, J., 1972. Geological map of Greece, 1:50.000, Lesbos Island-Plomari/Mytilene.

Helbling, A., 2011. Lithium, Beryllium and Boron in high-K Rhyolites from Lesbos Island, Greece. PhD Thesis, Heidelberg University, pp. 305.

Highley, D.E., Hetherington, L.E., Brown, T.J., Harrison, D.J., Jenkins, G.O., 2007. The strategic importance of the marine aggregate industry to the UK. British Geological Survey Research Report, OR/07/019.

ICES, 2005. Report of the Working Group on the Effects of Extraction of Marine Sediments on the Marine Ecosystem (WGEXT). San Sebastián, Spain 5–8 April, ICES CM 2005/E:06, 102 p.

ICES, 2006. Report of the Working Group on the Effects of Extraction of Marine Sediments on the Marine Ecosystem (WGEXT). 4-7 April 2006, Cork, Ireland, ICES CM 2006/E:06, 91p.

Jacobshagen, V., 1986. Geologie von Griechenland. Borntrager, Berlin.

Jolivet, L., Faccenna, C., Goffé, B., Burov, E., Agard, P., 2003. Subduction tectonics and exhumation of high-pressure metamorphic rocks in the Mediterranean orogen. Am. J. Sci., 303, 353–409.

Jolivet, L., Brun, J.P., 2010. Cenozoic geodynamic evolution of the Aegean. Int. J. Earth Sci., 99, 109–138.

Leeder, M.R., 1999. Sedimentology and Sedimentary Basins: from Turbulence to Tectonics. Oxford: Blackwell Science, 591 p.

Kanellopoulos, T.D., Kapsimalis, V., Poulos, S.E., Angelidis, M.O., Karageorgis, A.P., Pavlopoulos, K., 2007. The influence of the Evros River on the recent sedimentation of the inner shelf of the NE Aegean Sea.Environmental Geology, doi:10.1007/s00254-007-0754-2.

Kantiranis, N., Stamatakis, M., Filippidis, A., Squires, C., 2004. The uptake ability of the clinoptilolitic tuffs of Samos Island, Greece. Bulletin of the Geological Society of Greece. 36. 89-96. 10.12681/bgsg.16583.

Kapsimalis, V., Rousakis, G., Hatiris, G., Kalogirou, S., Hasiotis, T., Karditsa, A., Petrakis, S., Poulos S.E., Stamatakis, M., 2013. Searching for Marine Aggregates deposits in the Afandou bay (Rhodes island, Greece) 40th CIESM Congress – Marseille, France, 28 Oct - 1 Nov.

Karageorgis, A., Anagnostou, Ch., Sioulas, A., Eleftheriadis, G., Tsirabides, A., 2000. Distribution of surficial sediments in the Southern Evoikos and Petalioi Gulfs, Greece. Mediterranean Marine Science 1 (1), 111–121.

Karageorgis, A., Kanellopoulos, Th., Papageorgiou A., Taxiarchi M., Kambouri G., 2009. Geochemistry of Major And Minor Elements From Surface Sediments Of Lakonikos Gulf, Greece. 9th Panhellenic Symposium on Oceanography and Fisheries, Patras, Greece, pp. 223-227.

Karditsa, A., 2010. Study of the modern sedimentation of the Gulf (inner continental shelf) of Alexandroupolis. PhD thesis, National and Kapodistrian University of Athens, pp. 251.

Karymbalis, E., Papanastassiou, D., Gaki-Papanastassiou, K., Tsanakas, K., Maroukian, H., 2013. Geomorphological study of Cephalonia Island, Ionian Sea, Western Greece. Journal of Maps. 9. 121-134. 10.1080/17445647.2012.758423.

Katsikatsos, G., 1969. Age of the metamorphic system of S. Evia and its stratigraphic structure (in Greek). Praktika Acad. Athinon, 44, 223-238.

Katsikatsos, G., Migiros, G., Triantaphyllis, M., Mettos, A., 1986. Geological Structure of Internal Hellenides (E. Thessaly-SW Macedonia. Euboea-Attica-Northern Cyclades Islands and Lesvos). IGME, Geol. and Geoph. Res., Special Issue, 191-212.

Katzir, Y., Avigad, D., Matthews, A., Garfunkel, Z., Evans, B.W., 2000. Origin, HP/LT metamorphism and cooling of ophiolitic melanges in southern Evia (NW Cyclades), Greece. Journal of Metamorphic Geology, 18, 699–718.

Kelepertsis, A., Velitzelos, E., 1992. Oligocene swamp sediments of Lesvos Island, Greece (geochemistry and mineralogy). Facies, 27, 113-118.

Kelepertsis, A., 2002. Mineralogy and geochemistry of the Pliocene iron-rich laterite in the Vatera Area, Lesvos Island, Greece and its genesis. Chinese Journal of Geochemistry, 21(3).

Koglin, N., Kostopoulos, D., Reischmann, Th., 2009. The Lesvos mafic-ultramafic complex, Greece: Ophiolite or incipient rift? Lithos, 108, 243-261.

Kontogianni, V., Tsoulos, N., Stiros, S., 2002. Coastal uplift, earthquakes and active faulting of Rhodes Island (Aegean Arc): modeling based on geodetic inversion. Marine Geology, 186 (3–4), 299-317,https://doi.org/10.1016/S0025-3227(02)00334-1.

Kontopanou, D., 2019. Silica Sand in Construction. A case study from Skala, Kefallinia Island, Ionian islands, Greece. Bachelor thesis, National and Kapodistrian University of Athens.

Kontopoulos, N., 2004. Notes on Sedimentology. Departments of Geology, University of Patras, p. 26.

Korre, A., Durucan, S., 2009. Life Cycle Assesment of Aggregates. Imperial College London, EVA025 –Final Report: Aggregates Industry Life Cycle Assessment Model: Modelling Tools and Case Studies, Published by Waste and Resources Action Programme.

Koufogiannis, I., 2015. Metamorphic rocks of Karystos (Southern Evoia). Master Thesis, University of Patras, p. 160.

Kraus, N.C., Larson, M., Wise, R. 1999. Depth of closure in beach-fill design. Proceedings of the 12th National Conference on Beach Preservation Technology. Florida Shore and Beach Preservation Association, pp. 271–286.

Krausmann, F., Gingrich, S., Eisenmenger, N., Erb, K. H., Haber, H., Fischer-Kowalski, M., 2009. Growth in global materials use, GDP and population during the 20th century. Ecological Economics 68, 2696-2705.

Kudrass, H.R., 2000. Marine placer deposits and sea-level changes. In:Cronan, D.S. (Ed.), Handbook of Marine Mineral Deposits. CRC Press, Boca Raton, FL, pp. 3-26.

Lamera, S., Seymour, K., Vamvoukakis, C., Kouli, M., Paraskevas, E., Pe-Piper, G., 2001. The Polychnitos Ignimbrite of Lesvos Island. Bulletin of the Geological Society of Greece XXXIV (3): 917–921. doi: 10.12681/bgsg.17118.

Lekkas, E., Danamos, G., Skourtsos, E., 2007. Implications for the Correlation of the Hellenic Nappes in SW Aegean: the Geological Structure of the Archangelos Region, Rhodes Island. Bulletin of the Geological Society of Greece, 40(1), 374-385. doi:http://dx.doi.org/10.12681/bgsg.16622.

Liati, A., Skarpelis, N., Fanning, C.M., 2013. Late Permian–Early Triassic igneous activity in the Attic Cycladic Belt (Attica): New geochronological data and geodynamic implications. Tectonophysics, Vol. 595–596, 140-147, doi.org/10.1016/j.tecto.2012.05.009.

Litinas, N., 2008. New requirements for aggregates in construction. Experience from CE application in Greece. 1st Panhellenic Conference on Structural Materials and Data, TEE, Athens, 21-23 May, 2008.

Mahaney, W.C., 2002. Atlas of Sand Grain Surface Textures and Applications. Oxford University Press, New York (2002), p. 237.

Maluski, H., Vergely, P., Bavay, D., Bavay, P., Katsikatsos, G., 1981. 39Ar/40Ar dating of glaucophanes and phengites in southern Euboa (Greece): geodynamic implications. Bull Soc Géol Fr, 23, 469–476.

Mangor, K., Drønen, N. K., Kaergaard, K.H., Kristensen, N.E., 2017. Shoreline management guidelines. DHI.

Margolis, S.V., Krinsley, D.H., 1974. Processes of formation and environmental occurrence of microfeatures on detrital quartz grains. Am. J. Sci., 274 (1974), pp. 449-464.

Martins, L., Barboza, E., 2005. Sand-Gravel Marine Deposits and Grain-Size Properties. Gravel - 1678-5975. 3. 59-70.

Martsouka, F., Hasiotis, T., Maneas, G., Kostopoulou, M., 2009. Sediment Distribution and Sedimentary Processes in the Coastal Zone of SE Lesvos Island. Proceedings of 9th National Symposium of Oceanography and Fisheries. Patras 13–16 May, Proceedings 1: 202–207.

Mathers, S., Terrington, R., Waters, C., Leslie, A., 2014. GB3D – a framework for the bedrock geology of Great Britain. Geoscience Data Journal. 1. 10.1002/gdj3.9.

Mayer, L., Mosher, D., 2018. Setting the Context: The Scientific Aspects of Article 76. In Setting the Context: The Scientific Aspects of Article 76. Leiden, The Netherlands: Brill.

McManus, D.A., 1975. Modern versus relict sediments on continental shelf. Geological Society America Bulletin, 86, 1154-1160.

Menegaki, E.M., Kaliampakos, C.D., 2010. European aggregates production: Drivers, correlations and trends. Resources Policy 35 (2010), 235-244.

Miall, A.D., 1996. The Geology of Fluvial Deposits: Sedimentary Facies, Basin Analysis and Petroleum Geology. Springer, Berlin.

Migiros, G., Hatzipanagiotou, K., Gartzos, E., Serelis, K., Tsikouras, B., 2000. Petrogenetic evolution of ultramafic rocks from Lesvos Island (NE Aegean, Greece). Chemie der Erde, 60: 27–46.

Morang, A., Birkemeier, W.A., 2005. Depth of Closure on Sandy Coasts. In: Schwartz M.L. (eds) Encyclopedia of Coastal Science. Encyclopedia of Earth Science Series. Springer, Dordrecht.

Moustaka, E, 2011. Structural analysis and geochemical stydy of minerals of the metamorphic rocks of Mt. Ochi, Southern Evia. MSc Thesis, Faculty of Geology & Geoenvironment. NKUA, Athens, 169.

Mutti E., Orombelli G., Pozzi R., 1970. Geological studies of the Dodecanese Islands (Aegean Sea). Geological map of the Island of Rhodes and Explanatory Notes. Ann. Géol. Pays Hellén. 22, 77–226.

Newell, R., Woodcock, T., 2013. Aggregate dredging and the marine environment: an overview of recent research and current industry practice. BMAPA, The Crown Estate.

Nikolaides, A., Manthos, E., Sarafidou, M., 2007. Sand equivalent and methylene blue value of aggregates for highway engineering. Foundations of Civil and Environmental Engineering. 10.

Ott, R., Willett, S., Herman, F., Gallen, S., Biswas, R., Wegmann, K., 2019. Pleistocene terrace formation, Quaternary rock uplift rates and geodynamics of the Hellenic Subduction Zone revealed from dating of paleoshorelines on Crete, Greece. Earth and Planetary Science Letters, 525.

Palanques, A., Guillen, J., Puig, P., 2001. Impact of bottom trawling on water turbidity and muddy sediment of an unfished continental shelf. Limnology and Oceanography 46 (5): 1100–1110.

Papadopoulos, A., Tzifas, I., Tsikos, H., 2019. The Potential for REE and Associated Critical Metals in Coastal Sand (Placer) Deposits of Greece: A Review. Minerals, 9(8), 469.

Papanikolaou, D., 1984. The three metamorphic belts of the Hellenides: a review and a kinematic interpretation. In: Dixon, J.E., Robertson, A.H.F. (Eds.), The Geological Evolution of the Eastern Mediterranean: Geological Society, London, Special Publication, 17, 551–561.

Papanikolaou, D.J., 1987. Tectonic Evolution of the Cycladic Blueschist Belt (Aegean Sea, Greece). In: Helgeson H.C. (eds) Chemical Transport in Metasomatic Processes. NATO ASI Series (Series C: Mathematical and Physical Sciences), 218, Springer, Dordrecht.

Papanikolaou, D., Lekkas E., Sakellariou, D., J995. Tectonic units and terrane analysis in Rhodos and adjacent Dodekanese islands, Greece, XV Congr. Carpatho-Balcan Geol. Assoc., Symp. Tectonostratigraphic Terranes in CB Region, 20.

Papanikolaou, D., 1999. The Triassic ophiolites of Lesvos Island within the Cimmeride Orogene event. European Union of Geosciences conference abstracts; EUG 10. Journal of Conference Abstracts, 4, 315.

Papanikolaou, D., Bargathi, H., Dabovski, C., Dimitriu, R., El-Hawat, A., Ioane, D., Kranis, H., Obeidi, A., Oaie, G., Seghedi, A., Zagorchev, I., 2004. Transect VII: East European Craton – Scythian Platform – Dobrogea – Balkanides – Rhodope Massif – Hellenides – East Mediterranean – Cyrenaica. In: Cavazza W., Roure F.M., Spakman W., Stampfli G.M., Ziegler P.A., (eds.), The TRANSMED Atlas: The Mediterranean Region from Crust to Mantle.

Papanikolaou, D., Papanikolaou, I., 2007. Geological, geomorphological and tectonic structure of NE Attica and seismic hazard implications for the northern edge of the Athens plain. Bulletin of the Geological Society of Greece. 40. 425-438. 10.12681/bgsg.16634.

Papanikolaou, D., Vassilakis, E., 2010. Thrust faults and extensional detachment faults in Cretan tectono-stratigraphy: Implications for Middle Miocene extension. Tectonophysics, 488.

Papanikolaou, D., 2015. Geology of Greece. ISBN 978-960-16-6343-2.

Pascual, M., Jones, H., 2018. MSP as a Tool to Support Blue Growth. Sector Fiche: Marine Aggregates and Marine Mining. Technical Study for European Commission.

Pehlivanoglou, K., Tsirabides, A., Trontsios, G., 2000. Origin and distribution of clay minerals in the Alexandroupolis Gulf, Aegean Sea, Greece. Estuarine Coastal & Shelf Science 51, 61–73.

Pe-Piper, G., Piper, D., 1993. Revised Stratigraphy of the Miocene Volcanic Rocks of Lesbos, Greece. Neues Jahrbuch fuer Geologie und Palaeontologie. Monatshefte 2: 97–110.

Pe-Piper, G., Piper, D.J.W., 1993. Revised stratigraphy of the Miocene volcanic rocks of Lesbos, Greece. Neues Jahrbuch für Geologie und Paläontologie / Monatshefte 1993: 97–110.

Pe-Piper, G., Piper, D.J.W., Matarangas, D., Varti-Matarangas, M., 2001. The subophiolitic melange of the island of Lesbos, Greece. Neues Jahrbuch für Mineralogie, Monatshefte, (6), 241–260.

Pe-Piper, G., Imperial, A., Piper, D.J.W., Zouros, N., Anastasakis, G., 2019. Nature of the hydrothermal alteration of the Miocene Sigri Petrified Forest and host pyroclastic rocks, western Lesbos, Greece. J. Volc. Geol. Res. 369, 172–187.

Pettijohn, F.G., Potter, P.D., Siever, R., 1972. Sand and Sandstone. New York: Springer-Verlag, 618 p.

Phua, C., Van Den Akker, S., Baretta, J., Van Dalfs en, M., 2004. Ecological Effects of Sand Extraction in the North Sea. Report, p. 22.

Pirazzoli, P.A., Montaggioni, L., Saliege, J., Segonzac, G., Thommeret, Y., Vergnaud-Grazzini, C., 1989. Crustal block movements from Holocene shorelines: Rhodes island (Greece).Tectonophysics 170, 89-114.

Plaiti, W., Sympoura, N., Naletaki, M., Salomidi, M., Di Liberto, S., Pancucci, M.A., 2006. Study of benthic biocommunities of hard substrate on the shores of Rhodes. 8th Panhellenic Symposium on Oceanography & Fisheries, Thessaloniki, pp. 693-699.

Poulos, S.E., 2009. Origin and distribution of the terrigenous component of the unconsolidated surface sediment of the Aegean floor A synthesis. Continental Shelf Research, 29(16), 2045–2060.

Poulos, S., Koukounari, I., Tsoutsia, A., 2015. The current knowledge about marine aggregates presence in Greece. Technical Report, NSRF Project "Thalis – Mare/MIS 375655", NKUA.

Pranzini, E., Cinelli, I., Cipriani, L., Anfuso, G., 2020. An Integrated Coastal Sediment Management Plan: The Example of the Tuscany Region (Italy). Journal of Marine Science and Engineering. 8. 33. 10.3390/jmse8010033.

Radzevičius, R., Velegrakis, A., Bonne, W., Kortekaas, S., Gare, E., Blažauskas, N., Asariotis, R., 2010. Marine Aggregate Extraction Regulation in EU Member States. Journal of Coastal Research 51, 15-38.

Rona, P.A., 2008. The changing vision of marine minerals. Ore Geology Reviews, 33 (3-4) 618-666.

Roos, PC, 2004. Seabed Pattern Dynamics and Offshore Sand Extraction, 166pp. PhD Thesis, University of Twente, The Netherlands, ISBN 90-365-2067-3.

Roy, P.S., 1999. Heavy mineral beach placers in southeastern Australia—Their nature and genesis: Economic Geology. V94,4, pp. 567–588.

Poppe, L.J., McMullen, K.Y., Williams, S.J., Paskevich, V.F., eds., 2014. USGS east-coast sediment analysis: Procedures, database, and GIS data (ver. 3.0, November 2014): U.S. Geological Survey Open-File Report 2005-1001, http://pubs.usgs.gov/of/2005/1001/.

Poulos, S., 2009. Origin and distribution of the terrigenous component of the unconsolidated surface sediment of the Aegean floor: A synthesis. Continental Shelf Research. Cont. Shelf Res., 29, 2045-2060. 10.1016/j.csr.2008.11.010.

Ramadan, R., Gad, A., Yehia, M., & Dawood, Y., Nilly, K., 2019. Grain size and mineralogical characteristics of the stream sediments, east of Abu Zeneima area, southwestern Sinai, Egypt. Arabian Journal of Geosciences. 12. 10.1007/s12517-019-4362-8.

Reilinger, R., McClusky, S., Paradissis, D., Ergintav, S., Vernant, P., 2010. Geodetic constraints on the tectonic evolution of the Aegean region and strain accumu-lation along the Hellenic subduction zone. Tectonophysics, 488, 22–30.

Ring, U., Glodny, J., Will, T., Thomson, S., 2007. An Oligocene extrusion wedge of blueschist-facies nappes on Evia, Aegean Sea, Greece: implications for the early exhumation of high-pressure rocks. Journal of the Geological Society, London 164, 637–652.

SARMA Glossary, 2011. Eds: Imeri S., Šolar S., O'Brien J., Blengini G.A., Hamor T., Garbarino E., Tiess G., Agioutantis Z., http://www.sarmaproject.eu/uploads/media/Glossary_2011_03_01.pdf.

Sarris, A., Karakoudis, S., Vidaki, Ch., Soupios, P., 2005. Study of the Morphological Attributes of Crete through the Use of Remote Sensing Techniques. IASME Trans. 6.

Seidel, E., Kreuzer, H., Harre, W., 1982. A late Oligocene/early Miocene high pressure belt in the external Hellenides. Geol. Jb., 23, 165–206.

Seidel, M., 2003. Tectono-Sedimentary Evolution of Middle Miocene Supra-Detachment Basins (Western Crete, Greece). Unpubl. doctoral dissertation, University of Cologne, 106 pp.

Seidel, M., Seidel, E., Stöckhert, B., 2007. Tectono-sedimentary evolution of Lower to Middle Miocene half-graben basins related to an extensional detachment fault (Western Crete, Greece). Terra Nova, 19, 39 - 47.

Shaked, Y., Avigad, D., Garfunkel, Z., 2000. Alpine high-pressure metamorphism at the Almyropotamos window (southern Evia, Greece). Geological Magazine, 137, 367-380.

Shaffer, N.R., 2006. The Time of Sands: quartz-rich sand deposits as a Renewable Resource. University of Idaho 1-22.

Sirivivatnanon, V., Thomas, W.A., Waye, K., 2011. Determination of Free Chlorides in Aggregates and Concrete, Australian Journal of Structural Engineering, 12:2, 151-158

Skourtsos, E., Kranis, H., Zambetakis-Lekkas, A., Gawthorpe, R., Leeder, M., 2016. Alpine basement outcrops at northern Peloponnesus: implications for the early stages in the evolution of the Corinth Rift. Bulletin of the Geological Society of Greece, 50(1), 153-163.

Spagnoli, F., Dell'Anno, A., Marco, A., Dinelli, E., Fabiano, M., Gadaleta, M., Ianni, C., Loiacono, F., Manini, E., Marini, M., & Mongelli, G., Rampazzo, G., Rivaro, P., Vezzulli, L., 2010. Biogeochemistry, grain size and mineralogy of the central and southern Adriatic sea sediments: A review. Chemistry and Ecology. 26. 19-44. 10.1080/02757541003689829.)

Stamatakis, M., 1989a. A boron-bearing potassium feldspar in volcanic ash and the tuffaceous rocks from Miocene lake depositis, Samos Island, Greece, American Mineralogist 74, 230-235.

Stamatakis, M., 1989b. Authigenic silicates and silica polymorphs in the Miocene saline alkaline deposits of the Karlovassi basin, Samos Island, Greece, Economic Geology 84, 788-798.

Stamatakis, M., Poulos, S., Tsoutsia, A., Anastasatou, M., Karditsa, K., Koukounari, I., Papavlassopoulou, N., Velegrakis, A.F., Hasiotis, T., Evaggelopoulos, A, Koutsoumbas, D., Kapsimalis, V., Roussakis, G., Panagiotopoulos, I., 2015. Marine Aggregates Prospecting and Exploitation (MARE project) in Greek waters: Methods, Environmental Impact and Usage possibilities. 11th Panhellenic Symposium on Oceanography and Fisheries, Mytilene, 13-17 May, Lesvos island, Greece, pp. 1053-1056.

Stamatakis, M., Anastasatou, M., Tsoutsia, A., Petrakis, S., Kapsimalis, V., Roussakis, G., Poulos, S., Karditsa, A., Mitsis, I., Voudouris, P., Aspiotis, K., Stamatakis, G., Velegrakis, A., Papavlassopoulou, N., 2015. Quality factors concerning possible exploitation of Marine Aggregates in NW Crete Island inner shelf. 11thPanhellenic Symposium on Oceanography and Fisheries, Mytilene, Lesvos island, Greece, pp. 1081-1084.

Steele, J., Thorpe, S., Turekian, K., 2010. Marine Policy and Economics, Encyclopedia of Ocean Sciences, Elsevier Ltd., 2nd edition.

Taylor, R.K., 1985. Cation exchange in clays and mudrocks by methylene blue. J. Chem. Tech. Biotechnol., Vol. 35A, pp.195-207.

Topal, T., 1996. The use of methylene blue adsorption test to assess the clay content of the Cappadocian tuff, 8th. Int. Cong. on the Deterioration and Conservation of Stone, Berlin, Vol.2, 791-799.

Tsakiris, 2012. Effect of the granulometry of limestone aggregates in the determination of Bond project index, Postgraduate thesis, National and Technical University of Athens, Greece.

Tsimplis, M., 1994. Tidal Oscillations in the Aegean and Ionian Seas. Estuarine, Coastal and Shelf Science 39 (2): 201–208. doi:10.1006/ ecss.1994.1058.

Tsirabidis, A., Filippidis, A., 2013. Mineral Resources of Greece: Reserves and Value. Department of Mineralogy-Petrology-Economic Geology, Department of Geology, Aristotle University of Thessaloniki, p. 46.

Tsoutsia, A., Anastasatou, M., Petrakis, S., Stamatakis, G., Poulos, S., Stamatakis, M., Kapsimalis, V., Roussakis, G., 2014. Sedimentological and mineralogical analysis of seabed sediments of Afantou Bay, Rhodes Island, NE Greece. 10th International Congress of the Hellenic Geographical Society, Thessaloniki, 22 – 24/10/2014, p.p. 179-180.

UEPG, 2019. Annual review 2018 – 2019. European Aggregates Association, pp. 30.

Ulses, C., Estournel, C., Durrieu de Madron, X., Palanques, A., 2008. Suspended sediment transport in the Gulf of Lions (NW Mediterranean): Impact of extreme storms and floods. Continental shelf Research 28: 2048-2070.

UNEP, 2014. Sand, rarer than one thinks. United Nations Environment Programme, 14pp.

UNEP, 2019. Sand and Sustainability: Finding new solutions for environmental governance of global sand resources. United Nations Environment Programme, 56 pp.

UNESCO, 2006. The Petrified Forest of Lesvos, A Unique Natural Monument Recording the Evolutionary Process of Life on Earth. UNESCO Global Geoparks Network.

United Nations, 2015. 2030 Agenda of Sustainable Development: 17 Sustainable Development Goals (SDGs).

US Army Corps of Engineers, 1984. Shore protection manual. Coastal engineering Research Center, Department of the Army, Waterways Experiment Station, pp. 337.

USGS, 2014. Deposit model for heavy-mineral sands in coastal environments. Van Gosen, B.S., Fey, D.L., Shah, A.K., Verplanck, P.L., and Hoefen, T.M., Report 2010–5070–L, pp. 62.

USGS, 2020. Mineral commodities summaries 2020. U.S. Geological Survey, 200 p., https://doi.org/10.3133/.

Velegrakis, A.F., Collins, M.B., Bastos, A.C., Paphitis, D., Brampton, A., 2007. Seabed sediment transport pathway investigations: review of scientific approach and methodologies. In: Balson, P.S. and Collins, M.B. (eds.), Coastal and Shelf Sediment Transport. Geological Society of London Special Publication No. 274, pp. 127-146.

Velegrakis, A.F., Vousdoukas, M.I., Andreadis, O., Adamakis, G., Pasakalidou, E., Meligonitis, R., Kokolatos, G., 2008. Influence of Dams on Downstream Beaches: Eressos, Lesbos, Eastern Mediterranean, Marine Georesources & Geotechnology, 26:4, 350-371, DOI: 10.1080/10641190802425598.

Velegrakis, A., Ballay, A., Poulos, S., Radzevicius, R., Bellec, V., Manso, F., 2010. European marine aggregates resources: Origins, usage, prospecting and dredging techniques. Journal of Coastal Research. SI 51.

Velegrakis, A., Karditsa, A., Paramana, Th., Poulos, S., Anastasatou, M., Tsoutsia, A., Papavlassopoulou, N., Stamatakis, M., Hasiotis, T., 2015. Marine Aggregates extraction regulations in Greece in accordance to European Practices. 11th Panhellenic Symposium on Oceanography and Fisheries, 13-17 May, Mytilene, Lesvos island, Greece, pp. 1073-1076.

Verikiou-Papaspiridakou, E., Bathrellos, G., Skilodimou, H., 2004. Physico-geographical observations of the coastal zone of the northeastern part of island Rhodes. Bull. Geol. Soc. Greece, 36, 958-967.

Vernant, P., Reilinger, R., McClusky, S., 2014. Geodetic evidence for low coupling on the Hellenic subduction plate interface. Earth Planet. Sci. Lett.385, 122–129.

Vincent, C.E., Stolk, A., Porter, C.F.C., 1998. Sand suspension and transport on the Middelkerke Bank (southern North Sea) by storms and tidal currents. Marine Geology, 150, 113-129.

Voudouris, P., Spry, P., Sakellaris, G.A., Mavrogonatos, C., 2011. A cervelleite-like mineral and other Ag-Cu-Te-S minerals [Ag2CuTeS and (Ag,Cu)2TeS] in gold-bearing veins in metamorphic rocks of the Cycladic Blueschist Unit, Kallianou, Evia Island, Greece. Mineralogy and Petrology, 101, 169-183.

Voudouris, P., Mavrogonatos, C., Melfos, V., Spry, P.G., Magganas, A., Alfieris, D., Soukis, K., Tarantola, A., Periferakis, A., Kołodziejczyk, J., Scheffer, C., Repstock, A., Zeug, M., 2019. The geology and mineralogy of the Stypsi porphyry Cu-Mo-Au-Re prospect, Lesvos Island, Aegean Sea, Greece. Ore Geology Reviews, Vol. 112, 103023.

Wan Mohtar, H., Bassa, S., Porhemmat, M., 2017. Grain Size Analysis of Surface Fluvial Sediments in Rivers in Kelantan, Malaysia. Sains Malaysiana. 46. 685-693. 10.17576/jsm-2017-4605-02.

Warrier, A.K., Pednekar, H. Mahesh, B.S. Mohan, R. Gazi, S., 2015. Sediment grain size and surface textural observations of quartz grains in late quaternary lacustrine sediments from Schirmacher Oasis, East Antarctica: paleoenvironmental significance. Polar Sci., 10.1016/j.polar.2015.12.005

Winter, 2001. An introduction to igneous and metamorphic petrology. Prenitce Hall, 695.

Xypolias, P., Kokkalas, S., Skourlis, K. 2003. Upward extrusion and subsequent transpression as a possible mechanism for the exhumation of HP/ LT rocks in Evia Island (Aegean Sea, Greece). Journal of Geodynamics, 35, 303–332.

Xypolias, P., Iliopoulos, I., Chatzaras, V., Kokkalas, S., 2012. Subduction- and exhumation-related structures in the Cycladic Blueschists: Insights from south Evia Island (Aegean region, Greece). Tectonics, 31, TC2001.

Zachariasse, W.J., van Hinsbergen, D.J.J., Fortuin, A.R., 2008. Mass wasting and uplift on Crete and Karpathos during the early Pliocene related to initiation of south Aegean left-lateral, strike-slip tectonics. Geol. Soc. Am. Bull.120, 976–993.

Zouros, N., 2010. Lesvos Petrified Forest geopark, Greece: geoconservation, Geotourism and Local development. Journal of Parks, Protected Areas and Cultural sites. 27. 19-28.

ANNEX I – Catalogue of the sample locations

N°	Sample ID	Sampling Area	Sampling Date	Latitude	Longitude	Depth (m)	Sampler Type	Type of Sample
1	**KD-1**	SE Evia Isl.	07-Jun-14	38.16768	24.34137	17.5	Box Corer	Offshore
2	**KD-2**	SE Evia Isl.	07-Jun-14	38.16872	24.34173	19.6	Box Corer	Offshore
3	**KD-3**	SE Evia Isl.	07-Jun-14	38.17007	24.34167	43.2	Box Corer	Offshore
4	**KD-4**	SE Evia Isl.	07-Jun-14	38° 10,9306	24° 21,1588	76	Gravity Core	Offshore
5	**KD-5**	SE Evia Isl.	07-Jun-14	38° 10,4771	24° 20,8046	144	Gravity Core	Offshore
6	**KD-6**	SE Evia Isl.	07-Jun-14	38.16964	24.35164	52.1	Box Corer	Offshore
7	**KD-7**	SE Evia Isl.	07-Jun-14	38.16326	24.35503	41	Box Corer	Offshore
8	**KD-8**	SE Evia Isl.	07-Jun-14	38.16468	24.35571	44.8	Box Corer	Offshore
9	**KD-9**	SE Evia Isl.	07-Jun-14	38.16909	24.35908	83.2	Box Corer	Offshore
10	**KD-10**	SE Evia Isl.	07-Jun-14	38.14686	24.46564	37.4	Box Corer	Offshore
11	**KD-11**	SE Evia Isl.	07-Jun-14	38.14886	24.46679	46.1	Box Corer	Offshore
12	**KD-12**	SE Evia Isl.	07-Jun-14	38.14548	24.45734	19.8	Box Corer	Offshore
13	**KD-13**	SE Evia Isl.	07-Jun-14	38.14880	24.45909	42.5	Box Corer	Offshore
14	**KD-14**	SE Evia Isl.	07-Jun-14	38.15268	24.46151	79.9	Box Corer	Offshore
15	**KD-15**	SE Evia Isl.	07-Jun-14	38.14838	24.47309	40.3	Box Corer	Offshore
16	**KD-16**	SE Evia Isl.	07-Jun-14	38.14977	24.47354	50.1	Box Corer	Offshore
17	**KD-18**	SE Evia Isl.	07-Jun-14	38° 09,5165	24° 32,9900	218	Gravity Core	Offshore
18	**KIS-1A**	NW Crete Isl., Kissamos	19-May-13	35.51850	23.63035	12.6	Smith-McIntyre Grab	Offshore
19	**KIS-1B**	NW Crete Isl., Kissamos	19-May-13	35.52288	23.63110	20.1	Smith-McIntyre Grab	Offshore
20	**KIS-1C**	NW Crete Isl., Kissamos	19-May-13	35.52560	23.63312	31.5	Smith-McIntyre Grab	Offshore
21	**KIS-1D**	NW Crete Isl., Kissamos	19-May-13	35.53105	23.63515	43.8	Smith-McIntyre Grab	Offshore
22	**KIS-2A**	NW Crete Isl., Kissamos	19-May-13	35.50757	23.65795	10.9	Smith-McIntyre	Offshore

							Grab	
23	**KIS-2B**	NW Crete Isl., Kissamos	19-May-13	35.51320	23.65860	18.4	Smith-McIntyre Grab	Offshore
24	**KIS-2C**	NW Crete Isl., Kissamos	19-May-13	35.51843	23.65903	26.7	Smith-McIntyre Grab	Offshore
25	**KIS-2D**	NW Crete Isl., Kissamos	19-May-13	35.52473	23.65953	38.9	Smith-McIntyre Grab	Offshore
26	**KIS-3A**	NW Crete Isl., Kissamos	19-May-13	35.51068	23.67845	15.0	Smith-McIntyre Grab	Offshore
27	**KIS-3B**	NW Crete Isl., Kissamos	19-May-13	35.51372	23.67847	23.0	Smith-McIntyre Grab	Offshore
28	**KIS-3C**	NW Crete Isl., Kissamos	19-May-13	35.51958	23.67903	33.6	Smith-McIntyre Grab	Offshore
29	**KIS-3D**	NW Crete Isl., Kissamos	19-May-13	35.52482	23.67948	41.3	Smith-McIntyre Grab	Offshore
30	**KIS-4A**	NW Crete Isl., Kissamos	19-May-13	35.51153	23.69793	12.0	Smith-McIntyre Grab	Offshore
31	**KIS-4B**	NW Crete Isl., Kissamos	19-May-13	35.51530	23.69838	20.0	Smith-McIntyre Grab	Offshore
32	**KIS-4C**	NW Crete Isl., Kissamos	19-May-13	35.52147	23.69880	25.7	Smith-McIntyre Grab	Offshore
33	**KIS-4D**	NW Crete Isl., Kissamos	19-May-13	35.52953	23.69950	36.6	Smith-McIntyre Grab	Offshore
34	**SFI-1**	NW Crete Isl., Sfinari	16-May-13	35.4239	23.54776667	32.5	Smith-McIntyre Grab	Offshore
35	**SFI-2**	NW Crete Isl., Sfinari	16-May-13	35.4185	23.56	17.3	Smith-McIntyre Grab	Offshore
36	**SFI-3**	NW Crete Isl., Sfinari	16-May-13	35.41917	23.55867	8.2	Smith-McIntyre Grab	Offshore
37	**L-E1**	South Lesvos Isl., Eressos	11-Jul-14	39^{O} 07' 49.5"	025^{O} 55' 44.5"	13	Smith-McIntyre Grab	Offshore
38	**L-E2**	South Lesvos Isl., Eressos	11-Jul-14	39^{O} 07' 47.3"	025^{O} 55' 37.3"	28	Smith-McIntyre Grab	Offshore
39	**L-E3**	South Lesvos Isl., Eressos	11-Jul-14	39^{O} 07' 44.2"	025^{O} 55' 34.1"	42	Smith-McIntyre	Offshore

							Grab	
40	**L-E4**	South Lesvos Isl., Eressos	11-Jul-14	39^{O} 08' 01.8"	025^{O} 54' 56.8"	18	Smith-McIntyre Grab	Offshore
41	**L-E5**	South Lesvos Isl., Eressos	11-Jul-14	39^{O} 08' 00.0"	025^{O} 54' 55.5"	29	Smith-McIntyre Grab	Offshore
42	**L-E6**	South Lesvos Isl., Eressos	11-Jul-14	39^{O} 07' 58.3"	025^{O} 54' 53.4"	43.5	Smith-McIntyre Grab	Offshore
43	**L-E7**	South Lesvos Isl., Eressos	11-Jul-14	39^{O} 07' 43.2"	025^{O} 55' 02.4"	65	Smith-McIntyre Grab	Offshore
44	**L-E8**	South Lesvos Isl., Eressos	11-Jul-14	39^{O} 08' 07.5"	025^{O} 54' 30.7"	16	Smith-McIntyre Grab	Offshore
45	**L-E9**	South Lesvos Isl., Eressos	11-Jul-14	39^{O} 08' 02.6"	025^{O} 54' 28.8"	47	Smith-McIntyre Grab	Offshore
46	**L-V1**	South Lesvos Isl., Vatera	13-Jul-14	39^{O} 00' 31.5"	026^{O} 14' 40.6"	31.5	Smith-McIntyre Grab	Offshore
47	**L-V2**	South Lesvos Isl., Vatera	13-Jul-14	39^{O} 00' 25.4"	026^{O} 14' 41.2"	45	Smith-McIntyre Grab	Offshore
48	**L-V3**	South Lesvos Isl., Vatera	13-Jul-14	39^{O} 00' 19.6"	026^{O} 13' 56.6"	62.5	Smith-McIntyre Grab	Offshore
49	**L-V4**	South Lesvos Isl., Vatera	13-Jul-14	39^{O} 00' 31.8"	026^{O} 14' 00.3"	45.5	Smith-McIntyre Grab	Offshore
50	**L-V5**	South Lesvos Isl., Vatera	13-Jul-14	39^{O} 00' 38.2"	026^{O} 14' 01.1"	33.5	Smith-McIntyre Grab	Offshore
51	**L-V6**	South Lesvos Isl., Vatera	13-Jul-14	39^{O} 00' 52.0"	026^{O} 13' 02.9"	17.5	Smith-McIntyre Grab	Offshore
52	**L-V7**	South Lesvos Isl., Vatera	13-Jul-14	39^{O} 00' 41.7"	026^{O} 13' 01.3"	35.5	Smith-McIntyre Grab	Offshore
53	**L-V8**	South Lesvos Isl., Vatera	13-Jul-14	39^{O} 00' 32.5"	026^{O} 12' 59.5"	51	Smith-McIntyre Grab	Offshore
54	**L-V9**	South Lesvos Isl., Vatera	13-Jul-14	39^{O} 00' 14.4"	026^{O} 12' 04.2"	76.5	Smith-McIntyre Grab	Offshore
55	**L-V10**	South Lesvos Isl., Vatera	13-Jul-14	39^{O} 00' 45.0"	026^{O} 12' 05.1"	34	Smith-McIntyre Grab	Offshore
56	**L-V11**	South Lesvos Isl., Vatera	13-Jul-14	39^{O} 00' 33.1"	026^{O} 11' 14.2"	34	Smith-McIntyre	Offshore

							Grab	
57	**L-V12**	South Lesvos Isl., Vatera	13-Jul-14	39^{O} 00' 16.1"	026^{O} 11' 19.4"	63	Smith-McIntyre Grab	Offshore
58	**L-S3**	East Lesvos Isl., Mytilene Strait	14-Jul-14	39^{O} 15' 14.2"	026^{O} 28' 17.2"	53.5	Smith-McIntyre Grab	Offshore
59	**L-S4**	East Lesvos Isl., Mytilene Strait	14-Jul-14	39^{O} 15' 16.8"	026^{O} 29' 17.9"	57	Smith-McIntyre Grab	Offshore
60	**L-S7**	East Lesvos Isl., Mytilene Strait	14-Jul-14	39^{O} 13' 50.6"	026^{O} 29' 00.8"	46	Smith-McIntyre Grab	Offshore
61	**L-S11**	East Lesvos Isl., Mytilene Strait	16-Jul-14	39^{O} 02' 12.7'	026^{O} 38' 47.1"	50	Smith-McIntyre Grab	Offshore
62	**L-S12**	East Lesvos Isl., Mytilene Strait	16-Jul-14	39^{O} 03' 46.0"	026^{O} 39' 56.3"	47	Smith-McIntyre Grab	Offshore
63	**L-S16**	East Lesvos Isl., Mytilene Strait	16-Jul-14	39^{O} 03' 59.3"	026^{O} 37' 33.6"	38	Smith-McIntyre Grab	Offshore
64	**L-S19**	East Lesvos Isl., Mytilene Strait	16-Jul-14	39^{O} 06' 08.6"	026^{O} 38' 31.5"	41	Smith-McIntyre Grab	Offshore
65	**L-S22**	East Lesvos Isl., Mytilene Strait	16-Jul-14	39^{O} 07' 26.7"	026^{O} 33' 41.2"	31.5	Smith-McIntyre Grab	Offshore
66	**L-S24**	East Lesvos Isl., Mytilene Strait	16-Jul-14	39^{O} 08' 21.4"	026^{O} 37' 28.2"	39	Smith-McIntyre Grab	Offshore
67	**L-S25**	East Lesvos Isl., Mytilene Strait	16-Jul-14	39^{O} 09' 55.8"	026^{O} 35' 45.0"	42	Smith-McIntyre Grab	Offshore
68	**L-S26**	East Lesvos Isl., Mytilene Strait	16-Jul-14	39^{O} 11' 33.9"	026^{O} 34' 08.8"	38.5	Smith-McIntyre Grab	Offshore
69	**L-S28**	East Lesvos Isl., Mytilene Strait	16-Jul-14	39^{O} 12' 09.3"	026^{O} 32' 03.2"	43	Smith-McIntyre Grab	Offshore
70	**L-S29**	East Lesvos Isl., Mytilene Strait	16-Jul-14	39^{O} 11' 46.8"	026^{O} 31' 10.8"	36	Smith-McIntyre Grab	Offshore
71	**L-S32**	East Lesvos Isl., Mytilene Strait	16-Jul-14	39^{O} 13' 14.9"	026^{O} 31' 15,2"	44	Smith-McIntyre Grab	Offshore
72	**AFA-1A**	NE Rhodes Isl., Afantou	27-Nov-13	36.29508	28.19031	13.1	Smith-McIntyre Grab	Offshore

73	**AFA-1B**	NE Rhodes Isl., Afantou	27-Nov-13	36.29456	28.193	25.4	Smith-McIntyre Grab	Offshore
74	**AFA-1C**	NE Rhodes Isl., Afantou	27-Nov-13	36.29419	28.19408	36.5	Smith-McIntyre Grab	Offshore
75	**AFA-1D**	NE Rhodes Isl., Afantou	27-Nov-13	36.29406	28.19547	44.7	Smith-McIntyre Grab	Offshore
76	**AFA-2A**	NE Rhodes Isl., Afantou	27-Nov-13	36.28503	28.19083	15.2	Smith-McIntyre Grab	Offshore
77	**AFA-2B**	NE Rhodes Isl., Afantou	27-Nov-13	36.28544	28.18931	23.8	Smith-McIntyre Grab	Offshore
78	**AFA-2C**	NE Rhodes Isl., Afantou	27-Nov-13	36.28592	28.18847	35.3	Smith-McIntyre Grab	Offshore
79	**AFA-2D**	NE Rhodes Isl., Afantou	27-Nov-13	36.28631	28.18617	43.5	Smith-McIntyre Grab	Offshore
80	**AFA-3A**	NE Rhodes Isl., Afantou	27-Nov-13	36.27797	28.18214	15.8	Smith-McIntyre Grab	Offshore
81	**AFA-3B**	NE Rhodes Isl., Afantou	27-Nov-13	36.27697	28.18506	25.4	Smith-McIntyre Grab	Offshore
82	**AFA-3C**	NE Rhodes Isl., Afantou	27-Nov-13	36.27625	28.18739	35.2	Smith-McIntyre Grab	Offshore
83	**AFA-3D**	NE Rhodes Isl., Afantou	27-Nov-13	36.27561	28.18978	46.2	Smith-McIntyre Grab	Offshore
84	**NST-1**	East - Central Evia Isl.	22-Nov-13	38.434169	24.181340	3.0	Swimming/Manual	Coastal
85	**NST-2**	East - Central Evia Isl.	22-Nov-13	38.434188	24.181391	0.0	Swimming/Manual	Coastal
86	**NST-3**	East - Central Evia Isl.	22-Nov-13	38.428093	24.184476	3.0	Swimming/Manual	Coastal
87	**NST-4**	East - Central Evia Isl.	22-Nov-13	38.428120	24.184510	0	Swimming/Manual	Coastal
88	**PSA-1**	East - Central Evia Isl.	22-Nov-13	38.391786	24.183809	4	Swimming/Manual	Coastal
89	**PSA-2**	East - Central Evia Isl.	22-Nov-13	38.391821	24.183845	0	Swimming/Manual	Coastal
90	**PSA-3**	East - Central Evia Isl.	22-Nov-13	38.393393	24.182553	5	Swimming/Manual	Coastal
91	**PSA-4**	East - Central Evia Isl.	22-Nov-13	38.393413	24.182615	0	Swimming/Manual	Coastal
92	**EV-1**	East - Central Evia Isl.	22-Nov-13	38.366402	24.213992	3	Swimming/Manual	Coastal
93	**EV-2**	East - Central Evia Isl.	22-Nov-13	38.366430	24.214026	0	Swimming/Manual	Coastal

94	**EV-3**	East - Central Evia Isl.	22-Nov-13	38.368734	24.210713	2	Swimming/Manual	Coastal
95	**EV-4**	East - Central Evia Isl.	22-Nov-13	38.368738	24.210729	0	Swimming/Manual	Coastal
96	**K-13**	NW Crete Isl., Kissamos	18-May-13	35.495381	23.657877	1.8	Swimming/Manual	Coastal
97	**K-14**	NW Crete Isl., Kissamos	18-May-13	35.496025	23.673397	0	Swimming/Manual	Coastal
98	**K-15**	NW Crete Isl., Kissamos	18-May-13	35.309310	23.374450	3.5	Swimming/Manual	Coastal
99	**K-24**	NW Crete Isl., Kissamos	18-May-13	35.496999	23.685832	0	Swimming/Manual	Coastal
100	**K-23**	NW Crete Isl., Kissamos	18-May-13	35.499484	23.700266	0	Swimming/Manual	Coastal
101	**K-36**	NW Crete Isl., Kissamos	18-May-13	35.495651	23.662205	0	Swimming/Manual	Coastal
102	**KIS-1**	NW Crete Isl., Kissamos	25-Jul-12	35.515828	23.621693	0	Swimming/Manual	Coastal
103	**KIS-2**	NW Crete Isl., Kissamos	25-Jul-12	35.515933	23.623633	3	Swimming/Manual	Coastal
104	**KIS-3**	NW Crete Isl., Kissamos	25-Jul-12	35.516067	23.625633	4	Swimming/Manual	Coastal
105	**SFN-1**	NW Crete Isl., Sfinari	25-Jul-12	35.436238	23.569260	0	Swimming/Manual	Coastal
106	**SFN-2**	NW Crete Isl., Sfinari	25-Jul-12	35.416839	23.562566	0	Swimming/Manual	Coastal
107	**KAMP-1**	West Crete Isl., Kampos	23-Jul-12	35.395561	23.550792	0	Swimming/Manual	Coastal
108	**KAMP-2**	West Crete Isl., Kampos	23-Jul-12	35.395700	23.550550	2	Swimming/Manual	Coastal
109	**TAV-1**	NW Crete Isl., Tavronitis	24-Jul-12	35.534503	23.813786	0	Swimming/Manual	Coastal
110	**OAM-1**	W-SW Crete Isl., Orthi Ammos	04-Jun-14	35.182050	24.242983	3	Swimming/Manual	Coastal
111	**AST-1**	Argolic Gulf, Coastal Astros	22-Jun-12	37.430329	22.760120	0	Swimming/Manual	Coastal
112	**KAM-1**	Corinthian Gulf, Kamari	23-Jun-12	38.098083	22.575517	0	Swimming/Manual	Coastal
113	**LYK-1**	Corinthian Gulf, Lykoporia	23-Jun-12	38.115513	22.523683	0	Swimming/Manual	Coastal
114	**DER-1**	Corinthian Gulf, Derveni	23-Jun-12	38.199617	22.390484	0	Swimming/Manual	Coastal
115	**AL-1**	Corinthian Gulf, Alepochori	30-Jun-12	38.073411	23.168277	3	Swimming/Manual	Coastal
116	**SXN-1**	South Euboean Gulf, Schinias	Jun-12	38.143026	24.049574	2	Swimming/Manual	Coastal
117	**SXN-3**	South Euboean Gulf, Schinias	Jun-12	38.140860	24.032007	0	Swimming/Manual	Coastal
118	**PL-1**	North Milos Isl., Plathiena	04-Jul-12	36.753982	24.412731	0	Swimming/Manual	Coastal
119	**SAM-1**	SE Samos Isl., Psili Ammos	12-Jul-12	37.707469	27.016348	0	Swimming/Manual	Coastal
120	**BAL-1**	S-SW Samos Isl., Marathokampos, Mpalos	12-Jul-12	37.697393	26.751874	0	Swimming/Manual	Coastal
121	**SKK-1**	SE Kefalonia Isl., Skala	18-Dec-18	38.073834	20.800920	0	Swimming/Manual	Coastal

122	**Italian Sand**	NW Italy, Tuscany	Jul-15	43.823978°	10.254867°	–	Manual	Coastal
123	**Bournemouth Beach**	South UK, Bournemouth	10-Apr-15	50° 42.966'N	1° 52.398'W	–	Manual	Coastal
124	**Bournemouth Coastline**	South UK, Bournemouth	10-Apr-15	50° 42.947'N	1° 52.388'W	–	Manual	Coastal
125	**Boscombe Beach**	South UK, Boscombe	10-Apr-15	50° 43.186'N	1° 50.475'W	–	Manual	Coastal
126	**Boscombe Coastline**	South UK, Boscombe	10-Apr-15	50° 43.171'N	1° 50.471'W	–	Manual	Coastal
127	**Nairobi**	Nairobi Dessert	Unknown	Unknown	Unknown	–	Manual	Terrestrial
128	**Strymonas 1**	NW of Sidirokastro, Strymonas	Autumn 2015	41.262205°	23.328330°	–	Manual	Terrestrial/River
129	**Strymonas 2**	NW of Sidirokastro, Strymonas	Autumn 2015	41.262205°	23.328330°	–	Manual	Terrestrial/River
130	**Aliartos 1**	Central Greece, Aliartos	2014	38.368017°	23.142907°	–	Manual	Terrestrial
131	**Aliartos 2**	Central Greece, Aliartos	2014	38.368017°	23.142907°	–	Manual	Terrestrial
132	**GK**	Area between South Evia Isl. & North Kea Isl.	2014	Unknown	Unknown	–	Unknown	Offshore

ANNEX II – Grain Size Analysis

Table I. Extensive Catalogue of grain size analysis parameters for all samples.

No	Samples	Gravel %	Sand %	Silt %	Clay %	Median	Mean	StdDev	Skewness	Kurtosis	Characterization
1	**KD-1**	0.03	99.93	0.04	0	2.86	2.87	0.6	-0.02	0.95	MODERATELY WELL SORTED; NEAR SYMMETRICAL; MESOKURTIC
2	**KD-2**	0	99.95	0.05	0	2.68	2.72	0.58	0.09	1.09	MODERATELY WELL SORTED; NEAR SYMMETRICAL; MESOKURTIC
3	**KD-3**	0	99.95	0.05	0	2.61	2.64	0.56	0.08	1.22	MODERATELY WELL SORTED; NEAR SYMMETRICAL; LEPTOKURTIC
4	**KD-6**	0	44.73	48.2	7.07	4.2	4.67	1.71	0.45	1.09	POORLY SORTED; STRONGLY FINE SKEWED; MESOKURTIC
5	**KD-7**	0	89.52	8.8	1.68	2.73	2.86	1.03	0.42	1.99	POORLY SORTED; STRONGLY FINE SKEWED; VERY LEPTOKURTIC
6	**KD-8**	0	85.73	12.14	2.13	2.88	2.94	1.24	0.28	1.72	POORLY SORTED; FINE SKEWED; VERY LEPTOKURTIC
7	**KD-9**	0.46	39.7	52.19	7.65	4.36	4.79	1.71	0.43	1.07	POORLY SORTED; STRONGLY FINE SKEWED; MESOKURTIC
8	**KD-10**	90.57	9.35	0.08	0	-2.21	-2.11	0.86	0.3	1.43	MODERATELY SORTED; FINE SKEWED; LEPTOKURTIC

9	**KD-11**	0	50.56	43.78	5.66	3.98	4.49	1.52	0.56	1.3	POORLY SORTED; STRONGLY FINE SKEWED; LEPTOKURTIC
10	**KD-12**	0	99.91	0.09	0	2.53	2.55	0.59	0.02	1.27	MODERATELY WELL SORTED; NEAR SYMMETRICAL; LEPTOKURTIC
11	**KD-13**	0.11	99.78	0.11	0	2.48	2.46	0.66	-0.07	1.27	MODERATELY WELL SORTED; NEAR SYMMETRICAL; LEPTOKURTIC
12	**KD-14**	0	38.52	54.25	7.23	4.39	4.81	1.63	0.45	1.05	POORLY SORTED; STRONGLY FINE SKEWED; MESOKURTIC
13	**KD-15**	16.29	83.66	0.05	0	-0.12	-0.15	0.86	-0.06	1.02	MODERATELY SORTED; NEAR SYMMETRICAL; MESOKURTIC
14	**KD-16**	55.21	44.71	0.08	0	-1.11	-1.06	0.69	0.1	0.99	MODERATELY WELL SORTED; FINE SKEWED; MESOKURTIC
15	**4-1**	0	65.21	30.61	4.18	3.46	3.83	1.59	0.44	1.11	POORLY SORTED; STRONGLY FINE SKEWED; LEPTOKURTIC
16	**4-2**	0	66.38	29.24	4.38	3.38	3.81	1.61	0.49	1.12	POORLY SORTED; STRONGLY FINE SKEWED; LEPTOKURTIC
17	**4-3**	0	58.19	36.45	5.36	3.62	4.05	1.8	0.43	0.97	POORLY SORTED; STRONGLY FINE SKEWED; MESOKURTIC
18	**4-4**	0	75.51	21.14	3.35	3.11	3.5	1.41	0.51	1.48	POORLY SORTED; STRONGLY FINE SKEWED; LEPTOKURTIC
19	**4-5**	0	76.37	20.42	3.21	3.16	3.49	1.31	0.5	1.52	POORLY SORTED; STRONGLY FINE SKEWED; VERY LEPTOKURTIC
20	**4-6**	0	66.86	29.31	3.83	3.43	3.77	1.54	0.43	1.14	POORLY SORTED; STRONGLY FINE SKEWED; LEPTOKURTIC
21	**4-7**	0	52.24	42.34	5.42	3.9	4.17	1.73	0.34	1.05	POORLY SORTED; STRONGLY FINE SKEWED; MESOKURTIC
22	**4-8**	0	66.83	29.25	3.92	3.44	3.78	1.53	0.43	1.18	POORLY SORTED; STRONGLY FINE SKEWED; LEPTOKURTIC
23	**4-9**	0	30.75	60.72	8.53	4.94	5.01	1.88	0.15	1.15	POORLY SORTED; FINE SKEWED; LEPTOKURTIC
24	**4-10**	0	58.09	36.91	5	3.68	4.02	1.69	0.4	1.05	POORLY SORTED; STRONGLY FINE SKEWED; MESOKURTIC
25	**4-11**	0	63.26	32.3	4.44	3.53	3.88	1.62	0.43	1.1	POORLY SORTED; STRONGLY FINE SKEWED; MESOKURTIC
26	**4-12**	0	75.42	21.23	3.35	3.22	3.55	1.33	0.5	1.51	POORLY SORTED; STRONGLY FINE SKEWED; VERY LEPTOKURTIC
27	**4-13**	0	61.53	34.07	4.4	3.59	3.91	1.6	0.4	1.11	POORLY SORTED; STRONGLY FINE SKEWED; LEPTOKURTIC
28	**4-14**	0	60.8	35.06	4.14	3.63	3.94	1.55	0.39	1.11	POORLY SORTED; STRONGLY FINE SKEWED; LEPTOKURTIC
29	**5-1**	0	57.34	36.25	6.41	3.64	4.07	1.88	0.44	1	POORLY SORTED; STRONGLY FINE SKEWED; MESOKURTIC
30	**5-2**	0	54.28	38.59	7.13	3.78	4.18	1.95	0.41	1	POORLY SORTED; STRONGLY FINE SKEWED; MESOKURTIC
31	**5-3**	0	57.55	35.88	6.57	3.65	4.07	1.88	0.44	1.03	POORLY SORTED; STRONGLY FINE SKEWED; MESOKURTIC
32	**5-4**	0	45.51	46.75	7.74	4.25	4.47	1.95	0.29	1.06	POORLY SORTED; FINE SKEWED; MESOKURTIC
33	**5-5**	0	39.54	52.29	8.17	4.57	4.71	1.94	0.22	1.09	POORLY SORTED; FINE SKEWED; MESOKURTIC
34	**5-6**	0	51.97	40.96	7.07	3.89	4.24	1.94	0.37	0.99	POORLY SORTED; STRONGLY FINE SKEWED; MESOKURTIC
35	**5-7**	0	51.58	41.43	6.99	3.92	4.26	1.9	0.37	1.03	POORLY SORTED; STRONGLY FINE SKEWED; MESOKURTIC
36	**5-8**	0	52.86	40.29	6.85	3.87	4.22	1.87	0.39	1.08	POORLY SORTED; STRONGLY FINE SKEWED; MESOKURTIC
37	**5-9**	0	52	41.77	6.23	3.91	4.21	1.79	0.36	1.1	POORLY SORTED; STRONGLY FINE SKEWED; MESOKURTIC

38	**5-10**	0	47.75	45.76	6.49	4.11	4.33	1.81	0.3	1.1	POORLY SORTED; STRONGLY FINE SKEWED; MESOKURTIC
39	**5-11**	0	41.53	51.25	7.22	4.42	4.57	1.86	0.23	1.1	POORLY SORTED; FINE SKEWED; LEPTOKURTIC
40	**5-12**	0	34.23	56.68	9.09	4.78	4.91	1.94	0.21	1.16	POORLY SORTED; FINE SKEWED; LEPTOKURTIC
41	**5-13**	0	38.7	53.41	7.89	4.56	4.7	1.9	0.22	1.12	POORLY SORTED; FINE SKEWED; LEPTOKURTIC
42	**5-14**	0	37.38	55.36	7.26	4.58	4.69	1.8	0.21	1.17	POORLY SORTED; FINE SKEWED; LEPTOKURTIC
43	**5-15**	0	38.2	55.03	6.77	4.54	4.63	1.76	0.2	1.16	POORLY SORTED; FINE SKEWED; LEPTOKURTIC
44	**5-16**	0	32.8	60.26	6.94	4.72	4.78	1.73	0.16	1.22	POORLY SORTED; FINE SKEWED; LEPTOKURTIC
45	**5-17**	0	33.11	59.78	7.11	4.73	4.78	1.76	0.16	1.21	POORLY SORTED; FINE SKEWED; LEPTOKURTIC
46	**5-18**	0	36.14	57.3	6.56	4.6	4.66	1.73	0.17	1.17	POORLY SORTED; FINE SKEWED; LEPTOKURTIC
47	**5-19**	0	35.02	58.51	6.47	4.63	4.69	1.7	0.17	1.2	POORLY SORTED; FINE SKEWED; LEPTOKURTIC
48	**5-20**	0	47.71	47.22	5.07	4.1	4.26	1.63	0.27	1.12	POORLY SORTED; FINE SKEWED; LEPTOKURTIC
49	**5-21**	0	38.69	55.56	5.75	4.48	4.55	1.66	0.18	1.15	POORLY SORTED; FINE SKEWED; LEPTOKURTIC
50	**18-1**	0	30.4	58.44	11.16	5.1	5.19	2.1	0.16	1.08	VERY POORLY SORTED; FINE SKEWED; MESOKURTIC
51	**18-2**	0	25.07	60.45	14.48	5.37	5.52	2.23	0.17	1.08	VERY POORLY SORTED; FINE SKEWED; MESOKURTIC
52	**18-3**	0	26.45	58.87	14.68	5.3	5.5	2.24	0.19	1.05	VERY POORLY SORTED; FINE SKEWED; MESOKURTIC
53	**18-4**	0	26.35	59.84	13.81	5.27	5.45	2.19	0.19	1.08	VERY POORLY SORTED; FINE SKEWED; MESOKURTIC
54	**18-5**	0	25.36	61.04	13.6	5.29	5.45	2.19	0.18	1.12	VERY POORLY SORTED; FINE SKEWED; LEPTOKURTIC
55	**18-6**	0	31.08	56.82	12.1	5.04	5.2	2.16	0.2	1.08	VERY POORLY SORTED; FINE SKEWED; MESOKURTIC
56	**18-7**	0	22.65	64.72	12.63	5.34	5.48	2.06	0.17	1.17	VERY POORLY SORTED; FINE SKEWED; LEPTOKURTIC
57	**18-8**	0	21.84	64.91	13.25	5.4	5.54	2.1	0.16	1.17	VERY POORLY SORTED; FINE SKEWED; LEPTOKURTIC
58	**18-9**	0	24.83	61.82	13.35	5.34	5.45	2.18	0.15	1.12	VERY POORLY SORTED; FINE SKEWED; LEPTOKURTIC
59	**18-10**	0	28.87	57.91	13.22	5.2	5.34	2.22	0.17	1.06	VERY POORLY SORTED; FINE SKEWED; MESOKURTIC
60	**18-11**	0	26.12	59.34	14.54	5.25	5.47	2.24	0.21	1.09	VERY POORLY SORTED; FINE SKEWED; MESOKURTIC
61	**18-12**	0	30.18	56.4	13.42	5.08	5.28	2.24	0.21	1.08	VERY POORLY SORTED; FINE SKEWED; MESOKURTIC
62	**18-13**	0	25.87	60.13	14	5.3	5.46	2.21	0.18	1.1	VERY POORLY SORTED; FINE SKEWED; LEPTOKURTIC
63	**18-14**	0	25.1	59.74	15.16	5.35	5.55	2.26	0.19	1.08	VERY POORLY SORTED; FINE SKEWED; MESOKURTIC
64	**18-15**	0	27.01	58.73	14.26	5.26	5.42	2.27	0.17	1.09	VERY POORLY SORTED; FINE SKEWED; MESOKURTIC
65	**18-16**	0	24.51	61.25	14.24	5.29	5.49	2.19	0.2	1.14	VERY POORLY SORTED; FINE SKEWED; LEPTOKURTIC
66	**18-17**	0	26.96	59.56	13.48	5.21	5.37	2.21	0.19	1.13	VERY POORLY SORTED; FINE SKEWED; LEPTOKURTIC

67	**18-18**	0	25.66	62.27	12.07	5.23	5.33	2.1	0.16	1.16	VERY POORLY SORTED; FINE SKEWED; LEPTOKURTIC
68	**18-19**	0	27.24	61.62	11.14	5.14	5.23	2.06	0.15	1.16	VERY POORLY SORTED; FINE SKEWED; LEPTOKURTIC
69	**18-20**	0	27.2	61.14	11.66	5.18	5.27	2.1	0.15	1.13	VERY POORLY SORTED; FINE SKEWED; LEPTOKURTIC
70	**18-21**	0	23.91	64.34	11.75	5.3	5.39	2.05	0.15	1.16	VERY POORLY SORTED; FINE SKEWED; LEPTOKURTIC
71	**18-22**	0	36.43	53.14	10.43	4.79	4.93	2.13	0.2	1.04	VERY POORLY SORTED; FINE SKEWED; MESOKURTIC
72	**18-23**	0	34.06	52.87	13.07	4.97	5.15	2.29	0.21	1.03	VERY POORLY SORTED; FINE SKEWED; MESOKURTIC
73	**18-24**	0	32.83	54.06	13.11	5.02	5.21	2.26	0.21	1.04	VERY POORLY SORTED; FINE SKEWED; MESOKURTIC
74	**18_25**	0	39.7	48.99	11.31	4.67	4.87	2.24	0.24	0.99	VERY POORLY SORTED; FINE SKEWED; MESOKURTIC
75	**18_26**	0	55.03	37.6	7.37	3.67	4.11	2.09	0.38	0.99	VERY POORLY SORTED; STRONGLY FINE SKEWED; MESOKURTIC
76	**KIS-1A**	18.75	81.13	0.12	0	-0.03	0.12	1.36	0.19	1.26	POORLY SORTED; FINE SKEWED; LEPTOKURTIC
77	**KIS-1B**	0	99.66	0.34	0	2.48	2.47	0.56	-0.06	1.45	MODERATELY WELL SORTED; NEAR SYMMETRICAL; LEPTOKURTIC
78	**KIS-1C**	0.08	99.48	0.44	0	2.38	2.32	0.62	-0.13	1.25	MODERATELY WELL SORTED; COARSE SKEWED; LEPTOKURTIC
79	**KIS-1D**	0.25	61.74	25.4	12.61	3.64	4.59	2.3	0.64	1.21	VERY POORLY SORTED; STRONGLY FINE SKEWED; LEPTOKURTIC
80	**KIS-2A**	0	99.05	0.95	0	3.19	3.13	0.51	-0.17	0.94	MODERATELY WELL SORTED; COARSE SKEWED; MESOKURTIC
81	**KIS-2B**	0	98.57	1.43	0	3.07	3.05	0.53	-0.05	0.9	MODERATELY WELL SORTED; NEAR SYMMETRICAL; MESOKURTIC
82	**KIS-2C**	0.07	91.28	8.65	0	3.12	3.12	0.65	0.04	0.99	MODERATELY WELL SORTED; NEAR SYMMETRICAL; MESOKURTIC
83	**KIS-2D**	0.09	65.3	34.6	0	4.15	4.69	1.67	0.6	1.49	POORLY SORTED; STRONGLY FINE SKEWED; LEPTOKURTIC
84	**KIS-3A**	0	99.18	0.82	0	3.23	3.16	0.5	-0.2	0.97	MODERATELY WELL SORTED; COARSE SKEWED; MESOKURTIC
85	**KIS-3B**	0	96.51	3.49	0	3.21	3.15	0.54	-0.15	0.95	MODERATELY WELL SORTED; COARSE SKEWED; MESOKURTIC
86	**KIS-3C**	0.2	74.3	25.5	0	4.57	5.13	1.84	0.54	1.2	POORLY SORTED; STRONGLY FINE SKEWED; LEPTOKURTIC
87	**KIS-3D**	0.6	68.1	31.3	0	5.23	5.79	1.95	0.47	1.12	POORLY SORTED; STRONGLY FINE SKEWED; LEPTOKURTIC
88	**KIS-4A**	0	99.25	0.75	0	3.15	3.1	0.52	-0.14	0.92	MODERATELY WELL SORTED; COARSE SKEWED; MESOKURTIC
89	**KIS-4B**	0.16	96.51	3.33	0	3.39	3.34	0.46	-0.24	1.26	WELL SORTED; COARSE SKEWED; LEPTOKURTIC
90	**KIS-4C**	4.4	91.3	4.3	0	4.3	4.61	3.09	0.15	1.07	VERY POORLY SORTED; FINE SKEWED; MESOKURTIC
91	**KIS-4D**	2.7	72	25.2	0	5.68	6	2.11	0.27	1.06	VERY POORLY SORTED; FINE SKEWED; MESOKURTIC
92	**SFI-1**	0	99.75	0.25	0	2.3	2.25	0.61	-0.09	1.06	MODERATELY WELL SORTED; NEAR SYMMETRICAL; MESOKURTIC
93	**SFI-2**	0	98.98	1.02	0	2.9	2.9	0.61	-0.02	0.95	MODERATELY WELL SORTED; NEAR SYMMETRICAL; MESOKURTIC
94	**SFI-3**	0	99.44	0.56	0	2.64	2.68	0.6	0.07	1.2	MODERATELY WELL SORTED; NEAR SYMMETRICAL; LEPTOKURTIC
95	**L-E1**	0	99.8	0.2	0	2.14	2.09	0.58	-0.13	0.94	MODERATELY WELL SORTED; COARSE SKEWED; MESOKURTIC

96	**L-E2**	0	99.56	0.44	0	2.24	2.18	0.55	-0.17	0.97	MODERATELY WELL SORTED; COARSE SKEWED; MESOKURTIC
97	**L-E3**	0.18	95.18	4.64	0	2.78	2.85	0.67	0.11	1.05	MODERATELY WELL SORTED; FINE SKEWED; MESOKURTIC
98	**L-E4**	0	99.92	0.08	0	1.08	1.12	0.66	0.13	0.98	MODERATELY WELL SORTED; FINE SKEWED; MESOKURTIC
99	**L-E5**	0	99.36	0.64	0	1.45	1.53	0.93	0.15	0.86	MODERATELY SORTED; FINE SKEWED; PLATYKURTIC
100	**L-E6**	1.34	90.32	8.34	0	3.31	3.23	0.64	-0.16	1.14	MODERATELY WELL SORTED; COARSE SKEWED; LEPTOKURTIC
101	**L-E7**	0.61	81.77	17.62	0	3.46	3.42	0.72	-0.08	1.32	MODERATELY SORTED; NEAR SYMMETRICAL; LEPTOKURTIC
102	**L-E8**	0	99.8	0.2	0	1.48	1.51	0.85	0.06	0.81	MODERATELY SORTED; NEAR SYMMETRICAL; PLATYKURTIC
103	**L-E9**	0.23	95.63	4.14	0	2.87	2.79	0.84	-0.18	0.99	MODERATELY SORTED; COARSE SKEWED; MESOKURTIC
104	**L-V1**	0.66	63.53	29.3	6.51	3.7	4.13	1.52	0.55	2.13	POORLY SORTED; STRONGLY FINE SKEWED; VERY LEPTOKURTIC
105	**L-V2**	0.23	58.28	33.63	7.86	3.79	4.38	1.71	0.58	1.82	POORLY SORTED; STRONGLY FINE SKEWED; VERY LEPTOKURTIC
106	**L-V3**	1.72	70.37	23.32	4.59	3.39	3.47	1.72	0.19	1.82	POORLY SORTED; FINE SKEWED; VERY LEPTOKURTIC
107	**L-V4**	0.53	64.06	30.69	4.72	3.7	3.91	1.35	0.37	2.37	POORLY SORTED; STRONGLY FINE SKEWED; VERY LEPTOKURTIC
108	**L-V5**	1.87	66.87	26.78	4.48	3.64	3.82	1.53	0.23	3	POORLY SORTED; FINE SKEWED; VERY LEPTOKURTIC
109	**L-V6**	*Posidonia Oceanica*									
110	**L-V7**	0.53	50.8	42.39	6.28	3.97	4.21	1.41	0.44	2.06	POORLY SORTED; STRONGLY FINE SKEWED; VERY LEPTOKURTIC
111	**L-V8**	4.64	67.97	23.19	4.2	3.42	3.26	2.08	-0.08	2.09	VERY POORLY SORTED; NEAR SYMMETRICAL; VERY LEPTOKURTIC
112	**L-V9**	0.52	63.58	30.04	5.86	3.71	4.16	1.43	0.61	2.01	POORLY SORTED; STRONGLY FINE SKEWED; VERY LEPTOKURTIC
113	**L-V10**	0.29	36.8	53.5	9.41	4.33	4.82	1.73	0.53	1.54	POORLY SORTED; STRONGLY FINE SKEWED; VERY LEPTOKURTIC
114	**L-V11**	0.21	63.57	29.89	6.33	3.71	4.14	1.48	0.58	2.09	POORLY SORTED; STRONGLY FINE SKEWED; VERY LEPTOKURTIC
115	**L-V12**	0.19	55.4	39.41	5	3.87	4.04	1.17	0.47	1.99	POORLY SORTED; STRONGLY FINE SKEWED; VERY LEPTOKURTIC
116	**L-S3**	9.11	52.59	29.37	8.93	3.54	3.36	3.25	-0.03	1.21	VERY POORLY SORTED; NEAR SYMMETRICAL; LEPTOKURTIC
117	**L-S4**	4.28	49	37.15	9.57	3.83	3.85	2.96	0.04	1.21	VERY POORLY SORTED; NEAR SYMMETRICAL; LEPTOKURTIC
118	**L-S7**	10.88	58.52	23.98	6.62	2.98	2.81	3.07	-0.01	1.14	VERY POORLY SORTED; NEAR SYMMETRICAL; LEPTOKURTIC
119	**L-S11**	7.73	91.48	0.79	0	0.38	0.63	1.35	0.26	0.91	POORLY SORTED; FINE SKEWED; MESOKURTIC
120	**L-S12**	4.77	94.85	0.38	0	0.78	0.87	1.23	0.11	0.97	POORLY SORTED; FINE SKEWED; MESOKURTIC
121	**L-S16**	7.87	78.71	9.6	3.82	0.63	1.12	2.3	0.46	1.36	VERY POORLY SORTED; STRONGLY FINE SKEWED; LEPTOKURTIC
122	**L-S19**	3.19	95.94	0.87	0	0.98	1.04	1.05	0.05	1.02	POORLY SORTED; NEAR SYMMETRICAL; MESOKURTIC
123	**L-S22**	9.14	54.54	28.17	8.15	2.71	2.94	3.27	0.15	0.9	VERY POORLY SORTED; FINE SKEWED; MESOKURTIC
124	**L-S24**	6.24	93.38	0.38	0	1.28	1.15	1.36	-0.14	0.76	POORLY SORTED; COARSE SKEWED; PLATYKURTIC

125	**L-S25**	7.18	91.45	1.37	0	1.41	1.33	1.47	-0.11	1	POORLY SORTED; COARSE SKEWED; MESOKURTIC
126	**L-S26**	3.3	96.15	0.55	0	0.92	1	1.25	0.1	0.94	POORLY SORTED; FINE SKEWED; MESOKURTIC
127	**L-S28**	3.61	69.68	19.5	7.21	3.5	3.79	2.26	0.19	3.35	VERY POORLY SORTED; FINE SKEWED; EXTREMLY LEPTOKURTIC
128	**L-S29**	12.73	64.85	17.68	4.74	2.51	2.25	2.92	-0.03	1.11	VERY POORLY SORTED; NEAR SYMMETRICAL; LEPTOKURTIC
129	**L-S32**	2.78	65.03	24.14	8.05	3.04	3.47	2.66	0.26	1.32	VERY POORLY SORTED; FINE SKEWED; LEPTOKURTIC
130	**AFA-1A**	0	94.73	3.68	1.59	3.01	3.01	0.62	0.01	0.95	MODERATELY WELL SORTED; NEAR SYMMETRICAL; MESOKURTIC
131	**AFA-1B**	0.07	92.94	4.78	2.21	2.81	2.9	0.74	0.34	1.38	MODERATELY SORTED; STRONGLY FINE SKEWED; LEPTOKURTIC
132	**AFA-1C**	0.46	88.88	7.69	2.97	2.75	2.89	1.05	0.43	2.02	POORLY SORTED; STRONGLY FINE SKEWED; VERY LEPTOKURTIC
133	**AFA-1D**	0.03	74.53	18.62	6.82	3.57	3.89	1.37	0.6	3.44	POORLY SORTED; STRONGLY FINE SKEWED; EXTREMLY LEPTOKURTIC
134	**AFA-2A**	0	94.35	4.01	1.64	2.83	2.91	0.63	0.25	1.08	MODERATELY WELL SORTED; FINE SKEWED; MESOKURTIC
135	**AFA-2B**	0.05	93.77	3.9	2.28	2.72	2.82	0.71	0.38	1.49	MODERATELY WELL SORTED; STRONGLY FINE SKEWED; LEPTOKURTIC
136	**AFA-2C**	0.01	89.16	8.02	2.81	2.99	3.06	0.99	0.36	1.87	MODERATELY SORTED; STRONGLY FINE SKEWED; VERY LEPTOKURTIC
137	**AFA-2D**	0.11	72.71	20.62	6.56	3.27	3.61	1.61	0.53	1.83	POORLY SORTED; STRONGLY FINE SKEWED; VERY LEPTOKURTIC
138	**AFA-3A**	0	92.88	4.49	2.63	2.72	2.84	0.86	0.48	2.11	MODERATELY SORTED; STRONGLY FINE SKEWED; VERY LEPTOKURTIC
139	**AFA3B**	10.26	80.99	5.89	2.86	-0.28	-0.1	1.58	0.51	3.2	POORLY SORTED; STRONGLY FINE SKEWED; EXTREMLY LEPTOKURTIC
140	**AFA-3C**	0.26	76.7	17.1	5.94	3.51	2.92	2.34	-0.16	3.92	VERY POORLY SORTED; COARSE SKEWED; EXTREMLY LEPTOKURTIC
141	**AFA-3D**	0.01	95.76	2.54	1.69	2.48	2.44	0.83	-0.07	1.46	MODERATELY SORTED; NEAR SYMMETRICAL; LEPTOKURTIC
142	**NST-1**	76.3%	23.7%	0.0%	0.0%	-2.298	-2.009	1.138	0.281	0.840	POORLY SORTED; FINE SKEWED; PLATYKURTIC
143	**NST-2**	90.1%	9.9%	0.0%	0.0%	-1.689	-1.779	0.790	-0.029	1.191	MODERATELY SORTED; SYMMETRICAL; LEPTOKURTIC
144	**NST-3**	100.0%	0.0%	0.0%	0.0%	-2.376	-2.326	0.509	0.241	1.103	MODERATELY WELL SORTED; FINE SKEWED; MESOKURTIC
145	**NST-4**	100.0%	0.0%	0.0%	0.0%	-2.783	-2.856	0.613	-0.174	0.785	MODERATELY WELL SORTED; COARSE SKEWED; PLATYKURTIC
146	**PSA-1**	0.0%	99.9%	0.1%	0.0%	2.016	2.000	0.628	-0.034	0.738	MODERATELY WELL SORTED; SYMMETRICAL; PLATYKURTIC
147	**PSA-2**	11.5%	88.4%	0.1%	0.0%	1.099	0.729	1.248	-0.405	0.902	POORLY SORTED; VERY COARSE SKEWED; MESOKURTIC
148	**PSA-3**	0.0%	100.0%	0.0%	0.0%	2.411	2.411	0.456	-0.171	1.121	WELL SORTED; COARSE SKEWED; LEPTOKURTIC
149	**PSA-4**	0.0%	100.0%	0.0%	0.0%	2.373	2.313	0.528	-0.265	1.143	MODERATELY WELL SORTED; COARSE SKEWED; LEPTOKURTIC

150	**EV-1**	97.3%	2.7%	0.0%	0.0%	-2.286	-2.474	1.103	-0.235	0.792	POORLY SORTED; COARSE SKEWED; PLATYKURTIC
151	**EV-2**	79.4%	20.6%	0.0%	0.0%	-1.597	-1.650	0.897	-0.074	1.066	MODERATELY SORTED; SYMMETRICAL; MESOKURTIC
152	**EV-3**	82.6%	17.4%	0.0%	0.0%	-1.933	-2.320	1.052	0.292	0.296	POORLY SORTED; FINE SKEWED; VERY PLATYKURTIC
153	**EV-4**	98.0%	2.0%	0.0%	0.0%	-1.941	-2.011	0.748	-0.199	0.868	MODERATELY SORTED; COARSE SKEWED; PLATYKURTIC
154	**K-13**	0.00	100.00	0.00	0.00	2.29	2.20	0.59	-0.26	0.92	MODERATELY WELL SORTED; COARSE SKEWED; MESOKURTIC
155	**K-14**	67.00	33.00	0.00	0.00	-4.68	-2.45	2.94	0.94	0.49	VERY POORLY SORTED; VERY FINE SKEWED; VERY PLATYKURTIC
156	**K-15**	0.00	100.00	0.00	0.00	1.48	1.48	0.50	-0.05	1.27	MODERATELY WELL SORTED; SYMMETRICAL; LEPTOKURTIC
157	**K-24**	24.70	75.30	0.00	0.00	1.55	0.08	2.69	-0.67	1.39	VERY POORLY SORTED; VERY COARSE SKEWED; LEPTOKURTIC
158	**K-23**	0.10	99.90	0.00	0.00	1.65	1.73	0.69	0.09	1.11	MODERATELY WELL SORTED; SYMMETRICAL; MESOKURTIC
160	**K-36**	0.00	100.00	0.00	0.00	2.10	2.06	0.61	-0.10	0.75	MODERATELY WELL SORTED; COARSE SKEWED; PLATYKURTIC
161	**KIS-1**	16.42	83.57	0.01	0.00	-0.43	-0.39	1.02	-0.14	2.56	POORLY SORTED; COARSE SKEWED; VERY LEPTOKURTIC
162	**KIS-2**	0.00	99.96	0.04	0.00	0.86	0.87	0.63	-0.02	0.98	MODERATELY WELL SORTED; NEAR SYMMETRICAL; MESOKURTIC
163	**KIS-3**	0.19	99.81	0.00	0.00	0.89	0.92	0.55	0.06	0.91	MODERATELY WELL SORTED; NEAR SYMMETRICAL; MESOKURTIC
164	**SFN-1**	99.17	0.80	0.03	0.00	-3.14	-3.13	0.68	-0.03	1.00	MODERATELY WELL SORTED; NEAR SYMMETRICAL; MESOKURTIC
165	**SFN-2**	99.86	0.13	0.01	0.00	-2.68	-2.85	0.84	-0.29	1.20	MODERATELY SORTED; COARSE SKEWED; LEPTOKURTIC
166	**KAMP-1**	5.33	94.63	0.04	0.00	0.83	0.75	0.86	-0.22	1.06	MODERATELY SORTED; COARSE SKEWED; MESOKURTIC
167	**KAMP-2**	69.43	30.51	0.06	0.00	-1.63	-1.44	1.62	0.19	1.09	POORLY SORTED; FINE SKEWED; MESOKURTIC
168	**TAV-1**	10.62	89.28	0.10	0.00	0.18	0.09	0.84	-0.14	1.08	MODERATELY SORTED; COARSE SKEWED; MESOKURTIC
169	**OAM-1**	0.00	100.00	0.00	0.00	2.34	2.27	0.46	-0.26	1.14	WELL SORTED; COARSE SKEWED; LEPTOKURTIC
170	**AST-1**	40.29	59.34	0.37	0.00	0.48	-0.67	2.68	-0.50	0.58	VERY POORLY SORTED; STRONGLY COARSE SKEWED; VERY PLATYKURTIC
171	**KAM-1**	99.76	0.24	0.00	0.00	-2.23	-2.20	0.78	-0.15	1.64	MODERATELY SORTED; COARSE SKEWED; VERY LEPTOKURTIC
172	**LYK-1**	10.35	89.63	0.02	0.00	1.84	1.57	1.25	-0.48	1.67	POORLY SORTED; STRONGLY COARSE SKEWED; VERY LEPTOKURTIC
173	**DER-1**	15.22	84.71	0.07	0.00	1.25	0.85	1.53	-0.39	1.08	POORLY SORTED; STRONGLY COARSE SKEWED; MESOKURTIC
174	**AL-1**	0.00	99.75	0.25	0.00	2.42	2.37	0.58	-0.12	1.31	MODERATELY WELL SORTED; COARSE SKEWED; LEPTOKURTIC
175	**SXN-1**	0.00	99.31	0.69	0.00	2.43	2.34	0.59	-0.35	1.74	MODERATELY WELL SORTED; STRONGLY COARSE SKEWED; VERY LEPTOKURTIC
176	**SXN-3**	0.00	98.77	1.23	0.00	2.89	2.93	0.53	0.12	0.92	MODERATELY WELL SORTED; FINE SKEWED; MESOKURTIC
177	**PL-1**	15.85	84.00	0.15	0.00	0.99	0.72	1.86	-0.40	1.46	POORLY SORTED; STRONGLY COARSE SKEWED; LEPTOKURTIC

178	**SAM-1**	0.39	99.34	0.27	0.00	2.33	2.26	0.49	-0.26	1.14	WELL SORTED; COARSE SKEWED; LEPTOKURTIC
179	**BAL-1**	0.35	99.62	0.03	0.00	0.68	0.73	0.64	0.08	1.09	MODERATELY WELL SORTED; NEAR SYMMETRICAL; MESOKURTIC
180	**SKK-1**	32.59	67.11	0.30	0.00	-0.66	-0.64	0.83	0.15	1.25	MODERATELY SORTED; FINE SKEWED; LEPTOKURTIC

ANNEX III – Chemical Analysis

Table III.1 – Major Elements

Samples	SiO_2	Al_2O_3	Fe_2O_3	MgO	CaO	Na_2O	K_2O	TiO_2	P_2O_5	MnO	SO_3	LOI	Total
	%	%	%	%	%	%	%	%	%	%	%	%	%
KIS-1A	55.87	0.92	0.86	1.32	21.33	0.21	0.26	0.08	0.03	0.04	0.14	18.94	100.00
KIS-1B	51.38	1.30	0.84	1.28	23.39	0.31	0.33	0.14	0.04	0.04	0.13	20.81	99.99
KIS-1C	37.31	1.35	0.62	1.79	27.24	0.76	0.26	0.09	0.06	0.03	0.31	30.16	99.98
KIS-1D	29.89	2.03	1.47	2.08	32.23	0.45	0.39	0.21	0.06	0.03	0.38	30.56	99.78
KIS-2A	67.64	2.30	1.61	0.86	14.10	0.37	0.43	0.31	0.05	0.05	0.10	12.39	100.21
KIS-2B	67.25	2.20	1.37	0.85	14.21	0.41	0.41	0.26	0.04	0.04	0.09	12.78	99.91
KIS-2C	65.29	2.42	1.59	0.88	14.69	0.45	0.45	0.27	0.05	0.04	0.13	13.73	99.99
KIS-2D	49.10	4.90	1.56	0.10	19.16	0.12	0.66	0.36	0.61	0.03	0.29	22.87	99.76
KIS-3A	70.35	2.29	1.44	0.72	13.12	0.32	0.41	0.26	0.04	0.04	0.06	10.91	99.96
KIS-3B	60.14	2.92	1.84	0.95	16.60	0.95	0.54	0.27	0.05	0.05	0.24	15.45	100.00
KIS-3C	57.53	4.34	2.34	1.16	15.63	1.06	0.76	0.44	0.08	0.03	0.60	16.00	99.97
KIS-3D	50.83	4.30	2.04	0.17	17.19	0.07	1.02	0.46	0.63	0.03	0.53	22.53	99.80
KIS-4A	70.60	2.27	1.55	0.67	12.71	0.36	0.38	0.32	0.04	0.04	0.11	10.94	99.99
KIS-4B	64.39	2.40	1.27	0.87	14.88	0.79	0.40	0.36	0.04	0.04	0.21	13.83	99.48
KIS-4C	34.17	3.57	2.11	1.71	27.39	1.00	0.68	0.30	0.07	0.03	1.17	27.47	99.67
KIS-4D	48.83	6.12	2.46	0.08	17.50	0.18	1.31	0.53	0.68	0.03	0.82	21.12	99.66
SFI-1	79.75	0.86	1.15	0.17	7.25	0.00	0.43	0.28	0.38	0.01	0.07	9.59	99.94
SFI-3	82.08	0.97	1.42	0.70	6.48	0.00	0.45	0.38	0.33	0.01	0.06	7.54	100.42
AFA 1A	14.04	0.43	1.76	12.47	30.47	0.08	0.25	0.31	0.06	0.06	0.07	40.33	100.34
AFA 1B	8.98	0.70	1.70	14.47	31.06	0.09	0.30	0.20	0.07	0.06	0.12	42.11	99.85
AFA 1C	1.31	0.80	2.40	21.15	27.17	0.07	0.35	0.19	0.06	0.06	0.33	45.76	99.63
AFA 1D	3.00	1.67	2.45	18.95	30.31	0.10	0.38	0.29	0.08	0.06	0.20	42.50	100.00
AFA 2A	13.64	0.42	1.80	12.34	30.49	0.07	0.23	0.33	0.08	0.07	0.06	40.12	99.65

AFA 2B	11.00	0.68	1.66	13.78	31.66	0.08	0.27	0.22	0.06	0.06	0.14	40.24	99.84
AFA 2C	1.52	1.13	2.38	20.14	29.09	0.07	0.36	0.23	0.07	0.06	0.20	45.34	100.59
AFA 2D	2.92	1.87	2.48	18.81	30.26	0.06	0.41	0.30	0.08	0.06	0.22	42.64	100.11
AFA 3A	26.20	2.79	3.30	6.21	27.40	0.50	0.27	0.56	0.06	0.11	0.09	32.35	99.84
AFA 3B	2.60	0.68	1.36	13.67	36.60	0.09	0.21	0.16	0.06	0.05	0.37	44.46	100.30
AFA 3C	0.52	1.22	1.93	16.44	35.10	0.07	0.27	0.26	0.07	0.06	0.33	44.18	100.46
AFA 3D	4.80	5.10	0.50	4.14	39.80	0.50	0.08	0.05	0.07	0.03	0.36	44.28	99.70
KD 1	77.89	1.81	1.83	1.15	8.51	0.85	0.47	0.38	0.06	0.05	0.05	6.81	99.86
KD 2	80.42	3.23	1.66	2.66	4.63	0.27	0.49	0.36	0.06	0.06	0.09	5.39	99.32
KD 3	80.46	2.27	1.75	1.47	5.53	1.36	0.61	0.34	0.04	0.06	0.07	6.34	100.30
KD 6	68.74	4.57	2.69	1.51	8.41	2.09	0.87	0.53	0.05	0.06	0.23	10.19	99.94
KD 7	51.82	7.05	3.82	1.77	17.08	2.63	0.67	1.09	0.15	0.06	0.14	12.95	99.23
KD 8	61.59	5.39	2.38	2.13	11.24	1.18	0.75	0.53	0.05	0.05	1.20	9.64	96.13
KD 9	60.03	4.53	2.72	1.89	10.21	2.56	0.88	0.55	0.08	0.05	0.17	16.13	99.80
KD 10	66.75	0.00	1.22	1.82	14.59	1.12	0.39	0.13	0.05	0.09	0.04	14.18	100.38
KD 11	75.60	5.10	3.05	1.59	4.96	1.85	0.94	0.53	0.09	0.06	0.08	6.08	99.93
KD 12	73.51	4.53	2.92	1.78	6.59	1.55	0.75	0.68	0.09	0.06	0.02	7.61	100.09
KD 13	72.39	4.53	2.62	1.50	6.75	1.53	0.80	0.50	0.04	0.06	0.04	9.23	99.99
KD 14	70.46	5.23	3.19	2.60	7.06	1.32	0.98	0.56	0.08	0.06	0.15	8.62	100.31
KD 15	85.88	2.57	2.04	2.13	1.54	1.25	0.79	0.32	0.07	0.05	0.15	3.33	100.12
KD 16	83.76	3.97	1.32	4.28	2.06	1.56	0.56	0.18	0.05	0.06	0.12	2.43	100.35
KD-5 (5-7)	37.00	9.04	4.77	4.57	14.93	2.63	1.40	0.53	0.14	0.08	0.37	25.82	101.28
KD-5 (60-62)	35.39	9.23	5.44	4.87	16.47	2.80	1.60	0.56	0.14	0.10	1.27	24.20	102.07
KD-5 (110--112)	38.79	10.83	5.96	5.49	14.50	2.60	1.79	0.65	0.16	0.11	0.73	22.59	104.18
KD-5 (160-162)	39.63	10.60	6.00	6.06	16.22	2.38	1.73	0.62	0.14	0.13	0.42	21.05	104.97
KD-5 (190-192)	39.69	10.35	6.18	5.96	12.91	2.57	1.73	0.61	0.14	0.11	0.55	13.35	106.45
KD-18 (5-7)	41.47	12.73	6.58	5.35	11.71	2.30	2.22	0.71	0.18	0.10	0.08	21.80	105.23
KD-18 (50-52)	42.73	14.51	7.47	5.30	9.35	2.36	2.56	0.75	0.17	0.11	0.34	21.04	106.68
KD-18 (80-82)	37.22	11.75	6.08	4.97	15.30	2.08	2.06	0.62	0.14	0.10	0.26	22.84	103.41

KD-18 (120-122)	36.59	11.47	6.18	5.34	16.24	2.13	2.22	0.63	0.14	0.11	0.22	22.14	103.40
KD-18 (150-152)	37.89	11.89	6.63	5.09	13.44	2.60	2.36	0.67	0.14	0.09	1.12	22.20	104.13
KD-18 (200-202)	40.73	12.22	6.23	4.91	10.52	2.13	2.34	0.65	0.17	0.09	0.27	24.04	104.30
TH NST 1	90.88	0.28	0.23	1.64	1.03	0.11	0.21	0.03	0.09	0.01	0.18	5.02	94.69
TH NST 2	93.49	0.24	0.10	1.94	0.60	0.07	0.10	0.02	0.10	0.00	0.02	3.22	96.69
TH NST 3	91.88	0.18	0.11	1.56	0.51	0.06	0.11	0.01	0.15	0.00	0.01	4.78	94.58
TH NST 4	92.64	0.26	0.06	1.59	0.38	0.04	0.09	0.01	0.06	0.00	0.02	4.55	95.15
TH EV 1	68.50	3.95	1.14	1.27	8.30	2.27	3.96	0.23	0.40	0.01	0.03	10.31	90.05
TH EV 2	79.47	4.24	0.84	1.02	1.68	1.95	4.50	0.18	0.52	0.01	0.03	5.27	94.43
TH EV 3	85.40	2.73	1.14	0.55	1.73	3.01	3.11	0.16	0.37	0.01	0.01	1.96	98.21
TH EV 4	88.79	1.20	0.57	0.22	1.51	2.82	2.69	0.11	0.34	0.00	0.00	1.70	98.25
K-24	69.74	0.13	1.27	0.00	13.97	0.00	0.16	0.18	0.08	0.03	0.06	14.47	100.09
BOURNEMOUTH Coastline	87.08	2.26	0.35	2.46	0.99	4.57	0.16	0.07	0.01	0.04	0.09	2.09	100.17
BOSCOMBE Coastline	87.01	2.13	1.21	2.27	0.72	4.41	0.13	0.08	0.04	0.03	0.15	2.11	100.30
ALIARTOS 1	65.12	0.11	1.34	1.17	14.29	2.93	0.63	0.12	0.04	0.03	0.05	14.17	99.98
STRYMONAS 1	75.77	11.32	1.29	0.09	1.72	5.49	2.70	0.28	0.12	0.03	0.02	1.11	99.93
GK	60.10	6.93	3.85	0.21	10.49	4.15	0.83	0.69	0.11	0.05	0.10	12.28	99.79

Table III.2 – Trace Elements

Samples	**Ag**	**As**	**Ba**	**Bi**	**Br**	**Cd**	**Ce**	**Cl**	**Co**	**Cr**	**Cs**	**Cu**	**Ga**	**Ge**	**Hf**	**Hg**	**I**	**La**	**Mn**	**Mo**	**Nb**
	ppm	**ppm**	**ppm**	**ppm**	**ppm**	**ppm**	**ppm**	**%**	**ppm**	**ppm**	**ppm**	**ppm**	**ppm**	**ppm**	**ppm**	**ppm**	**ppm**	**ppm**	**ppm**	**ppm**	**ppm**
KIS-1A	0.0	31.0	28.2	2.1	7.9	0.0	7.7	-	18.4	34.7	0.0	9.4	0.0	0.0	7.0	0.0	2.7	4.8	358.2	1.7	0.7
KIS-1B	0.0	20.9	29.2	2.4	12.2	0.0	27.0	-	8.8	65.1	0.0	9.5	0.0	0.0	6.9	0.0	6.3	6.2	357.0	2.3	2.7
KIS-1C	0.2	16.4	43.6	0.0	13.3	0.2	23.1	-	5.8	82.5	5.0	12.2	4.9	1.0	6.9	0.0	10.8	14.1	0.0	1.0	1.6
KIS-1D	0.0	30.2	51.7	5.7	27.1	0.0	36.8	-	11.5	67.2	0.0	12.1	0.0	0.0	11.5	0.0	42.2	12.6	298.4	3.7	3.1

KIS-2A	0.0	24.3	54.9	0.5	10.2	0.0	34.3	-	19.6	82.1	0.0	7.0	0.0	0.0	9.1	0.0	0.8	14.2	429.3	4.4	6.9
KIS-2B	0.0	27.6	53.3	1.8	12.7	0.0	30.9	-	16.8	56.5	0.0	6.2	0.0	0.0	5.4	0.0	0.0	12.9	422.3	3.3	6.3
KIS-2C	0.0	29.1	55.3	4.2	16.1	0.0	36.3	-	16.1	60.6	0.0	7.6	0.0	0.0	10.2	0.0	6.8	12.0	381.3	3.9	7.2
KIS-2D	0.4	15.8	104.5	0.0	30.1	0.0	55.7	-	10.8	100.1	4.9	13.2	8.8	1.6	5.3	0.0	30.8	29.5	0.0	1.5	9.6
KIS-3A	0.0	22.9	51.1	3.3	8.8	0.0	26.7	-	18.4	43.3	0.0	4.7	0.0	0.0	6.6	0.0	0.1	8.1	403.1	3.1	7.3
KIS-3B	0.0	32.6	66.4	3.4	40.8	0.0	26.3	-	4.9	50.5	0.0	9.1	0.0	0.0	8.7	0.0	6.3	16.6	412.6	2.8	6.8
KIS-3C	0.0	18.3	101.3	2.3	61.9	0.0	41.6	-	5.1	71.7	0.0	14.6	0.0	0.0	8.8	0.0	37.8	20.7	274.7	5.3	11.2
KIS-3D	0.0	12.8	148.8	0.0	47.2	0.2	66.7	-	17.3	108.3	5.3	19.4	11.4	1.5	5.7	0.0	52.9	34.1	0.0	2.0	11.7
KIS-4A	0.0	25.7	45.4	1.8	9.3	0.0	38.1	-	17.6	39.3	0.0	5.2	0.0	0.0	9.3	0.0	0.0	10.0	420.4	4.3	8.2
KIS-4B	0.0	17.6	59.1	3.2	36.6	0.0	43.7	-	3.6	73.4	0.0	7.3	0.0	0.0	9.0	0.0	0.6	23.9	326.2	6.4	9.7
KIS-4C	0.0	26.5	77.3	2.6	112.5	0.0	44.0	-	9.7	60.5	0.0	13.2	0.0	0.0	11.8	0.0	66.0	19.2	307.8	6.3	7.3
KIS-4D	0.4	14.4	177.4	0.0	51.5	0.0	66.2	-	19.2	107.3	7.0	33.5	9.6	1.1	3.2	0.2	46.5	37.4	0.0	0.7	12.9
SPH 1	0.5	14.9	70.5	0.0	4.6	0.0	32.8	-	9.5	29.2	4.1	8.8	6.4	2.3	3.8	0.0	3.6	19.1	0.0	0.6	9.6
SPH 3	0.7	17.1	80.1	0.0	5.2	0.5	52.3	-	6.4	30.3	3.7	8.6	8.3	1.9	6.3	0.0	3.7	26.8	0.0	0.1	13.2
KD 1	0.2	10.3	96.7	0.0	25.8	0.0	22.2	0.2	48.4	130.3	3.6	73.5	4.7	4.2	0.0	0.0	2.4	11.8	0.0	0.6	4.7
KD 2	0.3	9.3	92.6	0.0	28.6	0.1	18.4	0.2	53.0	130.3	4.1	56.6	5.5	4.8	1.1	0.0	2.3	10.8	0.0	1.1	4.7
KD 3	0.9	10.9	120.7	0.0	22.7	0.0	19.1	0.2	43.8	138.7	5.4	96.5	5.5	3.6	0.0	0.0	3.9	10.5	0.0	0.8	3.1
KD 6	0.4	11.2	156.9	0.0	71.2	0.4	38.1	0.2	49.0	177.5	3.8	78.1	6.8	3.0	0.0	0.0	91.0	20.9	0.0	0.4	5.2
KD 7	0.0	13.1	111.1	0.0	22.1	0.8	56.4	0.1	30.5	159.1	2.5	94.1	11.4	3.3	0.0	0.0	3.8	27.8	0.0	6.7	0.4
KD 8	0.7	10.2	105.0	0.0	34.6	0.0	25.6	0.2	36.6	116.8	4.8	45.4	6.3	3.1	0.0	0.0	8.0	14.1	0.0	1.1	3.7
KD 10	0.5	11.9	61.1	0.0	6.7	1.1	14.1	0.2	28.5	84.2	3.7	71.5	4.3	2.9	0.6	0.0	6.0	11.7	0.0	1.5	2.2
KD 11	0.2	14.2	154.6	0.0	42.1	0.0	35.1	0.1	62.5	211.9	4.2	124.3	7.7	3.8	0.0	0.0	17.0	19.7	0.0	0.9	7.6
KD 12	0.5	15.5	120.7	0.0	23.7	0.3	36.8	0.2	63.7	171.5	4.7	115.3	8.5	5.7	0.0	0.0	1.5	20.6	0.0	0.4	8.6
KD 13	0.0	16.4	129.8	0.0	29.4	0.0	26.3	0.2	63.0	175.4	4.1	24.4	7.6	4.8	0.0	0.0	6.1	14.1	0.0	1.4	6.5
KD 14	0.5	13.9	171.3	0.0	59.5	0.5	38.6	0.2	63.0	218.6	5.1	52.0	7.2	4.4	0.0	0.0	66.6	21.9	0.0	0.8	6.8
KD 15	0.1	11.0	108.1	0.0	7.7	0.1	18.7	0.2	70.0	121.2	3.9	50.2	6.8	6.4	0.0	-14.2	2.0	11.6	0.0	1.7	3.6
KD 16	0.2	6.5	75.6	0.0	4.8	0.0	12.9	0.2	54.6	75.6	3.2	39.6	5.1	4.5	0.3	-12.4	5.2	9.1	0.0	1.3	2.1
KD-5 (5-7)	<2.8	0.4	161.0	<1.3	49.3	<3.1	-	1.0	84.0	316.0	-	27.1	8.2	0.5	-	0.6	43.5	-	639.0	<22	-

KD-5 (60-62)	<2.8	15.7	203.0	<1.3	47.5	<3.2	-	0.9	87.0	331.0	-	36.0	13.5	1.8	-	3.3	23.5	-	797.0	<19	-
KD-5 (110--112)	<2.9	11.1	216.0	<1.3	38.4	<3.2	-	0.8	94.0	378.0	-	39.0	11.8	<0.9	-	2.3	<12	-	875.0	<21	-
KD-5 (160-162)	3.6	6.7	316.0	<1.3	40.3	<2.9	-	0.8	91.0	418.0	-	37.6	11.2	1.2	-	1.6	<12	-	969.0	<20	-
KD-5 (190-192)	<2.5	7.1	249.0	<1.3	34.5	<3.1	-	0.7	74.0	460.0	-	30.4	<0.8	7.1	-	1.3	17.8	-	844.0	<21	-
KD-18 (5-7)	<2.5	16.7	241.0	<1.4	53.4	<2.9	-	1.1	101.0	328.0	-	46.3	11.4	1.6	-	<1.5	51.1	-	740.0	<20	-
KD-18 (50-52)	<2.9	21.3	350.0	<1.5	43.4	<2.9	-	0.9	108.0	394.0	-	63.7	17.3	1.1	-	0.7	16.5	-	816.0	<18	-
KD-18 (80-82)	<3	9.9	248.0	<1.4	44.3	<3.2	-	0.9	99.0	321.0	-	42.9	13.9	2.5	-	<1.6	<12	-	760.0	<21	-
KD-18 (120-122)	<2.7	8.5	307.0	<1.4	41.7	<3	-	0.9	82.0	353.0	-	48.2	14.0	0.4	-	3.0	15.3	-	823.0	<21	-
KD-18 (150-152)	<2.7	18.3	393.0	<1.4	59.8	3.2	-	1.0	95.0	316.0	-	45.5	15.6	1.9	-	<1.5	23.4	-	731.0	<21	-
KD-18 (200-202)	7.8	10.5	321.0	<1.4	32.9	<3	-	0.8	98.0	295.0	-	49.5	13.1	1.4	-	1.0	<12	-	692.0	<19	-
K 24	1.2	14.9	36.0	0.0	1.3	0.0	26.3	-	7.2	54.9	4.3	9.1	4.6	2.0	6.7	0.0	1.6	16.7	0.0	1.0	6.8
TH NST 1	0.6	0.0	35.5	0.0	0.0	0.0	6.6	0.1	14.2	19.7	3.0	8.7	3.2	2.7	3.1	0.0	0.6	6.3	0.0	0.8	1.2
TH NST 2	0.3	0.1	17.0	0.1	0.0	0.0	5.1	0.0	17.8	10.3	3.2	7.1	3.1	3.1	2.9	0.0	0.4	4.9	0.0	1.0	0.1
TH NST 3	0.1	0.1	32.8	0.4	0.0	0.0	6.1	0.0	18.6	9.1	2.7	7.2	3.0	2.9	3.1	0.0	0.3	5.7	0.0	0.7	0.0
TH NST 4	0.4	0.0	15.4	0.4	0.0	0.0	4.7	0.0	12.6	10.9	3.6	8.5	2.5	2.2	4.8	0.0	1.0	4.4	0.0	0.7	0.0
TH EV 1	0.7	0.4	568.9	0.0	0.4	-0.4	46.2	0.0	9.3	63.7	3.3	10.5	13.7	2.1	5.6	0.0	0.0	25.8	0.0	0.2	7.7
TH EV 2	1.4	0.5	589.7	0.1	1.4	0.0	41.8	0.1	9.3	-0.7	2.9	8.6	9.5	2.1	6.0	0.0	1.8	21.8	0.0	0.4	6.4
TH EV 3	0.4	1.3	355.4	0.0	0.2	0.0	29.6	0.0	12.8	2.5	3.9	9.7	6.4	2.9	5.5	0.0	1.2	16.8	0.0	1.0	5.0
TH EV 4	0.6	0.4	265.4	0.0	0.2	0.0	24.7	0.0	13.5	13.3	3.2	8.6	4.5	3.2	4.4	0.0	0.7	14.0	0.0	1.2	2.9
BOURNEMOUTH Coastline	0.5	1.8	48.9	0.0	12.3	0.5	13.7	0.6	14.5	56.1	4.1	5.9	2.2	2.1	5.0	0.0	1.6	9.1	15.5	0.3	1.3
BOSCOMBE Coastline	0.4	8.7	36.2	0.0	11.7	0.4	25.4	0.5	20.0	61.9	2.5	5.9	2.6	3.3	3.2	0.0	0.3	12.9	31.0	1.2	2.6
ALIARTOS 1	0.6	2.7	157.4	0.0	0.1	0.3	11.7	0.0	26.2	484.1	4.2	13.1	5.2	1.9	4.8	0.0	0.9	9.5	209.1	0.1	1.7
STRYMONAS 1	0.5	4.5	505.3	0.0	0.4	0.1	36.5	0.0	13.6	38.1	3.9	12.5	12.8	2.8	4.0	0.0	0.4	19.7	232.3	1.3	5.5
GK	1.0	11.1	170.1	0.0	10.0	0.5	43.9	-	28.9	106.4	3.7	51.4	12.5	1.8	0.9	0.0	0.6	23.0	0.0	3.2	8.1

Table III.3 – Trace Elements

Samples	Nd	Ni	Pb	Rb	Se	Sb	Sc	Sm	Sn	Sr	Te	Th	Tl	U	V	W	Y	Yb	Zn	Zr
	ppm	ppm	ppm	ppm	ppm	ppm	ppm	ppm	ppm	ppm	ppm	ppm	ppm	ppm	ppm	ppm	ppm	ppm	ppm	ppm
KIS-1A	1.5	18.6	0.0	12.1	0.0	2.0	10.7	7.7	4.0	647.5	0.0	16.0	0.0	-	19.0	0.0	9.5	0.0	11.7	10.1
KIS-1B	12.8	23.2	0.0	14.1	0.0	1.6	14.2	2.8	5.3	633.0	0.0	16.9	0.0	-	22.7	0.0	11.4	0.0	15.8	38.6
KIS-1C	11.5	12.6	3.2	9.1	4.2	0.8	0.0	7.4	1.1	822.4	0.3	1.8	0.9	-	40.5	28.8	10.5	0.0	21.6	39.9
KIS-1D	16.6	22.3	4.6	22.9	0.0	2.7	14.3	4.9	3.3	1491.2	0.0	31.6	0.0	-	35.5	0.0	15.7	0.0	30.3	81.0
KIS-2A	17.4	21.4	0.0	15.8	0.0	1.2	11.0	6.9	3.7	264.8	0.0	12.9	0.0	-	36.9	0.0	13.7	0.0	19.8	153.1
KIS-2B	12.7	20.8	0.5	15.5	0.0	1.7	10.3	7.1	6.4	281.4	0.0	13.5	0.0	-	36.4	0.0	12.3	0.0	17.2	103.3
KIS-2C	13.9	22.1	1.1	17.1	0.0	1.5	12.2	2.8	5.2	298.8	0.0	14.7	0.0	-	42.4	0.0	13.5	0.0	20.6	122.4
KIS-2D	27.3	16.8	7.7	22.5	7.7	1.0	0.0	8.4	1.8	345.3	0.5	0.0	0.9	-	68.1	68.9	18.1	0.0	30.3	172.0
KIS-3A	11.8	18.9	0.0	16.1	0.0	1.0	11.5	6.7	5.3	216.4	0.0	12.9	0.0	-	36.6	0.0	11.6	0.0	17.8	83.7
KIS-3B	13.8	24.6	2.3	21.1	0.0	1.4	8.6	6.3	3.0	344.6	0.0	13.9	0.0	-	52.9	0.0	13.0	0.0	24.4	78.5
KIS-3C	15.1	33.4	8.0	30.4	0.0	1.6	9.4	7.4	4.3	317.3	0.0	16.6	0.0	-	61.8	0.0	18.7	0.0	34.5	182.8
KIS-3D	30.6	34.8	13.0	36.4	6.4	0.2	0.0	9.9	2.6	327.7	0.3	2.4	1.7	-	91.4	49.9	18.6	0.0	45.4	199.0
KIS-4A	18.7	15.8	0.5	14.1	0.0	2.1	9.7	4.9	6.1	198.0	0.0	11.3	0.0	-	36.8	0.0	12.9	0.0	18.3	148.3
KIS-4B	17.9	16.8	0.6	15.8	0.0	1.2	8.2	4.2	3.7	262.9	0.0	14.3	0.0	-	38.4	0.0	16.4	0.0	18.5	255.2
KIS-4C	19.1	29.4	4.4	34.8	0.0	3.2	16.4	7.1	5.3	1579.4	0.0	31.9	0.0	-	62.5	0.0	16.4	0.0	33.7	96.4
KIS-4D	29.3	44.3	14.2	47.2	3.5	1.7	3.2	8.3	2.1	356.3	0.8	0.7	0.7	-	99.5	17.5	19.6	0.0	51.4	191.2
SPH 1	14.1	4.3	4.4	13.1	14.4	0.4	0.0	7.4	1.4	348.8	0.4	1.4	0.6	-	32.0	172.7	11.1	0.0	99.6	204.3
SPH 3	20.7	7.7	4.0	14.1	9.1	0.8	0.0	7.9	0.4	283.1	0.7	0.2	0.9	-	38.0	100.4	17.1	0.0	23.1	372.9
KD 1	7.9	64.7	8.1	17.6	40.2	0.8	29.8	5.4	1.3	103.2	1.0	7.1	0.7	-	51.5	485.8	11.5	0.0	67.0	48.9
KD 2	6.8	67.5	6.3	16.8	44.8	0.6	24.1	6.0	1.3	100.2	0.6	1.1	0.4	-	37.5	572.2	9.3	0.0	54.7	42.2
KD 3	6.5	84.8	8.3	22.4	30.6	0.8	19.5	4.9	2.1	121.8	0.6	0.2	1.2	-	49.2	382.2	10.9	0.0	85.4	44.9
KD 6	18.3	105.9	14.7	28.8	24.7	1.6	14.4	6.0	1.5	310.3	0.0	0.5	0.6	-	86.3	299.4	19.1	0.0	84.3	94.7
KD 7	30.7	49.1	17.2	15.7	12.5	1.9	0.3	7.5	3.3	425.3	1.8	0.2	3.6	-	202.5	138.5	29.0	0.0	109.1	92.3
KD 8	11.2	54.2	10.3	18.4	24.4	1.9	29.1	4.2	2.0	397.2	0.5	2.3	1.5	-	95.0	279.6	17.8	0.0	62.7	72.5
KD 10	7.7	41.6	7.9	13.6	27.2	1.3	33.3	5.9	2.2	277.5	1.0	2.4	0.7	-	51.9	320.4	9.1	0.0	56.9	26.3

KD 11	14.0	138.8	14.4	32.5	36.5	1.7	12.0	5.0	1.7	152.8	1.3	1.4	1.5	-	70.1	453.4	14.9	0.0	127.8	87.3
KD 12	18.3	113.6	12.3	24.3	46.3	1.3	10.1	7.2	1.2	121.4	0.5	1.4	0.9	-	74.7	561.7	18.9	0.0	118.3	71.3
KD 13	11.2	113.4	8.5	27.4	43.7	1.2	11.9	5.9	2.3	119.1	1.3	1.4	0.9	-	66.9	544.8	13.6	0.0	62.3	69.5
KD 14	18.6	138.3	15.2	34.3	33.4	1.1	12.2	7.7	1.6	182.8	0.6	1.8	0.8	-	81.6	404.9	15.9	0.0	77.5	98.6
KD 15	7.3	80.9	7.9	24.1	61.0	0.5	7.1	6.6	1.6	43.6	0.5	2.3	1.3	-	52.0	786.5	7.2	0.0	69.4	52.6
KD 16	3.2	50.3	7.1	17.6	52.4	0.9	14.1	4.5	1.6	46.7	1.6	0.0	0.3	-	29.8	670.8	4.3	0.0	47.0	35.1
KD-5 (5-7)	-	156.2	19.9	45.7	0.4	<4.5	-	-	<4.8	487.3	10.9	8.5	<1.5	6.8	114.0	6.2	20.4	-	58.1	-
KD-5 (60-62)	-	181.1	16.0	55.8	<0.6	<4.2	-	-	<5	483.2	<6.8	8.5	<1.5	3.5	135.0	<5.4	20.4	-	68.9	-
KD-5 (110--112)	-	204.8	14.9	64.3	<0.6	3.4	-	-	<4.1	410.7	<6.4	7.7	0.8	<2.8	131.0	9.3	24.7	-	77.3	-
KD-5 (160-162)	-	208.2	16.2	61.5	<0.6	<4.4	-	-	<4.2	364.9	<6.5	8.8	<1.5	<2.9	141.0	5.2	23.1	-	80.2	-
KD-5 (190-192)	-	230.3	17.2	58.6	<0.5	<4.3	-	-	<4.7	323.5	<6.9	8.7	<1.4	4.5	116.0	<5.9	24.0	-	78.1	-
KD-18 (5-7)	-	211.8	33.6	75.7	<0.6	7.5	-	-	<4.4	327.5	<5.9	11.6	<1.6	5.1	190.0	<5.8	25.5	-	91.8	-
KD-18 (50-52)	-	252.3	33.0	94.0	0.5	4.0	-	-	<4.9	246.3	<6.5	9.9	<1.6	3.6	180.0	<6.2	25.8	-	104.5	-
KD-18 (80-82)	-	191.4	20.4	74.3	<0.6	<4.3	-	-	<4.8	429.0	<6.8	10.0	<1.6	5.1	149.0	5.9	24.6	-	80.5	-
KD-18 (120-122)	-	198.5	22.9	76.1	<0.6	<4.2	-	-	<4.3	406.9	<6.1	10.2	<1.6	6.4	162.0	<5.7	23.9	-	84.4	-
KD-18 (150-152)	-	201.1	19.1	3242.0	1.1	3.4	-	-	<4.7	324.2	8.6	9.3	<1.6	5.3	181.0	<5.7	25.1	-	93.3	-
KD-18 (200-202)	-	171.8	29.5	74.0	<0.5	<4.2	-	-	<4.3	297.9	<6.6	10.1	<1.5	6.1	167.0	4.8	28.4	-	96.3	-
K 24	11.4	5.0	4.6	5.8	9.9	0.5	0.0	6.5	1.4	176.8	1.0	0.8	0.9	-	33.2	103.0	9.1	0.0	16.6	156.0
TH NST 1	0.0	4.7	5.4	6.1	21.4	1.1	11.4	3.9	0.9	11.8	1.4	0.6	0.3	-	5.4	260.4	3.7	0.0	64.0	16.5
TH NST 2	0.0	1.8	2.0	1.3	23.8	0.9	5.1	4.1	0.8	7.9	0.7	0.0	0.1	-	0.8	318.9	2.2	0.0	4.9	9.0
TH NST 3	0.0	1.2	3.0	1.6	25.0	0.7	6.6	4.2	1.0	4.4	0.7	0.0	0.5	-	0.5	337.8	2.2	0.0	6.1	10.4
TH NST 4	0.0	1.4	2.0	0.9	20.1	0.6	5.5	4.4	1.0	4.0	1.5	1.4	0.1	-	0.6	270.3	2.2	0.0	5.0	6.5
TH EV 1	19.5	3.6	9.8	87.0	0.0	0.8	0.0	5.9	2.5	17.5	0.0	6.7	1.3	-	30.7	135.8	25.2	0.0	33.5	209.9
TH EV 2	17.3	1.6	8.6	73.7	13.5	0.4	2.7	6.3	1.8	28.9	0.9	5.3	0.2	-	23.4	169.3	18.7	0.0	20.4	180.2
TH EV 3	11.2	1.2	8.5	52.9	14.5	0.8	1.7	6.4	2.1	45.8	0.8	3.4	0.4	-	21.8	182.3	15.8	1.0	19.9	121.6
TH EV 4	7.7	1.0	6.0	34.4	21.7	0.7	0.8	4.5	1.5	22.3	0.0	5.1	0.2	-	15.8	288.8	8.8	0.0	13.5	85.4
BOURNEMOUTH Coastline	1.7	0.2	6.4	3.7	21.6	1.2	8.6	4.2	2.3	23.8	0.4	0.7	0.6	-	7.7	306.8	6.1	0.0	7.6	104.8
BOSCOMBE Coastline	8.7	3.4	5.1	3.3	28.0	1.0	2.0	4.6	4.6	21.2	0.9	0.9	0.1	-	23.7	379.3	7.2	0.0	14.4	178.0

ALIARTOS 1	4.3	84.1	4.5	14.2	14.4	0.3	8.4	4.6	1.7	77.1	0.8	1.9	1.2	-	45.5	151.8	7.8	0.0	11.6	46.1
STRYMONAS 1	15.2	7.3	22.6	87.2	23.5	0.5	0.0	5.1	1.9	188.1	0.0	2.7	0.0	-	31.3	268.5	14.0	0.0	28.8	100.0
GK	20.8	53.3	18.5	22.9	8.2	1.0	13.3	4.8	2.0	249.0	1.0	0.4	2.4	-	138.9	80.0	21.5	0.0	79.1	98.9

ANNEX IV – Correlation Matrices

Table IV.1.1 – SE Evia Island

	SiO_2	**Al_2O_3**	**Fe_2O_3**	**MgO**	**CaO**	**Na_2O**	**K_2O**	**TiO_2**	**P_2O_5**	**MnO**	**SO_3**	**LOI**	***Ag***	***As***	***Ba***	***Bi***	***Br***	***Cd***	***Ce***	***Co***	***Cr***	***Cs***	***Cu***	***Ga***
SiO_2	1.00																							
Al_2O_3	-0.51	1.00																						
Fe_2O_3	-0.60	0.84	1.00																					
MgO	0.30	0.10	-0.32	1.00																				
CaO	-0.90	0.16	0.34	-0.39	1.00																			
Na_2O	-0.61	0.59	0.65	-0.16	0.38	1.00																		
K_2O	-0.20	0.66	0.73	-0.12	-0.17	0.52	1.00																	
TiO_2	-0.68	0.82	0.92	-0.32	0.49	0.61	0.44	1.00																
P_2O_5	-0.52	0.59	0.74	-0.09	0.42	0.55	0.24	0.81	1.00															
MnO	-0.10	-0.45	-0.30	0.02	0.35	-0.12	-0.42	-0.30	-0.11	1.00														
SO_3	-0.35	0.31	0.06	0.08	0.22	-0.05	0.16	0.11	-0.15	-0.33	1.00													
LOI	-0.88	0.13	0.35	-0.42	0.85	0.52	0.10	0.38	0.27	0.30	0.11	1.00												
Ag	0.09	-0.26	-0.27	-0.06	0.01	-0.34	-0.12	-0.26	-0.41	0.21	0.36	-0.05	1.00											
As	-0.27	0.30	0.64	-0.57	0.20	0.24	0.47	0.50	0.31	0.16	-0.23	0.27	-0.11	1.00										
Ba	-0.22	0.56	0.71	-0.31	-0.09	0.49	0.91	0.46	0.22	-0.39	-0.03	0.20	-0.04	0.47	1.00									

Bi	—	—	—	—	—	—	—	—	—	—	—	—	—	—	—	1.00								
Br	-0.39	0.45	0.53	-0.27	0.12	0.39	0.69	0.35	0.06	-0.30	0.16	0.41	0.04	0.20	0.86	—	1.00							
Cd	-0.61	-0.08	0.18	-0.11	0.73	0.31	-0.15	0.22	0.41	0.68	-0.19	0.71	-0.02	0.20	-0.11	—	0.03	1.00						
Ce	-0.72	0.78	0.95	-0.32	0.50	0.75	0.59	0.93	0.79	-0.22	0.01	0.51	-0.27	0.50	0.64	—	0.57	0.35	1.00					
Co	0.60	0.12	0.14	0.15	-0.81	-0.12	0.54	-0.11	-0.09	-0.42	-0.32	-0.56	-0.28	0.28	0.44	—	0.14	-0.54	-0.06	1.00				
Cr	-0.27	0.57	0.80	-0.41	0.01	0.43	0.82	0.58	0.39	-0.27	-0.17	0.23	-0.14	0.67	0.94	—	0.76	-0.02	0.72	0.43	1.00			
Cs	0.26	-0.10	-0.03	-0.18	-0.35	-0.34	0.33	-0.19	-0.42	-0.13	0.21	-0.17	0.72	0.25	0.39	—	0.28	-0.35	-0.18	0.33	0.33	1.00		
Cu	-0.19	0.11	0.37	-0.45	0.20	0.40	0.14	0.38	0.50	0.08	-0.28	0.20	0.15	0.28	0.28	—	0.18	0.19	0.46	-0.10	0.39	0.07	1.00	
Ga	-0.57	0.81	0.91	-0.21	0.34	0.70	0.53	0.93	0.84	-0.24	-0.03	0.30	-0.40	0.56	0.46	—	0.23	0.23	0.89	0.07	0.58	-0.24	0.35	1.00
Ge	0.67	-0.10	-0.09	0.23	-0.69	-0.40	0.04	-0.14	-0.01	-0.26	-0.32	-0.69	-0.23	0.16	-0.11	—	-0.42	-0.40	-0.27	0.76	-0.04	0.13	-0.21	0.03
Hf	0.23	-0.43	-0.57	0.39	-0.05	-0.59	-0.63	-0.45	-0.22	0.49	-0.17	-0.10	0.03	-0.39	-0.57	—	-0.31	0.19	-0.49	-0.21	-0.47	-0.17	-0.22	-0.45
Hg	-0.56	0.16	0.37	-0.61	0.58	0.08	0.06	0.40	0.11	0.20	0.07	0.60	0.29	0.46	0.33	—	0.51	0.26	0.43	-0.38	0.49	0.27	0.39	0.17
I	-0.34	0.28	0.35	-0.07	0.10	0.48	0.61	0.16	0.00	-0.13	0.03	0.45	-0.01	0.01	0.73	—	0.89	0.24	0.45	0.10	0.55	0.11	0.07	0.11
La	-0.73	0.73	0.92	-0.28	0.50	0.76	0.61	0.87	0.78	-0.11	-0.02	0.57	-0.25	0.51	0.65	—	0.59	0.45	0.98	-0.05	0.73	-0.16	0.49	0.85
Mn	—	—	—	—	—	—	—	—	—	—	—	—	—	—	—	—	—	—	—	—	—	—	—	—
Mo	-0.49	0.40	0.41	0.00	0.54	0.38	-0.15	0.61	0.71	0.11	-0.02	0.21	-0.38	0.11	-0.22	—	-0.32	0.42	0.46	-0.44	-0.09	-0.63	0.04	0.64
Nb	0.20	0.17	0.32	-0.25	-0.38	-0.09	0.56	0.08	-0.09	-0.20	-0.16	-0.12	0.03	0.58	0.61	—	0.48	-0.32	0.18	0.70	0.69	0.56	0.23	0.10
Nd	-0.79	0.72	0.91	-0.31	0.60	0.75	0.51	0.92	0.80	-0.11	0.01	0.61	-0.26	0.48	0.55	—	0.51	0.50	0.98	-0.16	0.63	-0.23	0.43	0.87
Ni	0.09	0.35	0.54	-0.26	-0.35	0.25	0.82	0.23	0.07	-0.22	-0.25	-0.02	-0.04	0.61	0.88	—	0.65	-0.21	0.40	0.70	0.89	0.52	0.29	0.30
Pb	-0.69	0.72	0.89	-0.26	0.45	0.78	0.69	0.79	0.70	-0.14	0.05	0.53	-0.15	0.43	0.72	—	0.67	0.39	0.95	-0.05	0.74	-0.09	0.50	0.76
Rb	0.04	0.39	0.53	-0.17	-0.34	0.35	0.91	0.19	0.03	-0.30	-0.13	0.01	-0.06	0.48	0.93	—	0.71	-0.20	0.40	0.67	0.85	0.47	0.17	0.28
Se	0.87	-0.33	-0.44	0.38	-0.86	-0.51	-0.08	-0.52	-0.34	-0.20	-0.30	-0.79	-0.21	-0.12	-0.24	—	-0.45	-0.55	-0.59	0.76	-0.24	0.11	-0.33	-0.34

Sb	-0.74	0.60	0.60	-0.25	0.63	0.52	0.32	0.60	0.40	0.15	0.46	0.48	0.06	0.37	0.23	—	0.29	0.32	0.61	-0.44	0.29	-0.16	0.30	0.52
Sc	0.06	-0.65	-0.67	-0.09	0.17	-0.59	-0.56	-0.61	-0.62	0.27	0.30	0.15	0.45	-0.39	-0.44	—	-0.07	0.00	-0.59	-0.44	-0.47	0.22	-0.18	-0.81
Sm	-0.32	0.27	0.57	-0.13	0.25	0.29	0.29	0.54	0.63	0.07	-0.42	0.34	-0.30	0.49	0.35	—	0.22	0.57	0.61	0.19	0.47	-0.13	0.16	0.59
Sn	-0.54	0.28	0.31	-0.16	0.61	0.37	-0.11	0.45	0.39	0.30	0.10	0.35	-0.11	0.25	-0.18	—	-0.28	0.40	0.31	-0.57	-0.09	-0.37	-0.04	0.47
Sr	-0.95	0.42	0.47	-0.27	0.85	0.57	0.19	0.55	0.38	0.06	0.50	0.84	0.05	0.06	0.20	—	0.44	0.55	0.61	-0.68	0.17	-0.21	0.19	0.42
Te	-0.28	0.23	0.13	0.21	0.26	0.43	-0.15	0.21	0.42	0.08	-0.24	0.19	-0.59	-0.02	-0.21	—	-0.31	0.13	0.18	-0.21	-0.10	-0.60	0.02	0.31
Th	0.09	-0.42	-0.20	-0.38	0.10	-0.36	-0.24	-0.20	-0.13	-0.23	0.04	0.04	-0.12	-0.04	-0.15	—	-0.03	-0.12	-0.20	0.00	-0.09	-0.02	-0.07	-0.36
Tl	-0.66	0.56	0.66	-0.30	0.58	0.62	0.20	0.79	0.80	-0.17	0.16	0.41	-0.27	0.27	0.15	—	-0.01	0.31	0.70	-0.38	0.23	-0.35	0.36	0.79
V	-0.84	0.70	0.80	-0.28	0.72	0.69	0.29	0.91	0.80	-0.11	0.20	0.57	-0.25	0.33	0.27	—	0.25	0.46	0.87	-0.41	0.35	-0.38	0.28	0.85
W	0.87	-0.33	-0.44	0.40	-0.87	-0.49	-0.08	-0.53	-0.34	-0.20	-0.31	-0.79	-0.22	-0.14	-0.23	—	-0.44	-0.55	-0.59	0.76	-0.25	0.10	-0.33	-0.34
Y	-0.85	0.73	0.87	-0.43	0.67	0.68	0.43	0.94	0.70	-0.18	0.21	0.63	-0.12	0.46	0.49	—	0.51	0.38	0.94	-0.30	0.57	-0.15	0.44	0.82
Yb	—	—	—	—	—	—	—	—	—	—	—	—	—	—	—	—	—	—	—	—	—	—	—	—
Zn	-0.32	0.49	0.74	-0.46	0.17	0.60	0.52	0.67	0.67	-0.13	-0.19	0.21	-0.06	0.56	0.57	—	0.34	0.11	0.74	0.14	0.69	0.09	0.87	0.70
Zr	-0.59	0.80	0.91	-0.28	0.26	0.68	0.86	0.76	0.52	-0.39	0.17	0.42	-0.20	0.47	0.87	—	0.81	0.11	0.89	0.18	0.86	0.08	0.29	0.73
Density	-0.47	0.36	0.19	0.15	0.53	0.29	-0.28	0.43	0.45	0.18	0.32	0.14	-0.01	-0.07	-0.43	—	-0.44	0.28	0.24	-0.63	-0.36	-0.47	0.05	0.42
Qz	—	—	—	—	—	—	—	—	—	—	—	—	—	—	—	—	—	—	—	—	—	—	—	—
Ab	-0.07	0.36	0.06	-0.04	0.04	-0.11	-0.11	0.23	-0.11	-0.30	0.55	-0.24	0.24	-0.09	-0.15	—	-0.05	-0.50	0.01	-0.23	-0.13	0.05	0.00	0.06
Cc	0.35	0.01	-0.40	0.84	-0.38	0.02	-0.24	-0.37	-0.18	0.02	-0.06	-0.44	-0.14	-0.58	-0.38	—	-0.37	-0.22	-0.37	0.07	-0.49	-0.35	-0.32	-0.26
MgCc	—	—	—	—	—	—	—	—	—	—	—	—	—	—	—	—	—	—	—	—	—	—	—	—
Dol	—	—	—	—	—	—	—	—	—	—	—	—	—	—	—	—	—	—	—	—	—	—	—	—
Ar	—	—	—	—	—	—	—	—	—	—	—	—	—	—	—	—	—	—	—	—	—	—	—	—
Ill	0.35	0.01	-0.40	0.84	-0.38	0.02	-0.24	-0.37	-0.18	0.02	-0.06	-0.44	-0.14	-0.58	-0.38	—	-0.37	-0.22	-0.37	0.07	-0.49	-0.35	-0.32	-0.26
ChlG	0.35	0.01	-0.40	0.84	-0.38	0.02	-0.24	-0.37	-0.18	0.02	-0.06	-0.44	-0.14	-0.58	-0.38	—	-0.37	-0.22	-0.37	0.07	-0.49	-0.35	-0.32	-0.26

Hem	—	—	—	—	—	—	—	—	—	—	—	—	—	—	—	—	—	—	—	—	—	—	—	—
Hl	—	—	—	—	—	—	—	—	—	—	—	—	—	—	—	—	—	—	—	—	—	—	—	—
Sme	—	—	—	—	—	—	—	—	—	—	—	—	—	—	—	—	—	—	—	—	—	—	—	—
Bas	—	—	—	—	—	—	—	—	—	—	—	—	—	—	—	—	—	—	—	—	—	—	—	—
Kfs	0.35	0.01	-0.40	0.84	-0.38	0.02	-0.24	-0.37	-0.18	0.02	-0.06	-0.44	-0.14	-0.58	-0.38	—	-0.37	-0.22	-0.37	0.07	-0.49	-0.35	-0.32	-0.26
Act	—	—	—	—	—	—	—	—	—	—	—	—	—	—	—	—	—	—	—	—	—	—	—	—
Cctl	—	—	—	—	—	—	—	—	—	—	—	—	—	—	—	—	—	—	—	—	—	—	—	—
Aug	—	—	—	—	—	—	—	—	—	—	—	—	—	—	—	—	—	—	—	—	—	—	—	—
Glc	0.09	0.31	0.07	-0.08	-0.08	-0.06	-0.18	0.24	-0.03	-0.21	0.12	-0.34	0.07	-0.01	-0.11	—	-0.09	-0.50	0.05	-0.10	-0.04	-0.08	0.15	0.12
Tlc	0.00	-0.06	-0.20	-0.13	0.19	-0.17	-0.51	0.00	-0.15	0.32	0.05	-0.12	0.19	0.00	-0.44	—	-0.31	-0.11	-0.16	-0.43	-0.32	-0.19	0.16	-0.12
Ed	-0.19	0.38	0.11	0.55	0.17	0.39	-0.22	0.29	0.46	0.03	-0.07	-0.09	-0.36	-0.32	-0.33	—	-0.37	0.17	0.20	-0.29	-0.32	-0.70	-0.08	0.35
Mn-Ox	0.36	-0.10	-0.13	0.05	-0.16	-0.48	-0.26	-0.09	-0.11	0.27	0.01	-0.56	0.25	0.14	-0.33	—	-0.44	-0.11	-0.26	0.00	-0.23	0.02	-0.16	-0.11

Table IV.1.2 – SE Evia Island

	Ge	***Hf***	***Hg***	***I***	***La***	***Mn***	***Mo***	***Nb***	***Nd***	***Ni***	***Pb***	***Rb***	***Se***	***Sb***	***Sc***	***Sm***	***Sn***	***Sr***	***Te***	***Th***	***Tl***	***V***	***W***	***Y***
SiO_2																								
Al_2O_3																								
Fe_2O_3																								
MgO																								
CaO																								
Na_2O																								
K_2O																								
TiO_2																								

P_2O_5																								
MnO																								
SO_3																								
LOI																								
Ag																								
As																								
Ba																								
Bi																								
Br																								
Cd																								
Ce																								
Co																								
Cr																								
Cs																								
Cu																								
Ga																								
Ge	1.00																							
Hf	0.04	1.00																						
Hg	-0.56	0.00	1.00																					
I	-0.42	-0.26	0.23	1.00																				
La	-0.29	-0.45	0.42	0.52	1.00																			
Mn	—	—	—	—	—	1.00																		
Mo	-0.11	-0.03	-0.04	-0.31	0.39	—	1.00																	
Nb	0.34	-0.22	0.32	0.26	0.21	—	-0.62	1.00																
Nd	-0.30	-0.42	0.43	0.44	0.98	—	0.51	0.09	1.00															

Ni	0.19	-0.43	0.25	0.51	0.43	—	-0.43	0.85	0.29	1.00														
Pb	-0.39	-0.52	0.39	0.61	0.97	—	0.31	0.20	0.92	0.48	1.00													
Rb	0.10	-0.52	0.13	0.64	0.44	—	-0.41	0.72	0.30	0.96	0.53	1.00												
Se	0.88	0.17	-0.68	-0.38	-0.59	—	-0.38	0.29	-0.64	0.11	-0.62	0.06	1.00											
Sb	-0.57	-0.34	0.46	0.15	0.61	—	0.38	-0.01	0.61	0.05	0.64	0.06	-0.69	1.00										
Sc	-0.38	0.44	0.29	-0.09	-0.57	—	-0.48	-0.10	-0.55	-0.40	-0.52	-0.41	-0.11	-0.15	1.00									
Sm	0.26	-0.09	0.12	0.30	0.65	—	0.34	0.18	0.67	0.31	0.52	0.26	-0.10	-0.02	-0.53	1.00								
Sn	-0.35	-0.13	0.14	-0.29	0.26	—	0.85	-0.59	0.37	-0.36	0.22	-0.32	-0.53	0.51	-0.29	0.09	1.00							
Sr	-0.78	-0.19	0.49	0.42	0.62	—	0.38	-0.30	0.68	-0.17	0.63	-0.07	-0.90	0.72	0.06	0.15	0.45	1.00						
Te	-0.18	-0.03	-0.11	-0.26	0.15	—	0.54	-0.37	0.18	-0.23	0.12	-0.22	-0.14	0.14	-0.25	-0.03	0.50	0.13	1.00					
Th	0.06	-0.11	0.12	-0.10	-0.21	—	-0.27	0.14	-0.21	-0.11	-0.22	-0.13	0.13	-0.23	0.52	-0.07	-0.34	-0.11	-0.08	1.00				
Tl	-0.27	-0.39	0.16	-0.10	0.63	—	0.82	-0.38	0.71	-0.13	0.59	-0.09	-0.56	0.53	-0.49	0.31	0.73	0.60	0.47	-0.18	1.00			
V	-0.38	-0.38	0.33	0.16	0.82	—	0.77	-0.26	0.90	-0.05	0.77	-0.01	-0.71	0.68	-0.49	0.47	0.67	0.75	0.33	-0.21	0.90	1.00		
W	0.88	0.18	-0.70	-0.37	-0.59	—	-0.37	0.27	-0.64	0.10	-0.62	0.06	1.00	-0.71	-0.13	-0.11	-0.52	-0.90	-0.13	0.10	-0.55	-0.71	1.00	
Y	-0.41	-0.45	0.57	0.35	0.91	—	0.48	0.06	0.95	0.20	0.86	0.19	-0.74	0.72	-0.40	0.48	0.42	0.76	0.12	-0.15	0.74	0.92	-0.74	1.00
Yb	—	—	—	—	—	—	—	—	—	—	—	—	—	—	—	—	—	—	—	—	—	—	—	—
Zn	-0.07	-0.50	0.35	0.17	0.74	—	0.17	0.40	0.68	0.54	0.74	0.46	-0.31	0.46	-0.53	0.35	0.09	0.25	0.09	-0.18	0.54	0.51	-0.31	0.66
Zr	-0.25	-0.59	0.38	0.67	0.89	—	0.13	0.40	0.83	0.64	0.92	0.70	-0.47	0.55	-0.52	0.45	0.08	0.53	-0.02	-0.16	0.46	0.65	-0.47	0.80
Density	-0.27	-0.01	-0.04	-0.45	0.18	—	0.81	-0.66	0.30	-0.61	0.14	-0.59	-0.42	0.57	-0.22	-0.08	0.80	0.44	0.45	-0.37	0.67	0.62	-0.42	0.38
Qz	—	—	—	—	—	—	—	—	—	—	—	—	—	—	—	—	—	—	—	—	—	—	—	—
Ab	-0.16	-0.08	0.23	-0.35	-0.11	—	0.08	-0.01	-0.07	-0.22	-0.10	-0.27	-0.15	0.45	0.12	-0.57	0.16	0.11	-0.06	-0.09	0.10	0.13	-0.16	0.19
Cc	0.11	0.15	-0.62	-0.14	-0.35	—	-0.01	-0.31	-0.38	-0.31	-0.30	-0.24	0.36	-0.18	-0.09	-0.37	-0.09	-0.33	0.40	-0.28	-0.30	-0.31	0.38	-0.46

MgCc	–	–	–	–	–	–	–	–	–	–	–	–	–	–	–	–	–	–	–	–	–	–	–	–
Dol	–	–	–	–	–	–	–	–	–	–	–	–	–	–	–	–	–	–	–	–	–	–	–	–
Ar	–	–	–	–	–	–	–	–	–	–	–	–	–	–	–	–	–	–	–	–	–	–	–	–
Ill	0.11	0.15	-0.62	-0.14	-0.35	–	-0.01	-0.31	-0.38	-0.31	-0.30	-0.24	0.36	-0.18	-0.09	-0.37	-0.09	-0.33	0.40	-0.28	-0.30	-0.31	0.38	-0.46
ChlG	0.11	0.15	-0.62	-0.14	-0.35	–	-0.01	-0.31	-0.38	-0.31	-0.30	-0.24	0.36	-0.18	-0.09	-0.37	-0.09	-0.33	0.40	-0.28	-0.30	-0.31	0.38	-0.46
Hem	–	–	–	–	–	–	–	–	–	–	–	–	–	–	–	–	–	–	–	–	–	–	–	–
Hl	–	–	–	–	–	–	–	–	–	–	–	–	–	–	–	–	–	–	–	–	–	–	–	–
Sme	–	–	–	–	–	–	–	–	–	–	–	–	–	–	–	–	–	–	–	–	–	–	–	–
Bas	–	–	–	–	–	–	–	–	–	–	–	–	–	–	–	–	–	–	–	–	–	–	–	–
Kfs	0.11	0.15	-0.62	-0.14	-0.35	–	-0.01	-0.31	-0.38	-0.31	-0.30	-0.24	0.36	-0.18	-0.09	-0.37	-0.09	-0.33	0.40	-0.28	-0.30	-0.31	0.38	-0.46
Act	–	–	–	–	–	–	–	–	–	–	–	–	–	–	–	–	–	–	–	–	–	–	–	–
Cctl	–	–	–	–	–	–	–	–	–	–	–	–	–	–	–	–	–	–	–	–	–	–	–	–
Aug	–	–	–	–	–	–	–	–	–	–	–	–	–	–	–	–	–	–	–	–	–	–	–	–
Glc	-0.04	-0.03	0.22	-0.36	-0.08	–	0.12	0.05	-0.04	-0.11	-0.10	-0.22	-0.04	0.30	-0.06	-0.43	0.13	-0.11	0.05	-0.16	0.05	0.08	-0.05	0.15
Tlc	-0.24	0.24	0.32	-0.48	-0.22	–	0.15	-0.13	-0.18	-0.37	-0.25	-0.50	-0.17	0.38	0.25	-0.48	0.28	-0.01	0.09	-0.12	-0.04	-0.01	-0.18	0.01
Ed	-0.08	0.02	-0.38	-0.22	0.16	–	0.70	-0.62	0.22	-0.47	0.14	-0.41	-0.11	0.20	-0.44	0.04	0.50	0.12	0.67	-0.39	0.42	0.42	-0.10	0.15
Mn-Ox	0.32	0.13	-0.11	-0.53	-0.31	–	0.21	-0.06	-0.28	-0.18	-0.31	-0.26	0.23	0.12	-0.05	-0.14	0.25	-0.39	-0.26	-0.08	-0.13	-0.12	0.22	-0.23

Table IV.1.3 – SE Evia Island

	Yb	***Zn***	***Zr***	***Density***	***Qz***	***Ab***	***Cc***	***MgCc***	***Dol***	***Ar***	***Ill***	***Chl***	***Hem***	***Hl***	***Sme***	***Bas***	***Kfs***	***Act***	***Cctl***	***Aug***	***Glc***	***Tlc***	***Ed***	***Tdk***
SiO_2																								
Al_2O_3																								
Fe_2O_3																								

MgO																								
CaO																								
Na_2O																								
K_2O																								
TiO_2																								
P_2O_5																								
MnO																								
SO_3																								
LOI																								
Ag																								
As																								
Ba																								
Bi																								
Br																								
Cd																								
Ce																								
Co																								
Cr																								
Cs																								
Cu																								
Ga																								
Ge																								
Hf																								
Hg																								
I																								
La																								

Mn																								
Mo																								
Nb																								
Nd																								
Ni																								
Pb																								
Rb																								
Se																								
Sb																								
Sc																								
Sm																								
Sn																								
Sr																								
Te																								
Th																								
Tl																								
V																								
W																								
Y																								
Yb	1.00																							
Zn	—	1.00																						
Zr	—	0.63	1.00																					
Density	—	0.08	-0.05	1.00																				
Qz	—	—	—	—	1.00																			
Ab	—	0.02	0.00	0.45	—	1.00																		
Cc	—	-	-	0.22	—	0.11	1.00																	

		0.38	0.37																					
MgCc	—	—	—	—	—	—	—	1.00																
Dol	—	—	—	—	—	—	—	—	1.00															
Ar	—	—	—	—	—	—	—	—	—	1.00														
Ill	—	-0.38	-0.37	0.22	—	0.11	1.00	—	—	—	1.00													
ChlG	—	-0.38	-0.37	0.22	—	0.11	1.00	—	—	—	1.00	1.00												
Hem	—	—	—	—	—	—	—	—	—	—	—	—	1.00											
Hl	—	—	—	—	—	—	—	—	—	—	—	—	—	1.00										
Sme	—	—	—	—	—	—	—	—	—	—	—	—	—	—	1.00									
Bas	—	—	—	—	—	—	—	—	—	—	—	—	—	—	—	1.00								
Kfs	—	-0.38	-0.37	0.22	—	0.11	1.00	—	—	—	1.00	1.00	—	—	—	—	1.00							
Act	—	—	—	—	—	—	—	—	—	—	—	—	—	—	—	—	—	1.00						
Cctl	—	—	—	—	—	—	—	—	—	—	—	—	—	—	—	—	—	—	1.00					
Aug	—	—	—	—	—	—	—	—	—	—	—	—	—	—	—	—	—	—	—	1.00				
Glc	—	0.14	-0.05	0.36	—	0.89	0.18	—	—	—	0.18	0.18	—	—	—	—	0.18	—	—	—	1.00			
Tlc	—	-0.01	-0.34	0.46	—	0.74	0.14	—	—	—	0.14	0.14	—	—	—	—	0.14	—	—	—	0.83	1.00		
Ed	—	-0.03	-0.05	0.73	—	0.16	0.68	—	—	—	0.68	0.68	—	—	—	—	0.68	—	—	—	0.26	0.21	1.00	
Mn-Ox	—	-0.16	-0.34	0.31	—	0.39	0.08	—	—	—	0.08	0.08	—	—	—	—	0.08	—	—	—	0.44	0.53	0.11	1.00

Table IV.2.1 – Kissamos Bay, NW Crete Island

	SiO_2	**Al_2O_3**	**Fe_2O_3**	**MgO**	**CaO**	**Na_2O**	**K_2O**	**TiO_2**	**P_2O_5**	**MnO**	**SO_3**	**LOI**	***Ag***	***As***	***Ba***	***Bi***	***Br***	***Cd***	***Ce***	***Co***	***Cr***	***Cs***	***Cu***	***Ga***
SiO_2	1.00																							

Al_2O_3	-0.14	1.00																						
Fe_2O_3	-0.01	0.85	1.00																					
MgO	-0.51	-0.63	-0.42	1.00																				
CaO	-0.94	-0.19	-0.26	0.72	1.00																			
Na_2O	-0.15	-0.07	0.16	0.54	0.16	1.00																		
K_2O	-0.19	0.93	0.84	-0.58	-0.14	-0.15	1.00																	
TiO_2	0.15	0.89	0.87	-0.69	-0.46	-0.05	0.86	1.00																
P_2O_5	-0.24	0.81	0.48	-0.71	-0.06	-0.53	0.82	0.66	1.00															
MnO	0.70	-0.47	-0.24	-0.07	-0.51	0.04	-0.46	-0.27	-0.51	1.00														
SO_3	-0.63	0.63	0.65	0.09	0.41	0.33	0.68	0.46	0.40	-0.64	1.00													
LOI	-0.99	0.10	-0.09	0.47	0.92	0.06	0.15	-0.20	0.28	-0.70	0.55	1.00												
Ag	-0.31	0.61	0.16	-0.44	0.10	-0.32	0.49	0.31	0.73	-0.46	0.27	0.35	1.00											
As	0.14	-0.55	-0.19	0.48	0.09	0.21	-0.54	-0.52	-0.67	0.55	-0.28	-0.20	-0.56	1.00										
Ba	-0.19	0.94	0.78	-0.62	-0.15	-0.20	0.98	0.86	0.88	-0.51	0.62	0.18	0.56	-0.63	1.00									
Bi	-0.01	-0.40	-0.08	0.53	0.20	0.35	-0.42	-0.30	-0.61	0.21	-0.16	-0.08	-0.59	0.68	-0.48	1.00								
Br	-0.48	0.59	0.68	0.08	0.27	0.51	0.58	0.48	0.25	-0.47	0.93	0.38	0.07	-0.17	0.52	-0.01	1.00							
Cd	-0.33	-0.01	-0.17	0.01	0.22	-0.09	0.13	-0.05	0.30	-0.38	0.11	0.45	0.10	-0.50	0.23	-0.48	-0.01	1.00						
Ce	-0.18	0.87	0.71	-0.61	-0.13	-0.22	0.85	0.88	0.82	-0.52	0.55	0.16	0.48	-0.66	0.88	-0.38	0.50	0.18	1.00					
Co	0.34	0.05	0.12	-0.41	-0.33	-0.75	0.18	0.12	0.25	0.14	-0.17	-0.31	0.04	0.11	0.15	-0.23	-0.34	-0.08	0.09	1.00				
Cr	-0.36	0.68	0.37	-0.44	0.09	-0.25	0.69	0.58	0.81	-0.50	0.40	0.40	0.64	-0.79	0.77	-0.60	0.27	0.45	0.79	-0.04	1.00			
Cs	-0.38	0.61	0.21	-0.48	0.11	-0.40	0.65	0.40	0.87	-0.57	0.36	0.45	0.82	-0.74	0.74	-0.73	0.13	0.58	0.62	0.12	0.81	1.00		
Cu	-0.47	0.76	0.57	-0.33	0.20	-0.19	0.88	0.58	0.79	-0.60	0.69	0.45	0.65	-0.55	0.87	-0.44	0.47	0.24	0.68	0.10	0.72	0.78	1.00	

Ga	-0.31	0.67	0.30	-0.60	0.04	-0.49	0.71	0.50	0.95	-0.56	0.34	0.39	0.72	-0.74	0.80	-0.70	0.17	0.57	0.73	0.18	0.84	0.96	0.74	1.00
Ge	-0.35	0.59	0.16	-0.52	0.10	-0.44	0.56	0.37	0.88	-0.57	0.27	0.44	0.76	-0.74	0.68	-0.72	0.11	0.61	0.63	0.07	0.81	0.94	0.62	0.97
Hf	-0.15	-0.36	0.01	0.66	0.30	0.58	-0.42	-0.24	-0.64	0.15	0.10	0.07	-0.61	0.56	-0.48	0.68	0.26	-0.25	-0.26	-0.31	-0.44	-0.68	-0.47	-0.66
Hg	-0.13	0.61	0.46	-0.41	-0.06	-0.26	0.71	0.51	0.58	-0.26	0.42	0.09	0.64	-0.35	0.67	-0.33	0.20	-0.10	0.49	0.30	0.45	0.59	0.83	0.49
I	-0.71	0.67	0.65	0.02	0.47	0.09	0.71	0.49	0.56	-0.76	0.91	0.66	0.29	-0.34	0.69	-0.13	0.82	0.21	0.67	-0.08	0.54	0.44	0.70	0.51
La	-0.23	0.89	0.66	-0.60	-0.10	-0.11	0.87	0.83	0.86	-0.49	0.58	0.23	0.60	-0.70	0.93	-0.50	0.53	0.28	0.91	-0.06	0.85	0.75	0.78	0.81
Mn	0.55	-0.58	-0.18	0.31	-0.29	0.26	-0.59	-0.35	-0.81	0.74	-0.45	-0.62	-0.76	0.78	-0.69	0.63	-0.25	-0.63	-0.61	0.09	-0.82	-0.95	-0.74	-0.92
Mo	0.20	-0.10	0.24	0.29	-0.14	0.61	-0.20	0.17	-0.52	0.17	0.16	-0.30	-0.60	0.26	-0.25	0.49	0.40	-0.40	-0.01	-0.29	-0.32	-0.68	-0.43	-0.62
Nb	0.25	0.86	0.83	-0.74	-0.55	-0.02	0.80	0.98	0.62	-0.22	0.39	-0.30	0.30	-0.54	0.81	-0.30	0.45	-0.05	0.85	0.08	0.53	0.37	0.48	0.47
Nd	-0.19	0.83	0.64	-0.62	-0.10	-0.28	0.79	0.82	0.84	-0.44	0.48	0.19	0.52	-0.64	0.84	-0.45	0.42	0.22	0.97	0.10	0.80	0.66	0.63	0.76
Ni	-0.21	0.74	0.81	-0.32	-0.03	-0.02	0.90	0.70	0.56	-0.35	0.69	0.14	0.20	-0.31	0.81	-0.18	0.60	0.01	0.63	0.16	0.48	0.38	0.82	0.43
Pb	-0.43	0.86	0.68	-0.43	0.11	-0.18	0.92	0.72	0.87	-0.69	0.67	0.43	0.57	-0.63	0.95	-0.45	0.52	0.36	0.82	0.05	0.78	0.79	0.91	0.83
Rb	-0.36	0.88	0.87	-0.35	0.06	-0.02	0.95	0.78	0.70	-0.53	0.83	0.28	0.37	-0.39	0.91	-0.22	0.74	0.04	0.79	0.10	0.58	0.51	0.85	0.57
Se	-0.34	0.54	0.11	-0.51	0.10	-0.44	0.49	0.33	0.85	-0.55	0.21	0.44	0.72	-0.71	0.62	-0.69	0.08	0.59	0.60	0.04	0.77	0.89	0.52	0.94
Sb	-0.35	-0.12	0.13	0.56	0.45	0.31	-0.13	-0.18	-0.38	-0.11	0.40	0.23	-0.21	0.58	-0.25	0.51	0.39	-0.57	-0.19	-0.02	-0.46	-0.46	-0.04	-0.51
Sc	0.09	-0.46	-0.06	0.55	0.13	0.29	-0.42	-0.34	-0.72	0.36	-0.04	-0.21	-0.67	0.72	-0.57	0.74	0.08	-0.65	-0.47	0.04	-0.69	-0.86	-0.47	-0.85
Sm	-0.20	0.53	0.37	-0.36	-0.02	-0.19	0.55	0.37	0.61	-0.38	0.40	0.24	0.41	-0.41	0.61	-0.67	0.30	0.44	0.36	0.23	0.46	0.61	0.51	0.65
Sn	0.50	-0.36	-0.03	0.13	-0.32	0.08	-0.35	-0.14	-0.57	0.36	-0.22	-0.56	-0.65	0.50	-0.46	0.45	-0.09	-0.52	-0.32	0.26	-0.69	-0.75	-0.56	-0.69
Sr	-0.85	-0.17	-0.08	0.76	0.92	0.29	-0.12	-0.36	-0.18	-0.44	0.54	0.80	-0.09	0.27	-0.17	0.34	0.46	0.05	-0.11	-0.25	-0.07	-0.10	0.11	-0.15
Te	-0.30	0.72	0.34	-0.55	0.04	-0.41	0.74	0.50	0.88	-0.51	0.40	0.34	0.91	-0.65	0.79	-0.64	0.16	0.26	0.65	0.19	0.75	0.93	0.85	0.87
Th	-0.25	-0.37	0.01	0.73	0.43	0.45	-0.35	-0.31	-0.63	0.08	0.20	0.14	-0.64	0.66	-0.46	0.78	0.32	-0.46	-0.35	-0.19	-0.54	-0.76	-0.35	-0.73
Tl	-0.33	0.48	0.15	-0.45	0.09	-0.41	0.55	0.35	0.81	-0.54	0.26	0.43	0.52	-0.72	0.65	-0.68	0.12	0.79	0.61	0.10	0.77	0.88	0.57	0.94

V	-0.26	0.94	0.79	-0.57	-0.09	-0.09	0.96	0.83	0.85	-0.52	0.68	0.24	0.55	-0.59	0.98	-0.48	0.60	0.30	0.88	0.07	0.75	0.74	0.83	0.80
W	-0.30	0.50	0.08	-0.50	0.09	-0.43	0.41	0.29	0.80	-0.51	0.15	0.40	0.67	-0.65	0.54	-0.65	0.07	0.54	0.56	0.01	0.72	0.80	0.41	0.88
Y	-0.26	0.89	0.80	-0.43	-0.05	0.03	0.83	0.89	0.69	-0.55	0.65	0.20	0.40	-0.55	0.85	-0.20	0.65	0.01	0.91	-0.11	0.71	0.46	0.67	0.55
Yb	—	—	—	—	—	—	—	—	—	—	—	—	—	—	—	—	—	—	—	—	—	—	—	—
Zn	-0.45	0.88	0.79	-0.35	0.14	-0.06	0.94	0.76	0.79	-0.64	0.77	0.42	0.48	-0.53	0.94	-0.33	0.64	0.27	0.85	0.04	0.74	0.68	0.89	0.73
Zr	0.26	0.66	0.59	-0.62	-0.50	-0.01	0.57	0.87	0.49	-0.17	0.22	-0.28	0.22	-0.57	0.63	-0.25	0.30	-0.02	0.79	-0.03	0.56	0.28	0.32	0.38
Density	0.49	-0.52	-0.55	-0.11	-0.35	-0.17	-0.57	-0.39	-0.27	0.57	-0.78	-0.38	-0.27	0.09	-0.48	-0.19	-0.66	0.28	-0.44	0.03	-0.21	-0.18	-0.65	-0.12
Qz	—	—	—	—	—	—	—	—	—	—	—	—	—	—	—	—	—	—	—	—	—	—	—	—
Ab	0.23	0.28	0.29	-0.31	-0.32	-0.16	0.27	0.28	0.18	-0.06	0.05	-0.25	0.21	-0.11	0.28	0.00	-0.02	-0.08	0.12	0.40	-0.04	0.18	0.16	0.14
Cc	-0.70	-0.02	0.01	0.50	0.71	-0.02	0.14	-0.17	0.06	-0.59	0.42	0.67	-0.02	-0.09	0.11	0.21	0.23	0.24	-0.01	-0.03	0.09	0.15	0.39	0.11
MgCc	-0.61	-0.47	-0.51	0.61	0.79	-0.23	-0.38	-0.63	-0.15	-0.23	-0.06	0.64	-0.08	0.21	-0.36	0.23	-0.21	0.16	-0.38	0.02	-0.10	-0.04	-0.05	-0.06
Dol	-0.23	0.09	0.24	0.18	0.19	-0.02	0.22	0.14	0.02	-0.31	0.31	0.21	-0.09	-0.22	0.16	-0.01	0.14	0.25	0.22	0.22	0.18	0.11	0.24	0.07
Ar	-0.75	-0.28	-0.49	0.57	0.86	-0.03	-0.32	-0.60	-0.05	-0.40	0.18	0.77	0.21	0.07	-0.31	0.02	0.08	0.10	-0.28	-0.26	-0.02	0.08	0.01	0.02
Ill	—	—	—	—	—	—	—	—	—	—	—	—	—	—	—	—	—	—	—	—	—	—	—	—
ChlG	0.36	0.50	0.48	-0.50	-0.58	0.25	0.38	0.59	0.24	0.01	0.18	-0.35	0.22	-0.35	0.42	-0.39	0.28	0.18	0.45	-0.01	0.29	0.27	0.08	0.26
Hem	-0.08	0.18	0.07	-0.18	0.04	-0.36	0.33	0.04	0.32	-0.10	0.19	0.07	0.38	-0.01	0.29	-0.24	-0.02	-0.14	-0.02	0.41	0.04	0.33	0.55	0.25
Hl	-0.17	0.04	0.10	0.22	0.15	0.49	0.00	0.12	-0.17	-0.10	0.45	0.11	-0.17	-0.05	-0.03	0.19	0.61	-0.14	0.15	-0.41	-0.03	-0.21	-0.07	-0.21
Sme	0.37	0.30	0.29	-0.42	-0.44	0.04	0.15	0.36	0.10	0.33	0.04	-0.42	0.22	0.03	0.14	-0.16	0.15	-0.43	0.21	0.14	-0.04	-0.03	-0.08	-0.04
Bas	—	—	—	—	—	—	—	—	—	—	—	—	—	—	—	—	—	—	—	—	—	—	—	—
Kfs	—	—	—	—	—	—	—	—	—	—	—	—	—	—	—	—	—	—	—	—	—	—	—	—
Act	—	—	—	—	—	—	—	—	—	—	—	—	—	—	—	—	—	—	—	—	—	—	—	—
Cctl	—	—	—	—	—	—	—	—	—	—	—	—	—	—	—	—	—	—	—	—	—	—	—	—
Aug	—	—	—	—	—	—	—	—	—	—	—	—	—	—	—	—	—	—	—	—	—	—	—	—

Glc	–	–	–	–	–	–	–	–	–	–	–	–	–	–	–	–	–	–	–	–	–	–	–	–
Tlc	–	–	–	–	–	–	–	–	–	–	–	–	–	–	–	–	–	–	–	–	–	–	–	–
Ed	–	–	–	–	–	–	–	–	–	–	–	–	–	–	–	–	–	–	–	–	–	–	–	–
Mn-Ox	–	–	–	–	–	–	–	–	–	–	–	–	–	–	–	–	–	–	–	–	–	–	–	–

Table IV.2.2 – Kissamos Bay, NW Crete Island

	Ge	*Hf*	*Hg*	*I*	*La*	*Mn*	*Mo*	*Nb*	*Nd*	*Ni*	*Pb*	*Rb*	*Se*	*Sb*	*Sc*	*Sm*	*Sn*	*Sr*	*Te*	*Th*	*Tl*	*V*	*W*	*Y*
SiO_2																								
Al_2O_3																								
Fe_2O_3																								
MgO																								
CaO																								
Na_2O																								
K_2O																								
TiO_2																								
P_2O_5																								
MnO																								
SO_3																								
LOI																								
Ag																								
As																								
Ba																								
Bi																								
Br																								

Cd																								
Ce																								
Co																								
Cr																								
Cs																								
Cu																								
Ga																								
Ge	1.00																							
Hf	-0.63	1.00																						
Hg	0.34	-0.52	1.00																					
I	0.44	0.06	0.32	1.00																				
La	0.73	-0.41	0.55	0.64	1.00																			
Mn	-0.94	0.53	-0.43	-0.57	-0.74	1.00																		
Mo	-0.63	0.75	-0.39	0.03	-0.15	0.57	1.00																	
Nb	0.37	-0.25	0.43	0.40	0.80	-0.31	0.19	1.00																
Nd	0.69	-0.29	0.45	0.61	0.88	-0.63	-0.10	0.78	1.00															
Ni	0.24	-0.25	0.67	0.69	0.63	-0.33	-0.08	0.61	0.54	1.00														
Pb	0.74	-0.42	0.60	0.80	0.88	-0.81	-0.34	0.64	0.78	0.78	1.00													
Rb	0.41	-0.20	0.65	0.85	0.79	-0.50	-0.04	0.70	0.72	0.92	0.88	1.00												
Se	0.99	-0.58	0.22	0.41	0.69	-0.91	-0.60	0.33	0.67	0.15	0.68	0.34	1.00											
Sb	-0.55	0.57	0.05	0.27	-0.31	0.40	0.42	-0.26	-0.24	0.08	-0.19	0.12	-0.56	1.00										
Sc	-0.89	0.67	-0.28	-0.14	-0.66	0.83	0.60	-0.36	-0.52	-0.09	-0.59	-0.21	-0.88	0.72	1.00									
Sm	0.64	-	0.25	0.46	0.56	-	-	0.33	0.38	0.37	0.63	0.48	0.62	-	-	1.00								

		0.52				0.59	0.39							0.30	0.61									
Sn	-0.74	0.33	-0.31	-0.32	-0.58	0.80	0.53	-0.10	-0.39	-0.14	-0.57	-0.26	-0.71	0.44	0.76	-0.49	1.00							
Sr	-0.12	0.51	-0.10	0.55	-0.15	-0.07	0.15	-0.46	-0.11	0.03	0.03	0.15	-0.12	0.68	0.38	-0.05	-0.07	1.00						
Te	0.82	-0.70	0.80	0.43	0.76	-0.84	-0.63	0.46	0.67	0.49	0.78	0.60	0.75	-0.28	-0.72	0.52	-0.66	-0.13	1.00					
Th	-0.75	0.80	-0.36	0.16	-0.49	0.62	0.65	-0.36	-0.41	-0.05	-0.40	-0.07	-0.72	0.80	0.89	-0.45	0.52	0.68	-0.68	1.00				
Tl	0.94	-0.55	0.23	0.45	0.69	-0.89	-0.57	0.34	0.65	0.28	0.73	0.41	0.93	-0.61	-0.86	0.65	-0.67	-0.10	0.68	-0.69	1.00			
V	0.70	-0.39	0.60	0.74	0.93	-0.71	-0.22	0.79	0.85	0.77	0.94	0.90	0.64	-0.23	-0.57	0.62	-0.47	-0.09	0.75	-0.43	0.68	1.00		
W	0.95	-0.52	0.09	0.37	0.64	-0.84	-0.54	0.31	0.63	0.06	0.61	0.27	0.99	-0.55	-0.84	0.58	-0.66	-0.12	0.66	-0.68	0.88	0.57	1.00	
Y	0.47	-0.09	0.43	0.75	0.88	-0.52	0.17	0.83	0.84	0.68	0.82	0.84	0.44	-0.03	-0.33	0.36	-0.33	0.00	0.53	-0.13	0.42	0.83	0.42	1.00
Yb	—	—	—	—	—	—	—	—	—	—	—	—	—	—	—	—	—	—	—	—	—	—	—	—
Zn	0.61	-0.26	0.62	0.86	0.86	-0.69	-0.18	0.68	0.81	0.84	0.96	0.95	0.54	-0.05	-0.43	0.55	-0.48	0.14	0.71	-0.23	0.61	0.95	0.46	0.86
Zr	0.31	-0.11	0.27	0.25	0.74	-0.28	0.34	0.88	0.72	0.35	0.48	0.47	0.29	-0.30	-0.36	0.17	-0.16	-0.43	0.33	-0.32	0.29	0.58	0.29	0.79
Density	0.00	-0.07	-0.64	-0.69	-0.39	0.22	-0.14	-0.31	-0.32	-0.67	-0.50	-0.73	0.07	-0.60	-0.23	-0.01	-0.02	-0.48	-0.38	-0.34	0.07	-0.46	0.15	-0.55
Qz	—	—	—	—	—	—	—	—	—	—	—	—	—	—	—	—	—	—	—	—	—	—	—	—
Ab	0.08	-0.28	0.38	0.01	0.14	-0.06	-0.12	0.32	0.09	0.16	0.15	0.23	0.03	-0.15	-0.11	0.33	-0.03	-0.22	0.27	-0.19	0.04	0.25	-0.02	0.08
Cc	0.06	0.07	0.16	0.54	-0.03	-0.28	-0.19	-0.28	-0.06	0.33	0.33	0.31	0.02	0.29	0.14	0.15	-0.20	0.66	0.10	0.35	0.14	0.08	-0.04	0.09
MgCc	-0.01	0.18	-0.22	0.12	-0.38	-0.09	-0.28	-0.73	-0.33	-0.25	-0.12	-0.24	0.01	0.25	0.18	-0.02	-0.23	0.66	-0.13	0.36	0.02	-0.39	0.03	-0.32
Dol	0.00	0.22	0.17	0.35	-0.02	-0.12	0.06	0.09	0.21	0.33	0.23	0.28	-0.05	0.09	0.16	-0.11	0.08	0.24	0.06	0.13	0.11	0.18	-0.11	0.14
Ar	0.15	0.13	-0.20	0.25	-0.24	-0.26	-0.25	-0.65	-0.22	-0.29	-0.08	-0.18	0.19	0.36	0.08	-0.02	-0.25	0.73	0.02	0.27	0.06	-0.26	0.23	-0.22
Ill	—	—	—	—	—	—	—	—	—	—	—	—	—	—	—	—	—	—	—	—	—	—	—	—
ChlG	0.27	-0.13	0.12	0.05	0.48	-0.19	0.21	0.68	0.44	0.13	0.24	0.25	0.26	-0.37	-0.41	0.32	-0.08	-0.46	0.24	-0.44	0.26	0.51	0.24	0.36

Hem	0.14	-0.45	0.68	0.09	0.15	-0.22	-0.47	-0.03	-0.08	0.38	0.28	0.30	0.06	0.16	-0.13	0.31	-0.22	-0.02	0.49	-0.20	0.07	0.18	-0.03	0.01
Hl	-0.21	0.42	-0.10	0.24	0.17	0.10	0.68	0.16	0.09	-0.02	-0.11	0.14	-0.21	0.35	0.27	-0.15	0.14	0.36	-0.19	0.41	-0.20	0.03	-0.19	0.24
Sme	-0.05	-0.12	0.23	-0.14	0.22	0.19	0.23	0.41	0.29	-0.04	-0.10	0.11	-0.05	0.09	0.01	0.13	0.15	-0.26	0.14	-0.11	-0.19	0.16	-0.04	0.15
Bas	—	—	—	—	—	—	—	—	—	—	—	—	—	—	—	—	—	—	—	—	—	—	—	—
Kfs	—	—	—	—	—	—	—	—	—	—	—	—	—	—	—	—	—	—	—	—	—	—	—	—
Act	—	—	—	—	—	—	—	—	—	—	—	—	—	—	—	—	—	—	—	—	—	—	—	—
Cctl	—	—	—	—	—	—	—	—	—	—	—	—	—	—	—	—	—	—	—	—	—	—	—	—
Aug	—	—	—	—	—	—	—	—	—	—	—	—	—	—	—	—	—	—	—	—	—	—	—	—
Glc	—	—	—	—	—	—	—	—	—	—	—	—	—	—	—	—	—	—	—	—	—	—	—	—
Tlc	—	—	—	—	—	—	—	—	—	—	—	—	—	—	—	—	—	—	—	—	—	—	—	—
Ed	—	—	—	—	—	—	—	—	—	—	—	—	—	—	—	—	—	—	—	—	—	—	—	—
Mn-Ox	—	—	—	—	—	—	—	—	—	—	—	—	—	—	—	—	—	—	—	—	—	—	—	—

Table IV.2.3 – Kissamos Bay, NW Crete Island

	Yb	***Zn***	***Zr***	***Density***	***Qz***	***Ab***	***Cc***	***MgCc***	***Dol***	***Ar***	***Ill***	***Chl***	***Hem***	***Hl***	***Sme***	***Bas***	***Kfs***	***Act***	***Cctl***	***Aug***	***Glc***	***Tlc***	***Ed***	***Tdk***
SiO_2																								
Al_2O_3																								
Fe_2O_3																								
MgO																								
CaO																								
Na_2O																								

K_2O																								
TiO_2																								
P_2O_5																								
MnO																								
SO_3																								
LOI																								
Ag																								
As																								
Ba																								
Bi																								
Br																								
Cd																								
Ce																								
Co																								
Cr																								
Cs																								
Cu																								
Ga																								
Ge																								
Hf																								
Hg																								
I																								
La																								
Mn																								
Mo																								
Nb																								
Nd																								
Ni																								

Pb																									
Rb																									
Se																									
Sb																									
Sc																									
Sm																									
Sn																									
Sr																									
Te																									
Th																									
Tl																									
V																									
W																									
Y																									
Yb	1.00																								
Zn	—	1.00																							
Zr	—	0.50	1.00																						
Density	—	-0.61	-0.17	1.00																					
Qz	—	—	—	—	1.00																				
Ab	—	0.19	0.12	-0.16	—	1.00																			
Cc	—	0.34	-0.35	-0.47	—	0.13	1.00																		
MgCc	—	-0.16	-0.60	0.02	—	-0.18	0.71	1.00																	
Dol	—	0.33	-0.02	-0.28	—	0.14	0.48	0.11	1.00																
Ar	—	-0.13	-0.58	-0.12	—	-0.38	0.48	0.77	-0.03	1.00															
Ill	—	—	—	—	—	—	—	—	—	—	1.00														
ChlG	—	0.29	0.58	0.08	—	0.37	-	-0.82	0.02	-	—	1.00													

							0.57			0.62														
Hem	—	0.21	-0.12	-0.37	—	0.24	0.24	0.16	-0.15	0.10	—	-0.30	1.00											
Hl	—	0.01	0.31	-0.34	—	-0.08	-0.08	-0.16	-0.15	0.10	—	0.18	-0.14	1.00										
Sme	—	0.00	0.35	-0.03	—	0.39	-0.55	-0.54	-0.32	-0.36	—	0.54	-0.05	0.33	1.00									
Bas	—	—	—	—	—	—	—	—	—	—	—	—	—	—	—	1.00								
Kfs	—	—	—	—	—	—	—	—	—	—	—	—	—	—	—	—	1.00							
Act	—	—	—	—	—	—	—	—	—	—	—	—	—	—	—	—	—	1.00						
Cctl	—	—	—	—	—	—	—	—	—	—	—	—	—	—	—	—	—	—	1.00					
Aug	—	—	—	—	—	—	—	—	—	—	—	—	—	—	—	—	—	—	—	1.00				
Glc	—	—	—	—	—	—	—	—	—	—	—	—	—	—	—	—	—	—	—	—	1.00			
Tlc	—	—	—	—	—	—	—	—	—	—	—	—	—	—	—	—	—	—	—	—	—	1.00		
Ed	—	—	—	—	—	—	—	—	—	—	—	—	—	—	—	—	—	—	—	—	—	—	1.00	
Mn-Ox	—	—	—	—	—	—	—	—	—	—	—	—	—	—	—	—	—	—	—	—	—	—	—	1.00

Table IV.3.1 – Afantou Bay, NE Rhodes Island

	SiO_2	Al_2O_3	Fe_2O_3	MgO	CaO	Na_2O	K_2O	TiO_2	P_2O_5	MnO	SO_3	LOI	*Ag*	*As*	*Ba*	*Bi*	*Br*	*Cd*	*Ce*	*Co*	*Cr*	*Cs*	*Cu*	*Ga*
SiO_2	1.00																							
Al_2O_3	0.06	1.00																						
Fe_2O_3	0.32	-0.23	1.00																					
MgO	-0.64	-0.61	0.37	1.00																				
CaO	-0.35	0.46	-0.85	-0.45	1.00																			
Na_2O	0.49	0.86	-0.06	-0.83	0.26	1.00																		

K_2O	-0.24	-0.47	0.74	0.84	-0.74	-0.58	1.00																	
TiO_2	0.72	-0.15	0.82	-0.10	-0.65	0.17	0.33	1.00																
P_2O_5	-0.23	0.06	0.24	0.35	-0.19	-0.21	0.50	0.10	1.00															
MnO	0.74	-0.15	0.84	-0.11	-0.69	0.22	0.33	0.96	0.02	1.00														
SO_3	-0.75	0.34	-0.38	0.15	0.59	0.06	-0.18	-0.64	-0.19	-0.61	1.00													
LOI	-0.96	-0.10	-0.47	0.55	0.38	-0.48	0.09	-0.83	0.08	-0.84	0.70	1.00												
Ag	-0.48	-0.54	0.08	0.64	-0.23	-0.57	0.34	-0.26	-0.28	-0.21	0.24	0.57	1.00											
As	-0.15	0.89	-0.40	-0.51	0.54	0.76	-0.57	-0.43	-0.19	-0.37	0.58	0.19	-0.23	1.00										
Ba	-0.09	-0.92	0.49	0.76	-0.66	-0.86	0.76	0.30	0.23	0.27	-0.42	0.05	0.50	-0.92	1.00									
Bi	0.37	0.92	-0.21	-0.82	0.37	0.98	-0.64	0.01	-0.19	0.05	0.15	-0.34	-0.55	0.85	-0.93	1.00								
Br	-0.56	0.53	-0.12	0.15	0.39	0.10	0.17	-0.32	0.43	-0.40	0.54	0.38	-0.19	0.37	-0.32	0.18	1.00							
Cd	0.42	-0.40	-0.17	-0.18	-0.13	-0.24	-0.21	0.18	-0.25	0.04	-0.60	-0.27	0.00	-0.47	0.29	-0.23	-0.52	1.00						
Ce	-0.55	-0.19	-0.45	0.29	0.37	-0.50	-0.06	-0.44	0.15	-0.61	0.26	0.56	0.24	-0.15	0.17	-0.38	0.27	0.39	1.00					
Co	-0.54	-0.43	0.53	0.95	-0.58	-0.65	0.91	0.03	0.47	0.01	0.08	0.43	0.52	-0.40	0.68	-0.66	0.23	-0.24	0.18	1.00				
Cr	0.87	0.10	0.61	-0.46	-0.45	0.49	-0.04	0.91	-0.14	0.90	-0.56	-0.91	-0.38	-0.12	-0.05	0.35	-0.41	0.21	-0.53	-0.32	1.00			
Cs	-0.42	-0.89	-0.03	0.71	-0.18	-0.95	0.42	-0.18	0.16	-0.21	-0.10	0.46	0.58	-0.73	0.81	-0.93	-0.29	0.26	0.45	0.50	-0.44	1.00		
Cu	-0.49	-0.39	0.50	0.89	-0.50	-0.64	0.93	0.05	0.61	0.03	0.01	0.33	0.30	-0.46	0.67	-0.66	0.37	-0.29	0.15	0.94	-0.34	0.46	1.00	
Ga	-0.34	-0.87	-0.03	0.68	-0.22	-0.95	0.46	-0.16	0.09	-0.21	-0.17	0.35	0.47	-0.80	0.83	-0.94	-0.16	0.39	0.47	0.50	-0.45	0.88	0.53	1.00
Ge	-0.46	-0.77	0.15	0.83	-0.33	-0.95	0.66	-0.07	0.41	-0.16	-0.15	0.43	0.42	-0.76	0.85	-0.93	-0.02	0.24	0.49	0.72	-0.42	0.88	0.73	0.88
Hf	0.33	0.08	0.26	-0.21	-0.12	0.35	-0.02	0.20	-0.41	0.40	0.04	-0.38	-0.10	0.15	-0.15	0.24	-0.17	-0.46	-0.79	-0.21	0.26	-0.33	-0.12	-0.28
Hg	-0.67	-0.44	0.12	0.77	-0.05	-0.66	0.58	-0.29	0.12	-0.24	0.40	0.54	0.44	-0.31	0.49	-0.65	0.30	-0.39	0.22	0.64	-0.58	0.55	0.72	0.58
I	-0.63	0.67	-0.50	-0.10	0.75	0.26	-0.28	-0.59	0.20	-0.66	0.77	0.55	-0.19	0.68	-0.63	0.39	0.83	-0.48	0.38	-0.08	-0.51	-0.33	-0.03	-0.34

La	-0.51	-0.68	-0.24	0.58	0.08	-0.88	0.24	-0.29	0.25	-0.41	0.02	0.54	0.42	-0.60	0.62	-0.81	-0.04	0.37	0.77	0.38	-0.51	0.90	0.37	0.81
Mn	0.72	0.57	0.38	-0.67	-0.13	0.87	-0.28	0.59	-0.22	0.66	-0.20	-0.76	-0.49	0.41	-0.53	0.76	-0.13	-0.20	-0.71	-0.49	0.81	-0.83	-0.48	-0.83
Mo	0.82	0.51	0.22	-0.71	-0.16	0.74	-0.30	0.58	0.02	0.55	-0.55	-0.82	-0.62	0.21	-0.41	0.67	-0.11	0.26	-0.36	-0.51	0.76	-0.73	-0.45	-0.62
Nb	0.53	-0.44	0.39	-0.01	-0.48	-0.22	0.17	0.64	0.30	0.56	-0.72	-0.53	-0.15	-0.64	0.49	-0.29	-0.49	0.51	0.07	0.00	0.55	0.30	0.01	0.21
Nd	-0.04	0.00	-0.13	-0.09	0.28	-0.06	-0.10	0.07	-0.30	-0.10	0.07	0.01	0.01	-0.11	-0.04	-0.06	0.23	0.34	0.29	-0.15	0.05	-0.04	-0.13	0.14
Ni	-0.48	-0.44	0.60	0.94	-0.63	-0.62	0.93	0.10	0.43	0.10	0.07	0.37	0.51	-0.41	0.69	-0.64	0.20	-0.27	0.09	0.99	-0.25	0.47	0.93	0.47
Pb	-0.56	-0.73	0.19	0.89	-0.29	-0.95	0.71	-0.09	0.45	-0.18	-0.02	0.49	0.48	-0.71	0.83	-0.93	0.11	0.10	0.52	0.79	-0.46	0.86	0.79	0.85
Rb	-0.25	0.88	-0.32	-0.29	0.38	0.58	-0.28	-0.42	0.23	-0.43	0.41	0.25	-0.34	0.84	-0.75	0.70	0.62	-0.37	0.05	-0.11	-0.25	-0.65	-0.10	-0.63
Se	-0.03	-0.77	-0.08	0.35	-0.21	-0.73	0.15	0.04	-0.02	-0.10	-0.39	0.14	0.38	-0.74	0.68	-0.72	-0.43	0.79	0.58	0.20	-0.11	0.76	0.12	0.77
Sb	0.48	0.84	-0.13	-0.80	0.21	0.92	-0.57	0.13	-0.16	0.12	-0.04	-0.42	-0.59	0.72	-0.83	0.94	0.09	-0.02	-0.37	-0.61	0.45	-0.90	-0.64	-0.88
Sc	0.68	0.65	0.29	-0.72	-0.05	0.92	-0.35	0.51	-0.22	0.58	-0.14	-0.71	-0.52	0.51	-0.62	0.83	-0.07	-0.22	-0.68	-0.54	0.76	-0.87	-0.53	-0.88
Sm	-0.33	-0.76	-0.16	0.52	-0.06	-0.86	0.25	-0.17	0.29	-0.26	-0.15	0.36	0.30	-0.70	0.69	-0.82	-0.23	0.41	0.63	0.34	-0.38	0.90	0.35	0.83
Sn	0.62	0.66	0.21	-0.69	-0.04	0.90	-0.36	0.39	-0.08	0.49	-0.13	-0.65	-0.61	0.55	-0.64	0.83	-0.11	-0.31	-0.71	-0.51	0.64	-0.83	-0.48	-0.88
Sr	-0.25	0.78	-0.72	-0.58	0.87	0.60	-0.77	-0.58	-0.21	-0.59	0.64	0.29	-0.29	0.87	-0.91	0.71	0.43	-0.27	0.17	-0.58	-0.28	-0.54	-0.58	-0.59
Te	-0.05	-0.59	-0.15	0.23	-0.11	-0.50	0.09	-0.11	-0.33	-0.16	-0.19	0.19	0.44	-0.47	0.44	-0.51	-0.33	0.47	0.08	0.08	-0.18	0.50	-0.01	0.59
Th	0.08	0.93	-0.51	-0.73	0.60	0.83	-0.72	-0.35	-0.14	-0.33	0.33	-0.01	-0.47	0.92	-0.97	0.92	0.32	-0.20	-0.09	-0.62	-0.01	-0.79	-0.62	-0.80
Tl	-0.26	-0.61	0.13	0.59	-0.31	-0.69	0.38	-0.01	0.30	-0.07	-0.16	0.24	0.30	-0.55	0.65	-0.67	-0.24	0.35	0.58	0.53	-0.23	0.67	0.48	0.64
V	0.50	-0.59	0.80	0.26	-0.75	-0.28	0.52	0.87	0.03	0.84	-0.62	-0.57	0.12	-0.74	0.67	-0.43	-0.50	0.32	-0.23	0.28	0.68	0.28	0.24	0.27
W	0.25	-0.49	-0.09	0.02	-0.19	-0.41	-0.02	0.19	0.17	0.04	-0.58	-0.13	0.02	-0.59	0.44	-0.40	-0.43	0.81	0.43	-0.04	0.15	0.47	-0.09	0.46
Y	-0.19	0.56	0.27	-0.01	0.14	0.42	0.17	0.07	0.30	0.14	0.41	-0.03	-0.24	0.43	-0.36	0.37	0.62	-0.79	-0.30	0.12	0.04	-0.50	0.24	-0.47
Yb	—	—	—	—	—	—	—	—	—	—	—	—	—	—	—	—	—	—	—	—	—	—	—	—
Zn	0.74	-0.12	0.80	-0.14	-0.66	0.21	0.28	0.98	0.08	0.95	-0.63	-0.82	-0.25	-0.38	0.26	0.06	-0.38	0.21	-0.43	0.00	0.94	-0.21	-0.02	-0.21

Zr	0.05	-0.71	0.64	0.60	-0.60	-0.65	0.73	0.55	0.42	0.50	-0.40	-0.20	0.11	-0.87	0.85	-0.75	-0.16	0.11	0.08	0.57	0.21	0.60	0.64	0.60
Density	0.74	0.40	0.03	-0.82	0.18	0.68	-0.58	0.53	-0.26	0.48	-0.29	-0.74	-0.60	0.22	-0.49	0.62	-0.25	0.23	-0.27	-0.77	0.77	-0.56	-0.73	-0.63
Qz	0.00	-0.64	0.39	0.55	-0.61	-0.54	0.58	0.20	0.07	0.21	-0.33	0.01	0.29	-0.61	0.68	-0.62	-0.32	0.22	-0.16	0.54	-0.01	0.45	0.48	0.60
Ab	0.02	-0.75	0.60	0.65	-0.71	-0.62	0.69	0.41	0.02	0.38	-0.32	-0.06	0.41	-0.75	0.83	-0.73	-0.33	0.29	0.02	0.64	0.14	0.51	0.55	0.65
Cc	-0.11	0.86	-0.67	-0.61	0.69	0.67	-0.71	-0.54	-0.08	-0.55	0.41	0.20	-0.38	0.89	-0.91	0.80	0.39	-0.16	0.10	-0.54	-0.23	-0.64	-0.54	-0.65
MgCc	0.23	-0.71	0.33	0.26	-0.43	-0.37	0.19	0.32	-0.23	0.41	-0.34	-0.18	0.38	-0.55	0.57	-0.49	-0.77	0.24	-0.19	0.15	0.23	0.50	0.06	0.41
Dol	0.38	-0.70	0.70	0.37	-0.73	-0.48	0.59	0.75	0.09	0.69	-0.61	-0.45	0.17	-0.87	0.80	-0.60	-0.39	0.37	-0.10	0.35	0.51	0.43	0.36	0.47
Ar	-0.15	0.65	-0.54	-0.58	0.84	0.58	-0.74	-0.35	-0.35	-0.35	0.66	0.15	-0.27	0.75	-0.83	0.64	0.30	-0.34	0.04	-0.63	-0.07	-0.49	-0.64	-0.60
Ill	—	—	—	—	—	—	—	—	—	—	—	—	—	—	—	—	—	—	—	—	—	—	—	—
ChlG	0.11	-0.86	0.67	0.61	-0.69	-0.67	0.71	0.54	0.08	0.55	-0.41	-0.20	0.38	-0.89	0.91	-0.80	-0.39	0.16	-0.10	0.54	0.23	0.64	0.54	0.65
Hem	—	—	—	—	—	—	—	—	—	—	—	—	—	—	—	—	—	—	—	—	—	—	—	—
Hl	—	—	—	—	—	—	—	—	—	—	—	—	—	—	—	—	—	—	—	—	—	—	—	—
Sme	—	—	—	—	—	—	—	—	—	—	—	—	—	—	—	—	—	—	—	—	—	—	—	—
Bas	—	—	—	—	—	—	—	—	—	—	—	—	—	—	—	—	—	—	—	—	—	—	—	—
Kfs	-0.10	-0.55	0.22	0.60	-0.61	-0.64	0.62	0.00	0.42	-0.03	-0.50	0.14	0.30	-0.59	0.71	-0.62	-0.14	0.37	0.21	0.63	-0.26	0.54	0.63	0.66
Act	0.11	-0.86	0.67	0.61	-0.69	-0.67	0.71	0.54	0.08	0.55	-0.41	-0.20	0.38	-0.89	0.91	-0.80	-0.39	0.16	-0.10	0.54	0.23	0.64	0.54	0.65
Cctl	0.11	-0.86	0.67	0.61	-0.69	-0.67	0.71	0.54	0.08	0.55	-0.41	-0.20	0.38	-0.89	0.91	-0.80	-0.39	0.16	-0.10	0.54	0.23	0.64	0.54	0.65
Aug	0.18	0.05	0.19	-0.26	0.23	0.26	-0.22	0.35	-0.40	0.38	0.28	-0.28	-0.08	0.07	-0.19	0.17	-0.10	-0.30	-0.29	-0.34	0.43	-0.17	-0.34	-0.30
Glc	—	—	—	—	—	—	—	—	—	—	—	—	—	—	—	—	—	—	—	—	—	—	—	—
Tlc	—	—	—	—	—	—	—	—	—	—	—	—	—	—	—	—	—	—	—	—	—	—	—	—
Ed	—	—	—	—	—	—	—	—	—	—	—	—	—	—	—	—	—	—	—	—	—	—	—	—
Mn-Ox	—	—	—	—	—	—	—	—	—	—	—	—	—	—	—	—	—	—	—	—	—	—	—	—

Table IV.3.2 – Afantou Bay, NE Rhodes Island

	Ge	*Hf*	*Hg*	*I*	*La*	*Mn*	*Mo*	*Nb*	*Nd*	*Ni*	*Pb*	*Rb*	*Se*	*Sb*	*Sc*	*Sm*	*Sn*	*Sr*	*Te*	*Th*	*Tl*	*V*	*W*	*Y*
SiO_2																								
Al_2O_3																								
Fe_2O_3																								
MgO																								
CaO																								
Na_2O																								
K_2O																								
TiO_2																								
P_2O_5																								
MnO																								
SO_3																								
LOI																								
Ag																								
As																								
Ba																								
Bi																								
Br																								
Cd																								
Ce																								
Co																								
Cr																								
Cs																								
Cu																								
Ga																								

Ge	1.00																								
Hf	-0.46	1.00																							
Hg	0.59	0.19	1.00																						
I	-0.22	-0.25	0.12	1.00																					
La	0.84	-0.64	0.42	-0.02	1.00																				
Mn	-0.83	0.53	-0.58	-0.12	-0.89	1.00																			
Mo	-0.63	0.08	-0.78	-0.18	-0.64	0.78	1.00																		
Nb	0.26	-0.30	-0.35	-0.61	0.30	0.07	0.34	1.00																	
Nd	0.10	-0.24	-0.01	0.20	0.14	-0.08	-0.01	-0.21	1.00																
Ni	0.68	-0.13	0.65	-0.13	0.32	-0.42	-0.48	0.01	-0.16	1.00															
Pb	0.97	-0.46	0.66	-0.12	0.84	-0.82	-0.67	0.22	0.07	0.75	1.00														
Rb	-0.47	-0.16	-0.25	0.74	-0.43	0.20	0.26	-0.53	-0.11	-0.15	-0.43	1.00													
Se	0.70	-0.61	0.03	-0.45	0.81	-0.63	-0.27	0.55	0.26	0.16	0.63	-0.61	1.00												
Sb	-0.82	0.09	-0.79	0.26	-0.75	0.74	0.74	-0.14	0.04	-0.60	-0.87	0.65	-0.54	1.00											
Sc	-0.87	0.50	-0.61	-0.03	-0.90	0.99	0.79	0.00	-0.08	-0.47	-0.87	0.30	-0.67	0.80	1.00										
Sm	0.82	-0.54	0.34	-0.23	0.94	-0.81	-0.54	0.48	-0.08	0.29	0.80	-0.54	0.82	-0.76	-0.84	1.00									
Sn	-0.84	0.51	-0.57	-0.02	-0.89	0.93	0.73	-0.01	-0.33	-0.45	-0.85	0.37	-0.73	0.78	0.94	-0.76	1.00								
Sr	-0.62	-0.07	-0.29	0.81	-0.28	0.17	0.09	-0.58	0.14	-0.62	-0.58	0.71	-0.49	0.58	0.27	-0.42	0.29	1.00							
Te	0.45	-0.19	0.03	-0.36	0.40	-0.45	-0.37	0.01	0.49	0.07	0.36	-0.50	0.65	-0.33	-0.47	0.35	-0.58	-0.31	1.00						
Th	-0.79	0.02	-0.55	0.62	-0.58	0.46	0.45	-0.45	-0.02	-0.64	-0.79	0.84	-0.61	0.85	0.56	-0.65	0.59	0.89	-0.44	1.00					
Tl	0.70	-0.45	0.39	-0.27	0.68	-0.59	-0.33	0.43	-0.27	0.50	0.70	-0.34	0.60	-0.65	-0.63	0.78	-0.52	-0.49	-0.05	-0.57	1.00				
V	0.32	0.07	-0.01	-0.76	0.10	0.20	0.20	0.68	0.10	0.34	0.29	-0.74	0.40	-0.30	0.09	0.21	-0.02	-0.83	0.20	-0.72	0.30	1.00			
W	0.46	-	-	-	0.59	-	0.11	0.74	0.14	-	0.36	-	0.87	-	-	0.67	-	-	0.48	-	0.44	0.37	1.00		

		0.70	0.39	0.42		0.35				0.08		0.41		0.17	0.37		0.40	0.36		0.35				
Y	-0.36	0.36	0.25	0.50	-0.49	0.40	0.13	-0.42	-0.11	0.16	-0.21	0.43	-0.80	0.16	0.41	-0.53	0.43	0.28	-0.65	0.28	-0.27	-0.17	-0.75	1.00
Yb	—	—	—	—	—	—	—	—	—	—	—	—	—	—	—	—	—	—	—	—	—	—	—	—	—
Zn	-0.11	0.12	-0.40	-0.60	-0.30	0.61	0.61	0.69	0.01	0.07	-0.13	-0.38	0.06	0.19	0.53	-0.16	0.42	-0.55	-0.11	-0.29	0.00	0.86	0.26	0.02
Zr	0.69	-0.08	0.43	-0.50	0.48	-0.26	-0.20	0.63	-0.07	0.60	0.71	-0.70	0.46	-0.69	-0.36	0.59	-0.36	-0.84	0.09	-0.89	0.60	0.77	0.35	-0.06
Density	-0.65	0.15	-0.71	-0.09	-0.44	0.75	0.73	0.35	0.18	-0.73	-0.69	-0.01	-0.19	0.66	0.75	-0.40	0.65	0.27	-0.29	0.41	-0.41	0.21	0.11	0.00
Qz	0.59	-0.04	0.26	-0.54	0.22	-0.32	-0.27	0.13	0.08	0.56	0.53	-0.47	0.43	-0.46	-0.39	0.34	-0.35	-0.70	0.62	-0.67	0.33	0.50	0.30	-0.24
Ab	0.64	-0.08	0.35	-0.60	0.33	-0.29	-0.25	0.32	0.13	0.67	0.63	-0.63	0.53	-0.60	-0.38	0.42	-0.43	-0.83	0.46	-0.83	0.54	0.73	0.32	-0.20
Cc	-0.64	-0.13	-0.45	0.71	-0.39	0.22	0.28	-0.51	-0.01	-0.58	-0.64	0.87	-0.49	0.73	0.33	-0.49	0.39	0.92	-0.35	0.97	-0.46	-0.84	-0.27	0.20
MgCc	0.30	0.22	0.20	-0.72	0.20	-0.08	-0.18	0.32	-0.15	0.20	0.26	-0.75	0.38	-0.51	-0.15	0.36	-0.11	-0.60	0.28	-0.63	0.46	0.63	0.21	-0.21
Dol	0.49	-0.01	0.09	-0.74	0.28	-0.02	0.05	0.72	0.13	0.40	0.46	-0.79	0.55	-0.44	-0.12	0.38	-0.25	-0.88	0.34	-0.83	0.32	0.93	0.48	-0.33
Ar	-0.64	0.13	-0.20	0.69	-0.30	0.31	0.04	-0.50	0.23	-0.64	-0.58	0.42	-0.50	0.47	0.38	-0.42	0.35	0.90	-0.30	0.71	-0.52	-0.57	-0.43	0.35
Ill	—	—	—	—	—	—	—	—	—	—	—	—	—	—	—	—	—	—	—	—	—	—	—	—	—
ChlG	0.64	0.13	0.45	-0.71	0.39	-0.22	-0.28	0.51	0.01	0.58	0.64	-0.87	0.49	-0.73	-0.33	0.49	-0.39	-0.92	0.35	-0.97	0.46	0.84	0.27	-0.20
Hem	—	—	—	—	—	—	—	—	—	—	—	—	—	—	—	—	—	—	—	—	—	—	—	—	—
Hl	—	—	—	—	—	—	—	—	—	—	—	—	—	—	—	—	—	—	—	—	—	—	—	—	—
Sme	—	—	—	—	—	—	—	—	—	—	—	—	—	—	—	—	—	—	—	—	—	—	—	—	—
Bas	—	—	—	—	—	—	—	—	—	—	—	—	—	—	—	—	—	—	—	—	—	—	—	—	—
Kfs	0.70	-0.35	0.22	-0.44	0.44	-0.55	-0.17	0.33	-0.23	0.59	0.63	-0.19	0.55	-0.46	-0.58	0.52	-0.51	-0.67	0.33	-0.54	0.57	0.24	0.47	-0.43
Act	0.64	0.13	0.45	-0.71	0.39	-0.22	-0.28	0.51	0.01	0.58	0.64	-0.87	0.49	-0.73	-0.33	0.49	-0.39	-0.92	0.35	-0.97	0.46	0.84	0.27	-0.20
Cctl	0.64	0.13	0.45	-0.71	0.39	-0.22	-0.28	0.51	0.01	0.58	0.64	-0.87	0.49	-0.73	-0.33	0.49	-0.39	-0.92	0.35	-0.97	0.46	0.84	0.27	-0.20
Aug	-0.36	0.47	0.05	0.03	-0.23	0.46	0.00	-0.03	0.25	-0.27	-0.28	-0.35	-0.29	0.03	0.42	-0.25	0.30	0.15	-0.14	-0.03	-0.33	0.28	-0.34	0.34
Glc	—	—	—	—	—	—	—	—	—	—	—	—	—	—	—	—	—	—	—	—	—	—	—	—	—

Tlc	–	–	–	–	–	–	–	–	–	–	–	–	–	–	–	–	–	–	–	–	–	–	–	–
Ed	–	–	–	–	–	–	–	–	–	–	–	–	–	–	–	–	–	–	–	–	–	–	–	–
Mn-Ox	–	–	–	–	–	–	–	–	–	–	–	–	–	–	–	–	–	–	–	–	–	–	–	–

Table IV.3.3 – Afantou Bay, NE Rhodes Island

	Yb	*Zn*	*Zr*	*Density*	*Qz*	*Ab*	*Cc*	*MgCc*	*Dol*	*Ar*	*Ill*	*Chl*	*Hem*	*Hl*	*Sme*	*Bas*	*Kfs*	*Act*	*Cctl*	*Aug*	*Glc*	*Tlc*	*Ed*	*Tdk*
SiO_2																								
Al_2O_3																								
Fe_2O_3																								
MgO																								
CaO																								
Na_2O																								
K_2O																								
TiO_2																								
P_2O_5																								
MnO																								
SO_3																								
LOI																								
Ag																								
As																								
Ba																								
Bi																								

Br																								
Cd																								
Ce																								
Co																								
Cr																								
Cs																								
Cu																								
Ga																								
Ge																								
Hf																								
Hg																								
I																								
La																								
Mn																								
Mo																								
Nb																								
Nd																								
Ni																								
Pb																								
Rb																								
Se																								
Sb																								
Sc																								
Sm																								
Sn																								
Sr																								
Te																								
Th																								
Tl																								

V																								
W																								
Y																								
Yb	1.00																							
Zn	—	1.00																						
Zr	—	0.50	1.00																					
Density	—	0.55	-0.19	1.00																				
Qz	—	0.20	0.50	-0.50	1.00																			
Ab	—	0.40	0.72	-0.40	0.88	1.00																		
Cc	—	-0.49	-0.90	0.24	-0.63	-0.83	1.00																	
MgCc	—	0.32	0.48	-0.08	0.56	0.64	-0.67	1.00																
Dol	—	0.72	0.84	0.06	0.51	0.73	-0.90	0.47	1.00															
Ar	—	-0.34	-0.65	0.45	-0.68	-0.71	0.68	-0.36	-0.68	1.00														
Ill	—	—	—	—	—	—	—	—	—	—	1.00													
ChlG	—	0.49	0.90	-0.24	0.63	0.83	-1.00	0.67	0.90	-0.68	—	1.00												
Hem	—	—	—	—	—	—	—	—	—	—	—	—	1.00											
Hl	—	—	—	—	—	—	—	—	—	—	—	—	—	1.00										
Sme	—	—	—	—	—	—	—	—	—	—	—	—	—	—	1.00									
Bas	—	—	—	—	—	—	—	—	—	—	—	—	—	—	—	1.00								
Kfs	—	0.00	0.44	-0.62	0.59	0.54	-0.43	0.16	0.40	-0.92	—	0.43	—	—	—	—	1.00							
Act	—	0.49	0.90	-0.24	0.63	0.83	-1.00	0.67	0.90	-0.68	—	1.00	—	—	—	—	0.43	1.00						
Cctl	—	0.49	0.90	-0.24	0.63	0.83	-1.00	0.67	0.90	-0.68	—	1.00	—	—	—	—	0.43	1.00	1.00					
Aug	—	0.31	0.10	0.53	-0.24	-0.06	-0.17	0.26	0.14	0.56	—	0.17	—	—	—	—	-0.82	0.17	0.17	1.00				
Glc	—	—	—	—	—	—	—	—	—	—	—	—	—	—	—	—	—	—	—	—	1.00			

Tlc	–	–	–	–	–	–	–	–	–	–	–	–	–	–	–	–	–	–	–	–	1.00		
Ed	–	–	–	–	–	–	–	–	–	–	–	–	–	–	–	–	–	–	–	–	–	1.00	
Mn-Ox	–	–	–	–	–	–	–	–	–	–	–	–	–	–	–	–	–	–	–	–	–	–	1.00